*Edited by Bert Müller and*
*Marcel Van de Voorde*

**Nanoscience and**
**Nanotechnology for**
**Human Health**

## *Further Volumes of the Series "Nanotechnology Innovation & Applications"*

Axelos, M. A. V. and Van de Voorde, M. (eds.)

### Nanotechnology in Agriculture and Food Science

2017
Print ISBN: 9783527339891

Cornier, J., Kwade, A., Owen, A., Van de Voorde, M. (eds.)

### Pharmaceutical Nanotechnology

**Innovation and Production**

2017
Print ISBN: 9783527340545

Fermon, C. and Van de Voorde, M. (eds.)

### Nanomagnetism

**Applications and Perspectives**

2017
Print ISBN: 9783527339853

Mansfield, E., Kaiser, D. L., Fujita, D., Van de Voorde, M. (eds.)

### Metrology and Standardization for Nanotechnology

**Protocols and Industrial Innovations**

2017
Print ISBN: 9783527340392

Meyrueis, P., Sakoda, K., Van de Voorde, M. (eds.)

### Micro- and Nanophotonic Technologies

2017
Print ISBN: 9783527340378

Puers, R., Baldi, L., van Nooten, S. E., Van de Voorde, M. (eds.)

### Nanoelectronics

**Materials, Devices, Applications**

2017
Print ISBN: 9783527340538

Raj, B., Van de Voorde, M., Mahajan, Y. (eds.)

### Nanotechnology for Energy Sustainability

2017
Print ISBN: 9783527340149

Sels, B. and Van de Voorde, M. (eds.)

### Nanotechnology in Catalysis

**Applications in the Chemical Industry, Energy Development, and Environment Protection**

2017
Print ISBN: 9783527339143

*Edited by Bert Müller and Marcel Van de Voorde*

# Nanoscience and Nanotechnology for Human Health

WILEY-VCH
Verlag GmbH & Co. KGaA

**Volume Editors**

***Prof. Bert Müller***
University of Basel
Department of Biomedical Engineering
Biomaterials Science Center
Gewerbestrasse 14
4123 Allschwil, Switzerland

***Prof. Dr. Dr. h.c. Marcel H. Van de Voorde***
Member of the Science Council
of the French Senate and National
Assembly, Paris
Rue du Rhodania, 5
BRISTOL A, Appartement 31
3963 Crans-Montana
Switzerland

**Series Editor**

***Prof. Dr. Dr. h.c. Marcel H. Van de Voorde***
Member of the Science Council
of the French Senate and National
Assembly, Paris
Rue du Rhodania, 5
BRISTOL A, Appartement 31
3963 Crans-Montana
Switzerland

**Cover credits:** Top right 3D image inside blood vessel: fotolia_© abhijith3747
Background, heart and skeleton: fotolia_© psdesign1



**Library of Congress Card No.:** applied for

**British Library Cataloguing-in-Publication Data**
A catalogue record for this book is available from the British Library.

**Bibliographic information published by the Deutsche Nationalbibliothek**
The Deutsche Nationalbibliothek lists this publication in the Deutsche Nationalbibliografie; detailed bibliographic data are available on the Internet at http://dnb.d-nb.de.



**Print ISBN:** 978-3-527-33860-3
**ePDF ISBN:** 978-3-527-69204-0
**ePub ISBN:** 978-3-527-69206-4
**Mobi ISBN:** 978-3-527-69207-1
**oBook ISBN:** 978-3-527-69205-7

**Cover Design** Adam Design
**Typesetting** Thomson Digital, Noida, India
**Printing and Binding**

Printed on acid-free paper

*Thanks to my wife for her patience with me spending many hours working on the book series through the nights and over weekends.*
*The assistance of my son Marc Philip related to the complex and large computer files with many sophisticated scientific figures is also greatly appreciated.*

*Marcel Van de Voorde*

## Series Editor Preface

Since years, nanoscience and nanotechnology have become particularly important technology areas worldwide. As a result, there are many universities that offer courses as well as degrees in nanotechnology. Many governments including European institutions and research agencies have vast nanotechnology programmes and many companies file nanotechnology-related patents to protect their innovations. In short, nanoscience is a hot topic!

Nanoscience started in the physics field with electronics as a forerunner, quickly followed by the chemical and pharmacy industries. Today, nanotechnology finds interests in all branches of research and industry worldwide. In addition, governments and consumers are also keen to follow the developments, particularly from a safety and security point of view.

This books series fills the gap between books that are available on various specific topics and the encyclopedias on nanoscience. This well-selected series of books consists of volumes that are all edited by experts in the field from all over the world and assemble top-class contributions. The topical scope of the book is broad, ranging from nanoelectronics and nanocatalysis to nanometrology. Common to all the books in the series is that they represent top-notch research and are highly application-oriented, innovative, and relevant for industry.

The titles of the volumes in the series are as follows:

**Human-related nanoscience and nanotechnology**

- *Nanoscience and Nanotechnology for Human Health*
- *Pharmaceutical Nanotechnology*
- *Nanotechnology in Agriculture and Food Science*

**Nanoscience and nanotechnology in information and communication**

- *Nanoelectronics*
- *Micro- and Nanophotonic Technologies*
- *Nanomagnetism: Perspectives and Applications*

**Nanoscience and nanotechnology in industry**

- Nanotechnology for Energy Sustainability
- Metrology and Standardization of Nanomaterials
- Nanotechnology in Catalysis: Applications in the Chemical Industry, Energy Development, and Environmental Protection

The book series appeals to a wide range of readers with backgrounds in physics, chemistry, biology, and medicine, from students at universities to scientists at institutes, in industrial companies and government agencies and ministries.

Ever since nanoscience was introduced many years ago, it has greatly changed our lives – and will continue to do so!

March 2016 *Marcel Van de Voorde*

## About the Series Editor

Marcel Van de Voorde, Prof. Dr. ir. Ing. Dr. h.c., has 40 years' experience in European Research Organisations, including CERN-Geneva and the European Commission, with 10 years at the Max Planck Institute for Metals Research, Stuttgart. For many years, he was involved in research and research strategies, policy, and management, especially in European research institutions.

He has been a member of many Research Councils and Governing Boards of research institutions across Europe, the United States, and Japan. In addition to his Professorship at the University of Technology in Delft, the Netherlands, he holds multiple visiting professorships in Europe and worldwide. He holds a doctor honoris causa and various honorary professorships.

He is a senator of the European Academy for Sciences and Arts, Salzburg, and Fellow of the World Academy for Sciences. He is a member of the Science Council of the French Senate/National Assembly in Paris. He has also provided executive advisory services to presidents, ministers of science policy, rectors of Universities, and CEOs of technology institutions, for example, to the president and CEO of IMEC, Technology Centre in Leuven, Belgium. He is also a Fellow of various scientific societies. He has been honored by the Belgian King and European authorities, for example, he received an award for European merits in Luxemburg given by the former President of the European Commission. He is author of multiple scientific and technical publications and has coedited multiple books, especially in the field of nanoscience and nanotechnology.

# Contents

# Nanomedicine: Present Accomplishments and Far-Reaching Promises

The symbolic dawn of nanotechnology is often ascribed to Richard Feynman's address to the American Physical Society in 1959: "There is plenty of room at the bottom.." Possible applications to medicine rapidly appeared as of major importance encompassing *in vitro* diagnosis, *in vivo* imaging, and therapeutics. It has been, however, necessary to wait until 1995 to have the first nanodrug approved by the US Food and Drug Administration – a liposomal formulation of doxorubicin termed Doxil®. At present, there are over 300 nanodrugs in various stages of clinical development. All of them, that have been already approved, rely on passive targeting: These compounds are accumulated in tumor tissue due to the existence of leaky, abnormally fenestrated blood vessels and also due to altered lymphatic circulation (EPR (enhanced permeability and retention effect)). Nanocarriers conjugated with antibodies or physiological ligands and thus specifically targeted to cells expressing the corresponding markers are the next step in the development of nanotherapeutics. Such drugs are expected to display a markedly increased therapeutic index, that is, increased effect on tumor tissue and decreased general toxicity. Several of them are now in the late stages of clinical studies and should become available soon. Future developments include theranostics and personalized nanomedicine. Theranostics consist in the presence of therapeutic and imaging compounds in the same carriers specifically targeted to tumor cells. A major advantage of this technology would be the possibility of noninvasive monitoring of early response to therapy and thus to rapid adaptation of the treatment. Personalized nanomedicine will allow the selection of nanodrugs specifically for each patient according to molecular markers ("-omics" data). In this respect, RNA interference seems a promising approach. In parallel to this progress, in diagnostics and therapy, it will be necessary to develop toxicology. The toxicity of a compound changes markedly when the latter is reduced at the nanometer scale. Besides toxicity, due to their shape – "asbestos-like" properties of carbon nanotubes – nanoparticle detrimental effects derive from generation of reactive oxygen species, cellular structure disruption, and immunological reactions. A great progress in the clinical development of

nanodrugs would be the availability of *in vitro* assays able to predict *in vivo* toxicity.

Nanoparticles are rapidly extending their use in industry: paints, electronics, tires, sport equipment, sunscreens, and so on. The possible toxicity of these compounds present in our environment should be examined. We should also keep in mind and try to prevent the possibility of most dreadful developments: the weaponization of the processes and compounds. The future of nanomedicine is obviously bright. It is bound to become one of our most important tools for diagnosis and therapy.

Member of the French Academy of Medicine *Edwin Milgrom*

# Part One
# Introduction to Nanoscience in Medicine of the Twenty-First Century

# 1
# Challenges and Opportunities of Nanotechnology for Human Health

*Bert Müller*

*University of Basel, Department of Biomedical Engineering, Biomaterials Science Center, Gewerbestrasse 14, 4123 Allschwil, Switzerland*

Medical doctors have a wide variety of experiences with patients. Therefore, they are generally fast in the evaluation of the entire human body. For example, looking at the morphology of the human body, they can identify the chronic inflammatory disease of the axial skeleton, termed ankylosing spondylitis, previously known as Bekhterev's disease. For many natural scientists and engineers, these abilities are fascinating and surprising, at once.

For the diagnosis of an increasing number of diseases, however, a more detailed evaluation, for example, on the basis of radiological data, is necessary. The amount of high-resolution data obtained is huge and usually overburdens the medical experts. Interdisciplinary cooperation with computer scientists to (semi)automatically analyze the imaging data becomes more and more common. These assessments are often expensive and time-consuming. Nonetheless, the available clinical imaging modalities even with the best spatial resolution do not reach the resolution needed to visualize individual biological cells with sizes of about 10 μm. To this end, it appears dubious, why patients can benefit from nanotechnology.

Reading the instruction leaflets of currently available sun crèmes or sensitive toothpastes, we realize, however, that nanotechnology has reached our daily routine. This book will hardly deal with these well-established, systemic applications, we have known from pharmacy for decades, but with the impact of nanotechnology on dedicated future therapies for the most important diseases.

The leading cause of death in our society relates to cardiovascular diseases [1]. Therefore, the first part of this book, which consists of four chapters from medical experts, that is, cardiologist, internist, immunologist, and natural scientists, targets current research activities toward nonsystemic treatments. For example, nitroglycerin is currently administered to widen the constricted atherosclerotic arteries in a systemic fashion. The vasodilator widens all arteries and veins with serious side effects, including a drastic blood pressure drop. Therefore, the nitroglycerin dose has to be kept limited. Specific biomarkers

*Nanoscience and Nanotechnology for Human Health,* First Edition. Edited by Bert Müller and Marcel Van de Voorde.

for this prevalent inflammation do not exist. Consequently, researchers proposed to exploit the wall shear stress increased at constricted arteries with respect to the healthy parts as purely physical trigger to release drugs from mechanosensitive containers or particles of nanometer size [2,3]. These nanotechnology-based innovations are sweeping the established cardiovascular treatments, especially before the patients reach the operating room and endovascular devices for intra-arterial clot lysis, stent implantation, or arterial balloon dilatation could become effective [4].

Second most common cause of death is cancer. It is, therefore, not surprising that the second part of the book is dedicated to alternative diagnoses and treatments of cancer. Although one can cleverly combine pharmaceutical, surgical, and radiation treatments to heal patients, alternative strategies to fight against cancer are more than desirable. The four related chapters depict how contemporary methods and sophisticated materials can contribute to a reliable diagnosis and, more important, to powerful treatments of cancerous tissues even deeply inside the human body difficult to reach. Here, the deep understanding of the physical interactions between the probes such as photons or protons and the biological matter is essential for the selection and the future development of treatment strategies for the general public.

The third part of the book relates to the most common diseases, which are caries, musculoskeletal diseases, incontinence, and allergies. Although they often do not result in death, they massively influence our quality of life.

Caries is the most common infectious bacterial diseases in the world [5]. The disease first destroys the human enamel, which is a unique biologically ordered material with hydroxyapatite crystallites being organized into a fibrous continuum. In healthy state, it remains stable for decades and centuries or even millennia. Currently, no engineering process exists to biomimetically repair this unique biological material with a well-defined nanostructural organization. Therefore, the burden of dental caries lasts for a lifetime. Once the tooth structure is destroyed, it will usually need restoration and additional maintenance throughout life. In addition, the economic impact of such therapeutic approaches is enormous. The World Health Organization estimated that the dental treatment costs accounted for 5–10% of healthcare budgets in industrialized countries and additional costs are caused through absences from work [6,7]. So far, treatments rely on mechanical replacement of decayed tissue by inert biomaterials such as isotropic polymers or composites. Recently, the analysis of the healthy and diseased crowns down to the nanometer scale has led to the necessary anatomical knowledge to develop biomimetic dental fillings, which contain elongated nanostructures with the orientations present in dentin and enamel [8]. Furthermore, the detailed analysis of the caries pathology using X-ray scattering has shown that while bacterial processes dissolve the minerals in enamel and dentin, the dentinal collagen network remains unaffected, enabling the development of treatments to remineralize the dentin [9,10].

The musculoskeletal system demands increasingly frequent treatments with metallic load-bearing implants, which include artificial hips, knees, and dental implants. In general, these metals integrate well into the bone because the sand-blasted and etched oxide surface contains a multiplicity of features on the micro- and nanometer scale, which exhibit similarities to the nanometer-size minerals in bone. Therefore, it has been stated that the morphology of the implant's surface tends to have a greater effect than chemical patterns, when both chemical patterns and topographic ones are offered to biological cells [11]. The vital role of the nanostructures in avoiding inflammatory reactions and in reaching cytocompatibility was demonstrated using nanopyramids naturally formed in heteroepitaxy of semiconductors [12,13]. In contrast to metals, high-performance polymers are radiolucent and magnetic resonance imaging compatible, which allow the diagnostic examination of tissues in implant's vicinity. Only recently, the systematic polymer structuring on the nanometer scale for centimeter-size implants was explored [14]. It is relatively easy to produce micro- and nanostructures with a preferential orientation, which better mimic the anisotropy of the bony tissues within our body [15]. Therefore, one can reasonably expect that polymeric load-bearing implants will be employed in near future at least for dedicated cases.

The aging of our society has led to the increasing prevalence of social and economic burdening by age-related diseases, including urinary and fecal incontinence. In comparatively simple cases, conservative therapy is successful. Surgical therapy is advisable for more complex cases, where the extent of surgery depends on the severity. In severe cases, artificial sphincter systems are applied, which currently rely on fluid-filled cuffs. So far, they are not part of everyday surgical treatments owing to the large number of complications, including wound infection, postoperative pain, and consecutive resurgeries. One of the main drawbacks is the constant pressure acting on the hollow organ. The natural counterpart, however, adapts to external factors such as climbing stairs or resting in bed, so that the function is guaranteed and the tissue can regenerate. Hence, sensor-controlled devices with the necessary time response have to be developed [16]. As dielectric elastomer actuators (DEA) not only provide the necessary forces, strains, and response time but can also simultaneously be operated as sensors, these artificial muscles have a huge potential to become the basis of future active implants [17]. There are, however, several challenges to be solved, mainly related to the high voltages required to drive micrometer-thin DEA. Sandwiched nanometer-thin elastomer films with ultrathin compliant electrodes have to be made available to fabricate biomimetic artificial sphincters and finally to successfully treat incontinence.

The book *Nanotechnology for Human Health* should promote the prosperous use of nanotechnology in prevention, diagnosis, and therapy of the most relevant diseases of our century. It should comparably become a tool for research-interested medical doctors as well as natural scientists and engineers with a strong affinity to support curing patients [18,19]. In this manner, patients concerned will benefit from this collaborative initiative of an interdisciplinary team of researchers.

## References


1 Lloyd-Jones, D., Adams, R., Carnethon, M., Simone, G.D., Ferguson, T.B., Flegal, K., Ford, E., Furie, K., Go, A., Greenlund, K., Haase, N., Hailpern, S., Ho, M., Howard, V., Kissela, B., Kittner, S., Lackland, D., Lisabeth, L., Marelli, A., McDermott, M., Meigs, J., Mozaffarian, D., Nichol, G., O'Donnell, C., Roger, V., Rosamond, W., Sacco, R., Sorlie, P., Stafford, R., Steinberger, J., Thom, T., Wasserthiel-Smoller, S., Wong, N., Wylie-Rosett, J., and Hong, Y. (2009) Heart disease and stroke statistics – 2009 update: a report from the American Heart Association Statistics Committee and Stroke Statistics Subcommittee. *Circulation*, **119** (3), e21–e181.

2 Holme, M.N., Fedotenko, I.A., Abegg, D., Althaus, J., Babel, L., Favarger, F., Reiter, R., Tanasescu, R., Zaffalon, P.-L., Ziegler, A., Müller, B., Saxer, T., and Zumbuehl, A. (2012) Shear-stress sensitive lenticular vesicles for targeted drug delivery. *Nat. Nanotechnol.*, **7** (8), 536–543.

3 Korin, N., Kanapathipillai, M., Matthews, B.D., Crescente, M., Brill, A., Mammoto, T., Ghosh, K., Jurek, S., Bencherif, S.A., Bhatta, D., Coskun, A.U., Feldman, C.L., Wagner, D.D., and Ingber, D.E. (2012) Shear-activated nanotherapeutics for drug targeting to obstructed blood vessels. *Supramol. Sci.*, **337** (6095), 738–742.

4 Saxer, T., Zumbuehl, A., and Müller, B. (2013) The use of shear stress for targeted drug delivery. *Cardiovasc. Res.*, **99**, 328–333.

5 Marcenes, W., Kassebaum, N.J., Bernabé, E., Flaxman, A., Naghavi, M., Lopez, A., and Murray, C.J.L. (2013) Global burden of oral conditions in 1990–2010: a systematic analysis. *J. Dent. Res.*, **92** (7), 592–597.

6 Petersen, P.E. (2008) World Health Organization global policy for improvement of oral health: World Health Assembly 2007. *Int. Dent. J.*, **58** (3), 115–121.

7 Petersen, P.E. (2009) Global policy for improvement of oral health in the 21st century: implications to oral health research of World Health Assembly 2007, World Health Organization. *Community Dent. Oral Epidemiol.*, **37** (1), 1–8.

8 Deyhle, H., Bunk, O., Buser, S., Krastl, G., Zitzmann, N., Ilgenstein, B., Beckmann, F., Pfeiffer, F., Weiger, R., and Müller, B. (2009) Bio-inspired dental fillings. *Proc. SPIE*, **7401**, 74010E.

9 Deyhle, H., Bunk, O., and Müller, B. (2011) Nanostructure of healthy and caries-affected human teeth. *Nanomedicine*, **7** (6), 694–701.

10 Gaiser, S., Deyhle, H., Bunk, O., White, S.N., and Müller, B. (2012) Understanding nano-anatomy of healthy and carious human teeth: a prerequisite for nanodentistry. *Biointerphases*, **7** (4), 14.

11 Curtis, A. and Wilkinson, C. (1999) New depths in cell behaviour: reactions of cells to nanotopography. *Biochem. Soc. Symp.*, **65**, 15–26.

12 Müller, B. (2001) Natural formation of nanostructures: from fundamentals in metal heteroepitaxy to applications in optics and biomaterials sciences. *Surf. Rev. Lett.*, **8** (1 and 2), 169–228.

13 Müller, B., Riedel, M., Michel, R., De Paul, S.M., Hofer, R., Heger, D., and Grutzmacher, D. (2001) Impact of nanometer-scale roughness on contact-angle hysteresis and globulin adsorption. *J. Vac. Sci. Technol. B*, **19** (5), 1715–1720.

14 Althaus, J., Padeste, C., Köser, J., Pieles, U., Peters, K., and Müller, B. (2012) Nanostructuring polyetheretherketone for medical implants. *Eur. J. Nanomed.*, **4** (1), 7–15.

15 Althaus, J., Urwyler, P., Padeste, C., Heuberger, R., Deyhle, H., Schift, H., Gobrecht, J., Pieles, U., Scharnweber, D., Peters, K., and Müller, B. (2012) Micro- and nanostructured polymer substrates for biomedical applications. *Proc. SPIE*, **8339**, 83390Q.

16 Fattorini, E., Brusa, T., Gingert, C., Hieber, S.E., Leung, V., Osmani, B., Dominietto, M. D., Büchler, P., Hetzer, F., and Müller, B. (2016) Artificial muscle devices: Innovations and prospects for fecal incontinence

treatment. *Ann. Biomed Engin.*, **44**, 1355–1369.

17 Müller, B., Deyhle, H., Mushkolaj, S., and Wieland, M. (2009) The challenges in artificial muscle research to treat incontinence. *Swiss Med. Wkly.*, **139** (41–42), 591–595.

18 Müller, B., Zumbuehl, A., Walter, M.A., Pfohl, T., Cattin, P.C., Huwyler, J., and Hieber, S.E. (2015) *Translational Medicine: Nanoscience and Nanotechnology to Improve Patient Care*, Wiley-VCH Verlag GmbH, Weinheim, p. 15.

19 Müller, B. (2010) Tailoring biocompatibility: benefitting patients. *Mater. Today*, **13** (4), 58.

# 2
# Nanoscience and Nanotechnology and the Armory for the Twenty-First Century Health Care

*Marcel Van de Voorde*[1] *and Pankaj Vadgama*[2]

[1]*Assembly, Paris, Rue du Rhodania, 5, BRISTOL A, Appartement 31, 3963 Crans-Montana, Switzerland*
[2]*Queen Mary University, Centre for Materials Research, Mile end Road, London E1 4NS, UK*

## 2.1
## Conceptual Dream

The discovery of atomic structure in solids initiated the development of man-made materials and now allows us to exquisite control over their properties and functions. Similarly, our understanding of molecular and chemical processes has allowed us to better understand and predict chemical reactions. Perhaps, the seminal moment came with Feynman's lecture to the American Physical Society in 1959: "There is plenty of room at the bottom." The prospects for uptake of the nanoscale paradigm in medicine have galvanized interest, both in academia and industry [1–10].

## 2.2
## A Real World Encounter

Accelerating advances encompassing the nanoscale have enabled us to design therapeutic agents with ever-increased likelihood of clinical effectiveness [2] and our understanding of the pathophysiology of disease has also been enhanced. In the context of cell and tissue organization, such knowledge, coupled with our understanding of macro- and microanatomy has opened a path to the emerging field of nanoanatomy. Our newly found nanodomain bridges the gap between the molecular and the "macro," and it will be of crucial importance in the future, given that biology uses supramolecular entities, that is, nanostructures, as key engines of control and management of the cellular world [11,12]. With better understanding of the nanoscale we will be better equipped to create nanomaterials to augment our current armory of diagnostic and therapeutic systems. Furthermore, a thorough structural characterization of the subcellular/supramolecular will give us considerably greater mechanistic understanding. This will have an

*Nanoscience and Nanotechnology for Human Health,* First Edition. Edited by Bert Müller and Marcel Van de Voorde.

impact on internal medicine, but is already seeing application in cardiovascular and regenerative medicine along with a broader refining of targeted therapies. Structure–function relationships at the nanoscale also has huge implications for complex biomimetics, for example, in the reproduction of multifunction sensing and organ systems to hard tissue design in dentistry and orthopedics [2,13].

## 2.3 Mapping the Microcosm of Disease

Nanomedicine delivers nanotechnology and nanoscience to practical health care with unprecedented precision. It exploits the often improved, and often unexpected physical, chemical, and biological properties of materials at this extreme length scale. Here, man-made structures match the length scale of many natural functional units in living organisms, allowing scale-matched interactions [2,14].

As the population ages, in developed nations, and those in developing countries become more subject to environmental threats and infectious agents, medicine is confronted with exceptional health care challenges. Early diagnosis and therapy is now of vital importance [15].

By building up strength in nanoscience and nanotechnology, early disease detection, preventative measures, and targeted therapies can be developed that will benefit all mankind.

## 2.4 Delivery at the Clinical "Coal Face"

The immediate practical outcome will be to complement, and indeed augment, existing therapies [1,16–18]. Nowhere is this more obvious than in the tailoring of therapeutic carriers to deliver antibiotics in innovative ways to increasingly resistant microorganisms. In this way, many antibiotic agents that are currently considered to be coming to the end of their useful lifetimes could see resurgent use, reducing the demand for expensive *de novo* drug development. The quality of life is as important as its longevity, and here also the nanoscale can offer solutions. With failing cellular and tissue structures, it may be possible to supply nanoscale substitutes in the way that traditional biomaterials are being used for macrostructures [19,20]. Thus, while say an osteoporotic fracture is seen as a macroscale failure, in reality it is a failure of organization at the nanoscale, and is therefore amenable to management at this scale.

## 2.5 A High Precision Aim for Disease Targets

Scientific discoveries in nanomedicine will have to pass through time-consuming development stages, including preclinical and clinical studies, to reach

commercialization. However, reengineered agents are emerging and have been targeted variously to cancer treatment, hepatitis and other infectious diseases, anesthesia, cardiac/vascular disorders, inflammatory and immune disorders, endocrine and exocrine disorders, degenerative disorders, and so on [1,4,21–25]. Perhaps the major part of current research effort is focused on cancer treatment. We now have high-impact interventions built on nanoscale medicines and nanocarriers. Preliminary exploitation was applied to imaging agents and now targeting of drugs and even remotely trackable agents is becoming feasible [18,26–28].

## 2.6 A Materials Revolution for Clinical Care

Earlier research, developed model systems, laid the foundation for nano materials and showed the potential for revolutionizing medicine. Preliminary evidence was provided of reconfigured bulk and surface properties afforded by nanostructures and how these could be harnessed for better ways of detecting and managing diseases, and in some cases even preventing them. In parallel, manipulative and analytical tools have been devised that offer the underpinning infrastructure. These addressing the unique imaging, manipulation, and interrogation needs of such materials [29–31]. The same, of course, applies to their natural biological counterparts. The scene is set to apply our knowhow to advance soft nano-objects based around proteins and other biopolymers. Through this strategy we may also have a better understanding of how biology achieves supramolecular systems. We certainly have a fix on structure, such as that of the elegant ribosomal machine (Nobel Prize Chemistry, 2009), and a full functional understanding may come within reach. An extreme challenge would be how chromosomal DNA is exposed and read in real time [32].

Artificial nanostructures able to interfere with such complex, self-assembly nanosystems may allow for the manipulation of these processes to deliver therapeutic outcomes, for example, via gene silencing and gene amplification. Without experimentally interacting with biology at the nanoscale in the first place, we will not be able to understand this all important nanobiology realm.

A combination of advanced tailored nanomaterials and monitoring tools will provide us with closer information on the dynamics of nano–bio interactions. We are well placed to delve into even the most elusive of natural nanostructures [33,34]. A practical advance could be a reinvention of the current surgery paradigm, where selective addition and removal of components at the cellular level are affected. A potent exemplar is in neurointervention, where techniques for neuronal repair and nano scaffolds for axonal growth already seem feasible for clinical use. Future extended neuronal lifespan and control of nanoaggregate formation may provide resolution of age-related neurodegenerative disease, most notably dementia.

## 2.7
## Robotics for Microrepair and Healing

Future possibilities lie in the use of so-called nanorobots introduced through the vascular system but having the capability of reaching a specific cell type to undertake a preset surgical maneuver [35,36]. Already femtosecond lasers perform 100 nm incisions in eye surgery and in regard to materials we have hemostasis peptides that can self-assemble as nanoscale protective barriers for sealing up wounds.

Cross-referencing of the diseased and normal at the nanoscale will also provide deeper insights. This text provides some representative examples of nanotechnology-based tools, materials, and systems that are set to have an impact on both biology and medicine.

## 2.8
## A Dialog with Cells

Our ability to transport materials to the cell is essentially a function of length scale [37,38]. Nanoscale devices might be developed to achieve this for us automatically. While being a hundred or thousand times smaller than a cell and on a par with biomacromolecules such as enzymes and cell receptors, they might have a built-in smartness that allows targeting and recognition. The scales for such machines are already evident with sophisticated, interactive structures such as hemoglobin at 5 nm, DNA 2.5 nm, and quantum dots 10 nm. In principle, a nanostructure of 50 nm size could enter the cell, and one of 20 nm size could traverse a capillary bed. Surface charge, shape, and polarity will modulate these properties. For the innovative nanoengineer, a combination of surface design, bulk reactivity, and payload release are all open for massive exploitation and development. Viruses already achieve such desired combinations, with their unique negotiation of cell receptors. A progression of this natural technology to achieve the same with artificial constructs would pay major dividends without the health risks. Gene therapy, for example, need not take the risky route of natural viral carriers.

Nanolayers might be usable for masking or protection of cellular surfaces such as vascular endothelial cells in order to manipulate vascular access. Masking, however, is a far greater challenge for the artificial particle introduced into the body, susceptible to all that the body can throw at it by way of masking and rejection with inevitable loss of efficacy.

The payoff of targeted therapy is a huge one. There is now major analysis of cancer/patient genomes to tailor therapeutic agents for individual patients. Anything that diminishes toxic drug effects while maintaining potency is a magnet for research, also presenting is a distinct opportunity for big pharma to advance our drugs concepts.

## 2.9
## Stealth Materials for a More Potent Delivery

Nanostructures to package proteins and other biodegradable agents could be given orally as opposed to the intravenous or tissue injection route. Complex nanoengineering is required to both protect such agents from degradation and make them available for intestinal uptake and onward transmission. The dual need is for protection against chemical defense while allowing for effective penetration of physical barriers. The barrier problem is at its most extreme at the blood–brain barrier and intact skin. Assistive technologies such as electroporation and electrical fields gradients are showing great promise, for example, for melanoma, and with a nanotechnology synergy the effects will surely be dramatic. Beyond this surely there may be the opportunity to fine-tune delivery to reach specific subcellular, including nuclear, subcomponents. At close range weak magnetic and dielectric properties might well serve as strong field manipulative tools. The challenge is the design. Magnetic liposomes and binary shell polyferrofluids have already provided better particle loading and tissue localization through external magnetic fields [24,26,39].

In an era where the drug pipeline is no longer guaranteed, a standard drug injected into tissue or given intravenously can be made to profoundly alter its pharmacodynamics without any change in chemistry, simply by associating it with a nanocarrier. So, there are likely to be drug advances made without the need for always discovering completely new therapeutic agents. Beyond and major cost savings in drug development would be a timely development when we need so many antimicrobials to fit for an era of resistant superorganisms.

The vascular compartment is itself a disease focus. The high incidence of cardiovascular disease has profound healthcare implications [6]. Thus, carrier nanoparticles for dealing with atherosclerotic plaques and inflammatory cardiovascular disease would revolutionize cardiac medicine. Heart tissue regeneration via nano particles, for example, releasing tissue regenerative agents just where they are needed could pay the way for treating more dramatic diseases such as myocardial infarction and stroke.

## 2.10
## Improved Biointerrogation for a Better Understanding

Many diseases, including cancer, originate from mutations with alterations in cellular regulatory and metabolic pathways. Early sensitive diagnosis has been constrained by the lack of biosensors and probes capable of reaching the local diseased compartment as opposed to, say, the signals coming from that zone, such as circulating biomarkers. Nanomaterials interacting with specific intracellular signals with some form of optical, magnetic, or electrical relays could provide early alert for disease [26,35]. In this context, *in vivo* nanodiagnostics

will be a major challenge combining the need for device biocompatibility with the IT element of remote interrogation. Loaded nanoparticles with an indicator function offer some glimpse of what is possible here. Extension of this concept to the intact organism or tissue would be a further, major step forward.

The greater emphasis on point-of-care and self-testing for rapid and early diagnosis also means the diagnostics have to be operationally simple. There is also a premium on multiparameter testing. Using nanostructures and nanosensing surfaces allows for a sensing system that has exceptional redundancy, providing robust and fast results. A true "lab-on-a-chip" could be realized using nanoscale sample handling, and coupling with extreme miniaturization of optical, electrochemical, and other platforms becomes feasible [2,40]. The patient then becomes empowered to track their own health status. A further attribute of nanotechnology would be the provision of nanoporous membrane structures for scaling down of surface interaction, down to the molecular level. Nanoporous liquid membranes are already under development for DNA sequence identification.

Nanoendoscopy is a further diagnostic method that has its precursor in the Pill Cam capsule endoscope. Here, peristaltic movement of a videocamera capsule down the gut yields intermittent imaging of the small intestine. A pill-sized camera with nanocomponents could be used to replace existing, more invasive, colonoscopy.

The key strength of nanodevices for sensing is their nonintrusive nature. This has the added advantage of provoking less biorejection, avoiding tissue disruption in the patient. Again, disease alerts could be provided earlier, for example, for those with coronary artery disease to ensure that the cardiac cells are not under hypoxic stress or in glaucoma through real time intraocular pressure monitoring with a contact system. In the case of both the central and peripheral nervous system, nanoneuroprostheses might well be designed for intelligent functional electrical stimulation (FES) with high spatial resolution.

Nanotechnology could accelerate the move away from laboratory testing. At the wider societal level the nonintrusiveness could allow use in medical surveillance for preventative medicine in whole populations.

## 2.11
## Crossing the Structure–Function Threshold

Structural and functional imaging such as PET is advancing, but there is an even greater need for better spatial resolution to image intralesion heterogeneity, tissue viability, and delineation of disease margins. Nanostructures, here as imaging beacons, offer huge advantages [7,26]. Already, superparamagnetic particles have been used to effect imaging, but such systems able to respond to local chemistry could create a revolution in functional imaging. While complex and potentially expensive, better disease management would bring down overall health care costs. Recent progress in multifunctional contrast agents using compounds responsive to biological activity suggests the capability is on the horizon.

## 2.12
## Living Implants for a Living Matrix

Traditional implant materials have made major headway in therapy. Their limited surface bio/hemocompatibility, however, compromises their long-term function. Surface nanostructuring and triggering of desirable, as opposed to adverse tissue/blood responses, could radically change the device, and patient's, lifetime. Such design could include chemical functionalization with the presentation of sophisticated motifs and subtle types of environmental responsiveness and remodeling [10,14,41]. Cells react to both surface chemistry and topography, so engineering of such nanomotifs has decided advantages. In dentistry, dental implants with nanostructured surfaces might enhance osteoblast adhesion, esthetic presentation, and provide for on-going drug release and treatment of periodontal disease.

Tissue engineering uses artificial scaffolds to direct and differentiate cells. With nanoscale fibers, pores, and decoration, spatial organization and differentiation would enter a quite unprecedented order of control [2,42]. Eventual tissue mimicry is possible, not just of homogeneous tissue such as cartilage, but of the refined mesoarchitecture of large organs. Parallel developments in stem cell research will provide previously unimaginated types of cell composite, with more elegant nanoarchitectures now able to engineer the local cell environment for high precision cellular cues for differentiation.

## 2.13
## Taming the Nanointerface

The properties that make nanomaterials so attractive may also make them hazardous to cells and tissues [38]. Concerns have been raised about unintentional health and environmental impacts. For instance, metal oxide-based nanoparticles ($TiO_2$, ZnO, $Fe_3O_4$, $Al_2O_3$, and $Cr_2O_3$) and quantum dots have a core made up of relatively toxic metals (Cd, Se, etc.). So nontoxic analogues are a vital next step. This again brings in the fundamentals of materials science. Particle residence times in the human body, may also be a factor, so it will be necessary to be clear, as with standard drug agents, as to the pathways taken by nanomaterials in the body over time: how they accumulate, break-down and are excreted, and the degree to which they cause oxidative stress to the tissues that they contact.

The bystander effect relates to the widening action of radiation on tissues through cell signaling. Nanobeams, targeting individual organelles of a cell have been useful tools for studying such communication and also trigger mechanisms, for example, for DNA. While nanoparticles could also be used in an analogous way, this also highlights their potency and potential for causing damage if not properly designed.

Metal ions play a role in cell regulatory processes but can also provoke disease states through deficiency or excess. They are known to play a part in some

cancers and in neurodegenerative disease like Alzheimer's. Therefore, where nanoscale metallized components are in cell contact, it becomes necessary to understand the dynamics of ion release and microenvironmental effects. In parallel, agents for ion removal may allow therapeutic modulation where ion release is for therapeutic purposes.

The effect of nanostructures on the aggregation of fibrous proteins such as amyloid may also be of importance. Not only might they promote neurodegeneration pathways, but also a better understanding of aggregation processes may emerge of natural peptides and mitigation strategies may be of value for the design of selforganized structures for therapies [27].

## 2.14 Where are We Now?

Over the past decade, nanomedicine and nanobiology have undergone radical transformation from fantasy to real science. The days of discussing advances in this area in the context of nanobots are over, and systems and nanomaterials have emerged that provide realistic analytical and therapeutic advantages over conventional approaches. We now know that much of biology is executed at the nanoscale, but our understanding resides at the extreme molecular and macro levels. Nanostructures used alone, or coupled with active payloads, along with advanced manipulative tools are the missing bridge between these two worlds. We are moving from just creating nanostructures to a systems approach where the nanostructures are spatially positioned. The potential aim of this 3D organization is to mimic environments that can be seen as natural by tissue, and through this to accelerate replacement and repair [41]. At the other extreme, we are learning to design nanostructures that can survive and operate under hostile *in vivo* conditions.

Some of the foundations have been led to nanostructured scaffolds for the growth of human dermal fibroblasts, for example, for chronic diabetic wounds and burns, nanosilver-loaded wound dressings for broad-spectrum antimicrobial action, image enhancers in radiology. Associated analytical tools for imaging and manipulation of both particles and biological structures are now advanced in ways that would have been viewed as science fiction a few years ago.

In the next phase of development, we need to unravel the complexities of the biointeractions and through this to translate a technological revolution from the laboratory to the patient.

## 2.15 Where will the Revolution Take Us?

Innovations are likely to shift toward those associated with overall systems and their applications. It is this shift that will impact on medicine. We will see uses in both general medicine and surgery. Increasing attention will be toward complex

functional replacement of tissues that are either not capable of regeneration or that have sophisticated structures involving multiple cell types. Such structures have to be spatially and functionally integrated in a way that does not oversimplify what we have in the natural tissue. The use of nanoarchitectures will progressively reduce the need for artificial macrostructures and emphasis materials at the nanoscale. The latter should also allow for greater convergence of diverse material types into a single monolithic entity. In cancer, we need to identify tumor margins, micrometastases, and the residuum of tumor burden to a higher level of sensitivity than is currently possible. In tissue engineering, we need nanomaterials as the extracellular chaperone for cell guidance, a kind of artificial extracellular matrix. We need to learn the relation between natural healing and regeneration and the artificial nanophases we will create, answering such questions as material degradation rates, surface adsorption/adhesion, and nutrient transport and its anisotropy. Nanocarrier-aided targeted delivery will need to be designed in a way that losses in the reticuloendothelial system are not so great as to make therapy ineffective. This brings nanoscience into mainstream biology and the processes of phagocytosis and particle membrane interactions. Cardiovascular science may well show the earliest advances with nanofiber-based scaffolds for vascular grafts, nanostructured drug-eluting stents, and thromboresistive surfaces.

A key justification is that nanotechnology will aid doctors to address currently unsolvable problems, for example, sight-restoration in retinal degenerative disease. In dentistry, orthodontic manipulative nanostructures could manipulate periodontal tissues, and even the use of nanotechnology-based drug release agents could degrade organic compounds into harmless odorless structures and also break down calculi.

Despite the ultimate value of *in vivo* monitoring with nonintrusive nanostructures, the more accessible, and rapid advances are likely to be seen in *in vitro* diagnostics. *In vivo* toxicity is not a concern here and the diagnostic industry is capable of building on existing platforms. Improved diagnostics, lower cost, and a reduced materials burden will widen uptake and act as a further vehicle for stratified medicine.

All of the above will need to combine engineering advances with strategies for handling the biological environment, both for the benefit of the nanostructure and the host environment. To facilitate this, it will be necessary to implement alternative manufacturing approaches. New products, however, will need to address stringent safety and environmental compatibility standards. The more potent the action, the more likely is the undesirable effect. Lifecycle outcomes will also need to be addressed: nanoparticle use means a greater surface activity and subsequent impact on the environment, making it paramount to develop appropriate destruction and disposal capabilities in parallel.

## 2.16 Conclusions

Our understanding of the molecular world with regards to medicine has seen an astonishing development. Through this development we recognize that the

spatial orientation and arrangement of this world is also important. Biology is chiral, directional, spatially alert, and embodies complex anisotropies. The supramolecular domain represents the stuff of nanomedicine with the emerging understanding of the solid states. We are now on the threshold of converging the formalism of solid-state physics with soft matter. This is not just a scientific refinement but a potential scientific revolution. There are practical implications for our greater understanding of disease states and through this a better design of therapeutic agents.

A medical future without nanotechnology would have a reduced toolkit to tackle intractable conditions. Hospitals will not sustain the even escalating success of the past without the input from new methodologies. Nanotechnology offers readily available solutions. It may be that traditional specialties will undergo a refinement with the advent of nanotherapeutics. Without the nano-input, imaging and diagnostics would not keep pace with the escalating need for high structural resolution and sensitivity. This quality of diagnostic tools is indispensable, if we are to tackle disease at the earliest stage and to identify aberrations that allow for preventative steps – the target of population preventative medicine. Degenerative conditions, associated with the aging population, especially, will remain only partially manageable. Modern medicine will initially apply nanoconstructs and nanoparticles to Cinderella areas where no alternative exists but with improved engineering of materials the scope will widen. Any extension, however, needs also to take into account a wider societal and cultural stance on nanotechnologies, which if not succeeding will create a resistance to uptake to the detriment of those who need the technology the most. This is where beyond the science arena societal engagement will be vital and objective assessments vital as with any trial data used to move to new treatments in the evidence-based way. A clue to the future comes from our past and the way we have accommodated the toxic and damaging part of radiology, radiotherapy, and therapeutics in order to benefit from their benefits. The nanotechnology will make no difference. As a label nanotechnology has been highly beneficial in our better understanding of matter, but the message now to government and funders should be that of funding nanotechnology not as an isolated entity, but as a vital bridge between the molecular and structural that will help better understand our external and internal environment.

This book with the selected topics on nanomedicine will fuel the creativity of medical doctors, natural scientists, and engineers in analyzing the human body and developing nanotechnology-based treatments to improve human health.

## References

1 Aleassa, E.M., Xing, M., and Keijzer, R. (2015) Nanomedicine as an innovative therapeutic strategy for pediatric cancer. *Pediatr. Surg. Int.*, **31** (7), 611–616.

2 Jesion, I., Skibniewski, M., Skibniewska, E., Strupinski, W., Szulc-Dabrowska, L., Krajewska, A., Pasternak, I., Kowalczyk, P., and Pinkowski, R. (2015) Graphene and

carbon nanocompounds: biofunctionalization and applications in tissue engineering. *Biotechnol. Biotec. Eq.*, **29** (3), 415–422.
3 Pelipenko, J., Kocbek, P., and Kristl, J. (2015) Critical attributes of nanofibers: preparation, drug loading, and tissue regeneration. *Int. J. Pharm.*, **484** (1–2), 57–74.
4 Gregori, M., Masserini, M., and Mancini, S. (2015) Nanomedicine for the treatment of Alzheimer's disease. *Nanomedicine*, **10** (7), 1203–1218.
5 Peer, D., Karp, J.M., Hong, S.P. *et al.* (2007) Nanocarriers as an emerging platform for cancer therapy. *Nat. Nanotechnol.*, **2** (12), 751–760.
6 Bawarski, W.E., Chidlowsky, E., Bharali, D.J. *et al.* (2008) Emerging nanopharmaceuticals. *Nanomed. Nanotech. Biol. Med.*, **4** (4), 273–282.
7 Kingsley, J.D., Dou, H., Morehead, J. *et al.* (2006) Nanotechnology: a focus on nanoparticles as a drug delivery system. *J. Neuroimmune Pharmacol.*, **1** (3), 340–350.
8 Pison, U., Welte, T., Giersig, M. *et al.* (2006) Nanomedicine for respiratory diseases. *Eur. J. Pharmacol.*, **533** (1–3), 341–350.
9 Freitas, R.A. (1999) *Nanomedicine*, Volume I: Basic Capabilities, CRC Press, ISBN-13: 978-1570596803 ISBN-10: 1570596808.
10 Webster, T. (ed.) (2012) *Nanomedicine*, Woodhead PublishingPrint Book, ISBN: 97808570.
11 Baharvand, H. (2015) *Stem Cell Nanoengineering*, Wiley-Blackwell, ISBN: 978-1-118-54061-9, 432 p.
12 Milane, L., Trivedi, M., Singh, A., Talekar, M., and Amiji, M. (2015) Mitochondrial biology, targets, and drug delivery. *J. Control. Release*, **207**, 40–58.
13 Jain, K.K. (2008) *The Handbook of Nanomedicine*, Springer, ISBN: 978-1-603-27318-3.
14 Ruiz-Molina, D., Novio, F., Roscini, C., and Mano, J.F. (2014) *Bio- and Bioinspired Nanomaterials*, Wiley-VCH Verlag GmbH & Co. KGaA, ISBN: 978-3-527-33581-7.
15 Prasad, P.N. (2012) *Introduction to Nanomedicine and Nanobioengineering*, John Wiley & Sons, Inc., ISBN 978-1-118-09343-6, 608 p.
16 Li, J., Wang, Y., Liang, R. *et al.* (2015) Recent advances in targeted nanoparticles drug delivery to melanoma. *Nanomed. Nanotech. Biol. Med.*, **11** (3), 769–794.
17 Nguyen-Ngoc, T. and Raymond, E. (2015) Reinvention of chemotherapy: drug conjugates and nanoparticles. *Curr. Opin. Oncol.*, **27** (3), 232–242.
18 Mura, S., Bui, D.T., Couvreur, P., and Nicolas, J. (2015) Lipid prodrug nanocarriers in cancer therapy. *J. Control. Release*, **208**, 25–41.
19 Ding, H.M. and Ma, Y.Q. (2015) Theoretical and computational investigations of nanoparticle-biomembrane interactions in cellular delivery. *Small*, **11** (9–10), 1055–1071.
20 Lee, W.H., Loo, C.Y., Traini, D., and Young, P.M. (2015) Nano- and micro-based inhaled drug delivery systems for targeting alveolar macrophages. *Expert Opin. Drug Deliv.*, **12** (6), 1009–1026.
21 Medintz, I.L., Uyeda, H.T., Goldman, E.R. *et al.* (2005) Quantum dot bioconjugates for imaging, labelling and sensing. *Nat. Mater.*, **4** (6), 435–446.
22 Kesharwani, P. and Lyer, A.K. (2015) Recent advances in dendrimer-based nanovectors for tumor-targeted drug and gene delivery. *Drug Discov. Today*, **20** (5), 536–547.
23 Landriscina, A., Rosen, J., and Friedman, A.J. (2015) Biodegradable chitosan nanoparticles in drug delivery for infectious disease. *Nanomedicine*, **10** (10), 1609–1619.
24 Xu, X., Ho, W., Zhang, X. *et al.* (2015) Cancer nanomedicine: from targeted delivery to combination therapy. *Trends Mol. Med.*, **21** (4), 223–232.
25 Choudhary, S. and Devi, V.K. (2015) Potential of nanotechnology as a delivery platform against tuberculosis: current research review. *J. Control. Release*, **202**, 65–75.
26 Berry, C.C. and Curtis, A.S.G. (2003) Functionalisation of magnetic nanoparticles for applications in biomedicine. *J. Phys. D Appl. Phys.*, **36** (13), R198–R206.
27 West, J.L. and Halas, N.J. (2003) Engineered nanomaterials for

biophotonics applications: Improving sensing, imaging, and therapeutics. *Annu. Rev. Biomed. Eng.*, **5**, 285–292.

**28** Ballou, B., Ernst, L.A., and Waggoner, A.S. (2005) Fluorescence imaging of tumors *in vivo*. *Curr. Med. Chem.*, **12** (7), 795–805.

**29** Cai, W. and Chen, X. (2007) Nanoplatforms for targeted molecular imaging in living subjects. *Small*, **3** (11), 1840–1854.

**30** Singh, R. and Nalwa, H.S. (2011) Medical applications of nanoparticles in biological imaging, cell labeling, antimicrobial agents, and anticancer nanodrugs. *J. Biomed. Nanotechnol.*, **7** (4), 489–503.

**31** Qiao, Z. and Shi, X. (2015) Dendrimer-based molecular imaging contrast agents. *Prog. Polym. Sci.*, **44**, 1–27.

**32** Chan, K. and Ng, T.B. (2015) *In-vitro* nanodiagnostic platform through nanoparticles and DNA-RNA nanotechnology. *Appl. Microbiol. Biotechnol.*, **99** (8), 3359–3374.

**33** Enrique, M.-A., Mariana, O.-R., Mirshojaei, S.F. *et al.* (2015) Multifunctional radiolabeled nanoparticles: strategies and novel classification of radiopharmaceuticals for cancer treatment. *J. Drug Target.*, **23** (3), 191–201.

**34** Palekar, R.U, Jallouk, A.P., Lanza, G.M., Pan, H., and Wickline, S.A. (2015) Molecular imaging of atherosclerosis with nanoparticle-based fluorinated MRI contrast agents. *Nanomedicine (Lond.)*, **10** (11), 1817–1832.

**35** Erickson, D., Mandal, S., Yang, A.H.J. *et al.* (2008) Nanobiosensors: optofluidic, electrical and mechanical approaches to biomolecular detection at the nanoscale. *Microfluid. Nanofluidics*, **4** (1–2), 33–52.

**36** Mallapragada, S.K., Brenza, T.M., McMillan, J.M. *et al.* (2015) Enabling nanomaterial, nanofabrication and cellular technologies for nanoneuromedicines. *Nanomed. Nanotech. Biol. Med.*, **11** (3), 715–729.

**37** Le Poul, N. and Colasson, B. (2015) Electrochemically and chemically induced redox processes in molecular machines. *Chemelectrochem*, **2** (4), 475–496.

**38** Dobrovolskaia, M.A. and McNeil, S.E. (2010) Strategy for selecting nanotechnology carriers to overcome immunological and hematological toxicities challenging clinical translation of nucleic acid-based therapeutics. *Expert Opin. Drug Deliv.*, **12** (7), 1163–1175.

**39** Sun, C., Lee, J.S.H., and Zhang, M. (2008) Magnetic nanoparticles in MR imaging and drug delivery. *Adv. Drug Deliv. Rev.*, **60** (11), 1252–1265.

**40** Ferrari, M., Onuoha, S.C., and Pitzalis, C. (2015) Trojan horses and guided missiles: targeted therapies in the war on arthritis. *Nat. Rev. Rheumatol.*, **11** (6), 328–337.

**41** Salmasi, S., Kalaskar, D.M., Yoon, W.-W. *et al.* (2015) Role of nanotopography in the development of tissue engineered 3D organs and tissues using mesenchymal stem cells. *World J. Stem Cells*, **7** (2), 266–280.

**42** Lee, J., Cuddihy, M.J., and Kotov, N.A. (2008) Three-dimensional cell culture matrices: state of the art. *Tissue Eng. Part B-Rev.*, **14** (1), 61–86.

# 3
# Nanomedicine Activities in the United States and Worldwide

*Carlotta Borsoi, Joy Wolfram, and Mauro Ferrari*

*Houston Methodist Research Institute, Department of Nanomedicine, 6670 Bertner Ave., M.S. R12-219, Houston, TX 77030, USA*

Nanotechnology is typically defined by three criteria, which take into account the production, size, and properties of the elements that comprise the technology. Specifically, a nanoproduct is usually man-made, has elements that are in the nanosize range, and properties that emerge due to nanoscale dimensions [1]. Over the past few decades, nanoparticles have been exploited within the field of medicine as diagnostic and therapeutic tools [2–4]. In fact, an increasing number of nanosystems formulated for medical applications are described in the scientific literature [3,5–7]. Nanoparticles show a wide variety of potential medical applications, including targeted delivery of drugs, diagnostics for *in vitro* and *in vivo* use [8,9], and fabrication of scaffolds [3]. Accordingly, a vast range of materials has been exploited in nanomedicine, such as polymers [10–15], metals [16,17], and ceramics [18,19]. In particular, several types of nanocarriers have been used for drug delivery purposes, such as liposomes [20–23], polymeric micelles [10,11,24], gold particles [25,26], silica particles [27,28], and silicon particles [29–31]. Compared to conventional drugs nanodelivery vehicles usually enable a higher degree of specificity for pathological tissue as they are multicomponent systems, which can incorporate, for example, biosensors, stimuli-responsive drug release mechanisms, and transport enhancing components. One of the main limitations of therapeutic regimens is the incapability to determine which organs and cells are subject to systemically administered drugs. Indeed, the therapeutic window, a concentration range in which a drug is clinically effective without causing detrimental side effects, is largely determined by the extent of which a therapeutic agent is delivered to pathological tissue and confined within it.

In addition to nanoparticles, nanosurfaces and nanointerfaces provide solutions for addressing medical problems. For instance, several nanoparticle platforms have displayed promising capabilities for detection of pathological markers [32], such as virus components [33] and endogenous proteins [34]. In fact, diagnostic nanosystems can be exploited for early detection of diseases

*Nanoscience and Nanotechnology for Human Health,* First Edition. Edited by Bert Müller and Marcel Van de Voorde.

and for monitoring response to therapeutic regimens. Moreover, nanotechnology can be applied to regenerative medicine and tissue engineering through the utilization of nanoscale materials for the fabrication of scaffolds. Such materials are often used to support three-dimensional tissue cultures for *in vivo* applications. To date, scaffolds have been studied for multiple applications, including wound repair [35], bone augmentation [36], neocartilage formation [12], cardiovascular repair [37], and pancreatic islet cell transplants [38]. In conclusion, biological exploitation of nanoparticles is a continuously evolving field that yields new approaches for the diagnosis and treatment of illnesses. In particular, nanotechnology has the potential to substantially improve human health by aiding the development of personalized medicine. This introductory chapter will describe some of the main applications of nanomedicine, including drug delivery, diagnostics, and scaffolds for tissue regeneration. The chapter will conclude with a section discussing the major categories of clinically approved nanoproducts.

## 3.1 Drug Delivery

One of the most beneficial properties of nanotherapeutics is their potential to improve the transport of drugs, which typically show low accumulation at a target site. Indeed, nanotherapeutic delivery systems display considerable versatility, which can be exploited to design nanoparticles that preferentially accumulate in different parts of the body. An important mechanism that determines the biodistribution of nanoparticles is their ability to cross specific biological compartments (Figure 3.1) [39,40]. Most of these compartments are intended to be discriminative toward foreign substances, which make it difficult for nanoparticles to reach an intended location. In fact, once drugs enter the vascular system, they are subjected to degradation, recognized and processed by the immune system, and excreted through various routes, including renal and biliary. Moreover, after a drug has traveled across the endothelial barrier, it encounters other transport obstacles including the extracellular matrix and interstitial pressure. Finally, in order to enter cells, drugs are exposed to further hurdles such as the cell membrane, internal cell components, and efflux pumps. It is crucial to understand the mechanisms by which nanoparticles interface these biological barriers for the design of delivery systems that are able to localize in an area of interest. In addition, it is important to understand the final destination of nanoparticles, since they will ultimately be excreted, broken down, or stored in the body. In order to attain a favorable accumulation of nanoparticles, there are four major strategies that have been adopted: (1) taking advantage of the biophysical characteristics of the pathological tissue, (2) exploiting biomaterials that tend to localize in tumors, (3) attaching targeting ligands to the exterior surface of nanoparticles, and (4) activating nanoparticles at a particular location with external energy. Along with the above-mentioned strategies, a next

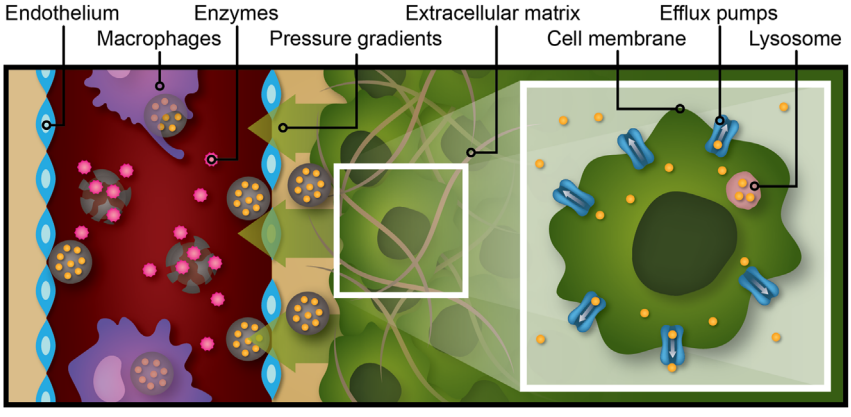


**Figure 3.1** Schematic representation of transport obstacles that are encountered upon intravenous administration of drugs (orange) in nanocarriers (gray). The first set of biological barriers is present in the circulation. These obstacles include enzymatic degradation, macrophage engulfment, and the endothelial barrier. The second set of obstacles resides in the tissue interstitium, where pressure gradients and extracellular matrix components impede drug transport. Finally, the third set of biological barriers, which can be found in the intracellular environment, consists of the cell membrane, efflux pumps, and lysosomal organelles. Although this schematic shows a diverse range of biological phenomenon that should be addressed to obtain efficient drug delivery, it is not intended to provide a complete representation of transport obstacles in the body.

generation of multifunctional drug delivery systems is surfacing. This chapter outlines these approaches in a more detailed manner.

### 3.1.1
### Strategies for Localized Delivery of Nanoparticles

In many cases, pathological cells are present in a difficult-to-reach location and dispersed throughout healthy tissue. Therefore, the blood circulation must be utilized for drugs to be delivered to diseased tissue. With reference to nanoparticles used for cancer treatment, approximately 5% of the administered dose successfully localizes in the tumor [41]. In contrast, less than 0.01% of systemically administered antibodies reach their target [42]. Likewise, small molecules typically accumulate in lower concentrations in pathological tissue in comparison to nanoparticles. In fact, the use of nanodelivery systems can result in a more than 10-fold increase in the amount of chemotherapeutic agents in tumor tissue [43,44]. Moreover, both effective transport across biological compartments and accurate identification of the pathological area determine the therapeutic outcome of nanotherapeutics. Therefore, there is an impetus toward the development of improved approaches to simultaneously attain the barrier penetration and target recognition goals. In this chapter, approaches that attempt to address both of these goals are discussed in greater detail.

#### 3.1.1.1 Physical Targeting

The first approach that has been used clinically to improve the localized accumulation of nanoparticles is physical targeting. The general idea of physical targeting is based on the supposition that pathological and healthy tissue show crucial dissimilarities, such as different hemodynamic characteristics and varying intracellular transport kinetics. Specifically, this strategy implies the adjustment of particle properties, namely, geometry, charge, and stiffness. For instance, the dimensions of nanoparticles significantly influence localization within the body. Previous studies have shown that nanoparticles in the 1.0–5.5 nm size range undergo renal clearance, while particles over 100 nm in size tend to deposit in the liver due to macrophage clearance [13,45]. In addition, the vasculature of pancreatic tumors typically prevents the uptake of particles that exceed 50 nm in size [13]. Accordingly, nanoparticles with specific features can be used to shed light upon how particle characteristics influence biodistribution. To evaluate the effect of particle dimensions on nanoparticle localization, other features such as surface charge and stiffness, should remain the same. Notably, since the dimensions and surface charge of nanoparticles could change considerably in biological fluids, it is crucial to evaluate how nanoparticle properties change following *in vivo* administration [46,47]. In this context, it is also important to assess how the transport of particles differs in healthy and pathological tissue. In fact, transport oncophysics is a term conceived for the analysis of transport in tumor tissue [40]. Such analysis can identify specific characteristics that govern the movement of molecules, particles, and cells within tumor tissue [40,48]. The main goal of transport oncophysics is to take advantage of differences in transport characteristics between diseased and healthy tissue. For instance, structural differences between tumor vasculature and normal blood vessels have been exploited for physical targeting. In particular, tumors utilize angiogenesis, a physiological process that results in the formation of new blood vessels from preexisting vessels, in order to provide nutrients and oxygen to the expanding mass of tumor cells [49]. A consequence of angiogenesis is the establishment of immature vascular networks characterized by a higher number of fenestrations attributable to a lack of tight junctions and pericytes. These fenestrations, which are typically less than 600 nm in diameter [50], enable most nanoparticles to permeate tumor tissue to a greater extent than healthy tissue. This phenomenon is referred to as the enhanced permeation and retention (EPR) effect [50,51]. Moreover, the enhanced retention of nanoparticles in tumors is generally a result of atypical hemodynamics [52,53], inefficient lymphatic drainage [52,53], and increased adhesive features of tumor tissue [39], of which the latter is due to the characteristic increase of extracellular matrix components in the tumor microenvironment [54,55]. The EPR effect is the most well known example of physical targeting, since the majority of nanoparticles take advantage of this phenomenon. For instance, liposomes, which are nanosized vesicles with one or more lipid bilayers, are usually in the size range of 50–400 nm, thereby enabling them to pass through fenestrations in tumor vasculature. In addition to improving biodistribution, liposomes also display several other benefits over their

conventional drug formulations [56,57], including possible circumvention of drug resistance as a result of alternative cellular internalization pathways [21]. Interestingly, the EPR effect can also be exploited in pathologies other than cancer, such as cardiovascular conditions and infections, since these diseases show comparable characteristics to those of tumor blood vessels [58–61].

One of the most common strategies for prolonging nanoparticle circulation time is functionalization with polyethylene glycol (PEG). Indeed, pegylation decreases particle recognition by opsonins, hence reducing phagocytosis by immune cells and avoiding potential immune reactions [47,62], consequently prolonging circulation half-life. For instance, the earliest nanoparticle drug to receive approval from the Food and Drug Administration (FDA) in the United States was Doxil, which is a pegylated liposomal formulation encapsulating doxorubicin. In fact, Doxil was initially approved in 1995 to treat Kaposi's sarcoma, [63] and has since then been used to treat several other cancer types. Following the approval of Doxil, many more nanotherapeutics have made it to the market, including albumin-bound paclitaxel (Abraxane), which was approved by the FDA in 2005 for adjuvant treatment of breast cancer [64]. In addition to the EPR effect, other forms of physical targeting have been utilized in nanotechnology, including the optimization of particle shape. Notably, traditional nanodelivery systems, such as liposomes and polymeric nanoparticles, are usually spherically shaped. However, particles with discoidal geometry generally display higher tumor accumulation in comparison to spheres [65]. In fact, once discoidal particles are intravenously injected, they exhibit increased margination against diseased vasculature and enhanced adhesion to the endothelium compared to spherical particles [66–68]. Indeed, improved adherence to tumor vasculature can be obtained with particles that display maximal surface area without substantially increasing dislodging forces [67,69]. In actuality, the utilization of disk-like geometries for nanodelivery vehicles is an example of biomimicry, since platelets that are discoidal in shape [70] are designed to bind to inflamed tissue [39,66]. It is notable that the human body consists of components with nanosized dimensions that exhibit distinct physical properties, such as shape, charge, and deformability, which facilitate specific biological processes. To conclude, drug delivery by means of physical targeting is a powerful approach that has already been used by nature for millions of years to ensure efficient and specific transport of biological elements within an organism.

#### 3.1.1.2 Biomaterials

The second approach for attaining increased accumulation of nanoparticles at a pathological site involves taking advantage of biomaterials that naturally localize in diseased tissue. For example, Abraxane exploits the properties of serum albumin, which acts as a carrier for endogenous and exogenous molecules with low water solubility. Albumin tends to accumulate in tumors as a result of both the EPR effect and receptor recognition on endothelial cells [71]. Moreover, it has been demonstrated that albumin is internalized in high amounts by cancer cells, thus enabling transport of albumin-associated molecules to tumors [71].

Furthermore, the use of endogenous proteins, such as albumin, eliminates toxicity caused by harmful excipients added for drug solubilization. For instance, the highly toxic solubilizing agent Cremophor EL is included in the standard formulation of paclitaxel used in the clinic [72]. In conclusion, Abraxane has a more favorable safety profile than conventional paclitaxel due to improved biodistribution and the lack of toxic excipients. Taken together, it is reasonable to utilize endogenous biomaterials for drug delivery applications, since these materials have been developed through natural selection to be compatible with the biological environment.

#### 3.1.1.3 Molecular Targeting

The third approach exploited to increase the transport of nanoparticles in diseased tissue is widely known as active targeting [4]. However, this denomination may be confusing, considering that particles move as a result of the systemic circulation and are unable to actively find the intended destination. Accordingly, this strategy implies the attachment of ligands on the nanoparticle in order to achieve recognition of pathological markers or biomolecules that are specific for a certain organ [73–76]. A major reason for enhanced accumulation of targeted nanoparticles is increased confinement in pathological tissue as a result of molecular binding events. Molecular targeting can also enhance particle internalization by diseased cells due to interactions between surface ligands and receptors, which can trigger receptor recycling and nanoparticle uptake [77]. However, active targeting may alter nanoparticle properties as conjugated moieties can enlarge particle dimensions, thereby hindering transport across biological compartments [78]. In addition, ligand binding can enhance chemical reactivity and increase recognition by the immune system [78,79]. Furthermore, nanoparticles functionalized with molecular moieties may be unable to maintain their recognition capabilities [80,81]. Namely, after intravenous administration, nanocarriers encounter plasma biomolecules that form a surrounding corona [47,82], which can have a predominant effect on particle biodistribution [81,83]. In fact, it is possible that the protein corona shields surface ligands, thereby preventing molecular recognition. Therefore, it is crucial to take into consideration such concerns when designing nanodelivery platforms. However, the surface of nanoparticles could be designed to specifically bind certain blood proteins that tend to accumulate in diseased tissue [47,82,84]. Despite several attempts to design nanotherapeutics that exploit targeting ligands, none have yet gained FDA approval. However, several nanoparticles that utilize active targeting are currently in clinical trials [85].

#### 3.1.1.4 External Activation

The fourth strategy for obtaining localized delivery of nanoparticles is the utilization of external energy sources [4]. With this approach the distribution of nanoparticles is less important, since the therapeutic mechanism can be activated at a specific site where the external energy is applied. For instance, gold nanoparticles can be used to thermally ablate pathological tissue in the presence

of infrared light or radio waves [86,87], while magnetic nanoparticles can be heated in an alternating magnetic field [88]. The use of external energy to attain selective heating has also been applied to carbon nanotubes, which are able to transform infrared radiation into heat [89–91]. Nevertheless, the aforementioned strategies can generally not be used in conjunction with intravenous injection of nanoparticles, as particle deposits are insufficient to thermally ablate tissue [87,92]. For this reason, it is probable that such approaches will not be suitable for the treatment of metastatic disease, which is the main cause of cancer morbidity. Moreover, the external activation strategy can also be exploited to increase infusion of particles into tumor tissue. In this case, nanoparticle-induced heating can be applied before injection of conventional drugs to achieve higher tumor permeability [93].

### 3.1.2 Next-generation Drug Delivery Vehicles

As previously mentioned, transport across biological compartments is one of the main problems that nanoparticles encounter after intravenous administration. Optimization of the biophysical properties of nanoparticles can improve their penetration across barriers, thereby permitting particles to deposit in the target tissue. Nevertheless, despite the use of physical, biomaterial, molecular, and external activation strategies, nanoparticles are generally unable to address a large portion of transport obstacles in the body. Consequently, there is a need to develop more sophisticated nanodelivery systems that are able to overcome a broad set of biological barriers. This goal can be reached through the utilization of various materials with multifunctional properties that can be exploited in a sequential manner.

#### 3.1.2.1 Sequential Drug Delivery

Two examples of next-generation sequential drug delivery systems include the nanocell and the multistage vector (MSV). The nanocell is designed to target tumor cells and tumor vasculature through sequential release of two small molecules, an angiogenesis inhibitor and a chemotherapeutic agent. Namely, the anti-angiogenic agent combretastatin was contained within a pegylated-lipid envelope surrounding a poly-(lactic-co-glycolic) acid (PLGA) nanoparticle with doxorubicin. In fact, PLGA is an FDA-approved biocompatible copolymer that permits sustained drug release. In essence, the nanocell enables the concurrent use of both chemotherapy and antiangiogenic therapy without impeding intratumoral delivery of cytotoxic agents, since polymeric doxorubicin nanoparticles are confined within the tumor before the vasculature is compromised [94]. In addition, this system increases the retention of doxorubicin nanoparticles inside the tumor due to a vasculature shutdown.

An additional example of a sequential drug delivery platform is the MSV. The MSV includes three stages, of which the first stage is a porous silicon-based micron-sized particle that can be loaded with two other stages consisting of

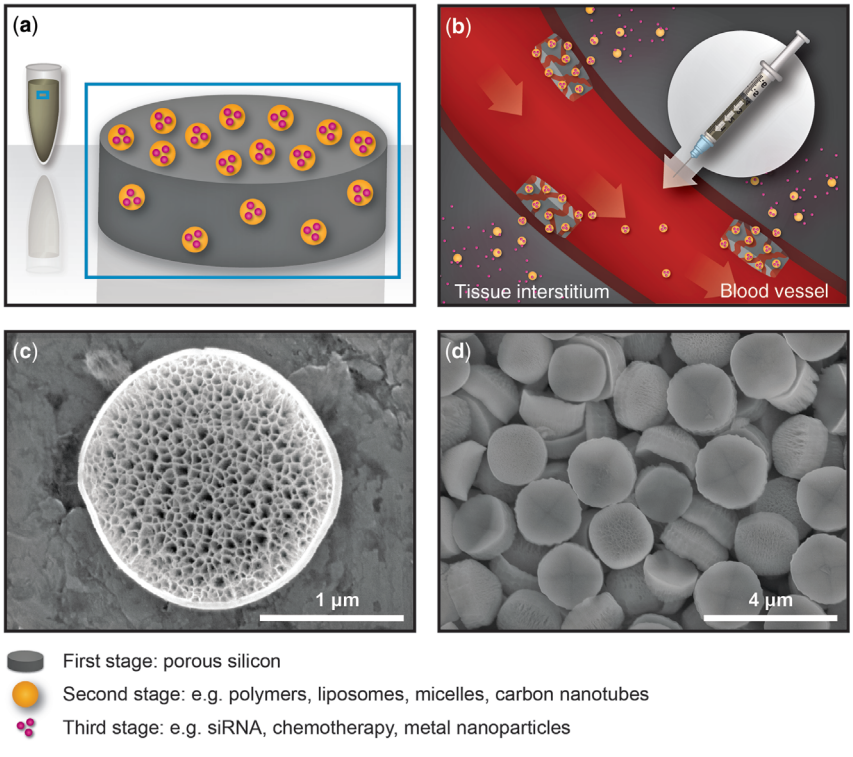


**Figure 3.2** The multistage vector (MSV). (a) The MSV is composed of three elements: a porous silicon microparticle, nanoparticles, and therapeutic agents. (b) Following intravenous injection, the first stage silicon particle binds to inflamed blood vessels and slowly degrades, releasing the second stage nanoparticles in diseased tissue. The third stage therapeutic agent is usually released after the nanoparticles have crossed the cell membrane. (c and d) Scanning electron microscopy (SEM) images of MSVs.

nanoparticles and therapeutic or diagnostic agents (Figure 3.2) [95,96]. Indeed, in the past few years, silicon has been exploited for the design of medical devices, since the material is biodegradable and nontoxic [97,98]. Moreover, silicon particles can be manufactured with specific geometries to be suitable for a wide range of applications. As previously mentioned, it was shown that disk-like particles display greater adhesion to pathological endothelium in comparison to spherical particles [65,66]. For this reason, MSVs are fabricated as discoidal particles that can take advantage of specific hemodynamics and structural features of pathological neovasculature in order to preferentially accumulate in tumor endothelium [99]. Moreover, it is possible to functionalize the surface of the MSV in order to modulate biodistribution, drug release, and degradation. During the degradation of the first MSV stage, second stage nanoparticles are continuously released from the silicon particle, subsequently permeating into the tumor interstitium [39]. Next, the nanoparticles release a third-stage payload, which consists

of a therapeutic or diagnostic agent. One of the major advantages of the MSV is extreme versatility, as a result of multiple possible combinations of first stage and second stage vectors. In particular, second stage carriers can consist of lipid-based micelles [100], liposomes [31,76,101–103], and polymer-based nanoparticles [29,30,104,105]. In addition, the MSV has been exploited for imaging applications, which include delivery of quantum dots [106,107], contrast agents [108–110], and carbon nanotubes [107]. The third stage payload can also be personalized depending on the intended use. For example, chemotherapeutic agents [100,105], antibiotics [111], small interfering RNAs (siRNAs) [29–31,76,101–104,112], and micro RNAs [29] have previously been used as cargo. In addition, thermal destruction of tumor tissue was achieved by exposing MSVs with gold nanoparticles to infrared light [87]. Furthermore, the first stage vector can also be modified in multiple ways to provide optimal transport of drugs. For instance, particle size, shape, pore size, degree of porosity, charge, and molecular functionalization can be changed to attain various biodistribution profiles [39]. Overall, the MSV system is a promising tool for personalized medicine as various combinations of nanostructures and payloads can be customized, permitting an individualized approach to the treatment of disease.

#### 3.1.2.2 Amplified Drug Delivery

Another approach to obtain localized accumulation of therapeutic agents is the use of an amplification strategy to enhance targeting. For example, Bhatia and coworkers designed a drug delivery platform where biological processes were exploited to sequentially amplify targeted delivery [113]. This nanoparticle platform uses nanoparticles or synthetic proteins to activate the coagulation cascade in the tumor microenvironment. Imaging or therapeutic agents are then delivered to the tumor by a second set of nanoparticles that are engineered to target blood clots. When this system was used, the accumulation of therapeutic agents in tumor tissue was 40 times higher than that achieved with a nonamplified approach.

#### 3.1.2.3 Biomimicry

Biomimetic therapies are inspired by mechanisms that regulate natural transport of endogenous and exogenous biological elements in the body. For instance, pathogens have developed a plethora of strategies to overcome biological barriers. As an illustration, viruses are able to penetrate the nuclear membrane, subsequently integrating their nucleic acids into the chromosomal DNA of the host. Furthermore, pathogens typically produce symptoms confined to specific organs, which could partially be due to preferential deposition in certain tissues. For these reasons, several nanodelivery platforms have incorporated elements from pathogenic organisms. For example, attenuated pathogens have been used in combination with nanoparticles to treat cancer. Specifically, a delivery system termed the microbot was constructed from *Listeria monocytogenes* bacteria, polysterene nanoparticles, and plasmid DNA [114]. Although the microbot strategy displayed low toxicity [114], the use of real pathogens for drug delivery purposes

will require extensive preclinical and clinical safety evaluations. In the case of viruses, an example of a biomimetic nanodelivery system is virus mimicking (VM) nanogel vehicle, composed of a nanoparticle with two hydrophilic polymer layers encapsulating a hydrophilic layer containing doxorubicin [115]. In addition, PEG, bovine serum albumin, and ligands for tumor recognition were also incorporated in this platform. The VM nanogel vehicle expands as the pH decreases, resulting in endosomal escape and release of doxorubicin. Notably, it was also found that the nanoparticles were able to infect multiple cells, moving from one cell to another as cells underwent apoptosis. Whereas this virus-resembling vehicle displays therapeutic potential *in vitro*, further experiments are necessary to assure anticancer efficacy in an *in vivo* environment.

A third example of a biomimetic nanoplatform is the leukolike vector developed by Tasciotti and coworkers. This drug delivery system consists of the MSV coated with cell membrane fragments from leukocytes [116]. After intravenous administration, the immune system is unable to recognize the drug delivery platform as a foreign object, enabling the particles to evade opsonization, therefore prolonging *in vivo* circulation times and increasing tumor accumulation. In addition, *in vitro* studies revealed enhanced permeation of leukolike vectors in pathological endothelium in comparison to uncoated MSVs [116]. In summary, the leukolike system can be exploited for the treatment of various illnesses associated with inflammation.

### 3.1.3 Implantable Devices

Over the past few decades, the average life span has continued to increase, causing chronic diseases to become more prevalent. Since this class of illnesses necessitates continuous administration of medication, drug delivery platforms that provide sustained release of therapeutic agents over prolonged periods of time, could substantially improve the well-being of patients suffering from chronic conditions. In addition, the utilization of implantable devices enables drug concentration to stay within the therapeutic window, thereby reducing toxicity and increasing therapeutic efficacy [117]. Moreover, maintaining a constant drug concentration in the body can reduce the risk of drug resistance as periods of recovery, characterized by low drug concentrations, could enable cancer cells [118] or bacterial cells [119] to evolve mechanisms of tolerance to cytotoxic agents. Furthermore, the integration of biosensors into implantable devices permits drug release adjustments in response to programmable features and physiological parameters, for example, body temperature and physical activity. In addition, implantable devices can be placed inside or in close proximity to the diseased area, hence maintaining high drug concentrations in pathological tissue.

In essence, there is a necessity to design implantable drug delivery systems that can provide sustained release of therapeutic agents over prolonged periods. Crucial considerations to make when creating an implantable system include long-term biocompatibility, biodegradability, stability [117,120], ability to control

drug release [121,122], and cost-to-benefit ratio compared to the standard of care. There are two main categories of implantable devices: implantable infusion pumps and implants [117]. While pumps mostly take advantage of pressure gradients, drug implants employ polymers or metallic materials to release drugs in a controlled fashion. In the case of polymeric devices, the drug can be uniformly distributed throughout the polymeric material or contained within a reservoir surrounded by a porous membrane. In addition, polymer-based devices can be divided into biodegradable and nondegradable implants. Notably, a major drawback of nondegradable systems is that they typically necessitate surgical removal after completion of therapy.

Although much progress has been made in the field of implantable devices, there still exists a need to develop new approaches in order to enhance therapeutic efficacy. Examples of new strategies include the work of Grattoni and coworkers, who have designed implantable silicon nanochannel platforms for drug delivery [123–125]. These devices were composed of a nanofluidic membrane comprising several nanochannels that regulated drug release through interactions between molecules and surfaces or electrokinetic modulation [126]. These platforms were biocompatible and displayed zero-order drug release kinetics for over 30 days. A major advantage of nanochannel drug delivery platforms is the possibility to obtain implants with highly specialized and distinct characteristics, since the size and number of channels can be fine-tuned to achieve customizable therapeutic regimens to accommodate individual patients.

## 3.2 Diagnostics

The field of nanodiagnostics is defined as the application of nanotechnology in molecular diagnostics [127] and can be used for *in vitro* or *in vivo* diagnosis in combination with standard imaging techniques. Recently, nanotechnology has started to play a part in early diagnosis and prevention of medical conditions. In particular, the use of nano-based diagnostics enables personalization of therapeutic regimens, immediate results from diagnostic testing, and real-time monitoring of treatment responses [128]. Early diagnosis is important for most diseases, especially cancer, where the chances of a complete response to treatment diminish over time. Moreover, nano-based tools such as lab-on-a-chip devices can aid the development of point-of-care testing, which permits rapid near-patient diagnosis. These devices are typically composed of biological and synthetic nanochannels or nanopores fabricated through a variety of techniques, including electron-beam lithography [129], sacrificial layer deposition [130], and track-etching polymer membranes [131]. This wide variety of fabrication techniques permits the design of versatile and personalized devices, where the geometry and chemistry of nanostructures can be adjusted. For example, nanotraps consist of engineered silica nanoporous thin films that can be tailored to achieve on-chip fractionation of a range of biomarkers. Hu and coworkers designed a

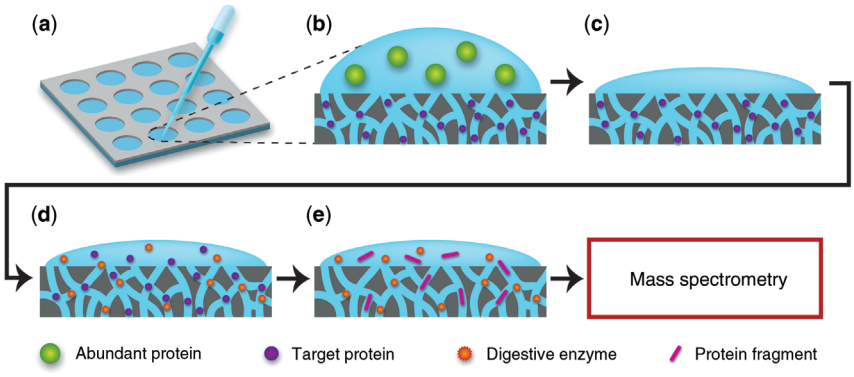


**Figure 3.3** Schematic representation of on-chip fractionation and digestion of proteins in the nanotrap. (a) A biological sample is placed in a sample reservoir. (b) Low-molecular-weight proteins, such as culture filtrate antigen 10 kDa (CFP-10) from *Mycobacterium tuberculosis*, enter the nanopores, while high-molecular-weight proteins remain in the upper part of the reservoir. (c) Washing steps remove proteins that are not confined within the nanopores, (d) A digestive enzyme is added to obtain peptide fragments. (e) Peptide fragments are then eluted prior to matrix-assisted laser desorption/ionization time-of flight-mass spectrometry (MALDI-TOF-MS) analysis.

nanotrap to rapidly isolate *Mycobacterium tuberculosis* (MTB) antigens from biospecimens with matrix-assisted laser desorption/ionization time-of flight-mass spectrometry (MALDI-TOF-MS) [132]. Notably, this nanotrap did not utilize antigen–antibody interactions as a means to isolate antigens. On the contrary, the physical and chemical properties of the nanopore film, such as pore size, pore morphology, and surface charge, were modified to permit detection of low-molecular-weight peptide biomarkers that are usually found in small amounts in the blood. Specifically, such peptides are able to enter nanopores through capillary motion, while high molecular weight proteins can be removed by washing as they remain outside the pores. This method permits enrichment of low-abundant peptides, resulting in improved mass spectrometry profiles (Figure 3.3). This nanotrap enabled up to 90% of recombinant CFP-10 (culture filtrate antigen 10 kDa), an antigen secreted by MTB, to be isolated from a quantified solution, while significant amounts of antigen could be detected in biological specimens. In addition, the same research group was able to exploit nanotraps in order to detect hepcidin, which is a biomarker for iron-related diseases, in biological samples [133]. Another illustration of a device for point-of-care and personalized diagnostics was developed by Qin and colleagues [134]. This device, termed the multiplexed volumetric bar-chart chip (V-Chip), utilizes ink bar charts to quantify oxygen created by a chemical reaction, resulting in rapid quantitative detection of DNA. An advanced version of this system, called the multistage propelled V-Chip (MV-Chip), was created by incorporating a multistage "rocket-like" propelling mechanism, which causes signal amplification, subsequently resulting in enhanced assay sensitivity [135]. The propellant reaction is obtained by a catalase

initiator that is conjugated to probe DNA, while signal amplification is achieved with platinum films. In particular, oxygen is produced in a reaction that takes place between catalase probes and hydrogen peroxide. The oxygen then causes the hydrogen peroxide to move forward and react with platinum films that contain nanoscale protrusions, enabling rapid decomposition of hydrogen peroxide. Subsequently, more oxygen is produced and used as a propeller to force hydrogen peroxide to react with a second set of platinum films. This platinum amplification cascade is taken through three stages, resulting in the production of a large quantity of oxygen that pushes ink through channels in order to generate visual bar charts. The resulting bar charts allow direct visual quantification of nucleic acids without the utilization of electronic or optical equipment.

In addition to nanostructured chips, nanoparticles can also be used for diagnosing disease. Namely, nanoparticles can act as labels or probes when bound to target biomolecules. In particular, quantum dots and gold nanoparticles have been extensively studied for this purpose. For instance, quantum dots conjugated with streptavidin or immunoglobulin G (IgG) were used for the *in vitro* detection of human epidermal growth factor receptor 2 (HER2) on breast cancer cells [136]. Moreover, quantum dots have been used extensively for *in vivo* imaging. For example, intravenously injected quantum dots were used to detect prostate-specific membrane antigen in mice bearing prostate cancer xenografts [137]. Similarly, gold nanoparticles can be functionalized with DNA or proteins, in order to enable binding to specific targets. Subsequently, these particles can be detected through plasmon–plasmon resonance imaging, an optical technique based on interaction between target-bound gold nanoparticles within close proximity of each other [138]. Gold nanoparticles have been used for the detection of, for example, prostate-specific antigen [139] and amyloid beta-derived diffusible ligands [140]. In conclusion, nanodiagnostics provide opportunities for faster, more accurate, and cheaper detection of disease. Especially for the developing world, where resources are limited and hospitals are scarce, point-of-care testing could dramatically improve healthcare.

## 3.3 Scaffolds

A major problem of transplantation medicine is the expanding gap between the demand and availability of tissue/organ grafts. Indeed, a solution has yet to be found to overcome the crucial matter of graft shortage. A major approach to address this problem is the use of regenerative medicine, which has been defined as “the replacement or regeneration of human cells, tissue, or organs, to restore or establish normal function” [141]. With the emergence of nanotechnology, the past couple of decades have witnessed the development of regenerative medicine as a promising strategy to repair and regenerate diseased tissues and organs [142]. For instance, the design of cell-based nanostructured scaffolds is a promising alternative to avoid graft shortage. Such scaffolds consist of a

structural matrix that has cells embedded within it. For example, multiple studies have utilized stem cells, since they have the potential to differentiate, thereby increasing the likelihood of tissue or organ recovery. Cell-based scaffolds should resemble the extracellular matrix that is found in the human body. This endogenous matrix provides cells with physical and biochemical support, displaying unique surface topography, porosity, and stiffness. Scaffolds that sufficiently mimic the extracellular matrix will increase the ability of cells to adhere, proliferate, differentiate, and migrate. The next sections discuss recent progress toward the development of nanostructures applied to regenerative medicine in three major tissues: bone, skin, and nerves.

### 3.3.1 Bone Tissue Regeneration

Bone tissue is a nanostructured matrix mainly composed of collagen and calcium phosphate, arranged in the form of hydroxyapatite crystals, which form nanosheets with a thickness, length, and width of 1–7 nm, 15–200 nm, and 10–80 nm, respectively [143]. This matrix also incorporates several types of cells, including osteoblasts, osteocytes, and osteoclasts. Since several conditions can cause the loss of bone tissue, such as fractures, infectious diseases, and organic diseases, there is a need to develop bone substitutes. Notably, bone reparation and regeneration is a lengthy process and seldom leads to complete recovery of bone function. In the past, bone regeneration has been attempted through graft transplantation, which typically has an unsatisfactory outcome due to infections, donor morbidity, and other threatening complications. Therefore, cell-based bone scaffolds are a promising alternative for bone replacement and regeneration [36,144,145]. Such scaffolds should be biocompatible, physically and biologically stable, able to induce osteogenesis, free of pathogens, and free of major antigenic factors. In order to enable cell embedment scaffolding materials should also display high porosity.

Several nanostructured matrices have been developed for bone tissue regeneration, including those composed of hydroxyapatite nanofibers, carbon nanotubes, and nanotitanium. Nanostructured hydroxyapatite can be synthetized through sol–gel, precipitation, hydrothermal, and electrospinning techniques [146,147]. For example, Tasciotti and coworkers developed a magnesium-doped hydroxyapatite/collagen scaffold that induced osteogenic differentiation of human bone marrow-derived mesenchymal stem cells *in vitro* and promoted bone tissue growth *in vivo* [36]. In addition, titanium implants coated with nanopolymeric hydroxyapatite were shown to be nontoxic and increase bone tissue proliferation *in vivo* [148,149]. An enhancement of bone growth was also observed when using a nanostructured scaffold employing hydroxyapatite and collagen in rats affected by calvarial defects [150]. In addition to hydroxyapatite nanofibers, vertically aligned multiwalled carbon nanotubes alone or in combination with hydroxyapatite have shown lamellar bone regeneration *in vitro* and *in vivo* [151]. Moreover, Yao and coworkers designed anodized

titanium-based nanotube scaffolds that permit high levels of calcium deposition when cultured with osteoblasts [152]. Interestingly, the shape of cell-embedded scaffolds can have a considerable effect on performance. In fact, Wang *et al.* demonstrated that spiral-structured nanofibrous poly(epsilon-caprolactone) scaffolds displayed higher levels of cell attachment, proliferation, differentiation, and mineralization *in vitro* in comparison to cylindrical scaffolds [153]. Furthermore, to improve the performance of scaffolds, antibacterial agents and growth factors can be included in the matrix. As an illustration, polymeric-based nanoscaffolds have previously been designed to release antibiotic agents [154] and bone morphogenetic proteins [155]. In addition, the inclusion of copper–zinc alloy nanoparticles in a hydroxyapatite and chitosan scaffold was shown to improve protein adsorption, antibacterial properties, and structural stability [156].

The ability of mesenchymal stem cells to undergo osteogenic differentiation, acquires osteoblastic markers, and secrete extracellular matrix and calcium phosphate [157] makes them ideal candidates for use in nanostructured scaffolds. For instance, mesenchymal stem cells have previously been embedded in three-dimensional scaffolds composed of porous nanofibrous polylactic acid [158], electrospun polylactic acid/nanohydroxyapatite [159], and porous silk fibroin/chitosan [160]. In addition to these nanomaterials, mesenchymal stem cells have also been seeded with carbon nanotubes [161]. In this case, the alignment of the nanotubes had an impact on cell growth and osteogenic differentiation. Although much progress has been made in the bone tissue regeneration field, there is still a need to improve the design of scaffolds that permit functional replacement of bone tissue.

### 3.3.2
### Skin Regeneration

Over the past few decades, the number of patients suffering with chronic wounds has increased. Indeed, multiple conditions, such as age, smoking, and chronic diseases, can increase the prevalence of chronic wounds and impede their healing process [162]. Non-healing wounds, for example, burns, are more likely to develop complications such as infections, malignant transformation, and compromised esthetics. Moreover, quality of life can also be reduced as a result of chronic pain. The standard treatment for wounds involves utilization of skin grafts, which can be harvested from the same patient (autograft), another person (allograft), or another species (xenograft). Among these skin grafts, autografts typically result in better outcomes, since the immunological profiles match. On the contrary, allografts and xenografts are used as temporary substitutes, since they are eventually rejected due to immune reactions [163]. In this regard, several studies have focused on the development of skin substitutes to avoid complications associated with skin grafts. Indeed, major advantages of skin equivalents include decreased cross-infection [164,165] and reduced pain, resulting in shorter patient hospitalization periods and reduced morbidity and mortality [165,166]. Notably, skin substitutes should display specific

characteristics, such as sterility, biocompatibility, barrier function, prevention of water loss, and minimal inflammatory responses [164,167]. Moreover, engineered skin grafts should exhibit precise mechanical and physical features, including flexibility, resistance to shear and linear stresses, prompt wound site adhesion, and controlled degradability [164]. In addition, when designing skin substitutes it is important to consider issues regarding production costs, shelf life, and storage conditions [168].

With the advent of nanomedicine, several research efforts have been undertaken to design nanostructured skin substitutes. For example, Chandrasekaran and coworkers demonstrated that plasma-treated electrospun poly(L-lactic acid)-co-poly(epsilon-caprolactone)/gelatin nanofibrous scaffolds were able to enhance skin regeneration through inducing proliferation of embedded fibroblasts [169]. Moreover, Sun and coworkers embedded keratinocytes and fibroblasts in a scaffold composed of rosette nanotubes and hydrogels, and demonstrated efficient cell proliferation *in vitro* [170]. Notably, *in vivo* studies show that the utilization of cell-embedded scaffolds composed of nanofibrin in a chitosan hydrogel matrix cause improved wound closure in rats as compared to non-treated wounds [171]. Additionally, a polyvinyl alcohol-based hydrogel containing epigallocatechin gallate was shown to increase angiogenesis and re-epithelialization, while decreasing inflammation *in vivo* in comparison to controls [172]. Notably, biological compounds that promote skin regeneration can also be embedded into scaffolds. For instance, Jin *et al.* designed an adipose-derived stem cell-embedded scaffold based on core-shell nanofibers with various epidermal induction factors [173]. Future studies will shed light upon the most cost-effective and optimal nanomaterials that can be used as alternatives to skin grafts.

### 3.3.3 Nerve Regeneration

Damage to the nervous system often leads to severe and chronic debilitation. Due to the intricate nature of the nervous system and the low proliferation capacity of adult nerve cells, nerve regeneration and recovery are arduous. Autografts have been used as an approach to heal nerve damage [174,175], although functional recovery of the damaged area seldom occurs and the donor site is usually harmed. Although several biomaterials have been assessed for nerve regeneration [176,177], attempts to reconstruct damaged nerves with the use of scaffolds typically result in glial scar tissue and low neural tissue regrowth. Neural scaffolds are generally cylindrical structures that connect the ends of a lesion, providing support for nerve cell proliferation and for axonal elongation. Recently, nanostructured scaffolds have gained attention for nerve regeneration as they can be used to mimic the mechanical and chemical features of the extracellular matrix in nervous tissue [142]. In particular, such scaffolds should provide physical and biological support for nerve regeneration by guiding axon elongation and releasing growth factors [178]. Two of the most commonly used nanomaterials for neural scaffolds are carbon nanotubes and carbon nanofibers,

which can be designed to display diameters similar to those of neurites. For example, it was shown that super-aligned carbon nanotubes permitted enhanced directional neuronal growth [179]. Notably, attachment of functional groups on multi-walled carbon nanotubes resulted in changes in neurite dimensions, branching, and number of growth cones [180]. Neuronal adhesion, guided elongation, and differentiation were also achieved by utilizing a positively charged single-walled carbon nanotube polymeric film [181]. The film maintained the electrophysiological characteristics of the neurons, which were able to conduct electrical signals between each other [182].

Notably, carbon nanofibers display similar characteristics as carbon nanotubes but they are cheaper and easier to fabricate [14]. For example, a vertically aligned carbon nanofiber electrode array was shown to induce the formation of electrical connections between cells and nanofibers [183,184]. Moreover, carbon nanofibers embedded with stem cells were injected into the brains of rats with stroke damage [185]. Three weeks after injection, the stem cells differentiated into neurons and minimal glial scarring was observed. In addition, Koh *et al.* demonstrated nerve regeneration *in vivo* by using intraluminal nanofibrous nerve guides coated with laminin and containing growth factors [186]. Another study used electrospun nanofiber scaffolds with self-assembling peptides and pro-regenerative cytokines to achieve increased electrophysiological recovery of nerves in a rat model of chronic spinal cord damage [187]. In addition, neural tissue scaffolds have also been fabricated through three-dimensional printing. For example, hydrogel scaffolds have been produced by inkjet bioprinting of cells, proteins, and growth factors [188]. Although important progress has been made in the realm of neural tissue engineering, considerable challenges remain in this field.

## 3.4 Clinically Approved Nanoproducts

A wide variety of nanoproducts have been developed for use in healthcare and some of these products have already gained clinical approval. This section discusses select nanotherapeutics, implantable nanodevices, nanoscaffolds, and nanodiagnostic devices that are currently on the market. A 2014 review by Weissig *et al.* identified 43 approved nanotherapeutics [16], while a 2012 review by Etheridge *et al.* identified 33 nanotherapeutics and 67 nanodevices on the market [189]. However, the exact number of clinically approved nanoproducts is highly dependent on the classification criteria. For example, Weissig *et al.* regard pegylated proteins, protein-drug conjugates, and surfactant-based formulations as nanotherapeutics [16], although these categories are less frequently considered to be nano-based drugs. A nanopharmaceutical can be broadly defined as a nanoengineered medicine that displays nano-scale characteristics that contribute to therapeutic effects. Based on this definition, approved nanopharmaceuticals can be classified into four major categories: lipid-based, polymer-based, protein-based, and metal-based medicines.

The lipid-based category of approved nanotherapeutics is dominated by liposomes. In addition to the approval of Doxil in 1995, DaunoXome, AmBisome, Inflexal V, and Depocyt were all approved before the year 2000 [16,190]. Daunoxome (liposomal daunorubicin citrate) and AmBisome (liposomal amphotericin) were approved by the FDA for Kaposi Sarcoma and fungal infections, respectively. Inflexal V (liposomal influenza virus antigen) was approved in Switzerland as a vaccine for influenza virus, while DepoCyt (liposomal cytarabine) was approved in the United States to treat lymphomatous malignant meningitis. In the year 2000, Myocet (liposomal doxorubicin) and Visudyme (liposomal verteporfin) received clinical approval [16,190]. Myocet was approved in Europe for metastatic breast cancer, while Visudyme was approved in the United States for photodynamic therapy to treat certain ocular disorders. In 2004, the FDA approved DepoDur (liposomal morphine sulfate) for chronic pain treatment. Recently, Mepact (liposomal mifamurtide) was approved in Europe for the treatment of non-metastatic resectable osteosarcoma [16,190], while Marqibo (liposomal vincristine sulfate) was approved by the FDA to treat relapsed or progressed acute lymphoid leukemia (Philadelphia chromosome-negative) [191]. Besides liposomes, nanotherapeutics in the form of lipid complexes have also gained regulatory approval, for example, Abelcet (amphotericin B) for the treatment of systemic fungal infections [16,190].

The second class of approved nanopharmaceuticals is protein-based. Following a stringent definition of nanotherapeutics, Abraxane would be considered the only protein-based nanoparticle on the market. As previously mentioned, Abraxane consists of albumin bound paclitaxel nanoparticles in the size range of 130 nm [64].

The third category of approved nanopharmaceuticals comprises a group of polymer-based nanoformulations. For example, Eligard, a poly(DL-lactide-co-glycolide) (PLGH) nanoparticle encapsulating leuprolide acetate, was approved in 2002 for the treatment of advanced prostate cancer [16]. Additionally, Opaxio, which is a polyglutamate-based nanoparticle conjugated to paclitaxel, was approved by the FDA in 2012 for the treatment of glioblastoma [16]. Another approved paclitaxel-containing polymeric nanoparticle is Genexol, which is based on PEG-poly(D,L-lactide) [15].

The fourth class of approved nanotherapeutics is metal nanoparticles. For instance, NanoTherm, based on aminosilane-coated superparamagnetic iron oxide nanoparticles, was approved in Europe in 2010 for local thermal ablation of glioblastoma [17]. After injection of the NanoTherm solution into the brain, the brain tissue is exposed to an alternating magnetic field, which causes particle oscillations that generate heat. Other approved metal nanoparticles include Feridex and Feraheme, which are superparamagnetic iron oxide nanoparticles coated with dextran that target the mononuclear phagocyte system [16]. The former was approved by the FDA in 1996 for magnetic resonance imaging (MRI), while the latter was approved by the FDA in 2006 for the treatment of kidney disease-related iron deficiency.

In regards to clinically approved nanodevices, a number of intravitreal implantable devices based on polymeric and silicone nanomaterials have entered

the market, including Ozurdex, Vitrasert, and Retisert [192]. For instance, Ozurdex is a biodegradable implant that was approved in 2009 for the treatment of macular edema. This device is composed of a Novadur solid polymer matrix, which is based on PLGA that slowly degrades over a six-month period forming lactic acid and glycolic acid, while releasing dexamethasone [192]. An example of an FDA approved nanoscaffold is Vitoss, which is composed of ultraporous beta-tricalcium phosphate nanoparticles [193]. This three-dimensional structure induces bone growth, thereby promoting bone reparation.

Moreover, several nano-based diagnostic tests have been approved by the FDA, including CellSearch, CombiMatrix DNAarray, and Verigene. For example, CellSearch was approved in 2004 for identification and quantification of circulating breast cancer cells in blood samples [194]. Verigene, in turn, was approved in 2007 as a diagnostic test for assaying warfarin metabolism. This diagnostic device is composed of gold nanoparticles conjugated to nucleotide sequences [193].

In the past two decades, multiple nanopharmaceuticals, implantable nanodevices, nanoscaffolds, and nanodiagnostics have received clinical approval. A much larger portion of nanoproducts is currently under clinical investigation and the next few years are likely to see an increase in the use of nanotechnology in the healthcare industry. Notably, the implementation of nanotechnology in medicine requires an interdisciplinary approach. In particular, the integration of medicine, biology, chemistry, physics, mathematics, and engineering is likely to provide the best nano-based products for improving healthcare. One of the most promising aspects of nanotechnology is the ability to provide the field of medicine with tools for multifunctional approaches to diagnose and treat disease. For instance, in the context of therapeutics, nanotechnology strategies can bestow drugs with transport, recognition, and release components, which can all be customized to permit an individualized approach to treatment. In addition, nanotechnology enables rapid or real-time theranostic approaches to manage disease. In this chapter we have introduced the main applications of nanotechnology in medicine, including drug delivery, diagnostics, and tissue regeneration. Additionally, we have provided an overview of the main classes of clinically approved nanoproducts. Currently, medicine is moving toward a multifaceted and personalized approach to patient care, in which next-generation nanotechnology products will play a dominant role. As the field of nanomedicine continues to grow, we are likely to experience radical advances in clinical care.

## References


1 Theis, T., Parr, D., Binks, P., Ying, J., Drexler, K.E., Schepers, E., Mullis, K., Bai, C., Boland, J.J., Langer, R. *et al.* (2006) nan'o.tech.nol'o.gy n. *Nat. Nanotechnol.*, **1**, 8–10.

2 Wolfram, J., Zhu, M., Yang, Y., Shen, J., Gentile, E., Paolino, D., Fresta, M., Nie, G., Chen, C., Shen, H. *et al.* (2015) Safety of nanoparticles in medicine. *Curr. Drug Targets.* doi: 10.2174/1389450115666140804124808

3 Ferrari, M. (2005) Cancer nanotechnology: opportunities and challenges. *Nat. Rev. Cancer*, **5**, 161–171.

4 Blanco, E., Shen, H., and Ferrari, M. (2015) Principles of nanoparticle design for overcoming biological barriers to drug delivery. *Nat. Biotechnol.*, **33**, 941–951.

5 Blanco, E., Hsiao, A., Mann, A.P., Landry, M.G., Meric-Bernstam, F., and Ferrari, M. (2011) Nanomedicine in cancer therapy: innovative trends and prospects. *Cancer Sci*, **102**, 1247–1252.

6 Molinaro, R., Wolfram, J., Federico, C., Cilurzo, F., Di Marzio, L., Ventura, C.A., Carafa, M., Celia, C., and Fresta, M. (2013) Polyethylenimine and chitosan carriers for the delivery of RNA interference effectors. *Expert Opin. Drug Deliv.*, **10**, 1653–1668.

7 Ma, X., Zhao, Y., and Liang, X.J. (2011) Theranostic nanoparticles engineered for clinic and pharmaceutics. *Acc. Chem. Res.*, **44**, 1114–1122.

8 Li, Y., Xuan, J., Song, Y., Wang, P., and Qin, L. (2015) A microfluidic platform with digital readout and ultra-low detection limit for quantitative point-of-care diagnostics. *Lab Chip*, **15**, 3300–3306.

9 Song, Y., Huang, Y.Y., Liu, X., Zhang, X., Ferrari, M., and Qin, L. (2014) Point-of-care technologies for molecular diagnostics using a drop of blood. *Trends Biotechnol.*, **32**, 132–139.

10 Blanco, E., Bey, E.A., Dong, Y., Weinberg, B.D., Sutton, D.M., Boothman, D.A., and Gao, J. (2007) Beta-lapachone-containing PEG-PLA polymer micelles as novel nanotherapeutics against NQO1-overexpressing tumor cells. *J. Control. Release*, **122**, 365–374.

11 Mu, C.F., Balakrishnan, P., Cui, F.D., Yin, Y.M., Lee, Y.B., Choi, H.G., Yong, C.S., Chung, S.J., Shim, C.K., and Kim, D.D. (2010) The effects of mixed MPEG-PLA/Pluronic copolymer micelles on the bioavailability and multidrug resistance of docetaxel. *Biomaterials*, **31**, 2371–2379.

12 Freed, L.E., Marquis, J.C., Nohria, A., Emmanual, J., Mikos, A.G., and Langer, R. (1993) Neocartilage formation *in vitro* and *in vivo* using cells cultured on synthetic biodegradable polymers. *J. Biomed. Mater. Res.*, **27**, 11–23.

13 Cabral, H., Matsumoto, Y., Mizuno, K., Chen, Q., Murakami, M., Kimura, M., Terada, Y., Kano, M.R., Miyazono, K., Uesaka, M. *et al.* (2011) Accumulation of sub-100nm polymeric micelles in poorly permeable tumours depends on size. *Nat. Nanotechnol.*, **6**, 815–823.

14 Kim, C., Jeong, Y.I., Ngoc, B.T., Yang, K.S., Kojima, M., Kim, Y.A., Endo, M., and Lee, J.W. (2007) Synthesis and characterization of porous carbon nanofibers with hollow cores through the thermal treatment of electrospun copolymeric nanofiber webs. *Small*, **3**, 91–95.

15 Oerlemans, C., Bult, W., Bos, M., Storm, G., Nijsen, J.F., and Hennink, W.E. (2010) Polymeric micelles in anticancer therapy: targeting, imaging and triggered release. *Pharm. Res.*, **27**, 2569–2589.

16 Weissig, V., Pettinger, T.K., and Murdock, N. (2014) Nanopharmaceuticals (part 1): products on the market. *Int. J. Nanomedicine.*, **9**, 4357–4373.

17 Thiesen, B., and Jordan, A. (2008) Clinical applications of magnetic nanoparticles for hyperthermia. *Int. J. Hyperthermia*, **24**, 467–474.

18 Yunus Basha, R., Sampath Kumar, T.S., and Doble, M. (2015) Design of biocomposite materials for bone tissue regeneration. *Mater. Sci. Eng. C Mater. Biol. Appl.*, **57**, 452–463.

19 Hu, J., Yang, Z., Zhou, Y., Liu, Y., Li, K., and Lu, H. (2015) Porous biphasic calcium phosphate ceramics coated with nano-hydroxyapatite and seeded with mesenchymal stem cells for reconstruction of radius segmental defects in rabbits. *J. Mater. Sci. Mater. Med.*, **26**, 257.

20 Pasut, G., Paolino, D., Celia, C., Mero, A., Joseph, A.S., Wolfram, J., Cosco, D., Schiavon, O., Shen, H., and Fresta, M. (2015) Polyethylene glycol (PEG)-dendron phospholipids as innovative constructs for the preparation of super stealth liposomes for anticancer therapy. *J. Control. Release*, **199**, 106–113.

21 Gentile, E., Cilurzo, F., Di Marzio, L., Carafa, M., Ventura, C.A., Wolfram, J., Paolino, D., and Celia, C. (2013) Liposomal chemotherapeutics. *Future Oncol.*, **9**, 1849–1859.

22 Wolfram, J., Suri, K., Huang, Y., Molinaro, R., Borsoi, C., Scott, B., Boom, K., Paolino, D., Fresta, M., Wang, J. *et al.* (2014) Evaluation of anticancer activity of celastrol liposomes in prostate cancer cells. *J. Microencapsul.*, **31**, 501–507.

23 Paolino, D., Cosco, D., Gaspari, M., Celano, M., Wolfram, J., Voce, P., Puxeddu, E., Filetti, S., Celia, C., Ferrari, M. *et al.* (2014) Targeting the thyroid gland with thyroid-stimulating hormone (TSH)-nanoliposomes. *Biomaterials*, **35**, 7101–7109.

24 Blanco, E., Sangai, T., Wu, S., Hsiao, A., Ruiz-Esparza, G.U., Gonzalez-Delgado, C.A., Cara, F.E., Granados-Principal, S., Evans, K.W., Akcakanat, A. *et al.* (2014) Colocalized delivery of rapamycin and paclitaxel to tumors enhances synergistic targeting of the PI3K/Akt/mTOR pathway. *Mol. Ther.*, **22**, 1310–1319.

25 Shen, J., Kim, H.C., Mu, C., Gentile, E., Mai, J., Wolfram, J., Ji, L.N., Ferrari, M., Mao, Z.W., and Shen, H. (2014) Multifunctional gold nanorods for siRNA gene silencing and photothermal therapy. *Adv. Healthc Mater*, **3**, 1629–1637.

26 You, J., Zhang, G., and Li, C. (2010) Exceptionally high payload of doxorubicin in hollow gold nanospheres for near-infrared light-triggered drug release. *ACS Nano*, **4**, 1033–1041.

27 Shen, J., Kim, H.C., Su, H., Wang, F., Wolfram, J., Kirui, D., Mai, J., Mu, C., Ji, L.N., Mao, Z.W. *et al.* (2014) Cyclodextrin and polyethylenimine functionalized mesoporous silica nanoparticles for delivery of siRNA cancer therapeutics. *Theranostics*, **4**, 487–497.

28 Chen, F., Hong, H., Shi, S., Goel, S., Valdovinos, H.F., Hernandez, R., Theuer, C.P., Barnhart, T.E., and Cai, W. (2014) Engineering of hollow mesoporous silica nanoparticles for remarkably enhanced tumor active targeting efficacy. *Sci. Rep.*, **4**, 5080.

29 Shen, J., Xu, R., Mai, J., Kim, H.C., Guo, X., Qin, G., Yang, Y., Wolfram, J., Mu, C., Xia, X. *et al.* (2013) High capacity nanoporous silicon carrier for systemic delivery of gene silencing therapeutics. *ACS Nano*, **7**, 9867–9880.

30 Shen, J., Wu, X., Lee, Y., Wolfram, J., Yang, Z., Mao, Z.W., Ferrari, M., and Shen, H. (2015) Porous silicon microparticles for delivery of siRNA therapeutics. *J. Vis. Exp.* doi: 10.3791/52075

31 Xu, R., Huang, Y., Mai, J., Zhang, G., Guo, X., Xia, X., Koay, E.J., Qin, G., Erm, D.R., Li, Q. *et al.* (2013) Multistage vectored siRNA targeting ataxia-telangiectasia mutated for breast cancer therapy. *Small*, **9**, 1799–1808.

32 Zheng, G., Patolsky, F., Cui, Y., Wang, W.U., and Lieber, C.M. (2005) Multiplexed electrical detection of cancer markers with nanowire sensor arrays. *Nat. Biotechnol.*, **23**, 1294–1301.

33 Barletta, J.M., Edelman, D.C., and Constantine, N.T. (2004) Lowering the detection limits of HIV-1 viral load using real-time immuno-PCR for HIV-1 p24 antigen. *Am. J. Clin. Pathol.*, **122**, 20–27.

34 Chen, X. and Kendler, K.S. (2008) Interleukin 3 and schizophrenia. *Am. J. Psychiatry*, **165**, 13–14.

35 Turner, N.J. and Badylak, S.F. (2015) The use of biologic scaffolds in the treatment of chronic nonhealing wounds. *Adv. Wound Care (New Rochelle)*, **4**, 490–500.

36 Minardi, S., Corradetti, B., Taraballi, F., Sandri, M., Van Eps, J., Cabrera, F.J., Weiner, B.K., Tampieri, A., and Tasciotti, E. (2015) Evaluation of the osteoinductive potential of a bio-inspired scaffold mimicking the osteogenic niche for bone augmentation. *Biomaterials*, **62**, 128–137.

37 Gori, T., Schulz, E., Hink, U., Wenzel, P., Post, F., Jabs, A., and Munzel, T. (2014) Early outcome after implantation of Absorb bioresorbable drug-eluting scaffolds in patients with acute coronary syndromes. *EuroIntervention*, **9**, 1036–1041.

38 Perez-Basterrechea, M., Briones, R.M., Alvarez-Viejo, M., Garcia-Perez, E., Esteban, M.M., Garcia, V., Obaya, A.J., Barneo, L., Meana, A., and Otero, J. (2009) Plasma-fibroblast gel as scaffold for islet transplantation. *Tissue Eng. Part A*, **15**, 569–577.

39 Wolfram, J., Shen, H., and Ferrari, M. (2015) Multistage vector (MSV)

therapeutics. *J. Control. Release.* doi: 10.1016/j.jconrel.2015.08.010

40 Ferrari, M. (2010) Frontiers in cancer nanomedicine: directing mass transport through biological barriers. *Trends Biotechnol.*, **28**, 181–188.

41 Bae, Y.H. and Park, K. (2011) Targeted drug delivery to tumors: myths, reality and possibility. *J. Control. Release*, **153**, 198–205.

42 Li, K.C., Pandit, S.D., Guccione, S., and Bednarski, M.D. (2004) Molecular imaging applications in nanomedicine. *Biomed. Microdevices*, **6**, 113–116.

43 Suzuki, R., Takizawa, T., Kuwata, Y., Mutoh, M., Ishiguro, N., Utoguchi, N., Shinohara, A., Eriguchi, M., Yanagie, H., and Maruyama, K. (2008) Effective anti-tumor activity of oxaliplatin encapsulated in transferrin-PEG-liposome. *Int. J. Pharm.*, **346**, 143–150.

44 Chau, Y., Dang, N.M., Tan, F.E., and Langer, R. (2006) Investigation of targeting mechanism of new dextran-peptide-methotrexate conjugates using biodistribution study in matrix-metalloproteinase-overexpressing tumor xenograft model. *J. Pharm. Sci.*, **95**, 542–551.

45 Choi, H.S., Liu, W., Misra, P., Tanaka, E., Zimmer, J.P., Itty Ipe, B., Bawendi, M.G., and Frangioni, J.V. (2007) Renal clearance of quantum dots. *Nat. Biotechnol.*, **25**, 1165–1170.

46 Wolfram, J., Suri, K., Yang, Y., Shen, J., Celia, C., Fresta, M., Zhao, Y., Shen, H., and Ferrari, M. (2014) Shrinkage of pegylated and non-pegylated liposomes in serum. *Colloids Surf B Biointerfaces*, **114**, 294–300.

47 Wolfram, J., Yang, Y., Shen, J., Moten, A., Chen, C., Shen, H., Ferrari, M., and Zhao, Y. (2014) The nano-plasma interface: Implications of the protein corona. *Colloids Surf B Biointerfaces*, **124**, 17–24.

48 Michor, F., Liphardt, J., Ferrari, M., and Widom, J. (2011) What does physics have to do with cancer? *Nat. Rev. Cancer*, **11**, 657–670.

49 Folkman, J. (1971) Tumor angiogenesis: therapeutic implications. *N. Engl. J. Med.*, **285**, 1182–1186.

50 Yuan, F., Dellian, M., Fukumura, D., Leunig, M., Berk, D.A., Torchilin, V.P., and Jain, R.K. (1995) Vascular permeability in a human tumor xenograft: molecular size dependence and cutoff size. *Cancer Res.*, **55**, 3752–3756.

51 Matsumura, Y. and Maeda, H. (1986) A new concept for macromolecular therapeutics in cancer chemotherapy: mechanism of tumoritropic accumulation of proteins and the antitumor agent smancs. *Cancer Res.*, **46**, 6387–6392.

52 Fang, J., Nakamura, H., and Maeda, H. (2011) The EPR effect: unique features of tumor blood vessels for drug delivery, factors involved, and limitations and augmentation of the effect. *Adv. Drug Deliv. Rev.*, **63**, 136–151.

53 Torchilin, V. (2011) Tumor delivery of macromolecular drugs based on the EPR effect. *Adv. Drug Deliv. Rev.*, **63**, 131–135.

54 Kalluri, R. and Zeisberg, M. (2006) Fibroblasts in cancer. *Nat. Rev. Cancer*, **6**, 392–401.

55 Gilkes, D.M., Semenza, G.L., and Wirtz, D. (2014) Hypoxia and the extracellular matrix: drivers of tumour metastasis. *Nat. Rev. Cancer*, **14**, 430–439.

56 Celia, C., Trapasso, E., Locatelli, M., Navarra, M., Ventura, C.A., Wolfram, J., Carafa, M., Morittu, V.M., Britti, D., DiMarzio, L. *et al.* (2013) Anticancer activity of liposomal bergamot essential oil (BEO) on human neuroblastoma cells. *Colloids Surf B Biointerfaces*, **112**, 548–553.

57 Wolfram, J., Suri, K., Huang, Y., Molinaro, R., Borsoi, C., Scott, B., Boom, K., Paolino, D., Fresta, M., Wang, J. *et al.* (2014) Evaluation of anticancer activity of celastrol liposomes in prostate cancer cells. *J. Microencaps*, **31**, 501–507.

58 Weis, S.M. (2008) Vascular permeability in cardiovascular disease and cancer. *Curr. Opin. Hematol.*, **15**, 243–249.

59 Azzopardi, E.A., Ferguson, E.L., and Thomas, D.W. (2013) The enhanced permeability retention effect: a new paradigm for drug targeting in infection. *J. Antimicrob. Chemother.*, **68**, 257–274.

60 Marti, C.N., Gheorghiade, M., Kalogeropoulos, A.P., Georgiopoulou, V.V., Quyyumi, A.A., and Butler, J. (2012) Endothelial dysfunction, arterial stiffness, and heart failure. *J. Am. Coll. Cardiol.*, **60**, 1455–1469.

61 Menon, C., Ghartey, A., Canter, R., Feldman, M., and Fraker, D.L. (2006) Tumor necrosis factor-alpha damages tumor blood vessel integrity by targeting VE-cadherin. *Ann. Surg.*, **244**, 781–791.

62 Pasut, G., Paolino, D., Celia, C., Mero, A., Joseph, A.S., Wolfram, J., Cosco, D., Schiavon, O., Shen, H., and Fresta, M. (2014) Polyethylene glycol (PEG)-dendron phospholipids as innovative constructs for the preparation of super stealth liposomes for anticancer therapy. *J. Control. Release*, **199**, 106–113.

63 Barenholz, Y. (2012) Doxil(R)–the first FDA-approved nano-drug: lessons learned. *J. Control. Release*, **160**, 117–134.

64 Ma, P. and Mumper, R.J. (2013) Paclitaxel nano-delivery systems: a comprehensive review. *J. Nanomed. Nanotechnol.*, **4**, 1000164.

65 Decuzzi, P., Godin, B., Tanaka, T., Lee, S.Y., Chiappini, C., Liu, X., and Ferrari, M. (2010) Size and shape effects in the biodistribution of intravascularly injected particles. *J. Control. Release*, **141**, 320–327.

66 van de Ven, A.L., Kim, P., Haley, O., Fakhoury, J.R., Adriani, G., Schmulen, J., Moloney, P., Hussain, F., Ferrari, M., Liu, X. *et al.* (2012) Rapid tumoritropic accumulation of systemically injected plateloid particles and their biodistribution. *J. Control. Release*, **158**, 148–155.

67 Adriani, G., de Tullio, M.D., Ferrari, M., Hussain, F., Pascazio, G., Liu, X., and Decuzzi, P. (2012) The preferential targeting of the diseased microvasculature by disk-like particles. *Biomaterials*, **33**, 5504–5513.

68 Decuzzi, P. and Ferrari, M. (2008) Design maps for nanoparticles targeting the diseased microvasculature. *Biomaterials*, **29**, 377–384.

69 Decuzzi, P. and Ferrari, M. (2006) The adhesive strength of non-spherical particles mediated by specific interactions. *Biomaterials*, **27**, 5307–5314.

70 Thon, J.N., Macleod, H., Begonja, A.J., Zhu, J., Lee, K.C., Mogilner, A., Hartwig, J.H., and Italiano, J.E. Jr. (2012) Microtubule and cortical forces determine platelet size during vascular platelet production. *Nat. Commun.*, **3**, 852.

71 Hawkins, M.J., Soon-Shiong, P., and Desai, N. (2008) Protein nanoparticles as drug carriers in clinical medicine. *Adv. Drug Deliv. Rev.*, **60**, 876–885.

72 Gelderblom, H., Verweij, J., Nooter, K., and Sparreboom, A. (2001) Cremophor EL: the drawbacks and advantages of vehicle selection for drug formulation. *Eur. J. Cancer*, **37**, 1590–1598.

73 Ruoslahti, E. (2012) Peptides as targeting elements and tissue penetration devices for nanoparticles. *Adv. Mater.*, **24**, 3747–3756.

74 Cardoso, M.M., Peca, I.N., and Roque, A.C. (2012) Antibody-conjugated nanoparticles for therapeutic applications. *Curr. Med. Chem.*, **19**, 3103–3127.

75 Paolino, D., Cosco, D., Gaspari, M., Celano, M., Wolfram, J., Voce, P., Puxeddu, E., Filetti, S., Celia, C., Ferrari, M. *et al.* (2014) Targeting the thyroid gland with thyroid stimulating hormone (TSH)-nanoliposomes. *Biomaterials*, **35**, 7101–7109.

76 Mai, J., Huang, Y., Mu, C., Zhang, G., Xu, R., Guo, X., Xia, X., Volk, D.E., Lokesh, G.L., Thiviyanathan, V. *et al.* (2014) Bone marrow endothelium-targeted therapeutics for metastatic breast cancer. *J. Control. Release*, **187**, 22–29.

77 Pollinger, K., Hennig, R., Ohlmann, A., Fuchshofer, R., Wenzel, R., Breunig, M., Tessmar, J., Tamm, E.R., and Goepferich, A. (2013) Ligand-functionalized nanoparticles target endothelial cells in retinal capillaries after systemic application. *Proc. Natl. Acad. Sci. USA*, **110**, 6115–6120.

78 Sperling, R.A. and Parak, W.J. (2010) Surface modification, functionalization and bioconjugation of colloidal inorganic nanoparticles. *Philos. Trans A Math Phys. Eng. Sci.*, **368**, 1333–1383.

79 Wang, A.Z., Gu, F., Zhang, L., Chan, J.M., Radovic-Moreno, A., Shaikh, M.R., and Farokhzad, O.C. (2008) Biofunctionalized targeted nanoparticles for therapeutic applications. *Expert Opin. Biol. Ther.*, **8**, 1063–1070.

80 Salvati, A., Pitek, A.S., Monopoli, M.P., Prapainop, K., Bombelli, F.B., Hristov, D.R., Kelly, P.M., Aberg, C., Mahon, E., and Dawson, K.A. (2013) Transferrin-functionalized nanoparticles lose their targeting capabilities when a biomolecule corona adsorbs on the surface. *Nat. Nanotechnol.*, **8**, 137–143.

81 Gaspar, R. (2013) Nanoparticles: pushed off target with proteins. *Nat. Nanotechnol.*, **8**, 79–80.

82 Lundqvist, M., Stigler, J., Elia, G., Lynch, I., Cedervall, T., and Dawson, K.A. (2008) Nanoparticle size and surface properties determine the protein corona with possible implications for biological impacts. *Proc. Natl. Acad. Sci. USA*, **105**, 14265–14270.

83 Monopoli, M.P., Aberg, C., Salvati, A., and Dawson, K.A. (2012) Biomolecular coronas provide the biological identity of nanosized materials. *Nat. Nanotechnol.*, **7**, 779–786.

84 Mahon, E., Salvati, A., Baldelli Bombelli, F., Lynch, I., and Dawson, K.A. (2012) Designing the nanoparticle-biomolecule interface for "targeting and therapeutic delivery". *J. Control. Release*, **161**, 164–174.

85 Davis, M.E., Chen, Z.G., and Shin, D.M. (2008) Nanoparticle therapeutics: an emerging treatment modality for cancer. *Nat. Rev. Drug Discov.*, **7**, 771–782.

86 Glazer, E.S., Zhu, C., Massey, K.L., Thompson, C.S., Kaluarachchi, W.D., Hamir, A.N., and Curley, S.A. (2010) Noninvasive radiofrequency field destruction of pancreatic adenocarcinoma xenografts treated with targeted gold nanoparticles. *Clin. Cancer Res.*, **16**, 5712–5721.

87 Shen, H., You, J., Zhang, G., Ziemys, A., Li, Q., Bai, L., Deng, X., Erm, D.R., Liu, X., Li, C. *et al.* (2012) Cooperative, nanoparticle-enabled thermal therapy of breast cancer. *Adv. Healthc. Mater*, **1**, 84–89.

88 Johannsen, M., Thiesen, B., Jordan, A., Taymoorian, K., Gneveckow, U., Waldofner, N., Scholz, R., Koch, M., Lein, M., Jung, K. *et al.* (2005) Magnetic fluid hyperthermia (MFH)reduces prostate cancer growth in the orthotopic Dunning R3327 rat model. *Prostate*, **64**, 283–292.

89 Chakravarty, P., Marches, R., Zimmerman, N.S., Swafford, A.D., Bajaj, P., Musselman, I.H., Pantano, P., Draper, R.K., and Vitetta, E.S. (2008) Thermal ablation of tumor cells with antibody-functionalized single-walled carbon nanotubes. *Proc. Natl. Acad. Sci. USA*, **105**, 8697–8702.

90 Ghosh, S., Dutta, S., Gomes, E., Carroll, D., D'Agostino, R. Jr., Olson, J., Guthold, M., and Gmeiner, W.H. (2009) Increased heating efficiency and selective thermal ablation of malignant tissue with DNA-encased multiwalled carbon nanotubes. *ACS Nano*, **3**, 2667–2673.

91 Sharma, A., Jain, N., and Sareen, R. (2013) Nanocarriers for diagnosis and targeting of breast cancer. *Biomed. Res. Int.*, **2013**, 960821.

92 Cervadoro, A., Giverso, C., Pande, R., Sarangi, S., Preziosi, L., Wosik, J., Brazdeikis, A., and Decuzzi, P. (2013) Design maps for the hyperthermic treatment of tumors with superparamagnetic nanoparticles. *PLoS One*, **8**, e57332.

93 Li, L., ten Hagen, T.L., Bolkestein, M., Gasselhuber, A., Yatvin, J., van Rhoon, G.C., Eggermont, A.M., Haemmerich, D., and Koning, G.A. (2013) Improved intratumoral nanoparticle extravasation and penetration by mild hyperthermia. *J. Control. Release*, **167**, 130–137.

94 Sengupta, S., Eavarone, D., Capila, I., Zhao, G., Watson, N., Kiziltepe, T., and Sasisekharan, R. (2005) Temporal targeting of tumour cells and neovasculature with a nanoscale delivery system. *Nature*, **436**, 568–572.

95 Wong, C., Stylianopoulos, T., Cui, J., Martin, J., Chauhan, V.P., Jiang, W., Popovic, Z., Jain, R.K., Bawendi, M.G., and Fukumura, D. (2011) Multistage nanoparticle delivery system for deep penetration into tumor tissue. *Proc. Natl. Acad. Sci. USA*, **108**, 2426–2431.

96 Tanaka, T., Decuzzi, P., Cristofanilli, M., Sakamoto, J.H., Tasciotti, E., Robertson, F.M., and Ferrari, M. (2009) Nanotechnology for breast cancer therapy. *Biomed. Microdevices*, **11**, 49–63.

97 Godin, B., Gu, J., Serda, R.E., Bhavane, R., Tasciotti, E., Chiappini, C., Liu, X., Tanaka, T., Decuzzi, P., and Ferrari, M. (2010) Tailoring the degradation kinetics of mesoporous silicon structures through PEGylation. *J. Biomed. Mater Res. A*, **94**, 1236–1243.

98 Anglin, E.J., Cheng, L., Freeman, W.R., and Sailor, M.J. (2008) Porous silicon in drug delivery devices and materials. *Adv. Drug Deliv. Rev.*, **60**, 1266–1277.

99 Godin, B., Tasciotti, E., Liu, X., Serda, R.E., and Ferrari, M. (2011) Multistage nanovectors: from concept to novel imaging contrast agents and therapeutics. *Acc. Chem. Res.*, **44**, 979–989.

100 Martinez, J.O., Evangelopoulos, M., Bhavane, R., Acciardo, S., Salvatore, F., Liu, X., Ferrari, M., and Tasciotti, E. (2014) Multistage Nanovectors Enhance the Delivery of Free and Encapsulated Drugs. *Curr. Drug Targets*, **16**, 1582–1590.

101 Tanaka, T., Mangala, L.S., Vivas-Mejia, P.E., Nieves-Alicea, R., Mann, A.P., Mora, E., Han, H.D., Shahzad, M.M., Liu, X., Bhavane, R. *et al.* (2010) Sustained small interfering RNA delivery by mesoporous silicon particles. *Cancer Res.*, **70**, 3687–3696.

102 Chen, X., Iliopoulos, D., Zhang, Q., Tang, Q., Greenblatt, M.B., Hatziapostolou, M., Lim, E., Tam, W.L., Ni, M., Chen, Y. *et al.* (2014) XBP1 promotes triple-negative breast cancer by controlling the HIF1alpha pathway. *Nature*, **508**, 103–107.

103 Shen, H., Rodriguez-Aguayo, C., Xu, R., Gonzalez-Villasana, V., Mai, J., Huang, Y., Zhang, G., Guo, X., Bai, L., Qin, G. *et al.* (2013) Enhancing chemotherapy response with sustained EphA2 silencing using multistage vector delivery. *Clin. Cancer Res.*, **19**, 1806–1815.

104 Zhang, M., Xu, R., Xia, X., Yang, Y., Gu, J., Qin, G., Liu, X., Ferrari, M., and Shen, H. (2014) Polycation-functionalized nanoporous silicon particles for gene silencing on breast cancer cells. *Biomaterials*, **35**, 423–431.

105 Blanco, E., Sangai, T., Hsiao, A., Ferrati, S., Bai, L., Liu, X., Meric-Bernstam, F., and Ferrari, M. (2013) Multistage delivery of chemotherapeutic nanoparticles for breast cancer treatment. *Cancer Lett.*, **334**, 245–252.

106 Chiappini, C., Tasciotti, E., Fakhoury, J.R., Fine, D., Pullan, L., Wang, Y.C., Fu, L., Liu, X., and Ferrari, M. (2010) Tailored porous silicon microparticles: fabrication and properties. *ChemPhysChem*, **11**, 1029–1035.

107 Tasciotti, E., Liu, X., Bhavane, R., Plant, K., Leonard, A.D., Price, B.K., Cheng, M.M., Decuzzi, P., Tour, J.M., Robertson, F. *et al.* (2008) Mesoporous silicon particles as a multistage delivery system for imaging and therapeutic applications. *Nat. Nanotechnol.*, **3**, 151–157.

108 Ananta, J.S., Godin, B., Sethi, R., Moriggi, L., Liu, X., Serda, R.E., Krishnamurthy, R., Muthupillai, R., Bolskar, R.D., Helm, L. *et al.* (2010) Geometrical confinement of gadolinium-based contrast agents in nanoporous particles enhances T1 contrast. *Nat. Nanotechnol.*, **5**, 815–821.

109 Gizzatov, A., Stigliano, C., Ananta, J.S., Sethi, R., Xu, R., Guven, A., Ramirez, M., Shen, H., Sood, A., Ferrari, M. *et al.* (2014) Geometrical confinement of Gd (DOTA) molecules within mesoporous silicon nanoconstructs for MR imaging of cancer. *Cancer Lett.*, **352**, 97–101.

110 Aryal, S., Key, J., Stigliano, C., Landis, M.D., Lee, D.Y., and Decuzzi, P. (2014) Positron emitting magnetic nanoconstructs for PET/MR imaging. *Small*, **10**, 2688–2696.

111 Yazdi, I.K., Murphy, M.B., Loo, C., Liu, X., Ferrari, M., Weiner, B.K., and Tasciotti, E. (2014) Cefazolin-loaded mesoporous silicon microparticles show sustained bactericidal effect against Staphylococcus aureus. *J. Tissue Eng.*, **5**, 2041731414536573.

112 Dave, B., Granados-Principal, S., Zhu, R., Benz, S., Rabizadeh, S., Soon-Shiong, P., Yu, K.D., Shao, Z., Li, X., Gilcrease, M. *et al.* (2014) Targeting RPL39 and MLF2 reduces tumor initiation and metastasis

in breast cancer by inhibiting nitric oxide synthase signaling. *Proc. Natl. Acad. Sci. USA*, **111**, 8838–8843.

**113** von Maltzahn, G., Park, J.H., Lin, K.Y., Singh, N., Schwoppe, C., Mesters, R., Berdel, W.E., Ruoslahti, E., Sailor, M.J., and Bhatia, S.N. (2011) Nanoparticles that communicate in vivo to amplify tumour targeting. *Nat. Mater.*, **10**, 545–552.

**114** Akin, D., Sturgis, J., Ragheb, K., Sherman, D., Burkholder, K., Robinson, J.P., Bhunia, A.K., Mohammed, S., and Bashir, R. (2007) Bacteria-mediated delivery of nanoparticles and cargo into cells. *Nat. Nanotechnol.*, **2**, 441–449.

**115** Lee, E.S., Kim, D., Youn, Y.S., Oh, K.T., and Bae, Y.H. (2008) A virus-mimetic nanogel vehicle. *Angew. Chem. Int. Ed. Engl.*, **47**, 2418–2421.

**116** Parodi, A., Quattrocchi, N., van de Ven, A.L., Chiappini, C., Evangelopoulos, M., Martinez, J.O., Brown, B.S., Khaled, S.Z., Yazdi, I.K., Enzo, M.V. *et al.* (2013) Synthetic nanoparticles functionalized with biomimetic leukocyte membranes possess cell-like functions. *Nat. Nanotechnol.*, **8**, 61–68.

**117** Dash, A.K. and Cudworth, G.C. 2nd (1998) Therapeutic applications of implantable drug delivery systems. *J. Pharmacol. Toxicol. Methods*, **40**, 1–12.

**118** Liang, X.J., Chen, C., Zhao, Y., and Wang, P.C. (2010) Circumventing tumor resistance to chemotherapy by nanotechnology. *Methods Mol. Biol.*, **596**, 467–488.

**119** Andersson, D.I. and Hughes, D. (2014) Microbiological effects of sublethal levels of antibiotics. *Nat. Rev. Microbiol.*, **12**, 465–478.

**120** Park, H. and Park, K. (1996) Biocompatibility issues of implantable drug delivery systems. *Pharm. Res.*, **13**, 1770–1776.

**121** Danckwerts, M. and Fassihi, A. (1991) Implantable controlled release drug delivery systems: a review. *Drug Dev. Ind. Pharm.*, **17**, 1465–1502.

**122** Staples, M., Daniel, K., Cima, M.J., and Langer, R. (2006) Application of micro- and nano-electromechanical devices to drug delivery. *Pharm. Res.*, **23**, 847–863.

**123** Sih, J., Bansal, S.S., Filippini, S., Ferrati, S., Raghuwansi, K., Zabre, E., Nicolov, E., Fine, D., Ferrari, M., Palapattu, G. *et al.* (2013) Characterization of nanochannel delivery membrane systems for the sustained release of resveratrol and atorvastatin: new perspectives on promoting heart health. *Anal. Bioanal. Chem.*, **405**, 1547–1557.

**124** Ferrati, S., Nicolov, E., Bansal, S., Hosali, S., Landis, M., and Grattoni, A. (2015) Docetaxel/2-hydroxypropyl beta-cyclodextrin inclusion complex increases docetaxel solubility and release from a nanochannel drug delivery system. *Curr. Drug Targets*, **16**, 1645–1649.

**125** Celia, C., Ferrati, S., Bansal, S., van de Ven, A.L., Ruozi, B., Zabre, E., Hosali, S., Paolino, D., Sarpietro, M.G., Fine, D. *et al.* (2014) Sustained zero-order release of intact ultra-stable drug-loaded liposomes from an implantable nanochannel delivery system. *Adv. Healthc Mater*, **3**, 230–238.

**126** Bruno, G., Geninatti, T., Hood, R.L., Fine, D., Scorrano, G., Schmulen, J., Hosali, S., Ferrari, M., and Grattoni, A. (2015) Leveraging electrokinetics for the active control of dendritic fullerene-1 release across a nanochannel membrane. *Nanoscale*, **7**, 5240–5248.

**127** Jain, K.K. (2003) Nanodiagnostics: application of nanotechnology in molecular diagnostics. *Expert Rev. Mol. Diagn.*, **3**, 153–161.

**128** Buxton, D.B., Lee, S.C., Wickline, S.A., Ferrari, M., and NationalHeart, Lung, and Blood Institute Nanotechnology Working, Group (2003) Recommendations of the national heart, lung, and blood institute nanotechnology working group. *Circulation*, **108**, 2737–2742.

**129** Saleh, O.A. and Sohn, L.L. (2001) Quantitative sensing of nanoscale colloids using a microchip Coulter counter. *Rev. Sci. Instrum.*, **72**, 4449–4451.

**130** Karnik, R., Castelino, K., Fan, R., Yang, P., and Majumdar, A. (2005) Effects of biological reactions and modifications on conductance of nanofluidic channels. *Nano Lett.*, **5**, 1638–1642.

131 Zhou, K., Kovarik, M.L., and Jacobson, S.C. (2008) Surface-charge induced ion depletion and sample stacking near single nanopores in microfluidic devices. *J. Am. Chem. Soc.*, **130**, 8614–8616.

132 Wu, H.J., Li, Y., Fan, J., Deng, Z., Hu, Z., Liu, X., Graviss, E.A., Ferrari, M., Ma, X., and Hu, Y. (2014) Antibody-free detection of Mycobacterium tuberculosis antigen using customized nanotraps. *Anal. Chem.*, **86**, 1988–1996.

133 Fan, J., Niu, S., Dong, A., Shi, J., Wu, H.J., Fine, D.H., Tian, Y., Zhou, C., Liu, X., Sun, T. *et al.* (2014) Nanopore film based enrichment and quantification of low abundance hepcidin from human bodily fluids. *Nanomedicine*, **10**, 879–888.

134 Song, Y., Zhang, Y., Bernard, P.E., Reuben, J.M., Ueno, N.T., Arlinghaus, R.B., Zu, Y., and Qin, L. (2012) Multiplexed volumetric bar-chart chip for point-of-care diagnostics. *Nat. Commun.*, **3**, 1283.

135 Song, Y., Wang, Y., and Qin, L. (2013) A multistage volumetric bar chart chip for visualized quantification of DNA. *J. Am. Chem. Soc.*, **135**, 16785–16788.

136 Wu, X., Liu, H., Liu, J., Haley, K.N., Treadway, J.A., Larson, J.P., Ge, N., Peale, F., and Bruchez, M.P. (2003) Immunofluorescent labeling of cancer marker Her2 and other cellular targets with semiconductor quantum dots. *Nat. Biotechnol.*, **21**, 41–46.

137 Michalet, X., Pinaud, F.F., Bentolila, L.A., Tsay, J.M., Doose, S., Li, J.J., Sundaresan, G., Wu, A.M., Gambhir, S.S., and Weiss, S. (2005) Quantum dots for live cells, *in vivo* imaging, and diagnostics. *Supramol. Sci.*, **307**, 538–544.

138 West, J.L. and Halas, N.J. (2003) Engineered nanomaterials for biophotonics applications: improving sensing, imaging, and therapeutics. *Annu. Rev. Biomed. Eng.*, **5**, 285–292.

139 Nam, J.M., Thaxton, C.S., and Mirkin, C.A. (2003) Nanoparticle-based bio-bar codes for the ultrasensitive detection of proteins. *Supramol. Sci.*, **301**, 1884–1886.

140 Fradinger, E.A. and Bitan, G. (2005) En route to early diagnosis of Alzheimer's disease--are we there yet? *Trends Biotechnol.*, **23**, 531–533.

141 Mason, C. and Dunnill, P. (2008) A brief definition of regenerative medicine. *Regen. Med.*, **3**, 1–5.

142 Zhang, L. and Webster, T.J. (2008) Nanotechnology and nanomaterials: promises for improved tissue regeneration. *Nano Today*, **1**, 66–80.

143 Qin, Z., Gautieri, A., Nair, A.K., Inbar, H., and Buehler, M.J. (2012) Thickness of hydroxyapatite nanocrystal controls mechanical properties of the collagen-hydroxyapatite interface. *Langmuir*, **28**, 1982–1992.

144 Navarro, M., Michiardi, A., Castano, O., and Planell, J.A. (2008) Biomaterials in orthopaedics. *J. R. Soc. Interface*, **5**, 1137–1158.

145 Giannoudis, P.V., Dinopoulos, H., and Tsiridis, E. (2005) Bone substitutes: an update. *Injury*, **36** Suppl (3), S20–S27.

146 Cardoso, A.M., Horn, M.B., Ferret, L.S., Azevedo, C.M., and Pires, M. (2015) Integrated synthesis of zeolites 4A and Na-P1 using coal fly ash for application in the formulation of detergents and swine wastewater treatment. *J. Hazard. Mater.*, **287**, 69–77.

147 Appleford, M.R., Oh, S., Oh, N., and Ong, J.L. (2009) In vivo study on hydroxyapatite scaffolds with trabecular architecture for bone repair. *J. Biomed. Mater Res. A*, **89**, 1019–1027.

148 Yamada, M., Ueno, T., Tsukimura, N., Ikeda, T., Nakagawa, K., Hori, N., Suzuki, T., and Ogawa, T. (2012) Bone integration capability of nanopolymorphic crystalline hydroxyapatite coated on titanium implants. *Int. J. Nanomedicine*, **7**, 859–873.

149 Wennerberg, A., Jimbo, R., Allard, S., Skarnemark, G., and Andersson, M. (2011) *In vivo* stability of hydroxyapatite nanoparticles coated on titanium implant surfaces. *Int. J. Oral Maxillofac. Implants*, **26**, 1161–1166.

150 Azami, M., Tavakol, S., Samadikuchaksaraei, A., Hashjin, M.S., Baheiraei, N., Kamali, M., and Nourani, M.R. (2012) A porous hydroxyapatite/gelatin nanocomposite scaffold for bone tissue repair: *in vitro* and *in vivo* evaluation. *J. Biomater. Sci. Polym. Ed.*, **23**, 2353–2368.

151 Lobo, A.O., Siqueira, I.A., das Neves, M.F., Marciano, F.R., Corat, E.J., and Corat, M.A. (2013) *In vitro* and *in vivo* studies of a novel nanohydroxyapatite/superhydrophilic vertically aligned carbon nanotube nanocomposites. *J. Mater. Sci. Mater. Med.*, **24**, 1723–1732.

152 Yao, C., Slamovich, E.B., and Webster, T.J. (2008) Enhanced osteoblast functions on anodized titanium with nanotube-like structures. *J. Biomed. Mater Res. A*, **85**, 157–166.

153 Wang, J., Valmikinathan, C.M., Liu, W., Laurencin, C.T., and Yu, X. (2010) Spiral-structured, nanofibrous, 3D scaffolds for bone tissue engineering. *J. Biomed. Mater Res. A*, **93**, 753–762.

154 Kim, K., Luu, Y.K., Chang, C., Fang, D., Hsiao, B.S., Chu, B., and Hadjiargyrou, M. (2004) Incorporation and controlled release of a hydrophilic antibiotic using poly(lactide-co-glycolide)-based electrospun nanofibrous scaffolds. *J. Control. Release*, **98**, 47–56.

155 Li, C., Vepari, C., Jin, H.J., Kim, H.J., and Kaplan, D.L. (2006) Electrospun silk-BMP-2 scaffolds for bone tissue engineering. *Biomaterials*, **27**, 3115–3124.

156 Tripathi, A., Saravanan, S., Pattnaik, S., Moorthi, A., Partridge, N.C., and Selvamurugan, N. (2012) Bio-composite scaffolds containing chitosan/nano-hydroxyapatite/nano-copper-zinc for bone tissue engineering. *Int. J. Biol. Macromol.*, **50**, 294–299.

157 Pittenger, M.F., Mackay, A.M., Beck, S.C., Jaiswal, R.K., Douglas, R., Mosca, J.D., Moorman, M.A., Simonetti, D.W., Craig, S., and Marshak, D.R. (1999) Multilineage potential of adult human mesenchymal stem cells. *Supramol. Sci.*, **284**, 143–147.

158 Hu, J., Feng, K., Liu, X., and Ma, P.X. (2009) Chondrogenic and osteogenic differentiations of human bone marrow-derived mesenchymal stem cells on a nanofibrous scaffold with designed pore network. *Biomaterials*, **30**, 5061–5067.

159 Spadaccio, C., Rainer, A., Trombetta, M., Vadala, G., Chello, M., Covino, E., Denaro, V., Toyoda, Y., and Genovese, J.A. (2009) Poly-L-lactic acid/hydroxyapatite electrospun nanocomposites induce chondrogenic differentiation of human MSC. *Ann. Biomed. Eng.*, **37**, 1376–1389.

160 Bhardwaj, N. and Kundu, S.C. (2012) Chondrogenic differentiation of rat MSCs on porous scaffolds of silk fibroin/chitosan blends. *Biomaterials*, **33**, 2848–2857.

161 Namgung, S., Baik, K.Y., Park, J., and Hong, S. (2011) Controlling the growth and differentiation of human mesenchymal stem cells by the arrangement of individual carbon nanotubes. *ACS Nano*, **5**, 7383–7390.

162 Menke, N.B., Ward, K.R., Witten, T.M., Bonchev, D.G., and Diegelmann, R.F. (2007) Impaired wound healing. *Clin. Dermatol.*, **25**, 19–25.

163 Swaim, S.F. (1990) Skin grafts. *Vet. Clin. North Am. Small Anim. Pract.*, **20**, 147–175.

164 MacNeil, S. (2007) Progress and opportunities for tissue-engineered skin. *Nature*, **445**, 874–880.

165 Supp, D.M. and Boyce, S.T. (2005) Engineered skin substitutes: practices and potentials. *Clin. Dermatol.*, **23**, 403–412.

166 Boyce, S.T. and Warden, G.D. (2002) Principles and practices for treatment of cutaneous wounds with cultured skin substitutes. *Am. J. Surg.*, **183**, 445–456.

167 Metcalfe, A.D. and Ferguson, M.W. (2007) Tissue engineering of replacement skin: the crossroads of biomaterials, wound healing, embryonic development, stem cells and regeneration. *J. R. Soc. Interface*, **4**, 413–437.

168 Shores, J.T., Gabriel, A., and Gupta, S. (2007) Skin substitutes and alternatives: a review. *Adv. Skin Wound Care*, **20**, 493–508 quiz 509-410.

169 Chandrasekaran, A.R., Venugopal, J., Sundarrajan, S., and Ramakrishna, S. (2011) Fabrication of a nanofibrous scaffold with improved bioactivity for culture of human dermal fibroblasts for skin regeneration. *Biomed. Mater*, **6**, 015001.

170 Sun, L., Li, D., Hemraz, U.D., Fenniri, H., and Webster, T.J. (2014) Self-assembled rosette nanotubes and poly(2-hydroxyethyl methacrylate) hydrogels

promote skin cell functions. *J. Biomed. Mater Res. A*, **102**, 3446–3451.

171 Sudheesh Kumar, P.T., Raj, N.M., Praveen, G., Chennazhi, K.P., Nair, S.V., and Jayakumar, R. (2013) In vitro and in vivo evaluation of microporous chitosan hydrogel/nanofibrin composite bandage for skin tissue regeneration. *Tissue Eng. Part A*, **19**, 380–392.

172 Jaiswal, M., Gupta, A., Agrawal, A.K., Jassal, M., Dinda, A.K., and Koul, V. (2013) Bi-layer composite dressing of gelatin nanofibrous mat and poly vinyl alcohol hydrogel for drug delivery and wound healing application: *in vitro* and *in vivo* studies. *J. Biomed. Nanotechnol.*, **9**, 1495–1508.

173 Jin, G., Prabhakaran, M.P., Kai, D., and Ramakrishna, S. (2013) Controlled release of multiple epidermal induction factors through core–shell nanofibers for skin regeneration. *Eur. J. Pharm. Biopharm.*, **85**, 689–698.

174 Norkus, T., Norkus, M., and Ramanauskas, T. (2005) Donor, recipient and nerve grafts in brachial plexus reconstruction: anatomical and technical features for facilitating the exposure. *Surg. Radiol. Anat.*, **27**, 524–530.

175 Ray, W.Z. and Mackinnon, S.E. (2010) Management of nerve gaps: autografts, allografts, nerve transfers, and end-to-side neurorrhaphy. *Exp. Neurol.*, **223**, 77–85.

176 Huang, Y.C. and Huang, Y.Y. (2006) Biomaterials and strategies for nerve regeneration. *Artif. Organs*, **30**, 514–522.

177 Subramanian, A., Krishnan, U.M., and Sethuraman, S. (2009) Development of biomaterial scaffold for nerve tissue engineering: Biomaterial mediated neural regeneration. *J. Biomed. Sci.*, **16**, 108.

178 Furth, M.E., Atala, A., and Van Dyke, M.E. (2007) Smart biomaterials design for tissue engineering and regenerative medicine. *Biomaterials*, **28**, 5068–5073.

179 Fan, L., Feng, C., Zhao, W., Qian, L., Wang, Y., and Li, Y. (2012) Directional neurite outgrowth on superaligned carbon nanotube yarn patterned substrate. *Nano Lett.*, **12**, 3668–3673.

180 Hu, H., Ni, Y., Montana, V., Haddon, R.C., and Parpura, V. (2004) Chemically functionalized carbon nanotubes as substrates for neuronal growth. *Nano Lett.*, **4**, 507–511.

181 Gheith, M.K., Sinani, V.A., Wicksted, J.P., Matts, R.L., and Kotov, N.A. (2005) Single-walled carbon nanotube polyelectrolyte multilayers and freestanding films as biocompatible platform for neuroprosthetic implants. *Adv. Mater.*, **22**, 2663–2670.

182 Lovat, V., Pantarotto, D., Lagostena, L., Cacciari, B., Grandolfo, M., Righi, M., Spalluto, G., Prato, M., and Ballerini, L. (2005) Carbon nanotube substrates boost neuronal electrical signaling. *Nano Lett.*, **5**, 1107–1110.

183 Nguyen-Vu, T.D., Chen, H., Cassell, A.M., Andrews, R.J., Meyyappan, M., and Li, J. (2007) Vertically aligned carbon nanofiber architecture as a multifunctional 3-D neural electrical interface. *IEEE Trans. Biomed. Eng.*, **54**, 1121–1128.

184 Nguyen-Vu, T.D., Chen, H., Cassell, A.M., Andrews, R., Meyyappan, M., and Li, J. (2006) Vertically aligned carbon nanofiber arrays: an advance toward electrical-neural interfaces. *Small*, **2**, 89–94.

185 Lee, J.E., Khang, D., Kim, Y.E., and Webster, T.J. (2006) Stem cell impregnated carbon nanofibers/nanotubes for healing damaged neural tissue. *Mater Res. Soc. Symp.Proc.*, **915**, 17–22.

186 Koh, H.S., Yong, T., Teo, W.E., Chan, C.K., Puhaindran, M.E., Tan, T.C., Lim, A., Lim, B.H., and Ramakrishna, S. (2010) In vivo study of novel nanofibrous intraluminal guidance channels to promote nerve regeneration. *J. Neural Eng.*, **7**, 046003.

187 Gelain, F., Panseri, S., Antonini, S., Cunha, C., Donega, M., Lowery, J., Taraballi, F., Cerri, G., Montagna, M., Baldissera, F. *et al.* (2011) Transplantation of nanostructured composite scaffolds results in the regeneration of chronically injured spinal cords. *ACS Nano*, **5**, 227–236.

188 Xu, T., Gregory, C.A., Molnar, P., Cui, X., Jalota, S., Bhaduri, S.B., and Boland, T. (2006) Viability and electrophysiology of

neural cell structures generated by the inkjet printing method. *Biomaterials*, **27**, 3580–3588.

**189** Etheridge, M.L., Campbell, S.A., Erdman, A.G., Haynes, C.L., Wolf, S.M., and McCullough, J. (2013) The big picture on nanomedicine: the state of investigational and approved nanomedicine products. *Nanomedicine*, **9**, 1–14.

**190** Chang, H.I. and Yeh, M.K. (2012) Clinical development of liposome-based drugs: formulation, characterization, and therapeutic efficacy. *Int. J. Nanomed.*, **7**, 49–60.

**191** Silverman, J.A. and Deitcher, S.R. (2013) Marqibo(R) (vincristine sulfate liposome injection) improves the pharmacokinetics and pharmacodynamics of vincristine. *Cancer Chemother. Pharmacol.*, **71**, 555–564.

**192** Kompella, U.B., Kadam, R.S., and Lee, V.H. (2010) Recent advances in ophthalmic drug delivery. *Ther. Deliv.*, **1**, 435–456.

**193** Ventola, C.L. (2012) The nanomedicine revolution: part 2: current and future clinical applications. *P T*, **37**, 582–591.

**194** Seigneuric, R., Markey, L., Nuyten, D.S., Dubernet, C., Evelo, C.T., Finot, E., and Garrido, C. (2010) From nanotechnology to nanomedicine: applications to cancer research. *Curr. Mol. Med.*, **10**, 640–652.

# Part Two
# Leading Cause of Death: Cardiovascular Diseases

# 4
# Challenges in Cardiovascular Treatments Using Nanotechnology-Based Approaches

*Till Saxer*[1] *and Margaret N. Holme*[2]

[1]*Cardiology, University Hospitals of Geneva, Rue Gabrielle Perret-Gentil 4, Geneva, Switzerland*
[2]*Department of Materials, Imperial College London, London, UK*

## 4.1
## Introduction

At the first glance, the cardiovascular system can be considered as a simple pump-and-pipe system in charge of delivering enough energy and oxygen to the organs. However, its dysfunction is the biggest cause of death and morbidity in the world. Cardiovascular diseases (CVDs) are numerous and complex and include coronary heart disease (leading to heart attack), stroke, peripheral arterial disease, aortic disease, and congenital heart disease. They lead to reduced blood flow to the heart, brain, and organs by either thrombosis, that is, blood clot, or atherosclerosis. Medical emergencies arise when there is an acute shortage of blood flow, termed ischemia, to for example the heart in the case of heart attack or brain in the case of stroke. Failure to treat such conditions immediately leads to oxygen starvation, that is, hypoxia. In between a quarter and half of patients, this leads to death, and survivors are often left with irreversible damage to the affected organ with lifelong implications for the patient's quality of life.

Cardiology has made huge progress in the domain of minimally invasive procedures, rhythmology devices, and pharmaceutical treatments. Nevertheless, cardiovascular diseases remain the main cause of burden of disease and mortality in the world, and even with state-of-the-art treatment patient prognosis can be bleak. This chapter presents present and future nanotechnology approaches for the treatment of CVD such as atherosclerosis and heart attack (*cf.* Figure 4.1), responsible for about half of all CVD-related deaths.

*Nanoscience and Nanotechnology for Human Health,* First Edition. Edited by Bert Müller and Marcel Van de Voorde.

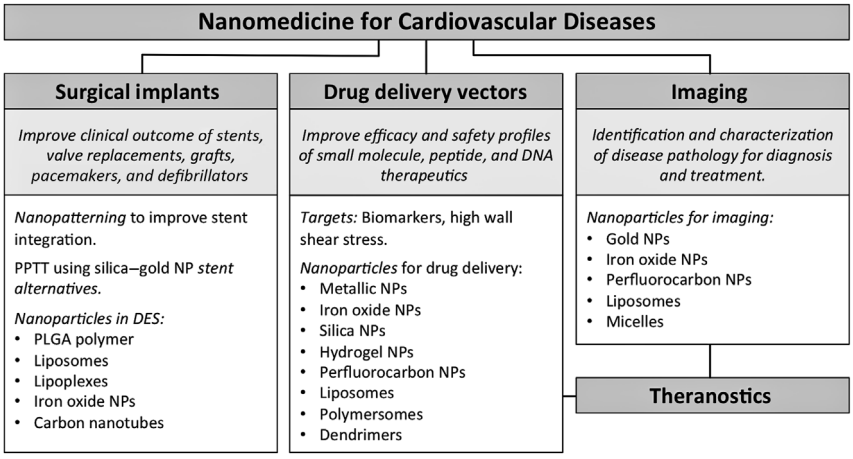


**Figure 4.1** Nanomedicine for cardiovascular diseases. Drug delivery vectors and surgical implants discussed in this publication, and examples of nanoparticles used in imaging.

## 4.2 Unmet Needs in Cardiology

One main drawback in the treatment of CVD with pharmacologically active compounds is that such treatments are often nonspecific. Medication that acts on the heart muscle, arteries, coagulation properties, or platelet function is sometimes specific to the organ but not disease specific. This limits optimal dosage administration to achieve the desired action because of dose-dependent side effects presenting a great therapeutic challenge that targeted drug delivery systems can help to overcome. For example, atherosclerosis, the narrowing of the vessels by a build-up of fatty lesions that become calcified plaques over time, is a general inflammatory disease. The thickening of a plaque is influenced by human metabolism and fundamental hydrodynamics, such as the local blood hemodynamics. Targeting general inflammation in this case does not lead to specific delivery of a drug. However, changes in the local hemodynamics can trigger localized release of pharmacological active units from engineered stimuli-responsive nanoparticles at sites of stenosis [1]. This approach calls for an interesting combination of different scientific disciplines leading to innovative medical solutions.

Small surgical procedures are routinely used to treat atherosclerosis. For example, blocked vessels are reopened using a balloon inserted by means of a catheter, followed by stent implantation to hold the vessel open. Although universally accepted and established in the operating theater, these treatments still require optimization to reduce procedure- or device-related complications. For example, in addition to simply covering stents with polymers containing active substances to deliver drugs locally, a better understanding of the influence of

stent geometry on the treated vessel's blood flow merits particular attention. This is particularly important since device-related endothelial wall stress can cause further damage to the treated vessel after surgery. Mechanical stress is a trigger for inflammation inside the vessel wall's intima, and responsible for restenosis around the stent by atherosclerosis formation. Recognition by the blood coagulation system of the stent as a foreign body risks an early in-stent stenosis by blood clot formation. An appropriate physiological structure of the stent material could limit both risks. This could be achieved by using nanoparticles capable of delivering small-molecule drugs, genes, or proteins in a spatiotemporal manner combined with appropriate nanotopographical structures on a biocompatible stent material.

### 4.2.1
### Nanomaterials for Medical Applications

Nanomaterials are typically defined as materials comprising particles or patterns with at least one dimension in the 0.1–100 nm size regime. Vesicles such as liposomes and polymersomes are the slight exception to this rule, since although they are considered as nanocarriers, that is, nanoparticles that can be used to transport an active agent, they are often larger than 100 nm. In the case of anisotropic particles such as carbon nanotubes, micrometer-scale characteristics may also be simultaneously present. In addition to nanoparticles, nanoscale-ordered topography is of particular importance in tissue regeneration on, for example, implanted stents, since it has a huge influence on cell behavior [2].

The diseased heart is an area of high physical stress. Treatment of CVD often involves administering vasodilators, statins, and thrombolytic drugs directly into the blood stream, but it is riddled with systemic toxicity problems. Effective diagnostics, targeting drugs at areas of disease, and ensuring implanted foreign objects such as stents do not move or cause an immunoresponse over time are areas of intense research [3–21]. Nanotechnology-based approaches offer a route into providing stable formulations to deliver such therapeutic agents and bypass their detrimental systemic side effects. Improving the safety and/or efficacy by passive or active targeted delivery, and improving solubility of drug candidates are two of the main goals of nanoparticle drug delivery systems. In addition to intravenous delivery, nanoparticle coatings and nanopatterning of implants such as stents and grafts can be hugely beneficial, for example, aiding appropriate tissue regeneration and alleviating side effects such as restenosis [13,22–24].

### 4.2.2
### Nanotechnology Applied to Medicine: A New Medical Discipline for Cardiology?

Nanomedicine, the application of nanotechnology for medical needs, is a highly interdisciplinary field combining biology, chemistry, physics, and medicine.

It requires a new understanding of the human body, because no traditional medical discipline has sufficiently studied the behavior of the body on the nanometer scale before. One example is anatomy. If we consider developing a treatment for a coronary artery, we must first understand its anatomy and physiology. For nanomedical approaches, this requires specialized technology to access this information and precisely observe and characterize physiology and physiopathology on the nanoscale. Many of these tools and competencies are common to the lab and animal research.

In the chapter, we discuss a cardio-specific subspecialty for nanomedicine, that is, nanocardiology.

### 4.2.3 Nano Approaches for Therapeutic Problems

*Primum non nocere*: Cardiology deals with life and death. The cardiovascular system's main task is to provide sufficient hemodynamic conditions to provide organs with enough energy and oxygen. When it fails, the human body has a huge range of protective mechanisms to maintain the required vital minimum and to compensate for the perfusion deficit of all or a part of an organ. Intervening in this complex system to help the patient reestablish normal hemodynamic conditions can become responsible for further deterioration of the protective mechanisms. In medicine, the first rule is not to harm the patient.

The second rule in medicine is to help the patient. It sounds trivial but is a balance in daily medical *business* and a mainstay of decision-making algorithms. This balance of not harming but helping is of particular importance in disease unspecific medication or nontargeted drug delivery procedures. One visible example relates to some chemotherapeutics in oncology, where a lot of progress has been made thanks to immunotherapy and nanoparticle drug delivery systems [25].

For nanocardiology drug delivery systems, one response lies in delivering an active drug selectively to the diseased organ, decreasing side effects at higher doses and increasing therapeutic effects at lower doses (see Figure 4.2). The ideal drug delivery system delivers the optimal treatment concentration at the desired site exclusively and without any side effects. Technologies using physical instead of the commonly employed biochemical stimuli could preferentially dispense an active drug to a stenosed artery in a high shear stress environment, either with a shear stress-activated mechnosensitive liposome carrier [1] or with a shear-activated nanotherapeutic aggregate [26].

In the field of invasive cardiology procedures, nanocardiology can help to better classify high-risk atherosclerotic lesions [27] to present a more differentiated risk–benefit analysis. Furthermore, anionic nanoparticles (NPs) could lower the cellular uptake of highly oxidized low-density lipoprotein molecules [28]. These approaches may lead to an improved detection of unstable plaque or vessels, where physiological structures are broken down by atherosclerosis.

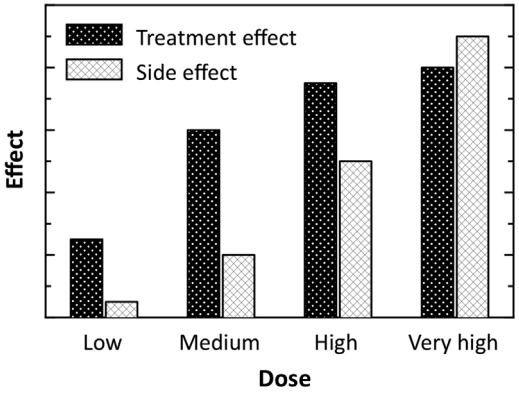


**Figure 4.2** The balance between desired action and side effects to be respected.

### 4.2.4
### Awareness of Risks Introducing Nanotechnology to Patient Treatment

The nanotechnologies presented here have the potential to be translated into the clinic for the treatment of CVD. However, relatively few nanotechnology approaches have been approved for use in man. The physical and chemical properties of bulk materials cannot be translated to the nanometer scale, as the surface/volume ratio becomes significantly large and suface properties dominate in this size regime. Surface chemistry, often negligible in bulk material, has a large effect on nanoparticle properties. For example, platinum is an inert metal on the macroscale but a highly active catalyst on the nanoscale. Little is know about the long-term risks of implementing nanoscale material**s** in the human being. Therefore, it is most important to thoroughly characterize the safety profiles for such technologies before they are brought to animals or humans [29,30]. Nursing [31] and medical ethical considerations [32] are beginning to be shared in the medical community. As the field of nanotoxicology emerges, safety profiles will become better understood and new legislation will be required to ensure the appropriate use of these powerful tools to the benefit of the patient.

### 4.2.5
### Decisional Analysis in Nanomedicine Development

An increased need for therapeutics that fight a disease more effectively or decrease side effects are two main drivers for optimizing existing treatment and innovating new technologies to improve the length and quality of patients' lives.

Nanotechnology applied in human beings requires a complete understanding of medical basic disciplines to get a measurable clinical effect, see Figure 4.3. Therefore, research projects are often labeled as high risk. This is a financial issue. On the medical side, nanotechnology has huge potential. Examples include rendering an already clinically approved material more biologically compatible,

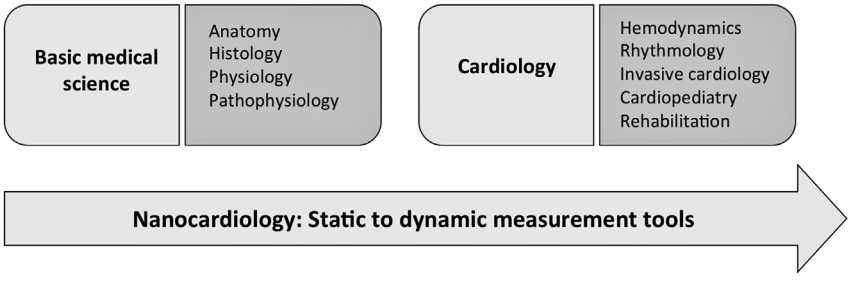


**Figure 4.3** Comprehensive approach for nanoengineering in cardiology.

engineering intelligent material, or targeting the delivery of active drugs at the disease. Ethical considerations are essential in both basic and clinical research, and of course when treatments are delivered to the patients.

## 4.3 Nanoparticles for Treatment of CVD

Nowadays, the use of nanoparticles for therapeutics is a large, diverse, and busy field. Particle sizes range from a couple of nanometers, for example gold nanoparticles and dendrimers, to over a hundred nanometers, for example liposomes and polymersomes. Particle composition might include metals such as gold or platinum and inorganic compounds such as iron oxide or silica [33,34] or self-assembly of organic molecules such as phospholipids [35], polymers [36,37], and dendrimers [38]. Shapes can vary wildly, with, for example, gold nanoparticles of spherical, star, rod, and shell and cage morphologies all commonly reported and well established [39]. Particles can be solid or contain oil or aqueous compartments. The release of encapsulated therapeutic agents from nanocarriers may be by passive or active targeting, which could include triggers from biological cues or external stimuli. Surface functionalization is used not only to tether active molecules to the surface of such particles but also to improve properties such as *in vivo* stability, which is vital to ensure, for example, low toxicity, and desirable solubility, aggregation, circulation, and clearance profiles. Many of the nanoparticles described here have also shown great promise in imaging CVD, although this is outside the scope of this chapter [4,8,9,12,15,40,41]. *Theranostic* formulations include a therapeutic and diagnostic moiety in a single nanoparticle-containing platform and can, therefore, track and treat disease simultaneously [42]. The field of theranostic nanoparticles is a young but promising technique for tackling CVD.

### 4.3.1 Delivery of Nitric Oxide Small-Molecule Donors

The vasodilator nitric oxide (NO) is frequently administered to reduce hypertension and to open a stenosed vessel that is causing heart pain, a dominant

symptom in atherosclerosis and heart attack. Due to its relative instability and short *in vivo* half-life, it is usually administered via NO precursor drugs such as nitroglycerin and nitroprusside. However, the *in vivo* half-life of the NO free radical is very short and drugs must be administrated repetitively or by a pump for continuous intravenous delivery. Then, NO acts on the whole arterial tree, limiting its local action on the stenosis, and often causes hypotension, further limiting blood perfusion distal to the stenosis. Encapsulating small-molecule NO donors in nanoparticles presents a solution to this problem. Liposomes are ideal candidates for such systems. Consisting of one or several phospholipid bilayers with an aqueous core, liposomes range in size from tens to thousands of nanometers. Sutton *et al.* showed that ultrasound-mediated release of a mixture of NO and perfluorocarbon gas from cationic liposomes causes NO deposition into vascular tissue [43]. This triggered potent vasorelaxation in an *ex vivo* pig model. The technique could also be used to deliver other vasodilators. Furthermore, liposomal formulations of the NO donor isosorbide mononitrate were found to have antimicrobial properties *in vitro* [44], suggesting that NO donor liposomes might also be useful in preventing bacterial infections in implanted stents.

Another potentially useful NO delivery method involves long-circulating chitosan-based hydrogel nanoparticles with incorporated NO donors. In an aqueous environment, these nanoparticles swell, releasing trapped NO over an extended period of several hours in hamster models. The rate of release is dependent on the swelling properties of the hydrogel and decomposition rate of the NO donor *in vivo* [45].

### 4.3.2 PLGA-based Nanoparticles for Gene Delivery

Poly(lactic-*co*-glycolic acid) (PLGA) is a copolymer that is FDA-approved for, among other things, drug delivery and diagnostics in a range of diseases [37]. Various formulation techniques give access to PLGA nanoparticles of different size, morphology, and Zeta-potential and allow for incorporation of both hydrophobic and hydrophilic drugs [36], which make them highly desirable for delivery of proteins, DNA, and RNA. Their *in vivo* biodegradability is thanks to ester hydrolysis in the presence of water and degradation rates can be tuned by tuning the polymer composition. Several examples of protein and peptide delivery exist in the literature [46–48]. For example, the mutant protein 1K1 has been shown to have strong angiogenic activity. When formulated into 60–140 nm nanoparticles with the copolymer PLGA, it was possible to alter downstream signaling through the mitogen-activated protein kinase pathway, leading to enhanced neovascularization [46].

The anti-inflammatory peptide Ac2-26 has been shown to be protective in reperfusion injury, when blood flow is reestablished after ischemia caused by heart attack [47]. Nanoparticles formulated from Ac2-26 and PLGA–PEG block copolymers and with collagen IV targeting peptide were significantly better at reducing the concentration of white blood cells (polymorphonuclear neutrophils) in extracted serum. Addition of a fluorescently labeled polymer allowed

the particles to be tracked in explanted specimens, showing preferential localization in injured tissue.

Injection of PLGA nanoparticles loaded with insulin-like growth factor has been shown to provide cardioprotection after heart attack [48]. With one injection only, prevention of cardiomyocyte apoptosis, reduction in the size of infarction, and increase in left ventricle ejection fraction was observed in mice. Particle size was also found to be a factor, with smaller particles of 60 nm proving more effective than 200 and 1000 nm sizes.

### 4.3.3 Perfluorocarbon Nanoparticles

Perfluorocarbon nanoparticles are lipid-encapsulated nanoemulsions with perfluorinated chemicals in their core [27]. They show promising theranostic properties and great potential for characterizing high-risk atherosclerotic plaques. For example, perfluorocarbon nanoparticles are in use for imaging of fibrin in unstable atherosclerotic plaques. Combined with an antifibrin antibody, high magnetic resonance contrast is achieved, which allows for the detection of unstable plaques with higher fibrin content. Ruptured plaques can be identified with the paramagnetic chemical exchange saturation transfer chelate technique for magnetic resonance imaging [3]. In another example, fibrin-coated perfluorocarbon nanoparticles have been shown *in vitro* to provide specific and rapid fibrinolysis and can be used for acoustic and MRI imaging, and are therefore proposed as a potential therapy for stroke reperfusion [49].

### 4.3.4 Targeting Vessel Geometry: a Physics-based Approach

Wall shear stresses (WSS) increase with the degree of stenosis, regardless of pathophysiology. Therefore, elevated WSS is potentially a more universal and region-selective target than biochemical markers. While biomarkers exist that can target specific organs, it is less trivial to *selectively* target specific disease pathologies with the speed required to treat medical emergencies such as heart attack or stroke. For example, creatinine kinase and troponin are known to be highly sensitive biomarkers for early myocardial infarction detection. But even these routinely used gold standard biomarkers can be elevated in conditions other than myocardial ischemia. As components of normal myocardial function, they are not useful for a targeted drug delivery process. Furthermore, possible inflammatory factor drug targets expressed on diseased artery surfaces, such as vascular cell adhesion molecule (VCAM-1) or intercellular adhesion molecule (ICAM-1), are not disease-specific. Fundamental changes to the morphology of stenotic or thrombosed vessels are a prevalent feature of cardiovascular diseases and can lead to significant effects on physical conditions, such as flow dynamics and wall shear stress. Nanoparticles capable of responding to physical changes present an exciting class of stimulus-responsive treatments for diseases such as atherosclerosis.

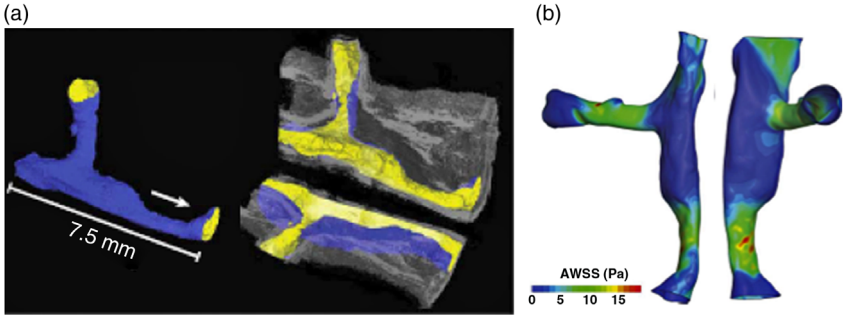


**Figure 4.4** WSS of a critically constricted human coronary artery (a), calculated average WSS (b). (Reproduced with permission from Ref. [51].)

WSS can be described as the tangential drag force caused by blood flowing along a vessel wall. It is directly proportional to blood velocity and inversely proportional to vessel diameter. Therefore, in the case of heart attack, where blood velocity is high and plaque rupture leads to a significantly decreased arterial diameter, WSS in the coronary arteries increase by at least an order of magnitude with respect to the healthy situation [50,51]. Typical WSS in healthy vessels are well understood thanks to computer simulations typically based on clinical observations and reconstructed 3D images acquired *in vivo* [52]. Recently, X-ray tomography, which allows access to reconstructed 3D images of explanted vessels with micrometer resolution, has also begun to afford suitable data sets for simulation of typical WSS in critically constricted coronary arteries, see Figure 4.4 [51].

In a first proof of concept of this technique, WSS-sensitive liposomes using the artificial phospholipid 1,3-dipalmitamidopropan-2-yl (2-(trimethylammonio)ethyl) phosphate (Pad-PC-Pad) were formulated [53] (see Figure 4.5 for chemical structure), which form lenticular vesicles with point dislocations. Such formulations can be loaded with a hydrophilic substance, are stable on the bench for weeks, and preferentially release their cargo in regions of high WSS, as seen in critically constricted arteries such as those found in pronounced atherosclerosis or heart attack [1]. The unique properties of these nanocarriers are due to the unusual chemical structure of the Pad-PC-Pad constituent phospholipids [54]. This effect has not been reported with naturally occurring phospholipids and is a powerful example of how nanoengineered materials can answer an unmet medical need.

Another recently published approach uses shear-active nanotherapeutics to deliver tissue plasminogen activator (tPA), an FDA-approved thrombolytic drug [26]. Nanoparticles of the polymer PLGA were coated with tPA and formed into micrometer-sized aggregates that dissociated into individual nanoparticles at high WSS. The tPA was effectively delivered to fibrin clots in *in vivo* studies.

These two examples use WSS in different ways, releasing an entrapped cargo or increasing the surface area and, therefore, the availability of conjugated drug. Importantly, both techniques offer not only active targeting toward the site of interest but also a *triggerable* exposure of the drug at the site.

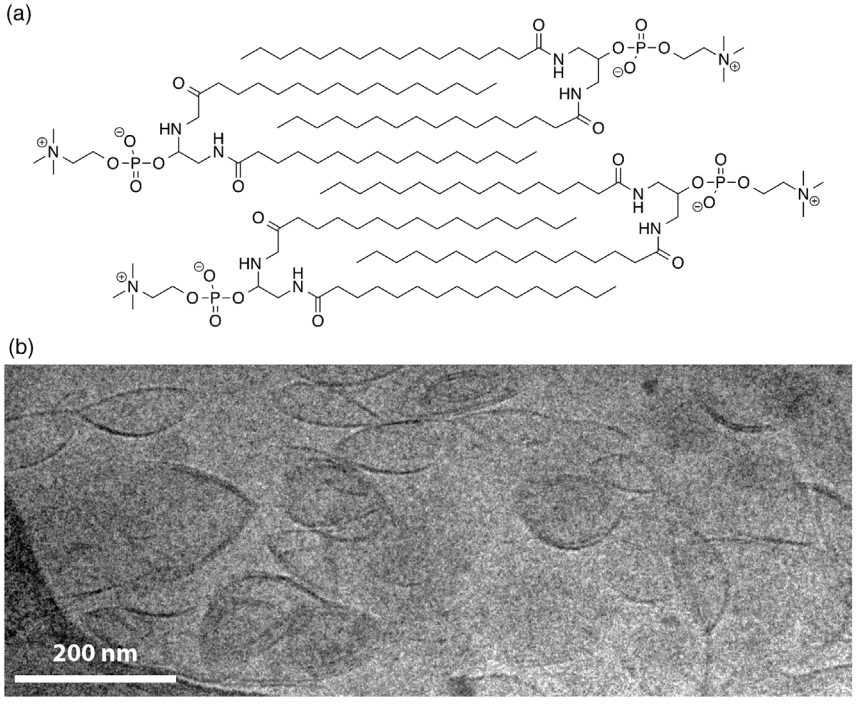


**Figure 4.5** Structure of Pad-PC-Pad and schematic of the interdigitated bilayer (a). Cryo-TEM of 100 nm Pad-PC-Pad liposomes showing lenticular geometry (b). (Reproduced with permission from Refs. [1,54].)

### 4.3.5
### Nanoparticles Endogenous to Atherosclerosis Pathology

The exact mechanism of plaque formation in atherosclerosis is not well understood. Recently, Bertazzo *et al.* discovered that in the early stages of disease, nanometer-sized calcium phosphate particles are found in tissue samples, by studying slices of human aortic valve using scanning electron microscopy [55]. As well as illuminating new insights into the early stages of this disease, understanding the role of such particles in disease progression opens the door to new targets for therapeutic agents.

## 4.4
## Nanotherapeutics in Surgical Interventions

In the case of heart attack, tissue death caused by oxygen deprivation is irreversible, and there is a huge need for treatments that allow regeneration of

tissue function. These can be broadly grouped into stent coatings to encourage reendothelialization while minimizing the risk of restenosis, grafts to encourage electrical stimulation and reestablishment of heart muscle function, aortic valve replacements, pacemakers, and defibrillators [18,24].

Here, we deal exclusively with the contribution of nanomedicine to improving patient prognosis after stent implantation.

### 4.4.1 Nanoparticles in Drug-eluting Stents

Typical treatment of occluded vessels in the operating theater comprises angioplasty by inserting a balloon to reopen the vessel, followed by stent implantation to support the reopened vessel geometry. The first-generation stents were bare metal; however, restenosis is a large problem, and after surgery the patient must be treated with an anticoagulant. To overcome the problem of restenosis, viable alternatives are nanopatterned and nanotherapeutic-containing stents [24]. Polymeric drug-eluting stents (DESs) have been implemented, with polymer coatings such as PLGA that include antiproliferative drugs. Inclusion of drugs such as sirolimus or paclitaxel reduces proliferation of vascular smooth muscle cells and inflammatory cells, decreasing the rate of restenosis to less than 10% [5,56]. However, DESs have drawbacks. Although there is a reduced rate of restenosis in the first 6 months after surgery compared to bare metal stents, the increased risk of late thrombosis has led to debate in the medical community about which has the best long-term outcome [57,58].

Current state-of-the-art drug coating techniques are limited to dipping or coating and are optimal only for highly lipophilic drugs. Delivery of hydrophilic drugs such as DNA, RNA, and proteins to cells requires crossing the lipophilic cell membrane. The use of cationic nanocarriers such as liposomes, polymersomes, and cell-derived vesicles overcomes this problem. Nakano *et al.* recently reported the first active nanoparticle coating on metallic stents, using biodegradable PLGA nanoparticles that encapsulated a hydrophilic fluorescent dye [56]. On incubation with human coronary artery smooth muscle cells, these polymeric nanoparticles showed almost 100% cellular uptake after only 5 min. In *in vivo* experiments, the nanoparticle-coated stent showed significant delivery of the dye to neointimal and medial layers of stented porcine coronary arteries, whereas no substantial fluorescence was observed in the case of a first-generation PLGA DES or bare metal stent.

Critically, the ability to intracellularly deliver hydrophilic moieties opens the door for gene eluting stents. Such gene therapies have the potential to address many of the current limitations such as proliferation, reendothelialization, thrombosis, and inflammation [59]. In addition to the inclusion of drug-loaded liposomes on DES for delivery of, for example, the hydrophilic drug heparin [60], DNA-loaded liposomes (lipoplexes) for gene delivery on both bare metal and DES surfaces were investigated [61,62]. It is postulated that such techniques may improve current DES by regenerating endothelium and inhibiting neointima

formation, both important factors for reducing in-stent thrombosis. *In vivo* delivery of endothelial nitric oxide synthase (eNOS) to the vessel wall was achieved using lipoplexes comprising lipofectin liposomes and plasmid DNA encoding eNOS deposited on polymer-coated stents [62]. Although this method resulted in accelerated reendothelialization, unlike adenoviral eNOS delivery methods it was unfortunately unable to reduce neointimal formation. However, intravenous injection of inducible NOS (iNOS) lipolexes before stent implantation has been shown to inhibit neointimial lesion formation [61]. The activity profile of such constructs depends on the method used for depositing the liposomal coating.

Other examples include iron oxide nanoparticles and carbon nanotubes. For example, iron oxide nanoparticles coated with the antimicrobial kojic acid [33] or the antibiotic nyst were proposed as possible candidates for incorporation into stents to reduce the risk of infection at the site of implantation [13]. They can also be used to guide cells within the body. To encourage reendothelialization, endothelial cells could even be loaded with magnetic iron oxide nanoparticles and guided to implanted stents using magnets [63]. The inclusion of carbon nanotubes into PLGA at a 50 : 50 ratio was shown to enhance cardiomyocyte function by mimicking the tensile strength and conductivity of native heart tissue and increasing adsorption of proteins that promote cardiomyocyte function, compared to PLGA alone [64].

### 4.4.2 Nanopatterning to Improve Stent Integration

First-generation DESs have been dogged with problems including an elevated risk of often fatal late-stent thrombosis, and patients must typically be treated long-term with two anticoagulants such as aspirin and Plavix. These problems are largely due to incomplete integration of the stent into the vessel due to underendothelialization leading to potentially fatal thrombosis, sometimes years after implantation. To overcome this problem, several groups are investigating the effect of nanopatterning on both DES [10] and bare metal stents, with the latter seeing a resurgence in popularity among the medial community thanks to the issue of late-stent thrombosis in DES. It is well known that the nanostructure of substrates greatly influences cell behavior. Plasma-induced nanopillars on bare metallic surfaces of MP35 N, the most common stent alloy, were found to significantly increase functionality, lower oxidative stress, and favor the presence of transmembrane tight junctions and organized monolayer formation of bovine aortic endothelial cells *in vitro*, compared to the smooth topology alternative [23].

These two nanotherapeutic technologies – drug-eluting nanomaterials and nanopatterning – have great potential to improve patient outcome after stent implantation, by reducing the risk of late thrombosis, allowing localized intracellular delivery of a variety of drugs and encouraging reendothelialization of favorable cell phenotypes.

### 4.4.3 Nanoparticle Alternatives to Stents

Stents, as with any implant, have the potential to be recognized by the immune and coagulation systems as a foreign body. This leads to increased risk of intraluminal thrombosis and vessel wall inflammatory reaction with late restenosis. Plasmonic photothermal therapy (PPTT) [65] has great potential to overcome the need for stent implantation. Irradiation with near-infrared (NIR) radiation causes coherent excitation of electrons in gold nanoparticles. The subsequent rapid relaxation leads to localized hyperthermia, which can be used to trigger cell death. This technique is already popular in localized treatment of cancer, where tumors can be targeted using the enhanced permeability and retention effect. Gabinsky and coworkers recently reported a first-in-man PPTT trial showing significant regression of coronary atherosclerosis [34] using either silica–gold core/shell nanoparticles incubated with stem cells and embedded in an implanted bioengineered NP-patch, or silica–gold core/shell and silica–gold iron-bearing NPs incubated with stem cells and microbubbles. This latter construct was infused into the target coronary artery using a minicatheter before microbubbles were destroyed using ultrasound and magnetic nanoparticles were guided to the atheroma using external magnets. Finally, in both constructs, PPTT using an NIR laser was used to locally burn the atheroma, leading to shrinkage and artery remodeling. In both approaches, a significant reduction of plaque burden was observed, with up to 60.3 $mm^3$ decrease in atheroma volume in the NP-patch patients, and physiologic arterial lumen was established and maintained for at least 12 months postintervention without a classical stent.

## 4.5 Conclusions

Despite huge progress in the domain of minimally invasive procedures, rhythmology devices, and pharmaceutical treatments, cardiovascular diseases remain the main cause of burden of disease and mortality in the world. Using nanoparticles and nanocarriers to locally deliver therapeutics to areas of CVD has the potential to greatly improve the efficacy and safety profiles of known therapeutic agents. Nanoparticle-containing stents could overcome many of the procedure- and device-related problems of DES, which, although capable of overcoming problems of bare metal stents such as restenosis, lead to other problems such as late in-stent thrombosis. Nanopatterning of stents can improve cell adhesion for reendothelialization, and there is the possibility to even replace stents entirely with nanoparticle-based therapies.

Mechanosensitive drug delivery systems that target increased wall shear stress in constricted arteries have huge potential to target drugs at atherosclerotic sites. This technique could enable localized vasodilation, fibrinolysis or plaque stabilization, and safely and *rapidly* limit hypoxic injury causing heart attack

symptoms. Critically, it could be administered during prehospital care and in developing countries, where hospitals do not have access to the high-tech equipment needed to carry out small surgeries such as angioplasty and stent implantation.

Europe is a leader in nanomedicine research activities (see etp-nanomedicine.eu; clinam.org). However, it is a highly interdisciplinary field, and research is rarely organized into a university department structure. There is a growing need for more cohesive nanomedicine research centers on an academic level, and an interdisciplinary nanomedicine innovating pool is required to unlock its huge potential. Flexible and quick private financing with organizational structures, such as those seen in Asian countries, offers a chance for synergic project developments and could enhance Europe's reactivity in this field.

Nanomedicine is a discipline that introduces a new scale for physiopathology understanding. Intelligent treatment devices can be designed for a specific therapeutic. Combining classical disciplines to address a specific need has huge potential for effective and safe treatments. Ethical and safety considerations for patients and the environment must be a first priority during the development process of any nanomedicine construct. A more official and structured organization of nanomedicine specialization in universities and the private industry will be helpful for a coordinated innovation process and sharing of collective knowledge.

## References


1 Holme, M.N., Fedotenko, I.A., Abegg, D., Althaus, J., Babel, L., Favarger, F., Reiter, R., Tanasescu, R., Zaffalon, P.-L., Ziegler, A., Muller, B., Saxer, T., and Zumbuehl, A. (2012) Shear-stress sensitive lenticular vesicles for targeted drug delivery. *Nat. Nanotechnol.*, **7** (8), 536–543.

2 Nozaki, K., Shinonaga, T., Ebe, N., Horiuchi, N., Nakamura, M., Tsutsumi, Y., Hanawa, T., Tsukamoto, M., Yamashita, K., and Nagai, A. (2015) Hierarchical periodic micro/nano-structures on nitinol and their influence on oriented endothelialization and anti-thrombosis. *Mater. Sci. Eng. C*, **57**, 1–6.

3 Wickline, S.A., Neubauer, A.M., Winter, P., Caruthers, S., and Lanza, G. (2006) Applications of nanotechnology to atherosclerosis, thrombosis, and vascular biology. *Arterioscler. Thromb. Vasc. Biol.*, **26** (3), 435–441.

4 Iverson, N., Plourde, N., Chnari, E., Nackman, G.B., and Moghe, P.V. (2008) Convergence of nanotechnology and cardiovascular medicine. *BioDrugs*, **22** (1), 1–10.

5 Serruys, P.W., Kutryk, M.J.B., and Ong, A.T.L. (2006) Coronary-artery stents. *N. Engl. J. Med.*, **354** (5), 483–495.

6 Buxton, D.B. (2009) Current status of nanotechnology approaches for cardiovascular disease: a personal perspective. *Wiley Interdisc. Rev.Nanomed. Nanobiotechnol.*, **1** (2), 149–155.

7 de Mel, A., Bolvin, C., Edirisinghe, M., Hamilton, G., and Seifalian, A.M. (2008) Development of cardiovascular bypass grafts: endothelialization and applications of nanotechnology. *Expert Rev. Cardiovasc. Ther.*, **6** (9), 1259–1277.

8 Tyler, P.D. and Kang, P.M. (2015) Diagnostic and therapeutic nanoparticles in cardiovascular diseases. *Curr. Pharm. Des.*, **21** (42), 6070–6080.

9 Godin, B., Sakamoto, J.H., Serda, R.E., Grattoni, A., Bouamrani, A., and Ferrari,

M. (2010) Emerging applications of nanomedicine for the diagnosis and treatment of cardiovascular diseases. *Trends Pharmacol. Sci.*, **31** (5), 199–205.
10 Caves, J.M. and Chaikof, E.L. (2006) The evolving impact of microfabrication and nanotechnology on stent design. *J. Vasc. Surg.*, **44** (6), 1363–1368.
11 Romana, B., Batger, M., Prestidge, C.A., Colombo, G., and Sonvico, F. (2014) Expanding the therapeutic potential of statins by means of nanotechnology enabled drug delivery systems. *Curr. Top. Med. Chem.*, **14** (9), 1182–1193.
12 Wickline, S.A., Neubauer, A.M., Winter, P.M., Caruthers, S.D., and Lanza, G.M. (2007) Molecular imaging and therapy of atherosclerosis with targeted nanoparticles. *J. Magn. Reson. Imaging*, **25** (4), 667–680.
13 Vellayappan, M.V., Balaji, A., Subramanian, A.P., John, A.A., Jaganathan, S.K., Murugesan, S., Supriyanto, E., and Yusof, M. (2015) Multifaceted prospects of nanocomposites for cardiovascular grafts and stents. *Int. J. Nanomed.*, **10**, 2785–2803.
14 Paul, A., Abbasi, S., Shum-Tim, D., and Prakash, S. (2010) Nano- and biotechnological approaches in current and future generation of cardiovascular stents. *Curr. Nanosci.*, **6** (5), 469–478.
15 Karagkiozaki, V., Logothetidis, S., and Pappa, A.M. (2015) Nanomedicine for atherosclerosis: molecular imaging and treatment. *J. Biomed. Nanotechnol.*, **11** (2), 191–210.
16 Psarros, C., Lee, R., Margaritis, M., and Antoniades, C. (2012) Nanomedicine for the prevention, treatment and imaging of atherosclerosis. *Nanomedicine*, **8**, S59–S68.
17 Binsalamah, Z.M., Paul, A., Prakash, S., and Shum-Tim, D. (2012) Nanomedicine in cardiovascular therapy: recent advancements. *Expert Rev. Cardiovasc. Ther.*, **10** (6), 805–815.
18 Ahmed, M., Yildirimer, L., Khademhosseini, A., and Seifalian, A.M. (2012) Nanostructured materials for cardiovascular tissue engineering. *J. Nanosci. Nanotechnol.*, **12** (6), 4775–4785.
19 Mironov, V., Kasyanov, V., and Markwald, R.R. (2008) Nanotechnology in vascular tissue engineering: from nanoscaffolding towards rapid vessel biofabrication. *Trends Biotechnol.*, **26** (6), 338–344.
20 Ghanbari, H., Viatge, H., Kidane, A.G., Burriesci, G., Tavakoli, M., and Seifalian, A.M. (2009) Polymeric heart valves: new materials, emerging hopes. *Trends Biotechnol.*, **27** (6), 359–367.
21 Silva, A.K.A., Letourneur, D., and Chauvierre, C. (2014) Polysaccharide nanosystems for future progress in cardiovascular pathologies. *Theranostics*, **4** (6), 579–591.
22 Naghavi, N., de Mel, A., Alavijeh, O.S., Cousins, B.G., and Seifalian, A.M. (2013) Nitric oxide donors for cardiovascular implant applications. *Small*, **9** (1), 22–35.
23 Loya, M.C., Brammer, K.S., Choi, C., Chen, L.H., and Jin, S.H. (2010) Plasma-induced nanopillars on bare metal coronary stent surface for enhanced endothelialization. *Acta Biomater.*, **6** (12), 4589–4595.
24 Arsiwala, A., Desai, P., and Patravale, V. (2014) Recent advances in micro/nanoscale biomedical implants. *J. Control. Release*, **189**, 25–45.
25 Barenholz, Y. (2012) Doxil(*R*) – the first FDA-approved nano-drug: lessons learned. *J. Control. Release*, **160** (2), 117–134.
26 Korin, N., Kanapathipillai, M., Matthews, B.D., Crescente, M., Brill, A., Mammoto, T., Ghosh, K., Jurek, S., Bencherif, S.A., Bhatta, D., Coskun, A.U., Feldman, C.L., Wagner, D.D., and Ingber, D.E. (2012) Shear-activated nanotherapeutics for drug targeting to obstructed blood vessels. *Supramol. Sci.*, **337** (6095), 738–742.
27 Lanza, G.M., Winter, P.M., Caruthers, S.D., Hughes, M.S., Cyrus, T., Marsh, J.N., Neubauer, A.M., Partlow, K.C., and Wickline, S.A. (2006) Nanomedicine opportunities for cardiovascular disease with perfluorocarbon nanoparticles. *Nanomedicine*, **1** (3), 321–329.
28 Chnari, E., Nikitczuk, J.S., Uhrich, K.E., and Moghe, P.V. (2006) Nanoscale anionic macromolecules can inhibit cellular uptake of differentially oxidized LDL. *Biomacromolecules*, **7** (2), 597–603.
29 Pietroiusti, A. (2012) Health implications of engineered nanomaterials. *Nanoscale*, **4** (4), 1231–1247.

30 Oberdorster, G. (2010) Safety assessment for nanotechnology and nanomedicine: concepts of nanotoxicology. *J. Intern. Med.*, **267** (1), 89–105.
31 Meetoo, D. (2009) Nanotechnology: is there a need for ethical principles? *Br. J. Nurs.*, **18** (20), 1264–1268.
32 Rasmussen, A.J. and Ebbesen, M. (2014) Why should nanoscience students be taught to be ethically competent? *Sci. Eng. Ethics*, **20** (4), 1065–1077.
33 Hussein-Al-Ali, S.H., Zowalaty, M.E.E., Hussein, M.Z., Ismail, M., Dorniani, D., and Webster, T.J. (2014) Novel kojic acid-polymer-based magnetic nanocomposites for medical applications. *Int. J. Nanomed.*, **9**, 351–362.
34 Kharlamov, A.N., Tyurnina, A.E., Veselova, V.S., Kovtun, O.P., Shur, V.Y., and Gabinsky, J.L. (2015) Silica–gold nanoparticles for atheroprotective management of plaques: results of the NANOM-FIM trial. *Nanoscale*, **7** (17), 8003–8015.
35 Levchenko, T.S., Hartner, W.C., and Torchilin, V.P. (2012) Liposomes for cardiovascular targeting. *Therap. Deliv.*, **3** (4), 501–514.
36 Astete, C.E. and Sabliov, C.M. (2006) Synthesis and characterization of PLGA nanoparticles. *J. Biomat. Sci. Polym. Ed.*, **17** (3), 247–289.
37 Lu, J.M., Wang, X.W., Marin-Muller, C., Wang, H., Lin, P.H., Yao, Q.Z., and Chen, C.Y. (2009) Current advances in research and clinical applications of PLGA-based nanotechnology. *Expert Rev. Mol. Diagn.*, **9** (4), 325–341.
38 Yu, M.M., Jie, X., Xu, L., Chen, C., Shen, W.L., Cao, Y.N., Lian, G., and Qi, R. (2015) Recent advances in dendrimer research for cardiovascular diseases. *Biomacromolecules*, **16** (9), 2588–2598.
39 Saha, K., Agasti, S.S., Kim, C., Li, X., and Rotello, V.M. (2012) Gold nanoparticles in chemical and biological sensing. *Chem. Rev.*, **112** (5), 2739–2779.
40 Kim, K.S., Khang, G., and Lee, D. (2011) Application of nanomedicine in cardiovascular diseases and stroke. *Curr. Pharm. Des.*, **17** (18), 1825–1833.
41 Mulder, W.J.M., Jaffer, F.A., Fayad, Z.A., and Nahrendorf, M. (2014) Imaging and nanomedicine in inflammatory atherosclerosis. *Sci. Transl. Med.*, **6** (239), 11.
42 Janib, S.M., Moses, A.S., and MacKay, J.A. (2010) Imaging and drug delivery using theranostic nanoparticles. *Adv. Drug Deliv. Rev.*, **62** (11), 1052–1063.
43 Sutton, J.T., Raymond, J.L., Verleye, M.C., Pyne-Geithman, G.J., and Holland, C.K. (2014) Pulsed ultrasound enhances the delivery of nitric oxide from bubble liposomes to *ex vivo* porcine carotid tissue. *Int. J. Nanomed.*, **9**, 4671–4683.
44 Jardeleza, C., Rao, S., Thierry, B., Gajjar, P., Vreugde, S., Prestidge, C.A., and Wormald, P.-J. (2014) Liposome-encapsulated ISMN: a novel nitric oxide-based therapeutic agent against *Staphylococcus aureus* biofilms. *PLOS One*, **9** (3), e92117.
45 Cabrales, P., Han, G., Roche, C., Nacharaju, P., Friedman, A.J., and Friedman, J.M. (2010) Sustained release nitric oxide from long-lived circulating nanoparticles. *Free Radic. Biol. Med.*, **49** (4), 530–538.
46 Roy, R.S., Soni, S., Harfouche, R., Vasudevan, P.R., Holmes, O., de Jonge, H., Rowe, A., Paraskar, A., Hentschel, D.M., Chirgadze, D., Blundell, T.L., Gherardi, E., Mashelkar, R.A., and Sengupta, S. (2010) Coupling growth-factor engineering with nanotechnology for therapeutic angiogenesis. *Proc. Natl. Acad. Sci. US A*, **107** (31), 13608–13613.
47 La, M., D'Amico, M., Bandiera, S., Di Filippo, C., Oliani, S.M., Gavins, F.N., Flower, R.J., and Perretti, M. (2001) Annexin 1 peptides protect against experimental myocardial ischemia-reperfusion: analysis of their mechanism of action. *FASEB J.*, **15** (12), 2247–2256.
48 Chang, M.Y., Yang, Y.J., Chang, C.H., Tang, A.C.L., Liao, W.Y., Cheng, F.Y., Yeh, C.S., Lai, J.J., Stayton, P.S., and Hsieh, P.C.H. (2013) Functionalized nanoparticles provide early cardioprotection after acute myocardial infarction. *J. Control. Release*, **170** (2), 287–294.
49 Marsh, J.N., Senpan, A., Hu, G., Scott, M.J., Gaffney, P.J., Wickline, S.A., and Lanza, G.M. (2007) Fibrin-targeted perfluorocarbon nanoparticles for targeted

thrombolysis. *Nanomedicine (Lond.)*, **2** (4), 533–543.

**50** Soulls, J.V., Farmakis, T.M., Giannoglou, G.D., and Louridas, G.E. (2006) Wall shear stress in normal left coronary artery tree. *J. Biomech.*, **39** (4), 742–749.

**51** Holme, M.N., Schulz, G., Deyhle, H., Weitkamp, T., Beckmann, F., Lobrinus, J.A., Rikhtegar, F., Kurtcuoglu, V., Zanette, I., Saxer, T., and Müller, B. (2014) Complementary X-ray tomography techniques for histology-validated 3D imaging of soft and hard tissues using plaque-containing blood vessels as examples. *Nat. Protocols*, **9** (6), 1401–1415.

**52** Doriot, P.A., Dorsaz, P.A., Dorsaz, L., De Benedetti, E., Chatelain, P., and Delafontaine, P. (2000) *In-vivo* measurements of wall shear stress in human coronary arteries. *Coron. Artery Dis.*, **11** (6), 495–502.

**53** Fedotenko, I.A., Zaffalon, P.-L., Favarger, F., and Zumbuehl, A. (2010) The synthesis of 1,3-diamidophospholipids. *Tetrahedron Lett.*, **51** (41), 5382–5384.

**54** Weinberger, A., Tanasescu, R., Stefaniu, C., Fedotenko, L.A., Favarger, F., Ishikawa, T., Brezesinski, G., Marques, C.M., and Zumbuehl, A. (2015) Bilayer properties of 1,3-diamidophospholipids. *Langmuir*, **31** (6), 1879–1884.

**55** Bertazzo, S., Gentleman, E., Cloyd, K.L., Chester, A.H., Yacoub, M.H., and Stevens, M.M. (2013) Nano-analytical electron microscopy reveals fundamental insights into human cardiovascular tissue calcification. *Nat. Mater.*, **12** (6), 576–583.

**56** Nakano, K., Egashira, K., Masuda, S., Funakoshi, K., Zhao, G., Kimura, S., Matoba, T., Sueishi, K., Endo, Y., Kawashima, Y., Hara, K., Tsujimoto, H., Tominaga, R., and Sunagawa, K. (2009) Formulation of nanoparticle-eluting stents by a cationic electrodeposition coating technology efficient nano-drug delivery via bioabsorbable polymeric nanoparticle-eluting stents in porcine coronary arteries. *JACC Cardiovasc. Interv.*, **2** (4), 277–283.

**57** Kastrati, A., Mehilli, J., Pache, J., Kaiser, C., Valgimigli, M., Kelbæk, H., Menichelli, M., Sabaté, M., Suttorp, M.J., Baumgart, D., Seyfarth, M., Pfisterer, M.E., and Schömig, A. (2007) Analysis of 14 trials comparing sirolimus-eluting stents with bare-metal stents. *N. Engl. J. Med.*, **356** (10), 1030–1039.

**58** Stettler, C., Wandel, S., Allemann, S., Kastrati, A., Morice, M.C., Schömig, A., Pfisterer, M.E., Stone, G.W., Leon, M.B., de Lezo, J.S., Goy, J.-J., Park, S.-J., Sabaté, M., Suttorp, M.J., Kelbaek, H., Spaulding, C., Menichelli, M., Vermeersch, P., Dirksen, M.T., Cervinka, P., Petronio, A.S., Nordmann, A.J., Diem, P., Meier, B., Zwahlen, M., Reichenbach, S., Trelle, S., Windecker, S., and Jüni, P. (2007) Outcomes associated with drug-eluting and bare-metal stents: a collaborative network meta-analysis. *Lancet*, **370** (9591), 937–948.

**59** Goh, D., Tan, A., Farhatnia, Y., Rajadas, J., Alavijeh, M.S., and Seifalian, A.M. (2013) Nanotechnology-based gene-eluting stents. *Mol. Pharm.*, **10** (4), 1279–1298.

**60** Antimisiaris, S.G., Koromila, G., Michanetzis, G., and Missirlis, Y.F. (2006) Liposome coated stents: a method to deliver drugs to the site of action and improve stent blood-compatibility. *J. Lipos. Res.*, **16** (3), 303–309.

**61** Muhs, A., Heublein, B., Schletter, J., Herrmann, A., Rudiger, M., Sturm, M., Grust, A., Malms, J., Schrader, J., and Von der Leyen, H.E. (2003) Preclinical evaluation of inducible nitric oxide synthase lipoplex gene therapy for inhibition of stent-induced vascular neointimal lesion formation. *Hum. Gene Ther.*, **14** (4), 375–383.

**62** Sharif, F., Hynes, S.O., McCullagh, K.J.A., Ganley, S., Greiser, U., McHugh, P., Crowley, J., Barry, F., and O'Brien, T. (2012) Gene-eluting stents: non-viral, liposome-based gene delivery of eNOS to the blood vessel wall *in vivo* results in enhanced endothelialization but does not reduce restenosis in a hypercholesterolemic model. *Gene Ther.*, **19** (3), 321–328.

**63** Polyak, B., Fishbein, I., Chorny, M., Alferiev, I., Williams, D., Yellen, B., Friedman, G., and Levy, R.J. (2008) High field gradient targeting of magnetic nanoparticle-loaded endothelial cells to

the surfaces of steel stents. *Proc. Natl. Acad. Sci. USA*, **105** (2), 698–703.

64 Stout, D.A., Yoo, J., Santiago-Miranda, A.N., and Webster, T.J. (2012) Mechanisms of greater cardiomyocyte functions on conductive nanoengineered composites for cardiovascular applications. *Int. J. Nanomed.*, **7**, 5653–5669.

65 Huang, X. and El-Sayed, M.A. (2011) Plasmonic photo-thermal therapy (PPTT). *Alexandria J. Med.*, **47** (1), 1–9.

# 5
# Smart Container for Targeted Drug Delivery

*Andreas Zumbuehl*

*University of Fribourg, Department of Chemistry, Chemin du Musée 9, 1700 Fribourg, Switzerland*

## 5.1
## Introduction

Nanomedicine, the application of nanotechnology in medicine, has spurred high hopes for new treatment technologies. These technologies can be old favorites in new clothes. This certainly applies to the field of liposome technology, which remains an interesting topic through the ages from the early *bangosomes* to todays' *nanocontainers*. This chapter summarizes our recent efforts in turning liposomes into *smart materials*.

Smart materials surfaced during the development of the second generation of drug delivery systems [1]. The first generation of these systems was introduced in the 1950s and focused on the controlled and sustained release of drugs using mechanisms such as diffusion, dissolution, osmosis, and ion exchange [1]. The second generation of drug delivery systems was introduced roughly 30 years later. These smart materials were not passive anymore and now reacted to an external trigger and released the drug molecules in zero order kinetics. Again, 30 years later, we are seeing the first third-generation materials, which are modulated, that is, the drug release can be turned on and off according to external stimuli. As this type of release mechanism is quite *smart* too, it does not make sense to label the second generation of drug delivery systems only as smart materials [1].

Aside from the three generations of drug delivery systems, the general problem of drug formulation prevailed. In an enthusiastic article from 2010, the authors discuss the formulation problems with new molecular entities [2]. Here lies a main hope in nanotechnology, because it should be possible to address shortcomings of drugs such as poor water solubility or very short blood circulating half-times or to even improve the properties of previously approved drugs [2]. The first generation of nontargeted nanomedical constructs could already have advantages over classical drug delivery such as a reduction in side effects and

*Nanoscience and Nanotechnology for Human Health,* First Edition. Edited by Bert Müller and Marcel Van de Voorde.

administration frequency. But out of these first generation nanomedicines, *smart* systems may be produced. In addition, theranostic approaches are feasible, combining targeting, visualization, and therapy. A multibillion market is waiting for smart personalized medical products.

## 5.2 Liposomes

### 5.2.1 General Characteristics

In 1965, Bangham *et al.* reported on cell-like structures that they were able to formulate from hydrated phospholipid molecules [3]. With this discovery, the field of phospholipid vesicles (or liposomes) was initiated – a success story at the nanoscale interface of chemistry, medicine, and physics. Phospholipids are surface-active agents that are cleverly put together from four components: two fatty acids, a phosphate ester, and a molecule of glycerol, see Figure 5.1 [4,5]. Three ester functionalities connect the molecules, with the glycerol being the central connecting molecule. From the beginning, the molecule of phospholipid was *designed* to be taken apart and again put together. This principle allows an organism to adapt very quickly to its environment by synthesizing phospholipids from the food provided. The process of homoviscous adaptation is, therefore, an important part of allowing life in different temperature environments on earth [6].

Phospholipids are amphiphiles with a hydrophobic fatty acyl chain region and a hydrophilic head group region. In water, the nonpolar $CH_2$ methylene units of

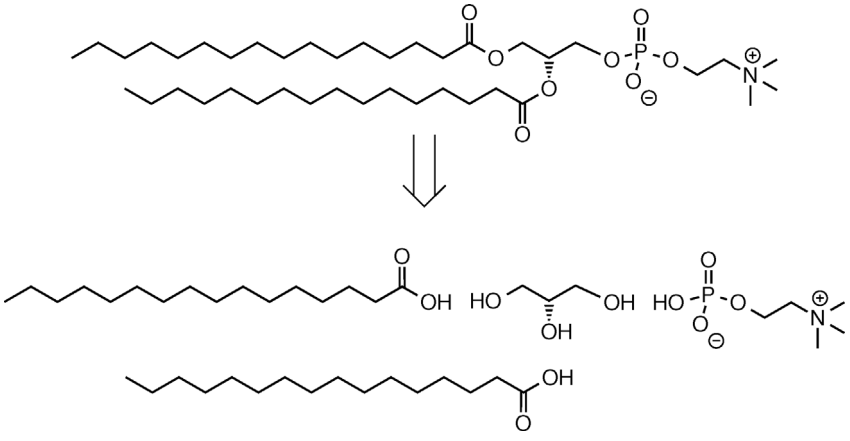

**Figure 5.1** The typical glycerol-phospholipid is made of four parts. Here, the structure of 1,2-dipalmitoyl-*sn*-glycero-3-phosphocholine can be divided into four interchangeable parts: two fatty acids, glycerol, and a zwitterionic phosphate ester.

the fatty acyl chains disturb the hydrogen-bonding pattern of water, creating a thermodynamic penalty. Therefore, the phospholipids arrange in such a way that the hydrophilic head groups point into the water phase and the hydrophobic tails point away from water and preferably interact with other hydrophobic tails. In addition, in water, the attraction between two hydrophobic molecule portions is bigger than the attraction between a hydrophobic and a hydrophilic portion. This effect is basically a van der Waals interaction and is named hydrophobic effect [7]. Overall, this leads to the formation of several possible phospholipid arrangements, depending mainly on the phospholipid molecular geometry [8]. The most interesting arrangements are the liposomes, water filled *sacks* enclosed by a bilayer membrane. In fact, such liposomes are so ubiquitously found in nature that they have been termed nature's preferred nanotechnology [9].

Vesicles are typically formulated from thin lipid films [10]: phospholipids are soluble in solvents such as methanol, dichloromethane, or chloroform. This lipid solution is transferred to a round-bottom flask and the solvent is slowly removed under reduced pressure while rapidly turning the round-bottom flask. This creates a continuous multilamellar sheet of phospholipids that is visible by eye as a white film. Upon addition of an aqueous buffer, the phospholipid head groups are hydrated. This leads to a swelling of the individual lamellar sheets on the glass wall and to the spontaneous formation of vesicles.

The volume entrapped by a large unilamellar vesicle of 100 nm diameter is surprisingly small, see Figure 5.2. A lipid vesicle formulated from a standard POPC phospholipid contains a mere $8.1 \times 10^4$ molecules in its bilayer membrane surrounding a volume of $4.16 \times 10^{-19}$ l (approx. 400 zl) [10]. In other words, if the vesicles are formulated in a buffer containing a 20 µM concentration of a small molecule drug, on average only five drug molecules will be encapsulated in a liposome [10]. This has to be put in relation to the typical drug load that is used today. For example, a pill with a dosage of 500 mg paracetamol contains $1.99 \times 10^{21}$ drug molecules. Needless to state that since their discovery in the 1960s, liposomes have spurred high hopes for drug delivery applications that

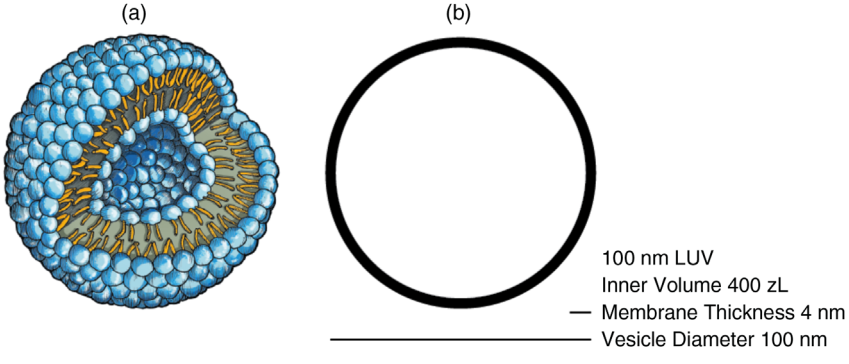


**Figure 5.2** Schematic of a liposome that is self-assembled from double-tail phospholipids. The true dimensions are depicted in (a). Typically, the membrane thickness is overrated in graphical representations of liposomes (b).

would deliver less molecules with higher precision and lower side effects as standard therapies. As of today, about 13 liposomal drug delivery formulations are approved for nanomedical applications [5].

### 5.2.2 Release of Vesicle-Entrapped Molecules

Most liposomes remain tight below the main phase transition of the bilayer membrane. Typically, this transition is set to above body temperature and the release of a drug molecule from a liposome can be triggered by any of several external triggers [5]. These triggers include changes in temperature or pH, introduction of enzymes or redox active substances, photochemical triggers, application of ultrasound, and, as is detailed in this chapter, changes in shear forces. Here is a concise overview of the possible triggers summarized from a recent review article, cf. Figure 5.3 [5].

#### 5.2.2.1 Temperature as Trigger

At the main transition temperature of the bilayer membrane ($T_m$), the acyl chains of the lipids undergo a change from an all-antiperiplanar (or all-trans) conformer to a chain with several gauche interactions. This leads to a decrease in membrane packing and an increase in packing defects and lateral density fluctuations. At the $T_m$, the passive flux through a membrane becomes maximal. The $T_m$ can be tuned by simply mixing together the correct lipids. A mixture consisting of DPPC:HSPC:Chol:DPPE-PEG2000 has, for instance, a $T_m$ of 41.9 °C [11]. This means a locally induced mild hyperthermia can lead to a triggered drug release [11].

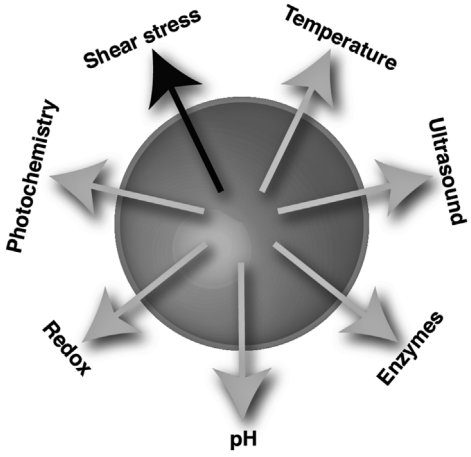


**Figure 5.3** Potential ways to trigger the release of a vesicle-entrapped agent. The ability to react to external triggers defines these liposomes as second-generation nanomaterials [1]. (Reproduced with permission from Ref. [5].)

#### 5.2.2.2 Ultrasound as Trigger

Low-frequency ultrasound leads to acoustic cavitation, in which gas bubbles induce high mechanical forces in the membrane leading to increased transmembrane flux [12]. Here, again, mixtures of lipids are used that have a $T_m$ close to the working temperature and typically contain less well-packed unsaturated phospholipids [12]. An additional factor is the fluid inside the vesicle, which can be an ultrasound-sensitive emulsion [13].

#### 5.2.2.3 Enzymes as Trigger

Phospholipase A2 (PLA2) is a family of enzymes that hydrolyze a phospholipid ester bond at the *sn*-2 position [14]. The enzymes are overexpressed in several human cancer types such as prostate, breast, and colon cancer [14]. This implies the possibility to release a cancer drug at the site, where it is needed. The prodrug is attached as tail to a synthetic phospholipid and is released from the *sn*-2 position via enzymatic cleavage [15].

The action of the enzymes on a liposome additionally leads to the formation of a lipid transmembrane pore, through which a vesicle-entrapped drug molecule can escape. This pore formation mechanism is also used by several insect and snake venoms [16].

#### 5.2.2.4 pH Changes as Trigger

Cancer cells lie in a low pH environment (pH 6–7), and this one to two orders of magnitude higher proton concentration compared to the rest of the body might serve as a external trigger for liposomal drug release [17]. Acid-labile groups such as ortho esters [18] or vinyl ethers [19] undergo acid-catalyzed hydrolysis. If these groups are strategically synthesized into phospholipid structures, the resulting liposomes will become leaky after a pH drop because of a change in the form factor of the lipids [8].

#### 5.2.2.5 Redox Reactions as Trigger

Because of the high sulfhydryl concentration (e.g., glutathione), the cell cytoplasm is a more reducing environment than the blood plasma [18]. The reduction of a dithiol bond in a phospholipid would, therefore, be a suited reaction to induce membrane permeability. This has, for example, been achieved using a dithiobenzyl-linked mPEG-DSPE that was present in 3 mol% in a vesicle formulation [20].

#### 5.2.2.6 Photoreactions as Trigger

Light offers an interesting toolbox for liposomal drug delivery, because diverse reactions are possible such as *trans/cis* isomerizations, uncaging, and polymerizations [5]. Diazo compounds can be photoswitched from a *trans* to a *cis* conformation using a 470 nm laser. Using a liposome with 6 mol% of a phospholipid containing two diazotylated acyl chains, it was shown that a single 10 ns laser pulse was sufficient to induce the total release of encapsulated calcein [21].

Most smart containers apply an all-or-none opening technique, that is, once the system is triggered, its entire content is released. Huang and coworkers presented another, milder form of release by simple deformation of the vesicle [22]. Upon UV radiation, the system develops hair-like protrusions similar to cilia found on the surface of bacteria. In the system of Huang, a helix-forming molecule is masked with beta-cyclodextrins where upon the masked molecules self-assemble into vesicles. UV radiation triggers a *trans–cis* azobenzene isomerization leading to the release of the cyclodextrins and the formation of helical vesicle protrusions.

#### 5.2.2.7 Shear Stress as Trigger

The purely physics-based trigger of shear stress is highly attractive for reaching areas of the human anatomy where no biological or chemical targeting is available, for example, in atherosclerotic plaques. Ours and other teams have presented this approach recently and the next section will explain this concept in more detail [17,23].

Overall, the liposomal self-assembly construct allows for a high flexibility in drug delivery approaches, because many amphiphiles can be combined in the same liposome. Therefore, liposomes are at the forefront of personalized, reactive third-generation materials for nanomedicine.

## 5.3 Shear Forces and Vesicles

### 5.3.1 Influence of Shear Forces on Vesicles

Shear forces are forces that act upon a body in opposite directions. In other words, one part of the body experiences a force in one direction, while the other part experiences a force in the opposite direction. This, of course, leads to significant effects on a soft material body such as a unilamellar liposome, and because of the quasi-inextensibility of the lipid membrane, the vesicle has to deform under shear [24]. The shape of the vesicle depends on the membrane elasticity [25] and on the strength of the applied force: in weak shear flow, the shape is close to equilibrium and in strong flows the vesicle resembles a prolate ellipsoid [26] because of the defects in the phospholipid tilt ordering that have to be present at the poles of a spherical vesicle [27]. The ellipsoid does not remain static but assumes one of the three dynamic modes: tank-treading, tumbling, and swinging [2]. In tank-treading the overall shape of the ellipsoidal vesicle stays static with a constant inclination angle, but the individual membrane phospholipids rotate along the vesicle like the chains of a tank [28]. If in addition the vesicle inclination angle slightly oscillates, the motion is called swinging [28]. Finally, if the vesicle starts to rotate like a rigid body would do, the motion is depicted as

tumbling [28]. These types of motion depend also on the difference of the viscosities of the vesicle internal and external fluids [25].

The liposomal membrane is a quasi two-dimensional liquid, which means that the shear modulus within the membrane plane vanishes [25]. The elastic membrane deforms in a shear field and assumes an ellipsoidal geometry. The membrane tension is highest at the waist of the ellipsoid and, here, the liposomal membrane will break if the tension gets too high. Holes form, through which liquid is ejected, in order to release the membrane tension. Eventually, the holes will close again because of the quasi two-dimensional liquid character of the membrane: if a hole is formed, hydrophobic parts of the membrane are exposed to the aqueous environment and a line tension is build up, which reseals the hole [25].

The curvature of a vesicle is made from two components: first, the local spontaneous membrane curvature from the intrinsic spontaneous curvature of each molecule and, second, the integrated membrane curvature arising from the difference in numbers of molecules in the outer and inner membrane leaflet [29]. Even small changes in phospholipid composition across bilayer leaflets can lead to significant shape changes in GUVs [30], because only minute concentration differences can be balanced out by the curvature energy [27]. These shape fluctuations get significantly bigger near instability boundaries [27].

However, a hexagonal, interdigitated bilayer membrane will have no curvature and a large bending modulus. If such a membrane is forced into forming vesicles, they are predicted to take polyhedral geometry with flat faces and sharp bends at the edges [31]. These edges should show defects of the inner membrane leaflet. The high curvature of the edges should be compensated by admixing a double-tail phospholipid with small amounts of a single-tail detergent with a large head group [32]. Indeed, when standard large unilamellar phospholipid vesicles from eggPC were doped with 1 mol% Brij 76, the vesicles became shear sensitive and would fuse at 10 000/s for 20 min [32]. However, in the absence of shear forces, these vesicles would revert to their basic spherical geometry. For medical purposes, it would be preferable if a vesicle would exist that shows the faceted geometry from the beginning and, therefore, could immediately release its cargo when shear forces are applied.

### 5.3.2
### Shear Force-Responsive Vesicles

Pad-PC-Pad is a synthetic 1,3-diamidophospholipid, see Figure 5.4 [33]. Compared to the natural 1,2-diesterphospholipids, the two fatty acyl chains of Pad-PC-Pad are forced wider apart [5]. This distance leads to an interdigitation of the fatty acyl chains of the phospholipids in the opposite membrane leaflets [34]. Through this physical cross-linking of the two membrane leaflets via phospholipid chain interdigitation, we created a capsule with finite shear elasticity [28]. Furthermore, the vesicle cannot be described by the area difference elasticity model [29], because the inner and outer membrane leaflets are intrinsically

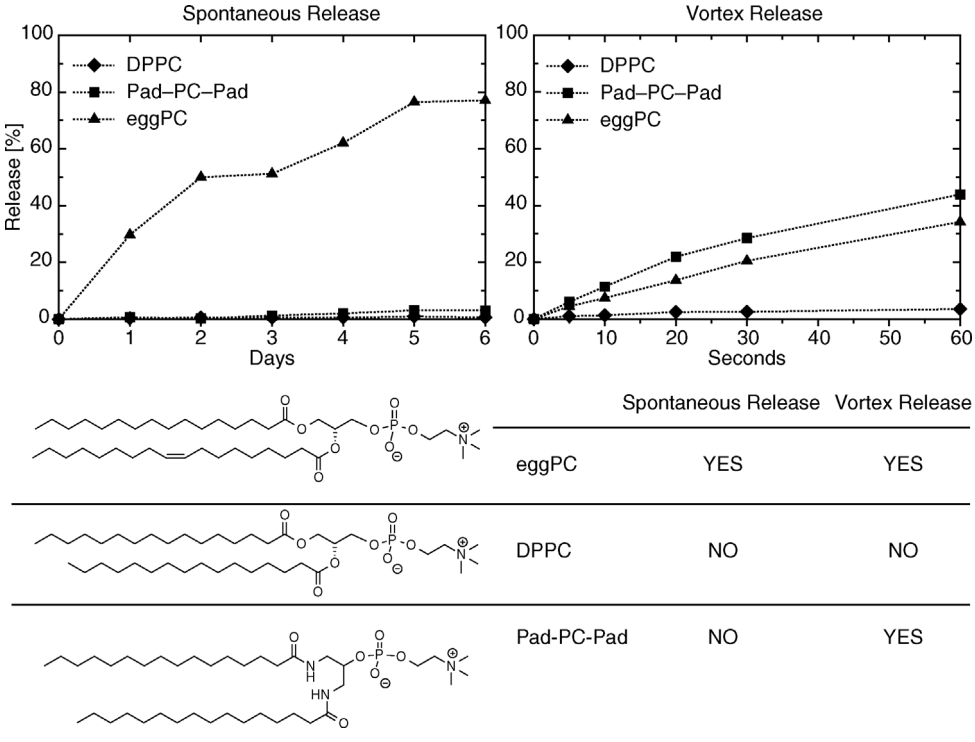


**Figure 5.4** Release of 5(6)-carboxyfluorescein from selected vesicles. The spontaneous release of the dye was measured in days. The shear stress-triggered release was measured in seconds. The lines in the graph serve as guide to the eyes.

connected. According to Noguchi a faceted vesicle should form. Indeed such structures are seen in cryo-TEM images represented in Figure 5.5 [23]. At the edges of the facets, membrane defects should form. It is expected that the application of shear forces attenuate the defects and lead to transient membrane pore formation.

Three vesicles were formulated from the natural and artificial phospholipids, eggPC, 1,2-dipalmitoyl-*sn*-glycero-3-phosphocholine (DPPC), and Pad-PC-Pad, see Figure 5.4 [23]. Each vesicle was filled with the self-quenching fluorescent dye 5(6)-carboxyfluorescein, a dye that allows measuring the release across a vesicle membrane [35]. At rest, the eggPC vesicle was leaky and the DPPC and Pad-PC-Pad vesicles remained tight over several days. When the vesicle suspension was shaken in a vortex shaker, both eggPC and Pad-PC-Pad vesicles did release a significant portion of their cargo and the DPPC vesicles remained tight, cf. Figure 5.4. Compared to the two natural phospholipid vesicles, the Pad-PC-Pad vesicles represent a new type of vesicle that reacts to shear stress as a trigger. As described in Chapter 4, such vesicles have unique potential for targeted drug delivery to the site of severe stenosis in arteries [23].

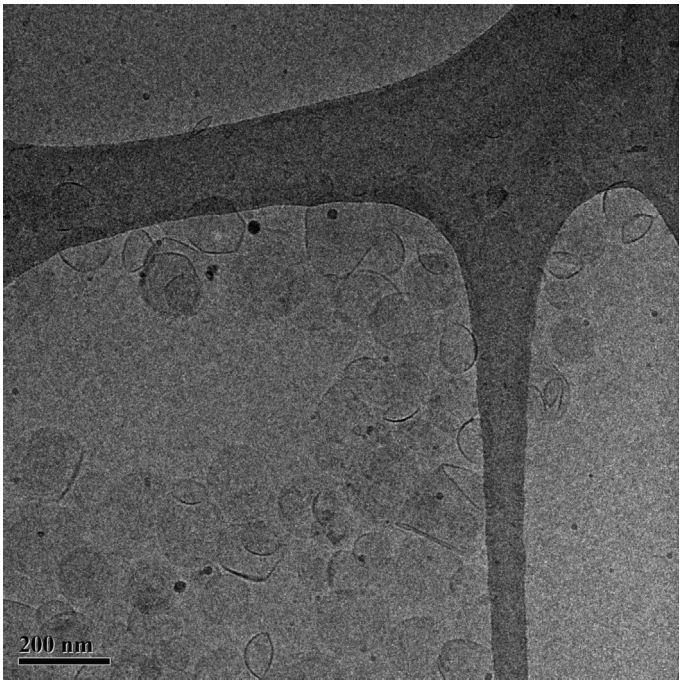


**Figure 5.5** Cryo-TEM image of Pad-PC-Pad vesicles. The faceted form of the vesicles is clearly visible. (The picture was taken by Dr. Takashi Ishikawa at the Paul Scherrer Institute, Switzerland.)

## 5.4 Conclusions

We have still a long way to go until responsive materials can be incorporated into future autonomous (robotic) devices as described in [36]. Nonetheless, significant advances have been made with the three generations of nanomaterials.

Self-assembled nanocontainers offer the very high flexibility needed both to address various medicinal questions and to personalize the drugs. Moving from classical passive self-assembly to guided self-assembly allows for nanocontainers with new properties such as vesicles that react to shear stress and have unlimited possibilities in nanomedicine for human health.

## References

1 Park, K. (2014) Controlled drug delivery systems: past forward and future back. *J. Control. Release*, **190**, 3–8.
2 Noguchi, H. (2010) Dynamic modes of microcapsules in steady shear flow: effects of bending and shear elasticities. *Phys. Rev. E*, **81**, 056319.
3 Bangham, A.D., Standish, M.M., and Watkins, J.C. (1965) Diffusion of univalent ions across the lamellae of swollen

phospholipids. *J. Mol. Biol.*, **13** (1), 238–252.
4 Zumbuehl, A. (2009) Nonnatural phospholipids: probing nature's modular platform. *Chimia*, **63** (1–2), 63–65.
5 Mellal, D. and Zumbuehl, A. (2014) Exit-strategies: smart ways to release phospholipid vesicle cargo. *J. Mater. Chem. B*, **2** (3), 247–252.
6 Hazel, J.R. (1995) Thermal adaptation in biological membranes: is homeoviscous adaptation the explanation? *Annu. Rev. Physiol.*, **57**, 19–42.
7 van Oss, C.J., Absolom, D.R., and Neumann, A.W. (1980) The "Hydrophobic effect": essentially a van der Waals interaction. *Colloid. Polym. Sci.*, **258**, 424–427.
8 Israelachvili, Jacob N. (2011) *Intermolecular and Surface Forces*, Academic Press, San Diego.
9 Mouritsen, O.G. and Zuckermann, M.J. (2004) What is so special about cholesterol? *Lipids*, **39** (11), 1101–1113.
10 Walde, P. (2004) Preparation of vesicles (liposomes), in *Encyclopedia of Nanoscience and Nanotechnology* (ed. H.S. Nalwa), American Scientific Publishers, Valencia, California, pp. 43–79.
11 de Smet, M., Heijman, E., Langereis, S., Hijnen, N.M., and Grull, H. (2011) Magnetic resonance imaging of high intensity focused ultrasound mediated drug delivery from temperature-sensitive liposomes: an *in vivo* proof-of-concept study. *J. Control. Release*, **150** (1), 102–110.
12 Schroeder, A., Kost, J., and Barenholz, Y. (2009) Ultrasound, liposomes, and drug delivery: principles for using ultrasound to control the release of drugs from liposomes. *Chem. Phys. Lipids*, **162** (1–2), 1–16.
13 Javadi, M., Pitt, W.G., Belnap, D.M., Tsosie, N.H., and Hartley, J.M. (2013) Encapsulating nanoemulsions inside eLiposomes for ultrasonic drug delivery. *Langmuir*, **28**, 14720–14729.
14 Hansen, A.H., Mouritsen, O.G., and Arouri, A. (2015) Enzymatic action of phospholipase A on liposomal drug delivery systems. *Int. J. Pharm.*, **491** (1–2), 49–57.
15 Davidsen, J., Jorgensen, K., Andresen, T.L., and Mouritsen, O.G. (2003) Secreted phospholipase A(2) as a new enzymatic trigger mechanism for localised liposomal drug release and absorption in diseased tissue. *BBA Biomembranes*, **1609** (1), 95–101.
16 Zimmerberg, J. and Chernomordik, L.V. (2005) Synaptic membranes bend to the wilt of a neurotoxin. *Supramol. Sci.*, **310** (5754), 1626–1627.
17 Korin, N., Kanapathipillai, M., Matthews, B.D., Crescente, M., Brill, A., Mammoto, T., Ghosh, K., Jurek, S., Bencherif, S.A., Bhatta, D., Coskun, A.U., Feldman, C.L., Wagner, D.D., and Ingber, D.E. (2012) Shear-activated nanotherapeutics for drug targeting to obstructed blood vessels. *Supramol. Sci.*, **337** (6095), 738–742.
18 Guo, X., MacKay, J.A., and Szoka, F.C. (2003) Mechanism of pH-triggered collapse of phosphatidylethanolamine liposomes stabilized by an ortho ester polyethyleneglycol lipid. *Biophys. J.*, **84** (3), 1784–1795.
19 Kim, H.K., Thompson, D.H., Jang, H.S., Chung, Y.J., and Van den Bossche, J. (2013) pH-responsive biodegradable assemblies containing tunable phenyl-substituted vinyl ethers for use as efficient gene delivery vehicles. *ACS Appl. Mater Interfaces*, **5** (12), 5648–5658.
20 Zalipsky, S., Qazen, M., Walker, J.A., 2nd, Mullah, N., Quinn, Y.P., and Huang, S.K. (1999) New detachable poly(ethylene glycol) conjugates: cysteine-cleavable lipopolymers regenerating natural phospholipid, diacyl phosphatidylethanolamine. *Bioconjug. Chem.*, **10** (5), 703–707.
21 Bisby, R.H., Mead, C., and Morgan, C.G. (2000) Active uptake of drugs into photosensitive liposomes and rapid release on UV photolysis. *Photochem. Photobiol.*, **72** (1), 57–61.
22 Zhao, Q., Wang, Y., Yan, Y., and Huang, J. (2016) Smart nanocarrier: self-assembly of bacteria-like vesicles with photoswitchable cilia. *ACS Nano*, 8 (11), 11341–11349.
23 Holme, M.N., Fedotenko, I.A., Abegg, D., Althaus, J., Babel, L., Favarger, F., Reiter, R., Tanasescu, R., Zaffalon, P.-L., Ziegler, A., Müller, B., Saxer, T., and Zumbuehl, A.

(2012) Shear-stress sensitive lenticular vesicles for targeted drug delivery. *Nat. Nanotechnol.*, **7**, 536–543.

24 Mader, M.A., Vitkova, V., Abkarian, M., Viallat, A., and Podgorski, T. (2006) Dynamics of viscous vesicles in shear flow. *Eur. Phys. J. E*, **19** (4), 389–397.

25 Marmottant, P., Biben, T., and Hilgenfeldt, S. (2008) Deformation and rupture of lipid vesicles in the strong shear flow generated by ultrasound-driven microbubbles. *Proc. Roy. Soc. Lond. A*, **464** (2095), 1781–1800.

26 Lebedev, V.V., Turitsyn, K.S., and Vergeles, S.S. (2008) Nearly spherical vesicles in an external flow. *New J. Phys.*, **10**, 043044.

27 Dobereiner, H.G., Evans, E., Kraus, M., Seifert, U., and Wortis, M. (1997) Mapping vesicle shapes into the phase diagram: a comparison of experiment and theory. *Phys. Rev. E*, **55** (4), 4458–4474.

28 Finken, R., Kessler, S., and Seifert, U. (2011) Micro-capsules in shear flow. *J. Phys. Condens. Matter*, **23**, 184113.

29 Döbereiner, H., Lehmann, A., Goedel, W., Selchow, O., and Lipowsky, R.R. (1998) Membrane curvature induced by sugar and polymer solutions. *Mat. Res. Soc. Symp. Proc.*, **489**, 101–106.

30 Farge, E. and Devaux, P.F. (1992) Shape changes of giant liposomes induced by an asymmetric transmembrane distribution of phospholipids. *Biophys. J.*, **61** (2), 347–357.

31 Noguchi, H. (2003) Polyhedral vesicles: a Brownian dynamics simulation. *Phys. Rev. E*, **67**, 041901.

32 Bernard, A.-L., Guedeau-Boudeville, M.-A., Marchi-Artzner, V., Gulik-Krzywicki, T., di Meglio, J.-M., and Jullien, L. (2005) Shear-induced permeation and fusion of lipid vesicles. *J. Colloid. Interface Sci.*, **287** (1), 298–306.

33 Fedotenko, I.A., Zaffalon, P.L., Favarger, F., and Zumbuehl, A. (2010) The synthesis of 1,3-diamidophospholipids. *Tetrahedron Lett.*, **51**, 5382–5384.

34 Weinberger, A., Tanasescu, R., Stefaniu, C., Fedotenko, L.A., Favarger, F., Ishikawa, T., Brezesinski, G., Marques, C.M., and Zumbuehl, A. (2015) Bilayer properties of 1,3-diamidophospholipids. *Langmuir*, **31** (6), 1879–1884.

35 Weinstein, J.N., Yoshikami, S., Henkart, P., Blumenthal, R., and Hagins, W.A. (1977) Liposome-cell interaction: transfer and intracellular release of a trapped fluorescent marker. *Supramol. Sci.*, **195** (4277), 489–492.

36 McEvoy, M.A. and Correll, N. (2015) Materials that couple sensing, actuation, computation, and communication. *Science*, **347** (6228), 1261689.

# 6
# Human Nano-Vesicles in Physiology and Pathology

*Arun Cumpelik and Jürg A. Schifferli*

*University Hospital Basel, Department of Biomedicine, Hebelstr. 20, 4031 Basel, Switzerland*

## 6.1
## Introduction

Micro- or nanovesicles (NVs) are nanosized spherical vesicles defined by a lipid bilayer and continuously shed from the surfaces of both quiescent and stimulated cells. NVs are ubiquitous and were successfully isolated from all extracellular spaces in humans. Initially, NVs were considered to be cell debris of no biological significance, intended for clearance and disposal by phagocytes. Over the past 30 years, however, it became increasingly evident that NVs take part in a unique and versatile form of intercellular communication. To overlook the rapid advances in our understanding of NV biology, an International Society of Extracellular Vesicles was founded in 2011.

NVs convey intercellular signals either by the surface interactions (cell–NV contact) or by the transfer of surface molecules and intravesicular content, such as mRNA, micro-RNA, proteins, lipids, and metabolites. The biological effects of NVs depend on the cell of origin, the nature of the stimulus that triggered their release and the compartment they were released into. Aside from intercellular communication, the shedding of NVs allows parent and target cells to rapidly lose or gain a particular surface phenotype. NVs can be targeted to specific cells. Given that they encapsulate a multitude of extra- and intravesicular signaling cues, their uptake can lead to global cellular reprogramming. The paracrine, endocrine, hemostatic, immune, and inflammatory functions of NV have been shown in multiple studies [1,2]. Apart from their physiological role, the clinical significance of NVs lies in their potential to serve as a diagnostic or prognostic marker of disease and, possibly, a platform for the development of semisynthetic nanovesicles. Thanks to their nanoscale size and the potential to express targeting ligands, native exosomes or semisynthetic vesicles have potential for nanomedical applications.

*Nanoscience and Nanotechnology for Human Health,* First Edition. Edited by Bert Müller and Marcel Van de Voorde.

In this chapter, we discuss the role of NVs in inflammation and coagulation, provide representative examples of their biological function and place them in clinical context. Specifically, we focus on (i) immune-modulatory function of neutrophil NVs (PMN-NVs) released in gout, (ii) the proinflammatory effects of erythrocyte NVs (RBC-NVs), which accumulate during RBC storage, and iii) the induction of the clotting cascade by the inadvertent release of platelet NVs (PLT-NVs) during therapeutic T-cell depletion in kidney transplantation.

## 6.2 Nomenclature and Definition

Nanosized vesicles perform a wide range of physiological tasks. They are heterogeneous with no distinctive structural features, uniform size, or phenotypic traits and vary significantly only in their mechanism of release and action. Aside from being smaller then 1 μm and enclosed by a double membrane, they have little in common. It is, therefore, understandable why a comprehensive functional definition and nomenclature still remains elusive. Over the past 30 years, with each new discovery multiple names for each vesicle subgroup were given, always with emphasis on their size (microparticles, microvesicles, and nanovesicles), their possible function (such as calcifying matrix for bone formation), tissue of origin (e.g., proteasome from the prostate), or their mode of formation (preformed: exosomes, versus budding and shedding from the cell surface: ectosomes), cf. Table 6.1 [1]. Although the distinction based on the mechanism of release

**Table 6.1** Overview of the biophysical properties of nanovesicles.

| Features | Exosomes | Ectosomes | Apoptotic vesicles |
|---|---|---|---|
| Size | 30–100 nm | 100–500 nm | 200–1000 nm |
| Buoyant density | 1.13–1.19 g/ml | ND | 1.16–1.28 g/ml |
| Electron microscopy | Cup shaped | Bilamellar round structures | Heterogeneous |
| Sedimentation | 100 000 g | 10 000 g | 1200–100 000 g |
| Lipid composition | Cholesterol<br>sphingomyelin<br>ceramide<br>PS | Cholesterol<br>DAG<br>PS | Heterogeneous |
| Main protein markers | Tetraspanins (CD63 CD9)<br>Alix<br>TSg101<br>FLOT1<br>TNFAR1 | CR1<br>Proteolytic enzymes<br>No CD63 | Histones |
| Intracellular origin | Multivesicular bodies | Plasma membrane | Plasma membrane |
| Type of generation | Constitutive | Cell regulated | Cell death |

has functional consequences, it is often difficult to differentiate between these two types of vesicle formation, when studying vesicles *in vivo*. The professional society, which is devoted to the field, decided to name itself the International Society for Extracellular Vesicles with a corresponding journal. Extracellular Vesicle (EV) is possibly a reasonable terminology for a biological reality that has no defined ends to date.

Due to the current limitations in vesicle isolation and analysis, the morphological definition of a nanovesicle as a spherical, double membrane, and submicron-sized vesicle seems to be most accurate and inclusive. Given that most vesicles range from 30 to 500 nm, the field should, however, adopt the more accurate *nano* terminology. All microvesicles should be called nanovesicles.

## 6.3
## Stimulus for Vesicle Release

The process of ectocytosis was first defined by Stein and Luzio in 1991, as the shedding of NVs from the surface of neutrophils during sublytic complement attack [3]. Since then, this form of NV release was consistently observed in erythrocytes [4], neutrophils [5], and platelets [6]. Given that NVs released by cells under complement attack are enriched in C5b–C9 (assembled lytic complex made of complement factors), ectocytosis is potentially a self-preserving mechanism, which allows cells to evade and survive complement attack by selectively shedding C5b–C9 in the form of NVs. Interestingly, vesicle release occurs in erythrocytes and platelets, which lack complex organelles and subcellular structures [4] (see Figure 6.1).

The C5b–C9 complex introduces a pore in the cell membrane and initiates flux of ions between the intra- and extracellular compartments. The influx of $Ca^{2+}$ in the vicinity of the C5b–C9 complex induces local ectocytosis. This involves lateral and vertical redistribution of plasma membrane constituents and depolymerization of cytoskeleton ultimately resulting in the budding of a vesicle and expulsion of C5b–C9. As a result of lipid redistribution, the outer membrane of ectosomes is enriched in phosphatidylserine, sphingomyelin, and cholesterol. The sorting of proteins does not show a consistent pattern and is cell specific.

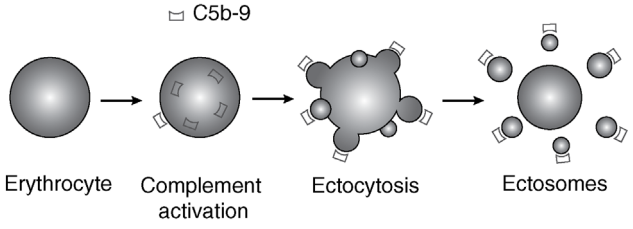


**Figure 6.1** Release of erythrocyte NV during sublytic complement attack.

Ectosome release is frequently associated with activation of complement, but complement is not the only trigger for vesicle release. Recently, T cells stimulated by a cognate antigen were shown to release NVs carrying the TCR. Subsequently, this NV-bound *soluble* TCR was able to engage with the antigen–MHC complex, form a functional immunological synapse, and deliver stimulatory signals to antigen presenting cells independent of the parent T cell [7].

The release of exosomes was first described in the 1980s by the group of R. Johnstone in reticulocytes as a mechanism that allowed the specific elimination of transferrin receptors [8,9]. At the same time, many other researchers described spontaneous release of vesicles from tumor cells in culture and could demonstrate a similar mechanism of formation and release [10]. Cancer cells frequently evade immunological surveillance or promote metastasis by releasing exosomes. Recently, exosomes derived from breast cancer cells were shown to induce malignant transformation in nontumorogenic epithelial cells by reprograming the target cell transcriptome with miRNA. The transfer of miRNA between malignant cells and cells of the immune system has widespread implications in cancer immunology.

Over the years, it became increasingly clear that vesicle release is a conserved mechanism across all cells, albeit serving different purposes. NVs are released even by prokaryotes. Bacteria can transmit virulence factors from one bacterium to another by shedding outer membrane vesicles (OMVs) [11–13]. In addition to DNA and RNA, these OMVs contain various other bacterial cell wall components [14]. This can be potentially exploited to develop vaccines once OMVs have been rid of all their infectious or toxic potential [15].

Many excellent reviews describe the field in depth from different perspectives [16–21]. We provide an overview about the physiological role such EVs may play and provide some examples looking at specific pathologies, where EVs may play a significant role.

## 6.4 Overview of Extracellular Vesicle Biology

For years, the release of NVs by living cells has been considered a mechanism to dispose of unnecessary or damaged intracellular or membrane-bound molecules. In addition to this, the release of *microparticles* by activated platelets was found to participate in hemostasis. This finding suggested that vesicles were not just *cell debris* but may be essential for various biological functions and responsible for specific pathologies. Indeed, in recent years, it became clear that vesicles from various sources play an important role in inflammation, hemostasis, and cell death. Consequently, the focus in the field shifted from the cellular housekeeping functions of NVs to assessing their wider pathophysiological significance in disease.

A typical example is bone formation. The process of calcification occurs in the so-called *matrix vesicles* that bud off the plasma membrane of osteoblasts and chondrocytes. Phosphatidylserine (PS) has a high affinity for calcium, and the PS–calcium complex along with phosphates nucleates to form hydroxyapatite crystals, which are essential for mineral formation on extracellular collagen fibers [22]. Without matrix vesicles, we would have soft bones and teeth. Pathological ectopic calcification occurs in many diseases including arteriosclerosis. Here, local cells such as pericytes and endothelial cells undergo oesteoblastic differentiation and initiate the process of calcification.

Urine is known to contain large quantities of NVs. Many research groups are trying to identify their exact origin within the nephron, [23,24]. The use of NVs as biomarkers for glomerular and tubular diseases is an attractive proposition, but it still remains elusive. Although to this point no function has been attributed to urinary NVs, one might postulate that they act as trophic factors for lower parts of the nephron/urinary tract or act as an antibacterial shield.

NVs released by dendritic cells might induce efficient T-cell immune response when loaded with a cognate antigen. Indeed, they may present arrays of particulate antigens in addition to helper molecules enhancing the interaction and activation of immune cells [25,26]. NVs shed by tumor cells have been shown to transfer specific antigens to dendritic cells, which could potentially induce a tumor-specific T-cell immune response [27]. This led to much enthusiasm among immunologists and oncologists initially. Later, however, it became increasingly evident that tumors exploit NVs to inhibit inflammation and the immune response by various mechanisms including the expression of specific immune inhibitors blocking NK cells or, less specifically, by the expression of PS, a molecule known to inhibit macrophage and dendritic cell activation [10,28]. Despite this, could NVs be modified and used to vaccinate against tumor? The concept would be that only foreign or modified autoantigens would be recognized by the immune system. A future avenue would be to produce NVs expressing specific tumor neoantigens, that is, modified protein sequences expressed from mutated genes of tumor cells, with surface proteins that enhance the immune response or block inhibitory signals, for example, CTLA-4 or PD-1 blockade [28]. Finally, NV must be able to circulate in the body and reach distant immune territories responsible for the immune response, for example, lymph nodes and spleen. Whether the immune-modulation by NV can aid in clearing tumors in humans remains to be established; however, findings in animal models would suggest that this is possible, and the recent data in melanoma patients are encouraging [29].

Erythrocytes, leukocytes, platelets, and endothelial cells release NVs in blood, even under normal conditions. However, the different leukocytes release NVs mainly in the extravascular compartment particularly at local inflammatory sites in tissues after having actively left the blood circulation. Let us illustrate in more detail the role of NVs of three origins, that is, polymorphonuclear(PMN) leukocytes, erythrocytes, and platelets in human pathologies.

## 6.5 NVs of Polymorphonuclear Leukocytes

Similar to other NVs, PMN-NVs were initially described as a means by which PMN leukocytes confer resistance to a complement attack by expelling C5b–C9 complexes by ectocytosis of vesicles. The shedding of vesicles has later been identified as a generalized phenomenon of neutrophil activation independent of the complement system. The soluble C5a complement factor and bacterial peptide fMLP are known to induce one of the strongest shedding responses in neutrophils [30]. Regardless of stimuli, the release of PMN-NVs is actually triggered by transient influx of $Ca^{2+}$ into the cells and is closely related to the redistribution of phospholipids across plasma membrane. In the quiescent cell, phosphatidylserine (PS) is actively translocated into the cytosolic leaflet of the plasma membrane by an enzyme called flippase [31]. Upon activation, the influx of $Ca^{2+}$ activates a lipid scramblase and inhibits flippase promoting the translocation of PS to the outer leaflet. The change in lipid distribution is followed by the release of PMN-NVs from the surface of cells and consequently PMN-NVs express PS on their surface. The expression of PS on PMN-NVs remains stable, since unlike cells, NVs lack the resources/energy to reestablish the asymmetrical distribution of lipids. The expression of PS on PMN-NVs is of great functional importance.

PMN-NVs are known to be anti-inflammatory and achieve their immunosuppressive effects by employing several independent mechanisms. First, PMN-NVs actively recruit annexin A1, a PS-binding protein in plasma, to their surface. Annexin A1 subsequently impairs the transmigration of circulating neutrophils in response to IL-1beta by inhibiting the interactions between neutrophil and endothelial cells [32]. Second, PMN-NVs deliver and induce the release of pro-resolving lipid mediators from macrophages termed resolvins, which reprogram antigen presenting cells to an anti-inflammatory phenotype [33]. Third, PMN-NVs express PS. PS is known to engage various receptors, including the MerTK (Mer receptor tyrosine kinase), which inhibits inflammatory responses to TLR ligands in macrophages and dendritic cells [34]. Similar response has been observed for other PS-expressing NVs or apoptotic cells [2,35,36]. Lastly, in addition to PS, PMN-NVs foster these anti-inflammatory effects by inducing the release of TGFβ in target cells. The release of TGFβ is independent of PS and relies on another membrane component of the PMN-NVs that has not yet been identified [37,38]. The relative contribution for all these mechanisms *in vivo* remains unknown.

The clinical relevance of PMN-NVs lies in their profound ability to suppress inflammation early on in its course. This mechanism is particularly effective in peripheral tissues with extensive complement activation, which induces neutrophil influx and NV release. Therefore, in conditions such as gout, large amounts of PMN-NVs are found in the synovial fluid of patients at the time of an acute attack. Interestingly, gouty attacks tend to resolve spontaneously and leave minimal residual damage to the joint. It has been recently shown that the release of

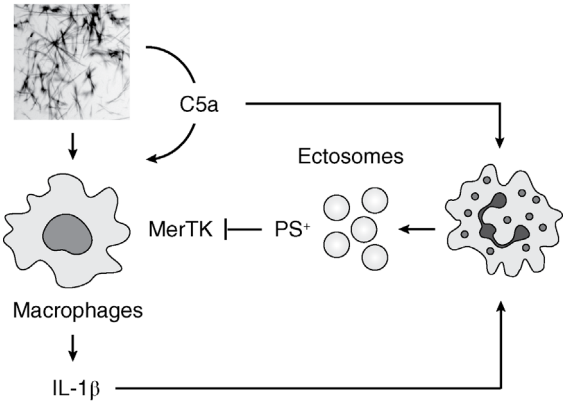


**Figure 6.2** Neutrophil NV limit inflammation in gout by inhibiting C5a priming of the inflammasome.

PMN-NVs contributes to this self-limiting nature of gout [39]. In gout, monosodium urate (MSU) crystals precipitate in joints and activate complement leading to the generation of C5a. This highly active chemotactic and anaphylatoxic factor primes the resident cells for the release of IL-1β [40], which is the principal cytokine driving gouty inflammation [41]. Although C5a drives the pro-inflammatory response, it can also trigger the release of PMN-NV, which contain inflammation and initiate is timely resolution [39]. The release of PMN-NVs completes what essentially is an internal regulatory mechanism in gout, where C5a simultaneously induces and resolves inflammation, see Figure 6.2. In a broader context, PMN-NV release may limit excessive inflammation in response to both exogenous and endogenous danger signals. The pathophysiological relevance of PMN-NVs likely extends to conditions other than gout. It is remarkable that the cells, which frequently cause tissue damage in attempt to fight off bacterial infections, responsibly release signals that limit excessive inflammation in the early stages of their activation anticipating the need for effective counterregulation.

## 6.6 Erythrocyte NVs

Erythrocytes can be stored up to 42 days before transfused according to most regulatory authorities. During this period of time, although erythrocytes remain stable, they are known to undergo an aging process, which involves the release of NVs by ectocytosis [42,43]. In fact, erythrocytes lose up to 20% of their hemoglobin content in the form of erythrocyte NVs during storage and these vesicles are given in significant amounts to patients along with erythrocytes at the time of transfusion. Evidently, the number of these NVs increases with storage time. Over the past few years, there have been several works reporting that when

transfused, older stored, compared to fresh, erythrocytes may have detrimental effects with a higher frequency of clotting disorders and increased morbidity and mortality in patients [44–47]. However, the issue remains controversial, since various other studies did not show significant differences [48,49]. Erythrocyte NVs are formed in blood or provided during erythrocyte transfusion, thus are mainly in the circulation as opposed to those of PMN-NVs, which are mainly found in tissues. Exposed to plasma containing annexins and platelets, the anti-inflammatory properties of erythrocyte NVs due to the expression of PS may play a minor role in the acute phase of transfusion [38]. It is known that PS surfaces initiate coagulation with PS serving as a platform for thrombin generation [50]. In addition, erythrocyte NVs bind complement fragments suggesting that they activate complement as well [38].

In a murine transfusion model, erythrocyte NVs purified from stored cells amplified systemic inflammation in endotoxemic mice. As expected, transfusion of erythrocyte NVs led to the generation of thrombin. The clotting phenomenon, however, was not the primary pathology. Thrombin induced by erythrocyte NVs acted as a direct complement C5 splitting agent and released C5a, a factor known to aggravate systemic inflammation and produce leukocyte aggregation in the lungs. The specific sequence of events demonstrated the complex interplay between the coagulation and the complement systems, which are too often looked at as separate entities. Consequently, the treatment of mice with a thrombin anticoagulant, such as lepirudin, prior to transfusion, alleviated the proinflammatory effects of transfusions by suppressing systemic C5a generation [51], see Figure 6.3. Although such an approach could be tested in more animal models, it would be difficult to translate even positive findings to human pathologies, since transfusions are mostly required for bleeding patients, in whom anticoagulation is not indicated.

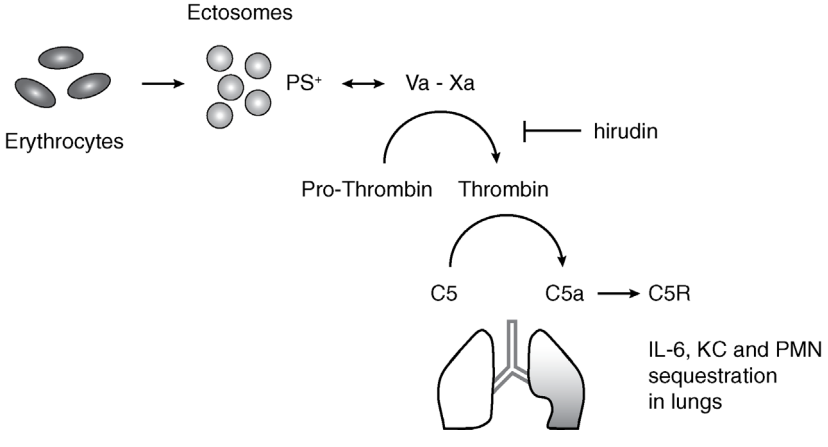


**Figure 6.3** The transfusion of erythrocyte NV triggers the sequential activation of the clotting and complement cascades, which amplify systemic inflammation.

The anti-inflammatory and immunosuppressive properties of erythrocytes toward activated macrophages and dendritic cells are due to the expression of PS as well [38]. It is unclear how these NVs, which are rapidly cleared from the circulation by Kupffer cells, would react and affect other cells. Some publications suggested that aged erythrocytes accelerate the development of tumors, that is, erythrocyte transfusion as such, all transfusion or erythrocytes include a variable load of NVs, reduce the survival in patients with colon carcinoma [52,53]. Although it is difficult to establish a direct link between erythrocyte NV transfusion and tumor development, the speed of tumor growth is likely to indirectly correlate with the immune competence.

## 6.7 Platelet NVs

Platelet NVs are released by activated platelets and constitute the dominant population of circulating NVs in humans [54]. The origin, quality, and properties of platelet NVs may differ depending on the stress, to which they are exposed. For instance, platelets simply stored prior to transfusion shed homogeneous NVs, which differ from those induced by strong activators such as complement. NVs released by activated platelets support hemostasis by generating thrombin on their negatively charged PS expressing surface. Early studies demonstrated that NV depletion prolonged the clotting time of human plasma and that activated platelets generated MV capable of activating thrombin in platelet-poor plasma. Patients with Scott syndrome can illustrate the functional significance of PS and platelet NV release for efficient clotting. These patients have a primary bleeding disorder caused by the inability of platelets to translocate PS to the outer leaflet of their plasma membrane. The budding of NVs is reduced as well [55,56].

The release of platelet NVs is induced by platelet stimuli such as thrombin or ADP. The shedding of NVs is, however, much stronger during complement activation on the surface of platelets. Platelets exposed to sublytic concentration of C5b–C9 were shown to release large amounts of small membrane vesicles capable of binding clotting factors and assembling the prothrombinase enzyme complex. This form of platelet activation may be relevant not only in idiopathic thrombocytopenic purpura (ITP), an autoimmune condition with antibodies against platelet surface antigens that initiates classical complement pathway activation and C5b–C9 deposition [57], but also during T-cell depletion therapy with antithymoglobulin (ATG), which cross-react with platelet antigens [58]. ATGs are T-cell depleting antibodies used for hematopoietic stem cell and solid organ transplant patients to prevent graft versus host disease (GvHD). Although designed to target T cell, ATG recognizes a wide range of epitopes, including those present on platelets. Consequently, the rapid infusion of ATGs triggers massive release of platelet NVs and frequently cause side effects associated with the overt activation of the clotting system called disseminated intravascular coagulopathy, which is mostly subclinical [59–61]. The release of NVs by platelets

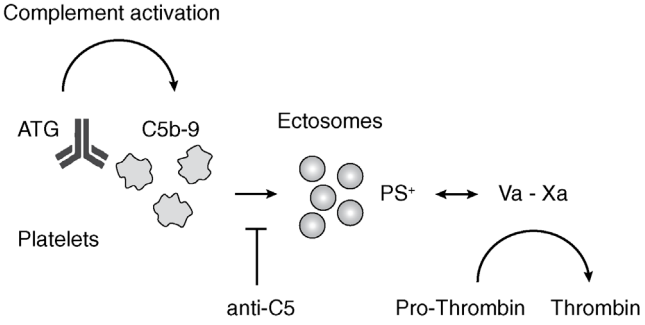


**Figure 6.4** Platelet NVs, induced by antithymoglobulins and complement, lead to a state of hypercoagulability.

exposed to ATGs in plasma is mainly due to complement activation with the binding of C5b–C9 to the platelet membrane leading to ectocytosis. Given that platelet NV release relied on complement activation, the use of a monoclonal anti-C5 antibody may prove to be beneficial in preventing thrombotic complications during ATG therapy, see Figure 6.4 [62].

All remains a question of balance. Although platelet NVs induce thrombosis, when they accumulate beyond a certain threshold, during physiological steady state PS on NVs might be responsible for baseline immune modulation. *In vitro*, platelet NVs have been shown to downregulate activated macrophages and modify the development of dendritic cells [36]. In addition, they foster the differentiation of CD4+ T cells into functional T regulatory cells, well known to control immunity [63]. These observations suggest that a continuous low level of platelet NVs represents a mechanism of inflammatory control and peripheral tolerance to low danger signals but evidently only up to a given threshold.

## 6.8 Conclusions

A complete overview of all functions of NVs found in humans would require a complete book for itself. Indeed, the field is exploding. We are only at the beginning of understanding when and how they are produced and what their functions are. It is worth emphasizing that communication between cells via NVs has over years been ignored, but it is now at the forefront. Indeed, a full organism needs constant regulation and for this makes sure that communication occurs at all levels: directly by cell–cell contact, by fluid phase molecules (proteins, lipids, metabolites, etc.) that can travel at a distance, *and* by NVs that not only travel at a distance but also expose surfaces and may serve as containers for transferring molecules (e.g., RNA) that would not resist the harsh enzymatic environment of the extracellular space. Looking at NVs from this angle, it is evident that much has still to be discovered as recently illustrated in the finding

of NVs with ectosomal properties in the immunological synapse [7]. It is also to be expected that anomalies in the formation, release, or content of NVs will be responsible for pathologies as indicated by the scott syndrome.

**Acknowledgment**

The Swiss National Science Foundation has supported the authors' work described in this review.

**References**

1 Théry, C., Ostrowski, M., and Segura, E. (2009) Membrane vesicles as conveyors of immune responses. *Nat. Rev. Immunol.*, **9** (8), 581–593.
2 Frey, B. and Gaipl, U.S. (2011) The immune functions of phosphatidylserine in membranes of dying cells and microvesicles. *Semin. Immunopathol.*, **33** (5), 497–516.
3 Stein, J.M. and Luzio, J.P. (1991) Ectocytosis caused by sublytic autologous complement attack on human neutrophils. The sorting of endogenous plasma-membrane proteins and lipids into shed vesicles. *Biochem. J.*, **274** (Pt 2), 381–386.
4 Iida, K., Whitlow, M.B., and Nussenzweig, V. (1991) Membrane vesiculation protects erythrocytes from destruction by complement. *J. Immunol.*, **147** (8), 2638–2642.
5 Morgan, B.P., Dankert, J.R., and Esser, A.F. (1987) Recovery of human neutrophils from complement attack: removal of the membrane attack complex by endocytosis and exocytosis. *J. Immunol.*, **138** (1), 246–253.
6 Sims, P.J., Faioni, E.M., Wiedmer, T., and Shattil, S.J. (1988) Complement proteins C5b-9 cause release of membrane vesicles from the platelet surface that are enriched in the membrane receptor for coagulation factor $V_a$ and express prothrombinase activity. *J. Biol. Chem.*, **263** (34), 18205–18212.
7 Choudhuri, K., Llodra, J., Roth, E.W., Tsai, J., Gordo, S., Wucherpfennig, K.W. *et al.* (2014) Polarized release of T-cell-receptor-enriched microvesicles at the immunological synapse. *Nature*, **507** (7490), 118–123.
8 Pan, B.T. and Johnstone, R.M. (1983) Fate of the transferrin receptor during maturation of sheep reticulocytes *in vitro*: selective externalization of the receptor. *Cell.*, **33** (3), 967–978.
9 Johnstone, R.M., Adam, M., Hammond, J.R., Orr, L., and Turbide, C. (1987) Vesicle formation during reticulocyte maturation. Association of plasma membrane activities with released vesicles (exosomes). *J. Biol. Chem.*, **262** (19), 9412–9420.
10 Taylor, D.D. and Gercel-Taylor, C. (2011) Exosomes/microvesicles: mediators of cancer-associated immunosuppressive microenvironments. *Semin. Immunopathol.*, **33** (5), 441–454.
11 Kulkarni, H.M. and Jagannadham, M.V. (2014) Biogenesis and multifaceted roles of outer membrane vesicles from Gram-negative bacteria. *Microbiology.*, **160** (Pt 10), 2109–2121.
12 Jager, J., Keese, S., Roessle, M., Steinert, M., and Schromm, A.B. (2014) Fusion of *Legionella pneumophila* outer membrane vesicles with eukaryotic membrane systems is a mechanism to deliver pathogen factors to host cell membranes. *Cell Microbiol.*, **17** (5), 607–620.
13 Unal, C.M., Schaar, V., and Riesbeck, K. (2011) Bacterial outer membrane vesicles in disease and preventive medicine. *Semin. Immunopathol.*, **33** (5), 395–408.
14 Ghosal, A., Upadhyaya, B.B., Fritz, J.V., Heintz-Buschart, A., Desai, M.S., Yusuf, D. *et al.* (2015) The extracellular RNA

complement of *Escherichia col. Microbiologyopen*, **4** (2): 252–266.
15 Acevedo, R., Fernandez, S., Zayas, C., Acosta, A., Sarmiento, M.E., Ferro, V.A. *et al.* (2014) Bacterial outer membrane vesicles and vaccine applications. *Front. Immunol.*, **5**, 121.
16 Lai, F.W., Lichty, B.D., and Bowdish, D.M. (2015) Microvesicles: ubiquitous contributors to infection and immunity. *J. Leukoc. Biol.*, **97** (2), 237–245.
17 Jaiswal, R., Raymond Grau, G.E., and Bebawy, M. (2014) Cellular communication via microparticles: role in transfer of multidrug resistance in cancer. *Future Oncol.*, **10** (4), 655–669.
18 Loyer, X., Vion, A.C., Tedgui, A., and Boulanger, C.M. (2014) Microvesicles as cell–cell messengers in cardiovascular diseases. *Circ. Res.*, **114** (2), 345–353.
19 Kittel, A., Falus, A., and Buzas, E. (2013) Microencapsulation technology by nature: cell derived extracellular vesicles with therapeutic potential. *Eur. J. Microbiol. Immunol. (Bp).*, **3** (2), 91–96.
20 van der Pol, E., Coumans, F., Varga, Z., Krumrey, M., and Nieuwland, R. (2013) Innovation in detection of microparticles and exosomes. *J. Thromb. Haemost.*, **11** (Suppl 1), 36–45.
21 Colombo, M., Raposo, G., and Thery, C. (2014) Biogenesis, secretion, and intercellular interactions of exosomes and other extracellular vesicles. *Annu. Rev. Cell Dev. Biol.*, **30**, 255–289.
22 Golub, E.E. (2011) Biomineralization and matrix vesicles in biology and pathology. *Semin. Immunopathol.*, **33** (5), 409–417.
23 Salih, M., Zietse, R., and Hoorn, E.J. (2014) Urinary extracellular vesicles and the kidney: biomarkers and beyond. *Am. J. Physiol. Renal Physiol.*, **306** (11), F1251–1259.
24 Pascual, M., Steiger, G., Sadallah, S., Paccaud, J.P., Carpentier, J.L., James, R. *et al.* (1994) Identification of membrane-bound CR1 (CD35) in human urine: evidence for its release by glomerular podocytes. *J. Exp. Med.*, **179** (3), 889–899.
25 Zitvogel, L., Regnault, A., Lozier, A., Wolfers, J., Flament, C., Tenza, D. *et al.* (1998) Eradication of established murine tumors using a novel cell-free vaccine: dendritic cell-derived exosomes. *Nat. Med.*, **4** (5), 594–600.
26 Pitt, J.M., Charrier, M., Viaud, S., Andre, F., Besse, B., Chaput, N. *et al.* (2014) Dendritic cell-derived exosomes as immunotherapies in the fight against cancer. *J. Immunol.*, **193** (3), 1006–1011.
27 Wolfers, J., Lozier, A., Raposo, G., Regnault, A., Thery, C., Masurier, C. *et al.* (2001) Tumor-derived exosomes are a source of shared tumor rejection antigens for CTL cross-priming. *Nat. Med.*, **7** (3), 297–303.
28 Snyder, A., Makarov, V., Merghoub, T., Yuan, J., Zaretsky, J.M., Desrichard, A. *et al.* (2014) Genetic basis for clinical response to CTLA-4 blockade in melanoma. *N. Engl. J. Med.*, **371** (23), 2189–2199.
29 Sznol, M. and Longo, D.L. (2015) Release the hounds! Activating the T-cell response to cancer. *N. Engl. J. Med.*, **372** (4), 374–375.
30 Hess, C., Sadallah, S., Hefti, A., Landmann, R., and Schifferli, J.A. (1999) Ectosomes released by human neutrophils are specialized functional units. *J. Immunol.*, **163** (8), 4564–4573.
31 Hankins, H.M., Baldridge, R.D., Xu, P., and Graham, T.R. (2015) Role of flippases, scramblases and transfer proteins in phosphatidylserine subcellular distribution. *Traffic*, **16** (1), 35–47.
32 Dalli, J., Norling, L.V., Renshaw, D., Cooper, D., Leung, K.Y., and Perretti, M. (2008) Annexin 1 mediates the rapid anti-inflammatory effects of neutrophil-derived microparticles. *Blood.*, **112** (6), 2512–2519.
33 Dalli, J. and Serhan, C.N. (2012) Specific lipid mediator signatures of human phagocytes: microparticles stimulate macrophage efferocytosis and pro-resolving mediators. *Blood.*, **120** (15), e60–72.
34 Eken, C., Martin, P.J., Sadallah, S., Treves, S., Schaller, M., and Schifferli, J.A. (2010) Ectosomes released by polymorphonuclear neutrophils induce a MerTK-dependent anti-inflammatory pathway in macrophages. *J. Biol. Chem.*, **285** (51), 39914–39921.
35 Gasser, O. and Schifferli, J.A. (2004) Activated polymorphonuclear neutrophils

disseminate anti-inflammatory microparticles by ectocytosis. *Blood.*, **104** (8), 2543–2548.

36 Eken, C., Gasser, O., Zenhaeusern, G., Oehri, I., Hess, C., and Schifferli, J.A. (2008) Polymorphonuclear neutrophil-derived ectosomes interfere with the maturation of monocyte-derived dendritic cells. *J. Immunol.*, **180** (2), 817–824.

37 Eken, C., Sadallah, S., Martin, P.J., Treves, S., and Schifferli, J.A. (2013) Ectosomes of polymorphonuclear neutrophils activate multiple signaling pathways in macrophages. *Immunobiology*, **218** (3), 382–392.

38 Sadallah, S., Eken, C., and Schifferli, J.A. (2008) Erythrocyte-derived ectosomes have immunosuppressive properties. *J. Leukoc. Biol.*, **84** (5), 1316–1325.

39 Cumpelik, A., Ankli, B., Zecher, D., and Schifferli, J.A. (2015) Neutrophil microvesicles resolve gout by inhibiting C5a-mediated priming of the inflammasome. *Ann. Rheum. Dis.*, **75** (6): 1236–45.

40 An, L.L., Mehta, P., Xu, L., Turman, S., Reimer, T., Naiman, B. *et al.* (2014) Complement C5a potentiates uric acid crystal-induced IL-1β production. *Eur. J. Immunol.*, **44** (12), 3669–3679.

41 Martinon, F., Pétrilli, V., Mayor, A., Tardivel, A., and Tschopp, J. (2006) Gout-associated uric acid crystals activate the NALP3 inflammasome. *Nature*, **440** (7081), 237–241.

42 Lutz, H.U., Liu, S.C., and Palek, J. (1977) Release of spectrin-free vesicles from human erythrocytes during ATP depletion. I. Characterization of spectrin-free vesicles. *J. Cell Biol.*, **73** (3), 548–560.

43 Pascual, M., Lutz, H.U., Steiger, G., Stammler, P., and Schifferli, J.A. (1993) Release of vesicles enriched in complement receptor 1 from human erythrocytes. *J. Immunol.*, **151** (1), 397–404.

44 Spinella, P.C., Carroll, C.L., Staff, I., Gross, R., Mc Quay, J., Keibel, L. *et al.* (2009) Duration of red blood cell storage is associated with increased incidence of deep vein thrombosis and in hospital mortality in patients with traumatic injuries. *Crit. Care*, **13** (5), R151.

45 Hendrickson, J.E., Shaz, B.H., Pereira, G., Atkins, E., Johnson, K.K., Bao, G. *et al.* (2012) Coagulopathy is prevalent and associated with adverse outcomes in transfused pediatric trauma patients. *J. Pediatr.*, **160** (2), 204–209 e203.

46 Koch, C.G., Li, L., Sessler, D.I., Figueroa, P., Hoeltge, G.A., Mihaljevic, T. *et al.* (2008) Duration of red-cell storage and complications after cardiac surgery. *N. Engl. J. Med.*, **358** (12), 1229–1239.

47 Wang, D., Sun, J., Solomon, S.B., Klein, H.G., and Natanson, C. (2012) Transfusion of older stored blood and risk of death: a meta-analysis. *Transfusion*, **52** (6), 1184–1195.

48 Edgren, G., Kamper-Jorgensen, M., Eloranta, S., Rostgaard, K., Custer, B., Ullum, H. *et al.* (2010) Duration of red blood cell storage and survival of transfused patients (CME). *Transfusion*, **50** (6), 1185–1195.

49 van de Watering, L., Biomedical Excellence for Safer Transfusion (BEST) Colloborative (2011) Pitfalls in the current published observational literature on the effects of red blood cell storage. *Transfusion*, **51** (8), 1847–1854.

50 Sweeney, J., Kouttab, N., and Kurtis, J. (2009) Stored red blood cell supernatant facilitates thrombin generation. *Transfusion*, **49** (8), 1569–1579.

51 Zecher, D., Cumpelik, A., and Schifferli, J.A. (2014) Erythrocyte-derived microvesicles amplify systemic inflammation by thrombin-dependent activation of complement. *Arterioscler. Thromb. Vasc. Biol.*, **34** (2), 313–320.

52 Atzil, S., Arad, M., Glasner, A., Abiri, N., Avraham, R., Greenfeld, K. *et al.* (2008) Blood transfusion promotes cancer progression: a critical role for aged erythrocytes. *Anesthesiology*, **109** (6), 989–997.

53 Jensen, L.S., Puho, E., Pedersen, L., Mortensen, F.V., and Sorensen, H.T. (2005) Long-term survival after colorectal surgery associated with buffy-coat-poor and leucocyte-depleted blood transfusion: a follow-up study. *Lancet*, **365** (9460), 681–682.

54 Aatonen, M., Gronholm, M., and Siljander, P.R. (2012) Platelet-derived microvesicles: multitalented participants in intercellular

communication. *Semin. Thromb. Hemost.*, **38** (1), 102–113.

55 Zwaal, R.F., Comfurius, P., and Bevers, E.M. (2004) Scott syndrome, a bleeding disorder caused by defective scrambling of membrane phospholipids. *Biochim. Biophys. Acta*, **1636** (2–3), 119–128.

56 Kodigepalli, K.M., Bowers, K., Sharp, A., and Nanjundan, M. (2015) Roles and regulation of phospholipid scramblases. *FEBS Lett.*, **589** (1), 3–14.

57 Najaoui, A., Bakchoul, T., Stoy, J., Bein, G., Rummel, M.J., Santoso, S. *et al.* (2012) Autoantibody-mediated complement activation on platelets is a common finding in patients with immune thrombocytopenic purpura (ITP). *Eur. J. Haematol.*, **88** (2), 167–174.

58 Beiras-Fernandez, A., Walther, S., Muenzing, S., Thein, E., and Hammer, C. (2004) *In vitro* assessment of dose-dependent platelet activation by polyclonal antithymocyte globulins: a flow-cytometric analysis. *Transplantation*, **78** (5), 751–754.

59 Trivedi, H.S., Lal, S.M., Gupta, N., and Ross, G., Jr. (1996) ATGAM associated coagulopathy in renal transplant patients: a report of two unusual cases. *Int. J. Artif. Organs*, **19** (8), 448–450.

60 Taylor, F.B., Jr., Toh, C.H., Hoots, W.K., Wada, H., Levi, M., and Scientific Subcommittee on Disseminated Intravascular Coagulation of the International Society on Thrombosis and Haemostasis (ISTH) (2001) Towards definition, clinical and laboratory criteria, and a scoring system for disseminated intravascular coagulation. *Thromb. Haemost.*, **86** (5), 1327–1330.

61 Inbal, A., Lubetsky, A., Shimoni, A., Dardik, R., Sela, B.A., Eskaraev, R. *et al.* (2004) Assessment of the coagulation profile in hemato-oncological patients receiving ATG-based conditioning treatment for allogeneic stem cell transplantation. *Bone Marrow Transplant.*, **34** (5), 459–463.

62 Cumpelik, A., Gerossier, E., Jin, J., Tsakiris, D., Dickenmann, M., Sadallah, S. *et al.* (2015) Mechanism of platelet activation and hypercoagulability by antithymocyte globulins (ATG). *Am. J. Transplant.*, **15**, 2588–2601.

63 Sadallah, S., Amicarella, F., Eken, C., Iezzi, G., and Schifferli, J.A. (2014) Ectosomes released by platelets induce differentiation of CD4+T cells into T regulatory cells. *Thromb. Haemost.*, **112** (6), 1219–1229.

# 7
# Challenges and Risks of Nanotechnology in Medicine: An Immunologist's Point of View

*János Szebeni*

*Semmelweis University & SeroScience Ltd, Nanomedicine Research and Education Center, Nagyvárad tér 4, Budapest 1089, Hungary*

## 7.1
## Introduction

Nanomedicines are often recognized by the immune system as foreign, leading to immune reactivity upon *in vivo* use. While this reactivity may have adverse effects on both the nanomedicine and the host, for immunologists it opens a new horizon to novel and yet poorly understood immune phenomena. This chapter focuses on three ill-understood adverse immune reactions to nanomedicines, that is, the complement activation-related pseudoallergy (CARPA), the triggering of specific anti-drug antibody (ADA) formation (immunogenicity), and the accelerated blood clearance (ABC phenomenon). These phenomena represent major immune barriers to the clinical use of immune reactive nanomedicines, and, when they stimulate each other in a circle, called immune stimulatory vicious cycle (ISVC), they can underlie severe toxic phenomena. For these reasons, their understanding and prediction by various *in vitro* and *in vivo* tests is essential for the safety and clinical success of nanomedicines. The goal of this chapter is to summarize the essentials on these phenomena, their molecular and cellular mechanisms, and to review the state of the art in their laboratory evaluation and prediction.

Nanomedicine, that is, the utilization of nanotechnology in medicine, is one of the most promising and intensely developing fields in biological sciences today. One of its visions is to use drug delivery systems in the nanodimension ($10^{-9}$–$10^{-6}$ m, <100 nm in at least one direction) to selectively target only abnormal cells and organs, and, thus, avoid side effects. There are numerous ingenious nanocarriers in clinical development that achieve this goal, yet a lack of information on their toxicities and environmental impact still slows down their advance into the clinic. In particular, the enlarged surface area and increased tissue and cell penetration of nanoparticles may lend them unique, unpredictable toxicities,

*Nanoscience and Nanotechnology for Human Health,* First Edition. Edited by Bert Müller and Marcel Van de Voorde.

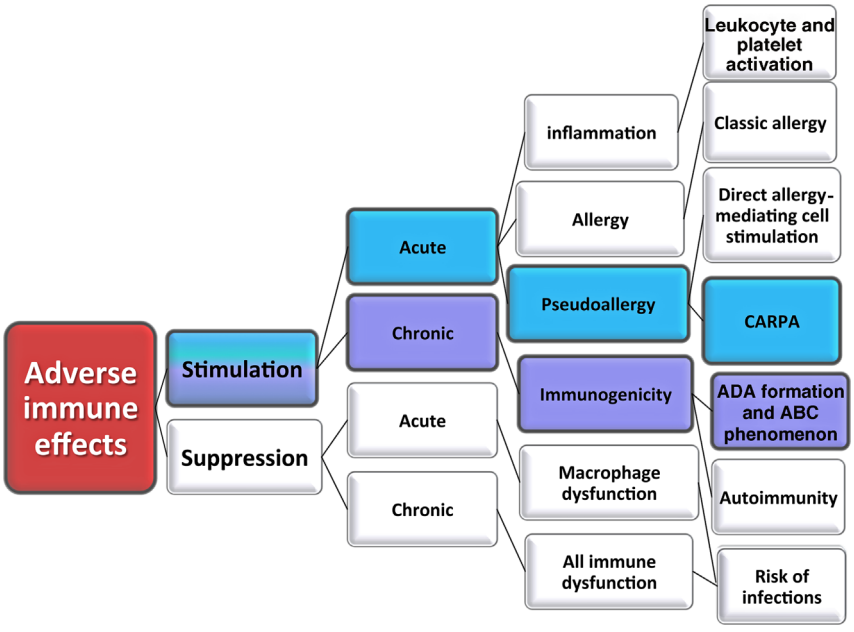


**Figure 7.1** Adverse immune effects of nanoparticles, classified according to their impact and time course. The pathways and side effects detailed in this chapter are shaded with color.

including novel yet poorly understood immune side effects [1,2]. Figure 7.1 categorizes the mentioned three adverse immune effects according to their impact and time course.

## 7.2 The Immune Stimulatory Vicious Cycle

Complement activation leading to CARPA, immunogenicity leading to ADA formation, and nanoparticle opsonization leading to the ABC phenomenon, each represents an abnormal immune activation that mutually accelerates each other in a vicious cycle, tentatively called immune stimulatory vicious cycle.

The different steps in ISCV are shown in Figure 7.2. These steps have been known for a long time and individually explored in substantial detail. It has also been recognized that C activation plays a causal role in ABC, that is, the abnormal pharmacokinetics of PEGylated liposomes [3–6]. Nevertheless, to the best knowledge of the author, the interdependence of these phenomena in a self-aggravating circular chain has not been emphasized to date. It should be added that the rate-limiting step in the cycle is immunogenicity, which takes place over days to weeks. Hence, the full manifestation of the ISCV symptoms is seen after

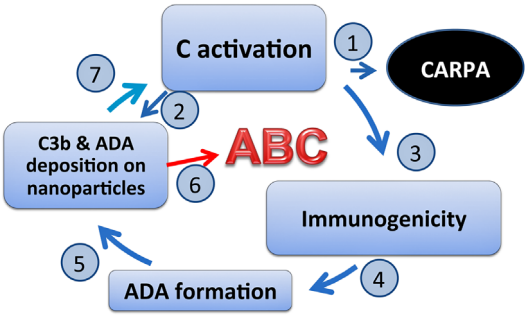


**Figure 7.2** The immune stimulatory vicious cycle caused by certain nanoparticles. The numbers indicate different steps in the cycle.

days to weeks following the first exposure of reactogenic nanoparticles to the blood.

Focusing on the processes in ISVC, the first step, C activation leading to CARPA, has been a subject of studies since the mid-1990s. Numerous papers and reviews detailed the processes involved, namely, the various pathways of C activation, the liberation of anaphylatoxins C3a and C5a, the stimulatory actions of anaphylatoxins on mast cells, basophils, secretory macrophages and other cells, the release of vasoactive mediators (histamine, thromboxane, leukotrienes, and PAF) from these cells and the effects of these mediators on endothelial, and smooth muscle and other effector cells causing the typical symptoms of pseudoallergy [7–18]. In step 2 of Figure 7.2, the C activation results in C3b deposition on nanoparticles, which initiates the alternative pathway amplification loop of the C cascade, and, thus, leads to more C activation. Furthermore, as a potent opsonin, C3b enhances the uptake of nanoparticles by the RES, that is, it initiates the ABC phenomenon.

In step 3 of ISVC, C activation promotes immunogenicity via a large number of different effects on antigen presenting cells (APCs), B and T cells (see Table 7.1) [19–36]. For this reason, C activation is often quoted as a bridge between innate and specific immunity.

The resulting production of ADAs by B cells (step 4) leads to deposition of these antibodies on nanoparticles (step 5) accelerating their uptake (ABC) via Fc receptors on RES cells (step 6) and further stimulating C activation via C1q binding (classical pathway activation) in step 7, thus closing the vicious cycle.

The consequences of ISVC are detrimental from many aspects, including the risk of severe CARPA with pain and discomfort, psychological stress on patients and health care professionals alike, financial loss in emergency care, denial of a potentially life-saving therapy to patients, and bad reputation of an otherwise useful state-of-art drug. Nevertheless, ISVC has a positive side as well for the benefit of immunologists. Namely, its study provides new insights into some mechanisms in innate immunity, such as nonspecific immune recognition and C activation by foreign particles, anaphylatoxin effects and anaphylactic shock,

**Table 7.1** Stimulation of specific (adaptive) immune response by C activation.

| Effects of C activation | Target cell(s) | References |
|---|---|---|
| Facilitation of the cooperation between APC and T cells | T cells and APC | [21,33] |
| Stimulation involving CD21/CD19/CD81 signaling | B cells follicular dentritic cells | [23,32–34] |
| Stimulation involving CD21/CD35 signaling | | |
| Increasing cell survival via CD21/CD19/Tapa-1 signaling | B cells | [28–31] |
| Stimulation of germinal center formation in lymph nodes | B cells, T cells | [24,25,35] |
| Increased cytotoxicity against CR2 (CD21)+ target cells via surface-bound C3b | CD8 T cells | [19] |
| Acceleration of antibody affinity maturation via ligation to CR2 | B cells | [36] |
| Induction of IL-1 and IL-10 production | Monocytes | [20,27] |
| Suppression of IL-6, IL-12, TNF-α | Monocytes, macrophages, dendritic cells, PBMC | [22,26,27,35] |

ADA formation via T-independent B-cell stimulation, and so on. In fact, research on CARPA led to the recognition of tachyphylactic hypersensitivity reactions (HSRs) to some nanomedicines, enabling their prevention by tachyphylactogenic pretreatment with placebo [37,38]. Also, the concept of ISVC represents a new concept in an uncharted cross section of immunology, pharmacology, and toxicology.

## 7.3 The Cause of Immune Recognition of Nanomedicines: Similarity to Viruses

A thought-provoking recognition in nanotoxicology is that the ultimate cause of immune recognition of nanoparticles is their relatively large size, which, considering their prefix *nano*, Greek word implying very small, is a paradox. In fact, nanomedicines are one–two orders of magnitude larger than conventional, small molecular weight drugs. As shown in Figure 7.3, their size in the 25–300 nm range exactly overlaps with the size range of pathogenic viruses, closely mimicking these pathogens, against which the immune system developed efficient defense over millions of years.

On the same token, reactogenic nanomedicines can be perceived as artificial, or *pseudoviruses*, which are fought by the immune system via *pseudoallergy*. This simply playing with words; however, the association of nanomedicines with viruses on the basis of physical similarity should be a reminder to their potential immune reactivity.

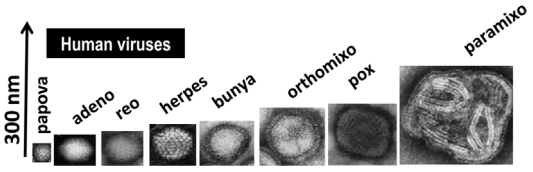


**Figure 7.3** Similarity between nanomedicines and viruses. Electron micrographs of human pathogenic viruses on the nanometer-size scale (Reproduced with permission from Ref. [13]. Copyright 2011 Elsevier).

## 7.4
## Processes in the Immune Stimulatory Vicious Cycle

The next sections provide further details on major processes in ISVC: CARPA, immunogenicity, ADA formation, and the ABC phenomena.

### 7.4.1
### Complement Activation-Related Pseudoallergy

#### 7.4.1.1 Definition and Basics

CARPA is essentially identical to the immune reactions termed infusion reaction, anaphylactoid, anaphylactic reaction, nonimmune HSR, nonallergic reaction, and idiosyncratic reaction. The introduction of a new name and its mnemonic acronym is in keeping with a long recognized and emphasized need to revise the classification of HSRs [12,39–42], as well as their extensive nomenclature, which is often redundant, cryptic, and controversial [16]. As pointed out recently, there are 12 descriptive or quantitative terms to describe HSRs [16]. Figure 7.4 shows that CARPA is an adverse immune stimulation caused primarily by intravenously administered drugs that contain liposomes, micelles, or polymers either as vehicle or active ingredient.

#### 7.4.1.2 Historic Leads

Complement activation as a possible cause of HSRs to radiocontrast agents was proposed in the late 1970s [43–45]; however, unfortunately, the concept was not pursued to gain wide acceptance. Subsequent studies on anaphylatoxins by Hugli *et al.* in the 1980s provided ample evidence that overproduction of these highly vasoactive small proteins explain the symptoms of anaphylactoid reactions and anaphylactic shock [46–48], but for some reason anaphylatoxin liberation was not linked to drug-induced HSRs at that time. In an independent line of research starting in the late 1960s, Alving *et al.* showed that liposomes can activate the C system [49–55] and that C activation by a liposomal vaccine can cause anaphylactoid reactions in pigs [56]. However, again, the phenomenon was not considered a mechanism of drug-induced HSRs. In the late 1990s and early 2000s, Rabinovici, Phillips, Goins and Awasthi were principal authors in numerous studies on the physiological effects of liposomes and liposome-encapsulated hemoglobin (LEH) in rats, showing essentially all symptoms of CARPA [57–77].

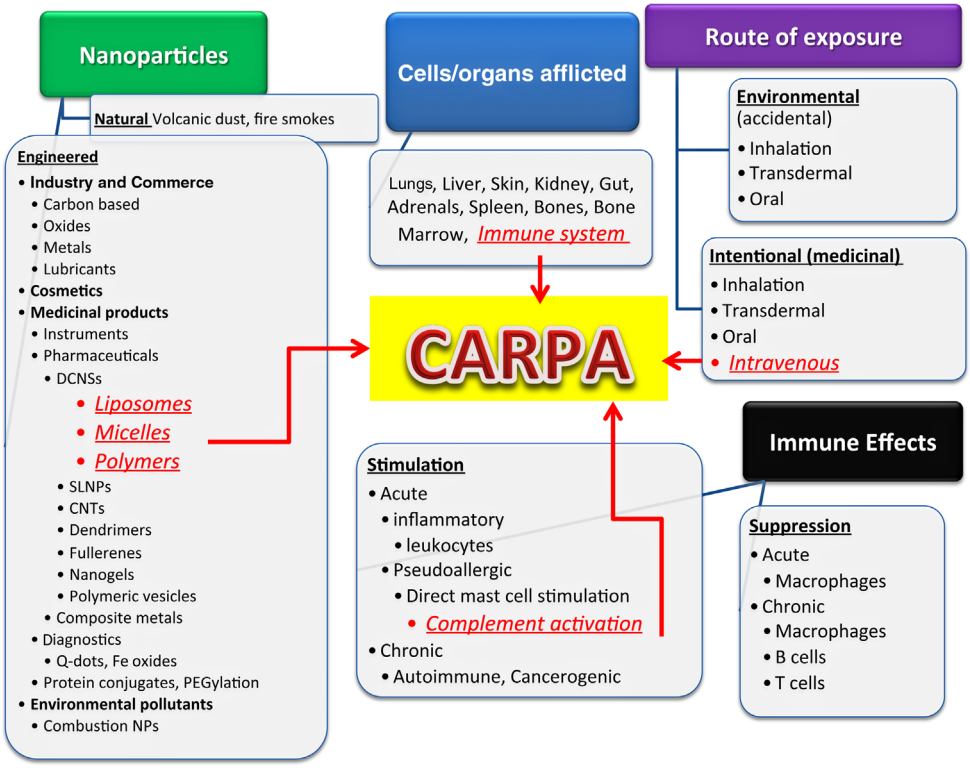


**Figure 7.4** The place of CARPA on the map of clinically relevant nanotoxicities: categorization of toxic reactions according to particle type (green heading), cells and organs afflicted (blue heading), route of exposure (purple heading), and type of immune reaction, if it occurs (black heading). The scheme represents an attempt to collect all variables that determine or characterize the toxic effects of nanoparticles. Abbreviations used only in this figure: DCNSSs, drug carrier nanosystems; SLNPs, solid lipid nanoparticles; CNTs, carbon nanotubes; Q-dots, quantum dots.

Nevertheless, the role of C activation behind these changes was not considered in these studies except for in one [68], where the thrombocytopenic effect of liposomes in rats was attributed to C activation on the basis that decomplementation of the animals prevented the effect.

The next critical lead in the progress of the CARPA concept was a series of clinical reports in the 1990s on unusual HSRs in patients treated with liposomal medicines, including the anticancer drug Doxil. It was puzzling in these reactions that the patients were not shown to be allergic to these drugs, the reaction arose at the first exposure, and that the symptoms soon vanished in most cases, so that the infusion could be continued [78–83]. Table 7.2 shows the symptoms recorded, which showed great individual variation in patients. Among them, the cardiovascular, bronchopulmonary, hematological, and mucocutaneous manifestations are also seen in the animal models of CARPA.

**Table 7.2** Symptoms of CARPA.

| Cardiovascular | Bronchopulmonary | Hematological | Mucocutaneous | Gastrointestinal | Neuropsycho-somatic | Systemic |
|---|---|---|---|---|---|---|
| Angioedema | Apnea | Leukopenia | Cyanosis | Nausea | Back pain | Chills |
| Arrhythmia | Bronchospasm | Granulopenia | Erythema | Vomiting | Chest pain | Diaphoresis |
| Cardiogenic shock | Coughing | Rebound leukocytosis | Flushing | Metallic taste | Chest tightness | Fever |
| Hypertension | Dyspnea | Rebound granulocytosis | Rash | Diarrhea | Headache | Sweating |
| Hypotension | Hyperventilation | Thrombocytopenia | Rhinitis | Cramping | Feeling of imminent death | Wheezing |
| Hypoxia | Laryngospasm | Lymphopenia | Swelling | Bloating | Fright | Rigors |
| Myocardial infarction | Stridor | | Urticaria | | Panic | Feeling of warmth |
| Tachycardia | Respiratory distress | | Nasal congestion | | Rigors | Loss of consciousness |
| Ventricular fibrillation | Shortness of breath | | Pruritus | | Anxiety | Death |
| Edema | Sneezing | | Tearing | | Confusion | |
| Syncope | Hoarseness | | Conjunctival erythema | | Dizziness | |

#### 7.4.1.3 Foundation of the CARPA Concept

The first proposal of causal relationship between C activation and hemodynamic and blood cell changes in rats following liposome injection came from the laboratory of Carl Alving in 1994 [7]. The conclusion was based on a remarkable parallelism between C consumption and hypotensive effects of liposomes, taken together with the fact that C activation can cause hypotension in rats [46,47,48]. Then, as mentioned above, Goins *et al.* showed in 1997 that the thrombocytopenic effect of liposomes was prevented by decomplementation of the animals, providing direct evidence for the causal role of C activation [68]. These rat studies were recently extended to show C activation progressing hand-in-hand with hypotension and blood cell changes [84,85].

In addition to rats, numerous pig studies served evidence for C activation underlying the physiological changes caused by i.v. liposomes [8,9,37,86,87]. The efficacy of soluble C receptor type 1 (sCR1) to prevent liposome-induced hemodynamic changes represented direct proof [8], while the indirect evidence included the mimicking of CARPA by the C activator zymosan and human C5a [86] and the quantitative correlation between *in vitro* C activation and *in vivo* reactogenicity in pigs [37,87].

In man, a correlation between C activation and HSRs to Doxil was shown by Chanan-Khan *et al.* [88], while a recent preliminary study extended this clinical research to Taxol, Taxotere, and Rituxan [89]. It was suggested that testing the C activating effect of these drugs in the serum or whole blood of patients (screening) can be used to predict the risk of CARPA in individual patients [89]. Today, there is a long list of nanoparticulate and/or protein-containing nanomedicines that are known to activate C and also cause HSRs in patients [14,18,90], although clinical studies on their correlation were done only for the drugs mentioned above. Table 7.3 provides a timeline for the progress of the CARPA concept until 2015.

#### 7.4.1.4 Prevalence, Symptoms, and Features

According to US statistics, allergic reactions to drugs occur in up to half a million patients per year, 77% of which is non-Ig-E mediated [102,103]. Pseudoallergy can have different mechanisms, that is, receptor-mediated and direct stimulation of mast cells [12], but the exact ratio of CARPA within pseudoallergy is unknown. However, a fraction even much lower than 77% of 500 000 patients still imply C-mediated acute illness in hundreds or thousands of patients every year in the United States of America, and proportionately less in other countries with advanced health care. Roughly, this translates to thousands of reactions every day. If we consider an estimate of 0.01–0.1% death rate in CARPA, this means many people dying every day because of these reactions.

Depending on the drug and its administration, the symptoms of allergic drug reactions (Table 7.2) vary among patients. Nevertheless, there are some common, unique features that distinguish CARPA from classical allergy. These include the following: (i) CARPA arises mostly at the first time, with no prior exposure, (ii) it decreases or disappears upon reexposure (tachyphylaxis), (iii) it

**Table 7.3** Milestones in the progress of the CARPA concept.

| Event | Period | References |
|---|---|---|
| Proposal of the role of C activation in radiocontrast reactions | 1976–1978 | [43–45] |
| Unveiling of the biological effects of anaphylatoxins that include the symptoms of CARPA | 1984–1987 | [46–48] |
| Studies on complement activation by liposomes *in vitro* and in pigs *in vivo* | 1969–1989 | [49–56] |
| Exploration of the adverse cardiopulmonary, hemodynamic, biochemical, and hematological effects of liposomes in rats | 1989–2004 | [57–77] |
| Clinical observations on HSRs to Doxil and other liposomes | 1995–2001 | [78–83] |
| Report on the involvement of C activation in the adverse physiological effects of liposomes in rats | 1994 | [7] |
| Indirect and direct evidence for a causal role of C activation in HSRs to various nanoparticulate drugs (mainly Taxol and Doxil) *in vitro* and *in vivo*. Reviews on CARPA | 1998–2014 | [8–10,12–14,38,86,88,91–99] |
| Regulatory recommendation of CARPA assays as preclinical safety tests | 2014 | [100] |
| Further addressing the regulatory relevance of CARPA assays; proposals that CARPA represents a *blood stress* and that it underlies HSRs to intravenous iron therapy and that in pigs it is mediated by pulmonary intravascular macrophages (PIM cells). | 2014–2015 | [14,16,18,101] |

spontaneously resolves in most cases, (iv) the strength of the reaction critically depends on the speed of infusion, (v) it responds to steroid and antihistamine premedication, (vi) the reaction rate is high (>2%), and (vii) the reaction is unpredictable by standard allergy tests. Among these features, the statement that CARPA mostly arises at the first treatment implies that there may be exceptions, that is, patients in whom the reaction arises at the second or third treatment. However, in these cases it is difficult to discern the impact of immunogenicity, that is, immunoglobulin (IgG and/or IgM) response to the first administration of the drug.

#### 7.4.1.5 **Mechanism**

As implied by its name, CARPA is an allergic reaction whose rise is related to C activation. It is not real allergy, as by textbook definition, *real* allergy is mediated by IgE. The word *related* in the name of CARPA is therefore critical, as it expresses uncertainty regarding causality, that is, whether C activation is the only cause of HSR or there are other co-stimuli as well. In fact, the relationship

between C activation and HSRs in this special subtype of pseudoallergy most likely involves stimulation of secretory cells by particle binding to their cell surface pattern recognition receptors (i.e., double hit) [13]. Another indirect contribution of C activation to CARPA might be cell sensitizing for other contributing processes, for example, endothelial cells for contraction or dilatation by vasoactive mediators. It is important to emphasize that CARPA is likely a consequence of the combination of C activation with other allergy triggers whose actions coincide with those of anaphylatoxins.

Over the past few years, several reviews [14,16,18,84] and book chapters [15,17,99,104] were published showing different schemes of the CARPA chain and physiological changes involved. Taken together, one can identify three pathways (classical, alternative, and lectin) of C activation by nanoparticles; two anaphylatoxins (C3a and C5a) liberated upon C activation; at least four vasoactive peptides (histamine, thromboxane, PAF, and leukotrienes) released from three types of anaphylatoxin reactive cells (macrophages, mast cells, and basophil leukocytes); three types of reactive blood cells (granulocytes, platelets, and monocytes) causing circulatory changes via three processes (leukocyte-platelet aggregation, microthrombus formation, and adherence to endothelial cells); three effector cells (endothel, smooth muscle, and glandular epithelial cells) directly involved in the symptoms in four major reactive organs or organ systems (heart, lung, circulatory system, and skin): a minimum of twenty-five processes and variables influencing the spectrum of individual symptoms, not including the contribution of *second hit* on macrophages [13].

### 7.4.2 Immunogenicity and Formation of Antidrug Antibodies

Immunogenicity means the capability of a drug or agent to induce a specific immune response, which can be antibody-mediated (humoral) or cell-mediated (cellular), or both. Accordingly, immunogenicity is assessed by measuring the production of specific antibodies or specific T-cell responses. Where immunogenicity becomes critical, in addition to vaccine research, is the field of biopharmaceuticals, whereupon monoclonal antibodies and other proteins are used via repeated or chronic administration protocols. Some of the patients treated this way mount an immune response against these drugs, mostly via production of ADAs. These antibodies can change the pharmacokinetics of the drug after the first or second administration and thus interfere with its therapeutic effect. In addition, ADAs can lead to adverse immune effects, sometimes they cause severe toxicities, including CARPA. Examples of such severe adverse responses to protein therapies include the antierythropoietin ADA-induced pure red cell aplasia [105]. Since the impact of immunogenicity can be quite severe, regulatory agencies have issued guidelines for immunogenicity screening of therapeutic proteins and biologicals [106,107].

Unlike with biologicals, the immunogenicity of nonbiological complex drugs (NBCDs), such as liposomes [108], is not widely recognized. Fortunately, no

catastrophic immunogenicity-related side effect has been reported to date for any liposome or other nanomedicine in the market, although PEGylated liposomes and some drug–polymer conjugates are highly immunogenic in animal models (see below).

### 7.4.3 Accelerated Blood Clearance (ABC Phenomenon)

#### 7.4.3.1 Essentials and Background

The ABC phenomenon, as its name indicates, is the accelerated clearance of nanoparticles from blood, a change from the expected long circulation *stealth*-type pharmacokinetics to rapid $T_{1/2}$, sometimes minutes instead of days or weeks. The phenomenon is due to rapid uptake of nanoparticles by macrophages of the RES, mainly because of their opsonization in blood via C activation and C3b deposition and ADA deposition (steps 2 and 5 given in Figure 7.2). The phenomenon has been the subject of numerous studies by the Japanese group of Ishida *et al.*, who dissected its mechanism to the utmost molecular detail. The ABC phenomenon has been shown to occur with PEGylated liposomes [3,4,109–122], micelles [123], microemulsions [124], and proteins [125].

Historically, the first observations on ABC upon repeated administration of $^{99m}$Tc-polyethylene glycol (PEG) liposomes were reported by Dams *et al.* [126], whose studies revealed the formation of a plasma factor following the first dose of such liposomes. However, at that time, the plasma factor was not yet identified as immunoglobulin [126]. In a parallel report, Laverman *et al.* [127] distinguished the induction phase and the effector phase of the ABC phenomenon. Later, Ishida *et al.* identified in rats and mice the plasma factor as immunoglobulin, mainly anti-PEG IgM with minor contribution of IgG [3,109–111]. Thus, the ABC phenomenon has been recognized as a consequence of PEGylated nanoparticle-induced immunogenicity.

#### 7.4.3.2 The Immunogenicity of PEG-Conjugated Nanomedicines

Coating of particles with various PEGs, termed PEGylation, is the state-of-the-art technology for extending the circulation time of proteins and liposomes via inhibition of their uptake by the mononuclear phagocyte system (MPS) [128,129]. However, PEGylation may also lend immunogenicity to the carrier to which it is conjugated, and vice versa, the carrier lends immunogenicity to PEG. Given the wide use of PEGylation, the latter effect, that is, the immunogenicity of PEG, has got exceptional attention over the past decade and the validity of its measurement is still debated [130].

As mentioned, Ishida *et al.* have clarified many details of the immunogenicity of PEGylated nanoparticles, including the fact that the ADAs causing the ABC phenomenon are mainly IgM subtype antibodies produced by marginal zone B cells in the spleen [114,131]. Because the production of these antibodies does not require T-cell help, the process is referred to as thymus

independent (TI) immunogenicity [132]. Consistent with TI B-cell response, the ABC phenomenon was shown to be present in T-cell-deficient (BALB/c nu/nu) mice but not in T- and B-cell-deficient (BALB/c SCID) mice [133,134]. TI anti-PEG IgM can be directed against both PEG and the phospholipid backbone in case of liposomes, with binding sites being close to the liposomal bilayer [125]. Moghimi *et al.* showed that in case of mPEG coating, it is the phosphate group of phospholipid head groups that binds the anti-PEG IgM [135]. Although TI B-cell responses lack memory, and the antibodies produced have low affinity to the antigen, the strong C1q binding to IgM and subsequent C activation explains the ABC and acceleration of C activation, when anti-PEG ADA binds to nanoparticles. Thus, IgM binding to PEGylated nanoparticles help their clearance by RES via at least two mechanisms: C3b opsonization and Fc receptor-mediated uptake (step 6 in Figure 7.2). As to the route of immunization with PEGylated nanoparticles, i.v. and s.c. administrations are both effective [133].

### 7.4.4 Mechanism of PEG Immunogenicity

There are two types of TI responses depending on whether mediated by T-1 or T-2 antigens. T-1 antigens activate B cells in a concentration-dependent manner: at low concentration, they induce antigen-specific IgM, while at high(er) concentration they act as potent B-cell mitogens, leading to polyclonal IgM production [136,137]. In contrast, T-2 antigens activate only mature B cells and induce specific IgM and IgG after extensive cross-linking the cell surface immunoglobulins [136,137]. Such activations are typically caused by repetitive surface molecules on a carrier, the latter acting as adjuvant. This type of immune response does not involve class switching and affinity maturation and, hence, long-term memory. Based on the fact that some IgG also takes part in the immune response against PEGylated nanoparticles [3,109–111] and that the PEG coat on the surface of nanoparticles may be seen by B cells as pattern-forming repetitive surface structures, it is possible that PEGylated nanoparticles set in motion both T-1 and T-2 B cell responses.

Regarding the role of particle surface morphology in TI B-cell stimulation, what seems likely to be a critical factor is the spacing of surface epitopes. Studies with polymer-conjugated dinitrophenyl (DNP) antigen showed maximal B-cell response when the spacing of DNP conjugates on the polymer was at 5–10 nm [138]. Furthermore, the number of repeat epitopes was also critical, with a minimum of 10–20 DNP units needed for immune response [138]. Based on the above polymer–DNP model, one might hypothesize that only those PEGylated liposomes are immune reactive where the PEG moieties are spaced on the vesicle surface in a density that interdigitates and, hence, cross-links the B-cell receptors (surface IgM). This then triggers their proliferation to antibody-producing plasma cells, which, in the absence of further signaling via T cells, typically leads to a transient IgM response, see Figure 7.5.

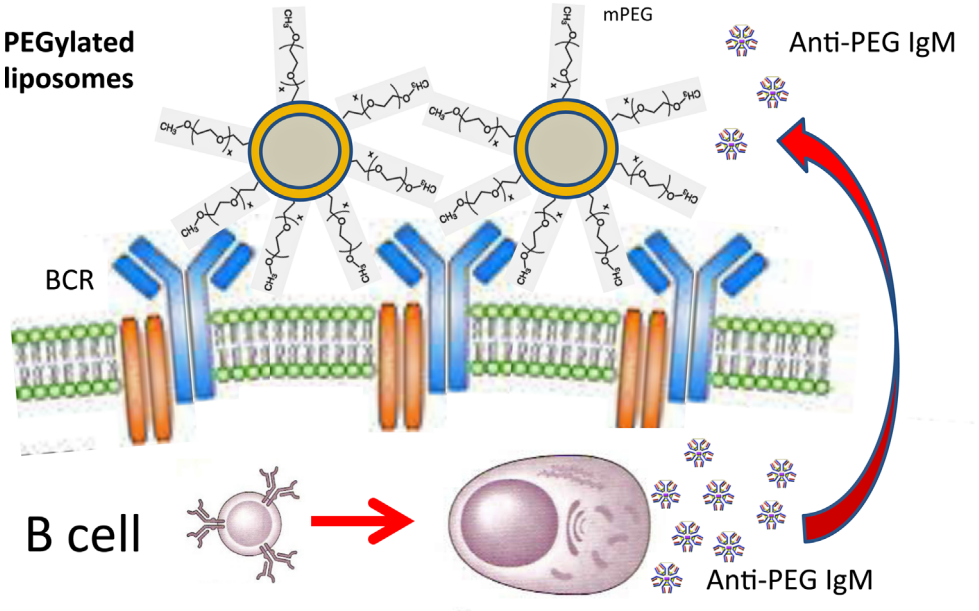


**Figure 7.5** Mechanism of ADA production against PEGylated liposomes via TI immunogenicity.

## 7.5 Particle Features Influencing the Immune Side Effects of Nanomedicines

Previous reviews provided long lists of particle features influencing C activation and CARPA by liposomes [10–13,18,94,139]. These lists included large versus small size (multi- versus unilamellar) vesicles, inhomogeneity, endotoxin contamination, the presence of aggregates, the presence of doxorubicin (or, assumedly, similar amphipathic weak base) in the extraliposome medium that promotes aggregation, oversaturating (>50%) amounts of cholesterol in the membrane, PEGylation of liposomes via negatively charged phospholipid anchor, for example, phosphatidyethanolamine, and coating of liposomes with polyaminoacids.

As for immunogenicity and ABC phenomenon caused by PEGylated nanoparticles, most studies found maximal immune response at PEG mole ratios between 5 and 10%. Ishida *et al.*, for example, found the optimal dose for ABC induction at 5 mol% mPEG2000-DSPE in liposomes [140], Li *et al.* [141] at 9 versus 3%, while Zhao *et al.* [142] found that solid lipid nanoparticles (SLNs) containing 10 mol% PEG induced stronger ABC than 5 mol% PEG-SLNs. In addition to PEG surface density, the molecular weight and, hence, chain length of PEG was also found to have critical impact on immunogenicity and ABC. In a study by Ishida *et al.* [111], 2K-PEG liposomes caused faster hepatic clearance of a second dose than 5K-PEG liposomes, while Shimizu showed that

30K-PEG-bovine serum albumin induced higher anti-PEG IgM response and greater C activation than 2K-PEG-BSA [120].

## 7.6 Experimental Analysis of the Adverse Immune Effects of Nanomedicines

### 7.6.1 Measurement of C Activation

There are several approaches to measure C activation by liposomes and other nanoparticles *in vitro*, the easiest being the incubation of particles with normal human serum (NHS) followed by the measurement of C split products with one or more ELISAs (C3a, C5a, SC5b-9, Bb, C4d, and iC3b). The sheep red blood cell (SRBC) hemolysis assay is less expensive and is also less sensitive than the ELISAs, but it is applicable and useful, and in case of animal studies, it is the only applicable C activation assay next to a recently commercialized ELISA (PAN-C3) that measures C3 consumption in pigs, dogs, rats, mice, and in essentially all animal species that utilize C3 as a central protein in C activation [143]. Nevertheless, *in vitro* C assays provide only partial, semiquantitative evaluation of the risk of CARPA, since they report only on the activity of afferent arm of the process, the extent of anaphylatoxin formation. The efferent arm, the body's response to anaphylatoxins, remains unknown. These can be measured only in *in vivo* animal models.

### 7.6.2 Prediction of Immunogenicity

The animal studies discussed in relation to immunogenicity highlight the possibility to predict in man the immunogenicity of PEGylated liposomes or other nanoparticles. If a product is immunogenic in rats and mice, there is no known reason for assuming that it will not be immunogenic in man. However, what is less certain and still not explored in experimental studies, what is the clinical impact of liposome immunogenicity in man? Clinical experience on this issue is available only for therapeutic proteins, but not liposomes or other nanomedicines. The doubt regarding the clinical relevance of natural and induced anti-PEG antibodies in man [130,144,145] has been based, in part, on the clinical success of PEGylated proteins and the archetype PEGylated liposome, Doxil [146]. Regarding PEGylated proteins, it should be noted that many of them, if not the majority, do cause CARPA in up to 5–10% of patients [90], very similar ratio to that seen with liposomes [90]. As for Doxil, one explanation is that doxorubicin in liposomes suppresses the B-cell response to the dug. This hypothesis has indirect support via the clinical observation on the reduced rate of immune reactions against cisplatin, when it is coadministered with Doxil [147].

### 7.6.3
### Prediction of CARPA

Preliminary clinical studies raise the possibility that CARPA in man may be roughly predicted by *in vitro* assessment of C activation and the presence of certain biomarkers in the screening serum or plasma of patients [88,89,148]. The studies that provide basis for this claim include the measurement of plasma terminal complex (SC5b-9) levels as a biomarker of C activation in cancer patients *in vivo*, while they were treated with Doxil [88], and another recent clinical study where three parameters of C activation (C3a, C5a, and SC5b-9) were measured in cancer patients treated with rituximab (Rituxan) and Taxanes (Taxol and Taxotere) [89]. In both studies, we observed the presence of HSRs and C activation in a high percentage of patients (>30– 50%), but C activation occurred in higher percentage than HSRs, suggesting that it cannot be the sole cause or rate-limiting factor in HSR. In fact, only major C activation displayed direct relationship with HSRs, for example, in the Doxil study only an elevation of SC5b-9 five–tenfold higher than baseline and, in addition, the infusion speed was also a critical factor in the rise of HSRs. In the Rituxan and Taxol study, we found a major rise of C3a to correlate best with HSRs [89], while in the biomarker analysis study, low level of factor H was among the significant changes that characterized *reactive sera* [148]. These endpoints data *made sense* as CARPA predictors, but not enough to prove conclusively their sufficient sensitivity and specificity for a clinically valid laboratory or bedside test. More clinical studies will hopefully lead to identifying the best CARPA predictive biomarkers.

Parallel with the human studies delineated above, substantial efforts have been devoted to establish animal models of CARPA, see Figure 7.6. These models,

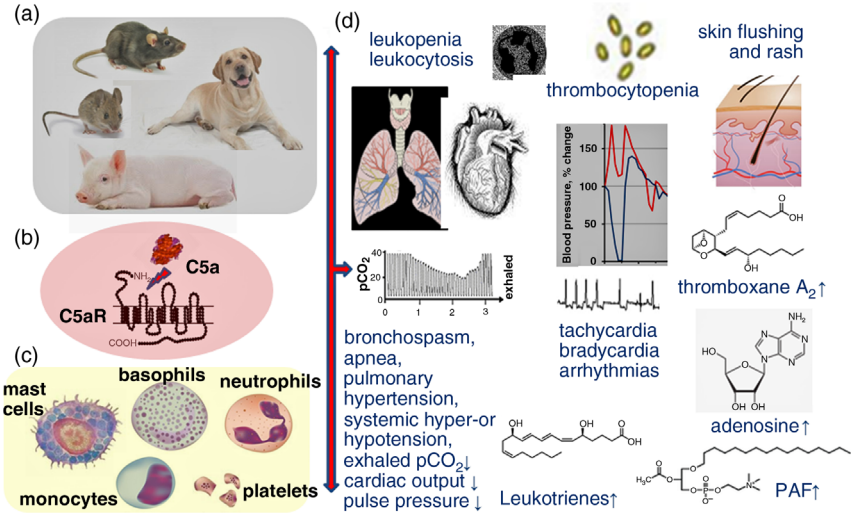


**Figure 7.6** Essentials of CARPA: (a) animal models, (b) role of anaphylatoxins, (c) blood cells involved, and (d) symptoms in pigs.

also listed in Table 7.2, enable both screening of drugs for CARPAgenicity and exploring biomarkers and the mechanism of the reaction. Thus, studies have been conducted in pigs [8,37,38,86,87,149,150], dogs [151], rats [84,85], and mice [152], inducing CARPA with a variety of soft and solid nanoparticles, including coated and bare, targeted and untargeted, liposomes, micelles, polymers, dendrimers, carbon nanotubes, and so on [150].

Among the animal models, the porcine model has got the most attention, since it turned out to be a highly sensitive yet astonishingly consistent model of CARPA [8,37,38,86,87,149,150]. It reproduces most symptoms of human CARPA, as given in Table 7.4, and provides conveniently measurable and quantifiable end points, most significantly the rise of pulmonary arterial pressure (PAP) (Figure 7.6).

**Table 7.4** Identities, similarities, and differences between CARPA in men and pigs (reproduced with permission from Ref. [150]).

| Comparison | Reaction features | Symptoms | |
|---|---|---|---|
| | | Human | Pig |
| Identical | Some cardiopulmonary and hemodynamic alterations | Difficulty of breathing, hypo- or hypertension, arrhythmia, tachycardia, bradycardia, edema | |
| | Body temperature | Fever | |
| | Blood cell changes | Leukopenia/leukocytosis, thrombocytopenia | |
| | Skin changes | Erythema, rash | |
| | Range of minimum reactogenic PL dose in infusion or bolus | 1–10 μg/(kg s) | |
| Similar | Blood chemistry | Rise of SC5b-9 | Rise of TXB2 |
| | Cardiopulmonary and hemodynamic alterations | Shortness of breath, fatigue, dizziness, fainting, swelling of the ankles, abdomen or legs, cyanosis, chest pain, passing out, or dizziness | Rise of PAP |
| | Time course | Symptoms start within 10 min after infusion and subside within 30–60 min | PAP rises between 3–15 min, returns to normal within 30–60 min |
| | Minimum reactogenic phospholipid dose | 0.15 mg/(kg min) phospholipid initially | 0.01 mg/kg bolus |
| Different | Sensitivity to emulsifiers | Yes | Yes |
| | Reaction frequency | < 10% | > 90% |

In particular, the symptoms observed during CARPA in pigs include hemodynamic, hematological, laboratory, and skin changes, referred to as *CARPA tetrad* [150], see Figure 7.6. Among the hemodynamic symptoms, the rise of PAP is the most prominent and reproducible measure of CARPA, which is invariably present with all reactogenic liposomes and other nanoparticles. However, depending on the reaction trigger and intensity of reactions, the PAP waveforms can substantially differ, which reflects the complex pathomechanism [150].

## 7.7
## Decision Tree to Guide the Evaluation of the CARPAgenic Potential of Nanomedicines

We have previously suggested a basic algorithm, a decision tree to guide the evaluation of the CARPAgenic potential of liposomes and other drug candidates, which is shown in Figure 7.7. According to this scheme, the test agent (drug candidate) is first incubated with a few normal human sera (NHS) to explore possible major C activation. If the result is positive, the agent is likely to carry a high risk for CARPA *in vivo*. As for the threshold for considering C activation as *major*, an activation factor (e.g., a rise of sC5b-9 above baseline over 20–30 min incubation at a temperature of 37 °C) of 5–10-fold may be a realistic predictor of clinical reaction, since such rises of SC5b-9 were shown to correlate with clinical symptoms of patients treated with Doxil [88]. However, the correlation between C activation by a drug *in vitro* and the clinical symptoms *in vivo* remains to be

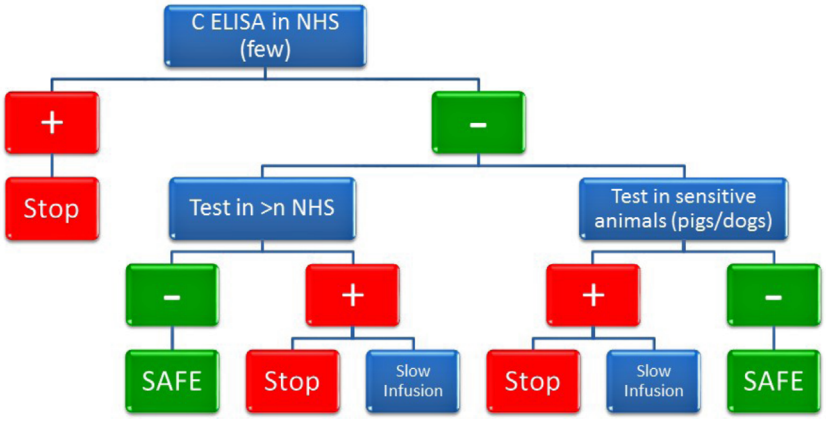


**Figure 7.7** Decision tree about the risk of CARPA. Abbreviations: NHS, normal human sera; blue entries are tests: C ELISA = ELISA of C activation byproducts (C3a, C5a, sC5b-9, Bb, C4d). plus and minus signs, reaction and no reaction, respectively, where major is defined in the text. *>n* = large number of human NHS; SAFE means that the tested drug candidate is unlikely to cause CARPA, while *slow infusion* means the possibility to develop a safe administration protocol by slow infusion. STOP means high risk for CARPA. (Reproduced with permission from Ref. [14]. Copyright 2014 Elsevier.)

established in the future with higher precision. If the *in vitro* C assay in NHS is not showing C activation, based on the substantial individual variation of C response, testing in a much larger number of NHS in the range of 10–100 can be recommended, and/or testing in sensitive large animals (pig and/or dogs) with bolus administration.

## 7.8 Outlook

The field of nanomedicine suffers from a fear from long-term toxicities or other unidentified adverse effects. As specified by the EU Commission's Scientific Committee on Emerging and Newly Identified Health Risks (SCENIHR), the contributing factors to this shortcoming are the "lack of methodologies for exposure estimation, hazard identification and risk assessment" [153,154]. This critique very much applies to the immune side effects discussed in this chapter, since the mandated preclinical toxicology tests fail to predict them and measure their risk. The present summary of progress and methods may help advance in this field.

## References


1 Buzea, C., Pacheco, I.I., and Robbie, K. (2007) Nanomaterials and nanoparticles: sources and toxicity. *Biointerphases*, **2**, MR17–MR21.

2 Smith, M.J., Brown, J.M., Zamboni, W.C., and Walker, N.J. (2014) From immunotoxicity to nanotherapy: the effects of nanomaterials on the immune system. *Toxicol. Sci.*, **138**, 249–255.

3 Wang, X., Ishida, T., and Kiwada, H. (2007) Anti-PEG IgM elicited by injection of liposomes is involved in the enhanced blood clearance of a subsequent dose of PEGylated liposomes. *J. Control. Release*, **119** (2), 236–244. Epub 2007/04/03.

4 Abu Lila, A.S., Kiwada, H., and Ishida, T. (2013) The accelerated blood clearance (ABC) phenomenon: clinical challenge and approaches to manage. *J. Control. Release*, **172** (1), 38–47. Epub 2013/08/13.

5 Verhoef, J.J., Carpenter, J.F., Anchordoquy, T.J., and Schellekens, H. (2014) Potential induction of anti-PEG antibodies and complement activation toward PEGylated therapeutics. *Drug Discov. Today*, **19** (12), 1945–1952. Epub 2014/09/11.

6 Hashimoto, Y., Shimizu, T., and Mima, Y. Abu Lila, A.S., Ishida T., Kiwada H. (2014) Generation, characterization and *in vivo* biological activity of two distinct monoclonal anti-PEG IgMs. *Toxicol. Appl. Pharmacol.*, **277** (1), 30–38. Epub 2014/03/19.

7 Szebeni, J., Wassef, N.M., Spielberg, H., Rudolph, A.S., and Alving, C.R. (1994) Complement activation in rats by liposomes and liposome-encapsulated hemoglobin: evidence for anti-lipid antibodies and alternative pathway activation. *Biochem. Biophys. Res. Comm.*, **205**, 255–263.

8 Szebeni, J., Fontana, J.L., Wassef, N.M., Mongan, P.D., Morse, D.S., Dobbins, D.E. *et al.* (1999) Hemodynamic changes induced by liposomes and liposome-encapsulated hemoglobin in pigs: a model for pseudoallergic cardiopulmonary reactions to liposomes. Role of complement and inhibition by soluble CR1 and anti-C5a antibody.

*Circulation.*, **99** (17), 2302–2309. Epub 1999/05/05.

9 Szebeni, J., Baranyi, B., Savay, S., Bodo, M., Morse, D.S., Basta, M. *et al.* (2000) Liposome-induced pulmonary hypertension: properties and mechanism of a complement-mediated pseudoallergic reaction. *Am. J. Physiol.*, **279**, H1319–H1328.

10 Szebeni, J. (2001) Complement activation-related pseudoallergy caused by liposomes, micellar carriers of intravenous drugs and radiocontrast agents. *Crit. Rev. Ther. Drug Carr. Syst.*, **18**, 567–606.

11 Szebeni, J. (2004) Complement activation-related pseudoallergy: mechanism of anaphylactoid reactions to drug carriers and radiocontrast agents, in *The Complement System: Novel Roles in Health and Disease* (ed. J. Szebeni), Kluwer, Boston, pp. 399–440.

12 Szebeni, J. (2005) Complement activation-related pseudoallergy: a new class of drug-induced acute immune toxicity. *Toxicology.*, **216** (2–3), 106–121.

13 Szebeni, J., Muggia, F., Gabizon, A., and Barenholz, Y. (2011) Activation of complement by therapeutic liposomes and other lipid excipient-based therapeutic products: prediction and prevention. *Adv. Drug Deliv. Rev.*, **63** (12), 1020–1030. Epub 2011/07/27.

14 Szebeni, J. (2014) Complement activation-related pseudoallergy: a stress reaction in blood triggered by nanomedicines and biologicals. *Mol. Immunol.*, **61**, 163–173.

15 Szebeni, J. (2016) Complement activation: a capricious immune barrier to the clinical use of nanomedicines, in *Handbook of Clinical Nanomedicine: Law, Business, Regulation, Safety, and Risk* (eds R. Bawa, G.F. Audette, and B.E. Reese), Pan Stanford Publishing, Singapore, pp. 845–862.

16 Szebeni, J., Fishbane, S., Hedenus, M., Howaldt, S., Locatelli, F., Patni, S. *et al.* (2015) Hypersensitivity to intravenous iron: classification, terminology, mechanisms and management. *Br. J. Pharmacol.*, **172**, 5025–5036. Epub 2015/08/13.

17 Szebeni, J., Muggia, F., and Barenholz, Y. (2015) Case study: complement activation related hypersensitivity reactions to pegylated liposomal doxorubicin, experimental and clinical evidence, mechanisms and approaches to inhibition, in *Handbook of Immunological Properties of Engineered Nanomaterials*, 2nd edn (eds M.A. Dobrovolskaia and S.E. McNeil). World Scientific Publishing Co Pte Ltd, New jersey, London, Singapore, Beijing, Shanghai, Hong Kong, Taipei, Chennai, Tokyo, pp. 331–362.

18 Szebeni, J. and Storm, G. (2015) Complement activation as a bioequivalence issue relevant to generic liposome development. *Biochem. Biophys. Res. Commun.* doi: 10.1016/j.bbrc.2015.06.177.

19 Ramos, O.F., Algarra, I., Sarmay, G., Yefenof, E., Gergely, J., and Klein, E. (1989) Lymphocytes stimulated by allogeneic B cell lines cleave the third component of complement and fix C3 fragments. Their nonspecific lytic capacity is elevated against complement receptor type 2-carrying targets. *J. Immunol.*, **142**, 217–223.

20 Bacle, F., Haeffner-Cavaillon, N., Laude, M., Couturier, C., and Kazatchkine, M.D. (1990) Induction of IL-1 release through stimulation of the C3b/C4b complement receptor type one (CR1, CD35) on human monocytes. *J. Immunol.*, **144**, 147–152.

21 Erdei, A., Köhler, V., Schéfer, H., and Burger, R. (1992) Macrophage-bound C3 fragments as adhesion molecules modulate presentation of exogenous antigens. *Immunobiology.*, **185** (2–4), 314–326.

22 Yentis, S.M., Gooding, R.P., and Riches, P.G. (1994) The effects of IgG and immune complexes on the endotoxin-induced cytokine response. *Cytokine.*, **6**, 247–254.

23 Roberts, M.L., Luxembourg, A.T., and Cooper, N.R. (1996) Epstein-Barr virus binding to CD21, the virus receptor, activates resting B cells via an intracellular pathway that is linked to B cell infection. *J. Gen. Virol.*, **77** (Pt 12), 3077–3085.

24 Molina, H., Holers, V.M., Li, B., Fung, Y., Mariathasan, S., Goellner, J. *et al.* (1996) Markedly impaired humoral immune response in mice deficient in complement receptors 1 and 2. *Proc. Natl. Acad. Sci. USA*, **93** (8), 3357–3361.

25 Ahearn, J.M., Fischer, M.B., Croix, D., Goerg, S., Ma, M., Xia, J. *et al.* (1996) Disruption of the Cr2 locus results in a reduction in B-1a cells and in an impaired B cell response to T-dependent antigen. *Immunity*, **4**, 251–262.

26 Marth, T. and Kelsall, B.L. (1997) Regulation of interleukin-12 by complement receptor 3 signaling. *J. Exp. Med.*, **185**, 1987–1995.

27 Yoshida, Y., Kang, K., Berger, M., Chen, G., Gilliam, A.C., Moser, A. *et al.* (1998) Monocyte induction of IL-10 and down-regulation of IL-12 by iC3b deposited in ultraviolet-exposed human skin. *J. Immunol.*, **161** (11), 5873–5879.

28 Carroll, M.C. (1998) CD21/CD35 in B cell activation. *Semin. Immunol.*, **10** (4), 279–286.

29 Carroll, M.C. and Prodeus, A.P. (1998) Linkages of innate and adaptive immunity. *Curr. Opin. Immunol.*, **10** (1), 36–40.

30 Carroll, M.C. (1998) The role of complement and complement receptors in induction and regulation of immunity. *Annu. Rev. Immunol.*, **16**, 545–568.

31 Carroll, M. (1999) Role of complement receptors CD21/CD35 in B lymphocyte activation and survival. *Curr. Top. Microbiol. Immunol.*, **246**, 63–69.

32 Roberts, T. and Snow, E.C. (1999) Cutting edge: recruitment of the CD19/CD21 coreceptor to B cell antigen receptor is required for antigen-mediated expression of Bcl-2 by resting and cycling hen egg lysozyme transgenic B cells. *J. Immunol.*, **162** (8), 4377–4380.

33 Ara, Y., Saito, T., Takagi, T., Hagiwara, E., Miyagi, Y., Sugiyama, M. *et al.* (2001) Zymosan enhances the immune response to DNA vaccine for human immunodeficiency virus type-1 through the activation of complement system. *Immunology*, **103**, 98–105.

34 Clemenza, L., Dieli, F., Cicardi, M., and Salerno, A. (2003) Research on complement: old issues revisited and a novel sphere of influence. *Trends Immunol.*, **24**, 292–296.

35 Erdei, A., Molnár, E., Csomor, E., Bajtay, Z., and Prechl, J. (2004) Coordination of adaptive immune responses by C3, in *The Complement System: Novel Roles in Health and Disease* (ed. J. Szebeni), Kluwer, Boston, pp. 77–96.

36 Holers, V.M.l. (2005) Complement receptors and the shaping of natural antibody repertoire. *Springer Semin. Immunopathol.*, **26**, 405–423.

37 Szebeni, J., Bedőcs, P., Urbanics, R., Bunger, R., Rosivall, L., Tóth, M. *et al.* (2012) Prevention of infusion reactions to PEGylated liposomal doxorubicin via tachyphylaxis induction by placebo vesicles: a porcine model. *J. Contr. Rel.*, **160**, 382–387.

38 Szebeni, J., Bedocs, P., Csukas, D., Rosivall, L., Bunger, R., and Urbanics, R. (2012) A porcine model of complement-mediated infusion reactions to drug carrier nanosystems and other medicines. *Adv. Drug Deliv. Rev.*, **64** (15), 1706–1716.

39 Choquet-Kastylevsky, G. and Descotes, J. (1998) Value of animal models for predicting hypersensitivity reactions to medicinal products. *Toxicology*, **129** (1), 27–35.

40 Descotes, J. and Choquet-Kastylevsky, G. (2001) Gell and Coombs's classification: is it still valid? *Toxicology*, **158**, 43–49.

41 Rajan, T.V. (2003) The Gell–Coombs classification of hypersensitivity reactions: a re-interpretation. *Trends Immunol.*, **24**, 376–379.

42 Pichler, W.J. (2006) Adverse side-effects to biological agents. *Allergy*, **61**, 912–920.

43 Lasser, E.C., Sovak, M., and Lang, J.H. (1976) Development of contrast media idiosyncrasy in the dog. *J. Radiol.*, **119**, 91–95.

44 Lang, J.H., Lasser, E.C., and Kolb, W.P. (1976) Activation of serum complement by contrast media. *Invest. Radiol.*, **11** (4), 303–308.

45 Kolb, W.P., Lang, J.H., and Lasser, E.C. (1978) Nonimmunologic complement activation in normal human serum

induced by radiographic contrast media. *J. Immunol.*, **121** (4), 1232–1238.
46 Hugli, T.E. (1984) Structure and function of the anaphylatoxins. *Springer Semin. Immunopathol.*, **7** (2–3), 193–219. Epub 1984/01/01.
47 Marceau, F., Lundberg, C., and Hugli, T.E. (1987) Effects of anaphylatoxins on circulation. *Immunopharmacology*, **14**, 67–84.
48 Lundberg, C., Marceau, F., and Hugli, T.E. (1987) C5a-induced hemodynamic and hematologic changes in the rabbit. Role of cyclooxygenase products and polymorphonuclear leukocytes. *Am. J. Pathol.*, **128** (3), 471–483. Epub 1987/09/01.
49 Alving, C.R., Kinsky, S.C., Haxby, J.A., and Kinsky, C.B. (1969) Antibody binding and complement fixation by a liposomal model membrane. *Biosci. Biotechnol. Biochem.*, **8**, 1582–1587.
50 Kinsky, S.C., Haxby, J.A., Zopf, D.A., Alving, C.R., and Kinsky, C.B. (1969) Complement-dependent damage to liposomes prepared from pure lipids and Forssman hapten. *Biosci. Biotechnol. Biochem.*, **8** (10), 4149–4158.
51 Alving, C.R., Richards, R.L., and Guirguis, A.A. (1977) Cholesterol-dependent human complement activation resulting in damage to liposomal model membranes. *J. Immunol.*, **118**, 342–347.
52 Richards, R.L., Gewurz, H., Osmand, A.P., and Alving, C.R. (1977) Interactions of C-reactive protein and complement with liposomes. *Proc. Natl. Acad. Sci. USA*, **74**, 5672.
53 Cunningham, C.M., Kingzette, M., Richards, R.L., Alving, C.R., Lint, T.F., and Gewurz, H. (1979) Activation of human complement by liposomes: a model for membrane activation of the alternative pathway. *J. Immunol.*, **122** (4), 1237–1242.
54 Alving, C.R., Urban, K.A., and Richards, R.L. (1980) Influence of temperature on complement-dependent immune damage to liposomes. *Biochim. Biophys. Acta.*, **600**, 117.
55 Richards, R.L., Habbersett, R.C., Scher, I., Janoff, A.S., Schieren, H.P., Mayer, L.D. *et al.* (1986) Influence of vesicle size on complement-dependent immune damage to liposomes. *Biochim. Biophys. Acta*, **855** (2), 223–230.
56 Wassef, N.M., Johnson, S.H., Graeber, G.M., Swartz, G.M., Jr., Schultz, C.L., Hailey, J.R. *et al.* (1989) Anaphylactoid reactions mediated by autoantibodies to cholesterol in miniature pigs. *J. Immunol.*, **143** (9), 2990–2995. Epub 1989/11/01.
57 Rabinovici, R., Rudolph, A.S., and Feuerstein, G. (1989) Characterization of hemodynamic, hematologic and biochemical responses to administration of liposome-encapsulated hemoglobin in the conscious, freely moving rat. *Circ. Shock*, **29**, 115–132.
58 Rabinovici, R., Rudolph, A.S., Yue, T.-L., and Feuerstein, G. (1990) Biological responses to liposome-encapsulated hemoglobin (LEH) are improved by a PAF antagonist. *Circ. Shock*, **31**, 431–445.
59 Rabinovici, R., Rudolph, A.S., Ligler, F.S., Yue, T.-L., and Feuerstein, G. (1990) Liposome-encapsulated hemoglobin: an oxygen-carrying fluid. *Circ. Shock*, **32**, 1–17.
60 Rabinovici, R., Rudolph, A.S., Ligler, F.S., and Smith, EF., III (1992) Feuerstein G. Biological responses to exchange transfusion with liposome-encapsulated hemoglobin. *Circ. Shock*, **37** (2), 124–133.
61 Rabinovici, R., Rudolph, A.S., Vernick, J., and Feuerstein, G. (1993) A new salutary resuscitative fluid: liposome encapsulated hemoglobin/hypertonic saline solution. *J. Trauma*, **35**, 121–127.
62 Rabinovici, R., Rudolph, A.S., Vernick, J., and Feuerstein, G. (1994) Lyophilized liposome-encapsulated hemoglobin: evaluation of hemodynamic, biochemical, and hematologic responses. *Crit. Care Med.*, **22**, 480–485.
63 Rudolph, A.S., Cliff, R.O., Klipper, R., Goins, B., and Phillips, W.T. (1994) Circulation persistence and biodistribution of lyophilized liposome-encapsulated hemoglobin: an oxygen-carrying resuscitative fluid. *Crit. Care Med.*, **22** (1), 142–150.
64 Rudolph, A.S. (1995) Encapsulation of hemoglobin in liposomes, in *Blood*

*Substitutes Physiological Basis of Efficacy* (eds R.M. Winslow, K.D. Vandegriff, and M. Intaglietta), Birkhauser, Boston, pp. 98–104.

65 Rudolph, A.S., Sulpizio, T., Kwasiborski, V., Cliff, R.O., Rabinovici, R., and Feurstein, G. (1996) Infusion of liposome-encapsulated hemoglobin in normovolemic primates. *Artif. Cells Blood Subst. Immob. Biotechnol.*, **24**, 415.

66 Rudolph, A.S., Sulpizio, A., Hieble, P., MacDonald, V., Chavez, M., and Feurstein, G. (1997) Liposome encapsulation attenuates hemoglobin-induced vasoconstriction in rabbit arterial segments. *J. Appl. Physiol.*, **82**, 1826–1835.

67 Rudolph, A.S., Cliff, R., Kwasiborski, V., Neville, L., Abdullah, F., and Rabinovici, R. (1997) Liposome-encapsulated hemoglobin modulates lipopolysaccharide-induced tumor necrosis-alpha production in mice. *Crit. Care Med.*, **25**, 460–468.

68 Goins, B., Phillips, W.T., Klipper, R., and Rudolph, A.S. (1997) Role of complement in rats injected with liposome-encapsulated hemoglobin. *J. Surg Res.*, **68**, 99–105.

69 Phillips, W.T., Klipper, R., Fresne, D., Rudolph, A.S., Javors, M., and Goins, B. (1997) Platelet reactivity with liposome-encapsulated hemoglobin in the rat. *Exp. Hematol.*, **25**, 1347–1356.

70 Phillips, W. (1999) Polyethylene glycol-modified liposome-encapsulated hemoglobin: A long circulating red cell substitute. *J. Pharmacol. Exp. Ther.*, **288**, 665–670.

71 Phillips, W.T., Klipper, R.W., Awasthi, V.D., Rudolph, A.S., Cliff, R., Kwasiborski, V. *et al.* (1999) Polyethylene glycol-modified liposome-encapsulated hemoglobin: a long circulating red cell substitute. *J. Pharmacol. Exp. Ther.*, **288** (2), 665–670.

72 Phillips, W.T., Klipper, R., and Goins, B. (2000) Novel method of greatly enhanced delivery of liposomes to lymph nodes. *J. Pharmacol. Exp. Ther.*, **295** (1), 309–313.

73 Phillips, W.T., Klipper, R., and Goins, B. (2001) Use of ($^{99m}$)Tc-labeled liposomes encapsulating blue dye for identification of the sentinel lymph node. *J. Nucl. Med.*, **42** (3), 446–451.

74 Phillips, W.T., Andrews, T., Liu, H., Klipper, R., Landry, A.J., Blumhardt, R. *et al.* (2001) Evaluation of [($^{99m}$)Tc] liposomes as lymphoscintigraphic agents: comparison with [($^{99m}$)Tc] sulfur colloid and [($^{99m}$)Tc] human serum albumin. *Nucl. Med. Biol.*, **28** (4), 435–444.

75 Awasthi, V.D., Garcia, D., Goins, B.A., and Phillips, W.T. (2003) Circulation and biodistribution profiles of long-circulating PEG-liposomes of various sizes in rabbits. *Int. J. Pharm.*, **253** (1–2), 121–132.

76 Awasthi, V.D., Garcia, D., Klipper, R., Phillips, W.T., and Goins, B.A. (2004) Kinetics of liposome-encapsulated hemoglobin after 25% hypovolemic exchange transfusion. *Int. J. Pharm.*, **283** (1–2), 53–62.

77 Awasthi, V.D., Garcia, D., Klipper, R., Goins, B.A., and Phillips, W.T. (2004) Neutral and anionic liposome-encapsulated hemoglobin: effect of postinserted poly(ethylene glycol)-distearoylphosphatidylethanolamine on distribution and circulation kinetics. *J. Pharmacol. Exp. Ther.*, **309** (1), 241–248.

78 Uziely, B., Jeffers, S., Isacson, R., Kutsch, K., Wei-Tsao, D., Yehoshua, Z. *et al.* (1995) Liposomal doxorubicin: antitumor activity and unique toxicities during two complementary phase I studies. *J. Clin. Oncol.*, **13** (7), 1777–1785.

79 de Marie, S. (1996) Liposomal and lipid-based formulations of amphotericin B. *Leukemia*, **10** (Suppl 2), S93–S100.

80 Muggia, F.M., Hainsworth, J.D., Jeffers, S., Miller, P., Groshen, S., Tan, M. *et al.* (1997) Phase II study of liposomal doxorubicin in refractory ovarian cancer: antitumor activity and toxicity modification by liposomal encapsulation. *J. Clin. Oncol.*, **15**, 987–993.

81 Gabizon, A.A. and Muggia, F.M. (1998) Initial clinical evaluation of pegylated liposomal doxorubicin in solid tumors, in *Long-Circulating Liposomes: Old Drugs, New Therapeutics* (eds M.C. Woodle and G. Storm), Landes Bioscience, Austin, TX, pp. 155–174.

82 Muggia, F.M., Blessing, J.A., Sorosky, J., and Reid, G.C. (2002) Phase II trial of the pegylated liposomal doxorubicin in previously treated metastatic endometrial cancer: a Gynecologic Oncology Group study. *J. Clin. Oncol.*, **20**, 2360–2364.

83 Muggia, F. and Hamilton, A. (2001) Phase III data on Caelyx(R) in ovarian cancer. *Eur. J. Cancer*, **37** (Suppl 9), 15–18.

84 Dézsi, L., Fülöp, T., Mészáros, T., Szénási, G., Urbanics, R., Vázsonyi, C. *et al.* (2014) Features of complement activation-related pseudoallergy to liposomes with different surface charge and PEGylation: comparison of the porcine and rat responses. *J. Control. Release*, **195**, 2–10.

85 Dézsi, L., Rosivall, L., Hamar, P., Szebeni, J., and Szénási, G. (2015) Rodent models of complement activation-related pseudoallergy: inducers, symptoms, inhibitors and reaction mechanisms. *Eur. J. Nanomed.*, **7** (1), 15–25.

86 Szebeni, J., Baranyi, L., Savay, S., Bodo, M., Milosevits, J., Alving, C.R. *et al.* (2006) Complement activation-related cardiac anaphylaxis in pigs: role of C5a anaphylatoxin and adenosine in liposome-induced abnormalities in ECG and heart function. *Am. J. Physiol. Heart Circ. Physiol.*, **290** (3), H1050–H1058.

87 Szebeni, J., Bedőcs, P., Rozsnyay, Z., Weiszhár, Z., Urbanics, R., Rosivall, L. *et al.* (2012) Liposome-induced complement activation and related cardiopulmonary distress in pigs: factors promoting reactogenicity of Doxil and AmBisome. *Nanomedicine*, **8**, 176–184.

88 Chanan-Khan, A., Szebeni, J., Savay, S., Liebes, L., Rafique, N.M., Alving, C.R. *et al.* (2003) Complement activation following first exposure to pegylated liposomal doxorubicin (Doxil): possible role in hypersensitivity reactions. *Ann. Oncol.*, **14** (9), 1430–1437. Epub 2003/09/05.

89 Kozma, T.G., Mészáros, T., Weiszhárt, Z., Schneider, T., Rosta, A., Urbanics, R. *et al.* (2015) Variable association of complement activation by rituximab and paclitaxel in cancer patients *in vivo* and in their screening serum *in vitro* with clinical manifestations of hypersensitivity: a pilot study. *Eur. J. Nanomed.*. doi 10.1515/ejnm-2015-0026

90 Szebeni, J. (2012) Hemocompatibility testing for nanomedicines and biologicals: predictive assays for complement mediated infusion reactions. *Eur. J. Nanomed.*, **5**, 33–53.

91 Szebeni, J., Wassef, N.M., Rudolph, A.S., and Alving, C.R. (1996) Complement activation in human serum by liposome-encapsulated hemoglobin: the role of natural anti-phospholipid antibodies. *Biochim. Biophys. Acta*, **1285**, 127–130.

92 Szebeni, J., Spielberg, H., Cliff, R.O., Wassef, N.M., Rudolph, A.S., and Alving, C.R. (1997) Complement activation and thromboxane secretion by liposome-encapsulated hemoglobin in rats *in vivo*: inhibition by soluble complement receptor type 1. Artificial cells, blood substitutes, and immobilization biotechnology. *Artif. Cells Blood Subst. Immob. Biotechnol.*, **25** (4), 347–355. Epub 1997/07/01.

93 Szebeni, J., Wassef, N.M., Hartman, K.R., Rudolph, A.S., and Alving, C.R. (1997) Complement activation *in vitro* by the red blood cell substitute, liposome-encapsulated hemoglobin: mechanism of activation and inhibition by soluble complement receptor type 1. *Transfusion (Paris)*, **37**, 150–159.

94 Szebeni, J. (1998) The interaction of liposomes with the complement system. *Crit. Rev. Ther. Drug Carrier Syst.*, **15** (1), 57–88.

95 Szebeni, J., Muggia, F.M., and Alving, C.R. (1998) Complement activation by Cremophor EL as a possible contributor to hypersensitivity to paclitaxel: an *in vitro* study. *J. Natl. Cancer Inst.*, **90** (4), 300–306. Epub 1998/03/05.

96 Szebeni, J., Baranyi, B., Savay, S., Lutz, L.U., Jelezarova, E., Bunger, R. *et al.* (2000) The role of complement activation in hypersensitivity to pegylated liposomal doxorubicin (Doxil®). *J. Lipos. Res.*, **10**, 347–361.

97 Szebeni, J., Baranyi, L., Savay, S., Milosevits, J., Bodo, M., Bunger, R. *et al.* (2003) The interaction of liposomes with the complement system: *in vitro* and

*in vivo* assays. *Methods Enzymol.*, **373**, 136–154.

98 Moghimi, M.S., Hunter, C., Dadswell, C.M., Savay, S., Alving, C., and Szebeni, J. (2004) Causative factors behind poloxamer 188 (Pluronic F68, Flocor trade mark)-induced complement activation in human sera: a protective role against poloxamer-mediated complement activation by elevated serum lipoprotein levels. *Biochim. Biophys. Acta*, **1689**, 103–113.

99 Szebeni, J. and Jiskoot, W. (2014) Immunological issues with nanomedicines: immunogenicity, hypersensitivity, accelerated clearance and immune suppression, in *Handbook of Nanobiomedical Research* (ed V. Torchillin), World Scientific, Singapore, pp. 45–73.

100 EMA (2013) Committee for Human Medicinal Products (CHMP): Reflection paper on the data requirements for intravenous liposomal products developed with reference to an innovator liposomal product. EMA/CHMP/806058/2009/Rev 02. http://www.ema.europa.eu/docs/en_GB/document.../WC500140351.pdf (accessed Oct. 19, 2016).

101 Csukas, D., Urbanics, R., Weber, G., Rosivall, L., and Szebeni, J. (2015) Pulmonary intravascular macrophages: prime suspects as cellular mediators of porcine CARPA. *Eur. J. Nanomed.*, **7** (1), 27–36.

102 Lazarou, J., Pomeranz, B.H., and Corey, P.N. (1998) Incidence of adverse drug reactions in hospitalized patients. A meta-analysis of prospective studies. *JAMA*, **279**, 1200–1205.

103 Adkinson, N.F.J., Essayan, D., Gruchalla, R., Haggerty, H., Kawabata, T., Sandler, J.D. *et al.* (2002) Task force report: future research needs for the prevention and management of immune-mediated drug hypersensitivity reactions. *J. Allergy Clin. Immunol.*, **109**, S461–S478.

104 Szebeni, J. (2015) Complement activation by nanomaterials, in *Handbook of Safety Assessment of Nanomaterials: From Toxicological Testing to Personalized Medicine* (ed. B. Fadeel), Pan Stanford Publishing Pte. Ltd., Singapore pp. 289–318.

105 Casadevall, N. (2003) Pure red cell aplasia and anti-erythropoietin antibodies in patients treated with epoetin. *Nephrol. Dial. Transplant.*, **18** (Suppl 8), 37–41.

106 FDA (2014) Guidance for industry: immunogenicity assessment for therapeutic protein products. http://wwwfdagov/downloads/drugs/guidancecomplianceregulatory-information/guidances/ucm338856pdf (accessed Oct. 19, 2016).

107 EMEA (2015) Guideline on immunogenicity assessment of biotechnology-derived therapeutic proteins, EMEA/CHMP/BMWP/14327/2006 Rev. 1 http://wwwemaeuropaeu/docs/en_GB/document_library/Scientific_guideline/2015/10/WC500194507pdf (accessed Oct. 19, 2016).

108 Crommelin, D.J.A., Shah, V.P., Klebovich, I., McNeil, S., Weinstein, V., and Flühmann, et al., (2015) The similarity question for biologicals and non-biological complex drugs. *Eur. J. Pharm. Sci.* **76**, 10–17.

109 Ishida, T., Kojima, H., Harashima, H., and Kiwada, H. (2000) Biodistribution of liposomes and C3 fragments associated with liposomes: evaluation of their relationship. *Int. J. Pharm.*, **205**, 183–193.

110 Ishida, T., Maeda, R., Ichihara, M., Irimura, K., and Kiwada, H. (2003) Accelerated clearance of PEGylated liposomes in rats after repeated injections. *J. Control. Release*, **88** (1), 35–42.

111 Ishida, T., Ichikawa, T., Ichihara, M., Sadzuka, Y., and Kiwada, H. (2004) Effect of the physicochemical properties of initially injected liposomes on the clearance of subsequently injected PEGylated liposomes in mice. *J. Control. Release*, **95**, 403–412.

112 Ishida, T., Harada, M., Wang, X.Y., Ichihara, M., Irimura, K., and Kiwada, H. (2005) Accelerated blood clearance of PEGylated liposomes following preceding liposome injection: effects of lipid dose and PEG surface-density and chain length of the first-dose liposomes. *J. Control. Release*, **105**, 305–317.

113 Wang, X.Y., Ishida, T., Ichihara, M., and Kiwada, H. (2005) Influence of the physicochemical properties of liposomes on the accelerated blood clearance phenomenon in rats. *J. Control. Release*, **104**, 91–102.

114 Ishida, T., Ichihara, M., Wang, X., Yamamoto, K., Kimura, J., Majima, E. *et al.* (2006) Injection of PEGylated liposomes in rats elicits PEG-specific IgM, which is responsible for rapid elimination of a second dose of PEGylated liposomes. *J. Control. Release*, **112**, 15–25.

115 Ishida, T., Wang, X., Shimizu, T., Nawata, K., and Kiwada, H. (2007) PEGylated liposomes elicit an anti-PEG IgM response in a T cell-independent manner. *J. Control. Release*, **122** (3), 349–355. Epub 2007/07/06.

116 Ishida, T. and Kiwada, H. (2008) Accelerated blood clearance (ABC) phenomenon induced by administration of PEGylated liposome. *Yakugaku Zasshi*, **128** (2), 233–243. Epub 2008/02/02.

117 Ishihara, T., Takeda, M., Sakamoto, H., Kimoto, A., Kobayashi, C., Takasaki, N. *et al.* (2009) Accelerated blood clearance phenomenon upon repeated injection of PEG-modified PLA-nanoparticles. *Pharm. Res.*, **10**, 2270–2279.

118 Koide, H., Asai, T., Hatanaka, K., Akai, S., Ishii, T., Kenjo, E. *et al.* (2010) T cell-independent B cell response is responsible for ABC phenomenon induced by repeated injection of PEGylated liposomes. *Int. J. Pharm.*, **392** (1–2), 218–223. Epub 2010/03/17.

119 Tagami, T., Uehara, Y., Moriyoshi, N., Ishida, T., and Kiwada, H. (2011) Anti-PEG IgM production by siRNA encapsulated in a PEGylated lipid nanocarrier is dependent on the sequence of the siRNA. *J. Control. Release*, **151** (2), 149–154. Epub 2011/01/13.

120 Shimizu, T., Ichihara, M., Yoshioka, Y., Ishida, T., Nakagawa, S., and Kiwada, H. (2012) Intravenous administration of polyethylene glycol-coated (PEGylated) proteins and PEGylated adenovirus elicits an anti-PEG immunoglobulin M response. *Biol. Pharm. Bull.*, **35** (8), 1336–1342. Epub 2012/08/07.

121 Suzuki, T., Ichihara, M., Hyodo, K., Yamamoto, E., Ishida, T., Kiwada, H. *et al.* (2012) Accelerated blood clearance of PEGylated liposomes containing doxorubicin upon repeated administration to dogs. *Int. J. Pharm.*, **436** (1–2), 636–643. Epub 2012/08/02.

122 Ichihara, M., Moriyoshi, N., Lila, A.S., Ishida, T., and Kiwada, H. (2013) Anti-PEG IgM production via a PEGylated nano-carrier system for nucleic acid delivery. *Methods Mol. Biol.*, **948**, 35–47. Epub 2012/10/17.

123 Koide, H., Asai, T., Hatanaka, K., Urakami, T., Ishii, T., Kenjo, E. *et al.* (2008) Particle size-dependent triggering of accelerated blood clearance phenomenon. *Int. J. Pharm.*, **362**, 197–200.

124 Joshi, M., Pathak, S., Sharma, S., and Patravale, V. (2008) Solid microemulsion preconcentrate (NanOsorb) of artemether for effective treatment of malaria. *Int. J. Pharm.*, **362**, 172–178.

125 Lu, W., Wan, J., She, Z., and Jiang, X. (2007) Brain delivery property and accelerated blood clearance of cationic albumin conjugated pegylated nanoparticle. *J. Control. Release*, **118**, 38–53.

126 Dams, E.T., Laverman, P., Oyen, W.J., Storm, G., Scherphof, G.L., van Der Meer, J.W. *et al.* (2000) Accelerated blood clearance and altered biodistribution of repeated injections of sterically stabilized liposomes. *J. Pharmacol. Exp. Ther.*, **292**, 1071–1079.

127 Laverman, P., Brouwers, A.H., Dams, E.T., Oyen, W.J., Storm, G., van Rooijen, N. *et al.* (2000) Preclinical and clinical evidence for disappearance of long-circulating characteristics of polyethylene glycol liposomes at low lipid dose. *J. Pharmacol. Exp. Ther.*, **293** (3), 996–1001. Epub 2000/06/28.

128 Pisal, D.S., Kosloski, M.P., and Balu-Iyer, S.V. (2010) Delivery of therapeutic proteins. *J. Pharm. Sci.*, **99**, 2557–2575.

129 Papahadjopoulos, D., Allen, T.M., Gabizon, A., Mayhew, E., Matthay, K., Huang, S.K. *et al.* (1991) Sterically stabilized liposomes: improvements in pharmacokinetics and antitumor

therapeutic efficacy. *Proc. Natl. Acad. Sci. USA*, **88**, 11460–11464.

130 Schellekens, H., Hennink, W.E., and Brinks, V. (2013) The immunogenicity of polyethylene glycol: facts and fiction. *Pharm. Res.*, **30** (7), 1729–1734. Epub 2013/05/16.

131 Shimizu, T., Ishida, T., and Kiwada, H. (2013) Transport of PEGylated liposomes from the splenic marginal zone to the follicle in the induction phase of the accelerated blood clearance phenomenon. *Immunobiology*, **218**, 725–732.

132 Vinuesa, J.C.G. and Chang, P.P. (2013) Innate B cell helpers reveal novel types of antibody responses. *Nat. Immunol.*, **14**, 119–126.

133 Semple, S.C., Harasym, T.O., Clow, K.A., Ansell, S.M., Klimuk, S.K., and Hope, M.J. (2005) Immunogenicity and rapid blood clearance of liposomes containing polyethylene glycol–lipid conjugates and nucleic acid. *J. Pharm. Exp. Ther.*, **312**, 1020–1026.

134 Ichihara, M., Shimizu, T., Imoto, A., Hashiguchi, Y., Uehara, Y., Ishida, T. *et al.* (2011) Anti-PEG IgM response against PEGylated liposomes in mice and rats. *Pharmaceuticals*, **3**, 1–11.

135 Moghimi, S.M., Hamad, I., Andresen, T.L., Jörgensen, K., and Szebeni, J. (2006) Methylation of the phosphate oxygen moiety of phospholipid-methoxy (polyethylene glycol) conjugate prevents PEGylated liposome-mediated complement activation and anaphylatoxin production. *FASEB J.*, **20**, 2591–2593.

136 Mond, J.J., Lees, A., and Snapper, C.M. (1995) T cell-independent antigens type 2. *Annu. Rev. Immunol.*, **13**, 655–692.

137 Mond, J.J., Vos, Q., Lees, A., and Snapper, C.M. (1995) T cell independent antigens. *Curr. Opin. Immunol.*, **7**, 349–354.

138 Dintzis, H.M., Dintzis, R.Z., and Vogelstein, B. (1976) Molecular determinants of immunogenicity: the immunon model of immune response. *Proc. Natl. Acad. Sci. USA*, **73**, 3671–3675.

139 Szebeni, J., Alving, C.R., Baranyi, L., and Bunger, R. (2006) Interactions of liposomes with complement leading to adverse reactions, in *Liposome Technology, Volume III: Interactions of Liposomes with the Biological Milieu*. 3nd edn, (ed. Gregory Gregoriadis), Informa Healthcare, New York, London pp. 1–25.

140 Ishida, T. and Kiwada, H. (2008) Accelerated blood clearance (ABC) phenomenon upon repeated injection of PEGylated liposomes. *Int. J. Pharm.*, **354**, 56–62.

141 Li, C., Cao, J., Wang, Y., Zhao, X., Deng, C., Wei, N. *et al.* (2012) Accelerated blood clearance of pegylated liposomal topotecan: influence of polyethylene glycol grafting density and animal species. *J. Pharm. Sci.*, **101** (10), 3864–3876. Epub 2012/07/11.

142 Zhao, Y., Wang, L., Yan, M., Ma, Y., Zang, G., She, Z. *et al.* (2012) Repeated injection of PEGylated solid lipid nanoparticles induces accelerated blood clearance in mice and beagles. *Int. J. Nanomed.*, **7**, 2891–2900.

143 Corporation, Q. (2014) MicroVue Complement Pan-Specific C3 reagent kit: procedure summary. https://wwwquidelcom/sites/default/files/product/documents/20261_MicroVue%20Pan-Specific_C3_Reagent_Kit_pip df (accessed Oct. 19, 2016).

144 Sroda, K., Rydlewski, J., Langner, M., Kozubek, A., Grzybek, M., and Sikorski, A.F. (2005) Repeated injections of PEG-PE liposomes generate anti-PEG antibodies. *Cell. Mol. Biol. Lett.*, **10** (1), 37–47. Epub 2005/04/06.

145 Sherman, M.R., Williams, L.D., Sobczyk, M.A., Michaels, S.J., and Saifer, M.G. (2012) Role of the methoxy group in immune responses to mPEG-protein conjugates. *Bioconjug. Chem.*, **23** (3), 485–499. Epub 2012/02/16.

146 Barenholz, Y. (2012) Doxil – the first FDA-approved nano-drug: from and idea to product, in *Handbook of Harnessing Biomaterials in Nanomedicine* (ed. D. Peer), Pan Standford Publishing Pte. Ltd., Singapure, p. 335–398.

147 Lyass, O., Hubert, A., and Gabizon, A.A. (2001) Phase I study of doxil-cisplatin combination chemotherapy in patients

with advanced malignancies. *Clin. Cancer Res.*, **7**, 3040–3046.

**148** Szebeni, J., Weiszhár, Z., Rozsnyay, Z., Martinsky, T., Kádas, J., Lázár, J. *et al.* (2013) Plasma proteome profiling with monoclonal antibody libraries: a pilot biomarker analysis for nanomedicine-induced complement activation.

**149** Bodo, M., Szebeni, J., Baranyi, L., Savay, S., Pearce, F., Alving, C. *et al.* (2005) Rheoencephalographic evidence of complement activation-related cerebrovascular changes in pigs. *J. Cereb. Blood Flow Metab.*, **25**, S550.

**150** Urbanics, R., Bedőcs, P., and Szebeni, J. (2015) Lessons learned from the porcine model of CARPA: constant and variable responses to different nanomedicines and administration protocols. *Eur. J. Nanomed.*, **7**, 219–231.

**151** Szebeni, J., Alving, C.R., Rosivall, L., Bunger, R., Baranyi, L., Bedocs, P. *et al.* (2007) Animal models of complement-mediated hypersensitivity reactions to liposomes and other lipid-based nanoparticles. *J. Liposome Res.*, **17** (2), 107–117.

**152** Mészáros, T., Szénási, G., Rosivall, L., Szebeni, J., and Dézsi, L. (2015) Paradoxical rise of hemolytic complement in the blood of mice during zymosan- and liposome-induced CARPA: a pilot study. *Eur. J. Nanomed.*, **7** (3), 257–262.

**153** SCENIHR (2009) Risk Assessment of Products of Nanotechnologies. http://eceuropaeu/health/ph_risk/committees/04_scenihr/docs/scenihr_o_023pdf (accessed Oct. 19, 2016).

**154** SCENIHR (2009) Risk Assessment of Products of Nanotechnologies: Opininon paper by Scientific Committee on Emerging and Newly Identified Health Risks, SCENIHR. http://eceuropaeu/health/archive/ph_risk/committees/04_scenihr/docs/scenihr_o_012pdf (accessed Oct. 19, 2016).

# Part Three
# Second Most Common Cause of Death: Cancer

# 8
# Challenges of Applying Targeted Nanostructures with Multifunctional Properties in Cancer Treatments

*Jean-Luc Coll and Jungyoon Choi*

*Institute for Advanced Biosciences, CR UGA/INSERM U1209 / CNRS UMR5309, Site Santé Allée des Alpes 38700 La Tronche, France*

## 8.1
## Introduction

The efficacy of both the conventional chemotherapy and that of the targeted therapy using small molecules is very often hampered by the poor pharmacodynamic properties of the molecules and, importantly, their toxicity. Now, the access to innovative nanostructured objects with particular functional properties not only allows us to reformulate *old* drugs but also allows the formulation of other drugs that were not suitable for systemic administration.

Nanovectors can target cancer cells while avoiding healthy tissues. They can be engineered in order to be rapidly cleared from the body or, on the contrary, to remain in circulation for extended period of time. In addition, nanomaterials can also combine multiple modalities of cancer diagnostic and treatment such as radiosensitization or photodynamic therapy. Finally, they can also deliver the drugs directly in subcellular compartments and avoid the multidrug resistance system. The specific and passive accumulation of these nanomedicines in tumors is due to the so-called *enhanced permeability and retention* (EPR) effect. Several attempts were made also to introduce specific ligands on their surfaces in order to generate an active targeting and uptake by the receptor-overexpressing tumor cells only, but the efficacy of this strategy is not yet completely established. Only, a very restricted amount of targeted formulations are tested in humans so far. The interest and limitations of this strategy will be presented in this chapter, based on the description of representative examples.

Delivery of drugs or contrast agents to tissues, cells, or intracellular molecular targets is a major challenge, particularly for poorly soluble drug candidates. In all cases, it is important to obtain first a favorable tumor/normal tissue ratio of accumulation of the delivered molecules and second the lowest nonspecific accumulation to reduce toxicity and contaminating signal.

*Nanoscience and Nanotechnology for Human Health,* First Edition. Edited by Bert Müller and Marcel Van de Voorde.

Targeted molecules can be schematically grouped into two categories: small molecules that diffuse freely until they reach their target and large macromolecules that exhibit difficulty in reaching the target but that carry a large cargo and are often multifunctional.

Because small, targeted molecules enter easily into cells, their biological functions and toxicity will rely on their specific activity and on rapid washout. Accordingly, during the past decade, targeted therapies such as epidermal growth factor receptor-tyrosine kinase inhibitors (EGFR-TKIs) represented a crucial innovation that has significantly altered the quality of life and overall survival rate of cancer patients. Unfortunately, they still present some side effects and frequently result in resistant tumors and relapse.

In contrast, several efficient small molecules do not function properly after systemic administration because of their poor solubility, fast metabolism, and/or rapid clearance from the bloodstream [1] or because of efficient detoxification *pumps* on tumor cells, such as P-glycoprotein, conferring a multidrug resistance (MDR) phenotype. Although the use of nanocarriers constitutes an interesting alternative for alleviating these problems, nanovectors tend to diffuse very poorly within tissues. Fortunately, nanoparticles (NPs) can accumulate passively in tumors due to the so-called *enhanced permeability and retention* (EPR) effect initially described by Yasuhiro Matsumura and Hiroshi Maeda in 1986 [2,3], which allows *stealth* macromolecules with a MW>40 kDa (>5 nm) to accumulate in tumors.

Starting from such NPs that accumulate passively in tumors, it is also possible to add specific tumor-homing ligands on their surface. This can increase their targeted accumulation in the tumor vasculature and, importantly, augment their internalization by target tumor cells. This strategy has resulted in the design of some NPs with improved therapeutic performances compared to their passively targeting counterparts, but to date the gain is still uncertain and only a restricted number of targeted NPs were translated for clinical evaluation [4].

Before we focused on how the presence of a ligand can affect the targeting efficiency, it is necessary to understand how untargeted NP function and how the EPR effect operates.

## 8.2 Enhanced Permeability and Retention Effect

### 8.2.1 Biological Point of View

The EPR effect is primarily not only due to an elevated systolic blood pressure that pushes blood into tumor tissue but also due to tumor angiogenesis, which dictates the blood vessel's density and properties. This pathologic angiogenesis produces a tumor endothelium lacking pericytes, presenting a large fenestration

(±100 nm) and thus leaky blood vessels. In addition, because lymphangiogenesis is not very active in tumors, lymphatic drainage is inefficient. Although the impact of the EPR effect is unquestionable, albeit variable in mice, its importance or existence in humans remains under discussion. For example, it has been described that only human sarcoma tumors could present tumor accumulation of liposomes, whereas breast, lung, ovarian, head and neck, and glioblastoma tumors showed lower accumulation of liposomes than in the surrounding tissues [5]. Tumors grow rapidly in a confined environment (and this is particularly true in animal models as compared to human tumors), inducing pressure on the surrounding stroma and extracellular matrix that leads to an increase in elastic stress and to a 10- to 100-fold increase in interstitial fluid pressure (IFP) in the tumor as compared to healthy surrounding tissues. Accordingly, the convection flow, which can be represented by the difference in pressure between the therapeutic solution and the tumor, will push the fluid (and cancer cells) away from the tumor and into the surrounding tissue. This pressure gradient reduces the transport of macromolecules away from vessels [6,7] and should thus be overcome by an elevated blood pressure.

### 8.2.2
### Biophysical Perspective

The EPR effect also depends on the physicochemical properties of nanovectors (e.g., size, electric charge, etc.) that will allow NPs to move relatively freely. The first rule that applies to large molecules is that they must remain in the blood circulation for longer than 6 h to benefit from the EPR effect [3]. This is the reason why chemists have made great efforts to adapt their size and to create a surface as invisible as possible to avoid capture by the reticuloendothelial system (RES); in addition, a large diameter will prevent rapid elimination through the kidneys. This stealth quality, while preventing electrostatic interaction with extravascular matrices once in the tumor microenvironment [8,9], will also reduce the capacity of the NPs to interact with the target cell. The NPs will thus remain entrapped in the interstitium until they are degraded or until they are endocytosed. It is, thus, tempting to introduce a targeting molecule onto nanovectors at this step because the ligand could interact with the target receptor and allow intracellular delivery, as presented below [3,5,10–17].

## 8.3
## Physicochemical Factors that Influence NP Passive Properties

As shown in Figure 8.1, in addition to the presence of ligand, several parameters influence the properties of an NP, for instance, size, charge, shape, and hydrophobicity.

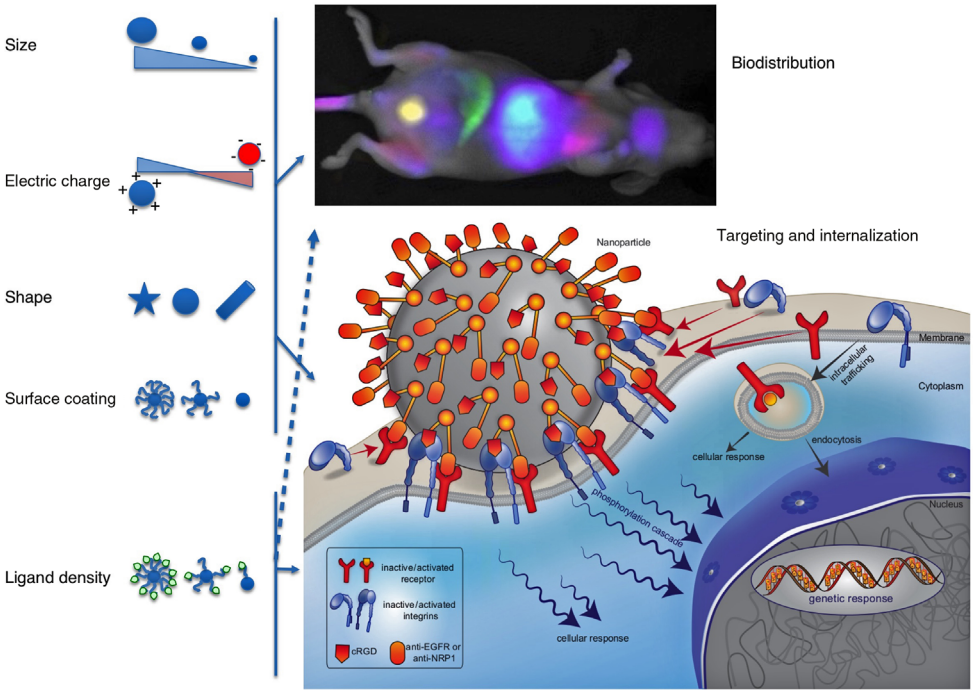


**Figure 8.1** Factors such as size, electric charge, surface coating, and the presence of targeting ligands can influence the biodistribution and intracellular uptake of nanoparticles.

### 8.3.1 Influence of the Size of the NP

Because the fenestration of the tumor-specific endothelium is around 100 nm, the NP smaller than this cut-off will be able to diffuse passively between endothelial cells. Macromolecules smaller than 6 nm accumulate more rapidly and penetrate deeper in the tumor than larger molecules; however, this is very transitory [18], and they are rapidly filtered through the kidneys [19] as demonstrated with imaging probes. Within 24 h, the majority of small-size imaging probes are usually filtered by the kidneys with a clearance efficiency greater than 50% of the injected dose (%ID) and a poor nonspecific accumulation in the main organs. This is the case for most of the hydrophilic intravenously injected and FDA-approved contrast agents used in humans for MRI, CT, SPECT, or PET imaging as well as for the near-infrared dyes used for optical imaging in preclinical studies. NPs of diameters smaller than 6 nm, such as gold nanoclusters [20,21] or gold NPs [22], quantum dots [19], silica [23], or gadolinium-polysiloxane-containing ultrasmall NPs [24,25], are also very rapidly cleared via the kidneys; however, despite their efficient renal clearance, ultrasmall inorganic NPs may be of great interest in theranostic applications, discussed below. Note that because of their small size and molecular weight below 40–50 kDa, such small NPs do

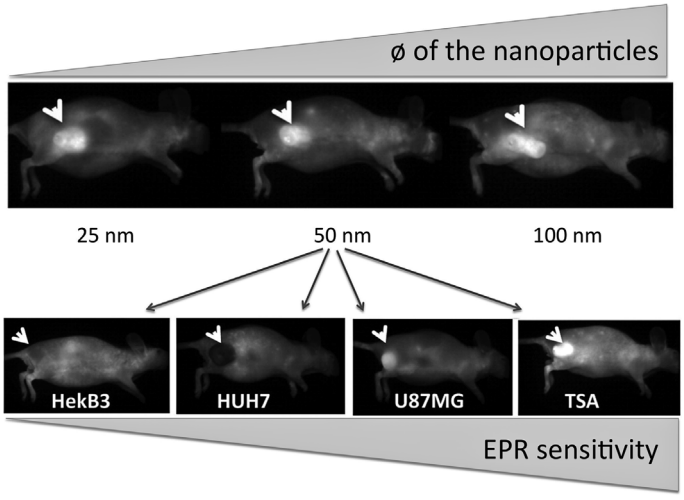


**Figure 8.2** Variability of the EPR effect in mice bearing different types of subcutaneous tumors (reproduced with permission from Ref. [28]. Copyright 2013 Elsevier Inc, graphical abstract).

not formally fall into the category of EPR-sensitive macromolecules. A recent and excellent review presents a broad view of our understanding of the behavior of such inorganic NPs [26].

We also investigated the EPR effect attained with larger NPs ranging from 25 to 100 nm. Although the smallest nanoemulsions (25 nm) disappeared from the blood circulation faster than the larger ones (50 and 100 nm) due to a rapid elimination and wider tissue distribution [27], the biodistribution profiles of all these particles were similar after 24 h and a positive but highly variable EPR effect was generally detected in different tumor types [28], see Figure 8.2. This was also observed using polymeric micelles with diameters of 30, 50, 70, and 100 nm [29]: all the micelles penetrated highly permeable tumors in mice, but only the smallest was able to penetrate poorly permeable tumors.

Clearly, the size and surface area of the NP also impacts the number of ligands that can be attached, cf. Figure 8.3, and thus NP reactivity and biological function. In addition, the surface elasticity and rigidity of the NP can change its binding efficiency toward the tumor cells [30]. The aspect ratio, that is, the ratio between the length and the diameter of an NP [31], may also play a very important role. Spherical NPs will not diffuse like rod-shaped or filamentous nanoobjects, and their interaction with the microenvironment and on the cell surface will differ, providing variable targeting properties [31].

### 8.3.2
### Surface Modification and Opsonization

As soon as they are diluted in serum-containing medium, NPs interact with serum components and in particular with abundant proteins that will form a

| Diameter of the NP | Antibody | Aptamer | Protein | Peptide | Small molecule | PEG2000 |
|---|---|---|---|---|---|---|
| **100 nm** | 140 | 314 | 558 | 13 956 | 125 600 | 7 850 |
| **50 nm** | 35 | 79 | 140 | 3 489 | 31 400 | 1 963 |
| **10 nm** | 1 | 3 | 6 | 140 | 1 256 | 79 |
| **5 nm** | <1 | 1 | 1 | 35 | 314 | 20 |
| **2.5 nm** | <1 | <1 | <1 | 9 | 78 | 5 |

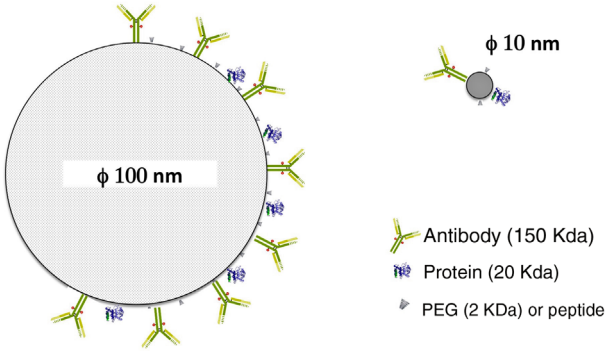


**Figure 8.3** Basic evaluation of the number of ligands that is physically possible to attach on NPs of different sizes, and the at scale representation.

*corona*. The quality, amount, and presentation of proteins in the corona are usually the main cause of the biological responses of nanovectors. Abundant proteins such as serum albumin, antibodies, or fibrinogen will be largely responsible for the formation of the corona, but these largely represented proteins may not have necessarily the most important biological activities. Less abundant proteins with high affinity for a receptor may sometime be very active. Among the proteins of the corona, IgG or proteins of the complement system [32], are termed opsonins because they are recognized and phagocytosed by RES cells and particularly macrophages present in the liver (Kupffer cells) and in the spleen. Their presence in the corona thus results in an unfavorable short circulation half-life and to a reduced EPR effect. Furthermore, the presence of the corona also affects the presentation of the ligands on the NP surface and usually reduces its accessibility and its targeting potential [33].

The formation of the corona can be reduced either by grafting the hydrophilic polymer polyethylene glycol (PEG) or, less frequently, by using polysaccharides, for example, dextran and chitosan, onto the NP surface [30]. The presence of PEG polymers is efficient in reducing opsonization and generating an augmented half-life in the circulation [34,35], ultimately leading to an augmented therapeutic activity [36]. However, several publications also describe that the PEG coating can generate an immune response, complement activation [37,38], and possible appearance of anti-PEG immunoglobulins [39]. This immunoglobulin could be responsible for the accelerated blood clearance (ABC), although a recent study indicated that the ABC phenomenon is not due to the opsonization of NPs with anti-PEG IgM [40,41].

A recent study also investigated the quality of the protein corona formed on intravenously injected liposomes and compared it with the situation *in vitro* [33].

This was achieved using bare, non-PEGylated, PEGylated, or antibody-targeted liposomes. The authors observed that the variety of proteins in the *in vivo* corona was more than that *in vitro* and that the presence of these proteins significantly reduced the activity of the targeting antibody, confirming previous observations [42].

In previous work, we also demonstrated that the nature (length) and net electric charge of PEG polymers linked to the surface of a 50 nm large silica NP strongly impacted biodistribution after intravenous injection in mice [43], underlining the importance of the size of PEG polymers and of the net electric charge on the surface [44].

### 8.3.3 Electric Charge

The tumor microenvironment presents different compartments with variable electric charges. In general, the glycocalyx renders the tumor blood vessels negatively charged as does the hyaluronic acid present in the interstitial space. In contrast, collagen fibers have a slightly positive charge. Thus, the presence of positive or negative electric charges on the surface of an NP will (i) increase its affinity for compounds or cell membranes presenting the opposite charge [45] and (ii) reduce its mobility within extracellular matrices. Neutral particles (zwitterionic) will lie in between these two situations and diffuse faster [46].

In mice, the presence of positive charges is usually associated with a stronger tumor accumulation. Using mesoporous silica NPs, which present a net negative electric charge after PEGylation or a positive one after the addition of polyethyleneimine (PEI), Meng *et al.* demonstrated that the presence of the positive charge improved EPR-mediated accumulation in tumors [47]. Such an effect could be related to the fact that positive charges favor electrostatic interaction with the negative charges of the glycocalyx of tumor-associated endothelial cells [48–50], but with a very poor diffusion within the tumor mass [51]. This is now being exploited in clinical trials using EndoTAGTM, a cationic liposome for the delivery of embedded paclitaxel for the treatment of pancreatic cancer [52], advanced cancers and liver metastasis [53], and recently in triple-negative breast cancer [54], and head and neck cancer [55]. Thus far, the results indicate that the use of these liposomes is safe, although their therapeutic impact was not obvious in phase I/II trials.

We demonstrated that the presence of negative charges due to the grafting of PEG-COOH onto silica-based 50 nm large NPs prevented their elimination by the RES [43]. Moreover, the use of shorter PEG250-COOH instead of PEG2000-COOH also allowed RES evasion, yet it dramatically augmented elimination through the kidneys; this reduced half-life in the blood is associated with a lower EPR accumulation.

A very good example of a negatively charged NP largely used in clinic is Abraxane®, a 130 nm particle composed of human serum albumin nonspecifically bound to paclitaxel [56]. Note that although it has been described that its

uptake could be mediated by albumin receptors such as gp60 and possibly by the secreted protein acidic and rich in cysteine (SPARC), Abraxane® is usually not considered an actively targeted NP [57,58]. The role of SPARC still remains an open debate [59].

Since positively charged NP are expected to target the tumor vasculature but diffuse less in the interstitial tissues than neutral ones, it could be of potential interest to design NP with positive charges that could become neutral once they enter the tumor interstitial space.

### 8.3.4 Density of Ligands

The strength of the noncovalent binding of a ligand to its receptor is defined as its affinity. This affinity of each ligand is not augmented, when it is presented by an NP. In fact, it is very often decreased because of eventual chemical modifications [60], steric hindrance, and possible inadequate presentation. It was demonstrated that PEGylation of EXP3174 with PEG 5000 reduced its affinity by 580 times. EXP3174 is a nonpeptidic ligand that binds the angiotensin receptor with a nanomolar affinity. However, if its grafting density on the surface is carefully tuned, the presentation of multiple copies of EXP3174 can generate a very strong cooperative effect, which represents its avidity. This cooperative effect derives from the fact that once the first ligand is bound, it increases the chances for others to find their target in the microenvironment. Indeed, when eleven copies of PEGylated EX3174 were covalently attached to 17 nm × 7 nm rod-shape quantum dots, the cooperative effect was capable of completely reversing the loss of affinity owing to the PEGylation [60]. It was also demonstrated that avidity can improve the efficiency of low-affinity ligands [61]. Multivalency also induces receptor clustering, which enhances the active internalization of nanosystems [62,63]. The ligand density should thus be finely defined [63,64], because, when the density is too low or too elevated, the binding efficiency of the targeted NP is suboptimal [65]. A rough calculation and a schematic representation of the number of molecules that can be mathematically attached to a given surface area are presented in Figure 8.3. The actual definition of the most efficient number of ligands per NP should be carefully investigated on a case-by-case basis [5].

## 8.4 Targeted NPs

Only a restricted number of actively targeted NPs are used in clinical trials [5]. However, as observed in the nonexhaustive list of common targets and targeting ligands recovered from a rapid search in PubMed, see Table 9.1, numerous publications describe the potential of this approach *in vitro* and in preclinical models. I will not present an extensive analysis of each system, as excellent recent reviews can be found [5,66,67], but I will rather attempt to present some selected

**Table 9.1** Results of PubMed queries

| Query performed with keywords | Total | In cancer | Percentage |
|---|---|---|---|
| Targeted nanoparticles | 6223 | 3377 | 54 |
| Folate receptor-targeted nanoparticles | 279 | 237 | 85 |
| Integrin-targeted nanoparticles | 273 | 173 | 63 |
| EGFR-targeted nanoparticles | 161 | 147 | 91 |
| HER2-targeted nanoparticles | 113 | 102 | 90 |
| Transferin receptor-targeted nanoparticles | 85 | 53 | 62 |
| CD44-targeted nanoparticles | 75 | 61 | 81 |
| PSMA-targeted nanoparticles | 40 | 37 | 93 |
| uPAR-targeted nanoparticles | 17 | 16 | 94 |
| Peptide-targeted nanoparticles | 1425 | 841 | 59 |
| Antibody-targeted nanoparticles | 908 | 550 | 61 |
| Folate-targeted nanoparticles | 526 | 417 | 79 |
| RGD-targeted nanoparticles | 176 | 128 | 73 |
| Aptamer-targeted nanoparticles | 146 | 106 | 73 |
| Transferrin-targeted nanoparticles | 138 | 92 | 67 |
| Lectin-targeted nanoparticles | 125 | 42 | 34 |
| Hyaluronic-acid-targeted nanoparticles | 108 | 80 | 74 |
| Glucose-targeted nanoparticles | 69 | 31 | 45 |
| Galactose-targeted nanoparticles | 43 | 16 | 37 |

works that describe the importance and complexity of using nanomedicines with targeting ligands of increasing molecular weight (small molecules, peptides, proteins, etc.).

### 8.4.1 Choice of Target Receptor

The most frequently chosen receptors are folate receptor (FR), integrins and in particular αvβ3 integrin, EGFR receptor, HER2, urokinase receptor (uPAR), transferrin receptor, CD44, and prostate-specific membrane antigen (PSMA), as they are cell-surface receptors and usually overexpressed in tumors.

### 8.4.2 Targeting Folate Receptor Using Folic Acid as an Example of a Small Ligand

Folic acid (FA, folate, also called vitamin B9), is an essential nutrient required for the biosynthesis of nucleotides and for cell proliferation. Two membrane-bound isoforms of FR have been identified in humans: α and β. FRα (FOLR1) has a dissociation constant ($K_d$) of 0.1 nM for FA and is overexpressed on the surface

of several cancers, including breast, kidney, lung, brain, and in particular in >90% ovarian cancers [68]. FOLR1 shows limited expression in normal tissues. It is normally present only on the apical surface of epithelial cells [69] and is thus poorly accessible from the bloodstream. FR+ tumor cells expressing $>10^6$ receptors present them on the basal surface, and activated macrophages are known to present between 100 000 and 200 000 receptors [11]. An anti-FOLR1 monoclonal antibody (farletuzumab) has entered clinical phases for the treatment of ovarian [70,71] and lung cancers [72]. Folic acid has been developed as a drug delivery system under the name of vintafolide (EC245), in which it is associated with a vinca alkaloid via a short hydrophilic peptide spacer and a disulfide-containing self-immolating linker [73–76].

#### 8.4.2.1 Folic Acid Receptor-Targeted NPs for Drug Delivery

Folic acid was attached to poly(ethylene glycol)-poly($\varepsilon$-caprolactone) to form large 70 nm micelles that also contained doxorubicin (Dox, 4.57 wt.%) covalently transported via a hydrazone linker (FA-hyd-PECL-hyd-Dox) [77]. Because of the presence of the hydrazine linker, Dox release is under pH control and should occur in the acidic environment of endosomes only after intracellular internalization. This resembles the disulfide self-immolating bridge present in the vintafoldine compound, although it reacts to pH rather than to a redox reaction. Indeed, 70% of the Dox content is released after 10 h at pH 5.0. Of note, this is also associated with swelling of the NP that may be beneficial for improved retention of NPs and eventually initiation of the drug release process in the acidic microenvironment of tumors, but such a phenomenon is not documented in the publication. The process is associated with an augmented $IC_{50}$ of the formulated Dox (0.51 mg/ml) that is three times higher than free Dox ($IC_{50}$, 1.51 mg/ml). The half-life of the formulated Dox is also significantly augmented (14 versus 1.5 h for free Dox), and its body distribution is largely affected. In particular, a 10-times augmented concentration of Dox in the tumor was found to be due to the targeted formulation, reaching a sustained concentration of the targeted particles of more than 6 μg/g in 24 h. In the absence of folic acid, the untargeted formulation also increases tumor targeting by the EPR effect, but the peak of concentration is reduced to 6 h. In terms of active targeting, the presence of folic acid reduced the accumulation of micelles in the liver, heart, spleen, and lungs, while augmenting its accumulation in the tumor. Overall, this was associated with a reduced general toxicity after treatment with a dose of 5 mg/kg of Dox and a dramatic increase in the survival rate after 45 days with targeted micelles (60%) versus naked micelles (30%); conversely, all the mice were dead at Day 33 with free Dox. These results are in the same range as that obtained with vintafolide because several SMDCs (small-molecule drug conjugates), such as vintafolide, which are being studied, provide safe delivery of 10–20-fold more drug to FR-expressing tumors compared to the unconjugated drug, when the latter was dosed at MTD (C. Leamon, personal communication). It is thus reasonable to assume that SMDCs that present a 1 : 1 ratio of FA:drug diffuse more efficiently than large 70 nm FA-hyd-PECL-hyd-Dox NPs, even though the latter

will deliver a larger amount of drug/vector. However, this comparison between the two types of vectors stands for the delivery of small drugs such as Dox, but SMDCs are expected to be less adapted than NPs for the delivery of larger drugs as well as poorly soluble or unstable payloads.

Another level of complexity in the formulation of Dox was recently published [78] and is based on the folic acid-mediated targeting of mesoporous silica NPs. Because mesoporous NPs contain empty cavities, they can be loaded with drugs that, however, will usually leak out as easily as they are loaded. In this study, folate-covered mesoporous NPs were covered by gelatin, which masked the holes and the surface of the NPs. PEGs were added to gelatin to improve bioavailability and the EPR effect. Folic acid is embedded and inaccessible. Therefore, such a nanomedicine will passively target a tumor via the EPR effect and encounter a favorable gradient of tumor-associated matrix metalloprotease 2 (MMP-2), which digests the gelatin and thus uncovers the folic acid. Thereafter, the folic acid enhances the internalization of NPs and the specific delivery of Dox. When injected intravenously, these NPs show improved performance in terms of Dox antitumor activity, without systemic toxicity.

The importance of nanomedicine in regard to NP multifunctionality was also recently demonstrated using a sequentially active multitargeted nanovector [79]. In this study, paclitaxel (PTX) was delivered *in vitro* and *in vivo* in mice using large, 200 nm FA-targeted dendrimers. In addition to targeting FA, the liberation of PTX was under the control of cathepsin B, a protease overexpressed in tumors, which was achieved through a cathepsin B-cleavable tetrapeptide conjugating PTX to the poly(amidoamine) dendrimer in the core of the particle.

Targeting NP with a small ligand was a successful strategy and resulted in the rapid clinical translation of a self-assembling 100 nm polymeric NP (BIND-014) that delivers docetaxel for cancer therapy via the active targeting of prostate-specific membrane antigen. Despite its name, PSMA is also expressed in other cancers [80] and BIND-014 is now in phase II trials in patients with NSCLC, urothelial carcinoma, cholangiocarcinoma, cervical cancer, and squamous cell carcinoma of the head and neck. The polymeric matrix consists of PEG-poly(D, L-lactic acid) (PEG5k-PLA16 k) mixed with PEG5k-PLA16k-ACUPA in a 97.5 to 2.5% ratio. The ACUPA (*S*,*S*-2-[3-[5-amino-1-carboxypentyl]-ureido]-pentanedioic acid) moiety is a PSMA substrate analog inhibitor. The pharmacokinetic profile of BIND-014 did not differ among mice, rats, monkeys, and human [81] and showed a blood circulation half-life of 20 h. The plasma levels of docetaxel were 100 times more elevated when administered in humans as BIND-014 compared to its usual solvent-based formulation. In terms of therapeutic efficacy in humans, the initial results are very promising [81].

#### 8.4.2.2 Folic Acid Receptor-Targeted NPs as Contrast Agents

For imaging purposes, the folic acid-targeted peptide derivative EC20, similar to that used for vintafolide, was labeled with $^{99m}$Tc [82] and used for SPECT imaging [83]. In parallel, folic acid labeled with FITC was injected in patients for intraoperative near-infrared optical-guided surgical resection of ovarian

cancer [84]. Based on the status of the receptors and the success of targeting, it is thus tempting to generate targeted nanoobjects, as recently performed [11], whereby folic acid was used to generate folate-PEG3400-DSPE liposomes of 100 nm loaded with a near-infrared dye (DiD) or with 3 H. In this preclinical study, two FR+ tumors were engrafted subcutaneously in mice. The animals also presented either ulcerative colitis or inflamed injured muscles to investigate how the targeted NPs behaved in the inflammatory milieu. The results clearly established not only that the folate-targeted and nontargeted NPs accumulate more efficiently at sites of inflammation than in solid tumors but also that the presence of the ligand was indeed improving targeting.

### 8.4.3 Targeting Integrin with Peptides

The integrin family is composed of 24 αβ heterodimeric members that mediate the attachment of cells to the extracellular matrix (ECM). Only eight recognize the RGD tripeptide sequence and in particular αVβ3, an integrin selectively overexpressed on the surface of neoangiogenic endothelial cells and in (migrating) tumor cells. One of the best studied RGD-peptide ligands for αVβ3 integrin is c (RGDf-N(Me)-V), which is also known as EMD121974 or cilengitide. This RGD peptide displays affinity in the subnanomolar range. Importantly, cilengitide displays a 1000-fold preference for αVβ3 over αIIbβ3, a very similar integrin expressed on platelets [85]. The multivalent binding of αVβ3 leads to their clustering, which in turn activates various kinases and signaling events [62].

Cilengitide [86–89] and several monoclonal antibodies, such as anti-αVβ3 (Vitaxin, Abegrin (etaracizumab) [90], CNTO-95 (intetumumab), and c7E3), were evaluated for possible antiangiogenic activity in clinical trials. To date, most have failed to demonstrate efficacy, and some even accelerated tumor progression, as demonstrated in prostate cancer patients [91]. Cilengitide failed in phase III trials because of a lack of antiangiogenic activity in glioblastoma [92]. It was also described that RGD-peptides or mimetic could present not only a very modest antiangiogenic activity at concentrations higher than 1 μM but also proangiogenic activity, if delivered at too low (nanomolar) concentration, in which case they promoted VEGF-mediated angiogenesis [93]. Indeed, intravenous injection of a dose of 200 mg/kg of RGD mimetic or cilengitide in mice was associated with micromolar plasma concentrations in a few hours, which rapidly decreased to nanomolar levels that persisted for 16–24 h after administration. This phenomenon should be kept in mind, when using targeted molecules that bind and cross-link homo- or heterodimeric receptors, thus generating different intracellular signaling cascades in a dose-dependent manner.

Nonetheless, RGD-based molecules are interesting targeted vectors for imaging, as was described for PET imaging in patients using $^{18}$F- or $^{68}$Ga-labeled\ Galacto-RGD [94–97]. These studies demonstrated a high level of detection of primary tumors (80–100%), but with reduced detection for distant metastasis or

invaded lymph nodes. However, inflammatory regions were also detected, and it is thus difficult to distinguish between benign and malignant lesions. Furthermore, atherosclerotic plaques were also detected [98] because activated macrophages express the integrin.

We also demonstrated the importance of RGD-based multimeric peptides for near-infrared optical imaging and PET and SPECT imaging of tumors as well as for the imaging of physiological and pathological angiogenesis in mice [99–105]. Concerning therapeutic applications, we reported that RGD-based peptides can be useful in optical-guided tumor surgery of head and neck cancer [106], peritoneal carcinomatosis [107], and infiltrative fibrosarcoma in cats [108]. We also proved the delivery of toxic peptides [109–111]. However, these studies noted that the 1: 1 ratio between the targeting RGD moiety and the toxic peptide was not sufficiently strong. Because we found that it was necessary to deliver larger amounts of the drug at the same time, we decided to generate a targeted NP. We used in parallel an NP of a size smaller than 5 nm [112,113] or as large as 50 nm [12]. Several other groups are also working in this direction, and numerous publications report the synthesis and use of RGD-targeted NPs (reviewed in [67]). In particular, a silica-based NP smaller than 7 nm was used as a multimodal NIR optical imaging and PET imaging contrast agent (labeled with 124I) [114] in the presence of an RGD-targeting ligand. In preclinical models, these targeted NPs provided a twofold increase in the targeting of a melanoma subcutaneous tumor with an overall modest 1.5% ID/g in 4 h due to the presence of RGD. This study was further extended to a phase I clinical trial in humans [16], which essentially confirmed the pharmacodynamics data obtained in mice but provided very modest tumor detection, with short retention times in a melanoma metastasis present in the liver [16]. These preclinical data are in agreement with our own, which also indicated a twofold increase in RGD-mediated targeting of U87MG glioblastoma subcutaneous tumors using gadolinium-based small rigid platforms [112]. Similarly, we also obtained a tumor versus skin fluorescence ratio of $1.53 \pm 0.07$ at 24 h after intravenous administration of large 35 nm lipid NPs in mice bearing subcutaneous tumors that overexpress very high levels of αVβ3 integrin. However, using larger NPs of 120 nm, the presence of RGD peptides did not augment active targeting [115] *in vivo*, as evidenced using $^{19}$F MRI.

These results are thus disappointing and raise questions concerning the added value of the presence of RGD in terms of gain in the efficacy of accumulation of NPs in tumors. Importantly, this targeting may be more helpful for the delivery of therapeutic agents, as demonstrated for siRNA [116]. The remainder of this chapter focuses on the work that has been performed using RGD-targeted gold NPs, because they serve as an example of promising inorganic theranostic agents that combine both diagnostic and therapeutic activities.

#### 8.4.3.1 RGD-Targeted Gold NPs

Gold (Au) is a very interesting product, because its assembly can produce NPs of different shapes in a controlled manner. AuNP shapes include nanoshell,

nanorod, nanocage, nanostar, and nanopopcorn [117], and they are used for drug delivery and imaging applications. Because of their high atomic number, small size, and chemical properties that make them amenable to functionalization, AuNPs have unique properties for medical purposes [118]. In particular, these nontoxic inert particles can serve as prodrugs because they absorb photons as a function of their size and aspect ratio and release this accumulated energy by converting it into heat [119] used for phototherapy under near-infrared illumination [120] or because of their radiosensitizing effect under X-ray irradiation [20,21,121,122]. They can serve as contrast agents both for X-ray imaging, with a three times greater attenuation than iodine, and for photoacoustic imaging, allowing tumor detection and imaging prior to remote activation [120].

Chen *et al.* used 26 nm large AuNPs to develop a chemical method of PEGylation that allowed the controlled addition of RGD-targeting ligands [123]. They proved *in vitro* that the presence of an increasing amount of RGD was associated with an increased efficacy of gold internalization in a dose-dependent manner, but this effect was mainly linked to unspecific binding when the peptide/AuNP ratio exceeded 50. Under optimized conditions, the presence of RGD increased internalization by 18 times. Starting with 32 nm large gold nanoclusters, another group covalently added RGD and Dox, thus forming larger Au-cRGD-DOX nanoclusters (58 nm of hydrodynamic radius) [124]. These targeted NPs were interestingly able to deliver Dox to the target cells, in contrast to Au-DOX NPs, and more importantly to generate a dual toxic effect by combining a near-infrared-induced thermal toxicity as well as Dox-mediated chemotherapeutic activity. This strategy was efficient in mice models after intratumoral or intravenous injection of the targeted NPs, confirming previous results that demonstrated the importance of gold nanorods in hyperthermia treatment of tumors [125,126] and the initial work by Hirsch *et al.* [127]. In a recent study, the impact of gold-mediated hyperthermia on tumors was evaluated noninvasively using a dendrimeric RGD-targeted multimodal nanoprobe followed by MRI. This study demonstrated that RGD targeting is indeed not only capable of inducing a high tumor/background ratio but can also serve to evaluate the therapeutic impact of a given treatment on the tumor vasculature [128].

Because it can provide photothermal destruction of malignant tissues and because of its apparent lack of toxicity in preclinical studies, gold is expected to be crucial in clinical applications. Nonetheless, long-term toxicity studies need to be performed [117] and a more precise standardization of the procedures needs to be implemented [129]. It should be noted that the covalent labeling of antibodies with 50 nm gold NPs prevented their capacity to generate the antibody-dependent cellular cytotoxicity (ADCC) that is normally present and part of the antibody-mediated antitumor effect [130]. Thus, the use of antibody-targeted gold NPs may not be feasible if we want to retain the innate and full activity of the therapeutic antibody. Nonetheless, this may also be the case with the covalent labeling of many other antibodies.

### 8.4.4 Protein-Targeted NPs

Among the eight targeted NPs used in clinical phases [5], four of them (MBP426, CALAA-01, SGT-53, and SGT-94) were directed against transferrin receptor (TfR).

#### 8.4.4.1 Targeting Transferrin Receptor

Transferrin (Tf) is a soluble protein that delivers iron to cells via its binding to TfR with an affinity ranging from 1 to 10 nM. Because cancer cells actively proliferate, they require iron and thus overexpress TfR [131], though it is normally ubiquitously expressed. After clathrin-mediated endocytosis, iron is released into early endosomes, and TfR is then recycled back to the cell surface. TfR is also abundantly expressed in the cerebral endothelium, where it can facilitate iron-loaded transferrin uptake from the bloodstream and its release into the brain parenchyma [132]. Depending on the transferrin content from low via moderate to high, NPs can fail to engage TfR on endothelial cells (low Tf content), adhere to the endothelium without being transferred (elevated Tf content), or undergo receptor-mediated transcytosis (moderate Tf content). This *bell curve* that correlates the Tf biological efficacy to its density on the NP surface is thus similar to that observed using RGD.

MBP-426 (Mebiopharm) is a transferrin–liposome–oxaliplatin conjugate. Transferrin is covalently attached via a pH sensitive *N*-glutarylphosphatidylethanolamine (NGPE) linker that allows oxaliplatin release in acidic (pH 5.5) endosomes (T. Fujisawa, Mebiopharm, personal communication). After the completion of a phase 1 and 1b studies on a total of 49 patients (clinical trial ID: NCT00355888), it is in phase 2a on 19 patients as a second-line treatment for gastric, gastro-esophageal, and esophageal adenocarcinomas (clinical trial ID: NCT00964080) in combination with leucovorin (folinic acid or FA) and fluorouracil (5-FU). The treatment was well tolerated (no over Gr 2 peripheral neurotoxicity reported) and a tumor reduction of more than 30% (PR) was observed in a patient resistant to platinum.

Based on initial preclinical works in mice and nonhuman primates [133–136], CALAA-01, a four-component NP [137], was made using the Rondel™ patented small RNA delivery technology. It was made of linear, cyclodextrin-containing cationic polymers (CDP s) targeted by transferrin (Tf) and siRNA was manufactured and tested in humans [138]. It was manufactured in two vials that were mixed just before injection so that the components could self-assemble. Vial 1 contained the polymers conjugated to human transferrin. Vial 2 contained a siRNA directed against the M2 subunit of ribonucleotide reductase (RRM2) [139]. Here also the preclinical pharmacokinetics data obtained in mice, rats, and nonhuman primates correlated well with those obtained in the 24 patients of the first clinical trial ever made in humans using siRNA. It should be noticed that the NP exhibited similar biodistribution and tumor localization in the presence or absence of the transferrin targeting ligand [135]. However, the

transferrin-targeted siRNA-NPs reduced the expression of their targeted gene relative by 50% compared to the nontargeted NP in preclinical studies, suggesting an improved cellular uptake due to the presence of active targeting. Because of adverse effects in this clinical trial [4], the development of the CALAA-01 product using the Rondel™ technology was then stopped and redirected to another delivery system that uses a Roche DPC technology product for the treatment of hepatitis B.

In terms of proteins, antibodies are major candidates for targeted delivery. Although antibodies have been the most widely investigated targeting ligands in the clinic, their use in NPs presents several drawbacks because of their important size as well as the fact that they are *naturally* designed to be rapidly cleared from the blood, once they bind to their antigen by the immune system. Indeed, the presence of a specific antibody does not always improve the global biodistribution and overall accumulation in the tumor [140]. The use of subfragments of antibodies missing the Fc domain (Fab fragments) or the one that contains only the antigen recognition domain (single-chain variable fragment scFv) should alleviate some of these problems and it has been shown that the presence of an scFv can augment blood circulation time and improve the biodistribution of targeted NPs [141]. Based on this concept, SGT-53 and SGT-94 nanovectors were studied. SGT-53 and SGT-94 are two formulations containing (1,2-dioleoyl-trimethylammonium-propane (DOTAP) and dioleoyl phosphatidylethanolamine (DOPE)) forming 60–100 nm large cationic liposomes and are able to target the TfR via a single-chain antibody fragment (TfRscFv). These liposomes are loaded with a plasmid expressing the tumor suppressor gene p53 (SGT-53) or the tumor suppressor gene RB94 (SGT-94) [142]. This scFv was preferred to transferrin itself, because it has a reduced molecular weight and size, and because it is a recombinant protein rather than a blood product [143,144]. In mice, SGT-53 was capable to deliver the plasmid to different tumors after a systemic injection and to provide antitumor activity, when combined with docetaxel. It was then translated to a phase I clinical trial in patients with advanced solid tumors [145]. It is now evaluated alone and in combination with topotecan and cyclophosphamide either in pediatric patients with recurrent or refractory solid tumors (clinical trial ID: NCT02354547) or in patients with metastatic pancreatic cancer in combination with gemcitabine/Nab-Paclitaxel (clinical trial ID: NCT02340117)) and in phase II study in combination with temozolomide for treatment of recurrent glioblastoma (clinical trial ID: NCT02340156). This latter study in particular demonstrates that because they target the TfR overexpressed in the cerebral endothelium, these immunoliposomes can cross the blood–brain barrier by TfR-mediated transcytosis and transfer the transported plasmids not only in the glioblastoma tumor cells but also in the tumor-associated cancer stem cells (CSCs), which have been implicated in resistance to treatments and recurrence [146–148]. Based also on preclinical basis [142], SGT-94 entered a phase I study in patients with solid tumors (clinical trial ID: NCT01517464).

#### 8.4.4.2 Targeting the Epithelial Growth Factor Receptor

PEGylated liposomal doxorubicin (Doxil®/Caelyx®) loaded with doxorubicin and presenting covalently linked Fab fragments of cetuximab (anti-EGFR ILs-dox) [149] were also used in a phase I clinical trial in patients with solid tumors (clinical trial ID: NCT01702129) [150] with promising results (one complete remission) that necessitate to be investigated in further trials. Biodistribution studies in mice showed extended half-life in blood ($t_{1/2}$ of 21 h). Here also, an efficient accumulation in tumors was observed (15% ID/g) but was not associated with the presence of the targeting agent in EGFR-overexpressing tumors. The targeting ligand augmented internalization of the drug carrier within tumor cells (92% of analyzed cells versus <5% for nontargeted liposomes) [151] and an improved antitumor activity of doxorubicin, epirubicin, and vinorelbine in preclinical models. Very interestingly also, the effect of such drug-loaded immunoliposomes did not depend on the inhibition of the EGFR receptor but on the internalization and intracellular delivery of the drug [152]. It was also proved using multidrug-resistant positive cells that Dox molecules released intracellularly by these immunoliposomes were able to bypass membrane-bound efflux [153] and thus produced 19–216-fold more cytotoxicity than free Dox *in vitro* and an augmented toxicity *in vivo* [152]. This is an important point, because it indicates that when Dox is delivered directly into the cytoplasm by a nanovector, it could bypass the membrane-associated P-glycoprotein (one of the main contributors to the MDR phenotype) present on some chemioresistant tumor cells, thus overcoming their resistance as demonstrated since a long time for several NPs [154–157].

## 8.5 Conclusions

There is still an important debate concerning the use of active versus passive targeting of nanovectors [5,10,11]. Although most studies present very positive and clear results *in vitro*, the final gain achieved *in vivo* may be modest in terms of targeting efficiency [11,12].

Conversely, if there is still a debate in terms of targeting efficiency, there is a large consensus on the fact that the presence of a ligand improves the receptor-mediated internalization and can improve therapeutic efficacy. This is particularly true for cancer drugs such DNA and siRNA molecules that cannot be internalized alone by cells and that are active only when delivered intact to the appropriate intracellular compartment [13,14]. In addition, this may be important also for drugs that are sensitive to the MDR phenotype. Finally, encapsulation and intracellular delivery will help solve problems of solubility and possible inactivation of drugs that are sensitive to degradation.

Ligands and/or prodrugs can also be hidden within the NPs and unmasked in the tumor only because their exposure or release can be controlled by activatable functions (protease-, pH-, thermo-, or oxidoreduction-sensitive links). The

physicochemical process that will control their unmasking and release can be specific to the tumor microenvironment (the presence of proteases, acidic pH, hypoxia, etc.) or remotely activated (laser light, X-rays, neutrons, ultrasounds, radiofrequency, etc.). This is opening huge possibilities and we can take advantage of the size of these nanovectors to combine multiple function and properties. This is a major advantage in favor of NPs as opposed to small molecules.

The controlled synthesis of such sophisticated nanosystems is not an easy task. It relies on a complex chemistry that must address many parameters (e.g., the NP composition and architecture, the presence of a large number of chemically reactive species, the necessity of mastering the geometry and orientation of the linked compounds, the quality of the coverage and density, and the presentation of the ligand) and because it is very often impossible to completely characterize the final products. All these problems need to be addressed very early in the design process, and all chemical steps should be perfectly mastered and adequately selected to comply with the legal recommendations on the definition of a nanomaterial. This is still a major bottleneck, but the progress made in particular in chemistry and biophysics is so impressive that this does not seem to be out of reach.

However, the additional cost in the production of targeted nanovectors versus passive, standard formulation of the drug should be proportional to the benefits in order to be acceptable. Because it is almost impossible to perform a side-by-side comparison in humans, preclinical data are extremely important because they are proven to be reliable [15,16]. These data must be sustained also by a precise knowledge of the biomarkers of the pathology being addressed in patients (i.e., the level and accessibility of the targeted receptors) and by a thorough understanding of the patient's pathological characteristics that will influence the access of nanovectors to their target [3]. In a recent review, Jain and Stylianopoulos concluded: "Given the highly heterogeneous and continuously evolving nature of the tumor microenvironment, the optimal design of NPs is likely to be disease specific. This is a formidable task, especially considering the difference from one tumor to the next, from primary tumor to its metastasis, from one day to the next in the same tumor and the changes induced by treatment" [17]. Furthermore, it is important to have in mind that at the end of the process, targeted NPs should be very sophisticated but as simple as possible to keep the development of such nanomedicine "reasonably simple, inexpensive, and scalable" [66].

Finally, the possibilities offered by the use of targeted nanomedicines are tremendous and only a part of them was discussed here. But we still need major concerted efforts of multidisciplinary groups before they are fully accepted for cancer diagnostic, treatment, or both.

**Acknowledgments**

Special thanks to Dr. Sandrine Dufort (Nano-H) and N. Mignet (Université Paris Descartes) for the help in the reviewing of this chapter.

This work was supported by the INSERM grants as well as the ANR CALIF (ANR-08-NANO-006), GdLung (ANR-12-P2N-0009), NanoLuc (ANR-11-BSV5-0018), Multimage (ANR-12-RPIB-0010-08), and the INCA PLBio PoroCombo.

## References


1 Gaudin, A., Yemisci, M., Eroglu, H., Lepetre-Mouelhi, S., Turkoglu, O.F., Donmez-Demir, B., Caban, S., Sargon, M.F., Garcia-Argote, S., Pieters, G., Loreau, O., Rousseau, B., Tagit, O., Hildebrandt, N., Le Dantec, Y., Mougin, J., Valetti, S., Chacun, H., Nicolas, V., Desmaele, D., Andrieux, K., Capan, Y., Dalkara, T., and Couvreur, P. (2014) Squalenoyl adenosine nanoparticles provide neuroprotection after stroke and spinal cord injury. *Nat. Nanotechnol.*, **9** 1054–1062.

2 Matsumura, Y. and Maeda, H. (1986) A new concept for macromolecular therapeutics in cancer chemotherapy: mechanism of tumoritropic accumulation of proteins and the antitumor agent smancs. *Cancer Res.*, **46**, 6387–6392.

3 Maeda, H. (2015) Toward a full understanding of the EPR effect in primary and metastatic tumors as well as issues related to its heterogeneity. *Adv. Drug Deliv. Rev.*, **91**, 3–6.

4 Stirland, D.L., Nichols, J.W., Miura, S., and Bae, Y.H. (2013) Mind the gap: a survey of how cancer drug carriers are susceptible to the gap between research and practice. *J. Control. Release*, **172**, 1045–1064.

5 Bertrand, N., Wu, J., Xu, X., Kamaly, N., and Farokhzad, O.C. (2014) Cancer nanotechnology: the impact of passive and active targeting in the era of modern cancer biology. *Adv. Drug Deliv. Rev.*, **66**, 2–25.

6 Torosean, S., Flynn, B., Axelsson, J., Gunn, J., Samkoe, K.S., Hasan, T., Doyley, M.M., and Pogue, B.W. (2013) Nanoparticle uptake in tumors is mediated by the interplay of vascular and collagen density with interstitial pressure. *Nanomed. Nanotech. Biol. Med.*, **9**, 151–158.

7 Munson, J.M. and Shieh, A.C. (2014) Interstitial fluid flow in cancer: implications for disease progression and treatment. *Cancer Manag. Res.*, **6**, 317–328.

8 Zhang, X., Hansing, J., Netz, R.R., and DeRouchey, J.E. (2015) Particle transport through hydrogels is charge asymmetric. *Biophys. J.*, **108**, 530–539.

9 Saito, R., Krauze, M.T., Noble, C.O., Tamas, M., Drummond, D.C., Kirpotin, D.B., Berger, M.S., Park, J.W., and Bankiewicz, K.S. (2006) Tissue affinity of the infusate affects the distribution volume during convection-enhanced delivery into rodent brains: implications for local drug delivery. *J. Neurosci. Methods*, **154**, 225–232.

10 Bazak, R., Houri, M., El Achy, S., Kamel, S., and Refaat, T. (2015) Cancer active targeting by nanoparticles: a comprehensive review of literature. *J. Cancer Res. Clin. Oncol.*, **141**, 769–784.

11 Poh, S., Chelvam, V., and Low, P.S. (2015) Comparison of nanoparticle penetration into solid tumors and sites of inflammation: studies using targeted and nontargeted liposomes. *Nanomedicine (Lond.)*, **10**, 1439–1449.

12 Goutayer, M., Dufort, S., Josserand, V., Royere, A., Heinrich, E., Vinet, F., Bibette, J., Coll, J.L., and Texier, I. (2010) Tumor targeting of functionalized lipid nanoparticles: assessment by *in vivo* fluorescence imaging. *Eur. J. Pharm. Biopharm.*, **75**, 137–147.

13 Choi, C.H., Alabi, C.A., Webster, P., and Davis, M.E. (2010) Mechanism of active targeting in solid tumors with transferrin-containing gold nanoparticles. *Proc. Natl. Acad. Sci. USA*, **107**, 1235–1240.

14 Huang, X., Peng, X., Wang, Y., Shin, D.M., El-Sayed, M.A., and Nie, S. (2010)

A reexamination of active and passive tumor targeting by using rod-shaped gold nanocrystals and covalently conjugated peptide ligands. *ACS Nano*, **4**, 5887–5896.

15 Eliasof, S., Lazarus, D., Peters, C.G., Case, R.I., Cole, R.O., Hwang, J., Schluep, T., Chao, J., Lin, J., Yen, Y., Han, H., Wiley, D.T., Zuckerman, J.E., and Davis, M.E. (2013) Correlating preclinical animal studies and human clinical trials of a multifunctional, polymeric nanoparticle. *Proc. Natl. Acad. Sci. USA*, **110**, 15127–15132.

16 Phillips, E., Penate-Medina, O., Zanzonico, P.B., Carvajal, R.D., Mohan, P., Ye, Y., Humm, J., Gonen, M., Kalaigian, H., Schoder, H., Strauss, H.W., Larson, S.M., Wiesner, U., and Bradbury, M.S. (2014) Clinical translation of an ultrasmall inorganic optical-PET imaging nanoparticle probe. *Sci. Transl. Med.*, **6**, 260ra149.

17 Jain, R.K. and Stylianopoulos, T. (2010) Delivering nanomedicine to solid tumors. *Nat. Rev. Clin. Oncol.*, **7**, 653–664.

18 Dreher, M.R., Liu, W., Michelich, C.R., Dewhirst, M.W., Yuan, F., and Chilkoti, A. (2006) Tumor vascular permeability, accumulation, and penetration of macromolecular drug carriers. *J. Natl. Cancer Inst.*, **98**, 335–344.

19 Choi, H.S., Liu, W., Liu, F., Nasr, K., Misra, P., Bawendi, M.G., and Frangioni, J.V. (2010) Design considerations for tumour-targeted nanoparticles. *Nat. Nanotechnol.*, **5**, 42–47.

20 Zhang, X.D., Chen, J., Luo, Z., Wu, D., Shen, X., Song, S.S., Sun, Y.M., Liu, P.X., Zhao, J., Huo, S., Fan, S., Fan, F., Liang, X.J., and Xie, J. (2014) Enhanced tumor accumulation of sub-2nm gold nanoclusters for cancer radiation therapy. *Adv. Healthcare Mater.*, **3**, 133–141.

21 Zhang, X.D., Luo, Z., Chen, J., Shen, X., Song, S., Sun, Y., Fan, S., Fan, F., Leong, D.T., and Xie, J. (2014) Ultrasmall Au (10–12)(SG)(10–12) nanomolecules for high tumor specificity and cancer radiotherapy. *Adv. Mater.*, **26**, 4565–4568.

22 Liu, J., Yu, M., Ning, X., Zhou, C., Yang, S., and Zheng, J. (2013) PEGylation and zwitterionization: pros and cons in the renal clearance and tumor targeting of near-IR-emitting gold nanoparticles. *Angew. Chem. Int. Ed. Engl.*, **52**, 12572–12576.

23 Burns, A.A., Vider, J., Ow, H., Herz, E., Penate-Medina, O., Baumgart, M., Larson, S.M., Wiesner, U., and Bradbury, M. (2009) Fluorescent silica nanoparticles with efficient urinary excretion for nanomedicine. *Nano Lett.*, **9**, 442–448.

24 Bianchi, A., Dufort, S., Lux, F., Courtois, A., Tillement, O., Coll, J.L., and Cremillieux, Y. (2014) Quantitative biodistribution and pharmacokinetics of multimodal gadolinium-based nanoparticles for lungs using ultrashort TE MRI. *Magma*, **27**, 303–316.

25 Lux, F., Mignot, A., Mowat, P., Louis, C., Dufort, S., Bernhard, C., Denat, F., Boschetti, F., Brunet, C., Antoine, R., Dugourd, P., Laurent, S., Elst, L.V., Muller, R., Sancey, L., Josserand, V., Coll, J.L., Stupar, V., Barbier, E., Remy, C., Broisat, A., Ghezzi, C., Le Duc, G., Roux, S., Perriat, P., and Tillement, O. (2011) Ultrasmall rigid particles as multimodal probes for medical applications. *Angew. Chem.*, **50**, 12299–12303.

26 Yu, M. and Zheng, J. (2015) Clearance pathways and tumor targeting of imaging nanoparticles. *ACS Nano*, **9**, 6655–6674.

27 Hirsjarvi, S., Sancey, L., Dufort, S., Belloche, C., Vanpouille-Box, C., Garcion, E., Coll, J.L., Hindre, F., and Benoit, J.P. (2013) Effect of particle size on the biodistribution of lipid nanocapsules: comparison between nuclear and fluorescence imaging and counting. *Int. J. Pharm.*, **453**, 594–600.

28 Hirsjarvi, S., Dufort, S., Gravier, J., Texier, I., Yan, Q., Bibette, J., Sancey, L., Josserand, V., Passirani, C., Benoit, J.P., and Coll, J.L. (2013) Influence of size, surface coating and fine chemical composition on the *in vitro* reactivity and *in vivo* biodistribution of lipid nanocapsules versus lipid nanoemulsions in cancer models. *Nanomed. Nanotech. Biol. Med.*, **9**, 375–387.

29 Cabral, H., Matsumoto, Y., Mizuno, K., Chen, Q., Murakami, M., Kimura, M., Terada, Y., Kano, M.R., Miyazono, K.,

Uesaka, M., Nishiyama, N., and Kataoka, K. (2011) Accumulation of sub-100nm polymeric micelles in poorly permeable tumours depends on size. *Nat. Nanotechnol.*, **6**, 815–823.

30 Hirsjarvi, S., Dufort, S., Bastiat, G., Saulnier, P., Passirani, C., Coll, J.L., and Benoit, J.P. (2013) Surface modification of lipid nanocapsules with polysaccharides: from physicochemical characteristics to *in vivo* aspects. *Acta. Biomater.*, **9**(5): 6686–6693.

31 Shukla, S., Eber, F.J., Nagarajan, A.S., DiFranco, N.A., Schmidt, N., Wen, A.M., Eiben, S., Twyman, R.M., Wege, C., and Steinmetz, N.F. (2015) The impact of aspect ratio on the biodistribution and tumor homing of rigid soft-matter nanorods. *Adv. Healthcare Mater.*, **4**, 874–882.

32 Liu, D., Liu, F., and Song, Y.K. (1995) Recognition and clearance of liposomes containing phosphatidylserine are mediated by serum opsonin. *Biochim. Biophys. Acta.*, **1235**, 140–146.

33 Hadjidemetriou, M., Al-Ahmady, Z., Mazza, M., Collins, R.F., Dawson, K., and Kostarelos, K. (2015) *In vivo* biomolecule corona around blood-circulating, clinically-used and antibody-targeted lipid bilayer nanoscale vesicles. *ACS Nano*, **9**, 8142–8156.

34 Laine, A.L., Gravier, J., Henry, M., Sancey, L., Bejaud, J., Pancani, E., Wiber, M., Texier, I., Coll, J.L., Benoit, J.P., and Passirani, C. (2014) Conventional versus stealth lipid nanoparticles: formulation and *in vivo* fate prediction through FRET monitoring. *J. Control. Release*, **188**, 1–8.

35 Allen, T.M., Hansen, C., Martin, F., Redemann, C., and Yau-Young, A. (1991) Liposomes containing synthetic lipid derivatives of poly(ethylene glycol) show prolonged circulation half-lives *in vivo*. *Biochim. Biophys. Acta.*, **1066**, 29–36.

36 Papahadjopoulos, D., Allen, T.M., Gabizon, A., Mayhew, E., Matthay, K., Huang, S.K., Lee, K.D., Woodle, M.C., Lasic, D.D., Redemann, C. *et al.* (1991) Sterically stabilized liposomes: improvements in pharmacokinetics and antitumor therapeutic efficacy. *Proc. Natl. Acad. Sci. USA*, **88**, 11460–11464.

37 Hamad, I., Al-Hanbali, O., Hunter, A.C., Rutt, K.J., Andresen, T.L., and Moghimi, S.M. (2010) Distinct polymer architecture mediates switching of complement activation pathways at the nanosphere-serum interface: implications for stealth nanoparticle engineering. *ACS Nano*, **4**, 6629–6638.

38 Hamad, I., Hunter, A.C., Szebeni, J., and Moghimi, S.M. (2008) Poly(ethylene glycol)s generate complement activation products in human serum through increased alternative pathway turnover and a MASP-2-dependent process. *Mol. Immunol.*, **46**, 225–232.

39 Schellekens, H., Hennink, W.E., and Brinks, V. (2013) The immunogenicity of polyethylene glycol: facts and fiction. *Pharm. Res.*, **30**, 1729–1734.

40 Hashimoto, Y., Shimizu, T., Abu Lila, A.S., Ishida, T., and Kiwada, H. (2015) Relationship between the concentration of anti-polyethylene glycol (PEG) immunoglobulin M (IgM) and the intensity of the accelerated blood clearance (ABC) phenomenon against PEGylated liposomes in mice. *Biol. Pharm. Bull.*, **38**, 417–424.

41 Mima, Y., Hashimoto, Y., Shimizu, T., Kiwada, H., and Ishida, T. (2015) Anti-PEG IgM is a major contributor to the accelerated blood clearance of polyethylene glycol-conjugated protein. *Mol. Pharm.*, **12**, 2429–2435.

42 Salvati, A., Pitek, A.S., Monopoli, M.P., Prapainop, K., Bombelli, F.B., Hristov, D.R., Kelly, P.M., Aberg, C., Mahon, E., and Dawson, K.A. (2013) Transferrin-functionalized nanoparticles lose their targeting capabilities when a biomolecule corona adsorbs on the surface. *Nat. Nanotechnol.*, **8**, 137–143.

43 Faure, A.C., Dufort, S., Josserand, V., Perriat, P., Coll, J.L., Roux, S., and Tillement, O. (2009) Control of the *in vivo* biodistribution of hybrid nanoparticles with different poly(ethylene glycol) coatings. *Small*, **5**, 2565–2575.

44 Dufort, S., Sancey, L., and Coll, J.L. (2012) Physico-chemical parameters that govern

nanoparticles fate also dictate rules for their molecular evolution. *Adv. Drug. Deliv. Rev.*, **64**, 179–189.

45 Wang, H., Zhao, P., Liang, X., Gong, X., Song, T., Niu, R., and Chang, J. (2010) Folate-PEG coated cationic modified chitosan–cholesterol liposomes for tumor-targeted drug delivery. *Biomaterials*, **31**, 4129–4138.

46 Stylianopoulos, T., Poh, M.Z., Insin, N., Bawendi, M.G., Fukumura, D., Munn, L.L., and Jain, R.K. (2010) Diffusion of particles in the extracellular matrix: the effect of repulsive electrostatic interactions. *Biophys. J.*, **99**, 1342–1349.

47 Meng, H., Xue, M., Xia, T., Ji, Z., Tarn, D.Y., Zink, J.I., and Nel, A.E. (2011) Use of size and a copolymer design feature to improve the biodistribution and the enhanced permeability and retention effect of Doxorubicin-loaded mesoporous silica nanoparticles in a murine xenograft tumor model. *ACS Nano*, **5**, 4131–4144.

48 Abu Lila, A.S., Ishida, T., and Kiwada, H. (2010) Targeting anticancer drugs to tumor vasculature using cationic liposomes. *Pharm. Res.*, **27**, 1171–1183.

49 Schmitt-Sody, M., Strieth, S., Krasnici, S., Sauer, B., Schulze, B., Teifel, M., Michaelis, U., Naujoks, K., and Dellian, M. (2003) Neovascular targeting therapy: paclitaxel encapsulated in cationic liposomes improves antitumoral efficacy. *Clin. Cancer Res.*, **9**, 2335–2341.

50 Campbell, R.B., Fukumura, D., Brown, E.B., Mazzola, L.M., Izumi, Y., Jain, R.K., Torchilin, V.P., and Munn, L.L. (2002) Cationic charge determines the distribution of liposomes between the vascular and extravascular compartments of tumors. *Cancer Res.*, **62**, 6831–6836.

51 Stylianopoulos, T., Soteriou, K., Fukumura, D., and Jain, R.K. (2013) Cationic nanoparticles have superior transvascular flux into solid tumors: insights from a mathematical model. *Ann. Biomed. Eng.*, **41**, 68–77.

52 Lohr, J.M., Haas, S.L., Bechstein, W.O., Bodoky, G., Cwiertka, K., Fischbach, W., Folsch, U.R., Jager, D., Osinsky, D., Prausova, J., Schmidt, W.E., Lutz, M.P., and Group, C.T.S. (2012) Cationic liposomal paclitaxel plus gemcitabine or gemcitabine alone in patients with advanced pancreatic cancer: a randomized controlled phase II trial. *Ann. Oncol.*, **23**, 1214–1222.

53 Fasol, U., Frost, A., Buchert, M., Arends, J., Fiedler, U., Scharr, D., Scheuenpflug, J., and Mross, K. (2012) Vascular and pharmacokinetic effects of EndoTAG-1 in patients with advanced cancer and liver metastasis. *Ann. Oncol.*, **23**, 1030–1036.

54 Awada, A., Bondarenko, I.N., Bonneterre, J., Nowara, E., Ferrero, J.M., Bakshi, A.V., Wilke, C., and Piccart, M. for the CT4002 Study Group (2014) A randomized controlled phase II trial of a novel composition of paclitaxel embedded into neutral and cationic lipids targeting tumor endothelial cells in advanced triple-negative breast cancer (TNBC). *Ann. Oncol.*, **25**, 824–831.

55 Strieth, S., Dunau, C., Michaelis, U., Jager, L., Gellrich, D., Wollenberg, B., and Dellian, M. (2014) Phase I/II clinical study on safety and antivascular effects of paclitaxel encapsulated in cationic liposomes for targeted therapy in advanced head and neck cancer. *Head Neck*, **36**, 976–984.

56 Miele, E., Spinelli, G.P., Miele, E., Tomao, F., and Tomao, S. (2009) Albumin-bound formulation of paclitaxel (Abraxane ABI-007) in the treatment of breast cancer. *Int. J. Nanomedicine*, **4**, 99–105.

57 Hoang, B., Ernsting, M.J., Roy, A., Murakami, M., Undzys, E., and Li, S.D. (2015) Docetaxel-carboxymethylcellulose nanoparticles target cells via a SPARC and albumin dependent mechanism. *Biomaterials*, **59**, 66–76.

58 Yardley, D.A. (2013) nab-Paclitaxel mechanisms of action and delivery. *J. Control. Release*, **170**, 365–372.

59 Schneeweiss, A., Seitz, J., Smetanay, K., Schuetz, F., Jaeger, D., Bachinger, A., Zorn, M., Sinn, H.P., and Marme, F. (2014) Efficacy of nab-Paclitaxel does not seem to be associated with SPARC expression in metastatic breast cancer. *Anticancer Res.*, **34**, 6609–6615.

60 Hennig, R., Pollinger, K., Veser, A., Breunig, M., and Goepferich, A. (2014) Nanoparticle multivalency

counterbalances the ligand affinity loss upon PEGylation. *J. Control. Release*, **194**, 20–27.

**61** Weissleder, R., Kelly, K., Sun, E.Y., Shtatland, T., and Josephson, L. (2005) Cell-specific targeting of nanoparticles by multivalent attachment of small molecules. *Nat. Biotechnol.*, **23**, 1418–1423.

**62** Sancey, L., Garanger, E., Foillard, S., Schoen, G., Hurbin, A., Albiges-Rizo, C., Boturyn, D., Souchier, C., Grichine, A., Dumy, P., and Coll, J.L. (2009) Clustering and internalization of integrin alphavbeta3 with a tetrameric RGD-synthetic Peptide. *Mol. Ther.*, **17**, 837–843.

**63** Stefanick, J.F., Ashley, J.D., Kiziltepe, T., and Bilgicer, B. (2013) A systematic analysis of peptide linker length and liposomal polyethylene glycol coating on cellular uptake of peptide-targeted liposomes. *ACS Nano*, **7**, 2935–2947.

**64** Hak, S., Helgesen, E., Hektoen, H.H., Huuse, E.M., Jarzyna, P.A., Mulder, W.J., Haraldseth, O., and Davies Cde, L. (2012) The effect of nanoparticle polyethylene glycol surface density on ligand-directed tumor targeting studied *in vivo* by dual modality imaging. *ACS Nano*, **6**, 5648–5658.

**65** Elias, D.R., Poloukhtine, A., Popik, V., and Tsourkas, A. (2013) Effect of ligand density, receptor density, and nanoparticle size on cell targeting. *Nanomedicine*, **9**, 194–201.

**66** Zamboni, W.C., Torchilin, V., Patri, A.K., Hrkach, J., Stern, S., Lee, R., Nel, A., Panaro, N.J., and Grodzinski, P. (2012) Best practices in cancer nanotechnology: perspective from NCI nanotechnology alliance. *Clin. Cancer Res.*, **18**, 3229–3241.

**67** Zhong, Y., Meng, F., Deng, C., and Zhong, Z. (2014) Ligand-directed active tumor-targeting polymeric nanoparticles for cancer chemotherapy. *Biomacromolecules*, **15**, 1955–1969.

**68** Parker, N., Turk, M.J., Westrick, E., Lewis, J.D., Low, P.S., and Leamon, C.P. (2005) Folate receptor expression in carcinomas and normal tissues determined by a quantitative radioligand binding assay. *Anal. Biochem.*, **338**, 284–293.

**69** Elnakat, H. and Ratnam, M. (2004) Distribution, functionality and gene regulation of folate receptor isoforms: implications in targeted therapy. *Adv. Drug Deliv. Rev.*, **56**, 1067–1084.

**70** Sasaki, Y., Miwa, K., Yamashita, K., Sunakawa, Y., Shimada, K., Ishida, H., Hasegawa, K., Fujiwara, K., Kodaira, M., Fujiwara, Y., Namiki, M., Matsuda, M., Takeuchi, Y., and Katsumata, N. (2015) A phase I study of farletuzumab, a humanized anti-folate receptor alpha monoclonal antibody, in patients with solid tumors. *Invest. New Drugs*, **33**, 332–340.

**71** Konner, J.A., Bell-McGuinn, K.M., Sabbatini, P., Hensley, M.L., Tew, W.P., Pandit-Taskar, N., Vander Els, N., Phillips, M.D., Schweizer, C., Weil, S.C., Larson, S.M., and Old, L.J. (2010) Farletuzumab, a humanized monoclonal antibody against folate receptor alpha, in epithelial ovarian cancer: a phase I study. *Clin. Cancer Res.*, **16**, 5288–5295.

**72** Bronte, G., Lo Vullo, F., Pernice, G., Galvano, A., Fiorentino, E., Cicero, G., Bazan, V., Rolfo, C., and Russo, A. (2015) Farletuzumab for NSCLC: exploiting a well-known metabolic pathway for a new therapeutic strategy. *Expert Opin. Investig. Drugs*, **24**, 125–132.

**73** Vergote, I. and Leamon, C.P. (2015) Vintafolide: a novel targeted therapy for the treatment of folate receptor expressing tumors. *Ther. Adv. Med. Oncol.*, **7**, 206–218.

**74** Leamon, C.P., Vlahov, I.R., Reddy, J.A., Vetzel, M., Santhapuram, H.K., You, F., Bloomfield, A., Dorton, R., Nelson, M., Kleindl, P., Vaughn, J.F., and Westrick, E. (2014) Folate-vinca alkaloid conjugates for cancer therapy: a structure–activity relationship. *Bioconjug. Chem.*, **25**, 560–568.

**75** Li, J., Sausville, E.A., Klein, P.J., Morgenstern, D., Leamon, C.P., Messmann, R.A., and LoRusso, P. (2009) Clinical pharmacokinetics and exposure–toxicity relationship of a folate-vinca alkaloid conjugate EC145 in cancer patients. *J. Clin. Pharmacol.*, **49**, 1467–1476.

76 Reddy, J.A., Dorton, R., Westrick, E., Dawson, A., Smith, T., Xu, L.C., Vetzel, M., Kleindl, P., Vlahov, I.R., and Leamon, C.P. (2007) Preclinical evaluation of EC145, a folate-vinca alkaloid conjugate. *Cancer Res.*, **67**, 4434–4442.

77 Guo, X., Shi, C., Wang, J., Di, S., and Zhou, S. (2013) pH-triggered intracellular release from actively targeting polymer micelles. *Biomaterials*, **34**, 4544–4554.

78 Zou, Z., He, X., He, D., Wang, K., Qing, Z., Yang, X., Wen, L., Xiong, J., Li, L., and Cai, L. (2015) Programmed packaging of mesoporous silica nanocarriers for matrix metalloprotease 2-triggered tumor targeting and release. *Biomaterials*, **58**, 35–45.

79 Satsangi, A., Roy, S.S., Satsangi, R.K., Tolcher, A.W., Vadlamudi, R.K., Goins, B., and Ong, J.L. (2015) Synthesis of a novel, sequentially active-targeted drug delivery nanoplatform for breast cancer therapy. *Biomaterials*, **59**, 88–101.

80 Wang, H.L., Wang, S.S., Song, W.H., Pan, Y., Yu, H.P., Si, T.G., Liu, Y., Cui, X.N., and Guo, Z. (2015) Expression of prostate-specific membrane antigen in lung cancer cells and tumor neovasculature endothelial cells and its clinical significance. *PLoS One*, **10**, e0125924.

81 Hrkach, J., Von Hoff, D., Mukkaram Ali, M., Andrianova, E., Auer, J., Campbell, T., De Witt, D., Figa, M., Figueiredo, M., Horhota, A., Low, S., McDonnell, K., Peeke, E., Retnarajan, B., Sabnis, A., Schnipper, E., Song, J.J., Song, Y.H., Summa, J., Tompsett, D., Troiano, G., Van Geen Hoven, T., Wright, J., LoRusso, P., Kantoff, P.W., Bander, N.H., Sweeney, C., Farokhzad, O.C., Langer, R., and Zale, S. (2012) Preclinical development and clinical translation of a PSMA-targeted docetaxel nanoparticle with a differentiated pharmacological profile. *Sci. Transl. Med.*, **4**, 128ra139.

82 Leamon, C.P., Parker, M.A., Vlahov, I.R., Xu, L.C., Reddy, J.A., Vetzel, M., and Douglas, N. (2002) Synthesis and biological evaluation of EC20: a new folate-derived, $^{99m}T_c$-based radiopharmaceutical. *Bioconjug. Chem.*, **13**, 1200–1210.

83 Fisher, R.E., Siegel, B.A., Edell, S.L., Oyesiku, N.M., Morgenstern, D.E., Messmann, R.A., and Amato, R.J. (2008) Exploratory study of $^{99m}$Tc-EC20 imaging for identifying patients with folate receptor-positive solid tumors. *J. Nucl. Med.*, **49**, 899–906.

84 van Dam, G.M., Themelis, G., Crane, L.M., Harlaar, N.J., Pleijhuis, R.G., Kelder, W., Sarantopoulos, A., de Jong, J.S., Arts, H.J., van der Zee, A.G., Bart, J., Low, P.S., and Ntziachristos, V. (2011) Intraoperative tumor-specific fluorescence imaging in ovarian cancer by folate receptor-alpha targeting: first in-human results. *Nat. Med.*, **17**, 1315–1319.

85 Dechantsreiter, M.A., Planker, E., Matha, B., Lohof, E., Holzemann, G., Jonczyk, A., Goodman, S.L., and Kessler, H. (1999) *N*-Methylated cyclic RGD peptides as highly active and selective alpha(V)beta(3) integrin antagonists. *J. Med. Chem.*, **42**, 3033–3040.

86 Stupp, R., Hegi, M.E., Gorlia, T., Erridge, S.C., Perry, J., Hong, Y.K., Aldape, K.D., Lhermitte, B., Pietsch, T., Grujicic, D., Steinbach, J.P., Wick, W., Tarnawski, R., Nam, D.H., Hau, P., Weyerbrock, A., Taphoorn, M.J., Shen, C.C., Rao, N., Thurzo, L., Herrlinger, U., Gupta, T., Kortmann, R.D., Adamska, K., McBain, C., Brandes, A.A., Tonn, J.C., Schnell, O., Wiegel, T., Kim, C.Y., Nabors, L.B., Reardon, D.A., van den Bent, M.J., Hicking, C., Markivskyy, A., Picard, M., Weller, M., and European Organisation for Research and Treatment of Cancer (EORTC), Canadian Brain Tumor Consortium, and CENTRIC Study Team. (2014) Cilengitide combined with standard treatment for patients with newly diagnosed glioblastoma with methylated MGMT promoter (CENTRIC EORTC 26071-22072 study): a multicentre, randomised, open-label, phase 3 trial. *Lancet Oncol.*, **15**, 1100–1108.

87 Millard, M., Odde, S., and Neamati, N. (2011) Integrin targeted therapeutics. *Theranostics*, **1**, 154–188.

88 Juliano, R.L., Ming, X., Nakagawa, O., Xu, R., and Yoo, H. (2011) Integrin targeted

delivery of gene therapeutics. *Theranostics*, **1**, 211–219.

89 Mas-Moruno, C., Rechenmacher, F., and Kessler, H. (2010) Cilengitide: the first anti-angiogenic small molecule drug candidate design, synthesis and clinical evaluation. *Anticancer Agents Med. Chem.*, **10**, 753–768.

90 Hersey, P., Sosman, J., O'Day, S., Richards, J., Bedikian, A., Gonzalez, R., Sharfman, W., Weber, R., Logan, T., Buzoianu, M., Hammershaimb, L., Kirkwood, J.M., and Etaracizumab Melanoma Study Group. (2010) A randomized phase 2 study of etaracizumab, a monoclonal antibody against integrin alpha(v)beta(3), + or − dacarbazine in patients with stage IV metastatic melanoma. *Cancer*, **116**, 1526–1534.

91 Heidenreich, A., Rawal, S.K., Szkarlat, K., Bogdanova, N., Dirix, L., Stenzl, A., Welslau, M., Wang, G., Dawkins, F., de Boer, C.J., and Schrijvers, D. (2013) A randomized, double-blind, multicenter, phase 2 study of a human monoclonal antibody to human $\alpha v$ integrins (intetumumab) in combination with docetaxel and prednisone for the first-line treatment of patients with metastatic castration-resistant prostate cancer. *Ann. Oncol.*, **24**, 329–336.

92 Williams, R. (2015) Discontinued in 2013: oncology drugs. *Expert Opin. Investig. Drugs*, **24**, 95–110.

93 Reynolds, A.R., Hart, I.R., Watson, A.R., Welti, J.C., Silva, R.G., Robinson, S.D., Da Violante, G., Gourlaouen, M., Salih, M., Jones, M.C., Jones, D.T., Saunders, G., Kostourou, V., Perron-Sierra, F., Norman, J.C., Tucker, G.C., and Hodivala-Dilke, K.M. (2009) Stimulation of tumor growth and angiogenesis by low concentrations of RGD-mimetic integrin inhibitors. *Nat. Med.*, **15**, 392–400.

94 Haubner, R., Maschauer, S., and Prante, O. (2014) PET radiopharmaceuticals for imaging integrin expression: tracers in clinical studies and recent developments. *Biomed. Res. Int.*, **2014**, 871609.

95 Schnell, O., Krebs, B., Carlsen, J., Miederer, I., Goetz, C., Goldbrunner, R.H., Wester, H.J., Haubner, R., Popperl, G., Holtmannspotter, M., Kretzschmar, H.A., Kessler, H., Tonn, J.C., Schwaiger, M., and Beer, A.J. (2009) Imaging of integrin alpha(v)beta(3) expression in patients with malignant glioma by [18F] galacto-RGD positron emission tomography. *Neuro. Oncol.*, **11**, 861–870.

96 Kenny, L.M., Coombes, R.C., Oulie, I., Contractor, K.B., Miller, M., Spinks, T.J., McParland, B., Cohen, P.S., Hui, A.M., Palmieri, C., Osman, S., Glaser, M., Turton, D., Al-Nahhas, A., and Aboagye, E.O. (2008) Phase I trial of the positron-emitting Arg-Gly-Asp (RGD) peptide radioligand 18F-AH111585 in breast cancer patients. *J. Nucl. Med.*, **49**, 879–886.

97 Beer, A.J., Haubner, R., Goebel, M., Luderschmidt, S., Spilker, M.E., Wester, H.J., Weber, W.A., and Schwaiger, M. (2005) Biodistribution and pharmacokinetics of the alphavbeta3-selective tracer 18F-galacto-RGD in cancer patients. *J. Nucl. Med.*, **46**, 1333–1341.

98 Beer, A.J., Pelisek, J., Heider, P., Saraste, A., Reeps, C., Metz, S., Seidl, S., Kessler, H., Wester, H.J., Eckstein, H.H., and Schwaiger, M. (2014) PET/CT imaging of integrin alphavbeta3 expression in human carotid atherosclerosis. *JACC Cardiovasc. Imaging*, **7**, 178–187.

99 Jin, Z.H., Razkin, J., Josserand, V., Boturyn, D., Grichine, A., Texier, I., Favrot, M.C., Dumy, P., and Coll, J.L. (2007) *In vivo* noninvasive optical imaging of receptor-mediated RGD internalization using self-quenched Cy5-labeled RAFT-c(-RGDfK-)(4). *Mol. Imaging*, **6**, 43–55.

100 Jin, Z.H., Josserand, V., Foillard, S., Boturyn, D., Dumy, P., Favrot, M.C., and Coll, J.L. (2007) *In vivo* optical imaging of integrin alphaV-beta3 in mice using multivalent or monovalent cRGD targeting vectors. *Mol. Cancer*, **6**, 41.

101 Jin, Z.H., Furukawa, T., Galibert, M., Boturyn, D., Coll, J.L., Fukumura, T., Saga, T., Dumy, P., and Fujibayashi, Y. (2011) Noninvasive visualization and quantification of tumor alphaVbeta3 integrin expression using a novel positron emission tomography probe,

64Cu-cyclam-RAFT-c(-RGDfK-)4. *Nucl. Med. Biol.*, **38**, 529–540.

**102** Briat, A., Wenk, C.H., Ahmadi, M., Claron, M., Boturyn, D., Josserand, V., Dumy, P., Fagret, D., Coll, J.L., Ghezzi, C., Sancey, L., and Vuillez, J.P. (2012) Gelofusine reduces renal uptake of RAFT-RGD. Gelofusine reduced renal uptake of RAFT-RGD, a tetrameric RGD-based peptide that specifically targets the integrin alphavbeta3, without affecting its local distribution. *Cancer Sci.*, **103**(6). DOI: 10.1111/j.1349-7006.2012.02278.x

**103** Jin, Z.H., Furukawa, T., Claron, M., Boturyn, D., Coll, J.L., Fukumura, T., Fujibayashi, Y., Dumy, P., and Saga, T. (2012) Positron emission tomography imaging of tumor angiogenesis and monitoring of antiangiogenic efficacy using the novel tetrameric peptide probe 64Cu-cyclam-RAFT-c(-RGDfK-)4. *Angiogenesis*, **15**, 569–580.

**104** Keramidas, M., Josserand, V., Feige, J.J., and Coll, J.L. (2013) Noninvasive and quantitative assessment of *in vivo* angiogenesis using RGD-based fluorescence imaging of subcutaneous sponges. *Mol. Imaging Biol.*, **15**, 239–244.

**105** Garanger, E., Boturyn, D., Jin, Z., Dumy, P., Favrot, M.C., and Coll, J.L. (2005) New multifunctional molecular conjugate vector for targeting, imaging, and therapy of tumors. *Mol. Ther.*, **12**, 1168–1175.

**106** Atallah, I., Milet, C., Henry, M., Josserand, V., Reyt, E., Coll, J.L., Hurbin, A., and Righini, C.A. (2014) Near-infrared fluorescence imaging-guided surgery improves the recurrence-free survival rate in a novel orthotopic animal model of HNSCC. *Head Neck.*, **38**, Suppl 1: E246–255.

**107** Kéramidas, M., Josserand, V., Righini, C.A., Wenk, C., Faure, C., and Coll, J.L. (2010) Intraoperative near-infrared image-guided surgery of peritoneal carcinomatosis in a preclinical mouse model. *Br. J. Surg.*, **97**, 737–743.

**108** Wenk, C.H., Ponce, F., Guillermet, S., Tenaud, C., Boturyn, D., Dumy, P., Watrelot-Virieux, D., Carozzo, C., Josserand, V., and Coll, J.L. (2013) Near-infrared optical guided surgery of highly infiltrative fibrosarcomas in cats using an anti-alphav beta3 integrin molecular probe. *Cancer Lett.*, **334**, 188–195.

**109** Foillard, S., Jin, Z.H., Garanger, E., Boturyn, D., Favrot, M.C., Coll, J.L., and Dumy, P. (2008) Synthesis and biological characterisation of targeted pro-apoptotic peptide. *ChemBioChem*, **9**, 2326–2332.

**110** Foillard, S., Sancey, L., Coll, J.L., Boturyn, D., and Dumy, P. (2009) Targeted delivery of activatable fluorescent pro-apoptotic peptide into live cells. *Org. Biomol. Chem.*, **7**, 221–224.

**111** Dufort, S., Sancey, L., Hurbin, A., Foillard, S., Boturyn, D., Dumy, P., and Coll, J.L. (2011) Targeted delivery of a proapoptotic peptide to tumors *in vivo*. *J. Drug. Target*, **19**, 582–588.

**112** Morlieras, J., Dufort, S., Sancey, L., Truillet, C., Mignot, A., Rossetti, F., Dentamaro, M., Laurent, S., Vander Elst, L., Muller, R.N., Antoine, R., Dugourd, P., Roux, S., Perriat, P., Lux, F., Coll, J.L., and Tillement, O. (2013) Functionalization of small rigid platforms with cyclic RGD peptides for targeting tumors overexpressing alphavbeta3-integrins. *Bioconjug. Chem.*, **24**, 1584–1597.

**113** Sancey, L., Lux, F., Kotb, S., Roux, S., Dufort, S., Bianchi, A., Cremillieux, Y., Fries, P., Coll, J.L., Rodriguez-Lafrasse, C., Janier, M., Dutreix, M., Barberi-Heyob, M., Boschetti, F., Denat, F., Louis, C., Porcel, E., Lacombe, S., Le Duc, G., Deutsch, E., Perfettini, J.L., Detappe, A., Verry, C., Berbeco, R., Butterworth, K., McMahon, S., Prise, K., Perriat, P., and Tillement, O. (2014) The use of theranostic gadolinium-based nanoprobes to improve radiotherapy efficacy. *Br. J. Radiol.*, **87**(1041): 20140134.

**114** Benezra, M., Penate-Medina, O., Zanzonico, P.B., Schaer, D., Ow, H., Burns, A., DeStanchina, E., Longo, V., Herz, E., Iyer, S., Wolchok, J., Larson, S.M., Wiesner, U., and Bradbury, M.S. (2011) Multimodal silica nanoparticles are effective cancer-targeted probes in a model of human melanoma. *J. Clin. Invest.*, **121**, 2768–2780.

**115** Diou, O., Fattal, E., Delplace, V., Mackiewicz, N., Nicolas, J., Meriaux, S.,

Valette, J., Robic, C., and Tsapis, N. (2014) RGD decoration of PEGylated polyester nanocapsules of perfluorooctyl bromide for tumor imaging: influence of pre or post-functionalization on capsule morphology. *Eur. J. Pharm. Biopharm.*, **87**, 170–177.

116 Ragelle, H., Colombo, S., Pourcelle, V., Vanvarenberg, K., Vandermeulen, G., Bouzin, C., Marchand-Brynaert, J., Feron, O., Foged, C., and Preat, V. (2015) Intracellular siRNA delivery dynamics of integrin-targeted, PEGylated chitosan-poly(ethylene imine) hybrid nanoparticles: a mechanistic insight. *J. Control. Release*, **211**, 1–9.

117 Hwang, S., Nam, J., Jung, S., Song, J., Doh, H., and Kim, S. (2014) Gold nanoparticle-mediated photothermal therapy: current status and future perspective. *Nanomedicine (Lond.)*, **9**, 2003–2022.

118 Jain, S., Hirst, D.G., and O'Sullivan, J.M. (2012) Gold nanoparticles as novel agents for cancer therapy. *Br. J. Radiol.*, **85**, 101–113.

119 Wang, Y., Black, K.C., Luehmann, H., Li, W., Zhang, Y., Cai, X., Wan, D., Liu, S.Y., Li, M., Kim, P., Li, Z.Y., Wang, L.V., Liu, Y., and Xia, Y. (2013) Comparison study of gold nanohexapods, nanorods, and nanocages for photothermal cancer treatment. *ACS Nano*, **7**, 2068–2077.

120 Jing, L., Liang, X., Deng, Z., Feng, S., Li, X., Huang, M., Li, C., and Dai, Z. (2014) Prussian blue coated gold nanoparticles for simultaneous photoacoustic/CT bimodal imaging and photothermal ablation of cancer. *Biomaterials*, **35**, 5814–5821.

121 Miladi, I., Alric, C., Dufort, S., Mowat, P., Dutour, A., Mandon, C., Laurent, G., Brauer-Krisch, E., Herath, N., Coll, J.L., Dutreix, M., Lux, F., Bazzi, R., Billotey, C., Janier, M., Perriat, P., Le Duc, G., Roux, S., and Tillement, O. (2014) The *in vivo* radiosensitizing effect of gold nanoparticles based MRI contrast agents. *Small*, **10**, 1116–1124.

122 Al Zaki, A., Joh, D., Cheng, Z., De Barros, A.L., Kao, G., Dorsey, J., and Tsourkas, A. (2014) Gold-loaded polymeric micelles for computed tomography-guided radiation therapy treatment and radiosensitization. *ACS Nano*, **8**, 104–112.

123 Chen, H., Paholak, H., Ito, M., Sansanaphongpricha, K., Qian, W., Che, Y., and Sun, D. (2013) 'Living' PEGylation on gold nanoparticles to optimize cancer cell uptake by controlling targeting ligand and charge densities. *Nanotechnology*, **24**, 355101.

124 Chen, H., Zhang, X., Dai, S., Ma, Y., Cui, S., Achilefu, S., and Gu, Y. (2013) Multifunctional gold nanostar conjugates for tumor imaging and combined photothermal and chemo-therapy. *Theranostics*, **3**, 633–649.

125 Larson, N., Gormley, A., Frazier, N., and Ghandehari, H. (2013) Synergistic enhancement of cancer therapy using a combination of heat shock protein targeted HPMA copolymer-drug conjugates and gold nanorod induced hyperthermia. *J. Control. Release*, **170**, 41–50.

126 Choi, W.I., Kim, J.Y., Kang, C., Byeon, C.C., Kim, Y.H., and Tae, G. (2011) Tumor regression *in vivo* by photothermal therapy based on gold-nanorod-loaded, functional nanocarriers. *ACS Nano*, **5**, 1995–2003.

127 Hirsch, L.R., Stafford, R.J., Bankson, J.A., Sershen, S.R., Rivera, B., Price, R.E., Hazle, J.D., Halas, N.J., and West, J.L. (2003) Nanoshell-mediated near-infrared thermal therapy of tumors under magnetic resonance guidance. *Proc. Natl. Acad. Sci. USA*, **100**, 13549–13554.

128 Bai, Y.Y., Zheng, S., Zhang, L., Xia, K., Gao, X., Li, Z.H., Li, C., He, N., and Ju, S. (2014) Non-invasively evaluating therapeutic response of nanorod-mediated photothermal therapy on tumor angiogenesis. *J. Biomed. Nanotechnol.*, **10**, 3351–3360.

129 Singh, M., Harris-Birtill, D.C., Markar, S.R., Hanna, G.B., and Elson, D.S. (2015) Application of gold nanoparticles for gastrointestinal cancer theranostics: a systematic review. *Nanomedicine*, **11**, 2083–2098.

130 Ahmed, M., Pan, D.W., and Davis, M.E. (2015) Lack of *in vivo* antibody dependent cellular cytotoxicity with

antibody containing gold nanoparticles. *Bioconjug. Chem.*, **26**, 812–816.

131 Daniels, T.R., Bernabeu, E., Rodriguez, J.A., Patel, S., Kozman, M., Chiappetta, D.A., Holler, E., Ljubimova, J.Y., Helguera, G., and Penichet, M.L. (2012) The transferrin receptor and the targeted delivery of therapeutic agents against cancer. *Biochim. Biophys. Acta.*, **1820**, 291–317.

132 Descamps, L., Dehouck, M.P., Torpier, G., and Cecchelli, R. (1996) Receptor-mediated transcytosis of transferrin through blood–brain barrier endothelial cells. *Am. J. Physiol.*, **270**, H1149–H 1158.

133 Bellocq, N.C., Pun, S.H., Jensen, G.S., and Davis, M.E. (2003) Transferrin-containing, cyclodextrin polymer-based particles for tumor-targeted gene delivery. *Bioconjug. Chem.*, **14**, 1122–1132.

134 Pun, S.H., Tack, F., Bellocq, N.C., Cheng, J., Grubbs, B.H., Jensen, G.S., Davis, M.E., Brewster, M., Janicot, M., Janssens, B., Floren, W., and Bakker, A. (2004) Targeted delivery of RNA-cleaving DNA enzyme (DNAzyme) to tumor tissue by transferrin-modified, cyclodextrin-based particles. *Cancer Biol. Ther.*, **3**, 641–650.

135 Bartlett, D.W., Su, H., Hildebrandt, I.J., Weber, W.A., and Davis, M.E. (2007) Impact of tumor-specific targeting on the biodistribution and efficacy of siRNA nanoparticles measured by multimodality *in vivo* imaging. *Proc. Natl. Acad. Sci. USA*, **104**, 15549–15554.

136 Heidel, J.D., Yu, Z., Liu, J.Y., Rele, S.M., Liang, Y., Zeidan, R.K., Kornbrust, D.J., and Davis, M.E. (2007) Administration in non-human primates of escalating intravenous doses of targeted nanoparticles containing ribonucleotide reductase subunit M2 siRNA. *Proc. Natl. Acad. Sci. USA*, **104**, 5715–5721.

137 Heidel, J.D. and Schluep, T. (2012) Cyclodextrin-containing polymers: versatile platforms of drug delivery materials. *J. Drug Deliv.*, **2012**, 262731.

138 Davis, M.E., Zuckerman, J.E., Choi, C.H., Seligson, D., Tolcher, A., Alabi, C.A., Yen, Y., Heidel, J.D., and Ribas, A. (2010) Evidence of RNAi in humans from systemically administered siRNA via targeted nanoparticles. *Nature*, **464**, 1067–1070.

139 Zuckerman, J.E., Gritli, I., Tolcher, A., Heidel, J.D., Lim, D., Morgan, R., Chmielowski, B., Ribas, A., Davis, M.E., and Yen, Y. (2014) Correlating animal and human phase Ia/Ib clinical data with CALAA-01, a targeted, polymer-based nanoparticle containing siRNA. *Proc. Natl. Acad. Sci. USA*, **111**, 11449–11454.

140 Kirpotin, D.B., Drummond, D.C., Shao, Y., Shalaby, M.R., Hong, K., Nielsen, U.B., Marks, J.D., Benz, C.C., and Park, J.W. (2006) Antibody targeting of long-circulating lipidic nanoparticles does not increase tumor localization but does increase internalization in animal models. *Cancer Res.*, **66**, 6732–6740.

141 Peng, X.H., Wang, Y., Huang, D., Wang, Y., Shin, H.J., Chen, Z., Spewak, M.B., Mao, H., Wang, X., Wang, Y., Chen, Z.G., Nie, S., and Shin, D.M. (2011) Targeted delivery of cisplatin to lung cancer using ScFvEGFR-heparin-cisplatin nanoparticles. *ACS Nano*, **5**, 9480–9493.

142 Pirollo, K.F., Rait, A., Zhou, Q., Zhang, X.Q., Zhou, J., Kim, C.S., Benedict, W.F., and Chang, E.H. (2008) Tumor-targeting nanocomplex delivery of novel tumor suppressor RB94 chemosensitizes bladder carcinoma cells *in vitro* and *in vivo*. *Clin. Cancer Res.*, **14**, 2190–2198.

143 Xu, L., Huang, C.C., Huang, W., Tang, W.H., Rait, A., Yin, Y.Z., Cruz, I., Xiang, L.M., Pirollo, K.F., and Chang, E.H. (2002) Systemic tumor-targeted gene delivery by anti-transferrin receptor scFv-immunoliposomes. *Mol. Cancer Ther.*, **1**, 337–346.

144 Xu, L., Tang, W.H., Huang, C.C., Alexander, W., Xiang, L.M., Pirollo, K.F., Rait, A., and Chang, E.H. (2001) Systemic p53 gene therapy of cancer with immunolipoplexes targeted by anti-transferrin receptor scFv. *Mol. Med.*, **7**, 723–734.

145 Senzer, N., Nemunaitis, J., Nemunaitis, D., Bedell, C., Edelman, G., Barve, M., Nunan, R., Pirollo, K.F., Rait, A., and Chang, E.H. (2013) Phase I study of a systemically delivered p53 nanoparticle in advanced solid tumors. *Mol. Ther.*, **21**, 1096–1103.

**146** Kim, S.S., Rait, A., Kim, E., Pirollo, K.F., Nishida, M., Farkas, N., Dagata, J.A., and Chang, E.H. (2014) A nanoparticle carrying the p53 gene targets tumors including cancer stem cells, sensitizes glioblastoma to chemotherapy and improves survival. *ACS Nano*, **8**, 5494–5514.

**147** Kim, S.S., Rait, A., Rubab, F., Rao, A.K., Kiritsy, M.C., Pirollo, K.F., Wang, S., Weiner, L.M., and Chang, E.H. (2014) The clinical potential of targeted nanomedicine: delivering to cancer stem-like cells. *Mol. Ther.*, **22**, 278–291.

**148** Kim, S.S., Rait, A., Kim, E., Pirollo, K.F., and Chang, E.H. (2015) A tumor-targeting p53 nanodelivery system limits chemoresistance to temozolomide prolonging survival in a mouse model of glioblastoma multiforme. *Nanomedicine*, **11**, 301–311.

**149** Wicki, A., Ritschard, R., Loesch, U., Deuster, S., Rochlitz, C., and Mamot, C. (2015) Large-scale manufacturing of GMP-compliant anti-EGFR targeted nanocarriers: production of doxorubicin-loaded anti-EGFR-immunoliposomes for a first-in-man clinical trial. *Int. J. Pharm.*, **484**, 8–15.

**150** Mamot, C., Ritschard, R., Wicki, A., Stehle, G., Dieterle, T., Bubendorf, L., Hilker, C., Deuster, S., Herrmann, R., and Rochlitz, C. (2012) Tolerability, safety, pharmacokinetics, and efficacy of doxorubicin-loaded anti-EGFR immunoliposomes in advanced solid tumours: a phase 1 dose-escalation study. *Lancet Oncol.*, **13**, 1234–1241.

**151** Mamot, C., Drummond, D.C., Noble, C.O., Kallab, V., Guo, Z., Hong, K., Kirpotin, D.B., and Park, J.W. (2005) Epidermal growth factor receptor-targeted immunoliposomes significantly enhance the efficacy of multiple anticancer drugs *in vivo*. *Cancer Res.*, **65**, 11631–11638.

**152** Mamot, C., Ritschard, R., Wicki, A., Kung, W., Schuller, J., Herrmann, R., and Rochlitz, C. (2012) Immunoliposomal delivery of doxorubicin can overcome multidrug resistance mechanisms in EGFR-overexpressing tumor cells. *J. Drug Target*, **20**, 422–432.

**153** Mamot, C., Drummond, D.C., Hong, K., Kirpotin, D.B., and Park, J.W. (2003) Liposome-based approaches to overcome anticancer drug resistance. *Drug Resist. Updat.*, **6**, 271–279.

**154** Thierry, A.R., Vige, D., Coughlin, S.S., Belli, J.A., Dritschilo, A., and Rahman, A. (1993) Modulation of doxorubicin resistance in multidrug-resistant cells by liposomes. *FASEB J.*, **7**, 572–579.

**155** Romsicki, Y. and Sharom, F.J. (1999) The membrane lipid environment modulates drug interactions with the P-glycoprotein multidrug transporter. *Biochemistry*, **38**, 6887–6896.

**156** Kabanov, A.V., Batrakova, E.V., and Alakhov, V.Y. (2002) Pluronic block copolymers for overcoming drug resistance in cancer. *Adv. Drug Deliv. Rev.*, **54**, 759–779.

**157** Wong, H.L., Bendayan, R., Rauth, A.M., Xue, H.Y., Babakhanian, K., and Wu, X.Y. (2006) A mechanistic study of enhanced doxorubicin uptake and retention in multidrug resistant breast cancer cells using a polymer-lipid hybrid nanoparticle system. *J. Pharmacol. Exp. Ther.*, **317**, 1372–1381.

# 9
# Highly Conformal Radiotherapy Using Protons

*Antony John Lomax*

*Paul Scherrer Institut, Zentrum für Protonentherapie, WPTA/140, 5232 Villigen PSI, Switzerland*

## 9.1
## Introduction

### 9.1.1
### Principles of Radiotherapy

After surgery, radiotherapy is the second most important treatment modality against cancer, with more than half of all patients being cured of cancer undergoing radiotherapy as part of their treatment [1]. The basic principles of radiotherapy are quite simple. Through the application of ionizing radiation, energy is deposited to the tumor, which in turn can result in cell sterilization through the production of highly reactive free radicals with the cell nucleus. Thus, if enough energy can be deposited to the whole tumor, tumor control (the arresting of uncontrolled cell division and tumor growth) can be achieved.

Unfortunately, a similar effect will take place in any normal tissues also irradiated as part of the treatment, and such colateral damage is an inevitable consequence of externally applied radiation therapy. The science or *art* of radiotherapy, therefore, is to concentrate the dose on the tumor, while sparing all surrounding normal tissues as much as possible. All technical developments in radiotherapy have been aimed at achieving this deceptively simple goal.

### 9.1.2
### Radiotherapy with X-Rays

Radiotherapy has a long and illustrious history, dating back to the end of the nineteenth century, when the first patients were treated using X-rays shortly after their discovery by Wilhelm Roentgen in 1895. Indeed, by 1902, more than 100 different tumor types could be listed that had been treated with X-ray radiation. Although first treatments necessarily used low-energy X-rays (in the

*Nanoscience and Nanotechnology for Human Health,* First Edition. Edited by Bert Müller and Marcel Van de Voorde.

kilovolt range), technical developments throughout the twentieth century were mainly in developing and implementing X-ray generators capable of ever-increasing energies, culminating in the widespread clinical deployment of dedicated linear accelerators (delivering X-rays/photons of 1–20 MV) for radiotherapy in the 1970s onward. The main advantage of these higher energies was the improved so-called *depth–dose* characteristics of such X-ray sources, an example of which is shown in Figure 9.1.

This diagram shows a typical depth–dose curve for 15 MV photons. The horizontal axis shows the depth of penetration of the X-rays in water, while the vertical axis shows the relative deposited energy, typically referred to as the deposited dose in radiotherapy. In physics terms, this deposited dose is expressed in the units of Joule/kilogram, that is, the energy deposited to unit mass, although in radiotherapy, this is expressed in terms of the Gray (1 Gy = 1 J/kg).

This curve is characterized by a sharp increase in dose in the first few millimeters of water, to a maximum dose at a depth of about 1.5 cm. This is followed by a more-or-less exponential reduction in deposited dose as the beam penetrates deeper through the water. From the physics point of view, as photons are uncharged particles, they deposit their energy indirectly by transferring their energy to secondary electrons. It is these that actually deposit the energy in the water or patient. This has two consequences. First, in their interactions with electrons, the photons are lost (absorbed) from the beam as they traverse through material, leading to the exponential drop in deposited dose as a function of depth beyond the maximum dose peak. Second, the dose build-up in the first few millimeters is due to the predominantly forward direction of secondary electrons, which always deposit their dose somewhat deeper than the initial interaction with the photon. This leads to a depletion of secondary electrons at the surface and, therefore, deposited dose, which eventually reaches an equilibrium

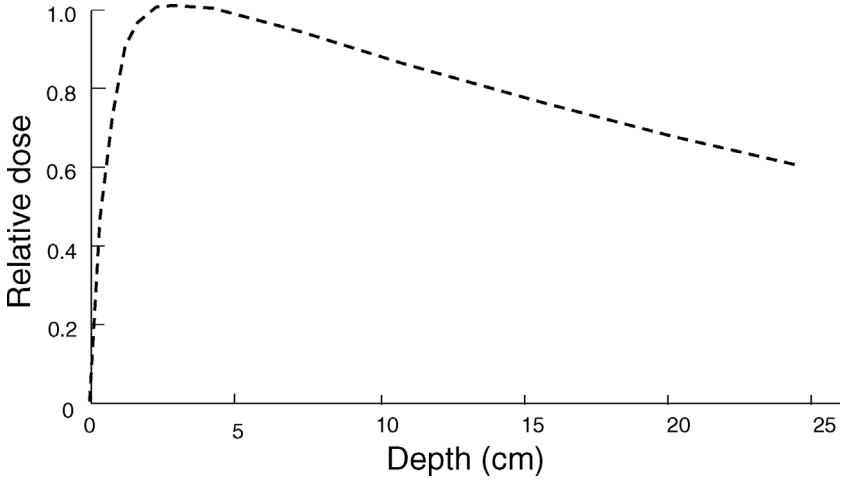


**Figure 9.1** The depth–dose curve for 15 MV X-rays (photons).

point, that is, the point where the dose deposited by secondary electrons released at shallower depths is compensated by secondary electrons released at the point of interest, close to the maximum dose point.

From the point of view of concentrating dose in the tumor, the curve shown in Figure 9.1 is less than optimal. If the tumor is at a depth more than the maximum dose, then the tumor will actually get less dose than the normal tissues directly in the path of the beam, while beyond the furthest extension of the tumor, the so-called distal end, any normal tissues will also receive an unwanted dose, even if this is somewhat lower than that delivered to the tumor, cf. Figure 9.2a. This is exactly what we do not want with radiotherapy. In practice, however, such a single X-ray beam will be rarely used, and the less than ideal characteristics of X-rays is typically compensated for by the use of multiple beams, each being delivered to the tumor from different directions around the patient. Indeed, in the state-of-the-art photon therapy, the trend is now toward fully rotational therapy combined with sophisticated intensity/fluence modulation of the individual fields so as to precisely and accurately shape the delivered dose in three dimensions to match the three-dimensional (3D) shape of the tumor, see, for example, Figure 9.2b. With such techniques, the fundamental physical disadvantages of photons can be overcome, and this is precisely the reason that radiotherapy has become such an important, and successful, treatment of cancer. However, the rather unfavorable depth–dose characteristics of X-rays/photons can never be fully avoided, and even with the most modern of delivery techniques, there is an inevitable *bath* of low-to-mid doses delivered to potentially large volumes of normal tissue [2,3].

### 9.1.3
### Radiotherapy Using Protons

In a similar way to Figure 9.1, Figure 9.3 shows the equivalent depth–dose curve achievable using protons instead of X-rays for therapy. In contrast to the curve

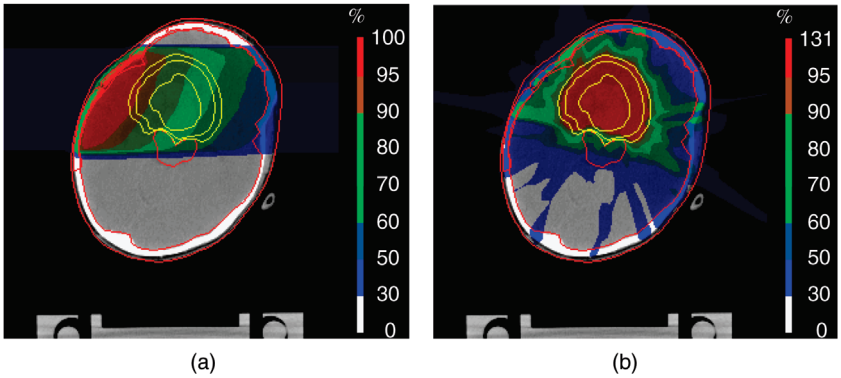


**Figure 9.2** The dose distribution for a single 6 MV field from the left-hand side (a) and a nine-field (all 6 MV) intensity-modulated (IMRT) plan to the same tumor (b).

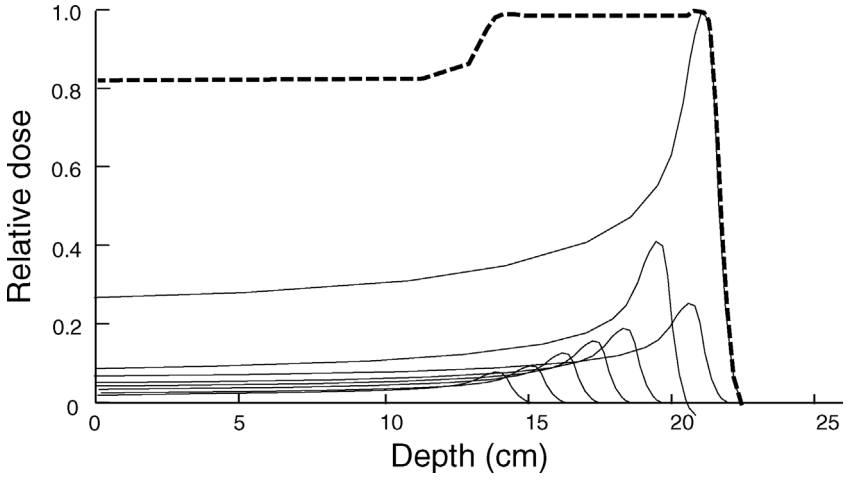


**Figure 9.3** A proton "spread-out Bragg peak", constructed from the superposition of multiple-range and magnitude modulated individual Bragg peaks.

shown in Figure 9.1, the curve for protons is characterized by a relatively flat entrance dose region, starting immediately at the surface of the patient, a flat dose region covering the region of the target, and a sharp dose fall-off immediately beyond the distal end of the target region. The reasons for this depth–dose characteristic will be covered in more detail in the next section. The potential advantages, however, are clear. In comparison to the photon curve, the entrance dose is lower, the target is irradiated with a homogeneous dose and immediately beyond the tumor virtually no dose is delivered. Only in the first few millimeters is there a slight advantage for photons, as protons exhibit no (or at least a very limited) build-up effect.

The use of protons for radiotherapy was first suggested by Robert Wilson in his seminal paper of 1946 [4], and it was in this paper that the potential advantages of protons as shown in Figure 9.3 for radiotherapy were first described. Based on this, the first patients were treated using protons in the 1950s in both the United States and Sweden [5], and by the time of writing, more than 120 000 patients have been treated worldwide using protons [6].

The aim of this chapter is to describe the physical principles and clinical practice of modern proton therapy. As such, it will begin with a section describing the main interaction processes of protons with matter and why these lead to the very different physical characteristics of protons compared to X-rays. The following sections will then describe how proton beams are generated, modulated, and optimally delivered to the patient. Finally, some clinical applications and results of proton therapy will be presented, followed by a *crystal ball* section discussing the likely future directions for proton therapy research and development, both technical and clinical, together with the potential role of nanotechnology.

## 9.2
## Proton Physics

The depth–dose curve for monoenergetic protons shown in Figure 9.3 is due to the interactions that protons undergo in comparison to photons, as they penetrate matter. These will be briefly discussed in this section.

### 9.2.1
### Energy Loss

The main difference between protons and photons from the point of view of physical interactions is that protons are charged particles. As such, the primary interaction of protons with matter is direct collision with orbiting electrons, which leads to the loss of proton energy rather than absorption of the particle. However, as protons are 1800 times heavier than electrons, protons lose only a tiny amount of their energy with each such collision, and thus deposit via these secondary electrons relatively small amounts of energy, at least when the proton energy is high. In addition, due to the large mass difference, only a relatively small amount of energy is transferred to the electron, and thus their energy is also relatively small, leading to much smaller secondary electron ranges than after the absorption of high-energy photons. This has two consequences. First, the energy deposited to matter at the entrance, where the protons have the highest energy, is relatively small, cf. the rather flat plateau dose seen on the left-hand part of the depth–dose curves for the monoenergetic proton curves shown in Figure 9.3, and there is no significant build-up effect as observed for photons, cf. Figure 9.1.

Nevertheless, as protons penetrate through matter, they continually lose energy due to many such interactions, with the amount of lost energy per interaction being roughly proportional to the inverse of the square of their velocity. So, as they lose energy, they lose velocity and thus deposit more and more energy as a function of penetration depth, also termed *range*. This inverse square relationship of deposited energy with velocity leads to a well-defined maximum range, beyond which no primary protons can penetrate as they have run out of energy, and also the characteristic peak of maximum dose, a few millimeters before the maximum range, in the so-called Bragg peak [7,8].

### 9.2.2
### Multiple Coulomb Scattering

In addition to energy loss due to electronic interactions, protons also undergo two other interactions, both of which are due to close encounters of the proton with atomic nuclei. The first, and most important, of these is multiple Coulomb scattering (MCS). As protons pass close to atomic nuclei, the positive charge of the proton and nucleus causes the proton to deflect

due to electrostatic repulsion. Thus, as protons transport through matter, they also gradually become *angularly confused* or, put another way, a perfectly narrow beam will generally tend to get broader. The nice thing about protons is that the effects of such scattering can be well approximated as a Gaussian distribution, which in turn can be parameterized by its standard deviation or sigma. Due to MCS alone, the sigma of a proton beam at the Bragg peak will increase by roughly 2% of the proton range. Thus, for 170 MeV protons with a range of 20 cm in water, the beam width due to MCS alone will be about 4 mm σ, equivalent to an increase in the full-width half-maximum (FWHM) of the pencil beam of about 1 cm. Consequently, MCS of protons is an important interaction to take into account when modeling proton beams for radiotherapy applications.

### 9.2.3 Nuclear Interactions and Secondary Particles

The second interaction of protons with nuclei is more direct and is the result of their elastic and/or inelastic collisions with atomic nuclei. In elastic collisions, the protons can be even more laterally deflected than from MCS interactions. However, as this is a rather rare event, it can generally be ignored, although in reality this leads to somewhat more dose in the lateral tails of the beam profile than would be expected from a pure Gaussian distribution. More important are inelastic collisions. In these events, protons can be lost from the beam completely, not only delivering some of their energy locally through the production of heavier secondary particles but also transferring energy into secondary protons, photons, and neutrons. The probability of such inelastic collisions is also rather low, but nevertheless leads to about 1% of protons being lost from the beam per centimeter of penetration, when the medium is water. Thus, for the selected 170 MeV beam with 20 cm range in water, only about 80% of protons actually make it to the Bragg peak, the other 20% being lost from the beam due to these inelastic nuclear interactions.

Such interactions lead to two main effects on the incident proton beam. First, the ratio of the height of the Bragg peak to the entrance dose (see Figure 9.3) will be reduced from that expected from pure energy loss considerations alone. Second, the secondary protons will tend to add dose to the lateral tails of the dose profile of the beam, and take dose out of the primary beam. Although the dose carried by these secondary protons is only a small percentage of the dose in the primary beam, this effect nevertheless is an important one, which needs to be taken into account in absolute dosimetry and treatment planning. Secondary photons and neutrons can be typically ignored, although the former can potentially be used for range verification, whereas secondary neutrons could have a role to play in secondary cancer induction and have been the cause of concern in proton therapy for a number of years, even if no evidence of increased secondary cancer due to proton therapy has been observed clinically [9,10].

### 9.2.4
### Linear Energy Transfer and Relative Biological Effectiveness

Up to now, we have looked at the pure physics effects of protons in matter. However, due to the interactions of protons with photons, there are also potentially characteristic biological effects as a result of proton irradiation. For instance, in the Bragg-peak region, the rate of deposited energy increases rapidly, meaning that the density of ionization, and therefore transferred energy, is also high. This parameter is known as the linear energy transfer (LET) and, as explained, is highest where the rate of the deposited energy is high and, therefore, where the proton energy is low. Thus, LET is highest in the Bragg peak and distal fall-off of the proton depth–dose curve. Evidence from *in vitro* experiments in cell cultures has shown that high LET can also result in a higher biological effect for the same deposited physical dose when that dose is applied using low LET radiation. This enhanced biological effect is known as relative biological effectiveness (RBE). The relationship between RBE and LET is, however, not trivial, and dependent on the tissue type, end point, and dose, to mention just a few [11]. Consequently, for proton therapy, a generic RBE value of 1.1 is generally assumed. Despite this, however, it should always be borne in mind that where LET may be enhanced, there is also a chance that the RBE, and therefore biological effect, could also be enhanced.

### 9.2.5
### Density Heterogeneities

Before moving to the more technical aspects of the generation of high-energy protons for radiation therapy, see the next section, a few words need to be said about the effects of density heterogeneities on proton beams.

Given the fact that proton range depends not only on energy but also on the density of the material, through which they pass, then density heterogeneities within the patient will have a profound effect on the accuracy of proton therapy. In the first instance, they will affect the actual range in the patient [8]. For instance, if passing through bone, due to its higher density, protons will lose more energy per millimeter than in water and will thus travel less far. In fact, this change of range is determined by the so-called proton stopping power of the material rather than its pure density, with stopping power being strongly correlated to physical density. On the other hand, if protons traverse air, they will lose very little energy and will obviously have a much longer range than in water. As both bone and air, for example, in the nasal cavities, are present within patients, not to mention soft tissues, whose stopping powers are actually close to water, it is hopefully clear that a detailed knowledge of the tissues, through which the tumor is irradiated, and their relative stopping powers, is a prerequisite for accurate *in vivo* range calculations.

The effect of density heterogeneities on clinical proton beams is actually even a little more complex than this. Typical treatment fields will have a finite size of

at least a few centimeters in all directions, and thus different parts of the field will pass through different anatomical regions of the patient. Thus, different protons will see different density variations in the patient, for instance, for a head and neck irradiation, some may pass through the nasal cavities, and some not; some may be irradiating the neck nodes and others the primary tumor close to the skull base. Thus, the energy of the irradiating field generally needs modulating so as to adapt to these range changes imposed by patient anatomy. In addition, however, there can often be an interplay between range variations and scatter, whereby beyond a sharp density interface, the amount of scattering from the high density portion is considerably higher than that from the low-density region. This, in turn, leads to a distortion of the proton fluence immediately beyond the density heterogeneity, with a shadowing effect immediately behind the high-density region and a peaking effect beyond the low-dose region. In a one-dimensional sense, this combination of range variation and variable scattering leads to a broadening and degradation of the pristine Bragg peak. As such, given that all patients are relatively heterogeneous, the sharp Bragg peak shown in Figure 9.3 is rarely the reality in therapy, with distortions and broadening of the distal dose fall-off being inevitable to a greater or lesser extent [12].

### 9.2.6 Generating High-Energy Proton Beams

A prerequisite for radiotherapy with protons is a source of protons with sufficient energy to penetrate the maximum depth of the target. In practice, this requires energies of up to 200 MeV or even more. There are at present two main categories of accelerator that can produce proton beams of such energies and that are used clinically: cyclotrons and synchrotrons [13]. The basic operating principles of both will be briefly discussed here.

#### 9.2.6.1 Cyclotron

Conceptually, the acceleration of charged particles such as protons is straightforward. As a result of the Lorenz forces on charged particles, the application of an electric field results in an acceleration of the particle. Thus, it is only required that a large enough electric potential is applied to the beam to accelerate protons to the required energies. In practice, of course, this would require potentials of many millions of volts, which is clearly impractical. As such, most high-energy accelerating techniques use the concept of repeated acceleration using much smaller voltages. The cyclotron is one such approach.

In the 1930s, Ernest Lawrence first proposed the idea of such a device [14]. He noted that, for lower-energy protons at least, the angular frequency of rotation of charged particles due to a vertically applied magnetic field is independent of energy or radius. Thus, by applying an alternating voltage across a gap between two sets of D-shaped magnets, the particle could be repeatedly accelerated across this gap as the particles rotate in the plane between magnetic poles. In addition, as the energy of the particle increases, so does the radius of rotation,

and thus the accelerated particles can be extracted at the outermost radius of the D-shaped magnets, where the particles have reached a specific energy level. Like most things, however, the devil is in the detail, and to reach energies of more than a few megaelectronvolts, the frequency/radius independence breaks down due to relativistic effects, and designs of cyclotrons for energies up to a few hundred megaelectronvolts are complicated. Nevertheless, the basic principle remains the same. The protons are accelerated multiple times across a gap, the radius of their track gradually increases as the energy increases, and they are eventually extracted at the outermost part of the magnet. Thus, by their very nature, cyclotrons are monoenergetic machines, but have the advantage of being able to operate in continuous mode, that is, they can provide a continuous stream of beam.

#### 9.2.6.2 Synchrotrons

Synchrotrons are also circular accelerators, but work on a different principle [15]. Instead of using a static magnetic field and allowing for a continually growing radius of accelerated particles, the synchrotron is designed to keep the rotational track of the particles constant while they are being accelerated, by continually varying the magnitude of the applied vertical magnetic field. Thus, a synchrotron typically consists of a set of curved magnets, each with the same radius of curvature, through which the accelerating beam line is placed. Particle acceleration is then performed in the gaps between these magnets, with the magnetic field of the following magnet being increased in order to keep the protons in the same radius. In contrast to cyclotrons, therefore, the energy of the extracted particles can be varied, by simply controlling the number of circuits the particles make. So, synchrotrons are capable of directly generating protons of any energy. On the other hand, as the field strengths of magnets have to be increased in synchrony with the energy of the protons, they are also inherently pulsed machines, accelerating bunches of protons at a time, with a repetition rate typically of a few seconds.

In summary, although somewhat different in their philosophy and design, both cyclotrons and synchrotrons are suitable accelerators for proton therapy, each having their advantages and disadvantages. As such, it should come as no surprise that all currently available commercial proton therapy systems are based on one of these accelerators, with a roughly 50–50 split between the existing manufacturers in the use of cyclotrons and synchrotrons.

## 9.3 Delivering Proton Therapy

### 9.3.1 Imaging and Treatment Planning

One of the great advantages of radiation and proton therapy over other forms of localized cancer treatment is the ability to utilize high-quality and state-of-the-

art imaging in order to precisely define the tumor volume to be treated, together with any neighboring critical organs, and to perform accurate predictions of the dose to be delivered.

For proton therapy, the most important imaging modality is X-ray CT, as this provides information about internal density variations of the patient, which are essential for proton dose and range calculations. However, both MRI and PET are extremely useful in order to identify and delineate the tumor (MRI) and its metabolic activity (PET) and to define the critical internal organs and structures that are important in treatment evaluation (CT/MRI).

Based on these imaging studies, proton therapy treatments are then preplanned in a process known as treatment planning. The first step in this process is to delineate the tumor volume and all neighboring critical structures – that are structures likely to be dose limiting during the treatment or for which the delivered dose needs to be evaluated. Although semiautomatic processes based on anatomical atlases are becoming more common, this is still a rather labor-intensive process, particularly the definition of the tumor and its microscopic spread, which is not always well defined in current imaging techniques. As such, in defining the tumor volume to be irradiated, the medical doctor is still very reliant on his or her experience and anatomical knowledge of where tumor microstructures are likely to spread.

Based on the defined tumor and critical structure volumes, the treatment planning process proceeds further through the definition of one or more field directions from which the proton irradiation will be delivered in order to best cover the target while sparing as necessary the various normal structures. The geometry of each field will then be defined, the process of which will be different depending on whether passive scattering or pencil beam scanning (PBS) is used (see below), followed by a prediction of the 3D dose distribution that will be delivered, calculated based on the underlying physics principles of proton interactions with matter (see Section 9.2). The resultant dose distribution is then the primary decision-making tool for the referring clinician about the quality of planned treatment, taking into account parameters such as target coverage and critical organ sparing, as predicted by the 3D dose distribution.

In the next sections, we will look into the two main methods of actually delivering proton therapy, and which have to be taken into account when calculating and designing treatment fields.

### 9.3.2 Passive Scattering

#### 9.3.2.1 Spread-out Bragg Peak

Both cyclotrons and synchrotrons provide monoenergetic proton beams, either continuous and with a fixed energy in the case of cyclotrons or with different energies within different pulses in the case of a synchrotron. However, a single, monoenergetic Bragg peak depth–dose curve is not really that useful for radiation therapy. As the present thinking in radiotherapy is that the probability of

controlling the tumor is maximized by irradiating it with a homogeneous dose, the narrowness of the monoenergetic Bragg peak makes it next to useless in a therapeutic setting. As such, the pristine beam emitted from an accelerator must be modulated in order to give it a clinically useful form.

For passive scattering [17], this is achieved through delivery of the so-called *spread-out B*ragg *Peak* (SOBP). In brief, this is formed through the delivery of multiple, energy (range) modulated Bragg peaks, which when combined produce a broad and flat plateau of high dose (see Figure 9.3), with the extent of this flat dose plateau being determined by the number of energy-modulated Bragg peaks added to the field. However, as can be seen in Figure 9.3, the fluence (amplitude) of each individual Bragg peak must also be modulated in order to achieve this flat dose. This is because each proximally shifted Bragg peak, that is, with lower energy, delivers its Bragg peak in the proximal build-up region of the next deepest, highest energy Bragg peak, and thus must only deliver sufficient dose to make up the difference in dose between this and the dose delivered by the highest energy Bragg peak. As more and more Bragg peaks are added distally, the dose from more distal Bragg peaks add up quickly, meaning that the amplitudes required for the lowest energy Bragg peaks reduce in a very nonlinear and rapid way.

The concept of the SOBP is central to passive scattered proton therapy and, in practice, can be constructed using one of the two methods: range shifter wheels and ridge filters. In the first of these, a rapidly rotating (~300 rpm) and suitably shaped propeller type device intersects with the monoenergetic beam, with the *blades* being made up of segments of varying width and thickness so as to perform the shifts and fluence modulations necessary for forming the SOBP. With such a device, varying extent SOBPs are produced either by using different modulators or by *gating* the incident beam to only intersect with particular segments of a standard wheel design, the wider the *gated* beam, correspondingly the wider the delivery of extent SOBPs. Alternatively, the ridge filter is a fixed device, shaped much like a pyramid so that the incident monoenergetic proton beam *sees* different thicknesses of the filter [18]. In this case, the effective cross-sectional areas of the segments of the filter each with different thicknesses, and as projected along the direction of the incident beam, are directly proportional to the required SOBP-weighted fluences, so that the probability of a proton passing through a particular segment is proportional to the required fluence relating to that thickness.

#### 9.3.2.2 Single and Double Scattering

The SOBP effectively broadens the homogeneous part of the depth–dose curve, but the initial proton beam, typically only a few millimeters wide when extracted from the accelerator, also needs to be broadened laterally in order to treat anything but the smallest tumor volume. For the passive scattering approach, there are two main methods to this.

The simplest is single scattering. As the name implies, this uses a single-scattering foil, usually constructed of a high-z material, in which the incident

protons are laterally scattered by the MCS process described above. As the material is high density, the amount of scattering can be large for even a thin foil, and the larger the scattering angle resulting from the foil, the larger the effective field size for therapy. However, as the practical thickness of the scatterer is ultimately limited by the inevitable range reduction due to energy loss in the scatterer, acceptable field sizes can be attained only by also having a large drift space between the scatterer and the patient. Typically, such drift spaces must be at least 2 m, which for single scattering allows for usable field sizes of up to about 20 cm × 20 cm. For larger field sizes, a double-scattering system needs to be used [19]. With this approach, a second carefully shaped second scatter is also used, which effectively flattens the profile of the initially scattered beam and allows for field sizes of up to 30 cm × 40 cm for the same drift space. The disadvantage of this approach is that the lateral penumbra of the resultant field is somewhat compromised in comparison to single scattering, basically due to a larger angular confusion of the proton field after the second scatterer. As such, both systems may need to be available in a facility, with single scattering being used for smaller tumors or where sharper penumbras are required, and double scattering for the treatment of larger tumors.

#### 9.3.2.3 Collimators and Compensators

Range shifter wheels or ridge filters and scattering alone produce an SOBP with a constant water-equivalent range at the distal end of the field across the whole field and a circularly shaped cross section of the maximum field size orthogonal to the field direction. Both can be further modulated to better conform the dose to the target volume through the use of patient- and field-specific hardware elements referred to as collimators and compensators [20]. Collimators are designed to cut off the lateral aspects of the scattered field, which will not deliver useful dose to the target volume. As such, they are typically made of thick slabs of high-density material, for example, tungsten or brass, in which apertures are milled, which match the shape of the projected shape of the target along the field direction.

Compensators, on the other hand, conform the distal end of the SOBP to the distal end of the target, and as such are formed of an easily workable block of material, such as PMMA, whose thickness in two dimensions can be individually defined so as to be thicker for the portion of the field, where the distal end of the field is shallower in the patient, and thinner, where the distal end is deeper. As such, the distal end of the field can be quite precisely molded to the distal end of the target volume, even when passing through relatively complex density heterogeneities.

#### 9.3.2.4 Passive Scattering in Practice

Passive scattering has been a successful modality for proton therapy for more than 50 years, and the vast majority of patients treated with protons have been treated using such an approach. However, it has its limitations.

Passive scattering is rather labor-intensive to plan, prepare, and deliver. Although complex plans and treatments can be designed, the inherent inflexibility

of a fixed SOBP extent for each field means that constructing complex dose distributions that can wrap around critical structures is time-consuming and difficult. Indeed, it is common that passive scattered plans for complex volumes consist of 10 or more fields, in which the distal ends of some fields are patched against the lateral edges of other fields. However, for each of these fields, individual collimators and compensators have to be manufactured, and on each day of delivery, both devices need to be changed for every delivered field. Although this can be mitigated by delivering different combinations of fields on different days of treatment as long as each combination fully covers the tumor volume, it is, nevertheless, a time-consuming daily process. The recent introduction of multileaf collimators into proton therapy helps only a little, as there are at present no solutions for automating compensator shapes and these thus need to be manually changed for every field every day.

An exception to this is the treatment of uveal melanoma, a tumor of the retina of the eye. These have been treated for many years using a single field, collimated approach, typically without the use of compensators, see for example, [21]. This treatment has been proven to be not only very efficient, with typical treatment times per patient per day are 15 min at our institute, but also extremely effective, see Section 9.4.1.1.

### 9.3.3 Pencil Beam Scanning

#### 9.3.3.1 Principle of PBS

As protons are charged particles, when passing through electromagnetic fields, they undergo two separate forces – the so-called Lorenz forces. The electric field component accelerates or deaccelerates depending on the polarity of the field of the particles, whereas a magnetic field will deflect them. This second characteristic of the Lorenz force can be directly exploited to construct therapeutically useful proton fields through a process now universally known as pencil beam scanning [22,23].

This concept is deceptively simple and is shown in Figure 9.4. If we consider the Bragg peak of a monoenergetic proton beam to be a 3D *spot* of delivered dose, then one can also imagine that this *spot* can be magnetically scanned in order to *paint* a homogeneous dose across the target. When combined with fast energy changes, such that different layers can be painted at different depths in the patient, then the concept of pencil beam scanning is complete, see, for example, Figure 9.4a. As such, PBS proton therapy is essentially the 3D *painting* of proton Bragg peaks throughout the selected tumor volume, with the fluence (number of protons) being delivered by each spot being individually optimized in order to obtain the desired dose distribution to the target volume. This optimization step is part of the treatment planning process, in which field directions are manually defined, spot (Bragg peak) positions calculated in the patient, fluences optimized, and then the final 3D dose distribution calculated, see for example, [24,25] and Figure 9.4b. In current terminology for PBS proton therapy,

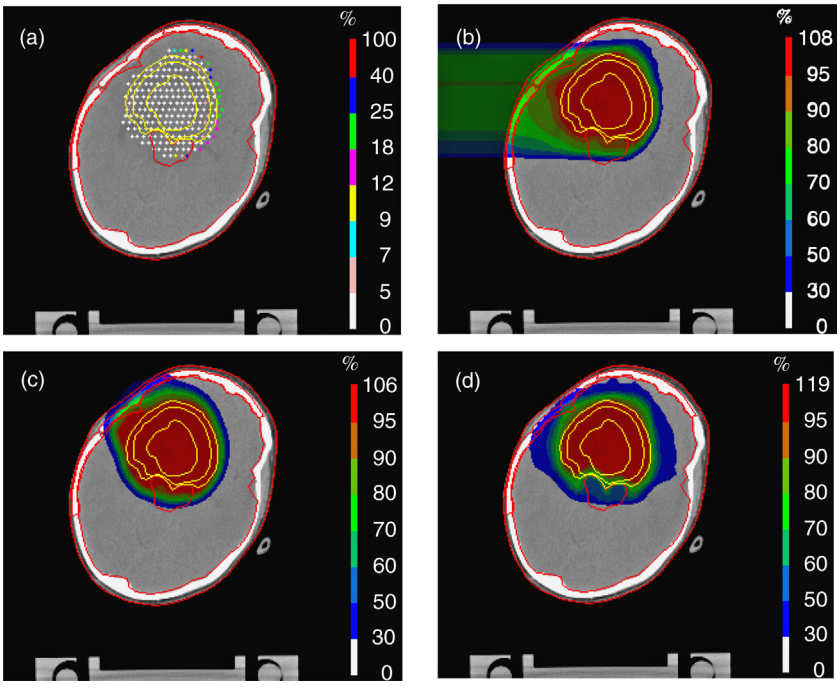


**Figure 9.4** Field geometry and dose distributions for PBS proton therapy. (a) Bragg peak positions (crosses) and optimized relative fluences (color) for a single, SFUD field incident from the left-hand side and (b) the resulting optimized dose distribution. (c) A three-field SFUD plan to the same tumor and (d) an IMPT plan, using the same field geometry as (c) but with dose constraints defined for the brain stem.

such optimization can be performed in two ways – either field by field, termed single-field uniform dose (SFUD) or single-field optimization (SFO) (Figure 9.4c) or for all fields simultaneously, typically referred to as intensity-modulated proton therapy (IMPT) or multiple field optimization (MFO), see Figure 9.4d [26]. Both are acceptable approaches, with SFUD resulting in homogeneous coverage of the target volume from each individual field, cf. passive scattering, and IMPT resulting in potentially very inhomogeneous individual field dose distributions, but generally more conformal, and more importantly, conformal avoidance of neighboring critical structures, when all fields are combined. As such, IMPT is the PBS equivalent of patched fields for passive scattering and intensity-modulated radiation therapy (IMRT) for photon therapy.

#### 9.3.3.2 PBS versus Passive Scattering

Although the vast majority of experience with proton therapy at the time of writing is with passive scattering, there is little doubt that the future of proton therapy lies with PBS. Due to the 3D active scanning of individual proton Bragg peaks within the selected target volume only, the need for collimators and

compensators is avoided, and even if for some cases, these can still bring advantages to PBS. In addition, and just as importantly, the planning process becomes a more automated procedure, with the optimization processes doing the *hard work* of combining and patching different fields in order to both cover the target volume and avoid as necessary any neighboring critical structures. This not only makes the treatment planning process significantly faster and more efficient but also results in significantly improved treatments than can ever be achieved using passive scattering. Finally, the treatment delivery process can also be fully automated, with many fields and treatments being delivered without the need to go into the treatment room between fields. This can have a significant impact on the patient throughput of such a facility (see Section 9.5.2.1). Although passive scattering still has some advantages, for example, for superficial tumors, where collimation still provides by far the best lateral fall-off, and for the treatment of mobile tumors, these problems are also being tackled and gradually solved with PBS. As such, nearly all new or planned proton facilities in the future will have at least the option of PBS, whereas many will provide PBS only. Indeed, by the end of 2015, it is forecast that, for the first time, the number of PBS-equipped proton treatment rooms worldwide will overtake passive scattering rooms [27]. This trend will certainly continue, if not accelerate, in future.

### 9.3.4
### Treatment Gantries

Even though protons can apply more-or-less homogeneous and conformal doses to a target from a single direction, there are nevertheless many good reasons why proton treatments should be designed using multiple, angularly spaced fields. These include improved sparing of critical structures using IMPT, as well as general treatment robustness. Indeed, multiple fields are, in the author's opinion, one of the best and certainly the simplest method of mitigating the potential effects of systematic errors such as *in vivo* uncertainties in proton range. The use of multiple fields implies the treatment machine has the ability to bring the beam in from different incident angles on to the tumor, ideally, at least in the head and neck region, with nearly $4\pi$ degrees of freedom. Although it is always possible to imagine moving and rotating the patient about a fixed beam line, in reality this is not always well tolerated by the patient and can add additional uncertainties in the treatment due to the motion of internal organs, particularly for extracranial treatments.

As such, for patient comfort and treatment precision, there is no real alternative to keeping the patient as still as possible and moving the treatment beam around the patient. Thus, the state-of-the-art proton therapy is typically applied using the so-called *gantries*, which can rotate the final beam line and delivery nozzle elements around the patient at least by 180° and more usually by 360°. The off-axis angles (called noncoplanar in radiotherapy jargon) are then achieved with an additional patient table rotation (yaw) as necessary [28].

The problem of gantries for proton therapy, and also the main problem of proton therapy, is their size.

First, as already pointed out for passive scattering, a minimal distance of at least 2 m is typically required between the scattering devices and the patient in order to have reasonable field sizes. A similar distance is also required for scanned beams in order to keep the angle of deflection and hence the required magnetic fields to a reasonable magnitude. Thus, as an absolute minimum, current proton gantries need a diameter of at least 4 m, if the patient is placed at the center of rotation of the gantry. In addition, however, as elementary particles go, protons are rather heavy – they are about 1800 times heavier than electrons – making them magnetically very rigid. Put another way, strong magnetic fields are required to significantly bend a proton beam of therapeutically useful energies larger or equal to 70 MeV. Although this is not a great problem for the magnets required for scanning proton beams with PBS, they only need to deflect the beam over a few degrees at most if the distance to the patient is kept reasonably large, this is a problem for gantries where, typically, the beam needs to be bent at least 90° to bring it onto the patient. As the radius of this bending is directly determined by the achievable magnetic field, this is, in the end, the limiting factor on the size of gantries. As such, typical proton gantries, whether passive scattering or PBS, are large beasts, with diameters of 10 m or more and weights well over 100 ton. Although many ideas have been proposed to reduce sizes and weights, for example, through off-center positioning of the patient [23] or by rotating a compact cyclotron so that it directly emits onto the patient [29], such solutions are not without their disadvantages, and as such, for the foreseeable future, it appears that proton therapy delivery facilities will remain large and, consequently, expensive.

## 9.4 Clinical Applications

### 9.4.1 Selected Clinical Indications

#### 9.4.1.1 Uveal Melanoma

One of the oldest indications for proton therapy is the treatment of uveal melanomas. These are malignant, aggressive tumors of the retina of the eye. Although small in absolute size, typically just a few millimeters, they are fast growing and metastasize easily. They are also histologically the same as skin melanoma.

There are two main treatments for this tumor – surgery and radiotherapy. Although surgery is a successful treatment, achieving very high local tumor control rates, it is a mutilating approach involving the removal of the whole involved eye. As such, proton therapy was proposed and introduced as an alternative treatment at Massachusetts General Hospital in the 1970s [30]. Since this first pioneering work, more than 22 000 uveal melanoma patients have been treated worldwide at 11 facilities. However, proton therapy of uveal melanomas is a rather specialized treatment, predominantly performed on dedicated beam lines and facilities, and is exclusively an indication for passive scattering. Given the

special anatomical position of these tumors, being just a few centimeters deep and approachable with the proton beam directly through the eye, low-energy, about 70 MeV, proton beams are used and the patient is treated in the sitting position. This is also one of the very few indications where a single field treatment is the optimum approach. Finally, it is also the only proton treatment that, as standard, is planned and calculated without the use of X-ray CT.

Paradoxically, the treatment of uveal melanoma with protons starts with a surgical intervention. In order to localize the tumor, and to make its position visible on planar X-rays (see below), small tantalum clips need to be attached to the orbit of the involved eye, as close to the tumor as possible. This, of course, needs to be performed by an experienced opthalmologic surgeon. Together with fundus images and ultrasound measurements of the length of the eye, the positions of these tantalum clips are the main input into the treatment planning system. From this information, the best incident direction for the proton beam can be determined so as to cover the target while avoiding critical structures – mainly the lens and optic nerves. However, in contrast to other radiotherapy techniques, the incident beam angle is not determined by defining a gantry and table angle but rather by defining a *gaze* angle for the involved eye. During treatment, this gaze angle is ensured by having the patient stare at an LED placed at a well-defined position in relation to the treatment nozzle, see Figure 9.5. As the typical treatment time is about 1 min, this is well tolerated by most patients.

From the clinical point of view, such tumors are treated to a total dose of 60 Gy in four sessions of 15 Gy each over 4 consecutive days – an approach called fractionation in radiotherapy terms. In fact, this treatment is actually a *hypofractionated* regime, meaning that the fraction dose is high and the whole

**Figure 9.5** The treatment chair and nozzle for the OPTIS facility at PSI. This is a passive scattering facility dedicated to the treatment of uveal melanomas, which are rather aggressive tumors of the retina.

treatment is delivered in a small number of sessions. Accurate positioning of the patient is performed on each treatment day by the use of orthogonal X-ray images of the eye from which the tumor position can be determined indirectly from the tantalum clips. Based on these images, the eye's position in relation to the beam is adjusted to the tenth of millimeter accuracy using a six-degree of freedom robotic chair positioning system.

Such a treatment has been delivered at our institutes since 1984, and at the time of writing, more than 6500 patients have been treated, with about 200 new patients being referred each year. Based on the last detailed analysis of the first 3000 patients treated, local tumor control at 5 years, that is, tumor growth has been arrested for a period of at least 5 years since the completion of treatment, is 98%, together with an eye-retention rate of more than 90% [31,32]. In fact, it is this latter figure that is the true success of this treatment, as surgery alone can achieve similar levels of tumor control, but only of course at the cost of full enucleation of the diseased eye.

#### 9.4.1.2 Skull-Base Chordomas

The next two indications to be discussed are both treatments that are usually conducted using gantry-based facilities. Although both can and are treated using both passive scattering and pencil beam scanning, we will concentrate on their treatment using PBS and our own clinical experience with these tumor types and sites.

Skull-base chordomas and their closely related, but histologically different cousins, chondrosarcomas are tumors of the bone that occur mainly in the base of skull and along the spinal axis. Standard of care for these is the use of surgery to remove as much of the bulk tumor as possible, followed by high-dose radiotherapy to the whole preoperative tumor volume if it cannot be totally removed through surgery. For skull-base chordomas/chondrosacomas, this is often the case due to the tumor's close proximity to many critical organs such as the brain stem and spinal cord for more caudally positioned or extending tumors, optic nerves, and chiasm, to mention just a few. However, the same structures also make high-dose radiotherapy a challenging proposition. As such, these tumors were identified as good candidates for proton therapy in the mid-1970s at Massachusetts General Hospital and have subsequently become a standard indication for proton therapy.

Skull-base chordomas have been treated with PBS at our institute for more than 15 years, with well over 200 patients now having been treated. Typical prescription doses are 74 Gy to the tumor volume, with maximum dose constraints of 63 and 60 Gy to the brain stem/spinal cord and all optical structures, respectively [33]. However, in contrast to ocular treatments, a conventional fractionation schedule of 37 fractions of 2 Gy each is used, delivered 5 days per week over 7–8 weeks. At our institute, a multiple series approach to treatment is taken, with the first 30–40 Gy of treatment being delivered using the somewhat simpler SFUD technique and the remaining 34–44 Gy being delivered using IMPT.

A SFUD approach is used in the first series in order to ensure a fully homogeneous dose distribution across the whole preoperative tumor bed, an example of

which is shown in Figure 9.6a. This is a three-field approach, consisting of a quasi-lateral field and two noncoplanar (apical) fields. This field arrangement achieves a high level of dose conformity to the target volume and exploits a wide angular separation of the fields in order to mitigate the potential degrading effects of density heterogeneities, particularly for the two apical fields, which only pass through the skull and brain and, therefore, pass through rather density-homogeneous anatomical regions. Given its robustness, this series is taken to as high a total dose as possible, but not so high that in the subsequent series, the constraint doses to the brain stem/spinal cord and optical structures cannot be met.

The more complex, but more flexible, IMPT approach is then used for the second series in order to *carve* out a dose from these critical organs and to ensure that for the whole treatment, the respective maximum dose constraints are not violated. A typical field arrangement and plan for this is shown in Figure 9.6b and consists of four fields in a shallow *cross* arrangement with a small angulation of 10–15° in the cranial direction. Such a beam arrangement has been adopted for the IMPT part of the treatment for two reasons. First, these angles have been found to best allow the planner to remove dose from the main critical structures, such as brain stem and optical structures, while maximizing target coverage, and second because this arrangement has been found to be also

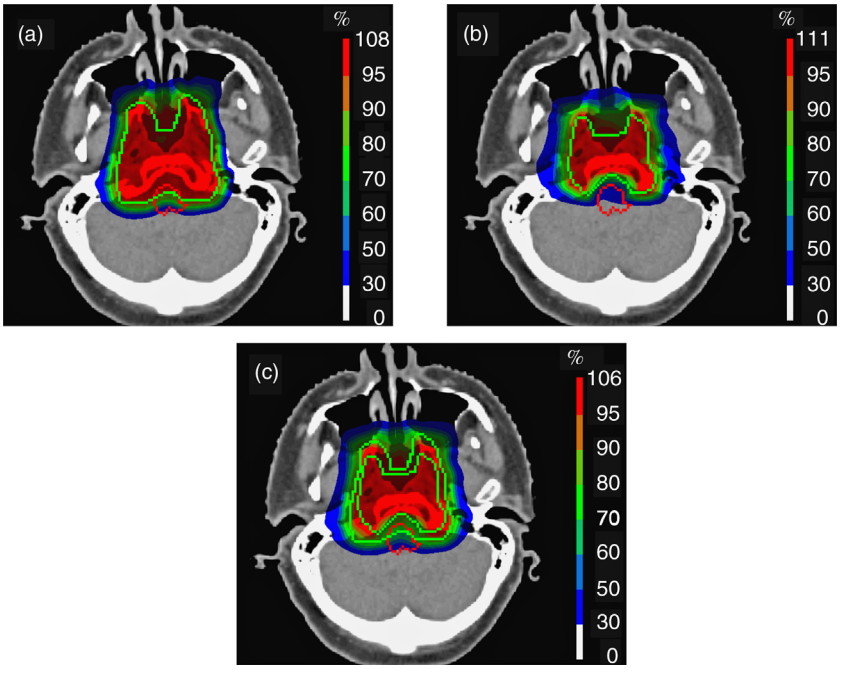


**Figure 9.6** An example skull base treatment using PBS proton therapy. (a) The first series, three field, SFUD plan and (b) the second series IMPT plan with dose constraints set on the brain stem and optical structures. (c) The total delivered dose constructed from the weighted addition of the SFUD and IMPT plans.

relatively robust to potential range uncertainties. The combined dose distribution for the whole treatment – the combination of the SFUD and IMPT series for this treatment – is shown in Figure 9.6c, showing the high dose homogeneity and conformity that can be achieved with PBS proton therapy for such a case.

In our most recent analysis of treatment outcome, based on 222 patients treated since 1999, local tumor control at 5 years post-treatment is 80% with higher grade side effects being restricted to the optical nerves and temporal node necrosis in very few patients. No brain stem/spinal cord toxicities have been observed. These results compare very favorably with other published data for protons with passive scattering as well as the conventional photon therapy [33,34].

#### 9.4.1.3 Ependymoma

Ependymomas are brain tumors that are typically in pediatric patients of even very young ages (less than 5 years old). Predominantly, these occur in the central brain, but can often abut against the brain stem. Such tumors are typically treated to a total of 54.0–59.4 Gy with 30–33 fractions of 1.8 Gy, with the patient being treated in the prone position, that is, lying on their belly. For children under the age of 5 years, a light anesthesia is generally required each treatment day.

Given the anatomical situation of such tumors, density heterogeneities are not too much of an issue. The field directions we use have been selected both to reduce the volume of developing brain that is irradiated and to avoid overdosing the brain stem. A typical example of such a treatment is shown in Figure 9.7. This consists of three series, each using different field arrangements, but with all fields incident from the posterior aspect. The relatively narrow separation of the fields is a compromise between robustness, where wider separations are generally more favorable, and minimizing the total volume of brain irradiated, which can be achieved using narrower separations or even a single posterior beam. In addition, however, this field arrangement *ranges out* in the brain stem, which is generally not advised in proton therapy due to worries about possible range uncertainties and enhanced RBE at the distal end of the field [11]. We have decided to nevertheless take this approach as reducing the volume of involved brain is considered to be the most important clinical factor with these cases. However, multiple series have been used to reduce the high-dose region to successively smaller target volumes, and in these later series, different beam arrangements have been used such as to make the overall treatment somewhat more robust to range/RBE uncertainties.

Over 50 ependymoma patients have been treated with PBS proton therapy at our institute. Mean age at treatment was 2.6 years and surgical gross tumor resection (GTR) had been achieved in only about 50% of the patients. At the last analysis, mean follow-up time after treatment was just over three and a half years and actuarial local control at 5 years post-treatment of over 80% has been achieved, which compares very well with published results with photons, especially given the very large proportion (~50%) of patients without GTR. In

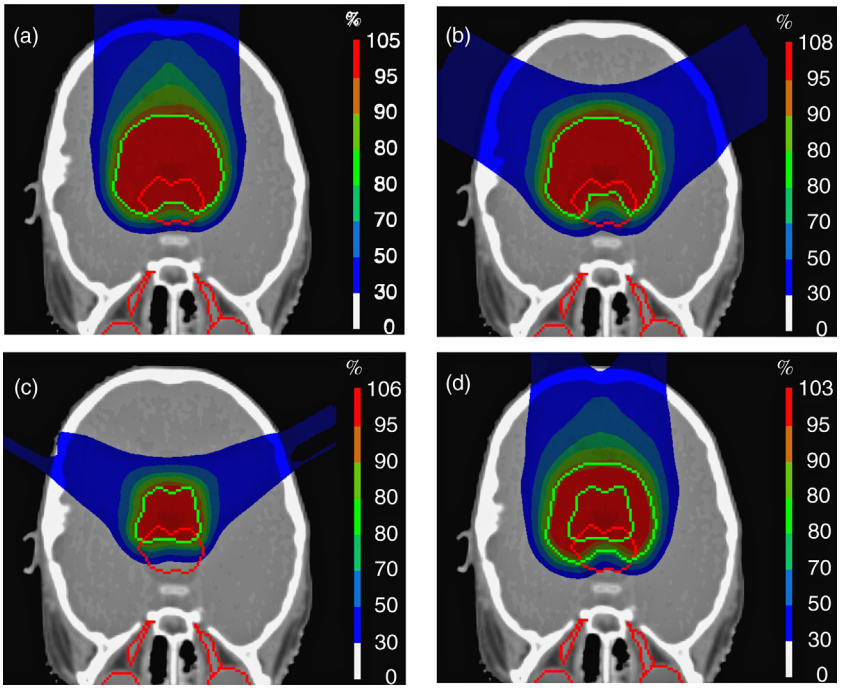


**Figure 9.7** An example treatment to a ependymoma (brain tumor). This consists of three SFUD series, with two–three fields per series (a–c). The combined dose distribution for all series is shown in (d). Different angles are used for each series in order to reduce the risk of high LET/RBE in the brain stem at the distal end of the target volume.

addition, only one patient (2%) developed a brain stem complication, which is also comparable to the incidence of similar toxicities in photon therapy. Cognitive development, the main benefit we would expect from reducing the irradiated brain volume, for these children is also being followed using quality-of-life questionnaires, and these are being assessed. However, it is too early to say whether a clinical advantage for PBS proton therapy in this end point can be demonstrated.

## 9.5 The Future of Proton Therapy

### 9.5.1 Future is PBS

It is becoming increasingly clear that the future of proton therapy lies with pencil beam scanning. It is more flexible, automated, and more effective than passive scattering in almost all cases apart from the very specialized treatment of uveal

melanoma described above. This is now being clearly recognized by both potential customers and manufacturers. Indeed, it is forecast that by the end of 2015, there would be, for the first time, more PBS proton treatment room worldwide than passive scattering, and this trend is bound to continue. In addition, of all the commercial firms offering proton therapy solutions, nearly half provide PBS-only solutions, while all others provide both PBS and passive scattering. Thus, the future of proton therapy is quite clearly PBS.

### 9.5.2 Current and Future Technological Developments

#### 9.5.2.1 Treatment Delivery

In addition to the more widespread installation of PBS-only proton therapy facilities, there are many other technological developments for proton therapy that can be envisaged.

From the economic point of view, the holy-grail of proton therapy is the development of small and cheap proton therapy systems. The size and cost of the available proton therapy equipment is clearly a limiting factor, with treatment gantries having diameters of typically 10 m or more, in the vast majority of cases without including the accelerator. Such large gantries are expensive and heavy, and require extensive shielding to meet radiation protection regulations. Although these vary from country to country, the basic equation remains the same: larger rooms require more volume of shielding, and the larger the volume of shielding required, the more expensive it will be. So, there are good reasons to try to reduce the size of proton facilities, and indeed, it may be the only way by which the costs of facilities can be drastically reduced [35,36].

Developments in this direction include single-room systems either with a compact cyclotron and shortened beam line or even the use of a very compact cyclotron mounted directly on the gantry, which avoids the beam line and last 90° magnet [29]. However, the latter solution is only for passive scattering at the moment, although a scanning solution is under development. Nevertheless, both systems have gantry diameters of 10 m or more, so although total volume can be reduced, the diameter remains more or less the same. Other suggestions for reducing costs include superconducting gantries, the main advantage being a considerable reduction in the weight of the gantry, or the utilization of alternative accelerator technologies [35,36].

In the last category, the most challenging is the use of laser-based accelerators. By using very powerful TW lasers impinging on thin metal foils, very high electric fields can be produced by the plasma of electrons emitted from the foil when it is obliterated by the laser. This electric field with strengths of megaelectronvolt/millimeter can then accelerate protons that are also ejected to hundreds of megaelectronvolts in just a few millimeters. The potential advantages of such an approach are clear. However, many challenges remain before such a system will come into clinical use, not least of which are problems with the energy spectrum, as the accelerated protons have a wide energy spectrum, rather than the

quasi monoenergetic characteristics that are ideally required for therapy, and the pulse rate of the laser, which in the TW/PW region are in the range of a single pulse every few seconds or even minutes. Thus, there is much work to be done before laser acceleration will be seen in the clinic.

In summary, at the time of writing, it seems that, although some advances are being made in reducing the size of proton facilities, for the foreseeable future, such systems will remain considerably larger than conventional radiotherapy facilities and, therefore, also more expensive.

#### 9.5.2.2 Treatment Efficiency

Another factor affecting the cost of proton therapy is treatment efficiency. Although for PBS proton therapy, relatively few treatment fields are required in order to obtain highly conformal treatments, at our institute the average number of fields per plan is just over three [24], the treatment time per field can be quite long, particularly for larger tumor volumes. As PBS is a three-dimensional method, which includes changes of the beam energy, the treatment time per field increases roughly in proportion to the volume of the tumor. For example, modern PBS proton therapy machines require roughly a minute or more to deliver 2 Gy to a 1 l volume from a single-field direction. Although this does not seem too long, it is considerably longer than is required for a single field with conventional, photon-based techniques. Indeed, in recent times, photon-based radiotherapy has developed into a rotational approach, with the fields being modulated simultaneously at high-dose rates, such that very complex, full treatments can be delivered in just a few minutes – basically the time it takes for the gantry to rotate around the patient [37]. As the effective cost of a facility also depends on the number of patients that can be treated per day, a less efficient delivery of proton therapy also has financial consequences. There is, therefore, a clear need for proton treatment times to be reduced.

One clear area of improvement for treatment efficiency is in the area of online imaging, which we will return to in the following section. However, there are also developments in treatment delivery that could contribute significantly to reducing treatment times. One is improving the speed of energy changes. This is a main limiting factor in delivery time at the moment, with many commercial PBS proton therapy systems requiring a second or more to change energy corresponding to a range change of only 5 mm. To put this in context, for the delivery of a liter volume, about 20 such energy changes will be required assuming a 5 mm separation of Bragg peaks in depth, meaning that 20 s, or a third of the total delivery time, is required just for such changes. Thus, a significant gain could be made, if energy change times can be reduced. This is in principle possible, with the gantry 2 at PSI already demonstrating that 5 mm range changes can be achieved in only 0.1 s, reducing the dead time in delivery for energy variation down to only 2 s [38].

Similar gains could also be made in the efficiency of orthogonal scanning as well. For example, the typical time for adjusting the pencil beam by 5 mm, a typical *spot* spacing for PBS, is about 3 ms – so considerably faster than the time

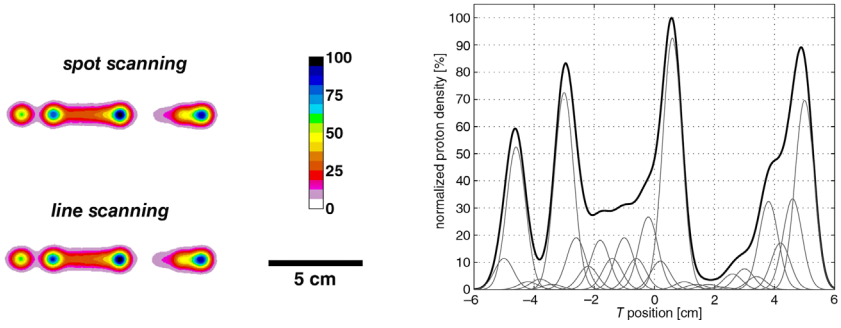


**Figure 9.8** A comparison of spot and continuous scanning. On the left, color-enhanced, relative-dose measurements of a spot scanned and continually scanned line delivering the same fluence modulated profile. On the right is shown the corresponding summed fluence profile of the individual pencil beams in spot scanning mode (light gray) and the sum of these fluences (dark line) as would be delivered in continuous line scanning mode.

required for range (energy) changes. However, there are also many more such adjustments to be made within the field delivery. Once again, assuming our 1 l $(10\,\text{cm})^3$ target volume and 5 mm spacing between pencil beams orthogonal to the beam direction, in each plane $20 \times 20 = 400$, such adjustments are required, leading to an additional 1 s dead time per energy layer and, therefore, an additional 20 s of dead time for the whole field. Alternatively, however, line scanning can be performed, where the beam is continuously scanned in combination with beam intensity and velocity modulations [39] (see Figure 9.8). In this case, delivery time is simply the total beam-on time required to deliver the full proton fluence required for the line, essentially eliminating the dead time for scanning in any line completely. This is a development that is currently being investigated at our institute with encouraging results. Finally, delivery times could be further reduced by upgrading and improving beam monitoring equipment such that higher beam intensities can be used, thus also effectively reducing the beam-on time per line or pencil beam position.

In all these approaches, there is lot of interesting and challenging physics and engineering to be done, and they will hopefully make their way into the clinic in the future.

#### 9.5.2.3 In-Room/Onboard 3D Imaging and Adaptive Therapy

In all developments aimed at improving workflow and patient throughput, such as those outlined above, it is important that treatment quality should not be compromised. However, can treatment quality also be improved while at least maintaining, if not increasing, patient throughput?

In the author's opinion, one of the biggest gains for both treatment quality and efficiency will be the introduction of state-of-the-art imaging devices on proton gantries. The ability to perform 3D imaging in the treatment room, immediately before treatment, has perhaps been one of the biggest advances in conventional therapy in the past few years [40]. In-room CT or onboard cone-beam imaging

**Figure 9.9** In-room CT will play an essential role in improving proton therapy.

allows for regular, maybe even daily, imaging of the patient for more accurate 3D positioning of the patient as well as providing a way of monitoring anatomical changes of the tumor and/or patient through the treatment course, cf. Figure 9.9.

Unfortunately, although this is slowly changing, in-room 3D imaging devices are somewhat lacking in the majority of proton therapy facilities. This is despite the fact that proton therapy is likely to benefit from regular 3D imaging more than conventional radiotherapy due to its much higher sensitivity to changes in densities in the entrance path of the beam, which consequently can cause significant range changes in the patient. For this, regular 3D imaging can help in two ways.

First, for many treatment sites, 3D imaging may be the only way to accurately detect rotational setup errors of the patient. For proton therapy, such rotations can potentially bring different densities in and out of the beam path, thus affecting the range of the field. In addition, a change in incidence of the beam with a density interface due to such rotations as bone–air interfaces in the nasal cavities can also potentially affect the distal shape of the Bragg peak [12] and, therefore, the form of the distal dose fall-off. Second, and perhaps more importantly, regular 3D imaging allows for a more detailed monitoring of anatomical changes during the course of treatment. These can be due, for example, to changes in the tumor volume, weight gain, and loss [41], or differential filling of internal cavities such as in the nasal region. All these can have a significant effect on proton range and, depending on the patient, can in the end be the most substantial contribution to range uncertainty for proton therapy. Three dimensional imaging is the only method of detecting and assessing the effects of such changes.

But if such changes are found, what can be done? The only solution, if the effect on the treatment has been judged to be clinically relevant, is to replan the treatment – a technique known as *adaptive therapy* [42]. This concept was proposed about 20 years ago for conventional therapy and, as argued above, such an approach may be even more important for proton therapy. As such, an important future development for PBS proton therapy will be a move toward *daily adapted proton therapy* (DAPT), where in-room/onboard, 3D X-ray-based

imaging will be a key feature. In-room because the imaging must be performed as close in time to the treatment delivery as possible, and 3D X-ray based because, currently, only X-ray CT/CBCT provides the necessary information on patient density to allow for accurate proton dose calculations and planning, see Section 9.3.1.

Although a technologically challenging approach, it is interesting to note that the challenges for DAPT are mainly computational. For instance, the imaging devices for such an approach already exist. CBCT is a standard imaging tool in conventional therapy now and is slowly being introduced into proton gantries, and a growing number of proton therapy facilities are installing in-room CT systems for a similar purpose, ours included. And with proton PBS, there is a delivery technology that is flexible enough to deliver any fluence pattern to any patient on any day, without the need for any externally manufactured patient- and field-specific hardware. The main problem for DAPT then is in the calculation, and quality assurance, of the *plan-of-the-day* and how this can be performed within a few minutes of the imaging. But with the introduction of GPU-based dose calculations [43] and algorithmic tools for helping with patient-specific QA [44], the author believes that, although much work still needs to be done, DAPT is just around the corner.

### 9.5.3 Clinical Future of Proton Therapy

In the previous sections, we have presented the clinical results of three example indications that have been treated using proton therapy at PSI. The results are certainly promising, but are not presented in order to prove that proton therapy is better than other techniques. In principle, this can only be proven in large-scale clinical trials, which are notoriously difficult to perform in radiotherapy. They have been presented more in order to show that this technique can be delivered safely and successfully.

It should be remembered that modern radiotherapy with X-rays or with other radiation-based techniques such as electrons and brachytherapy is already a very successful treatment of cancer, contributing to the treatment of more than half of all curable patients. As such, it is the second most important cancer treatment modality as well as being by a long way the cheapest. So, conventional radiotherapy is already an excellent approach, which is still further advancing with the introduction of ever more sophisticated modulation and calculation tools, and for many patients and indications, there is likely to be little, if any, additional gain from the use of the more complex and expensive proton therapy.

However, it is also true that there are still a disappointingly high proportion of individual patients and indications that cannot be adequately treated with conventional approaches. It is perhaps for these patients that proton therapy can play a role. Indeed, this is the rationale for the current indications with protons. For instance, uveal melanomas, although small in absolute terms, can be large in relation to the anatomical compartment, in which they are found, that is, the eye.

As such, although these could be treated using photons, there is little doubt that protons can reduce the integral dose to the whole eye, thus possibly reducing the probability of glaucoma and a subsequent treatment-related loss of the eye. For the skull-base chordomas, on the other hand, protons have become the radiation treatment modality of choice due to the challenging site of the primary tumor being so close to many critical organs and its radioresistance, which requires high doses. With their tissue sparing characteristics, protons seem to provide the best approach for the treatment of these lesions. Finally, for the last indication discussed in detail here, that is, pediatric ependymoma, protons will hopefully have a clinical advantage in longer-term clinical outcomes such as cognitive performance of the patient due to their ability to reduce the volume of irradiated brain. These are, however, just a few of the many indications including prostate and breast cancers being treated at various facilities around the world with protons.

So what exactly will be the role for proton radiotherapy in the future? The author's own opinion is that, while hopefully never completely replacing conventional radiotherapy, PBS proton therapy could bring clinically relevant advantages in up to 15–20% of patients who are being referred for radiotherapy. However, rather than this being indication driven, it may well become more and more patient driven. That is, patients for proton therapy could be selected based on the merits of the individual case rather than whether a patient has prostate cancer, breast cancer, or even a skull-base chordoma. Within each of these indications, there are likely to be individual patients, maybe few in the case of prostate or breast cancers, more for chordoma that, for various reasons, can benefit more from proton therapy than others. For example, due to a particularly large and complex tumor volume, advanced prostate cancer, which also requires irradiation of the pelvic nodes, comorbidity of the patient, for example, to reduce dose to an already damaged lung in the treatment of lung cancer, or the need to reduce overall integral dose to the patient, that is, for most pediatric cases, but possibly also some patients on particularly aggressive concomitant chemotherapy regimes. Of course, this list is not exhaustive, but hopefully gives the reader the feel for how proton therapy may best be deployed in the future – as a powerful modality for personalized radiotherapy.

## 9.6
## Is There a Role for Nanotechnology in Proton Therapy?

This is a book on nanotechnology, so it is befitting to finish this chapter by talking about what possible applications there are in proton therapy for this exciting field. In fact, as in many other areas of science and medicine, there is a growing interest in the use of nanotechnologies in proton therapy. In this last section, we will briefly look at potential nanotechnology applications that could have an impact on the accuracy and effectiveness of this treatment modality.

### 9.6.1 Tumor Imaging

As discussed in Section 9.3.1, imaging is a crucial and critical part of radiotherapy generally and for proton therapy in particular. Simply put, without having an accurate indication of the position and extent of the tumor, or even better the tumor cell density or activity, then the effectiveness of any form of localized tumor therapy will always be limited.

Typically, imaging for radiotherapy is based on the use of combined modalities consisting of X-ray CT, MRI, and increasingly, PET imaging. Although all of these give important and complementary information about the tumor and its environment, information on the microscopic spread and metabolic activity of the tumor is still very limited. As such, any developments in the imaging of tumors at the micro- and nanolevel would be a great step forward, and recent advances in nanoparticle imaging show great promise.

Tumor activity and metabolism can be monitored via nanoparticles by a number of processes, one of which is the monitoring of overexpressed or misregulated cell surface proteins. For example, the surface protein plectin, which although normally expressed intracellularly, is exceptionally found on the surface of pancreatic tumor cells, has recently been used as a radiolabel for targeting pancreatic cancer using single-photon emission computer tomography (SPECT) [45]. Alternatively, transferrin, a plasma protein that is expressed by highly proliferative cells, can be combined with viral nanoparticles (VNPs), which in turn can be manipulated to incorporate MRI contrast agents [46]. Similarly, using MRI, it may be possible to directly image tumorigenesis via telomerase activity through the use of magnetic nanoparticles [47], tumor vasculature with multifunctional nanoparticles [48], and tumor-associated macrophages using iron oxide-enhanced particles [49].

Although still very much in the research phase, and mostly not yet applied *in vivo* to humans, these preclinical results show the huge potential of nanotechnology for improving tumor imaging and eventually the ability of proton therapy to more accurately target the tumor in its entirety.

### 9.6.2 Dose Enhancement

Radiotherapy, and particularly proton therapy, is already a highly targeted therapy against cancer, which uses the physical characteristics of charged particles to conform the delivered dose to the target. Nevertheless, and as seen in Figures 9.6 and 9.7, there is unfortunately still some considerable dose delivered to normal tissues in the entrance path of the individual proton beams. As such, researchers are looking into ways of locally enhancing the delivered dose in the tumor to increase the ratio of target-to-normal tissue doses. One approach being investigated is the use of gold nanoparticles targeted to the tumor.

As the actual energy delivered to tissue from photon and proton therapy is mainly from secondary electrons rather than from primary particles, the local deposited dose can be enhanced by increasing the secondary electron yield resulting from proton interactions. One way of achieving this is by *seeding* the tumor with high-density, high-z material [50], for example, through the use of gold nanoparticles. Such seeding has been shown to produce a pronounced dose enhancement effect for kiloelectronvolt X-rays in mice [51], although the effect is smaller for photon beams with therapeutic energies in the megaelectronvolt range [52].

Dose enhancement effects have also been observed for proton irradiation, with a 50% increase in 1 year survival of mice being observed when combined with gold nanoparticles [53] and a 15% increase in cell killing in prostate cancer cells in *in vitro* experiments [54], compared to proton irradiation on its own. More recently, dose enhancement for both photon and proton irradiation has been studied in detail using Monte Carlo simulations [55]. This work concludes that although dose enhancement is likely to be independent of energy for protons, the enhancement factor will be smaller than for photons and, due to the much smaller range of secondary electrons resulting from proton irradiation, could be achieved only if the nanoparticles are well internalized in the cell. Nevertheless, these first studies into gold nanoparticle dose enhancement for proton irradiation are promising enough to warrant further research.

### 9.6.3
### Nanodosimetry

The final application of nanotechnologies for proton therapy reviewed here is in the field of dosimetry or radiation metrology.

As discussed in Section 9.2.4, an important parameter for proton therapy is the linear energy transfer, as this has been shown in *in vitro* experiments to be directly related to biological effectiveness. To be more precise, LET can be characterized as the lineal density of ionizations along a path, and has the units of kiloelectronvolt/micrometer. As such, LET is a characteristic of proton interactions that acts at the dimensions of DNA and can only be accurately measured at the nanometer scale. The science of nanodosimetry, therefore, attempts to directly measure LET at similar scales [56].

Given the challenges of constructing radiation detectors at the nanoscale, present developments in nanodosimetry concentrate, instead, on the measurement of ionization cluster distributions in low-pressure gases. By measuring at low pressures, and, therefore, under very low-density conditions, the size of the detection volume can be significantly increased, while still effectively measuring at the nanometer scale, when scaling back up to the density of water. Different approaches have been suggested in literature including the jet counter [57], the track nanodetector [58], and 2D GEM detectors for reconstructing the full 3D structure of ionization tracks [59]. Although much of this work is still in its infancy, its potential in proton therapy has already been demonstrated, at least

theoretically, by incorporating nanodosimetrical information into the optimization process for proton therapy in very simplified treatment geometries [60]. Whether such an approach has applications clinically, or will bring significant advantages, remains to be seen, and will depend on the success of nanodosimetry to accurately measure localized LET at the DNA scale. Nevertheless, the ability to measure deposited dose precisely at the DNA/nanoscale will undoubtedly improve our knowledge and understanding of the effect of proton therapy at the cellular level.

### 9.6.4 Summary

In this final section, we have outlined some areas, where nanotechnology could have an impact on proton therapy. Indeed, proton therapy itself could in some ways already be considered a *nanotechnology*. After all, proton interactions operate at the nanometer scale, and the primary biological effect is at the DNA level. As such, the exploitation of emerging technologies in nanotechnology, such as imaging, dose enhancement, and dosimetry, can only enhance this *alternative* form of nanotreatment, hopefully leading to significant clinical improvements through more accurate tumor targeting, more effective dose delivery, and more precise dosimetric measurements.

## References


1 Schlegel, W. (2005) *Scientific Forum*, IAEA.
2 Lomax, A.J., Goitein, M., and Adams, J. (2003) Intensity modulation in radiotherapy: photons versus protons. *Radiother. Oncol.*, **66**, 11–18.
3 Boyer, A.L., Goitein, M., Lomax, A.J., and Pedroni, E.S. (2002) Radiation in the treatment of cancer. *Physics Today*, **55** (9), 34–36.
4 Wilson, R.R. (1946) Radiological use of fast protons. *Radiology*, **47**, 487–491
5 Goitein, M. (2008) *Radiation Oncology: A Physicist's-Eye View*, Springer Science and Business Media, NY.
6 www.ptcog.ch/.
7 Lomax, A.J. (2009) Charged particle therapy: the physics of interaction. *Cancer J.*, **15**, 285–291.
8 Gottschalk, B. (2012) Physics of proton interactions in matter, in *Proton Therapy Physics* (ed. H. Paganetti), CRC Press, Boca Raton, FL, pp. 20–59.
9 Hall, E.J. (2006) Intensity-modulated radiation therapy, protons, and the risk of second cancers. *Int. J. Radiat. Oncol. Biol. Phys.*, **65**, 1–7.
10 Paganetti, H., Bortfeld, T., and Delaney, T.F. (2006) Neutron dose in proton radiation therapy: in regard to Eric J. Hall (Int J Radiat Oncol Biol Phys 2006; 65: 1–7). *Int. J. Radiat. Oncol. Biol. Phys.*, **66**, 1594–1595, author reply 1595.
11 Paganetti, H. (2014) Relative biological effectiveness (RBE) values for proton beam therapy. Variations as a function of biological endpoint, dose and linear energy transfer. *Phys. Med. Biol.*, **59**, R419–R472.
12 Urie, M., Goitein, M., Holley, W.R. *et al.* (1986) Degradation of the Bragg peak due to inhomogeneities. *Phys. Med. Biol.*, **31**, 1–15.
13 Schippers, M. (2015) Proton beam production and dose delivery techniques, in *Principle and Practice of Proton Beam Therapy* (eds I. Das and H. Paganetti),

Medical Physics Publishing, Madison, pp. 129–163.
14 Lawrence, E.O. (1934) Method and apparatus for the acceleration of ions, US Patent 1948384.
15 Veksler, V.I. (1944) A new method of accelerating relativistic particles. *Dokladv Acad. Nauk URSS*, **43**, 329–331.
16
17 Koehler, A.M., Schneider, R.J., and Sisterson, J.M. (1975) Range modulators for protons and heavy ions. *Med. Phys.*, **131**, 437–440.
18 Kostjuchenko, V., Nichiporov, D., and Luckjashin, V. (2001) A compact ridge filter for spread out Bragg peak production in pulsed proton clinical beams. *Med. Phys.*, **28**, 1427–1430.
19 Koehler, A.M., Schneider, R.J., and Sisterson, J.M. (1977) Flattening of proton dose distributions for large fields. *Nucl. Instrum. Meth.*, **4**, 297–301.
20 Mazal, A., Patriarca, A., Wessels, C., and Das, I.J. (2015) Field-shaping: scattered beam, in *Principle and Practice of Proton Beam Therapy* (eds I. Das and H. Paganetti), Medical Physics Publishing, Madison, pp. 191–208.
21 Zografos, L., Perret, C., Egger, E., Gailloud, C., and Greiner, R. (1990) Proton beam irradiation of uveal melanoma at Paul Scherrer Institute (former SIN). *Strahlenther. Onkol.*, **166**, 114.
22 Kanai, T., Kanai, K., Kumamoto, Y., Ogawa, H., Yamada, T., and Matsuzawa, H. (1980) Spot scanning system for radiotherapy. *Med. Phys.*, **7**, 365–369.
23 Pedroni, E., Bacher, E., Blattmann, H., Boehringer, T., Coray, A., Lomax, A.J., Lin, S., Munkel, G., Scheib, S., Schneider, U., and Tourovsky, A. (1995) The 200 MeV proton therapy project at PSI: conceptual design and practical realisation. *Med. Phys.*, **22**, 37–53.
24 Lomax, A.J., Boehringer, T., Bolsi, A., Coray, A., Emert, F., Jerman, M., Lin, S., Pedroni, E., Rutz, HP., Stadelmann, O., Timmermann, B., Verwey, J., Weber, D.C., and Goitein, G. (2004) Treatment planning and verification of proton therapy using spot scanning: initial experiences. *Med. Phys.*, **31**, 3150–3157.
25 Lomax, A.J. (1999) Intensity modulated methods for proton therapy. *Phys. Med. Biol.*, **44**, 185–205.
26 Lomax, T., Bolsi, A., Albertini, F., and Weber, D.W. (2015) Treatment planning for pencil beam scanning, in *Principle and Practice of Proton Beam Therapy* (eds I. Das and H. Paganetti), Medical Physics Publishing, Madison, pp. 667–707.
27 Jermann, M. (2014) PTCOG 53, Shanghai.
28 Schippers, J.M. (2009) Beam delivery systems for particle radiation therapy: current status and recent developments. *Rev. Accel. Sci. Tech.*, **2**, 179–200.
29 Gall, K. (2012) The single-room ion beam facility, in *Ion Beam Therapy* (ed. U. Linz), Springer-Verlag, Berlin, pp. 661–672.
30 Gragoudas, E.S., Goitein, M., Koehler, A.M., Verhey, L., Tepper, J., Suit, H.D., Brockhurst, R., and Constable, I.J. (1977) Proton irradiation of small choroidal malignant melnomas. *Am. J. Opththalmol.*, **83**, 665–673.
31 Egger, E., Schalenbourg, A., Zografos, L., Bercher, L., Boehringer, T., Chamot, L., and Goitein, G. (2001) Maximizing local tumor control and survival after proton beam radiotherapy of uveal melanoma. *Int. J. Radiat. Oncol. Biol. Phys.*, **51**, 138–147.
32 Egger, E., Zografos, L., Schalenbourg, A., Beati, D., Boehringer, T., Chamot, L., and Goitein, G. (2003) Eye retention after proton beam radiotherapy for uveal melanoma. *Int. J. Radiat. Oncol. Biol. Phys.*, **44**, 867–880.
33 Ares, C., Hug, E.B., Lomax, A.J., Bolsi, A., Timmermann, B., Rutz, H.P., Schuller, J.C., Pedroni, E., and Goitein, G. (2009) Effectiveness and safety of spot scanning proton radiation therapy for chordomas and chondrosarcomas of the skull base: first long-term report. *Int. J. Radiat. Oncol. Biol. Phys.*, **75**, 1111–1118.
34 Weber, D.C., Badiyan, S., Malyapa, R., Albertini, F., Bolsi, A., Lomax, A.J., and Schneider, R. (2015) Long term outcomes and prognostic factors of skull-base chondrosarcoma patients treated with pencil-beam scanning proton therapy at the Paul Scherrer Institute. *Neuro. Oncol.*, [Epub ahead of print].

35 Schippers, J.M. and Lomax, A.J. (2011) Emerging technologies in proton therapy. *Acta. Oncol.*, **50**, 838–850.

36 Owen, H., Lomax, A.J., and Jolly, S. (2015) Current and future accelerator technologies for charged particle therapy. *Nucl. Inst. Methods. Phys. Res. Sec. A.* doi: 10.106/j.nima2015.08.038

37 Georg, D., Knöös, T., and McClean, B. (2011) Current status and future perspective of flattening filter free photon beams. *Med. Phys.*, **38**, 1280–1293.

38 Pedroni, E., Bearpark, R., Bohringer, T., Coray, A., Duppich, J., Forss, S., George, D., Grossmann, M., Goitein, G., Hilbes, C., Jermann, M., Lin, S., Lomax, A.J., Negrazus, M., Schippers, M., and Kotle, G. (2004) The PSI Gantry 2: a second generation proton scanning gantry. *Z. Med. Phys.*, **14**, 25–34.

39 Schätti, A., Meer, D., and Lomax, A.J. (2014) First experimental results of motion mitigation by continuous line scanning of protons. *Phys. Med. Biol.*, **59**, 5707–5723.

40 Jaffray, D.A., Siewerdsen, J.H., Wong, J.W., and Martinez, A.A. (2002) Flat-panel cone-beam computed tomography for image-guided radiation therapy. *Int. J. Radiat. Oncol. Biol. Phys.*, **53**, 1337–1349.

41 Albertini, F., Bolsi, A., Lomax, A.J., Rutz, HP., Timmerman, B., and Goitein, G. (2008) Sensitivity of intensity modulated proton therapy plans to changes in patient weight. *Radiother. Oncol.*, **86**, 187–194.

42 Yan, D., Vicini, F., Wong, J., and Martinez, A. (1997) Adaptive radiation therapy. *Phys. Med. Biol.*, **42**, 123–132.

43 Jia, X., Schumann, J., Paganetti, H., and Jiang, S.B. (2012) GPU-based fast Monte Carlo dose calculation for proton therapy. *Phys. Med. Biol.*, **57**, 7783–7797.

44 Meier, G., Besson, R., Nanz, A., Safai, S., and Lomax, A.J. (2015) Independent dose calculations for commissioning, quality assurance and dose reconstruction of PBS proton therapy. *Phys. Med. Biol.*, **60**, 2819–2836.

45 Bausch, D., Thomas, S., Mino-Kenudson, M., Frenandez-del, C.C., Bauer, T.W., Williams, M., Warshaw, A.L., Thayer, S.P., and Kelly, K.A. (2011) Plectin-1 as a novel biomarker for pancreatic cancer. *Clin. Cancer Res.*, **17**, 302–309.

46 Rae, C., Koudelka, K.J., Destito, G., Estrada, M.N., Gonzalez, M.J., and Manchester, M. (2008) Chemical addressability of ultraviolet inactivated viral nanoparticles (VNP's). *PLoS*, **30**, e3315.

47 Grimm, J., Perez, J.M., Josephson, L., and Weissleder, R. (2004) Novel nanosensors for rapid analysis of telomerase activity. *Cancer Res.*, **64**, 639–643.

48 Reddy, G.R., Bhojani, M.S., McConville, P., Moody, J., Moffat, B.A., Hall, D.E., Kim, G., Koo, Y.E., Wooliscroft, M.J., Sugai, J.V., Johnson, T.D., Philbert, M.A., Kopelmann, R., Rehemtulla, A., and Ross, B.D. (2006) Vascular targeted nanoparticles for imaging and treatment of brain tumours. *Clin. Cancer Res.*, **12**, 6677–6686.

49 Daldrup-Link, H.E., Golovko, D., Ruffel, B., Denardo, D.G., Castaneda, R., Ansari, C., Rao, J., Tikhomirov, G.A., Wendland, M.F., Corot, C., and Coussens, L.M. (2011) MRI of tumor-associated macrophages with clinically applicable iron-oxide nanoparticles. *Clin. Cancer Res.*, **17**, 5695–5704.

50 Khan, F.M. (2010) *The Physics of Radiation Therapy*, Lippincott Williams & Wilkins, Philadelphia, PA.

51 Hainfeld, J.F., Slatkin, D.N., and Smilowitz, H.M. (2004) The use of gold nano-particles to enhance radiotherapy in mice. *Phys. Med. Biol.*, **49**, N309–N315.

52 Jain, S., Coulter, J.A., Hounsell, A.R., Butterworth, K.T., McMahon, S.J., Hyland, W.B., Muir, M.F., Dickson, G.R., Prise, K.M., and Currell, F.J. (2011) Cell-specific radiosensitization by gold nanoparticles at megavoltage radiation energies. *Int. J. Radiat. Oncol. Biol. Phys.*, **79**, 531–539.

53 Kim, J.-K., Seo, S.-L., Kim, H.-T., Kim, K.-H., Chung, M.-H., Kim, K.-R., and Ye, S.-J. (2012) Enhanced proton treatment in mouse tumours through proton irradiated nanoradiator effects on metallic nanoparticles. *Phys. Med. Biol.*, **57**, 8309.

54 Polf, J.C., Bronk, L.F., Driessen, W.H., Arap, W., Pasqualini, R., and Gillin, M. (2011) Enhanced relative biological effectiveness of proton radiotherapy in tumor cells with internalized gold

nanoparticles. *Appl. Phys. Lett.*, **98**, 193702.

55 Lin, Y., McMahon, S.J., Scarpelli, M., Paganetti, H., and Schuemann, J. (2014) Comparing gold nano-particle enhanced radiotherapy with protons, megavoltage photons and kilovoltage photons: a Monte Carlo simulation. *Phys. Med. Biol.*, **59**, 7675–7689.

56 Schulte, R.W. (2011) Nanodosimetry: principle and current status. *AIP Conf. Proc.*, **1345**, 249–261.

57 Pszona, S., Kula, J., and Marjanska, S. (2000) A new method for measuring ion clusters produced by charged particles in nanometre track section of DNA size. *Nucl. Instrum. Meth. A.*, **447**, 601–607.

58 De Nardo, L., Alkaa, A., Knamphan, C., Colautti, P., and Conte, V. (2004) Design of a 10 nm electron collector for a track-nanodosimetric counter. *Radiat. Prot. Dosimetry*, **110**, 859–862.

59 Casiraghi, M., Bashkirov, V., Hurley, F., and Schulte, R. (2014) A novel approach to study radiation track structure with nanometer-equivalent resolution. *Eur. Phys. J. D.*, **68**, 111–116.

60 Casiraghi, M. and Schulte, R.W. (2015) Nanodosimetry-based plan optimization for particle therapy. *Comput. Math. Meth. Med.*, Article ID 908971.

# 10
# Self-Organization on a Chip: From Nanoscale Actin Assemblies to Tumor Spheroids

*Cora-Ann Schoenenberger and Thomas Pfohl*

*University of Basel, Department of Chemistry, Klingelbergstr. 80, 4056 Basel, Switzerland*

Tissue architecture and functionality are defined by complex cell–cell and cell–matrix interactions that are specifically modulated by the local environment. To explore biochemical, genetic, and metabolic activities of living cells in a three-dimensional (3D) context *in vitro*, considerable efforts have been made over the past 50 years to establish culture models that closely resemble tissue-specific organization. The use of self-organized multicellular spheroid cultures is particularly widespread in cancer biology, as changes in the cross talk between cells and the microenvironment are key to tumor initiation and progression. To more closely capture *in vitro* the complexity and heterogeneity of a human cancer, methods that permit controlled changes in the environment, for example, pH, nutrients, and oxygen, both in 2D and 3D, are crucial.

Microfluidics allow for the spatiotemporal control over local chemical conditions at nanoscale precision. Besides the generation of solution and surface gradients, on-chip technology lends itself to the control of other microenvironmental parameters including cell–cell and cell–matrix interactions, as well as biophysical features. Therefore, microfluidics is rapidly emerging as a method to emulate tissue- and organ-level physiology. In combination with high-resolution real-time microscopy, microfluidic devices are designed to promote and analyze the self-organization of cells into multicellular microtissues. Owing to a noninvasive segregation of single cells in parallelized microenvironments, cell proliferation and spheroid formation can be individually observed and modulated *ab initio*. The option of fine-tuning microenvironmental parameters at the nanoscale should prove useful in unraveling their influence on cell functionality. Moreover, tumors on a chip enable not only to characterize but also to modify growth and the evolution of tumor phenotypes.

*Nanoscience and Nanotechnology for Human Health,* First Edition. Edited by Bert Müller and Marcel Van de Voorde.

## 10.1 Introduction

The integration of micro- and nanofabrication techniques with microfluidics provides exceptional opportunities to create structures of defined architecture and controlled environments. Benefits of the so-called *on-chip* technology include the small length scales, corresponding to those of the systems to be investigated, limited sample volumes, the controlled manipulation of minute amounts of fluids from nano- to femtoliter, the generation of spatiotemporal chemical gradients, and dynamic (mechanical) microenvironments [1]. Microfluidic chips lend themselves to sequestering individual macromolecules, cells, and tissues, which facilitates the spatiotemporal controlled self-assembly from subcellular structures to the self-organization of entire tissues. Such multifunctional miniaturized systems provide interfaces at the cell- and tissue level that ultimately allow mimicking the structure and function of complete organs *in vitro* [2–6]. Early 2015, an organ-on-chip was added to the permanent collection of the Museum of Modern Art (MoMA), as it could soon change the way scientists develop and test life-saving medicines [7].

Already a minimal continuous flow microfluidics device enables the complex hierarchical self-assembly of cellular components in a specific local microenvironment [8]. Figure 10.1a shows the design of a basic microfluidic device with a regulative channel that delivers solutions and the molecular reaction partners by advective flow. The main channel is connected to microchambers of different shapes and sizes via narrow channels, resulting in transport into and out of the microchambers that is exclusively mediated by diffusion. Thus, the flow-free microenvironment in the confinement can be fine-tuned by specifically regulating the addition of the reaction partners to the advective channel. Using a corresponding microfluidic device, we have recently demonstrated by fluorescence microscopy that disperse actin filaments can be assembled into bundled filament networks and subsequently disassembled by tuning the concentration of the entropic bundling agent polyethylene glycol (see Figure 10.1b) [9].

Microfluidic devices with controllable and flow-free reaction chambers can be also used for experiments on cell growth and organization in molecularly tunable environments (see Figure 10.2a). The addition of a second flow channel that connects by narrow channels to the reaction chambers opposite of the first flow channel allows for generating concentration gradients across the microchambers. With this design, where one flow channel serves as the concentration source and the other as the sink, it should be possible to observe cellular growth and organization in controlled gradients of either chemical reagents, for example, drugs or biomolecular constituents of the cell's natural microenvironment (see Figure 10.2b). The efficiency of the spatiotemporal control and the experimental variability of the reaction chambers can be specifically modified by adapting the device architecture. By adding chambers of defined geometries to the main reaction chamber with corresponding connection patterns, the emulation

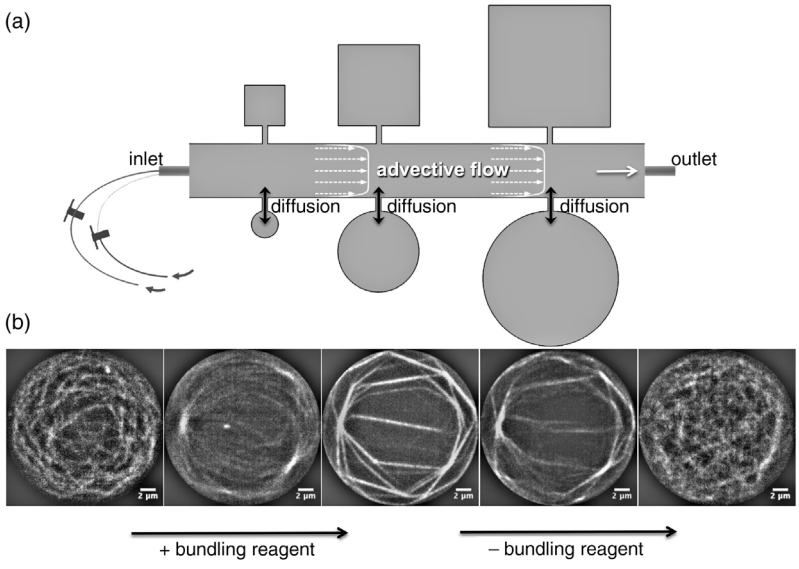


**Figure 10.1** Assembly and disassembly of actin networks in a microfluidic device. (a) Quasi two-dimensional microchambers of different shape and size are attached to a controlling channel via a narrow connecting channel, enabling exclusive diffusive transport into and out of the microchambers. Solutions or suspensions are infused through inlets into the controlling channel. (b) Formation of actin networks in a round microchamber and their subsequent disassembly upon addition and depletion of bundling reagent (polyethylene glycol, 5% w/v, MW 8000).

of more complex cellular reaction cascades and networks can be achieved (see Figure 10.2c).

Below we introduce adaptations of basic microfluidics platforms that allow for establishing microenvironments for individual cells, cellular assemblies that are linked together by cell–cell and cell–matrix contacts, or 3D, highly organized physiological tissues and tumors. For example, the microfluidic device in Figure 10.3 is adapted for a self-regulated loading of cells into the microchambers. Starting at the level of an individual cell in confinement, cell growth, proliferation, and the formation of 2D monolayers and 3D multilayers can be directly observed. Moreover, given suitable surface functionalization of the microchambers, structures that promote the growth of spheroidal cell clusters can be produced.

Microfluidic setups offer not only the ability to locally control the microenvironment as key determinant of cell structure and function, but also allow for the *in situ* observation and direct analysis of cellular dynamics, which is essential for cellular processes and signaling cascades. In order to probe the impact of confinement and diffusion barriers on cell growth and the development of tissues and tumors, microfluidic structures can be specialized in uncountable combinations with precisely defined geometries. Exploring the

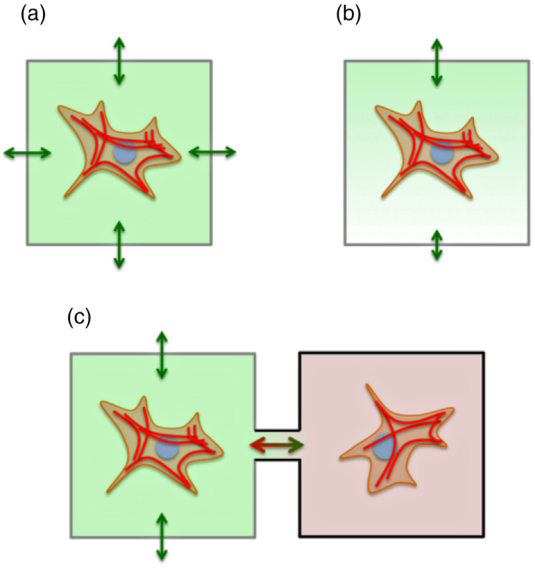


**Figure 10.2** Spatiotemporal control of cellular growth and organization. Schematic representation of potential cell growth experiments in spatiotemporal-controlled reaction chambers. Proliferation and organization in homogeneous environment (a), in concentration gradients of chemicals and biomolecular factors (b) or in biochemical and cellular cascades and networks (c).

effects of confinement by microfluidics are of particular interest in understanding tumor progression as breaking through the confining basement membrane is the initial step of a carcinoma *in situ* toward invasiveness and metastasis. In general, attempts to combine the features of microfluidics and 3D culture systems

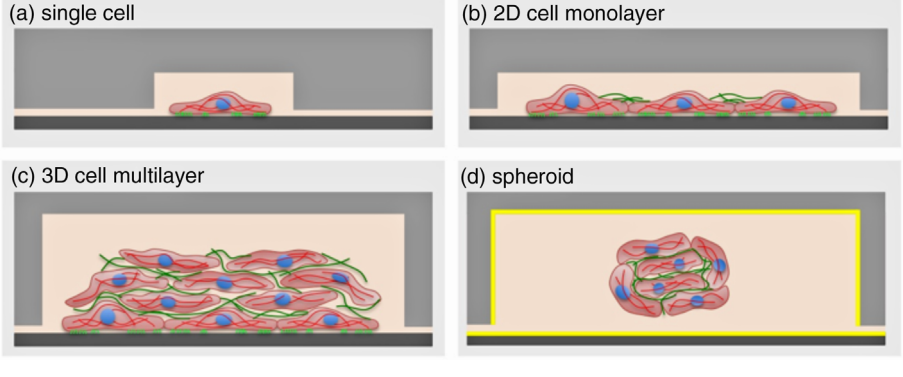


**Figure 10.3** Microfluidics platforms can be designed for single cell analysis (a), for cell growth and migration in 2D (b) and for 3D cell clusters with substrate attachment (c). Substrate-independent 3D spheroids or cysts can be grown in confinement after surface functionalization of the device walls (d).

are gaining momentum, since these models promote levels of cell differentiation and tissue organization which are not possible in conventional 2D cell systems [10–13].

In particular, microfluidic systems hold great promise as an emerging tool for understanding cancer biology. Moreover, evidence is increasing that they should be useful in rare cell detection from clinical samples, highlighting their potential in cancer diagnostics [14,15].

In cancer, it is in general not the primary tumor, but its metastases at distant sites that are the main cause of death. Thus, key issues in cancer research concern alterations of the tumor and the microenvironment that promote invasion and metastasis, such as the insufficient supply of oxygen in the growing tumor mass or the adhesion of circulating tumor cells to the microvascular endothelium.

Molecular oxygen plays a fundamental role in cell function and survival in health and disease. Consequently, cells have evolved a variety of mechanisms to sense and respond to changes in $O_2$. One of the main adaptive responses involves the activation of hypoxia-inducible transcription factor 1 (HIF-1) [16]. Hypoxia – the reduced level of tissue oxygen tension – modulates tissue architecture as well as cell adhesion and migration under physiological and pathological conditions. Reduced levels of oxygen is a typical feature of solid tumors, since the blood vessels formed in growing tumor masses are of very poor quality, which severely compromises delivery of oxygen. Despite this hypoxia, the tumor cells survive as they become adapted to the anaerobic conditions. Moreover, hypoxia induces a transcription program that promotes an aggressive tumor phenotype. Several studies have shown a deregulated HIF-1$\alpha$ expression in human tumors [17] and that the resulting high level of HIF-1 expression is associated with cancer progression.

As cancer cells become more aggressive, there can be a loss of adhesion to neighboring cells and of the integrin tethers to the extracellular matrix. Ultimately, the cells acquire the ability to attach to and grow on molecules that are not normally found in healthy tissues, but are found at sites of tumor metastases. The exact mechanism that allows cancer cells to detach from one site, spread, and then reattach themselves in a new site is not well understood [18].

Hypoxia-induced changes in the adhesion and spreading of cells are accompanied by variations in the expression of molecules that play a role in tumor spread such as the $\alpha$5 and $\alpha$2 integrins and fibronectin [19]. As integrin mediates the cross talk between the microenvironment and the actin cytoskeleton at the cell interior, their signaling affects cell shape and migration. Figure 10.4 illustrates different states of cell spreading in a fibroblast cell line: after 15–30 min, cells plated on a flat surface can be weakly attached with a rounded-up morphology, more firmly attached and starting to spread out or fully spread with extensive protrusions at the cell periphery (top panel). Under normoxic conditions (20% $O_2$, bottom panel), the parental Rat2 and the tumorigenic derivative Rat2-sm9 attach and spread out to a

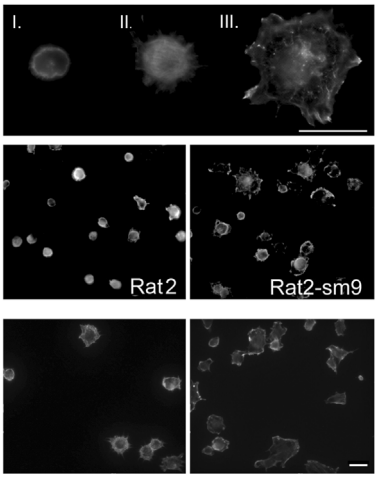


**Figure 10.4** Transformed cells exhibit increased spreading under low oxygen. Cells grown under normoxic and hypoxic conditions were suspended and allowed to reattach for 30 and 15 minutes, respectively, and then fixed. Cells were visualized by staining filamentous actin with phalloidin-FITC. Three spreading phenotypes could be distinguished: category I, round cells, weakly attached; category II, weakly attached cells in the course of spreading; category III, flat cells, well spread. Examples of each category are shown in the top panel. Under normoxia (bottom panels), most Rat2 and Rat2-sm9 belonged to category II or III; there was no significant difference between the spreading behavior of parental cells and transformed derivatives. Under hypoxic conditions (middle panels), tumorigenic Rat2-sm9 cells were well spread (category III), whereas Rat-2 predominantly showed a round morphology. Scale bars: 20 μm. (Image courtesy of Anke Zieseniss, University of Göttingen, Germany).

similar extent. In contrast, under hypoxic conditions (1% $O_2$, middle panel), Rat2 fibroblasts are deficient in spreading and stay rounded up, whereas many of the transformed Rat-sm9 cells are well attached and fully spread out. These data support the notion of a differential response of tumor cells to hypoxia. It also illustrates the extent of phenotypic variation that may not be apprehended in conventional 2D culture systems or bulk analyses. More indications for the importance of analyzing individual cells rather than bulk cell cultures come from the emerging field of quantitative biology and from the requirements for high-throughput, cell-based assays in drug development.

Recently, Yu *et al*. have designed a portable microfluidic device for the rapid diagnosis of cancer metastatic potential. Featuring a microsystem to control temperature and a bicarbonate-buffered environment, their device discriminates a rate of surface detachment as an index of the migratory ability of cells cultured on pH-responsive chitosan. These findings suggest that, as only few cells are needed for analysis, metastatic subpopulations could be determined from biopsies, for example, from fine-needle aspiration, on site and results immediately available to physicians [20].

## 10.2
## Microfluidic Cell Culture

Microfluidic cell culture systems are produced by microchip manufacturing methods. The most widely used approach for making devices for cell culture applications involves soft lithography of polydimethylsiloxane elastomers (PDMS). The main advantage of using PDMS is that its gas-permeation ensures basic oxygen supply of cultured cells. In addition, it is generally regarded as inert, nontoxic, and fully biocompatible.

First, a structure is designed depending on the task at hand and printed on a chrome-mask or on a high-resolution transparency. This is then used to produce a hard master of a specific height for molding structures of micrometer resolution into PDMS. The fabrication of PDMS devices involves mixing the PDMS elastomer base with a curing agent, pouring it onto the master and heating to accelerate the curing process. The cured PDMS can then be peeled off the master and trimmed as desired. Holes punched into the final PDMS cell culture device provide access to the microfluidic structure. Permanently bonding the PDMS device to a cover glass by plasma treatment not only seals off the structure but also allows for analysis by light and fluorescence microscopy. Finally, a plastic ring that surrounds the device is mounted on the cover glass. This reservoir can be filled with buffer to prevent evaporation of medium through the PDMS in long-term experiments (cf. Figure 10.5a).

The design of a basic microfluidic device, with which single living cells can be confined and analyzed, is shown in Figure 10.5b. The device consists of micrometer-sized chambers that are at least large enough for the cell to be analyzed. In the design shown, a series of microchambers are located next to each other. Each microchamber is connected via an entry and an exit channel to a 100 µm wide main channel on either side. While the entry channel is large enough to allow for unrestricted flow of cells into the microchamber, the exit channel is much smaller and will restrain mammalian cells from flowing out of the microchamber. In a typical microfluidic culture experiment, cell suspensions are loaded into the device through tubing attached to the inlet, either by gravity or by a syringe pump. A channel leads from the inlet to the two connected main channels. In the design shown, the main channel connecting to the entry channels of the microchambers remains closed at the end, whereas the second main channel opens up to an outlet. As indicated by the arrows, cells flow from the inlet into both main channels but can only reach the outlet from the main channel connected to the microchamber exits.

## 10.3
## Self-Regulated Loading of Cells into Microchambers

When suspended cells are added to the microfluidic device, the pressure difference established across the microchamber will cause cells flowing in the dead-

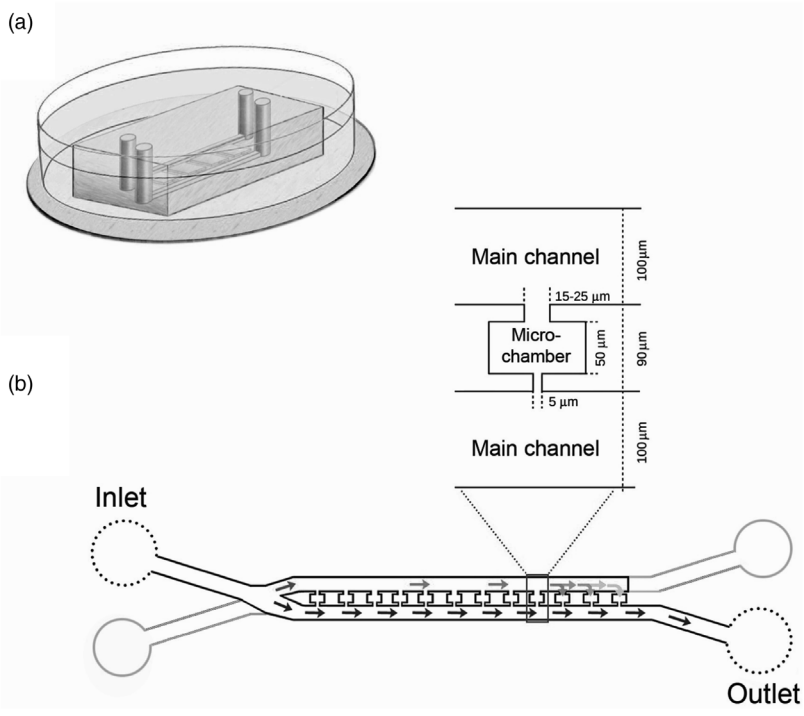


**Figure 10.5** Microfluidic device for single cell analysis. The inlet leads to two connected main channels, one end of which is closed, whereas the other leads to an outlet. A series of microchambers connect the dead-end channel with the open channel. The width of the entry channel into the microchamber allows unrestricted inflow of cells whereas the narrow exit channel obstructs free cell passage.

end channel to enter the microchamber (see Figure 10.6a). According to the design shown in Figure 10.5b, the exit channel is too small to allow for an unrestricted passage of the cell. As a consequence, a cell trying to exit will plug the channel and largely shut down the flow through the respective microchamber, which in turn will prevent more cells from entering the microchamber. An example of the self-regulated loading of microchambers is shown in Figure 10.6b. The microfluidic device was mounted on an inverted light microscope and three neighboring microchambers were monitored. A single-cell suspension of HeLa-H2B-GFP cells grown as conventional 2D cultures was infused via the inlet. The microchamber furthest away from the inlet was immediately loaded with a single cell that localized to the exit channel. Acting as a plug, the cell abolished the pressure difference and thus the flow through this microchamber. Flow in the remaining microchambers occurred freely until the exit of the next chamber was blocked by a cell. By this mechanism, confinement of single cells in many consecutive microchambers is rapidly achieved, provided the

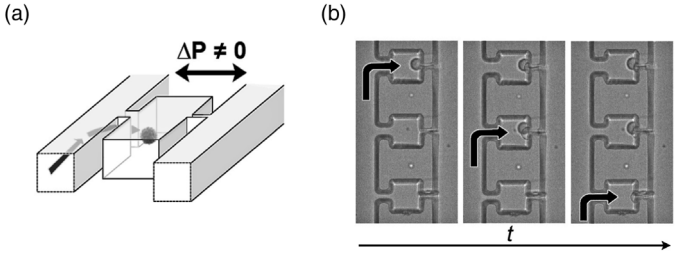


**Figure 10.6** Self-regulated loading of cells into microchambers. (a) Schematic representation of single cell confinement in microchambers. Cells flowing in the dead-end main channel enter the microchamber through a connecting channel due to a pressure difference between the two main channels. (b) Bright-field image time series of a HeLa-H2B-GFP cell suspension filled into a microfluidic device. A dispersed HeLa-H2B-GFP cell has flowed into the micro-chamber nearest the end of the main channel and stops further flow through this chamber by plugging the narrow exit. Flow will take place through the neighboring micro-chamber until a cell blocks the exit.

pressure difference is not so excessive as to squeeze cells through the exit channel into the draining main channel. As shown in Figure 10.6b, incomplete plugging of the exit channel might result in a small pressure difference that immobilizes cells at the exit site. This residual flow can easily be regulated by reducing the loading forces or by opening the dead-end main channel, which abolishes the pressure difference (see Figure 10.7a). The resulting flow-free conditions prevent further cells from entering the microchamber.

As many cutting-edge cell studies involve high-throughput single cell analysis, there have recently been a number of reports that describe cell trapping by different microfluidic procedures [21,22].

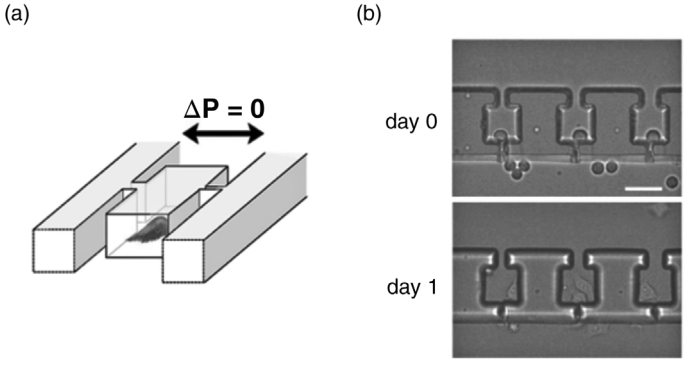


**Figure 10.7** Cell attachment and growth in microchambers. (a) In the absence of a pressure difference, cells attach to the substrate and spread. (b) Freshly trapped cells (day 0) are suspended and show a round morphology. After 24 hours in culture (day 1), cells are spread out on the glass surface as indicated by the different focal plane. The cell in the middle microchamber has divided. Scale bar: 50 μm.

## 10.4
## 2D Cell Culture in Microfluidics

Light microscopy of a basic microfluidic device loaded with HeLa-H2B-GFP cells reveals that single cells confined to microchambers begin to attach to the glass substrate shortly after loading (cf. Figure 10.7). After 24 h at 37 °C with continuous medium perfusion, cells were fully attached and spread out. In some microchambers, cell division had occurred demonstrating that cells are viable.

One of the first studies using a perfusion culture device constructed from two layers of PDMS to culture a human hepatocarcinoma cell line was reported by Leclerc *et al.* [23]. The authors also reported that gas transport through PDMS was sufficient to maintain a viable culture over days. Subsequently, the effects of the device geometry and of factors added to microfluidic culture systems were intensely investigated [24,25]. The possibility to modify the microenvironment at high spatial and temporal resolution increasingly attracted the attention of many researchers. Because microfluidic systems offer a high degree of control over culture conditions including biotic and abiotic factors such as mechanical signals, cell-based applications have experienced an unprecedented rise over the past few years (cf. reviews [26–28]).

## 10.5
## Expanding Microfluidic Cell Culture to the Third Dimension

Cells *in vivo* are in a 3D environment, where they experience characteristic biophysical and biochemical signals that influence cell functions like gene expression, proliferation, adhesion, and migration. The extracellular matrix (ECM) and the tissue architecture are key determinants of the microenvironment, and as such are responsible for tissue-specific differentiation and morphogenesis. In cancer, cell–cell and cell–ECM interactions are altered. As a result, cancer cells evolve with traits that promote their growth, invasion, and metastasis [29,30].

In order for *in vitro* culture systems to be effective experimental models, they need to recapitulate the basic unit of differentiated function in the tissue or organ. Cells have to be cultured in a format that mirrors the 3D microenvironment and native cell composition as closely as possible. In most cases, conventional 2D cultures, that is, on flat substrates, do not adequately represent the anatomical and physiological microenvironment, which a cell encounters in a living tissue. Foremost, cell–cell and cell–matrix interactions are limited in 2D cultures, but gradients in oxygen, nutrition, and growth factors also differ considerably. Accordingly, cellular function [31,32] and the composition of the cytoskeleton and the ECM varies between cells grown as monolayers and 3D cultures. Moreover, as cell-based assays are an inherent part of drug discovery and development, an *in vitro* cell model that is more representative of the *in vivo* biology is critical to predicting the *in vivo* response to biologicals and chemicals.

Among the various 3D cell culture models that have been developed since the 1950s, matrix-embedded culture and self-assembling multicellular structures

known as organoids or spheroids have been the most prominent. Due to its simplicity and similarity to physiological tissues, use of spheroids in biomedical research and drug screening is widespread [33,34]. A number of cancer cells grown as spheroids exhibit features of *in vivo* tumors [35]. For example, spheroids contain microenviromental variations and, in particular, regions of low oxygen concentration similar to those found in solid tumors [36]. Thus, research on tumorigenesis, invasion, metastasis, and tumor angiogenesis has been widely carried out using spheroid cultures [37,38].

An example of phenotypic differences related to tumorigenic transformation in spheroid cultures is shown in Figure 10.8. Spheroids formed by Rat2-sm9 cells, a tumorigenic derivative of Rat2 fibroblasts that express an actin mutant, exhibit a distinct surface morphology compared to the nontransformed parental Rat2 cells [39]. In addition, Rat2-sm9 spheroids are significantly larger than spheroids of nontransformed Rat2 cells. Studies involving conventional spheroid cultures are often hampered by a number of limitations including the struggle to generate reproducible spheroids. Microfluidic culture systems may overcome these limitations by geometrically controlling the cellular assembly process within a fluidic compartment and by providing perfusion conditions that more accurately mimic the *in vivo* situation, for example, that of vascularized tumors [40,41].

Interest in constructing reliable 3D microfluidic platforms is increasing as researchers strive to investigate reciprocal interactions between the ECM and cells under various conditions. Microfluidic cell culture devices that enable real-time imaging and *in vitro* analysis of biochemical, genetic, and metabolic activities of cells in a 3D context need to have corresponding geometries. Besides

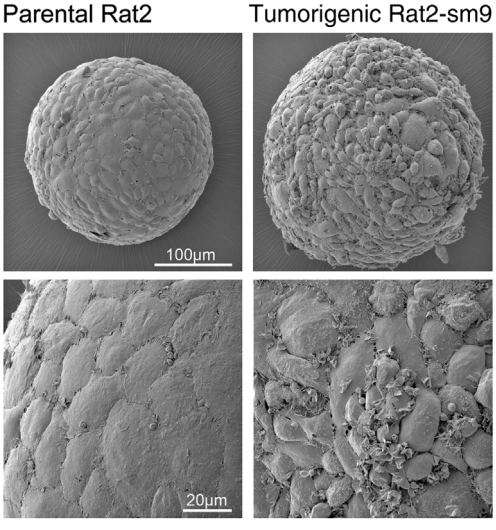


**Figure 10.8** Multicellular Rat2 and Rat2-sm9 spheroids. Scanning electron micrographs of whole mount specimens show differences in size and surface topography between 2-day old parental Rat-2 and tumorigenic Rat-2-sm9 spheroids. Tumorigenic spheroids are bigger with cells that exhibit morphological heterogeneity, in particular extensive membrane ruffling.

enough space to accommodate increasing cell numbers, a constant supply of nutrients and adequate gas exchange is required to maintain viability of cells over several days. Figure 10.9a shows the physical design of a device with differently sized microchambers that allow for multicellular aggregates to form in confinement. Bright field microscopy images of the two larger microchambers (see Figure 10.9b) revealed that at the given cell density and flow rate, more than one HeLa-H2B-GFP cell had entered each chamber before the pressure

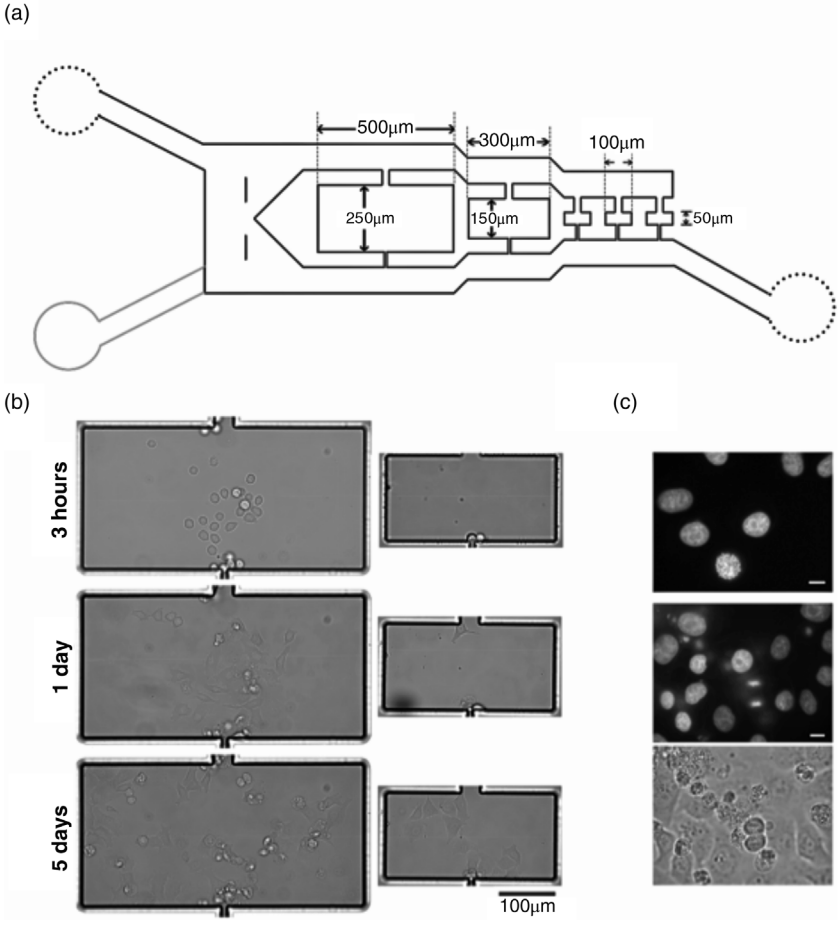


**Figure 10.9** Microfluidic device for 3D cell growth. (a) A microfluidic device with different sized microchambers for 3D cell cultures. (b) HeLa-H2B-GFP cells were added to the device and cultured for 5 days at 37 °C. Three hours after loading, cell morphology is still rather round but cells have started to attach. After 1 day in culture, cells are fully spread and have started to divide. On day 5, several rounds of cell division have occurred. (c) Fluorescence microscopy reveals different stages of mitosis - prophase nucleus (top) and telophase (middle)- in microfluidic HeLa-H2B-GFP cultures. The corresponding DIC image (bottom) shows the dividing cell. Scale bars: 10 μm.

difference was sufficiently decreased for the flow to stop. Attachment and the onset of spreading were evident after 3 h. Corresponding images showed that cells were not only viable, but their number had increased after an incubation time of 24 h at 37 °C. When the culture medium was replenished, cells continued to proliferate at least until day 5 after loading. Proliferation was further confirmed by live-cell fluorescence microscopy of HeLa cells expressing H2B-GFP in various cell cycle phases (see Figure 10.9c).

A fundamental step toward recapitulating biomimetic tissue architecture in microfluidic culture systems is the establishment of 3D cell–cell interactions within the confinement. As illustrated in Figure 10.10a, optical sections recorded at different heights of a 30 μm-high microchamber revealed cells in different layers that are contacting each other. In contrast 2D cultures on flat substrates, microfluidic structures can be modified to allow for spatial depth and cell connectivity.

For the past two decades, researchers, especially those working in cancer-related fields, have become increasingly aware of just how much a cell's context matters. As a result, they have been turning to 3D cell culture systems, where patterns of gene expression and other biological activities more closely mirror the complex conditions in living organisms. For example, embedding MDCK (Madin–Darby Canine Kidney) cells in an extracellular matrix is associated with apical–basal polarization [42] and lumen formation (cf. Figure 10.10b) [43,44]. Recently, Huang *et al.* have reported the enhancement of renal epithelial cell functions through microfluidic-based coculture of MDCK with adipose-derived stem cells [45]. The design of their microfluidic device was inspired by the anatomical structure of the Bowman's capsule in the human kidney. A number of scaffolds that promote multidimensional cell–cell/cell–matrix contacts in

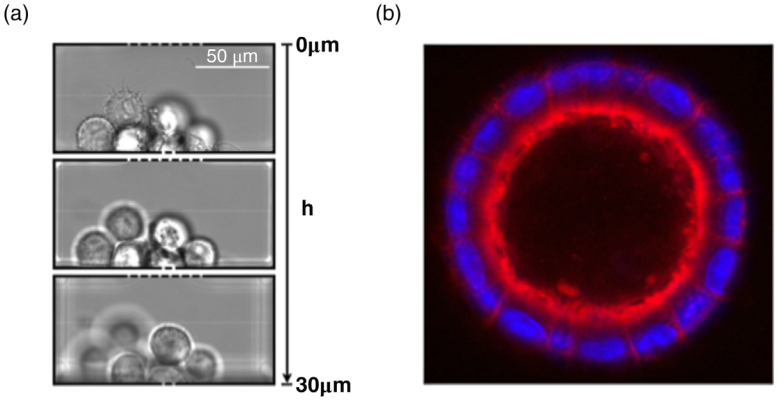


**Figure 10.10** 3D cell assemblies. (a) Bright field images of a medium-sized microchamber recorded at different heights reveal different layers of HeLa-GFP-H2B cells. (b) Cross-section through an MDCK cyst grown in Matrigel. TRITC-phalloidin staining shows an intense actin network at the apical side facing the lumen. Nuclei are counterstained with DAPI (blue; image courtesy of Aki Maninnen, University of Oulu, Finland).

conventional 3D culture systems [46] have also been employed in microfluidic cell cultures [47–51]. Furthermore, the formation of uniformly sized tumor spheroids largely depends on scaffolds.

Microfluidic methods that enable on-demand formation of arrays of microgels bearing arbitrary contents and shapes are rapidly evolving. For example, Eydelnant *et al.* have recently reported a digital microfluidic method (DMF) that has the capacity to generate a 3D gel structure containing any combination of constituents, where specific microgels can be addressed individually [52]. They used MDCK to validate that cells cultured in collagen or Matrigel® microgels on DMF can form multicellular clusters during the first 72 h, and a visible lumen resulting from cell polarization after 96 h.

Undoubtedly, many basic research areas and applied sciences such as tissue engineering and testing of novel therapeutic approaches will benefit from the ability to precisely micro- and nanofabricate and control the microenvironment for culturing and analyzing 3D cell constructs.

## 10.6 Microfluidic Biomimetic Models of Cancer

Cellular and structural aspects, that is, the ECM, of the microenvironment, but also the resulting mechanical features play a critical role in driving cancer progression. The possibility to address these parameters, either individually or at increasing complexity, in microfluidic platforms in real time has led to an explosion of microfluidic 3D culture applications in cancer research over the past few years [53–55]. For example, Hockemeyer *et al.* have introduced an intricate microfluidic device that made it possible to image cells migrating out from a spheroid in a controlled microenvironment [56]. With the objective to mimic the tumor microenvironment and the surrounding vasculature, these authors fabricated a device using femtosecond laser-etching technology [57], where a 200 μm channel coupled with a semicircular chamber is integrated with an array of capillary-like channels, all machined in glass. Besides the coculture of different cell types, this miniaturized bioreactor allowed for a spatially and temporally controlled recreation of a 3D microenvironment by the targeted delivery of reagents via the capillary-like channels that mimic blood vessels. In addition, the interactions of interstitial flow, endothelial cells, leukocytes, and fibroblasts with the tumor cells could be monitored.

## 10.7 Future Perspectives

Design and dimensions of microfluidic devices make it possible to analyze individual cells and monitor the formation of 3D cell assemblies under various biophysical and biochemical constraints in real time. Designs that allow for the

coculture of different cell types in precisely controllable microenvironments are increasingly attracting attention, in particular with regard to tissue regeneration and cancer progression. For example, the differentiation of stem cells that is mostly difficult to obtain and only available in small numbers can be induced and simultaneously analyzed *in situ* [58].

Based on the spatial and temporal control over local environmental parameters at the micro- to nanoscale and the minimal demands on volumes of medium and reagents, microfluidic platforms using 3D cell culture models, for example, spheroids, lend themselves to a broad range of applications from basic to applied science. The necessity to more accurately represent normal and diseased processes *in vitro* in many areas including drug testing and regenerative medicine will spur further development of multifunctional and highly integrated microdevices for 3D culture systems.

Under the premise that the system is optimized accordingly, tumor development and progression, as well as the response of solid tumors to potential drugs can be examined by microfluidics at the level of gene and/or protein expression, but also with regard to cell–cell and cell–matrix interactions. Of particular interest are studies addressing cell heterogeneity and the resulting signaling pathways, both, in tumor spheroids and physiological microtissues.

## Acknowledgments

We thank Fabian Bača, Siddharth Deshpande, Florian Herren, Andreas Reichmuth, Natalja Strelnikova, and Zoe Swank for their experimental support and fruitful discussions. We gratefully acknowledge Anke Zieseniss (University of Göttingen, Germany) and Aki Maninnen (University of Oulu, Finland) for providing images in Figure 10.4 and 10.10b, respectively. This work was supported by the NCCR Molecular Systems Engineering of the SNSF.

## References

1 Whitesides, G.M. (2006) The origins and the future of microfluidics. *Nature*, **442** (7101), 368–373.
2 Mammoto, T. *et al.* (2011) Mechanochemical control of mesenchymal condensation and embryonic tooth organ formation. *Dev. Cell*, **21** (4), 758–769.
3 van der Meer, A.D. and van den Berg, A. (2012) Organs-on-chips: breaking the *in vitro* impasse. *Integr. Biol.*, **4** (5), 461–470.
4 Zervantonakis, I.K. *et al.* (2012) Three-dimensional microfluidic model for tumor cell intravasation and endothelial barrier function. *Proc. Natl. Acad. Sci. USA*, **109** (34), 13515–13520.
5 Huh, D. *et al.* (2010) Reconstituting organ-level lung functions on a chip. *Supramol. Sci.*, **328** (5986), 1662–1668.
6 Lee, P.J., Hung, P.J., and Lee, L.P. (2007) An artificial liver sinusoid with a microfluidic endothelial-like barrier for primary hepatocyte culture. *Biotechnol. Bioeng.*, **97** (5), 1340–1346.
7 https://http://www.moma.org/explore/inside_out/2015/03/04/is-this-for-everyone-new-design-acquisitions-at-moma. Posted by P. Antonelli, M. Millar

Fisher, Department of architecture and design. Accessed 072315.
8 Deshpande, S. and Pfohl, T. (2012) Hierarchical self-assembly of actin in micro-confinements using microfluidics. *Biomicrofluidics*, **6** (3), 34120.
9 Deshpande, S. and Pfohl, T. (2015) Real-time dynamics of emerging actin networks in cell-mimicking compartments. *PLoS One*, **10** (3), e0116521.
10 Huh, D., Hamilton, G.A., and Ingber, D.E. (2011) From 3D cell culture to organs-on-chips. *Trends Cell Biol.*, **21** (12), 745–754.
11 Occhetta, P. *et al.* (2015) High-throughput microfluidic platform for 3D cultures of mesenchymal stem cells, towards engineering developmental processes. *Sci. Rep.*, **5**, 10288.
12 Ruppen, J. *et al.* (2014) A microfluidic platform for chemoresistive testing of multicellular pleural cancer spheroids. *Lab. Chip.*, **14** (6), 1198–1205.
13 Mehling, M. and Tay, S. (2014) Microfluidic cell culture. *Curr. Opin. Biotechnol.*, **25**, 95–102.
14 Karabacak, N.M. *et al.* (2014) Microfluidic, marker-free isolation of circulating tumor cells from blood samples. *Nat. Protoc.*, **9** (3), 694–710.
15 Sarioglu, A.F. *et al.* (2015) A microfluidic device for label-free, physical capture of circulating tumor cell clusters. *Nat. Methods*, **12** (7), 685–691.
16 Harris, A.L. (2002) Hypoxia—a key regulatory factor in tumour growth. *Nat. Rev. Cancer*, **2** (1), 38–47.
17 Bos, R. *et al.* (2001) Levels of hypoxia-inducible factor-1 alpha during breast carcinogenesis. *J. Natl. Cancer Inst.*, **93** (4), 309–314.
18 Reticker-Flynn, N.E. *et al.* (2012) A combinatorial extracellular matrix platform identifies cell-extracellular matrix interactions that correlate with metastasis. *Nat. Commun.*, **3**, 1122.
19 Indovina, P., Rainaldi, G., and Santini, M.T. (2008) Hypoxia increases adhesion and spreading of MG-63 three-dimensional tumor spheroids. *Anticancer Res.*, **28** (2A), 1013–1022.
20 Yu, I.F. *et al.* (2014) A portable microfluidic device for the rapid diagnosis of cancer metastatic potential which is programmable for temperature and CO2. *Lab. Chip.*, **14** (18), 3621–3628.
21 Jin, D. *et al.* (2015) A microfluidic device enabling high-efficiency single cell trapping. *Biomicrofluidics*, **9** (1), 014101.
22 Chen, H. *et al.* (2015) High-throughput, deterministic single cell trapping and long-term clonal cell culture in microfluidic devices. *Lab. Chip.*, **15** (4), 1072–1083.
23 Leclerc, E., Sakai, Y., and Fujii, T. (2003) Cell culture in 3-dimensional microfluidic structure of PDMS (polydimethylsiloxane). *Biomed. Microdevices*, **5** (2), 109–114.
24 Yu, H.M. *et al.* (2005) Diffusion dependent cell behavior in microenvironments. *Lab. Chip.*, **5** (10), 1089–1095.
25 Yu, H.M., Alexander, C.M., and Beebe, D.J. (2007) Understanding microchannel culture: parameters involved in soluble factor signaling. *Lab. Chip.*, **7** (6), 726–730.
26 Avesar, J., Arye, T.B., and Levenberg, S. (2014) Frontier microfluidic techniques for short and long-term single cell analysis. *Lab. Chip.*, **14** (13), 2161–2167.
27 Lin, B. and Levchenko, A. (2015) Spatial manipulation with microfluidics. *Front Bioeng. Biotechnol.*, **3**, 39.
28 Xiong, B. *et al.* (2014) Recent developments in microfluidics for cell studies. *Adv. Mater.*, **26** (31), 5525–5532.
29 Ravi, M. *et al.* (2015) 3D cell culture systems: advantages and applications. *J. Cell. Physiol.*, **230** (1), 16–26.
30 Bissell, M.J., Kenny, P.A., and Radisky, D.C. (2005) Microenvironmental regulators of tissue structure and function also regulate tumor induction and progression: the role of extracellular matrix and its degrading enzymes. *Cold Spring Harb. Symp. Quant. Biol.*, **70**, 343–356.
31 Smalley, K.S., Lioni, M., and Herlyn, M. (2006) Life isn't flat: taking cancer biology to the next dimension. *In Vitro Cell. Dev. Biol. Anim.*, **42** (8–9), 242–247.
32 Lin, R.Z. and Chang, H.Y. (2008) Recent advances in three-dimensional multicellular spheroid culture for biomedical research. *Biotechnol. J.*, **3** (9–10), 1172–1184.
33 Friedrich, J. *et al.* (2009) Spheroid-based drug screen: considerations and practical approach. *Nat. Protoc.*, **4** (3), 309–324.
34 Burdett, E. *et al.* (2010) Engineering tumors: a tissue engineering perspective in

cancer biology. *Tissue Eng. Part B Rev.*, **16** (3), 351–359.
35 Sutherland, R.M. (1988) Cell and environment interactions in tumor microregions: the multicell spheroid model. *Supramol. Sci.*, **240** (4849), 177–184.
36 Serganova, I. *et al.* (2004) Molecular imaging of temporal dynamics and spatial heterogeneity of hypoxia-inducible factor-1 signal transduction activity in tumors in living mice. *Cancer Res.*, **64** (17), 6101–6108.
37 Liu, J. *et al.* (2011) Three-dimensional spheroid cultures of A549 and HepG2 cells exhibit different lipopolysaccharide (LPS) receptor expression and LPS-induced cytokine response compared with monolayer cultures. *Innate Immun.*, **17** (3), 245–255.
38 Pampaloni, F., Reynaud, E.G., and Stelzer, E.H. (2007) The third dimension bridges the gap between cell culture and live tissue. *Nat. Rev. Mol. Cell Biol.*, **8** (10), 839–845.
39 Blache, U. *et al.* (2013) A tumorigenic actin mutant alters fibroblast morphology and multicellular assembly properties. *Cytoskeleton (Hoboken)*, **70** (10), 635–650.
40 Hsiao, A.Y. *et al.* (2009) Microfluidic system for formation of PC-3 prostate cancer co-culture spheroids. *Biomaterials*, **30** (16), 3020–3027.
41 Torisawa, Y.S. *et al.* (2007) Efficient formation of uniform-sized embryoid bodies using a compartmentalized microchannel device. *Lab. Chip.*, **7** (6), 770–776.
42 Schoenenberger, C.A. *et al.* (1994) Integrin expression and localization in normal mdck cells and transformed mdck cells lacking apical polarity. *J. Cell Sci.*, **107**, 527–541.
43 O'Brien, L.E., Zegers, M.M.P., and Mostov, K.E. (2002) Opinion - Building epithelial architecture: insights from three-dimensional culture models. *Nat. Rev. Mol. Cell Biol.*, **3** (7), 531–537.
44 Debnath, J. and Brugge, J.S. (2005) Modelling glandular epithelial cancers in three-dimensional cultures. *Nat. Rev. Cancer*, **5** (9), 675–688.
45 Huang, H.C. *et al.* (2013) Enhancement of renal epithelial cell functions through microfluidic-based coculture with adipose-derived stem cells. *Tissue Eng. Part A*, **19** (17–18), 2024–2034.
46 LaPlaca, M.C. *et al.* (2010) Three-dimensional neuronal cultures in *Methods in Bioengineering: 3D Tissue Engineering*, Artech House, 187–204.
47 Lii, J. *et al.* (2008) Real-time microfluidic system for studying mammalian cells in 3D microenvironments. *Anal. Chem.*, **80** (10), 3640–3647.
48 Sung, K.E. *et al.* (2009) Control of 3-dimensional collagen matrix polymerization for reproducible human mammary fibroblast cell culture in microfluidic devices. *Biomaterials*, **30** (27), 4833–4841.
49 Jeong, G.S. *et al.* (2011) Microfluidic assay of endothelial cell migration in 3D interpenetrating polymer semi-network HA-Collagen hydrogel. *Biomed. Microdevices*, **13** (4), 717–723.
50 Shin, Y. *et al.* (2013) Extracellular matrix heterogeneity regulates three-dimensional morphologies of breast adenocarcinoma cell invasion. *Adv. Healthc. Mater*, **2** (6), 790–794.
51 Jang, J.M. *et al.* (2015) Engineering controllable architecture in matrigel for 3D cell alignment. *ACS Appl. Mater Interfaces*, **7** (4), 2183–2188.
52 Eydelnant, I.A., Li, B.B., and Wheeler, A.R. (2014) Microgels on-demand. *Nat. Commun.*, **5**, 3355.
53 Zhang, Z. and Nagrath, S. (2013) Microfluidics and cancer: are we there yet? *Biomed. Microdevices*, **15** (4), 595–609.
54 Sung, K.E. and Beebe, D.J. (2014) Microfluidic 3D models of cancer. *Adv. Drug Deliv. Rev.*, **79–80**, 68–78.
55 van Duinen, V. *et al.* (2015) Microfluidic 3D cell culture: from tools to tissue models. *Curr. Opin. Biotechnol.*, **35**, 118–126.
56 Hockemeyer, K. *et al.* (2014) Engineered three-dimensional microfluidic device for interrogating cell–cell interactions in the tumor microenvironment. *Biomicrofluidics*, **8** (4), 044105.
57 Wright, G. *et al.* (2012) On-chip open microfluidic devices for chemotaxis studies. *Microsc. Microanal.*, **23** (4), 816–828.
58 Chen, Q. *et al.* (2013) Microfluidic isolation of highly pure embryonic stem cells using feeder-separated co-culture system. *Sci. Rep.*, **3**, 2433.

# 11
# The Nanomechanical Signature of Tissues in Health and Disease

*Daphne O. Asgeirsson,[1] Philipp Oertle,[1] Marko Loparic,[1,3] and Marija Plodinec[1,2]*

*[1]University of Basel, Biozentrum and the Swiss Nanoscience Institute, Klingelbergstrasse 70, CH-4056 Basel, Switzerland*
*[2]University Hospital Basel, Institute of Pathology, Spitalstrasse 21, 4056 Basel, Switzerland*
*[3]Nuomedis AG, Seltisbergstrasse 14, 4410 Liestal, Switzerland*

## 11.1
## Summary

Scientific interest in mechanics of biological materials has been steadily rising for the past decade, as their unique viscoelastic properties define the response to forces on all architectural levels of biology, from macroscopic tissue to the molecular level of proteins and DNA [1–7]. Living tissues are composed of various cell types, extracellular matrix (ECM) proteins, and other components, each exhibiting distinct mechanical properties such as plasticity, viscoelasticity, tensile strength, or stiffness [8]. These physical properties collectively define the material properties of a tissue and dictate how it will respond to mechanical load and how the tissue will sense and transmit load. A balance of forces is required to maintain tissue homeostasis during development and in adulthood, disruptions in tissue structure and force balance thereby leading to numerous diseases ranging from osteoarthritis to cancer [9–11]. Despite the importance of mechanical properties for physiological functions of living tissues, relatively little is known about how forces inherent to the cellular and noncellular microenvironment actually contribute to the regulation of tissue fate and function [12,13]. The link between functional changes and mechanics of cells and tissues is fundamental for our understanding of tissue-specific functions *in vivo* and might provide potential diagnostic and prognostic markers for diseases as well [14–16]. In order to achieve this goal, quantitative characterization of cell and tissue mechanics under physiological conditions plays an essential role. In particular, single cell and tissue level experimentation must be bridged to obtain a holistic understanding of mechanobiological properties at all length scales. In this chapter, we will provide a state-of-the-art overview of atomic force microscopy

*Nanoscience and Nanotechnology for Human Health,* First Edition. Edited by Bert Müller and Marcel Van de Voorde.

(AFM) in life sciences and discuss recent findings as to how AFM techniques can break new ground in the field of mechanobiology.

## 11.2 Tissue Mechanics Across Length Scales

Living tissues exhibit exceptional physical properties as defined by the complex interplay between cells and the ECM in which they are embedded. Living cells sense and convert mechanical cues from their microenvironment into biochemical responses to resist compression and adapt to changes in their surrounding [17]. These processes are directly coupled to gene regulation and protein expression, cellular development, motility, proliferation, and differentiation as factors that altogether define tissue mechanofunctionality [18].

Numerous studies have shown that the cellular response to mechanical forces is intrinsically coupled both to the internal organization of the cytoskeleton as well as cell adhesion to surrounding cells and ECM [19]. Several (nano)mechanosensors that respond to different magnitudes and types of force have been identified. Intracellular signaling cascades, for instance, can be activated by force-induced spatial reorganization of cell surface receptors such as integrin clusters [20] and the spatial restriction of ephrin receptors [21,22], which can lead to a global remodeling of cytoskeletal elements [23]. Indeed, for living cells to be mechanically active, a reliable and precisely tunable cytoskeleton machinery is essential. In this context, microtubules (MT), actin microfilaments (AF), and intermediate filaments (IF) are the main components of such a cell spanning scaffold, each exhibiting differential characteristics regarding structure, rigidity, assembly, and decomposition. The versatile nature of the cytoskeleton provides both stabilization and protection to cells, while at the same time being highly plastic in terms of its dynamic reorganization [24,25]. Nanomechanical measurements of living cells using AFM have shown that the disruption of the actin or microtubule cytoskeleton results in a decreased cellular stiffness [26–28]. On the other hand, high abundance of cell and tissue-specific IFs and the fact that they span the entire cell from the nucleus to the plasma membrane additionally suggested them to play an important role in providing tissue-specific mechanical stability [29].

The majority of cells in our body are anchorage dependent. Thus, in order to survive, proliferate and function properly, their attachment to physiologically relevant substrates is required [30]. The ECM is comprised of diverse proteins, such as collagens, fibronectin, proteoglycans, and glycoproteins that together form a strong physical and biochemical support for the inlaying cells. The tight control of homeostasis between cells and ECM is crucial for normal development, wound healing and organ functions, any disruption of this intricate balance leading to a series of biochemical and mechanical alterations that are associated with fibrotic diseases [31].

Despite the fact that cellular responses are both tissue- and context-dependent in terms of biochemical and mechanical cues [32,33], most cell mechanics

experiments are performed using cells cultured as 2D monolayers on plastic substrates. On the other hand, it is well established that cells cultured and/or studied in the context of a 3D tissue culture involving some sort of ECM, either as a primitive model *in vitro*, or by studying tissues *in situ*, exhibit completely different gene and protein expression profiles and consequently mechanical properties. In the context of various pathologies, the best way to accurately study cell–ECM biomechanical interactions is certainly either by assessing them *in vivo*, or alternatively *ex vivo* on tissue excisions. However, methodological limitations exist, since there is a clear length-scale division between single cell biophysical techniques [34–36] that lack a natural 3D tissue context and bulk tissue rheology, in which measurements are dominated by the most abundant structural elements (e.g., collagen or fat) and limited by low spatial resolution. In living tissues, cell–ECM interactions occur at the molecular, hence nanometer scale. Therefore, in this chapter we present AFM as a technique which is able to operate at a nanometer spatial resolution and picoNewton (pN) force range that could provide a more comprehensive understanding of cell–ECM interactions in the native unperturbed state of living tissues [37].

## 11.3 Atomic Force Microscopy (AFM) in Cell and Tissue Biology

Recent developments in AFM enable researchers to combine high-resolution nanometer scale imaging with quantitative mapping of physical, chemical, and biological properties [38]. Indentation techniques such as AFM can measure stiffness by indenting a probe into the sample surface and, by alterations of the probe size and shape, mechanical properties of the sample can be assessed both at the micrometer and nanometer scale. The AFM raster-scan technology allows for sequential indentation cycles across large areas and the gain of contextual information from biological materials.

### 11.3.1 Basic Operating Principles of AFM

The heart of an AFM consists of four components. A probe (1), referred to as cantilever, made from silicon or silicon-nitride with an indenter of spherical or pyramidal shape attached to its end. The actuator (2) is made from piezo elements owing to their extremely high spatial resolution in the picometer range [39] and is used to press the indenter into the sample, or to pull the cantilever away from a sample, respectively. The detection scheme (3) consists of a laser and a photodiode. The laser is directed onto the backside of the cantilever and reflected to the photodiode, thereby reporting the exact position of the cantilever while it is approaching, indenting and retracting from the sample (Figure 11.1a). Plotting the cantilever deflection against the actuator displacement yields the so-called force curves, from which quantities such as stiffness, topography, or adhesive

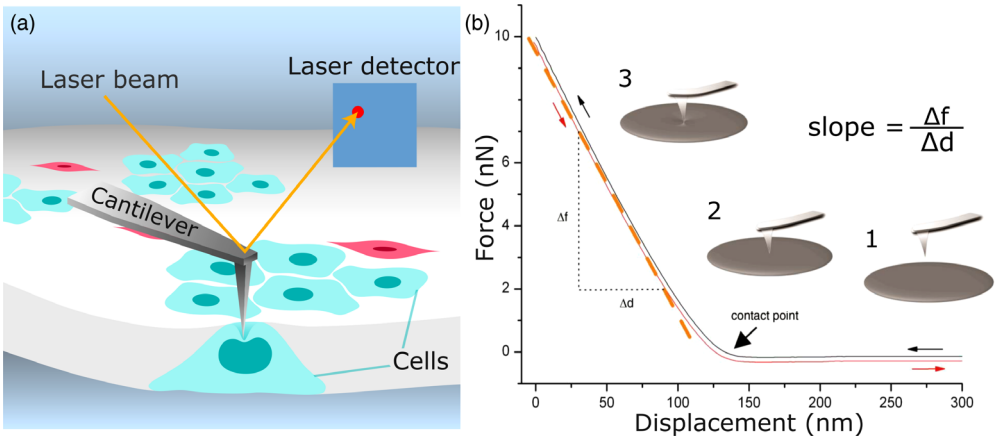


**Figure 11.1** AFM testing of biological samples. (a) The AFM scans and probes the surface of living samples (tissues or single cells) maintained in physiological buffer or culture medium. Surface corrugations are recorded using a laser beam that is focused onto a cantilever and upon interaction with the sample the beam is differentially deflected on a photodetector. (b) During mechanical loading of the sample, force measurements are recorded from the cantilever bending as the tip is brought into contact with the sample surface (black curve) and then retracted (red curve). The cantilever approaches the surface (1), the tip contacts the sample surface (2) and further indents the sample, thereby bending the lever upward (3). The slope (orange dashed line) of the contact area (3) of the recorded force curve $\Delta f / \Delta d$ reports the samples mechanical response (stiffness). (Modified with permission from [44], copyright 2011, Cold Spring Harbor Laboratory Press.)

forces are extracted (indentation mode) [40,41] (Figure 11.1b). Additional actuators for the *x*-, *y*-, and *z*-direction can be added to cover sample sizes ranging from nanometers to millimeters and enable scanning of large cells or complete tissue resection specimens. The *x*–*y* scanner (4) moves either the sample or the probe in order to record 2D maps of force curves, so-called force-maps, or to hover the probe across the sample surface at a constant cantilever deflection, recording the sample topography, as it occurs during imaging in contact mode. Furthermore, operational modes such as intermittent contact (or tapping mode), phase imaging, and noncontact mode can be employed for imaging of biological specimens. However, noncontact mode is rarely applied for biological samples due to numerous technical challenges when measuring in liquid environment [42], which is a prerequisite for physiologically relevant cell and tissue applications [43].

### 11.3.2 Scale Dependency and Resolution

The variety of combinations that can be made from different lever stiffness, indenter shapes (sphere, cone, pyramid, needle, etc.), and the high precision piezo positioning allow for the application of loading forces and mechanical measurements at a wide range of spatial and force resolutions and broaden the

scope of biological specimens that can be examined. AFM cantilevers typically measure a few hundred micrometers in length and some dozen micrometers in width, thereby exhibiting a rectangular or triangular shape. Geometry and the type of material will define the lever stiffness $k$ [45], which can range from 0.002 (SiN) to 80 N/m (Si). Very soft levers ($k < 0.01$ N/m) are commonly applied to characterize (bio-) polymer brushes, single proteins, or soft cells such as red blood cells. Soft levers ($0.01\ \text{N/m} < k < 0.2\ \text{N/m}$) are used to measure epithelial cells or fibroblasts and very soft tissues [46]. Stiffer cantilevers ($0.2\ \text{N/m} < k$) are useful for measuring cartilage, bone, or teeth. The size of the indenter represents the critical defining factor for the spatial resolution that can be achieved with AFM. The tip is either a micrometer-sized bead or an upside-down pyramidal tip with a diameter between 10 and 25 nanometers. Generally, spherical indenters are used to apply higher forces, in the micro- to millinewton range, at a comparably low spatial and force resolution. This is due to the fact that spheres have larger areas that come in direct contact with the sample compared to pyramids measuring forces in the pico- to micronewton range. Spherical indenters measure an average bulk stiffness of the components within the contact area and can therefore not resolve fine details such as cell compartments or individual ECM fibers (Figure 11.2a). However, the advantage is that measurements can be performed much faster, as long as no high spatial resolution is necessary. In contrast to this, nanometer-scale pyramidal tips are able to resolve structural details of individual ECM fibers, for example 67-nm axial repeat distances in collagen fibers [47] (Figure 11.2b), or the local stiffness heterogeneities resulting from complex cytoarchitecture (Figure 11.3). In summary, these considerations suggest that a spherical AFM tip is large enough to measure the bulk elastic modulus of entire tissues on the micrometer scale, similarly to other rheology methods, whereas the sharp pyramidal AFM tip depicts the elastic properties of the cell and tissue fine structure (Figures 11.2 and 11.3, respectively).

The most important point to consider when performing AFM measurements on biological specimens is the choice of an appropriate loading force. The

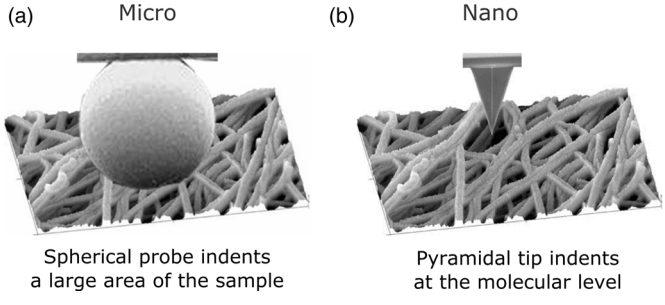


**Figure 11.2** Mechanical properties of living tissues are scale dependent. Cartoon showing the interaction of (a) a micrometer-sized spherical tip and (b) a nanometer-sized pyramidal AFM tip that is in contact with the tissue extracellular matrix. The spherical probes measure only bulk properties that average the mechanical properties of a large tissue area. In contrast to this, high-resolution pyramidal probes measure local sample differences at the nanometer scale.

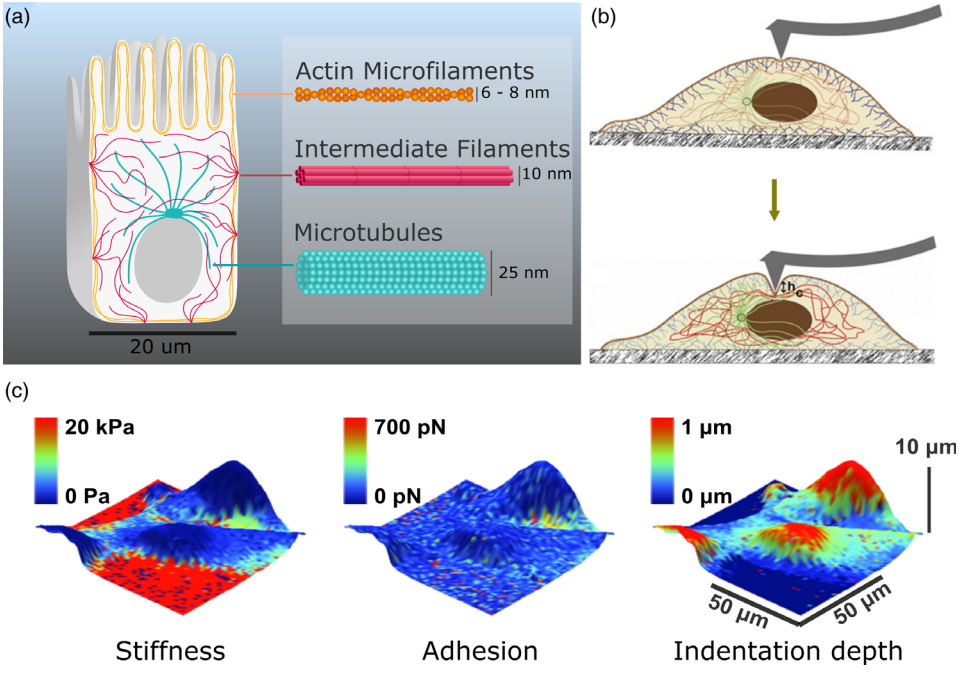


**Figure 11.3** Cytoarchitecture and nanomechanics of living cells. (a) The schematic displays the cytoskeleton of a living cell, the major determinant to the cells mechanical properties. The cytoskeletal elements actin, microtubules, and intermediate filaments build up a heterogeneous and dynamic structure that is involved in many cellular processes such as cell motion, division, and intracellular transport. The specific filament assembly, diameter, length, and position within a cell distinctly contribute to nanomechanical properties of living cells. (b) For instance, when indenting a cell ($h_c$), an AFM tip first encounters the plasma membrane (upper image, blue), below the actin cytoskeleton, followed by the intermediate filament network (lower image, red and green). (Modified with permission from Ref. [48]. Copyright 2011, Elsevier Inc.) (c) The nanomechanical assessment of living MCF10-A breast cells with AFM provides information about depth of tip indentation to probe specific cytoskeletal elements within cells (right) cell stiffness (left) and adhesion to the AFM tip (middle) as illustrated by the color-coded maps to depict local cellular heterogeneities (Modified with permission from Ref. [49]. Copyright 2009, Biophysical Society. Published by Elsevier Inc.).

necessity of a very precise force control comes from the fact that biomolecules and tissues probed with AFM are typically heterogeneous, respond nonlinearly, and are, due to their high water content, highly viscoelastic. Consequently, the stiffness will depend in a nonlinear fashion on the amplitude and rate of the applied load. Hence, applied loads and displacements have to be reproducible for the comparison of mechanical responses across specimens. A high interexperimental force control can be achieved by proper calibration of the AFM setup prior to each measurement, a process that includes the determination of the cantilevers spring constant $k$, the deflection sensitivity $DS$ relating to the cantilever

bending and laser deflection on the photodiode, as well as the actuator expansion for an applied voltage.

### 11.3.3 AFM in Cell Biology

Originally invented for research in physics with focus on condensed matter in 1986 [50], AFM was soon applied in life sciences, first to study macromolecules under nonphysiological conditions [51] and subsequently for studying cell cultures and primary cells [52–58]. In addition to cell stiffness measurements, AFM was readily used to directly measure individual ligand–receptor forces under near-physiological conditions to map antigenic sites on a cell surface by molecular recognition of an antigen by an antibody tethered to an AFM tip [59–61]. On the other hand, first AFM measurements on tissues started much later and were initially performed on stiff specimens such as bone, similarly to standard indenter measurements [62,63]. Only in recent years, AFM is being used for measuring a variety of soft tissues [43,64–66] and tissue biopsies to provide functional information about soft tissue properties ranging from the micrometer to nanometer scale, which is illustrated in detail in Table 11.1.

**Table 11.1** Atomic force microscopy for tissue measurement.

| Tissue type | Organ | Topic | Species, Stiffness [kPa] | Reference |
|---|---|---|---|---|
| Connective tissue | Cartilage | Mechanobiology | Bovine, 160–600(S)[a)] | [67] |
| | | | Porcine, 2600(OP)[b)], 20–30(C)[a)] | [47] |
| | | | Porcine, 1300(OP)[b)], 20–400(OP)[a)] | [68] |
| | | | Mouse, 800–5000 (OP)[b)], 20–60(C)[a)] | [9] |
| | | | Bovine, 200–900(D)[b)], 200–1100(D)[a)] | [69] |
| | | | Bovine, 50–600 (H + D)[b)] | [70] |
| | | | Porcine, 20–400(H)[b)] | [71] |
| | | Osteoarthritis | Human, 1300(OP)[b)], 5–90(C)[a)] | [9] |
| | | | Mouse, 10–10 000(D)[b)] | [72] |
| | Bone | Mechanobiology | Ewe, 16–24 GPa(H)[a)] | [73] |
| | Tendon | Collagen | Bovine, 1200(H)[a)] | [74] |
| | Basement | Mechanobiology | Human Ocular BMs, 40–200(OP)[a)] | [75] |
| | Membrane | | Human ILM, 1200–4200(S)[a)] | [76] |
| | | | Human ILM, 50–200(OP)[a)] | [77] |

(*continued*)

**Table 11.1** (*Continued*)

| Tissue type | Organ | Topic | Species, Stiffness [kPa] | Reference |
|---|---|---|---|---|
| | | | Chick ILM, 800–4400(S)[a)] | [78] |
| | | Diabetes | Human LC, 50–800 (OP)[a)] | [79] |
| Muscle tissue | EDL muscle | Muscular dystrophy | Mouse, 8–24(H)[a)] | [80] |
| | Paravertebral muscle | Muscular dystrophy | Human, 1.2–14.8(H)[a)] | [81] |
| | Tibialis anterior | Muscular dystrophy | Mouse, 1.2–3.9(S)[a)] | [82] |
| Nervous tissue | Retina | Mechanobiology | Guinea pig, 0.9–1.8(H)[b)] | [83] |
| | Hippocampus | Traumatic brain injury | Rat, 0.1–0.3(H)[b)] | [84] |
| | Cerebellum | Mechanobiology | Rat, 0.3–0.45(H)[b)] | [85] |
| | Cerebral Cortex | Development | Mouse, 0.1–0.7(H)[b)], 0.5–3(S)[a)] | [86] |
| Epithelial tissue (human) | Breast | Cancer | 0.5–10(OP)[a)] | [14] |
| | | | 0.3–2(H)[a)] | [87] |
| | | | 0.5–10(H)[a)] | [88] |
| | | | 0.1–6(H)[b)] | [89] |
| | | | 0.1–8(H)[a)] | [36] |
| | Uterus | Cancer | 0.5–6(H)[a)] | [87] |
| | Vulva | Cancer | 0.3–2(H)[a)] | [87] |
| | Liver | Cancer | 0.3–15(H)[a)] | [90] |

Contact model: (S)neddon, (O)liver-(P)harr, (H)ertz, (C)alibrator, (D)ynamic measurement.
a) Pyramidal indenter.
b) Spherical indenter.

Living cells or tissues exhibit rough surfaces that are in the range of micrometers or even millimeters. This is a challenge for AFM measurements, since the indenter is typically 5–15 μm long. Ideally, a sample surface should be planar with topology corrugations in a height range of the probe tip and not be obstructing the process of indentation. This problem can be easily bypassed by using longer indenters or mounting the whole sample in a way such that the region of interest is elevated [91].

Another key parameter that has to be considered as potential obstacle for the AFM setup is a macroscopic "waviness" of the tissue surface. Tissues exhibiting excessive surface waviness, for instance, can cause uneven leveling, which might result in cantilever breakage and measurement failure. Native breast tissue biopsies, for instance, exhibit a waviness between 250 and 500 μm (Figure 11.4a), a microscopic tissue "roughness" of approximately 1–5 μm, as well as a local ECM porosity of approximately 200 nm (Figure 11.4b). Such problems can be solved

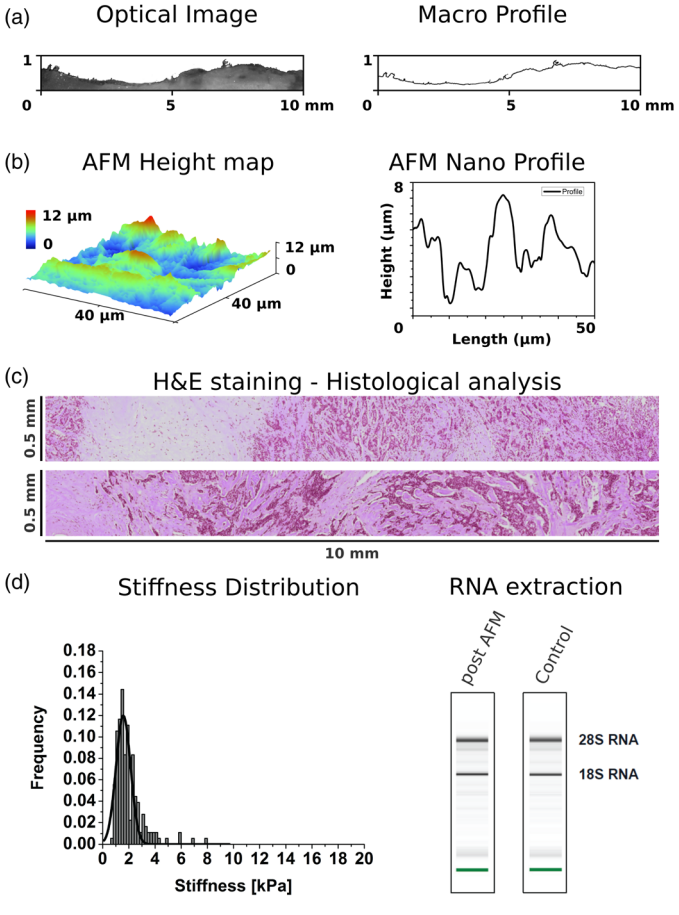


**Figure 11.4** Surface properties and quality control of isolated tissue specimens. (a) Optical image (left) and the extracted profile (right) reveal the surface waviness of up to 500 µm. (b) AFM topography and line profile (3 µm roughness) obtained on a representative human breast cancer biopsy containing cancer cells and ECM. (c) Post-AFM histological assessment reveals no damage to tissue appearance. Scale is 500 µm. (d) Stiffness profiles of normal murine mammary glands that were stored and measured in Ringer solution containing protease inhibitors. Data were recorded immediately after tissue excision (left) and comparison of total RNA extracted from the post-AFM specimens (right) reveals that AFM measurements do not affect RNA stability, as demonstrated by intact 28 S and 18 S RNA bands. (Modified with permission from Ref. [14]. Copyright 2012, Rights Managed by Nature Publishing Group.)

by implementing leveling algorithms and additional actuators that are able to circumvent waviness/roughness by controlled stepwise height changes in the $z$-direction. To obtain physiologically relevant measurements of living biological specimens, control of the culture medium pH, $CO_2$ concentration and temperature control should be implemented in the AFM setup. Animal organs and

human tissue samples are generally much more resilient than cultured cells, since they are embedded into a fully functional ECM scaffold. However, these samples should also be stored and measured in physiological buffers, such as Ringer solution supplemented with protease inhibitors, in order to prevent tissue alterations (Figure 11.4c) and RNA degradation (Figure 11.4d).

In the next sections, recent advances in the field of tissue nanomechanics using AFM are discussed in the context of articular cartilage and breast tissue.

## 11.4
## The Nanomechanical Signature of Articular Cartilage

### 11.4.1
### Articular Cartilage Composition and Function

Human hyaline articular cartilage (AC) is a highly specialized, 1–3 mm thick connective tissue with a unique three-dimensional structure that enables it to withhold tremendous mechanical forces during joint loading while its smooth surface lowers the friction between articular surfaces of the joint during movement [66]. The composition of AC can be subdivided into a fluid and a

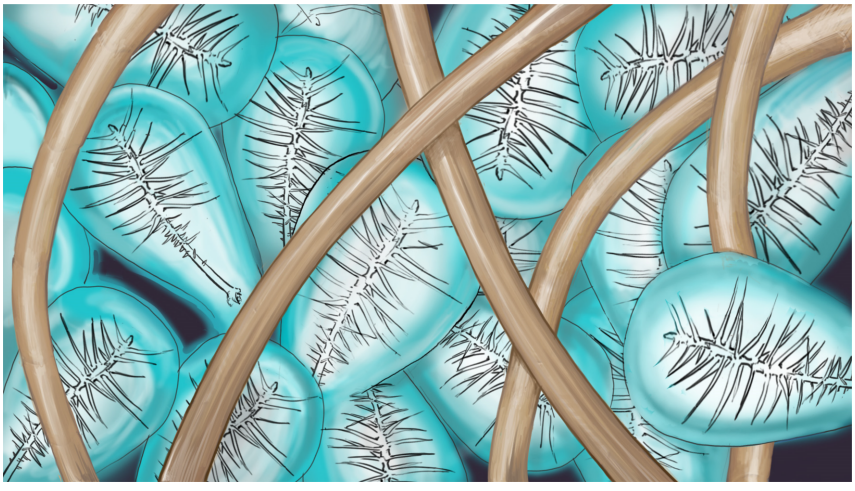

**Figure 11.5** Mechanical function of articular cartilage (AC). The compression resistance mechanism of AC is based on the interactions between proteoglycans and collagen II. Proteoglycans are condensed within the high-tensile collagen (brown) meshwork that is restraining the proteoglycans (blue) expansion. The proteoglycan gel swells because of its high osmotic pressure (Donnan effect), due to fixed negative charges on the proteoglycans. This provides a mechanism for constant prestrain of the collagen network and load dissipation. Disruptions of this mechanism, such as osteoarthritis, have tremendous impact on cartilage loading profile, which can result in degeneration and complete degradation of the tissue.

solid phase. The fluid phase, with water and electrolytes as the most prevalent components, accounts for 60–80% of the cartilage structure measured by wet weight. The solid phase is composed from the ECM proteins mainly represented by collagen II fibrils (15–20% by wet weight), proteoglycans (PG) (10% by wet weight), and chondrocytes (1–5%) [92], which mainly synthesize and maintain ECM components. The viscoelastic response of AC originates from the fluid friction that occurs through squeezing of the interstitial fluid phase, which flows through the low permeable solid phase originating from the intrinsic viscoelasticity of the solid matrix (flow independent viscoelasticity) [93,94]. Conversely, the AC is considered as a tough but at the same time highly compliant load-bearing tissue with mechanical characteristics depending on the integrity of the collagen network and concentration of the embedded PGs (Figure 11.5). For example, multiple aggrecan monomers are noncovalently bound to hyaluronic acid (hyaluronan) and together form a concentrated space-filling proteoglycan gel to ensure aggrecan retention within the collagen network (Figure 11.5) [95]. In case of injury or degenerative disease, PGs are secreted by chondrocytes at a much higher rate than collagen, which promotes the healing capacity of cartilage. During aging and degeneration, PGs undergo significant alterations in composition and organization with respect to both core protein and aggrecan length, sulphate pattern modification and the length of CS and KS side chains [96–98]. This in turn has a significant impact on the mechanical performance of PGs and consequently the AC function [99].

### 11.4.2
### The Nanomechanics of Articular Cartilage

In order to provide fundamental knowledge on cartilage properties from a molecular perspective, it is necessary to study nanomechanical properties of its individual ECM constituents in the context of physiological tissues [92]. Methods to study AC include visual inspection histology [66,100,101] and optical microscopy [102,103], methods which are limited to a spatial resolution of approximately 200 nm. In contrast to this, electron microscopy [104,105] reveals ultrastructural details at a molecular resolution but requires chemical fixation and dehydration of the AC, followed by metal staining or sputtering. AFM can be used both at the micrometer (tissue level) and nanometer (molecular level) scale (Figure 11.2) for measuring mechanical properties associated with functional states of the AC [106]. An advantage of AFM in comparison to magnetic resonance imaging (MRI) is the high sensitivity in measuring changes at the AC surface, especially since ECM degeneration typically starts in the superficial zones and then progresses to deeper regions of the tissue [106]. Micrometer scale measurements typically yield a unimodal stiffness distribution of 1.3 MPa from the collagen network as the predominantly contributing factor to bulk viscoelastic properties (Figure 11.6a) [68]. Conversely, nanometer scale measurements give rise to a bimodal stiffness

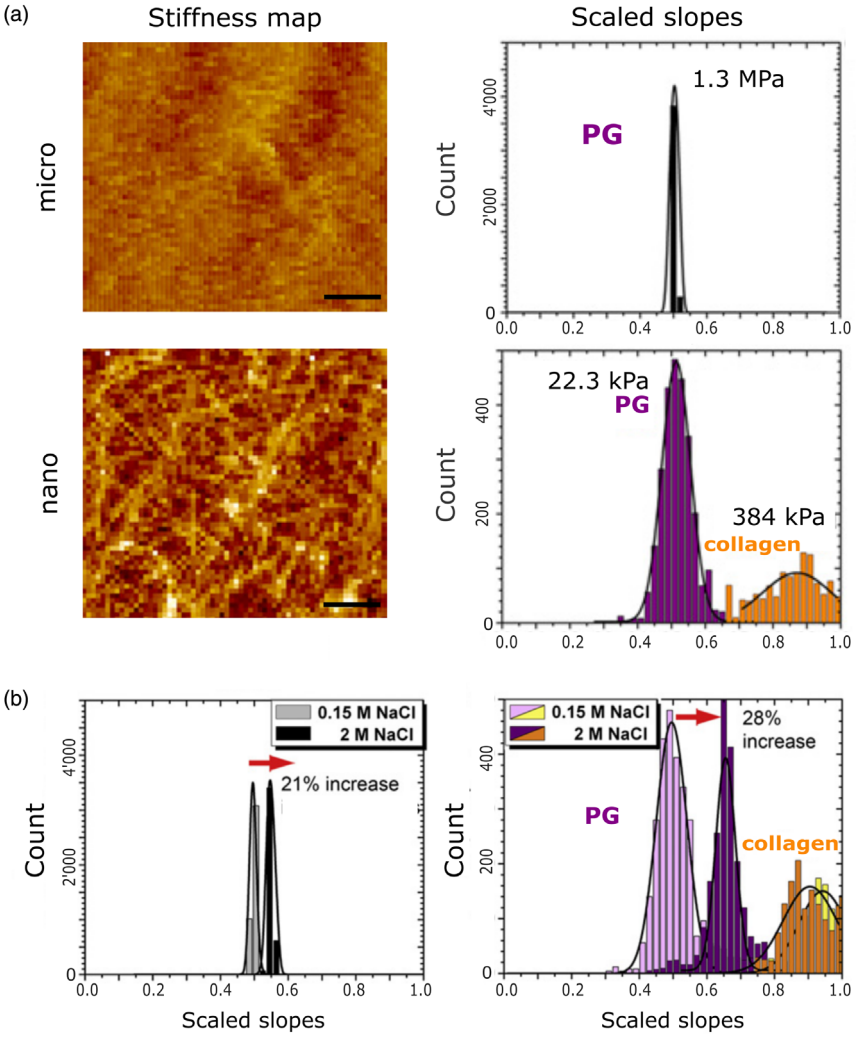


**Figure 11.6** Stiffness of the AC at the micro- and nanometer scales and the effects of different ionic strength. (a) AC was probed either at the micrometer scale using a 5-μm-diameter spherical bead (top) or at the nanometer scale with a sharp pyramidal tip (bottom). The stiffness map (top left, 64 × 64 pixels, corresponding to 4096 force curves) shows that the micrometer-sized probe is not able to resolve the cartilage structural elements. The stiffness distribution (top right) reveals that the scaled unloading slope histogram exhibits a narrow normal distribution centered around a scaled slope value of 0.53, yielding a micrometer scale stiffness of 1.3 ± 0.4 MPa (bottom, left). A nanometer-sized tip, however, can assess the stiffness of cartilage at the level of the individual cartilage ECM components, collagen fibrils and proteoglycan gel. In the high-resolution stiffness map (bottom left) representing a 12 μm × 12 μm area (64 × 64 pixels corresponding to a sampling of 187.5 nm) of the specimen individual collagen fibrils, are visualized on the surface of the AC. The histogram (bottom right) reveals a bimodal distribution with two normal distributions being centered scaled slope values of 0.51 and 0.87, respectively. From these, nanometer scale stiffness

distribution with stiffness peaks corresponding to values of the molecular AC constituents [68]. The stiffness distribution has revealed that PGs account for the soft ECM component with a stiffness of 23 kPa, while collagen II exhibits a 20 times higher stiffness of 384 kPa and emphazises that the nanomechanical measurements are sensitive to the soft, gel-like ECM components, while micrometer scale measurements are not (Figure 11.6b). As a result of osmotic effects, an increase in salt concentration reduces the water content and increases the stiffness of the PGs but without significantly changing collagen II stiffness (Figure 11.6c). On the micrometer scale, stiffness increases by 21% but does not affect its unimodal frequency distribution (Figure 11.6c, left). Upon exchanging the buffer from isotonic to hypertonic PBS, the bimodal nanomechanical distribution was observed to remain. However the slope of the lower PG peak has increased by 28%, whereas the increase in slope of the higher peak was insignificant (Figure 11.6c, right). Nanomechanical structures govern the functional behavior in the articular cartilage as shown by tuning the nanomechanical properties of cartilage ECM components. This could be valuable for interpreting and even predicting structure–mechanical property relationships on different length scales and the resulting data could be used for further optimization of *in vitro* engineered cartilage.

### 11.4.3
### The Nanomechanical Signature of Osteoarthritis

Osteoarthritis is a leading cause of disability among the working population; by 2030, 67 million people are projected to suffer from doctor-diagnosed arthritis only in the United States [107]. The absence of blood vessels and the age-dependent decline in metabolic activity of chondrocytes (1–5%) [108,109] impede such defects from healing and often lead to premature osteoarthritis. Currently, diagnostic methods (X-ray and MRI detection) are able to resolve only the irreversible phase of OA when the treatment options are limited and total knee replacement is the only available long-term treatment. Tissue engineered cartilage, which is considered as the most promising treatment option, has not yet reached routine clinical application due to mechanical variability of the engineered scaffolds and the lack of reliable quality controls. Hence, a comprehensive understanding of cartilage nanomechanics and its underlying biological

values of $22.3 \pm 1.5$ kPa for the soft proteoglycan phase and $384 \pm 50$ kPa for the stiffer collagen network were calculated. Scale bar 2 μm. (b) To demonstrate that nanometer-sharp tip specifically measures proteoglycans and the collagen network isotonic and hypertonic PBS buffers were used to provoke alterations of the proteoglycans driven by osmotic forces. An increase in salt concentration, due to osmotic effects, lead to an increase in cartilage stiffness on the micrometer scale by 21% but the distribution stayed unimodal (left). On the nanometer scale, the corresponding effects of the change from isotonic to hypertonic PBS resulted in an increased stiffness of the proteoglycan gel phase by 28% (right), whereas the stiffness increase of the collagen fraction was not significantly changed. (Modified with permission from Ref. [68].)

processes is crucial for the development of protocols and treatments which will allow early diagnostics and therewith better treatment options for OA patients. Recent evidence suggests that AFM is able to resolve nanomechanical changes associated with aging in mice (Figure 11.7a), which includes all grades of osteoarthritis in the mouse model of OA (Figure 11.7b) and human patients (Figure 11.7c), according to the Outerbridge classification system [110]. Moreover, functional states of the AC surface and its inner layers can be discerned from the

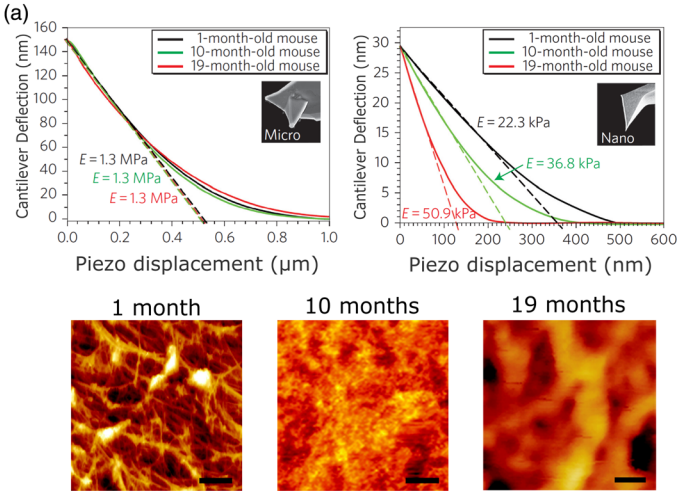


**Figure 11.7** The nanomechanical properties of AC during aging and osteoarthritis. Surface imaging and mechanical loading tests were performed on the hips of normal mice of various ages and those of osteoarthritic mice. (a) AFM imaging of AC with a nanometer tip (top left) in a buffer solution resolved individual collagen fibrils. Topography images (right) show that collagen fibrils appear thicker with aging. Scale bar 1 μm. Mechanical testing reveals that cartilage stiffness on the micrometer scale stays similar during aging (top left). In contrast, measurements on the nanometer scale depicted stiffness increase with increasing age of the mice (bottom left). (b) Surface imaging and mechanical testing of AC from wild-type control and Col9a1$^{-/-}$ knockout mice (osteoarthritis model) demonstrate disease related structural and mechanical changes. Surface topography (right) of AC shows individual collagen fibrils with different thicknesses, as the disease progressed from normal, intermediate to late stage. Scale bar 1 μm. Similar to the aging phenotype, micrometer scale stiffness cannot distinguish between wild-type and knockout mice (top left). Nano-stiffness (bottom left) increased with progression of the disease and in correlation with thickening of the collagen fibers. (Modified with permission from Ref. [68].) (c) The assessment of osteoarthritis in human patients has revealed no apparent changes in the collagen meshwork (top) for the early grades, according to the Outerbridge classification (grade 0 and 1), while in grade 2 fibrils start to show tangles and disarrangement. In grade 3, disruption of the superficial collagen meshwork and extensive splitting of collagen fibrils into thinner fibrils (white arrows) is revealed. Scale bars 0.5 μm. Microstiffness remained constant for all grades (bottom left), while nanostiffness significantly (in accordance to disruption of collagen network) decreased (bottom right) with increasing grades of osteoarthritis. (Modified with permission from Ref. [9]. Copyright 2009, Rights Managed by Nature Publishing Group.)

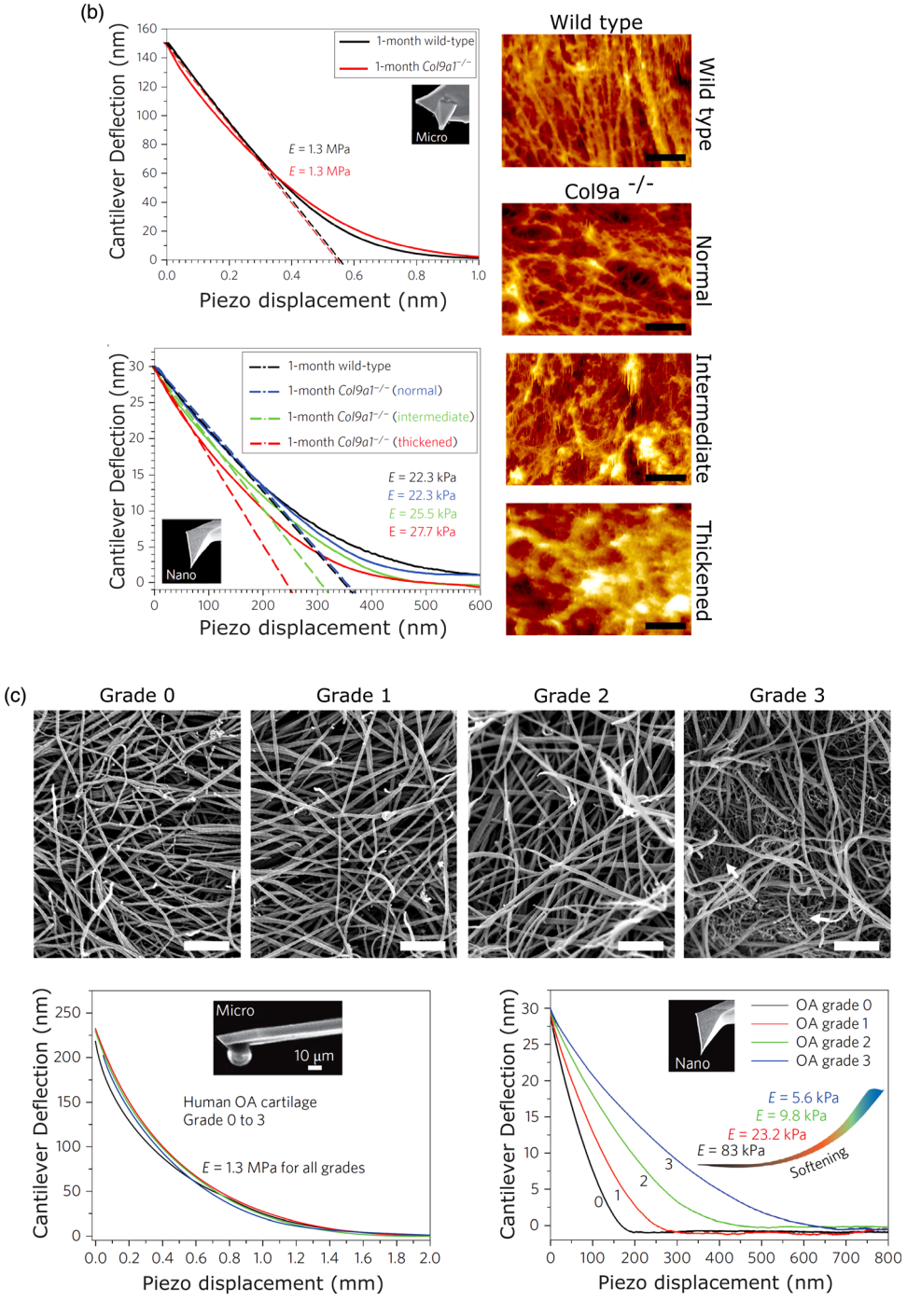


**Figure 11.7** Continued

AFM measurements. The protein lubricin secreted on the AC surface is mainly responsible for regulating its friction properties and any changes in the lubricin thickness or friction contributing to development and progression of OA [9]. Therefore, friction measurements could serve as an additional mechanical marker of cartilage wear disease state [68]. In summary, nanomechanical measurements using AFM show great potential for unraveling the molecular mechanisms that drive the onset of OA and could in future promote the development of novel therapeutic modalities which allow to reverse the progression of osteoarthritis or to cure this disease.

## 11.5 The Nanomechanical Signature of Mammary Tissues

### 11.5.1 Mammary Gland Composition and Mechanics

Mammary glands consist of ductal cells and milk producing alveolar epithelial cells, which all together embed in the stromal connective tissue and the mammary fat pad. Mammary epithelial cells are organized into three-dimensional structures that are strongly dependent on their polarized morphology, specialized cell–cell contacts, and the attachment to an underlying specialized basement membrane ECM [111]. Cell–cell and cell–ECM adhesive interactions regulate functions of the normal mammary gland and are critical for the maintenance of tissue homeostasis and mechanical equilibrium [112,113]. In particular, mechanical forces are prerequisite for proper control of cell proliferation, survival, differentiation, migration, and milk protein secretion during normal development, puberty, and adulthood [114]. At the onset of cancerous breast diseases, the normal tissue structure and its mechanical equilibrium become disrupted and undergo continuous changes and distinct mechanical characteristics as the tumor progresses [14,111]. A hyperplastic (benign) lesion typically involves loss of normal cell polarization and organization, disruption of cell–cell and cell–ECM adhesions, which then results in increased stromal response, increased matrix deposition, and changes in the mechanical properties that contribute to stiffening [115]. Most importantly in benign lesions, mechanical and biochemical signals do hinder invasion of nearby tissues. On the other hand, carcinomas *in situ* are characterized by uncontrolled cell growth due to genetic and epigenetic alterations and reduced cell death within an intact basement membrane and interstitial ECM [116]. Furthermore, cancer cells exhibit pleomorphic characteristics with varying size and shape [117]. Uncontrolled cell growth and consequently the increase in tumor mass within the restricted volume lead to elevated compression of surrounding ECM [118]. Due to tumor growth, factors such as intratumoral hypoxia can further contribute to mechanical changes. In response to hypoxia, tumor and stromal cells secrete various soluble factors, facilitating matrix remodeling including basement membrane breakdown and

angiogenesis, that will overall endorse cell invasion [119]. In the case of invasive cancer, intratumoral cell–cell interactions further decrease and tumor cells disseminate through the damaged basement membrane and interstitial ECM [120]. Invading cells are accompanied by surrounding stromal cells (fibroblasts and macrophages) and migrate through degraded matrix by following the biochemical gradients in the direction of the circulatory system [121,122]. In addition to genetic and external environmental factors, the interplay of biochemical and physical interactions of cancer cells with their environment and their modulation by mechanical forces are critical for the metastatic process [11] in which cancer cells can overcome boundaries between different tissues [1,123]. Clearly, the ability to target this key step in cancer progression can be improved by understanding the physical characteristics that metastatic cells exhibit and experience from their microenvironment.

### 11.5.2
### The Nanomechanical Signature of Breast Cancer

Until recently [14], efforts to understand cancer biomechanics had been largely polarized between tissue-level and single-cell experimentation. At the bulk level, it is alleged that continuous tissue stiffening promotes cancer [34,124] since tumors are macroscopically stiffer than healthy tissue [124,125], an observation that is in accordance with conventional knowledge from palpation (Figure 11.8, left). Furthermore, single isolated cancer cells are significantly softer than normal cells, suggesting that metastasis might be facilitated by cell compliance [58].

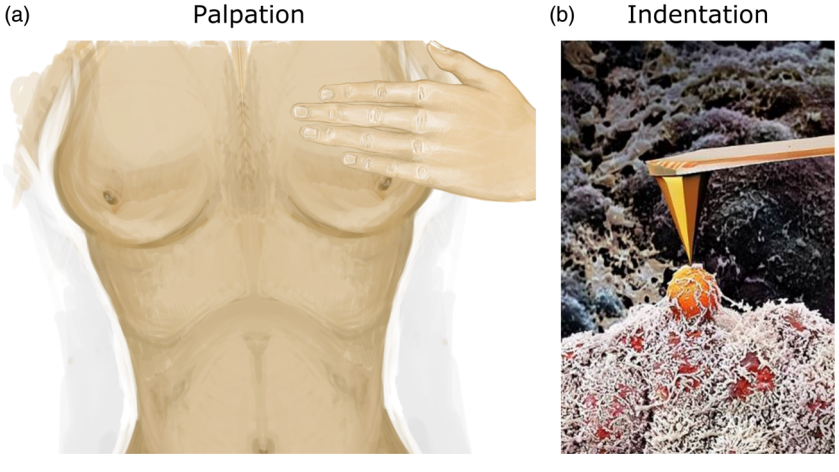


**Figure 11.8** Detection of breast diseases on different length scales. (a) Breast examination is typically initially performed by a palpation test where a clinician examines the breast for distinct lesions, irregularities, and changes in breast stiffness. (b) Similarly, a nanometer sized AFM probe is used to measure tissue stiffness by providing detailed information about the molecular and cellular level changes associated with benign or malignant lesions.

Efforts to bridge this controversy have led to the discovery that soft hypoxic cancer cells are responsible for the metastatic spread from a primary tumor to a secondary lesion [14]. This is based on AFM-type nanomechanical testing, which measures and spatially correlates local nanomechanical properties (Figure 11.8, right) across entire unadulterated human breast tissue biopsies (Figure 11.9) in close to native physiological conditions (Figure 11.9, right). Unprecedentedly, individual cells (approximately 0.5 kPa) can be distinguished from their

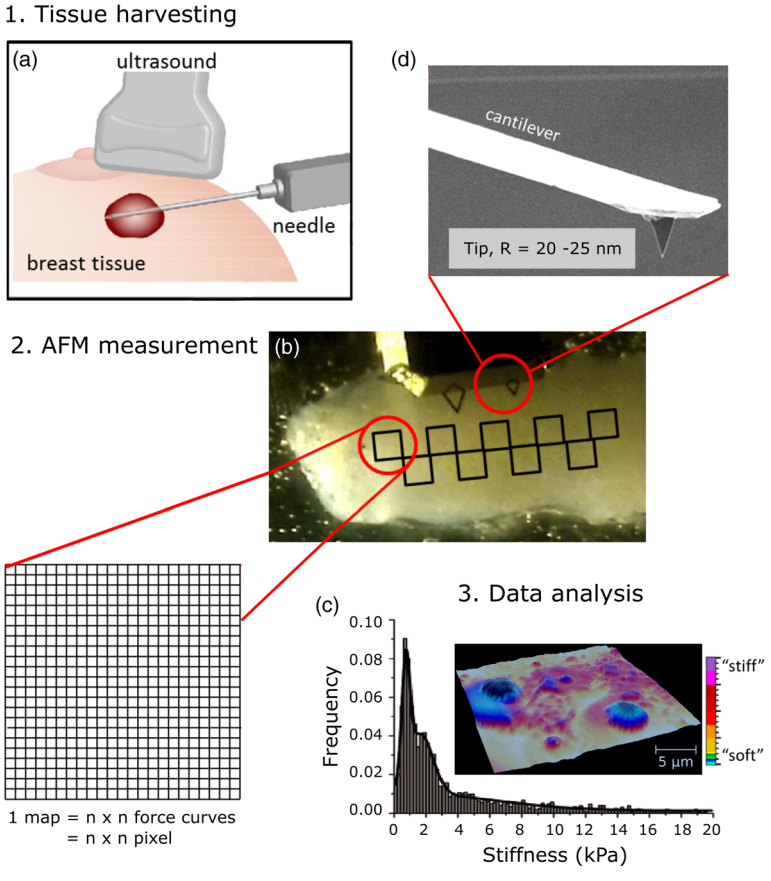


**Figure 11.9** Nanomechanical characterization of human tissues by AFM. (a) Schematic representation of an ultrasound-guided biopsy collected from a patient with a suspicious lesion. (b) Top-view of an immobilized biopsy in Ringer solution showing the cantilever positioned above the biopsy. Scale bar, 500 µm. Up to 20 stiffness maps ($20 \times 20\ \mu m^2$), each consisting of 1024–4096 indentation measurements are recorded homogeneously distributed across the entire specimen. (c) Subsequent analysis of the data provides a sample-wide stiffness distribution and individual areas can be visualized plotting color-coded stiffness maps. (d) The choice of dimensions for both the tip and the cantilever is critical for obtaining high-resolution topography and nanomechanical information on a correct length-scale.

surrounding ECM based on the sub-kilopascal (kPa) stiffness sensitivity of this method. Briefly, an AFM assay uses a 20 nm sharp tip to indent approximately 10 000 individual locations across a biopsy surface within a few hours (Figure 11.9, stiffness map). Each indentation measures the stiffness of local structures (e.g., ECM, cancer cells, etc.) that lie beneath the tip. In this manner, a quantitative biopsy-wide nanomechanical profile or signature of the biopsy is obtained that strongly correlates to the status and health of the tissue (Figure 11.9, stiffness distribution). Comprehensive analysis of native human breast biopsies, where nanomechanical properties were correlated with the specific histopathological markers, has determined whether a biopsy represents normal glandular tissue, a benign lesion or cancer (Figure 11.10a) [14]. In addition, individual stiffness peaks were assigned to specific tissue morphologies by performing more detailed measurements within defined regions of the biopsy (Figure 11.10b), particularly in the core and at the periphery. The correlation of local AFM data with matching histological findings corroborated that the soft peak is typical for cancer cells (Figure 11.10b, left), which are surrounded by stiffer peripheral stroma (Figure 11.10b, right). Moreover, these findings were validated by studying nanomechanical changes during tumor progression from normalcy to late metastasis in a standard transgenic mouse MMTV-PyMT (mouse mammary tumor virus polyoma middle T antigen) model that faithfully recapitulates human invasive ductal carcinoma [122,126] (Figure 11.11a). Recent studies [14,127–130] strongly indicate that cancer cell softness is essential for their mobility, intravasation and metastasis and further suggest that cancer cell softness may be a consequence of molecular pathways regulating cancer progression and metastasis (Figure 11.11b). For example, it has been widely considered that antiangiogenic therapy holds great promise in treating cancer by preventing and/or blocking the metastatic cascade through the induction of intratumoral hypoxia, and consequently cell death due to the lack of nutrients and oxygen [37]. Early preclinical studies showed that inhibiting the vascular endothelial growth factor (VEGF) pathway retards tumor growth [131]. However, long-term preclinical and clinical studies now show that these drugs (i.e., Bevacizumab and Sunitinib) provide only moderate increases in progression-free survival with little benefit in the overall survival of cancer patients [132,133]. In addition, recent evidence shows that antiangiogenic drugs in fact increase invasive and metastatic properties of cancer cells through the induction of hypoxia [128,134]. This could be due to alterations in HIF-1 alpha signaling, which is involved in almost every step of the metastatic cascade such as epithelial-to mesenchymal transition (EMT), stromal invasion, and vascular infiltration [135]. Recent data suggest a strong correlation between cancer cell softening and hypoxia [14] (Figure 11.11b). In particular, hypoxic cells increase in population and spread as the tumor progression enters into later stages as well as in metastases (Figure 11.11c). Indeed, emerging results show that hypoxic cells, by decreasing their stiffness, have a much higher propensity to metastasize and the alterations in the cancer metabolism are key players in the evolutionary selection for the softest and the most aggressive cancer phenotypes [136].

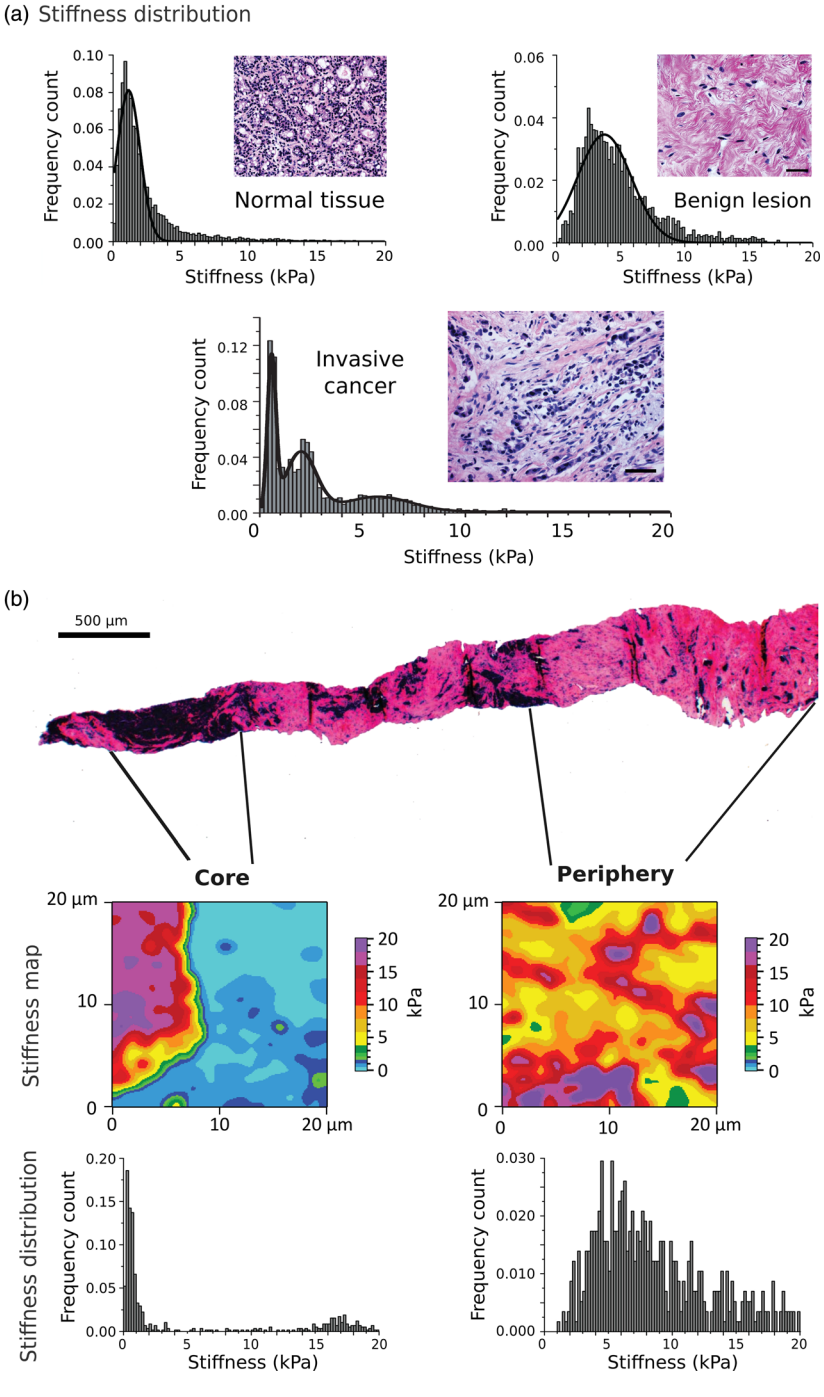
(a) Stiffness distribution
Frequency count
Stiffness (kPa)
Normal tissue
Benign lesion
Invasive cancer
(b)
500 µm
Core
Periphery
Stiffness map
20 µm
kPa
Stiffness distribution

## 11.6
## AFM – The Diagnostic and Prognostic Tool of the Future

Specific cell–cell and cell–ECM interactions play critical roles in cellular communication, tissue organization, embryonic development, and wound healing. Accordingly, a wide variety of diseases are associated with impaired cell–cell and cell–ECM interactions, and consequently mechanical responses, both on the level of tissues and single cells. The nanomechanical testing of soft biological tissues by AFM provides a key ability to address these interactions in an unperturbed, physiological state, and *in situ*. Nevertheless, testing of soft biological tissues represents a significant challenge for indenter-based setups since fundamental changes of the experimental systems are required. Despite many innovations, the AFM technology is still underdeveloped for routine biomedical applications. This is probably due to the fact that most AFMs available today are all-purpose devices asking for a very skilled and experienced user. Therefore, the future of AFM-based technology lies in its simplification and automation that will, in combination with other imaging modalities such as high-resolution light and fluorescence microscopy, provide new insights for cell and tissue mechanical functions. We conclude this chapter by recent examples from our own research, as to how nanomechanical measurements can be used as unique mechanomarkers of progressive stages of OA and cancer by providing relevant information at the molecular level and in native tissues. This is demonstrated by the ability of AFM to detect degradation from healthy to completely deteriorated cartilage [9,68] as shown in Figure 11.12.

Furthermore, the detection of soft phenotypes both in primary tumors and in lung metastasis suggests that compliance of malignant cells in the primary cancer

**Figure 11.10** The nanomechanical signature of human breast tissue. (a) Stiffness distribution of normal mammary gland tissue is unimodal (left). Post-AFM histology (inset) reveals the terminal ductal lobular unit of a normal mammary gland fenced by interstitial connective tissue. Biopsy-wide histogram for a benign lesion (middle) reveals a unimodal but broader stiffness distribution with an overall increase in stiffness. H&E stained section (inset) demonstrates extensive fibrotic stroma interspersed with fibroblasts typical fibroadenoma. Heterogeneous stiffness distribution (right) with a characteristic soft peak for malignant tumor tissue is consistent with the histopathology (inset) revealing an invasive breast carcinoma with infiltrating nests of cancer cells that have evoked a dense fibrous tissue response. Scale bar is 50 μm. (b) In breast cancer biopsies, stiffness varies from core to periphery in accordance with post-AFM histology. Post-AFM histological overview (top) of the entire cancer biopsy with reference to the areas mapped in detail. Representative AFM stiffness map (middle, $24 \times 24$ pixels) of the core region exhibited pronounced softness within a narrow peak of specific stiffness values (bottom). Accordingly, local histology (top left) shows that the core region is densely populated with cancer cells. The typical stiffness map (bottom) of the tumor periphery demonstrates increased stiffness. The corresponding stiffness distribution (bottom) is broader and shifted toward stiffer. Post-AFM histopathology (top right) reveals that the tumor periphery predominantly comprises fibrotic tissue. (Modified with permission from Ref. [14]. Copyright 2012, Rights Managed by Nature Publishing Group.)

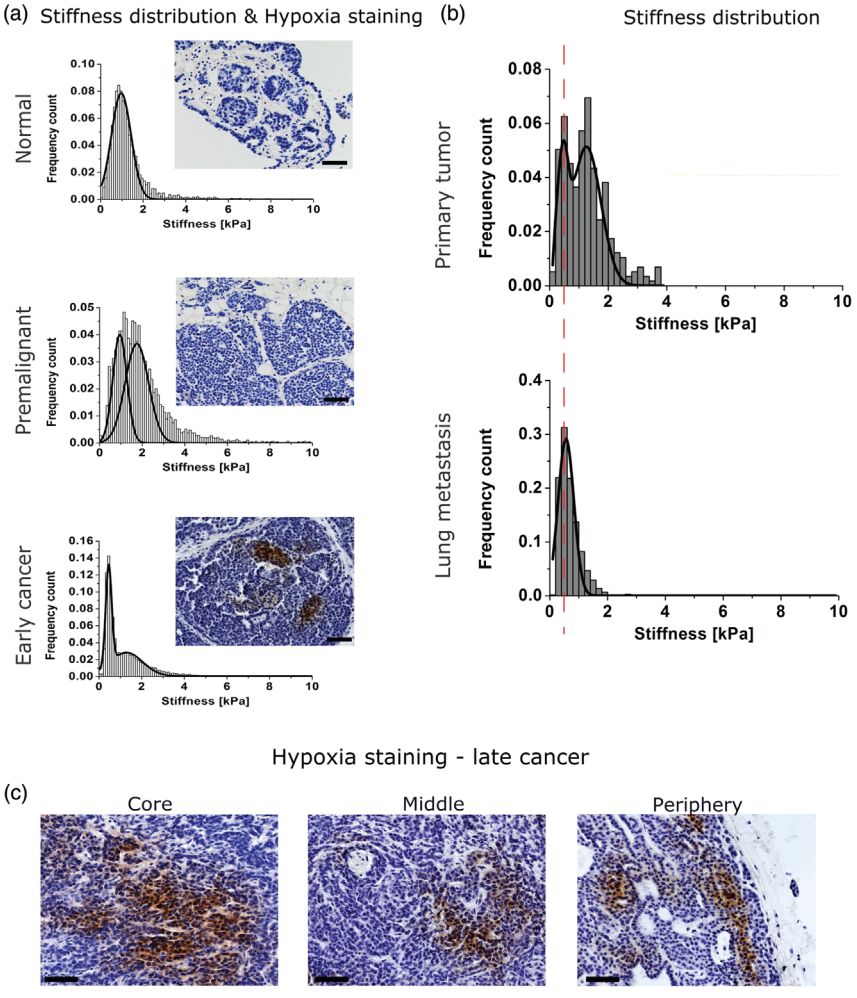


**Figure 11.11** Correlating the nanomechanical response with tumor progression and hypoxia in MMTV-PyMT. (a) Nanomechanical measurements showed that stiffness values of normal ductal epithelium (top) followed a uniform Gaussian distribution. In the premalignant lesion (middle), the contribution of stiffer features increased, as seen by a broader stiffness distribution with an indication of bimodality. The pimonidazole (hypoxyprobe) immunostaing did not indicate hypoxia in normal glandular tissue (top inset) or in the premalignant lesion (middle inset). In early cancer (bottom), significant softening produced a characteristic peak that dominated the prominent bimodal stiffness distribution. Hypoxia positive cells (brown staining) revealed central hypoxia in early cancer (bottom inset). Scale bars 50 μm. (b) Stiffness profiles of primary tumor (top) and lung metastasis (bottom) revealed a common phenotype. In the primary tumor, the corresponding stiffness distribution revealed two peaks representing distinct phenotypes of cancer cells, a softer one at $0.45 + 0.15$ kPa and another at $1.26 + 0.43$ kPa. The stiffness distribution of metastatic lesions from the same mice revealed a peak value that is almost identical to the softer peak detected at the primary tumor site (indicated by the red dashed line). (c) Accordingly, in this late cancer stage, hypoxic cells were abundant in the core region (left), streaming toward tumor blood vessels (middle) and have already disseminated to the tumor periphery (right). Scale bar 50 μm. (Modified with permission from Ref. [14]. Copyright 2012, Rights Managed by Nature Publishing Group.)

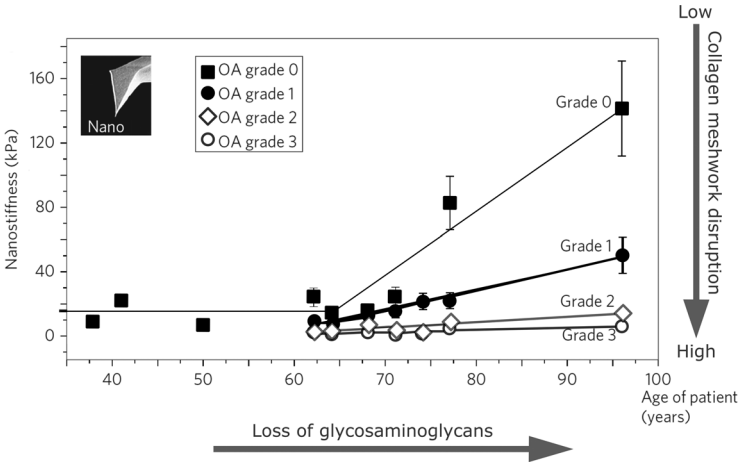


**Figure 11.12** The nanomechanical signature of osteoarthritis. Nanomechanical properties of cartilage from seven osteoarthritis patients and three healthy individuals have revealed that the stiffness increased with age. This was accompanied by reduced glycosaminoglycan content (horizontal arrow). As the slopes indicate, incremental reduction of stiffness depicted by the nanomechanical measurement, by osteoarthritis as a function of age, was largest between grades 0 and 1. This could be used as an early diagnostic method of OA. The disease progression to grades 2 and 3 correlates with the increased tendency of collagen meshwork disruption (vertical arrow) and further stiffness decrease. (Modified with permission from Ref. [9]. Copyright 2009, Rights Managed by Nature Publishing Group.)

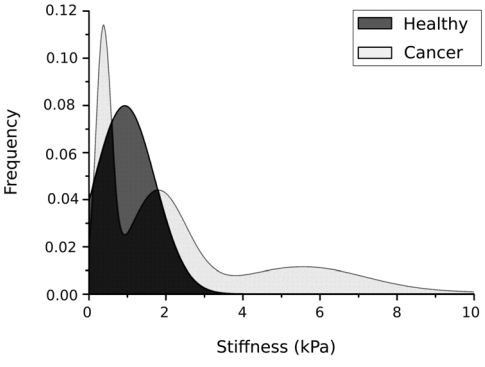


**Figure 11.13** The nanomechanical signature of breast cancer. Biopsy-wide histograms propose an inverse correlation between stiffness profiles for specimens obtained from healthy and invasive cancer patients. The measured twofold decrease in stiffness for invasive and more metastatic cancer cells could have prognostic indications. (Modified with permission from Ref. [14]. Copyright 2012, Rights Managed by Nature Publishing Group.)

is correlated to cancer aggressiveness by promoting migration and metastasis. As a result, detecting these soft peaks may not only serve as a nanomechanical marker for the onset of cancer but can have a prognostic value in the future as well (Figure 11.13). To bridge this gap, an AFM-based apparatus known as

ARTIDIS was developed ("Automated and Reliable Tissue Diagnostics") (Publication number WO2012076729 A9). ARTIDIS measures and spatially correlates local nanomechanical properties across entire unadulterated tissues in close to native physiological conditions.

The ability to measure nanomechanical changes at the molecular level and in living tissues has opened up the exciting prospect of developing this simple nanodevice into a clinical tool. Last but not the least, ARTIDIS is not limited to cartilage and mammary tissues but can be applied to a large variety of soft tissues (lung, liver, prostate, and lymph nodes) and 3D tissue cultures [137].

### Acknowledgments

This work was funded by the M. E. Müller Foundation of Switzerland, Commission for Technology and Innovation (CTI) Project 11977.2 PFNM-NM; ARTIDIS "Automated and Reliable Tissue Diagnostics" and Nanotera Project awarded to PATLiSci II Consortium.

The authors thank Annette Roulier for Figures 11.1 and 11.3 and Kjartan Asgeirsson for Figures 11.5 and 11.8.

### Competing Financial Interests

The University of Basel has filed patents on the technology and intellectual property related to this work based on the inventions of M.L., P.O, and M.P.

### References

1 Kumar, S. and Weaver, V.M. (2009) Mechanics, malignancy, and metastasis: the force journey of a tumor cell. *Cancer Metastasis Rev.*, **28**, 113–127. doi: 10.1007/s10555-008-9173-4

2 Discher, D.E., Janmey, P., and Wang, Y.-L. (2005) Tissue cells feel and respond to the stiffness of their substrate. *Science*, **310**, 1139–1143. doi: 10.1126/science.1116995

3 Ikai, A. (1996) STM and AFM of bio/organic molecules and structures. *Surf. Sci. Rep.*, **26**, 261–332.

4 Bustamante, C., Bryant, Z., and Smith, S.B. (2003) Ten years of tension: single-molecule DNA mechanics. *Nature*, **421**, 423–427. doi: 10.1038/nature01405

5 Wang, J.H.-C. and Thampatty, B.P. (2006) An introductory review of cell mechanobiology. *Biomech. Model. Mechanobiol.*, **5**, 1–16. doi: 10.1007/s10237-005-0012-z

6 Fisher, T.E., Oberhauser, A.F., Carrion-Vazquez, M., Marszalek, P.E., and Fernandez, J.M. (1999) The study of protein mechanics with the atomic force microscope. *Trends Biochem. Sci.*, **24**, 379–384. doi: 10.1016/S0968-0004(99)01453-X

7 Bao, G. and Suresh, S. (2003) Cell and molecular mechanics of biological materials. *Nat. Mater.*, **2**, 715–725. doi: 10.1038/nmat1001

8 Ingber, D.E. (1993) Cellular tensegrity: defining new rules of biological design that govern the cytoskeleton. *J. Cell Sci.*, **104** (Pt 3), 613–627.

9 Stolz, M., Gottardi, R., Raiteri, R., Miot, S., Martin, I., Imer, R., Staufer, U., Raducanu, A., Düggelin, M., Baschong, W., Daniels, A.U., Friederich, N.F., Aszodi, A., and Aebi, U. (2009) Early detection of aging cartilage and osteoarthritis in mice and patient samples using atomic force microscopy. *Nat. Nanotechnol.*, **4**, 186–192. doi: 10.1038/nnano.2008.410

10 Suresh, S. (2007) Biomechanics and biophysics of cancer cells. *Acta Mater.*, **55**, 3989–4014. doi: 10.1016/j.actamat.2007.04.022

11 Wirtz, D., Konstantopoulos, K., and Searson, P.C. (2011) The physics of cancer: the role of physical interactions and mechanical forces in metastasis. *Nat. Rev. Cancer*, **11**, 512–522. doi: 10.1038/nrc3080

12 Shawky, J.H. and Davidson, L.a. (2015) Tissue mechanics and adhesion during embryo development. *Dev. Biol.*, **401**, 152–164. doi: 10.1016/j.ydbio.2014.12.005

13 Janmey, P.a. and Miller, R.T. (2011) Mechanisms of mechanical signaling in development and disease. *J. Cell Sci.*, **124**, 9–18. doi: 10.1242/jcs.071001

14 Plodinec, M., Loparic, M., Monnier, C.a., Obermann, E.C., Zanetti-Dallenbach, R., Oertle, P., Hyotyla, J.T., Aebi, U., Bentires-Alj, M., Lim, R.Y.H., and Schoenenberger., C.-A. (2012) The nanomechanical signature of breast cancer. *Nat. Nanotechnol.*, **7**, 757–765. doi: 10.1038/nnano.2012.167

15 Wyss, H.M.H., Henderson, J.J.M., Byfield, F.J., Bruggeman, L.a., Ding, Y., Huang, C., Suh, J.H., Franke, T., Mele, E., Pollak, M.R., Miner, J.H., Janmey, P.a., Weitz, D.a., and Miller, R.T. (2011) Biophysical properties of normal and diseased renal glomeruli. *Am. J. Physiol. Cell Physiol.*, **300**, 397–405. doi: 10.1152/ajpcell.00438.2010

16 Bonnans, C., Chou, J., and Werb, Z. (2014) Remodelling the extracellular matrix in development and disease. *Nat. Rev. Mol. Cell Biol.*, **15**, 786–801. doi: 10.1038/nrm3904

17 Hoffman, B.D. and Crocker, J.C. (2009) Cell mechanics: dissecting the physical responses of cells to force. *Annu. Rev. Biomed. Eng.*, **11**, 259–288. doi: 10.1146/annurev.bioeng.10.061807.160511

18 Janmey, P.A. and McCulloch, C.A. (2007) Cell mechanics: integrating cell responses to mechanical stimuli. *Annu. Rev. Biomed. Eng.*, **9**, 1–34. doi: 10.1146/annurev.bioeng.9.060906.151927

19 Chen, C.S., Tan, J., and Tien., J. (2004) Mechanotransduction at cell-matrix and cell-cell contacts. *Annu. Rev. Biomed. Eng.*, **6**, 275–302. doi: 10.1146/annurev.bioeng.6.040803.140040

20 Paszek, M.J., Boettiger, D., Weaver, V.M., and Hammer, D.a. (2009) Integrin clustering is driven by mechanical resistance from the glycocalyx and the substrate. *PLoS Comput. Biol.*, **5**, e1000604. doi: 10.1371/journal.pcbi.1000604

21 Plodinec, M. and Schoenenberger, C.-A. (2010) Spatial organization acts on cell signaling: how physical force contributes to the development of cancer. *Breast Cancer Res.*, **12**, 308. doi: 10.1186/bcr2623

22 Salaita, K., Nair, P.M., Petit, R.S., Neve, R.M., Das, D., Gray, J.W., and Groves, J.T. (2010) Restriction of receptor movement alters cellular response: physical force sensing by EphA2. *Science*, **327**, 1380–1385. doi: 10.1126/science.1181729

23 Gao, M., Sotomayor, M., Villa, E., Lee, E.H., and Schulten, K. (2006) Molecular mechanisms of cellular mechanics. *Phys. Chem. Chem. Phys.*, **8**, 3692. doi: 10.1039/b606019f

24 Parsons, J.T., Horwitz, A.R., and Schwartz, M.A. (2010) Cell adhesion: integrating cytoskeletal dynamics and cellular tension. *Nat. Rev. Mol. Cell Biol.*, **11**, 633–643. doi: 10.1038/nrm2957

25 Ridley, A.J., Schwartz, M.A., Burridge, K., Firtel, R.A., Ginsberg, M.H., Borisy, G., Parsons, J.T., and Horwitz, A.R. (2003) Cell migration: integrating signals from front to back. *Science*, **302**, 1704–1709. doi: 10.1126/science.1092053

26 Rotsch, C. and Radmacher, M. (2000) Drug-induced changes of cytoskeletal structure and mechanics in fibroblasts: an atomic force microscopy study. *Biophys. J.*, **78**, 520–535. doi: 10.1016/S0006-3495(00)76614-8

27 Pelling, A.E., Dawson, D.W., Carreon, D.M., Christiansen, J.J., Shen, R.R., Teitell, M.A., and Gimzewski, J.K. (2007) Distinct contributions of microtubule subtypes to cell membrane shape and stability. *Nanomed. Nanotech. Biol. Med.*, **3**, 43–52. doi: 10.1016/j.nano.2006.11.006

28 Ofek, G., Wiltz, D.C., and Athanasiou, K. a. (2009) Contribution of the cytoskeleton to the compressive properties and recovery behavior of single cells. *Biophys. J.*, **97**, 1873–1882. doi: 10.1016/j.bpj.2009.07.050

29 Herrmann, H., Bär, H., Kreplak, L., Strelkov, S.V., and Aebi, U. (2007) Intermediate filaments: from cell architecture to nanomechanics. *Nat. Rev. Mol. Cell Biol.*, **8**, 562–573. doi: 10.1038/nrm2197

30 Schwartz, M.A. and Assoian, R.K. (2001) Integrins and cell proliferation: regulation of cyclin-dependent kinases via cytoplasmic signaling pathways. *J. Cell Sci.*, **114**, 2553–2560. doi: 10.1007/s10555-005-5130-7

31 DuFort, C.C., Paszek, M.J., and Weaver, V.M. (2011) Balancing forces: architectural control of mechanotransduction. *Nat. Rev. Mol. Cell Biol.*, **12**, 308–319. doi: 10.1038/nrm3112

32 Bissell, M.J. and Radisky, D. (2001) Putting tumours in context. *Nat. Rev. Cancer.*, **1**, 46–54. doi: 10.1038/35094059

33 Mammoto, T. and Ingber, D.E. (2010) Mechanical control of tissue and organ development. *Development*, **137**, 1407–1420. doi: 10.1242/dev.024166

34 Levental, K.R., Yu, H., Kass, L., Lakins, J.N., Egeblad, M., Erler, J.T., Fong, S.F.T., Csiszar, K., Giaccia, A., Weninger, W., Yamauchi, M., Gasser, D.L., and Weaver, V.M. (2009) Matrix crosslinking forces tumor progression by enhancing integrin signaling. *Cell*, **139**, 891–906. doi: 10.1016/j.cell.2009.10.027

35 Krouskop, T.A., Wheeler, T.M., Kallel, F., Garra, B.S., and Hall, T. (1998) Elastic moduli of breast and prostate tissues under compression. *Ultrason. Imaging*, **20**, 260–274.

36 Lopez, J.I., Kang, I., You, W.-K., McDonald, D.M., and Weaver, V.M. (2011) *In situ* force mapping of mammary gland transformation. *Integr. Biol.*, **3**, 910. doi: 10.1039/c1ib00043h

37 Staton, C.a., Brown, N.J., and Reed, M.W. (2009) Current status and future prospects for anti-angiogenic therapies in cancer. *Expert Opin. Drug Discov.*, **4**, 961–979. doi: 10.1517/17460440903196737

38 Pfreundschuh, M., Martinez-Martin, D., Mulvihill, E., Wegmann, S., and Muller, D.J. (2014) Multiparametric high-resolution imaging of native proteins by force-distance curve-based AFM. *Nat. Protoc.*, **9**, 1113–1130. doi: 10.1038/nprot.2014.070

39 Cai, J., Jelezko, F., and Plenio, M.B. (2014) Signal transduction and conversion with color centers in diamond and piezo-elements. *Nat. Commun.*, **5**, 1–10. doi: 10.1038/ncomms5065

40 Cappella, B. and Dietler, G. (1999) Force-distance curves by atomic force microscopy. *Surf. Sci. Rep.*, **34**, 1–104. doi: 10.1016/S0167-5729(99)00003-5

41 Oliver, W.C. and Pharr, G.M. (1992) An improved technique for determining hardness and elastic-modulus using load and displacement sensing indentation experiments. *J. Mater. Res.*, **7**, 1564–1583. doi: 10.1557/

42 Solares, S.D. (2014) Challenges and complexities of multifrequency atomic force microscopy in liquid environments. *Beilstein J. Nanotechnol.*, **5**, 298–307. doi: 10.3762/bjnano.5.33

43 Müller, D.J. and Dufrêne, Y.F. (2008) Atomic force microscopy as a multifunctional molecular toolbox in nanobiotechnology. *Nat. Nanotechnol.*, **3**, 261–269. doi: 10.1038/nnano.2008.100

44 Plodinec, M., Loparic, M., and Aebi, U. (2010) Atomic force microscopy for biological imaging and mechanical testing across length scales. *Cold Spring Harb. Protoc.*, **2010**, pdb. top86–pdb. top86. doi: 10.1101/pdb.top86

45 Sader, J.E., Chon, J.W.M., and Mulvane, P. (1999) Calibration of rectangular

atomic force microscope cantilevers. *Rev. Sci. Instrum.*, **70**, 3967.

46 Dufrêne, Y.F., Martínez-Martín, D., Medalsy, I., Alsteens, D., and Müller, D.J. (2013) Multiparametric imaging of biological systems by force-distance curve-based AFM. *Nat. Methods*, **10**, 847–854. doi: 10.1038/nmeth.2602

47 Stolz, M., Raiteri, R., Daniels, A.U., VanLandingham, M.R., Baschong, W., and Aebi, U. (2004) Dynamic elastic modulus of porcine articular cartilage determined at two different levels of tissue organization by indentation-type atomic force microscopy. *Biophys. J.*, **86**, 3269–3283. doi: 10.1016/S0006-3495(04)74375-1

48 Plodinec, M., Loparic, M., Suetterlin, R., Herrmann, H., Aebi, U., and Schoenenberger, C.a. (2011) The nanomechanical properties of rat fibroblasts are modulated by interfering with the vimentin intermediate filament system. *J. Struct. Biol.*, **174**, 476–484. doi: 10.1016/j.jsb.2011.03.011

49 Roduit, C., Sekatski, S., Dietler, G., Catsicas, S., Lafont, F., and Kasas, S. (2009) Stiffness tomography by atomic force microscopy. *Biophys. J.*, **97**, 674–677. doi: 10.1016/j.bpj.2009.05.010

50 Binnig, G., Quate, C.F., and Gerber, C. (1986) Atomic force microscope. *Phys. Rev. Lett.*, **56**, 930–933. doi: 10.1103/PhysRevLett.56.930

51 Engel, A. (1991) Biological applications of scanning probe microscopes. *Annu. Rev. Biophys*, **20**, 79–108.

52 Hoh, J.H. and Schoenenberger, C.a. (1994) Surface morphology and mechanical properties of MDCK monolayers by atomic force microscopy. *J. Cell Sci.*, **107** (Pt 5), 1105–1114.

53 Lekka, M., Laidler, P., Gil, D., Lekki, J., Stachura, Z., and Hrynkiewicz, aZ. (1999) Elasticity of normal and cancerous human bladder cells studied by scanning force microscopy. *Eur. Biophys. J.*, **28**, 312–316. doi: 10.1007/s002490050213

54 Radmacher, M., Fritz, M., Kacher, C.M., Cleveland, J.P., and Hansma, P.K. (1996) Measuring the viscoelastic properties of human platelets with the atomic force microscope. *Biophys. J.*, **70**, 556–567. doi: 10.1016/S0006-3495(96)79602-9

55 Park, S. and Lee, Y.J. (2013) Nano-mechanical compliance of müller cells investigated by atomic force microscopy. *Int. J. Biol. Sci.*, **9**, 702–706. doi: 10.7150/ijbs.6473

56 Lu, Y.B., Pannicke, T., Wei, E.Q., Bringmann, A., Wiedemann, P., Habermann, G., Buse, E., Käs, J.a., and Reichenbach, A. (2013) Biomechanical properties of retinal glial cells: comparative and developmental data. *Exp. Eye Res.*, **113**, 60–65. doi: 10.1016/j.exer.2013.05.012

57 Cross, S.E., Jin, Y.-S., Rao, J., and Gimzewski., J.K. (2007) Nanomechanical analysis of cells from cancer patients. *Nat. Nanotechnol.*, **2**, 780–783. doi: 10.1038/nnano.2007.388

58 Cross, S.E., Jin, Y.-S., Tondre, J., Wong, R., Rao, J., and Gimzewski., J.K. (2008) AFM-based analysis of human metastatic cancer cells. *Nanotechnology*, **19**, 384003. doi: 10.1088/0957-4484/19/38/384003

59 Ludwig, M., Dettmann, W., and Gaub, H.E. (1997) Atomic force microscope imaging contrast based on molecular recognition. *Biophys. J.*, **72**, 445–448. doi: 10.1016/S0006-3495(97)78685-5

60 Fritz, J., Katopodis, A.G., Kolbinger, F., and Anselmetti, D. (1998) Force-mediated kinetics of single P-selectin/ligand complexes observed by atomic force microscopy. *Proc. Natl. Acad. Sci. USA*, **95**, 12283–12288. doi: 10.1073/pnas.95.21.12283

61 Hinterdorfer, P., Baumgartner, W., Gruber, H.J., Schilcher, K., and Schindler, H. (1996) Detection and localization of individual antibody-antigen recognition events by atomic force microscopy. *Proc. Natl. Acad. Sci. USA*, **93**, 3477–3481. doi: 10.1073/pnas.93.8.3477

62 Diez-Perez, A., Güerri, R., Nogues, X., Cáceres, E., Peña, M.J., Mellibovsky, L., Randall, C., Bridges, D., Weaver, J.C., Proctor, A., Brimer, D., Koester, K.J., Ritchie, R.O., and Hansma., P.K. (2010) Microindentation for *in vivo* measurement of bone tissue mechanical properties in humans. *J. Bone Miner. Res.*, **25**, 1877–1885. doi: 10.1002/jbmr.73

63 Hansma, P., Yu, H., Schultz, D., Rodriguez, A., Yurtsev, E.a., Orr, J., Tang, S., Miller, J., Wallace, J., Zok, F., Li, C.,

Souza, R., Proctor, A., Brimer, D., Nogues-Solan, X., Mellbovsky, L., Pena, M.J., Diez-Ferrer, O., Mathews, P., Randall, C., Kuo, A., Chen, C., Peters, M., Kohn, D., Buckley, J., Li, X., Pruitt, L., Diez-Perez, A., Alliston, T., Weaver, V., and Lotz., J. (2009) The tissue diagnostic instrument. *Rev. Sci. Instrum.*, **80**, 54303. doi: 10.1063/1.3127602

64 Müller, D.J. and Dufrêne, Y.F. (2011) Atomic force microscopy: a nanoscopic window on the cell surface. *Trends Cell Biol.*, **21**, 461–469. doi: 10.1016/j.tcb.2011.04.008

65 Gautier, H.O.B., Thompson, A.J., Achouri, S., Koser, D.E., Holtzmann, K., Moeendarbary, E., and Franze, K. (2015) Atomic force microscopy-based force measurements on animal cells and tissues. *Methods Cell Biol.*, **125**, 211–235. doi. 10.1016/bs.mcb.2014.10.005

66 Mow, V.C., Ratcliffe, A., and Poole, A.R. (1992) Cartilage and diarthrodial joints as paradigms for hierarchical materials and structures. *Biomaterials*, **13**, 67–97. doi: 10.1016/0142-9612(92)90001-5

67 Weisenhorn, a.L., Khorsandi, M., Kasas, S., Gotzos, V., and Butt, H.-J. (1999) Deformation and height anomaly of soft surfaces studied with an AFM. *Nanotechnology*, **4**, 106–113. doi: 10.1088/0957-4484/4/2/006

68 Loparic, M., Wirz, D., Daniels, A.U., Raiteri, R., Vanlandingham, M.R., Guex, G., Martin, I., Aebi, U., and Stolz, M. (2010) Micro- and nanomechanical analysis of articular cartilage by indentation-type atomic force microscopy: validation with a gel-microfiber composite. *Biophys. J.*, **98**, 2731–2740. doi: 10.1016/j.bpj.2010.02.013

69 Han, L., Frank, E.H., Greene, J.J., Lee, H.Y., Hung, H.H.K., Grodzinsky, A.J., and Ortiz, C. (2011). Time-dependent nanomechanics of cartilage. *Biophys. J.*, **100**, 1846–1854. doi: 10.1016/j.bpj.2011.02.031

70 Nia, H.T., Han, L., Li, Y., Ortiz, C., and Grodzinsky, A. (2011) Poroelasticity of cartilage at the nanoscale. *Biophys. J.*, **101**, 2304–2313. doi: 10.1016/j.bpj.2011.09.011

71 Sanchez-Adams, J., Wilusz, R.E., and Guilak, F. (2013) Atomic force microscopy reveals regional variations in the micromechanical properties of the pericellular and extracellular matrices of the meniscus. *J. Biomech.*, **46**, 586–592. doi: 10.1016/j.jbiomech.2012.09.003

72 Nia, H.T., Gauci, S.J., Azadi, M., Hung, H.-H., Frank, E., Fosang, A.J., Ortiz, C., and Grodzinsky, A.J. (2015) High-bandwidth AFM-based rheology is a sensitive indicator of early cartilage aggrecan degradation relevant to mouse models of osteoarthritis. *J. Biomech.*, **48**, 162–165. doi: 10.1016/j.jbiomech.2014.11.012

73 Cueru, L., Trunfio sfarghiu, a.M., Bala, Y., Depalle, B., Berthier, Y., and Follet, H. (2011) Mechanical and physicochemical multiscale analysis of cortical bone. *Comput. Methods Biomech. Biomed. Engin.*, **14**, 223–225. doi: 10.1080/10255842.2011.595199

74 Grant, C.A., Brockwell, D.J., Radford, S.E., and Thomson, N.H. (2008) Effects of hydration on the mechanical response of individual collagen fibrils. *Appl. Phys. Lett.*, **92**, 2006–2009. doi: 10.1063/1.2937001

75 Halfter, W., Monnier, C., Müller, D., Oertle, P., Uechi, G., Balasubramani, M., Safi, F., Lim, R., Loparic, M., and Henrich, P.B. (2013) The bi-functional organization of human basement membranes. *PLoS One*, **8**, e67660. doi: 10.1371/journal.pone.0067660

76 Candiello, J., Cole, G.J., and Halfter, W. (2010) Age-dependent changes in the structure, composition and biophysical properties of a human basement membrane. *Matrix Biol.*, **29**, 402–410. doi: 10.1016/j.matbio.2010.03.004

77 Henrich, P.B., Monnier, C.a., Halfter, W., Haritoglou, C., Strauss, R.W., Lim, R.Y.H., and Loparic., M. (2012) Nanoscale topographic and biomechanical studies of the human internal limiting membrane. *Invest. Ophthalmol. Vis. Sci.*, **53**, 2561–2570. doi: 10.1167/iovs.11-8502

78 Candiello, J., Balasubramani, M., Schreiber, E.M., Cole, G.J., Mayer, U.,

Halfter, W., and Lin, H. (2007) Biomechanical properties of native basement membranes. *FEBS J.*, **274**, 2897–2908. doi: 10.1111/j.1742-4658.2007.05823.x

**79** To, M., Goz, A., Camenzind, L., Oertle, P., Candiello, J., Sullivan, M., Henrich, P.B., Loparic, M., Safi, F., Eller, A., and Halfter, W. (2013) Diabetes-induced morphological, biomechanical, and compositional changes in ocular basement membranes. *Exp. Eye Res.*, **116**, 298–307. doi: 10.1016/j.exer.2013.09.011

**80** Engler, A.J. (2004) Myotubes differentiate optimally on substrates with tissue-like stiffness: pathological implications for soft or stiff microenvironments. *J. Cell Biol.*, **166**, 877–887. doi: 10.1083/jcb.200405004

**81** van Zwieten, R.W., Puttini, S., Lekka, M., Witz, G., Gicquel-Zouida, E., Richard, I., Lobrinus, J.a., Chevalley, F., Brune, H., Dietler, G., Kulik, A., Kuntzer, T., and Mermod, N. (2014) Assessing dystrophies and other muscle diseases at the nanometer scale by atomic force microscopy. *Nanomedicine.*, **9**, 393–406.

**82** Puttini, S., Lekka, M., Dorchies, O.M., Saugy, D., Incitti, T., Ruegg, U.T., Bozzoni, I., Kulik, A.J., and Mermod, N. (2009) Gene-mediated restoration of normal myofiber elasticity in dystrophic muscles. *Mol. Ther.*, **17**, 19–25. doi: 10.1038/mt.2008.239

**83** Franze, K., Francke, M., Günter, K., Christ, A.F., Körber, N., Reichenbach, A., and Guck, J. (2011) Spatial mapping of the mechanical properties of the living retina using scanning force microscopy. *Soft Matter.*, **7**, 3147. doi: 10.1039/c0sm01017k

**84** Elkin, B.S., Azeloglu, E.U., Costa, K.D., and Morrison, B. III (2007) Mechanical heterogeneity of the rat hippocampus measured by atomic force microscope indentation. *J. Neurotrauma.*, **24**, 812–822. doi: 10.1089/neu.2006.0169

**85** Christ, A.F., Franze, K., Gautier, H.O.B., Moshayedi, P., Fawcett, J., Franklin, R.J.M., Karadottir, R.T., and Guck, J. (2010) Mechanical difference between white and gray matter in the rat cerebellum measured by scanning force microscopy. *J. Biomech.*, **43**, 2986–2992.

**86** Iwashita, M., Kataoka, N., Toida, K., and Kosodo, Y. (2014) Systematic profiling of spatiotemporal tissue and cellular stiffness in the developing brain. *Development*, **141**, 3793–3798. doi: 10.1242/dev.109637

**87** Lekka, M., Gil, D., Pogoda, K., Dulińska-Litewka, J., Jach, R., Gostek, J., Klymenko, O., Prauzner-Bechcicki, S., Stachura, Z., Wiltowska-Zuber, J., Okoń, K., and Laidler, P. (2012) Cancer cell detection in tissue sections using AFM. *Arch. Biochem. Biophys.*, **518**, 151–156. doi: 10.1016/j.abb.2011.12.013

**88** Mouw, J.K., Yui, Y., Damiano, L., Bainer, R.O., Lakins, J.N., Acerbi, I., Ou, G., Wijekoon, A.C., Levental, K.R., Gilbert, P.M., Hwang, E.S., Chen, Y.-Y., and Weaver, V.M. (2014) Tissue mechanics modulate microRNA-dependent PTEN expression to regulate malignant progression. *Nat. Med.*, **20**, 360–367. doi: 10.1038/nm.3497

**89** Acerbi, I., Cassereau, L., Dean, I., Shi, Q., Au, A., Park, C., Chen, Y.Y., Liphardt, J., Hwang, E.S., and Weaver, V.M. (2015) Human breast cancer invasion and aggression correlates with ECM stiffening and immune cell infiltration. *Integr. Biol.*, **7**, 1120–1134. doi: 10.1039/C5IB00040H

**90** Tian, M., Li, Y., Liu, W., Jin, L., Jiang, X., Wang, X., Ding, Z., Peng, Y., Zhou, J., Fan, J., Cao, Y., Wang, W., and Shi, Y. (2015) The nanomechanical signature of liver cancer tissues and its molecular origin. *Nanoscale*, **7**, 12998–13010. doi: 10.1039/c5nr02192h

**91** Plodinec, M. and Lim, R.Y.H. (2015) Nanomechanical characterization of living mammary tissues by atomic force microscopy. *Methods Mol. Biol.*, **1293**, 231–246. doi: 10.1007/978-1-4939-2519-3_14

**92** Han, L., Grodzinsky, A.J., and Ortiz., C. (2011) Nanomechanics of the cartilage extracellular matrix. *Annu. Rev. Mater. Res.*, **41**, 133–168. doi: 10.1146/annurev-matsci-062910-100431

**93** Mak, A.F. (1986) The apparent viscoelastic behavior of articular cartilage—the contributions from the

intrinsic matrix viscoelasticity and interstitial fluid flows. *J. Biomech. Eng.*, **108**, 128–130.

94 Mow, V.C., Kuei, S.C., Lai, W.M., and Armstrong, C.G. (1980) Biphasic creep and stress relaxation of articular cartilage in compression: theory and experiments. *J. Biomech. Eng.*, **102**, 73–84.

95 Maroudas, A., Bayliss, M.T., Uchitel-Kaushansky, N., Schneiderman, R., and Gilav, E. (1998) Aggrecan turnover in human articular cartilage: use of aspartic acid racemization as a marker of molecular age. *Arch. Biochem. Biophys.*, **350**, 61–71. doi: 10.1006/abbi.1997.0492

96 Bayliss, M.T. and Ali, S.Y. (1978) Age-related changes in the composition and structure of human articular-cartilage proteoglycans. *Biochem. J.*, **176**, 683–693.

97 Bayliss, M.T. and Roughley, P.J. (1985) The properties of proteoglycan prepared from human articular cartilage by using associative caesium chloride gradients of high and low starting densities. *Biochem. J.*, **232**, 111–117.

98 Roughley, P.J. and White, R.J. (1980) Age-related changes in the structure of the proteoglycan subunits from human articular cartilage. *J. Biol. Chem.*, **255**, 217–224.

99 Bank, R.A., Bayliss, M.T., Lafeber, F.P.J.G., Maroudas, A., and Tekoppele., J.M. (1998) Ageing and zonal variation in post-translational modification of collagen in normal human articular cartilage. *Biochem. J.*, **351**, 345–351.

100 Bhosale, A.M. and Richardson, J.B. (2008) Articular cartilage: structure, injuries and review of management. *Br. Med. Bull.*, **87**, 77–95. doi: 10.1093/bmb/ldn025

101 Aspden, R.M. and Hukins, D.W. (1981) Collagen organization in articular cartilage, determined by X-ray diffraction, and its relationship to tissue function. *Proc. R. Soc. Lond. B. Biol. Sci.*, **212**, 299–304. doi: 10.1098/rspb.1981.0040

102 Miller, E.J. and Gay, S. (1987) *Structural and Contractile Proteins Part D: Extracellular Matrix*, vol. **144**, Elsevier, pp 3–41.

103 Yasuda, T., Tchetina, E., Ohsawa, K., Roughley, P.J., Wu, W., Mousa, A., Ionescu, M., Pidoux, I., and Poole, A.R. (2006) Peptides of type II collagen can induce the cleavage of type II collagen and aggrecan in articular cartilage. *Matrix Biol.*, **25**, 419–429. doi: 10.1016/j.matbio.2006.06.004

104 Blaschke, U.K., Eikenberry, E.F., Hulmes, D.J.S., Galla, H.J., and Bruckner, P. (2000) Collagen XI nucleates self-assembly and limits lateral growth of cartilage fibrils. *J. Biol. Chem.*, **275**, 10370–10378. doi: 10.1074/jbc.275.14.10370

105 Bruckner, P. and van der Rest, M. (1994) Structure and function of cartilage collagens. *Microsc. Res Tech.*, **28**, 378–384.

106 McCutchen, C.W. (1959) Mechanism of animal joint sponge-hydrostatic and weeping bearings. *Nature*, **184**, 1284–1285.

107 Hootman, J.M. and Helmick, C.G. (2006) Projections of US prevalence of arthritis and associated activity limitations. *Arthritis Rheum.*, **54**, 226–229. doi: 10.1002/art.21562

108 Stockwell, R.A. (1967) The cell density of human articular and costal cartilage. *J. Anat.*, **101**, 753–763.

109 Vignon, E., Arlot, M., Patricot, L.M., and Vignon, G. (1976) Cell density of human femoral-head cartilage. *Clin. Orthop. Relat. Res.*, **121**, 303–308.

110 Scott, J.E., Bosworth, T.R., Cribb, a.M., and Taylor, J.R. (1994) The chemical morphology of age-related changes in human intervertebral disc glycosaminoglycans from cervical, thoracic and lumbar nucleus pulposus and annulus fibrosus. *J. Anat.*, **184** (Pt 1), 73–82.

111 Butcher, D.T., Alliston, T., and Weaver, V.M. (2009) A tense situation: forcing tumour progression. *Nat. Rev. Cancer.*, **9**, 108–122. doi: 10.1038/nrc2544

112 Naylor, M.J., Li, N., Cheung, J., Lowe, E.T., Lambert, E., Marlow, R., Wang, P., Schatzmann, F., Wintermantel, T., Schüetz, G., Clarke, A.R., Mueller, U., Hynes, N.E., and Streuli, C.H. (2005) Ablation of beta1 integrin in mammary epithelium reveals a key role for integrin in glandular morphogenesis and differentiation. *J. Cell Biol.*, **171**, 717–728. doi: 10.1083/jcb.200503144

113 Kass, L., Erler, J.T., Dembo, M., and Weaver, V.M. (2007) Mammary epithelial cell: Influence of extracellular matrix composition and organization during development and tumorigenesis. *Int. J. Biochem. Cell Biol.*, **39**, 1987–1994. doi: 10.1016/j.biocel.2007.06.025

114 Bissell, M.J., Radisky, D.C., Rizki, A., Weaver, V.M., and Petersen, O.W. (2002) The organizing principle: microenvironmental influences in the normal and malignant breast. *Differentiation*, **70**, 537–546. doi: 10.1046/j.1432-0436.2002.700907.x

115 Schwartz, M.A. and DeSimone, D.W. (2008) Cell adhesion receptors in mechanotransduction. *Curr. Opin. Cell Biol.*, **20**, 551–556. doi: 10.1016/j.ceb.2008.05.005

116 Anderson, A.R.a., Weaver, A.M., Cummings, P.T., and Quaranta., V. (2006) Tumor morphology and phenotypic evolution driven by selective pressure from the microenvironment. *Cell*, **127**, 905–915. doi: 10.1016/j.cell.2006.09.042

117 Elston, C.W. and Ellis, I.O. (1991) Pathological prognostic factors in breast cancer. I. The value of histological grade in breast cancer: experience from a large study with long-term follow-up. *Histopathology*, **19**, 403–410.

118 Sarntinoranont, M., Rooney, F., and Ferrari, M. (2003) Interstitial stress and fluid pressure within a growing tumor. *Ann. Biomed. Eng.*, **31**, 327–335. doi: 10.1114/1.1554923

119 Tlsty, T.D. and Coussens, L.M. (2006) Tumor stroma and regulation of cancer development. *Annu. Rev. Pathol. Mech. Dis.*, **1**, 119–150. doi: 10.1146/annurev.pathol.1.110304.100224

120 Sugarbaker, P.H. (1993) Metastatic inefficiency: the scientific basis for resection of liver metastases from colorectal cancer. *J. Surg. Oncol. Suppl.*, **3**, 158–160.

121 Wyckoff, J.B., Jones, J.G., Condeelis, J.S., and Segall, J.E. (2000) A critical step in metastasis: *in vivo* analysis of intravasation at the primary tumor. *Cancer Res.*, **60**, 2504–2511.

122 Condeelis, J. and Pollard, J.W. (2006) Macrophages: obligate partners for tumor cell migration, invasion, and metastasis. *Cell*, **124**, 263–266. doi: 10.1016/j.cell.2006.01.007

123 Fritsch, A., Höckel, M., Kiessling, T., Nnetu, K.D., Wetzel, F., Zink, M., and Käs, J.a. (2010) Are biomechanical changes necessary for tumour progression? *Nat. Phys.*, **6**, 730–732. doi: 10.1038/nphys1800

124 Paszek, M.J., Zahir, N., Johnson, K.R., Lakins, J.N., Rozenberg, G.I., Gefen, A., Reinhart-King, C.a., Margulies, S.S., Dembo, M., Boettiger, D., Hammer, D.a., and Weaver, V.M. (2005) Tensional homeostasis and the malignant phenotype. *Cancer Cell*, **8**, 241–254. doi: 10.1016/j.ccr.2005.08.010

125 Paszek, M.J. and Weaver, V.M. (2004) The tension mounts: mechanics meets morphogenesis and malignancy. *J. Mammary Gland Biol. Neoplasia.*, **9**, 325–342. doi: 10.1007/s10911-004-1404-x

126 Lin, E.Y., Jones, J.G., Li, P., Zhu, L., Whitney, K.D., Muller, W.J., and Pollard, J.W. (2003) Progression to malignancy in the polyoma middle T oncoprotein mouse breast cancer model provides a reliable model for human diseases. *Am. J. Pathol.*, **163**, 2113–2126. doi: 10.1016/S0002-9440(10)63568-7

127 Chen, K.D., Li, Y.S., Kim, M., Li, S., Yuan, S., Chien, S., and Shyy, J.Y. (1999) Mechanotransduction in response to shear stress. Roles of receptor tyrosine kinases, integrins, and Shc. *J. Biol. Chem.*, **274**, 18393–18400. doi: 10.1074/jbc.274.26.18393

128 Conley, S.J., Gheordunescu, E., Kakarala, P., Newman, B., Korkaya, H., Heath, a.N., Clouthier, S.G., and Wicha., M.S. (2012) Antiangiogenic agents increase breast cancer stem cells via the generation of tumor hypoxia. *Proc. Natl. Acad. Sci. USA*, **109**, 2784–2789. doi: 10.1073/pnas.1018866109

129 Sarioglu, a.F., Aceto, N., Kojic, N., Donaldson, M.C., Zeinali, M., Hamza, B., Engstrom, A., Zhu, H., Sundaresan, T.K., Miyamoto, D.T., Luo, X., Bardia, A., Wittner, B.S., Ramaswamy, S., Shioda, T., Ting, D.T., Stott, S.L., Kapur, R.,

Maheswaran, S., Haber, D.a., and Toner, M. (2015) A microfluidic device for label-free, physical capture of circulating tumor cell clusters. *Nat. Methods.*, **12**, 1–10. doi: 10.1038/nmeth.3404

**130** Aceto, N., Bardia, A., Miyamoto, D.T., Donaldson, M.C., Wittner, B.S., Spencer, J.a., Yu, M., Pely, A., Engstrom, A., Zhu, H., Brannigan, B.W., Kapur, R., Stott, S.L., Shioda, T., Ramaswamy, S., Ting, D.T., Lin, C.P., Toner, M., Haber, D.A., and Maheswaran., S. (2014) Circulating tumor cell clusters are oligoclonal precursors of breast cancer metastasis. *Cell*, **158**, 1110–1122. doi: 10.1016/j.cell.2014.07.013

**131** Folkman, J. (2007) Angiogenesis: an organizing principle for drug discovery? *Nat. Rev. Drug Discov.*, **6**, 273–286. doi: 10.1038/nrd2115

**132** Burstein, H.J., Elias, A.D., Rugo, H.S., Cobleigh, M.a., Wolff, A.C., Eisenberg, P.D., Lehman, M., Adams, B.J., Bello, C.L., DePrimo, S.E., Baum, C.M., and Miller, K.D. (2008) Phase II study of sunitinib malate, an oral multitargeted tyrosine kinase inhibitor, in patients with metastatic breast cancer previously treated with an anthracycline and a taxane. *J. Clin. Oncol.*, **26**, 1810–1816. doi: 10.1200/JCO.2007.14.5375

**133** Bergers, G. and Hanahan, D. (2008) Modes of resistance to anti-angiogenic therapy. *Nat. Rev. Cancer.*, **8**, 592–603. doi: 10.1038/nrc2442

**134** Pàez-Ribes, M., Allen, E., Hudock, J., Takeda, T., Okuyama, H., Viñals, F., Inoue, M., Bergers, G., Hanahan, D., and Casanovas, O. (2009) Antiangiogenic therapy elicits malignant progression of tumors to increased local invasion and distant metastasis. *Cancer Cell*, **15**, 220–231. doi: 10.1016/j.ccr.2009.01.027

**135** De Bock, K., Mazzone, M., and Carmeliet, P. (2011) Antiangiogenic therapy, hypoxia, and metastasis: risky liaisons, or not? *Nat. Rev. Clin. Oncol.*, **8**, 393–404. doi: 10.1038/nrclinonc.2011.83

**136** Hanahan, D. and Weinberg, R.A. (2011) Hallmarks of cancer: the next generation. *Cell*, **144**, 646–674. doi: 10.1016/j.cell.2011.02.013

**137** Blache, U., Silván, U., Plodinec, M., Suetterlin, R., Jakob, R., Klebba, I., Bentires-Alj, M., Aebi, U., and Schoenenberger, C.-A. (2013) A tumorigenic actin mutant alters fibroblast morphology and multicellular assembly properties. *Cytoskeleton (Hoboken)*, **70**, 635–650. doi: 10.1002/cm.21120

# Part Four
# Most Common Diseases: Caries, Musculoskeletal Diseases, Incontinence, Allergies

# 12
# Revealing the Nano-Architecture of Human Hard and Soft Tissues by Spatially Resolved Hard X-Ray Scattering

*Hans Deyhle and Bert Müller*

*University of Basel, Department of Biomedical Engineering, Biomaterials Science Center, Gewerbestrasse 14, 4123 Allschwil, Switzerland*

## 12.1
## Introduction

Human tissues are highly organized anisotropic structures, hierarchically ordered from the macroscopic down to the nanometer scale. These biologically generated materials are usually highly specialized and often provide a unique performance for the period of several decades. For example, human enamel consists of ordered hydroxyapatite crystallites organized in a fibrous continuum. The highly anisotropic organization and interaction of these components makes human enamel about three times tougher than its geological counterpart and much less brittle than sintered hydroxyapatite [1]. It is therefore of interest, to understand the synergetic structure of such tissues.

For this purpose, hard X-rays are of particular interest, because the deep penetration allows nondestructively probing the interior of specimens close to physiological conditions.

Radiography has been available for more than a century. Medical doctors routinely use this modality to image human tissues. Computed tomography (CT), or more precisely hard X-ray tomography in absorption contrast mode, has been implemented in daily clinical diagnosis. In both cases, the attenuation of the X-ray beam intensity traversing the tissues is measured. Because of the relatively low X-ray attenuation by the soft tissue components, the hard X-ray techniques concentrate on imaging hard tissues such as bone and tooth crowns. More recently, hard X-ray imaging techniques in phase contrast mode became available, which are much better suitable for the investigation of soft tissue components owing to their increased sensitivity for materials with low atomic numbers including carbon. These sophisticated methods allow detecting the phase shift generally described by the real part of the refractive index.

The spatial resolution of the real-space imaging techniques is ultimately limited by the wavelength of the probe. Hard X-rays have a wavelength of the order

*Nanoscience and Nanotechnology for Human Health,* First Edition. Edited by Bert Müller and Marcel Van de Voorde.

of 0.1 nm. The spatial resolution of CT and radiography, however, is not better than a fraction of a micrometer, if one sets special X-ray optics aside. These contemporary real-space imaging techniques gave the possibility to image individual human cells [2,3].

Subcellular components, that is, anatomical structures on the true nanometer level are commonly imaged using electron microscopy. These experiments need high-vacuum conditions and, thus, a specimen preparation procedure that transforms the tissues into states far from physiological conditions. As the electrons strongly interact with matter, the imaging restricts to surfaces or thin sections of the human tissue.

For about a century, we know that X-rays can reveal atomic structures. X-ray scattering allows for the exact determination of arrangements from periodic features on the nanometer scale. It has been shown that the minerals in bones and teeth as well as the myelin sheaths in human brain tissues and collagen fibers of cartilage give rise to such periodicities and the related signals in scattering pattern. X-ray scattering has found increasing application in the medical research for the characterization of the nanoarchitecture of tissues and their components. Its combination with two-dimensional scanning allows mapping quantities as nanoscale anisotropy or preferential orientation over macroscopic specimens with micrometer resolution [4,5]. The present chapter introduces the experimental principles and selected applications in studying soft and hard tissues, that is, the breast, brain, parts of joints, and tooth crowns.

## 12.2 Spatially Resolved Hard X-Ray Scattering

### 12.2.1 Introductory Remarks on X-Ray Scattering

As X-ray diffraction, the X-ray scattering techniques belong to the reciprocal space or *k*-space, as they are based on an inverse relationship between the angles of X-rays scattered by the tissues and real-space nanometer periodicities of the tissues.

One can distinguish between two experimental setups: X-ray diffraction, or *wide-angle X-ray scattering* (WAXS), which is used to gain insight about the atomic lattice structure of crystals or crystallites, and *small-angle X-ray scattering* (SAXS), which deals with structures between 1 and several 100 nm. The underlying physical principles, however, are the same. The X-rays impinging on the tissues excite electrons, which in return emit secondary waves that interfere with each other [6]. The scattered waves are coherent, and their amplitudes add linearly. Depending on the tissue morphology, constructive interference occurs at well-defined angles. By measuring these angles, information about the relative positions of the electrons can be derived. It should be noted that one can restrict the description on coherent scattering, since at small angles the incoherent portion is negligible [6].

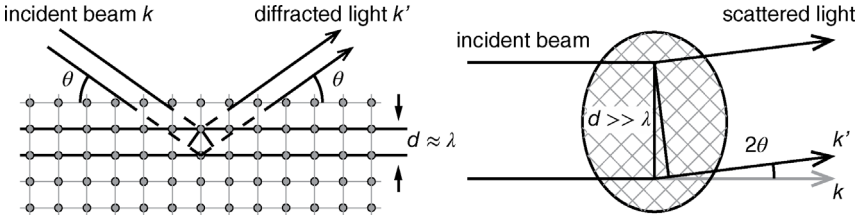


**Figure 12.1** Reciprocal relationship between scattering angle and scattering feature dimension. At dimension $d$ close to the wavelength of the X-rays, the electrons can be considered to be located at the position of the atoms, and information about the lattice structure of the specimen is obtained at large angles. At dimensions $d$ significantly larger than the wavelength, small-angle scattering occurs, providing information about the electron density distribution.

Within crystals the electrons are localized at the atoms. The relation between the crystallographic structure and the scattering angle can be described by the Bragg equation

$$\lambda = 2d \sin\theta, \tag{12.1}$$

where $\lambda$ denotes the wavelength of the X-rays, $d$ the spacing between atomic lattice planes, and $\theta$ the scattering angle, under which constructive interference occurs (cf. Figure 12.1). If the size of the inspected structures is of the order of magnitude of the X-ray wavelength, as is the case for crystal lattices, the scattering angles will be large, and the technique is termed WAXS. Diffraction peaks appear, when the Bragg equation is satisfied.

By collecting the positions of several diffraction peaks and comparing them with crystallographic databases, it is possible to reconstruct the lattice structure of the investigated crystal. It should be noted that the position of the diffraction peaks depends on crystal orientation; they lay in a plane parallel to the direction of the incident X-rays and perpendicular to the related lattice planes. Therefore, in anisotropic specimens, diffraction also provides information about crystal orientation.

If the dimension $d$ of the investigated objects becomes much larger than the wavelength, the scattering angle will conversely get small (cf. Figure 12.1). When observing objects orders of magnitude larger than the atomic scale, it is practical to consider the electron density distribution $\rho(x)$, that is, the number of electrons per unit volume, rather than electrons localized at defined positions. Then, all electrons contribute to the scattering, and the scattered signal is the superposition of all contributions. If a specimen presents a homogeneous electron density, the individual contributions will cancel each other out. Thus, small-angle scattering only occurs when electron density inhomogeneity in the nanometer range exists. Since the scattering angle is dependent on the wavelength $\lambda$ of the incident X-rays, it is useful and common to introduce the scattering vector or momentum transfer $q$, defined as

$$q = \frac{4\pi}{\lambda}\sin\theta = \frac{2\pi}{\lambda}|\boldsymbol{k}' - \boldsymbol{k}|, \tag{12.2}$$

where $\theta$ indicates the scattering angle. $\boldsymbol{k}$ and $\boldsymbol{k}'$ are unit vectors in the direction of the incoming and outgoing waves, respectively [6] (cf. Figure 12.1).

The resulting scattered amplitude $A$ is then given by integrating over the contribution from all electrons as

$$A(q) = \int dV \cdot \rho(r) e^{-iqr}, \tag{12.3}$$

when the observer is located at distances much greater than the specimen size. Note that in experiments, the intensity $I(q)$ is recorded. This implies that the phase information is lost, making a back transform of the recorded intensities to the electron density distribution impossible. Thus, only derived quantities can be obtained from diffraction or scattering patterns. For a thorough treatment of SAXS formalism, see references [6,7].

### 12.2.2 Experimental Setup for X-Ray Scattering

The scheme of a scattering experiment can be described as follows. A narrow incident beam impinges on the specimen, where the X-rays interact with the electrons, and the scattered intensity is collected some distance away. The precise distance between specimen and detector can be obtained by measuring standards with well-known periodicities, for example, silver behenate (http://www.esrf.eu/UsersAndScience/Experiments/CRG/BM26/SaxsWaxs/Silverbehenate).

Only a fraction of the incoming photons are scattered, the majority is either absorbed in the specimen or transmitted. The transmitted, or direct, beam is generally collected by a beamstop in front of the detector. This allows tuning the sensitivity of the detector to the intensity of the SAXS signal and avoiding possible damage to the detector. It should be noted that the beamstop not only effectively blocks the direct beam, but also the scattering at very small angles. Therefore, a small beamstop is generally desirable. By mounting a photon counting device, for example a diode, on the beamstop, it is possible to measure the X-ray attenuation simultaneously. This is of particular interest for inhomogeneous specimens, since also the scattered intensity is attenuated by the specimen. It is also directly proportional to specimen thickness. Thus, for a known wavelength $\lambda$ the scattered intensity I is proportional to

$$I \propto I_0 \cdot t \cdot e^{-\mu t}, \tag{12.4}$$

where $\mu$ is the linear attenuation coefficient for the specimen at wavelength $\lambda$, $I_0$ and $I$ are the incoming and scattered intensities, respectively, and $t$ is the specimen thickness. The optimal specimen thickness, where the scattered intensity is maximal, corresponds to $t=1/\mu$ [6]. The specimen thickness should always be chosen so that the beam illuminates a reasonable volume. If the attenuation is known, the scattered intensity can be corrected by the specimen transmission.

The smallest angles, where a SAXS signal can be measured, is given by the size of the beamstop, which in return is determined by the cross sectional size of the

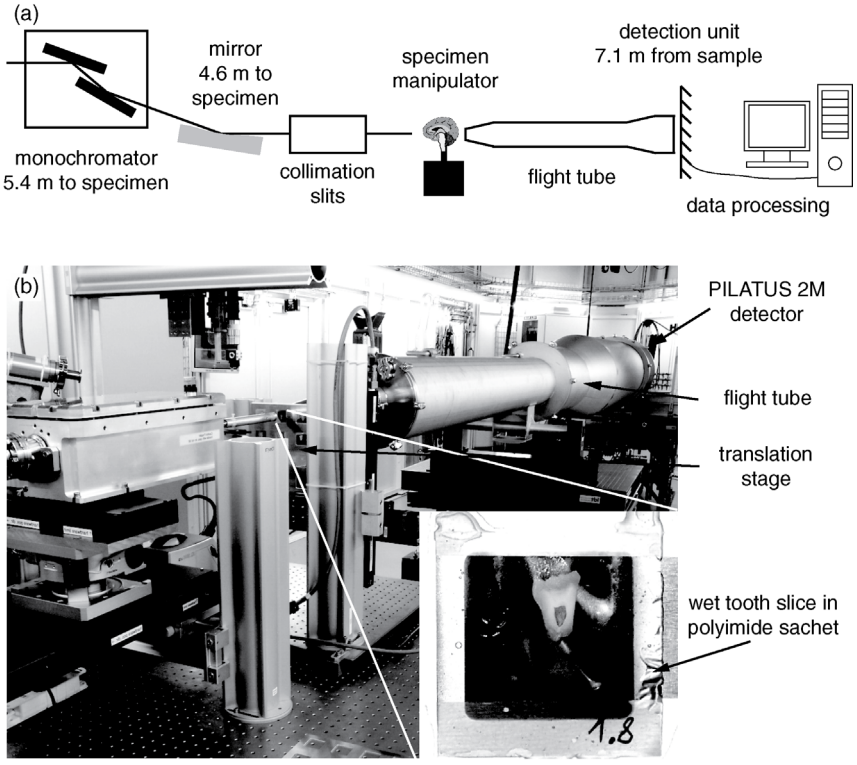


**Figure 12.2** (a) Schematic representation of the cSAXS beamline at the Swiss Light Source, Villigen, Switzerland. (Adapted from Ref. [9]. With permission from Springer-Verlag Berlin Heidelberg.) (b) The end station of the cSAXS beamline at the Swiss Light Source, Villigen, Switzerland. The tissue of interest, here a slice of a human tooth, can be kept under wet conditions at a predefined temperature. (Adapted from Ref. [9]. With permission from Springer-Verlag Berlin Heidelberg.)

direct beam. The small direct beam size is generally obtained with a system of collimation slits or pinholes, depending on setup, resulting in beam sizes generally below 200 µm at the position of the specimen.

Figure 12.2a shows a schematic representation of the SAXS setup at the cSAXS beamline located at the Swiss Light Source storage ring (Paul Scherrer Institut, Villigen, Switzerland) [4]. The wavelength for the experiment is selected by a monochromator, and the beam is focused to about 20 µm × 20 µm at the specimen location by the monochromator and a mirror. It is further collimated by a system of horizontal and vertical slits. The specimen is mounted on a motorized $x$–$y$-stage for positioning, and the scattered light is collected with a PILATUS single photon counting detector [8]. The direct beam is blocked by a beamstop in front of the detector, equipped with a proportional counting diode. A flight tube is placed between the specimen and the detector. It can be either

evacuated, or filled with inert gas, to minimize air scattering. Figure 12.2b shows a photograph of the end station.

In order to operate an efficient spatially resolved SAXS system, powerful personal computers and dedicated software are required.

### 12.2.3
### Two-Dimensional Scanning Small-Angle X-Ray Scattering

SAXS measurements can be combined with two-dimensional scanning to obtain information on the nanometer range over macroscopic areas [4,5]. Then, the specimen, here the tissue of interest, is scanned in raster fashion through the beam by means of a motorized $x$–$y$-stage. A scattering pattern is acquired at each position, allowing creating a two-dimensional map over extended areas (cf. Figure 12.3). Depending on the actual set-up, one may need about 1 h beamtime to record an area of 1 cm × 1 cm with a raster of 10 µm × 10 µm.

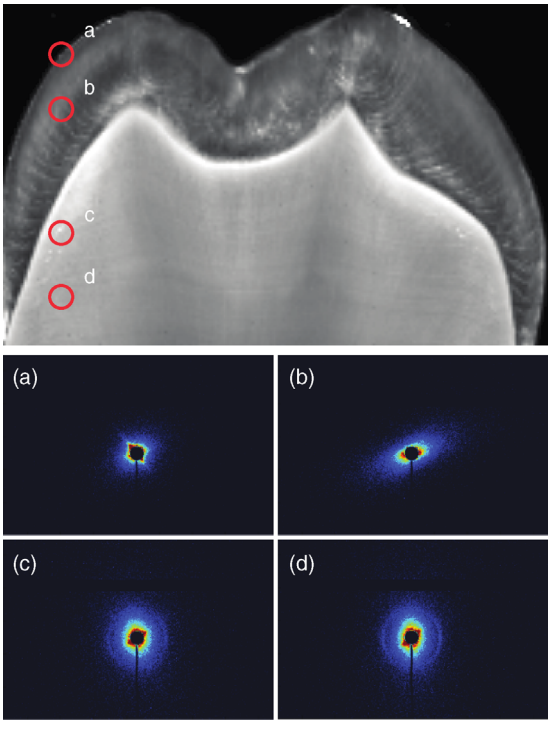


**Figure 12.3** The tooth slice several hundred micrometer thick is scanned through the collimated X-ray beam in $x$ and $y$ directions (cf. Figure 12.2). At each position a SAXS pattern is acquired, and nanoscale information is mapped over macroscopic areas. (Adapted from Ref. [10]. With permission from Springer Science+Business Media B.V.)

12.2.4
**Scattering Pattern Analysis**

After acquisition, the scattering pattern is further processed, integrating the intensity values in radial or azimuthal directions, as depicted in Figure 12.4. In practice, this is often performed by dividing the scattering patterns into radial segments, and averaging, in each segment, the intensity of all pixels with the same distance to the beam center [4]. Several bits of information can be extracted from the obtained curves. The radial plots, where the intensity $I$ is plotted against the scattering angle, or the scattering vector $q$, holds information about shape and size distribution of the scattering features within the specimen [6,7]. Alternatively, preferential orientation and anisotropy of periodicities of special interest can be observed by plotting the SAXS intensity against the azimuthal position. If the scattering features exhibit one preferential orientation, the azimuthal plot will display two peaks, reflecting the central symmetry of the scattering pattern. The preferential orientation can be extracted from the peak position with respect to the vertical direction. Since the scattering signal is

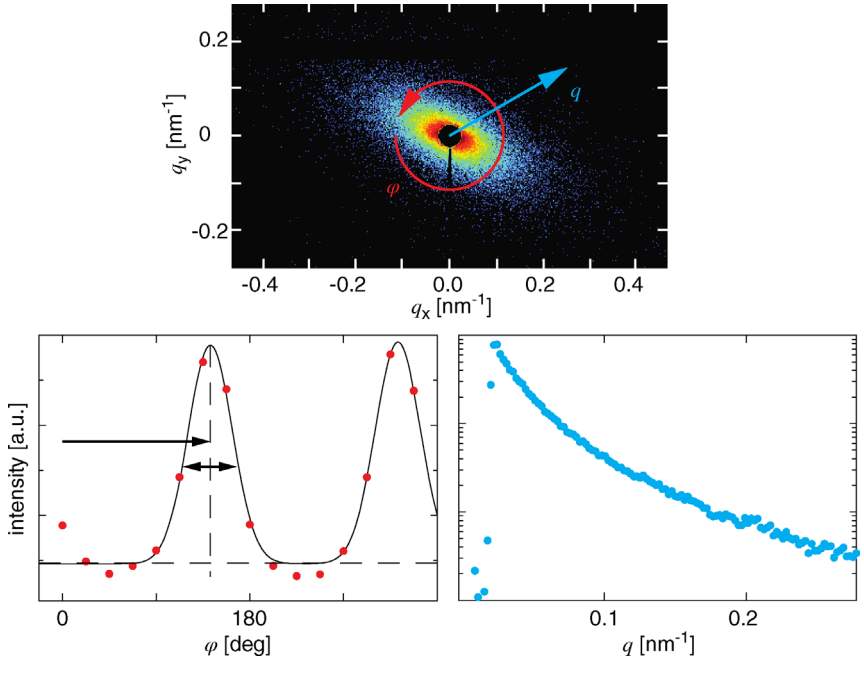


**Figure 12.4** The two-dimensional SAXS pattern can be integrated radially along q or azimuthally along $\varphi$. The I versus q plot is linked to the shape and the size distribution of the scattering features within the specimen/tissue. The azimuthal plot along $\varphi$ provides information about specimen/tissue anisotropy. The q-values smaller than a certain cut-off are inaccessible because of the beamstop.

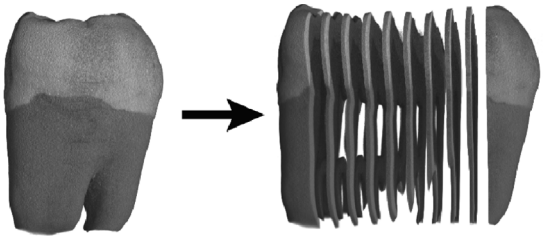

**Figure 12.5** Serial sectioning of a human third molar into slices each about 500 μm thin.

typically oriented perpendicular to the largest extension of structures like rods and platelets, the preferential orientation of these features can be deduced. A measure for the anisotropy and physical spread of the scattering nanofeatures can be deduced by analyzing the shape of the scattered intensity [5,11]. Thus, depending on the extracted information, several types of *contrast* can be obtained from a single SAXS measurement. Integration has the added benefit of drastically reducing data size. A thorough treatment and additional parameters can be found, for example, in references [4,12].

### 12.2.5
### Tissue Preparation

As stated in Section 12.2.4, specimen thickness has to be carefully chosen prior to performing the experiment. For specimens from human tissues, generally having a size in the range of a few to several cm, this involves sectioning into thin slices.

Scattered intensity increases linearly with specimen thickness; therefore, thickness should be chosen appropriately to ensure sufficient signal. Scattered intensity is, however, also attenuated within the specimen, requiring the specimen to be thin enough so that a reasonable amount of photons reaches the detector. Furthermore, SAXS measurements are of projective nature, meaning that resolution is limited to the specimen thickness. This is of particular interest for human specimens, where changes on structural organization might happen in the micrometer range, or even below, or interfaces between adjacent tissues are present. Different structures overlapping along the beam will be projected on the same spot. Separating their contribution to the scattering pattern obtained in this manner is often infeasible and thus hinders data interpretation. The projective nature of the method also implies that sequential sectioning might be required to obtain information on volumetric specimens (cf. Figure 12.5).

It should also be noted that SAXS is generally only sensitive to features lying in the plane perpendicular to the direction $\boldsymbol{k}$ of the incident X-ray beam, because for small scattering angles $\theta$, the scattering vector $q$ is almost perpendicular to $\boldsymbol{k}$. The sectioning direction of the specimen is therefore crucial. Highly oriented

structures might remain invisible in the scattering pattern if the sectioning plane is inappropriately selected.

Since vacuum is not a necessary requirement for X-ray experiments, specimen environment can be chosen to best suit specimen specifications. For example, a wet environment can be realized by storing specimens in sachets (cf. Figure 12.2). Special care should be taken that the sachet material exhibits low and especially uniform scattering (cf. Section 12.6). For example, polyimide is routinely used at the cSAXS beamline to hold specimens wet during the measurements.

## 12.3
## Nanoanatomy of Human Hard and Soft Tissues

### 12.3.1
### Human Tooth

Figure 12.6 shows processed scanning SAXS data of a human tooth slice for the range corresponding to 60 and 70 nm. In Figure 12.6a, the total scattered intensity is represented, which is related to the abundance of periodicities in this nanometer range.

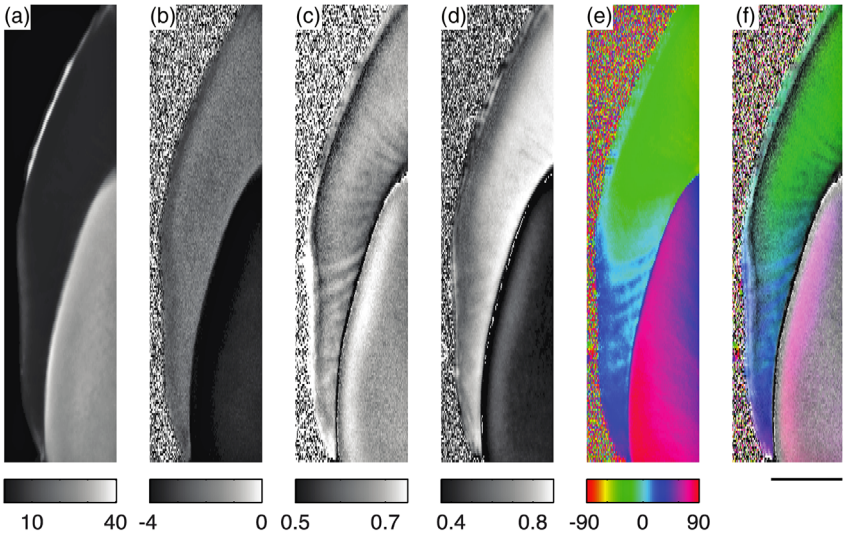


**Figure 12.6** Several types of contrast can be extracted from the scattering patterns. (a) Total scattered intensity in counts per pixel. (b) Intensity exponent. (c) FWHM of the azimuthal scattering distribution in radians. (d) Anisotropy, that is, the amount of anisotropic scattering. (e) Preferential orientation of the scattering signal with respect to the vertical direction. (f) Several contrast types can be combined within one image. Here, the color indicates the preferential orientation, the saturation gives the FWHM, or physical spread of the scatterers, and the intensity codes the anisotropy. The length bar corresponds to 1 mm.

Figure 12.6b displays the *intensity exponent* $\alpha$, which is derived fitting the $I$–$q$ curve with the power law $q^{\alpha}$. The exponent $\alpha$ is linked to the shape of the scattering features, corresponding to −1 for needle and rod-like structures and to −2 for platelets and disks [7]. Note that this relationship is only valid for specific $q$-ranges dependent on the scattering feature sizes and for dilute solutions [6,7]. Therefore, these conditions are hardly met in the densely packed enamel and dentin. Nonetheless, the exponent allows distinguishing enamel from dentin, and even gives rise to contrast within certain regions of the enamel. The images of Figure 12.6c and d show some aspects of the anisotropy within the tooth crown. The image in Figure 12.6c relates to the physical spread of the scattering features, whereas the image in Figure 12.6d shows the ratio of oriented to total scattering. The alternating brighter and darker regions in enamel correspond to the Hunter–Schreger bands well known from optical micrographs [13]. They originate from bundles of coaligned enamel rods [14]. In enamel, the scattering features are almost exclusively oriented. They are more isotropic in dentin. The preferential orientation of the scattering signal is visualized in Figure 12.6e using the color code according to the bar. Zero means vertical orientation.

In order to provide the information to the viewer in concentrated manner, the contrast of selected representations are often combined. Figure 12.6f shows such an example, which is appreciated by medical experts including anatomists.

Each periodic structure gives rise to a related peak in the $I$–$q$ plot. For example, the main organic component of dentin, collagen-I, exhibits periodic gap zones at the 67 nm spacing [15]. Figure 12.7a contains characteristic $I$–$q$ diagrams for dentin (red color) and enamel (blue color). The first order collagen peak causes a bump in the curve for dentin. Such a peak is absent for enamel. The intensity below the bump can be approximated with a power law $q^{\alpha}$ with $\alpha = -2.6$. Then, the intensity above the fit is exclusively associated with the occurrence of collagen-I [16], which can be processed separately. The associated results are given in the images of Figure 12.7b and d. Here, the scattering potential is coded by brightness, anisotropy by color saturation, and preferential orientation of the scattering signal by color according to the color wheel. In Figure 12.7b, the total intensity was processed, which mainly originates from the inorganic components [16]. The preferential orientation of the scattering signal in enamel is mostly parallel to the dentin–enamel junction (DEJ), whereas in dentin it is perpendicularly oriented. In Figure 12.7d, only the collagen-related intensity is displayed. In dentin, the preferential orientation of the collagen-related scattering signal is perpendicular to the one originating from the inorganic components, indicating a close organizational relation between these essential components.

The investigated $q$-range can be shifted to higher values by reducing the specimen-detector distance (cf. Figure 12.8). In this regime, termed wide-angle X-ray scattering (WAXS), diffraction patterns of crystallites can be accessed. Figure 12.9 shows spatially resolved WAXS data of a selected human tooth slice. Since the main inorganic component of the crown is hydroxyapatite, most peaks can be associated to this lattice structure. Similarly to SAXS data processing, the

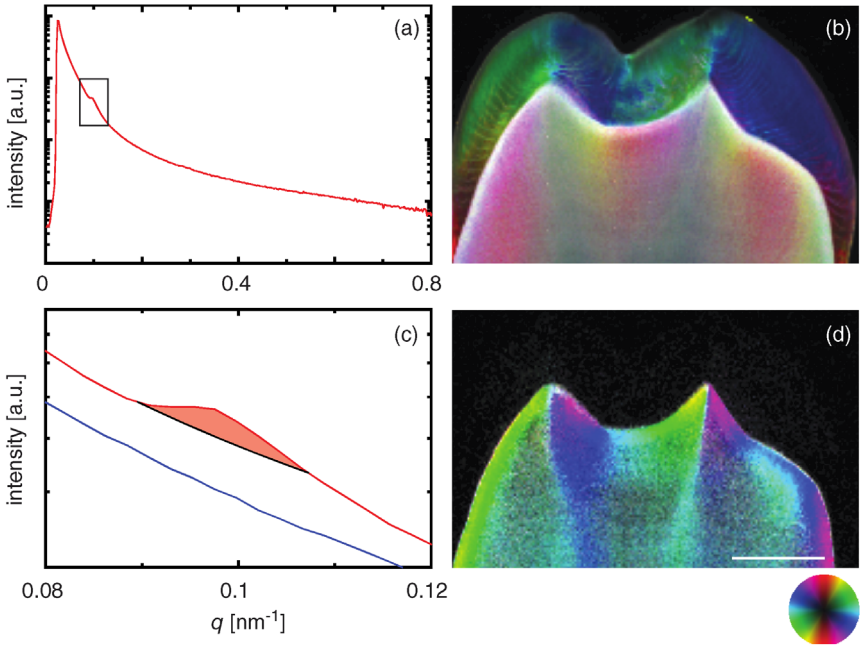


**Figure 12.7** The diagram (a) shows characteristic scattering curves of dentin in red color and of enamel in blue color. The image (b) is the locally processed SAXS signal, where the orientation of the scattering signal is according to the color-wheel, scattering potential is coded by brightness, and anisotropy by color saturation. The distinct periodicity of about 67 nm in the collagen fibers gives rise to a related peak in the scattering signal (c). This signal, related to collagen-I, can be extracted and allows generating descriptive images as displayed in (d). The scale bar corresponds to a length of 2 mm.

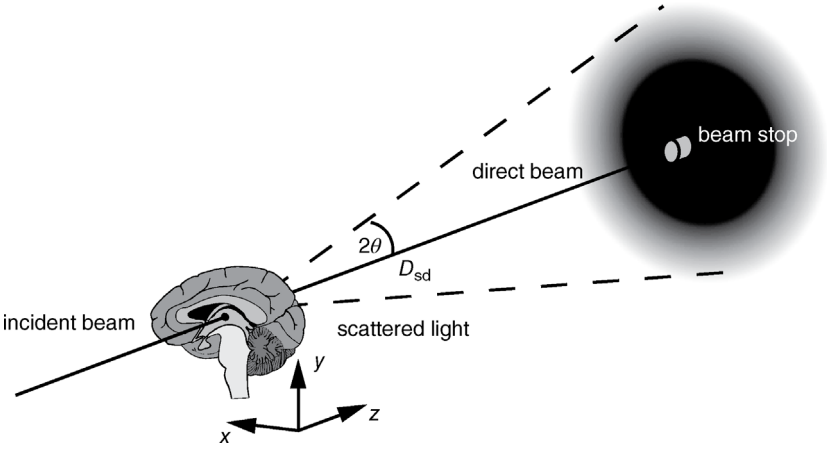


**Figure 12.8** Schematic representation of a standard scattering measurement setup. A collimated X-ray beam impinges on the tissue of interest. The scattered X-rays are collected on a detector, whereas the transmitted radiation is absorbed at the beam stop.

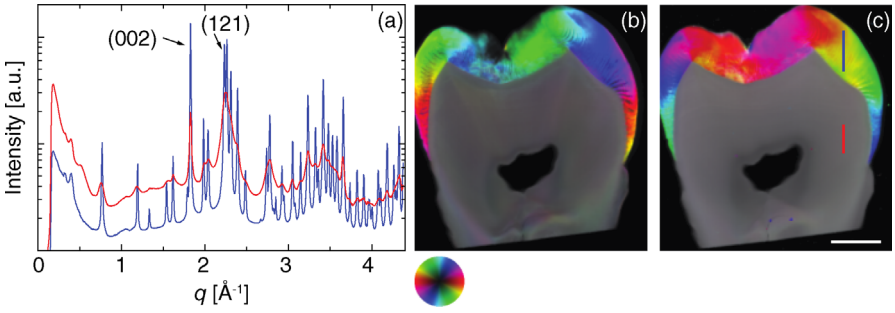


**Figure 12.9** The diagram (a) reveals the characteristic diffraction (WAXS) patterns of enamel in blue color and of dentin in red color. Most of the peaks are easily associated to hydroxyapatite. The images (b) and (c) present the locally processed signals of the (002) and (121) planes, respectively. The color corresponds to the orientation of the diffraction peak according to the color-wheel, whereas the color saturation indicates anisotropy in the plane of the specimen. The scale bar corresponds to a length of 2 mm.

intensity associated with individual peaks can be processed, as performed here for the families of (002) and (121) planes and depicted in the images of Figure 12.9b and c, respectively. In enamel, the (002) signal orients radially to the DEJ. The (121) signal is oriented parallel to the DEJ. The comparison with SAXS data reveals that the (002) direction, corresponding to the *c*-axis, aligns with the long axis of the needle-shaped crystallites. No distinct orientation can be identified for dentin.

The anatomical knowledge on the nanometer scale should be applied for the realization of nature-inspired, biomimetic fillings. Currently, the dentists repair caries lesions mechanically removing the affected parts of the crown and filling the cavity using advanced isotropic materials. These dental fillings usually do not reach the duration of the natural counterpart. Consequently, dental fillings should be inserted, which contain elongated nanostructures with the orientation of dentin and enamel [17].

The study of caries pathology using synchrotron radiation-based hard X-ray scattering has demonstrated that while bacterial processes do dissolve the ceramic components in enamel and dentin, the dentinal collagen network remains unaffected, enabling the development of future caries treatments that remineralize the dentin [16].

### 12.3.2 Femoral Head

The articular cartilage of the human femoral head is composed of layered tissues, as schematically depicted in Figure 12.10b [18]. This configuration illustrates the tissue's function as load bearing and shock absorbing anatomical structure [19,20]. Applying the two-dimensional position-resolved SAXS, it is possible to map the local orientation of collagen fibrils from the femoral head

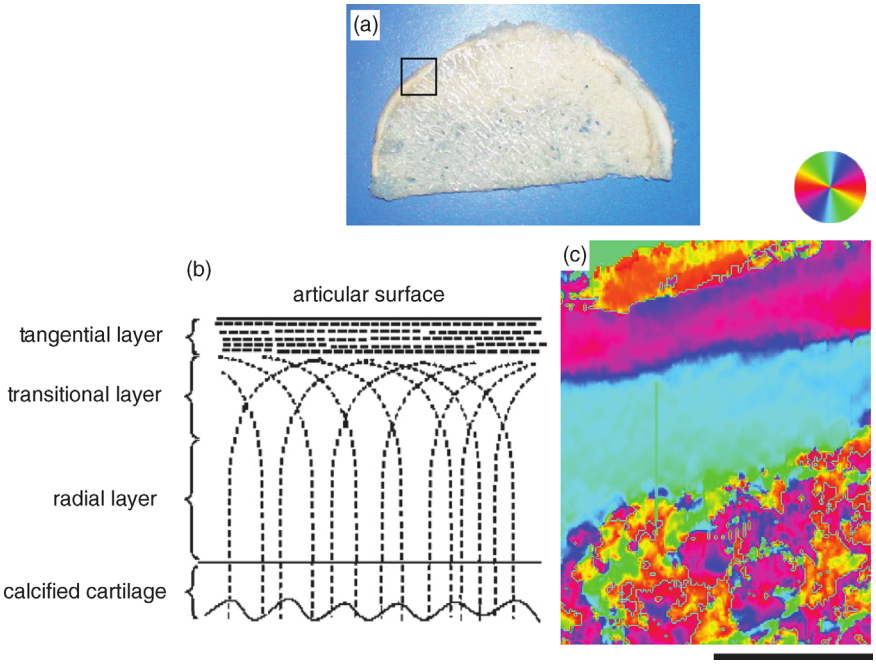


**Figure 12.10** The rectangle of the photograph (a) indicates the area of a section of decalcified femoral head selected for the scanning SAXS measurement. The scheme (b) shows the anatomical layered structure from the bone to the articular surface indicating the alignment of collagen fibers in knee cartilage. The spatially resolved SAXS data shown in the image (c) reveals the main orientation of the scattering signal in the range from 12.5 to 13.7 nm according to the color-wheel. The orientation of the signal changes from parallel to perpendicular to the surface. These data show results from the first scanning SAXS experiments performed at the cSAXS beamline in August 2007. The length bar corresponds to 500 µm. (Adapted from Ref. [18]. With permission from Elsevier.) (Adapted from Ref. [19]). With permission from Elsevier. SAXS data with permission by D. Bradley.)

surface down to the underlying subchondral plate and the trabecular bone. The SAXS data reveal the parallel alignment of the collagen fibers at the articular surface, which accommodate the gliding motion of the joint, then a change to a perpendicular arrangement in the direction of mechanical loading [19,21]. Such measurements can, for example, be utilized to track osteoarthritis, that is, the induced changes of the anatomy on the nanometer scale in affected joints, *ex vivo* [19].

Currently, the repair of joints is only partially possible. Once the joint, such as hip and knee, is severely damaged, it is replaced using medical implants. Although this surgical treatment is a standard medical procedure, rather complex complications can occur. Therefore, tissue engineering is still an interesting alternative. Related research activities are ongoing. The spatially resolved SAXS data underline the necessity (i) to incorporate anisotropic nanostructures into

the tissue-engineered constructs and (ii) to extend the two-dimensional arrangements of biological cells into the third dimension. Here, one finds some promising results concerning bone substitutes [22]. Nevertheless, the tissue engineering of joints is still at the very early stage of development. Research initiatives with durations of rather a decade than a year will be required to build the tissues in a biomimetic manner with ordered anisotropic nanostructures as revealed with the spatially resolved SAXS measurements.

### 12.3.3 Breast Tumor

In order to diagnose breast cancer, medical experts have to discriminate between normal tissue and benign as well as malignant lesions. This task is often challenging. The result has major impact on the survival and the quality of life of the affected patients. It has been demonstrated that SAXS allows classifying formalin-fixated human breast tissues as normal, benign, or malignant with a high sensitivity and specificity [23–28]. Here, the scientists have analyzed both the Bragg peaks of the collagen fibrils and the scattering of the packing of triglycerides in the lamellar phase present in normal tissue. Usually, several parameters are derived to improve the significance. Figure 12.11, for example, shows beside the histology slice, the related, simultaneously obtained spatially resolved SAXS data for the degree of orientation, the intensity exponent, the total scattered intensity, and the preferential orientation of the scattering signal corresponding to the range between 6 and 21 nm. One easily recognizes the similarities between conventional histology and spatially resolved SAXS data as well as the additional information SAXS can provide with respect to the conventional approach. Although laboratory set-ups are sufficient to discriminate the cancerous and healthy parts of the breast tissues, further efforts have to be invested to develop spatially resolved SAXS toward mammography screening.

### 12.3.4 Brain Tissue

Brain tissue contains prominent nanoscale periodicities, which include the myelin sheaths that surround the nerve axons. They have a spiral arrangement with a constant separation distance between the turns of about 17 nm and act as electrical isolation. Similar to collagen, this 17 nm periodicity gives rise to distinct peaks in the $I$–$q$ plots. Degenerative pathological events can alter its abundance and structure [29]. The images of Figure 12.12a and b show the total and myelin-related signals of a human brain slice. The image represented in Figure 12.12c depicts the relative frequency of the myelin signal. The central dark region belongs to the thalamus, where the myelin is hardly found. Around the thalamus, however, abundant myelin sheaths, that surround the nerve axons, are present.

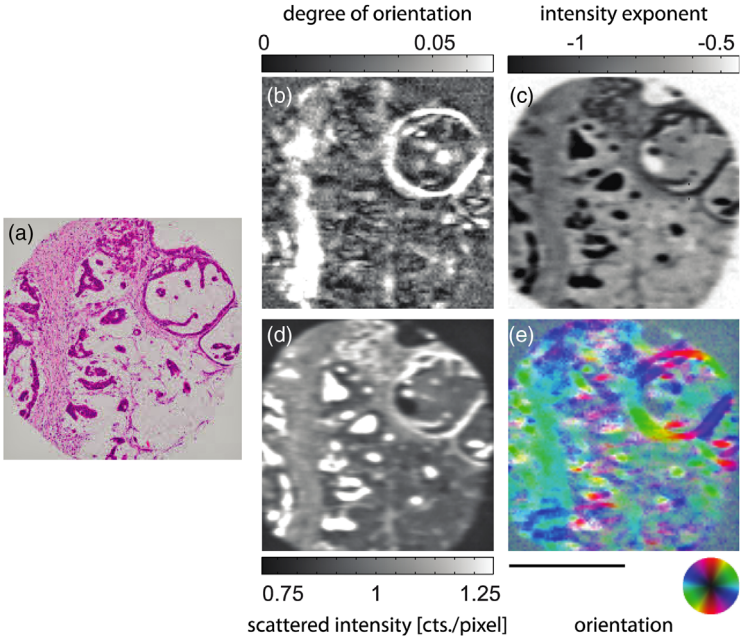


**Figure 12.11** (a) Histology slice of human breast tissue. (b) Degree of orientation. (c) Intensity exponent. (d) Total scattered intensity. (e) Orientation of the scattering signal, according to the color-wheel. The nanostructures in the range from 6 to 21 nm are considered. The scale bar corresponds to a length of 500 µm. Histology and SAXS data with permission by D. Bradley.

The two-dimensional SAXS measurements can be extended to the third dimension incorporating a rotation, for example, around *y*-axis (cf. Figure 12.2). In this manner, SAXS is combined with a tomographic setup. The well-known reconstruction schemes, that is, filtered back-projection, can be applied. The direction-dependent nature of the SAXS signal imposes limitations on the information that is obtained. The scattering intensity signal, related to the abundance of nanostructures, can only be meaningfully reconstructed, if the nanostructures are isotropic, meaning that scattered intensity is independent on specimen's orientation [30–32]. Using this method the preferential orientation of the scattering features cannot be reconstructed. Nonetheless, this basic approach can result in a remarkable contrast, as shown in the images of Figure 12.12d and e for rat brain. The images, displayed in Figure 12.12d and g, show conventional tomography slices in absorption-contrast mode. Only a few features can be identified. Conversely, improved contrast is found in the SAXS-CT data that are displayed in the images of Figure 12.12e and h. Similar to the two-dimensional data, the intensity associated with myelin can be processed and reconstructed separately, allowing for the access of the myelin density in each voxel [31]. These unique results are visible in the images of Figure 12.12f and i.

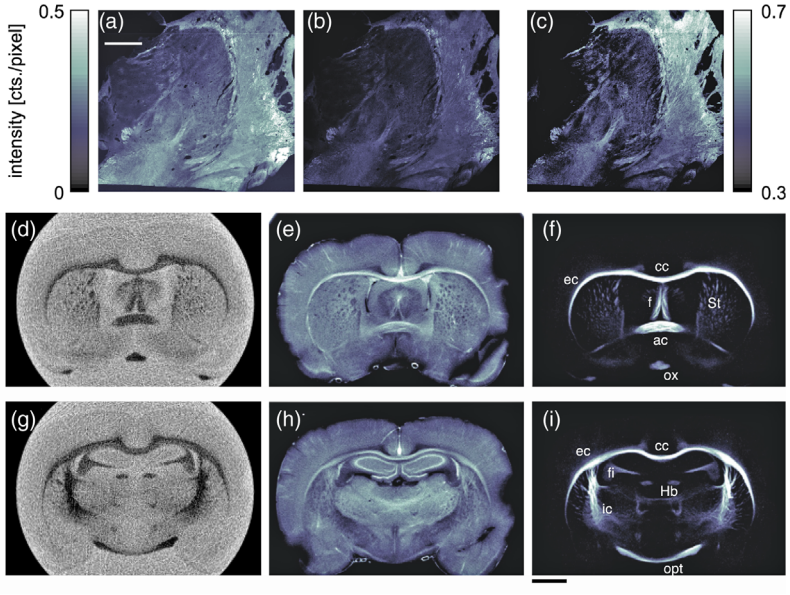


**Figure 12.12** In the top row (a) two-dimensional SAXS intensity of a histology slice from the human thalamus for the range between 8.2 and 9.0 nm. (b) Myelin-related signal. (c) Ratio of the images represented in (b) and (a), giving rise to the relative myelin abundance. The scale bar corresponds to a length of 5 mm. In the second and third row, one finds selected tomographic slices of SAXS-CT data reconstructed by filtered back-projection from a rat brain. (d) and (g) absorption contrast. (e) and (h) total scattering signal. (f) and (i) myelin-related signal. The scale bar corresponds to a length of 2 mm. ((d, g) Adapted from Ref. [30], with permission from IOP Publishing. (e, f, h, i) Adapted from Ref. [31], with permission from Elsevier.)

For specimens presenting a high degree of anisotropy on the nanometer scale the approach is, however, questionable, and more sophisticated measurements and reconstruction algorithms have to be developed. Very recently, Georgiadis *et al.* have proposed a method for the three-dimensional assessment of the local orientation of nanocomponents of bone using spatially resolved SAXS [33]. This method relies on the inspection of thin slices in a similar manner as for the projection approach in spatially resolved SAXS. Here, however, the measurement is repeated for a variety of incidence angles with respect to the beam, allowing for the reconstruction of the local preferential orientation of the nanostructures in three dimensions. As for the two-dimensional projection data, the spatial resolution is limited to the slice thickness. To investigate volumetric specimen, sequential sections can be scanned, as performed successfully for bone [33].

The two- and three-dimensional SAXS data allow for a detailed evaluation of brain tissues in health and disease. Based on the present results, the future SAXS experiments will expand our understanding of neurodegenerative diseases and the role of the nanostructures and their arrangement for the well and fit aging.

## 12.4 Conclusions and Outlook

Our body can be regarded as the arrangement of atomic and molecular species in hierarchical manner to offer the dedicated functionality. Radiologists, however, cannot resolve the individual atoms and molecules, because the spatial resolution of their modalities is not better than a fraction of a millimeter. Specialized computed tomography based on hard X-rays can reach the submicrometer level for specimens of a restricted size. Atoms and molecules within biopsies, however, are inaccessible so far. As a consequence, the diffraction- and scattering-based, *k*-space techniques are extremely helpful. We have known these techniques in the fields of crystallography, physics, and materials science for about a century. The detailed understanding of these methods, however, is demanding. More recently, however, the scattering techniques have been combined with scanning in two dimensions taking advantage of well-collimated hard X-ray beams. In this way, images of a reasonable tissue area with strong similarities with histology can be generated. In comparison with histology, however, staining procedures can be avoided, which allows investigations closer to the physiological stage. Even more important, SAXS permits the determination of the orientation and degree of anisotropy of the nanoscale ultrastructure that is impossible using conventional histology. This feature is essential, since the human tissues are almost exclusively anisotropic. The combination with tomographic reconstruction is still in its infancy and restricted to rather small volumes.

SAXS has been successfully applied to a variety of hard and soft tissues [21]. Diseases can be diagnosed even in quantitative manner. The results may be applied to develop next-generation treatment strategies, as, for example, being demonstrated for caries [16].

## References


1 White, S.N., Luo, W., Paine, M.L., Fong, H., Sarikaya, M., and Snead, M.L. (2001) Biological organization of hydroxyapatite crystallites into a fibrous continuum toughens and controls anisotropy in human enamel. *J. Dent. Res.*, **80** (1), 321–326.

2 Lareida, A., Beckmann, F., Schrott-Fischer, A., Glueckert, R., Freysinger, W., and Müller, B. (2009) High-resolution X-ray tomography of the human inner ear: synchrotron radiation-based study of nerve fiber bundles, membranes, and ganglion cells. *J. Microsc.*, **234** (1), 95–102.

3 Schulz, G., Weitkamp, T., Zanette, I., Pfeiffer, F., Beckmann, F., David, C., Rutishauser, S., Reznikova, E., and Müller, B. (2010) High-resolution tomographic imaging of a human cerebellum: comparison of absorption and grating based phase contrast. *J. R. Soc. Interface*, **7** (53), 1665–1676.

4 Bunk, O., Bech, M., Jensen, T.H., Feidenhans'l, R., Binderup, T., Menzel, A., and Pfeiffer, F. (2009) Multimodal x-ray scatter imaging. *New J. Phys.*, **11**, 123016.

5 Fratzl, P., Jakob, J.F., Rinnerthaler, S., Roschger, P., and Klaushofer, K. (1997) Position-resolved small-angle X-ray

scattering of complex biological materials. *J. Appl. Crystallogr.*, **30**, 765–769.
6 Glatter, O. and Kratky, O. (eds) (1982) *Small-Angle X-ray Scattering*, Academic Press, London.
7 Guinier, A. and Fournet, G. (eds) (1955) *Small Angle Scattering of X-rays*, John Wiley & Sons, Inc., New York.
8 Kraft, P., Bergamaschi, A., Broennimann, C., Dinapoli, R., Eikenberry, E.F., Henrich, B., Johnson, I., Mozzanica, A., Schlepütz, C.M., Willmott, P.R., and Schmitt, B. (2009) Performance of single-photon-counting PILATUS detector modules. *J. Synchrotron Radiat.*, **16**, 368–375.
9 Schulz, G. *et al.* (2012) Imaging the human body: micro- and nanostructure of human tissues, in *NanoScience and Technology* (ed. S. Logothetidis), Springer-Verlag Berlin Heidelberg.
10 Deyhle, H. *et al.* (2012) Imaging the human body down to the molecular level, in *Encyclopedia of Nanotechnology* (eds B. Bhushan and H.D. Winbigler), Springer Science+Business Media B.V.
11 Deyhle, H., White, S.N., Bunk, O., Beckmann, F., and Müller, B. (2014) Nanostructure of the carious tooth enamel lesion. *Acta Biomater.*, **10** (1), 355–364.
12 Pabisch, S., Wagermaier, W., Zander, T., Li, C., and Fratzl, P. (2013) Imaging the nanostructure of bone and dentin through small- and wide-angle X-ray scattering, in *Methods in Enzymology, Research Methods in Biomineralization Science* (ed. J.J. De Yoreo), Academic Press, pp. 391–413.
13 Gaiser, S., Deyhle, H., Bunk, O., White, S.N., and Müller, B. (2012) Understanding nano-anatomy of healthy and carious human teeth: a prerequisite for nanodentistry. *Biointerphases*, **7**, 4.
14 Mortell, J.F. and Peyton, F.A. (1956) Observation of Hunter-Schreger bands. *J. Dent. Res.*, **35** (5), 804–823.
15 Kinney, J.H., Pople, J.A., Marshall, G.W., and Marshall, S.J. (2001) Collagen orientation and crystallite size in human dentin: a small angle X-ray scattering study. *Calcif. Tissue Int.*, **69**, 31–27.
16 Deyhle, H., Bunk, O., and Müller, B. (2011) Nanostructure of healthy and caries-affected human teeth. *Nanomed. Nanotech. Biol. Med.*, **7**, 694–701.
17 Deyhle, H., Bunk, O., Buser, S., Krastl, G., Zitzmann, N., Ilgenstein, B., Beckmann, F., Pfeiffer, F., Weiger, R., and Müller, B. (2009) Bio-inspired dental fillings. *Proc. of SPIE*, **7401**, 74010E 11.
18 Kaabar, W., Daar, E., Gundogdu, O., Jenneson, P.M., Farquharson, M.J., Webb, M., Jeynes, C., and Bradley, D.A. (2009) Metal deposition at the bone-cartilage interface in articular cartilage. *Appl. Radiat. Isot.*, **67**, 475–479.
19 Kaabar, W., Gundogdu, O., Laklouk, A., Bunk, O., Pfeiffer, F., Farquharson, M.J., and Bradley, D.A. (2010) μ-PIXE and SAXS studies at the bone-cartilage interface. *Appl. Radiat. Isot.*, **68**, 730–734.
20 Stockwell, R.A. (ed.) (1970) *Biology of Cartilage Cells*, vol. **7**, Cambridge University Press, New York.
21 Müller, B., Deyhle, H., Bradley, D., Farquharson, M., Schulz, G., Müller-Gerbl, M., and Bunk, O. (2010) Scanning x-ray scattering: evaluating the nanostructure of human tissues. *Eur. J. Clin. Nanomed.*, **3**, 30–33.
22 Hoffmann, W., Bormann, T., Rossi, A., Müller, B., Schumacher, R., Martin, I., de Wild, M., and Wendt, D. (2014) Rapid prototyped porous nickel–titanium scaffolds as bone substitutes. *J. Tissue Eng.*, **5**, 1–14.
23 Conceicao, A.L., Antoniassi, M., and Poletti, M.E. (2009). Analysis of breast cancer by small angle X-ray scattering (SAXS). *Analyst*, **134** (6), 1077–1082.
24 Falzon, G., Pearson, S., Murison, R., Hall, C., Siu, K., Evans, A., Rogers, K., and Lewis, R. (2006) Wavelet-based feature extraction applied to small-angle x-ray scattering patterns from breast tissue: a tool for differentiating between tissue types. *Phys. Med. Biol.*, **51** (10), 2465–2477.
25 Fernandez, M., Keyrilainen, J., Serimaa, R., Torkkeli, M., Karjalainen-Lindsberg, M.L., Leidenius, M., von Smitten, K., Tenhunen, M., Fiedler, S., Bravin, A., Weiss, T.M., and Suortti, P. (2005) Human breast cancer *in vitro*: matching histo-pathology with small-angle x-ray scattering and diffraction enhanced x-ray imaging. *Phys. Med. Biol.*, **50** (13), 2991–3006.
26 Fernandez, M., Keyrilainen, J., Serimaa, R., Torkkeli, M., Karjalainen-Lindsberg, M.L.,

Tenhunen, M., Thomlinson, W., Urban, V., and Suortti, P. (2002) Small-angle x-ray scattering studies of human breast tissue samples. *Phys. Med. Biol.*, **47** (4), 577–592.

**27** Round, A.R., Wilkinson, S.J., Hall, C.J., Rogers, K.D., Glatter, O., Wess, T., and Ellis, I.O. (2005) A preliminary study of breast cancer diagnosis using laboratory based small angle x-ray scattering. *Phys. Med. Biol.*, **50** (17), 4159–4168.

**28** Sidhu, S., Siu, K.K.W., Falzon, G., Nazaretian, S., Hart, S.A., Fox, J.G., Susil, B.J., and Lewis, R.A. (2008) X-ray scattering for classifying tissue types associated with breast disease. *J. Med. Phys.*, **35** (10), 4660–4670.

**29** De Felici, M., Felici, R., Ferrero, C., Tartari, A., Gambaccini, M., and Finet, S. (2008) Structural characterization of the human cerebral myelin sheath by small angle x-ray scattering. *Phys. Med. Biol.*, **53**, 5675–5688.

**30** Jensen, T.H., Bech, M., Bunk, O., Thomsen, M., Menzel, A., Bouchet, A., LeDuc, G., Feidenhans'l, R., and Pfeiffer, F. (2011) Brain tumor imaging using small-angle x-ray scattering tomography. *Phys. Med. Biol.*, **56**, 1717–1726.

**31** Jensen, T.H., Bech, M., Bunk, O., Menzel, A., Bouchet, A., LeDuc, G., Feidenhans'l, R., and Pfeifer, F. (2011) Molecular x-ray computed tomography of myelin in a rat brain. *Neuroimage*, **57** (1), 124–129.

**32** Schroer, C.G., Kuhlmann, M., Roth, S.V., and Gehrke, R. (2006) Mapping the local nanostructure inside a specimen by tomographic small-angle x-ray scattering. *Appl. Phys. Lett.*, **88**, 164102.

**33** Georgiadis, M., Guizar-Sicairos, M., Zwahlen, A., Trüssel, A.J., Bunk, O., Müller, R., and Schneider, P. (2015) 3D scanning SAXS: A novel method for the assessment of bone ultrastructure orientation. *Bone*, **71**, 42–52.

# 13
# Regenerative Dentistry Using Stem Cells and Nanotechnology

*Thimios A. Mitsiadis*[1] *and Giovanna Orsini*[2]

[1]*University of Zurich, Medical Faculty, Centre for Dental Medicine, Institute of Oral Biology, Orofacial Development and Regeneration, Plattenstrasse 11, 8032 Zurich, Switzerland*
[2]*Polytechnic University of Marche, Department of Clinical Sciences and Stomatology, Via Tronto 10, 60126 Ancona, Italy*

## 13.1
## Introduction

New therapeutic approaches benefit from recent advances in stem cell biology and material sciences. The combination of stem cells with sophisticated nanostructured materials and scaffolds is increasingly beneficial in all areas of regenerative medicine [1,2]. Nanoparticles (i.e., 1–100 nm size) can be used both for the diagnosis and targeted therapy through *in vivo* imaging and drug delivery, and for the creation of biomimetic scaffolds and implants [2–7]. Nanostructured biomaterials can be personalized by engineering their structure, shape, size, and surface properties in order to be applied in precise anatomical sites. Stem cells are powerful tools for diseases that conventional medicine cannot cure presently [8–10]. However, significant hurdles remain for successful clinical translation, such as harmonization of methodologies and regulations of stem cell isolation and expansion, as well as attitudes to their clinical adoption. A fundamental requirement for the successful clinical application is the production of desired quantities of stem cells that display acceptable levels of comparability across different lines [1,8,10]. Variability in engineered nanomaterials, microenviromental fluctuations, and heterogeneous nature of patients (in terms of disease status and genetic background), creates additional inconsistencies that are challenging to control during the clinical procedures [1,2,8,10]. Therefore, standardized methodologies will reduce the impact of technical variability and validate clinical procedures associated with stem cells and nanostructured materials. To this end, we emphasize the role of stem cells combined with novel nanostructured materials and nanoparticles in dental tissue regeneration. Furthermore, we highlight here various applications of nanotechnology in current dentistry, ranging from diagnostics to dental materials.

*Nanoscience and Nanotechnology for Human Health,* First Edition. Edited by Bert Müller and Marcel Van de Voorde.

## 13.2 Repair of Dental Tissues

Enamel, dentin, and cementum constitute the hard tissues of the tooth that is formed as the outcome of sequential and reciprocal interactions between cells of the oral epithelium and the cranial neural crest-derived mesenchyme (Figure 13.1) [9–13]. The epithelium-derived ameloblasts are responsible for the formation of enamel, while the mesenchymal cells give rise to two distinct components: the dental pulp and the dental follicle. Cells of the dental pulp differentiate into odontoblasts and produce the dentin matrix, while cells from the dental follicle are involved in cementum and alveolar bone formation. The tooth anchors to the alveolar bone through the periodontal ligament (PDL). The fibers of the PDL connect the tooth root cementum with the alveolar bone, thus contributing to tooth stability and homeostasis [10,12]. The periodontal space also contains a variety of cells such as fibroblasts, epithelial rests of Malassez (ERM), and endothelial cells [12].

There is an increased need of specific dental biomaterials that can be used in clinics for dental tissue repair and regeneration [14]. Novel, tailor-made dental materials are successfully used for partial dental tissue repair, while sophisticated dental implants are used for tooth replacement [10]. These materials are often used in conjunction with signaling molecules to enhance the regeneration of the dental tissues and alveolar bone. Damaged enamel is usually substituted with sophisticated biomaterials, ceramics, and precious metals, since the enamel cannot be repaired naturally [15,16].

Novel, stem cell-based, therapeutic approaches are both promising and challenging, and they complement the traditional restorative or surgical techniques

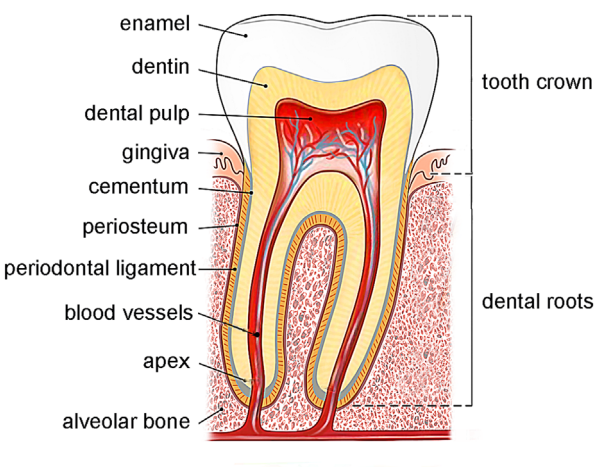


**Figure 13.1** Schematic representation of a molar indicating the various components of the tooth and the surrounding tissues. (Adapted from Ref. [13].)

for the repair and regeneration of dental tissues [1,10]. The generation of induced pluripotent stem cells (iPSCs) by reprogramming somatic cells via a cocktail of transcription factors represents another attractive source of cells for tooth repair and regeneration [8,17,18]. The administration to patients of stem cells or iPSCs in conjunction with nanomaterials, bioactive scaffolds, and nanoparticles might increase the regenerative capability of the damaged dental tissues [1,10]. Most studies focus on partial dental tissue repair/regeneration for diseases that commonly affect dental tissues. However, several attempts have also been made for the regeneration of entire teeth [15–22]. Recent advances, future developments, and raising new challenges in the field of dentistry are discussed in this chapter.

## 13.3
## Dental Stem Cells and Their Regenerative Potential

Stem cells are characterized by their potential to self-replicate and differentiate into a vast variety of cell populations [9,23]. Pluripotent epithelial and mesenchymal cell populations are present in the vast majority of adult human tissues and organs, including teeth. Dental mesenchymal stem cells (DMSCs) were found in the dental pulp of human permanent [24] and exfoliated deciduous teeth [25]. These cells were also identified in the apical part of dental papilla [26,27], dental follicle [28], and periodontal ligament [29,30]. DMSCs are responsible for homeostasis and regeneration of the dental pulp and periodontium [1,10,31], and are able to form dentin, cementum, and alveolar bone [31–33], thus indicating their potential for applications in dental treatments [1,10,15,26]. In contrast, dental epithelial stem cells (DESCs) are very rare in adult human teeth, thus making it difficult to naturally repair or regenerate enamel [12,16,34]. The current knowledge on DESCs has been obtained from studies in rodents, in which DESCs are found to be responsible for the renewal of the continuously growing incisors [9,12,16,23]. Here, we report on the various dental cell populations that are characterized and currently used for experimental regenerative purposes.

*Dental pulp stem cells* (DPSCs) were first isolated in 2000 and are the most common source of DMSCs [24] (Figure 13.2). Purification of the isolated pulp cells can be obtained after their labeling with fluorescent antibodies followed by fluorescence-activated cell sorting (FACS) [24,35]. Due to the lack of specific DMSCs markers, generic mesenchymal stem cell (MSC) markers such as STRO-1, CD146, and CD44 are commonly used for the identification of DMSC populations [1,10,24,31,35]. Additional identification procedures that rely on the morphology, selective adherence properties, proliferation and differentiation potential, and tissue repair abilities of these cell populations are in use [35]. DPSCs are capable to differentiate into odontogenic, osteogenic, chondrogenic, adipogenic, myogenic, and neurogenic cells *in vitro* and *in vivo* [1,10,35,36]. Pulp–dentin tissues have been generated after ectopic transplantation of DPSCs mixed with hydroxyapatite/tricalcium phosphate [11,24,37,38]. Furthermore,

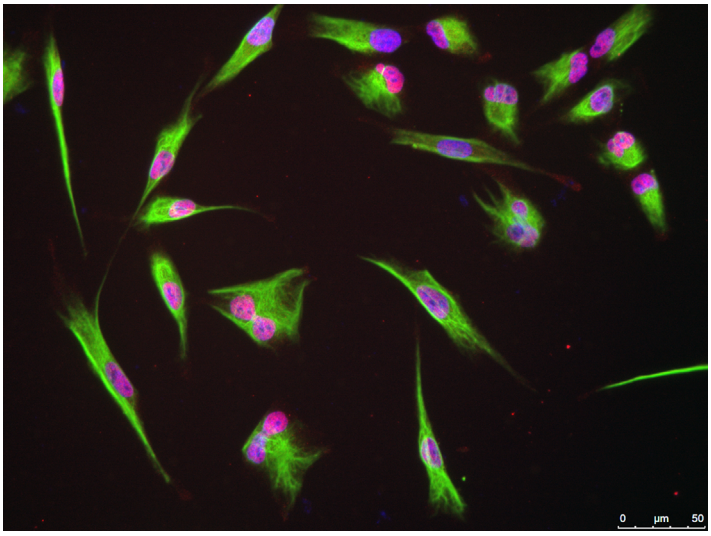


**Figure 13.2** Cultured human dental pulp stem cells (hDPSCs) after immunostaining with vimentin (fluorescent green color) and NuMA (pink/violet color). Vimentin staining illustrates the structure of the cytoskeleton, while NuMA staining indicates the nuclei of human cells. (Photo given by A. Woloszyk, Orofacial Development and Regeneration, University of Zurich, Zurich, Switzerland.)

clinical trials using autologous human DPSCs combined with collagen scaffolds for alveolar bone reconstruction have been successfully performed several years ago [39].

*Stem cells from human exfoliated deciduous teeth* (SHEDs) can be isolated using the same procedure as for DPSCs [25]. SHEDs express the surface molecules STRO-1 and CD146, and several neural and glial markers such as nestin and β-III tubulin [25]. These cells are capable to differentiate into odontogenic, osteogenic, chondrogenic, adipogenic, myogenic, and neurogenic cells *in vitro* [25,31,35]. SHEDs proliferate very fast, but they have a limited capacity to form dentin-pulp complexes *in vivo* [25,31]. However, transplantation of SHEDs seeded in biodegradable scaffolds into human tooth slices resulted in the formation of dental pulp-like tissue. In addition, it has been shown that SHEDs are able to induce bone and dentin formation *in vivo* [25,31].

*Stem cells from the apical part of the dental papilla* (SCAPs) are mesenchymal cells located at the apex of the developing root of the tooth [26,27]. SCAPs are highly proliferative, and exhibit increased migratory and regenerative potentials. These cells express the same DMSC surface markers, as well as the SCAP-specific marker CD24, for which DPSCs are negative [26,36]. SCAPs have the potential to generate odontogenic and adipogenic lineages *in vitro* and are able to form dentin *in vivo*, when transplanted on hydroxyapatite/tricalcium phosphate carriers [26,31].

*Stem cells from the dental follicle* (DFSCs) are progenitor cells for the PDL, alveolar bone, and cementum, and express the STRO-1 and CD44 markers, as well as the BMP receptor-IA, -IB, and –II [10,28]. DFSCs transplanted into immune-deficient animals were able to form cementum and PDL-like tissues [40,41].

*Periodontal ligament stem cells* (PDLSCs) also express the cell-surface markers STRO-1, CD146, and CD44 [10,29,30]. These cells are able to differentiate into adipogenic and osteogenic cells under defined culture conditions *in vitro*. PDLSCs can contribute to the regeneration of the periodontium by giving rise to cementum/PDL tissues, after their injection into immune-compromised animals *in vivo* [29]. Another PDLSC population that is located close to the alveolar bone (abPDLSCs) has shown higher osteogenic and adipogenic capabilities when compared to PDLSCs [30].

*Human dental epithelial stem cells* (hDESCs) can be isolated from the third molar that develops late after birth. Another source of hDESCs is the epithelial root sheath that disintegrates into strands of epithelial cells, also known as epithelial rests of Malassez [42–44], as well as from the dental pulp [45]. ERM cells express epithelial stem cell markers such as Bmi-1, E-CAM, and p75, as well as embryonic stem cell markers such as Oct-4 and Nanog, which are necessary for pluripotency and self-renewal of embryonic stem cells [42–44].

*Induced pluripotent stem cells* (iPSCs) may represent another source of hDESCs. Indeed, iPSCs have the capacity to differentiate into various cell lineages and can be technically produced from patient's cells [17,18]. The iPSCs technology can be progressively applied for the regeneration of dental tissues [46,47]. iPSCs are able to differentiate into ameloblast-like cells in the presence of ameloblastin expressing cells [46]. Also, iPSCs are capable to differentiate into mesenchymal odontogenic cells and form neurospheres in floating culture conditions that allow their differentiation into neural crest cells. In presence of serum or dental epithelial cell medium the neural crest cells start to express Pax9 and dentin sialophosphoprotein (DSPP), which are markers of odontogenic mesenchymal cells and odontoblasts [48].

## 13.4 Regenerative Dentistry

Dental pathologies (e.g., periodontal and carious diseases), fractures, injuries, and genetic aberrations represent a frequent socioeconomical problem [10]. In clinical practice, damaged dental tissues are usually substituted with artificial materials. We could imagine that in the near future dentists will focus on tissue regeneration methods for the treatment of several clinical cases [49,50]. So far, dental implants have been the only solution for the replacement of missing teeth. Although the development of novel biocompatible materials improved the quality of treatment, there are several limitations in functionality and longevity of dental implants due to their strong dependence on the quantity and quality of

the surrounding bone [10]. To overcome this problem, new ideas and approaches have emerged recently from the fields of stem cell biology, tissue engineering, and nanotechnology [12,15]. Different therapeutic approaches that depend on the degree of tooth damage are required. Current therapies are mainly oriented toward partial dental tissue repair, where injured dental tissues are substituted with appropriate materials. In contrast, dental tissue regeneration involves the replacement and functional restoration of the injured (or pathological) tissue by the same healthy biological tissue.

*Pulp-dentin regeneration*. Proper regeneration of the dentin-pulp complex allows new dentin formation under the pathological site and requires the revascularization and reinnervation of the pulp. Signaling molecules such as bone morphogenetic proteins (BMPs) have been used to stimulate and increase the natural regenerative response of the dental pulp. DPSCs are able to differentiate into odontoblasts, endothelial cells, and neurons when placed in contact with dentin *in vitro* [10,24,51,52]. *In vivo* studies in mice have shown that transplanted DPSCs can regenerate the pulp–dentin complex after pulpotomy [38]. Similarly, transplantation of human DPSCs and SCAPs seeded on a poly-D,L-lactide/glycole scaffold into the empty root canal space of mouse teeth gave rise to a brand new vascularized pulp–dentin complex [10,38]. Although these and other findings clearly show that DPSCs can be used for dental pulp regeneration, further studies and regulations are needed for their definitive application in dental clinics.

*Periodontal tissue regeneration*. Using different scaffolds has made it possible to induce differentiation of PDLSCs or DPSCs into the various cell types of the periodontium *in vitro* [10]. Human PDLSCs transplanted into immunecompromised animals participate in the regeneration of the periodontium [29], thus indicating their potential for future cell-based therapies in dentistry [10]. Equally important for the development of these therapies is the use of signaling molecules, such as PDGFs and BMPs [53,54]. PDGFs are able to stimulate periodontal healing and regeneration, while BMPs are capable to form new alveolar bone and cementum. However, BMPs may have undesirable effects on the periodontium by inducing tooth ankylosis [10,54]. In addition to these signaling molecules, commercialized amelogenin extracts are successfully used in dental clinics for the regeneration of periodontal tissues [55], but their mechanism of action is still unclear. The combination of stem cells, signaling molecules, and desirable scaffold materials is under investigation for the regeneration of periodontal tissues.

*Enamel regeneration*. It has been shown that porcine ERM can differentiate into ameloblast-like cells after coculture with dental pulp cells *in vitro* and that they can form enamel after transplantation *in vivo* [34].

*Root regeneration.* The regeneration of innervated dental roots composed of pulp, dentin, PDL, and cementum has been realized after subcutaneous transplantation of human dental follicle cells seeded into dentin matrix [56]. However, this approach still has to be tested *in vivo*, and it has to be determined whether the regenerated root can support a dental crown.

*Whole-tooth regeneration.* Formation of a brand new tooth would be the ideal therapeutic approach after tooth loss. The association of DESCs and DMSCs *in vitro* could allow the formation of a tooth germ that could then be transplanted into the alveolar bone, where the tooth germ would develop, erupt, and become a functional tooth [15,16,47,57]. Another approach to obtain a functional tooth is the implantation into the jaw of tooth-shaped polymeric biodegradable scaffolds that are filled with both DESCs and DMSCs [16,57]. The three-dimensional structure of the scaffolds should drive the differentiation of the transplanted cells into odontoblasts and ameloblasts. These bioengineered teeth have been produced in ectopic sites and are still missing some essential elements such as a complete root or the correct crown morphology [15,16]. However, recent experiments in mice have shown that it is possible to obtain functional teeth with roots using bioengineered approaches [19,21,22,57]. Indeed, tooth germs formed by dental epithelial and mesenchymal cells seeded into collagen drops, which served as scaffolds, have been implanted in the mandible of adult mice and gave rise to new functional teeth. Formation of all dental tissues allows the eruption and full integration of the bioengineered teeth into the recipient alveolar bone [19,21,22,57].

Recent studies have shown that the reaggregation of iPSC-derived neural crest cells and mouse odontogenic epithelial tissues is able to generate entire teeth after kidney capsule transplantation [15,47]. However, such results have not been obtained yet with human cells. Although further technical improvements may be needed, the iPSC technology is expected to open new horizons in regenerative dentistry [15,47].

## 13.5 Nanotechnology in Dentistry

The combination of the above-mentioned stem cell populations with novel nanotechnology platforms holds great promise for applications in regenerative dentistry [1]. The development of innovative nanostructured materials (i.e., on the scale of 1–100 nm) could be useful in manipulating stem cells for tooth regeneration. Nanomaterials can be also used for stem cell tracking, gene and protein delivery, and formation of artificial stem cell niches [1,4,6,7,58]. In addition, nanotechnology is used for improving biomaterials or creating new "smart" biomaterials used for specific dental disciplines [1]. Recent advances and potential applications in dentistry of several tools offered by nanotechnology are discussed below.

### *Tracking Stem Cells after Transplantation*

For the evaluation of the therapeutic efficacy of the transplanted stem cells into precise areas, it is important to track their survival, migration, fate, and regenerative impact *in vivo* [1,58]. Transplanted stem cells can be tracked *in vivo* for a long-term period with noninvasive imaging techniques using fluorescent dyes or the green fluorescence protein [59]. Furthermore, magnetic nanoparticles might

bring information about stem cell kinetics and fate during dental tissue (e.g., periodontium, pulp) regeneration. Light-emitting nanocrystals (i.e., quantum dots) can be also used to monitor the dynamics of dental stem cell niches in real time [58,59]. This knowledge could be used for the design of appropriate scaffolds for homing dental stem cells before transplantation. These approaches are necessary to evaluate the therapeutic effects of the various dental stem cell populations when exposed to specific microenvironments before any clinical application.

*Gene, Protein, and Drug Intracellular Delivery*

Another attractive concept in manipulating dental stem cell fate is the use of nanomaterials such as polymeric biodegradable nanoparticles, carbon nanotubes, and silicon nanowire arrays for gene and protein delivery [6,58,60].

*Artificial Stem Cell Niches: Nanofiber Scaffolds*

Nanotechnology could create artificial microenvironments that will direct dental stem cells toward a precise fate and function [4,60–62]. The size, surface, and shape of the artificial nanostructures are important parameters for the development of cell adhesion sites that monitor stem cell behavior [62]. Nanoscale structures such as nanotubes constitute the noncellular components of the stem cell niches [61] and could be used for the creation of particular dental microenvironments (e.g., apex of the root, pulp chamber) [1,35]. Furthermore, dental stem cells anchored to biocompatible and biodegradable nanofiber scaffolds, which are composed by natural or synthetic polymers (e.g., collagen, silk, polylactic acid polymers), could improve their survival, differentiation potential and three-dimensional organization [62]. Transplanted biodegradable scaffolds may act as temporary niches that guide, by controlling stem cell behavior, the formation of a new specific extracellular matrix (ECM) for dental tissue regeneration [1,46].

## 13.6 Nanoscale Surface Modifications of Dental Biomaterials

The trend in designing new dental biomaterials is based on the principle that nanoscale surface properties affect molecular and biological processes at the interface between the biomaterial and the involved tissue [63].

### 13.6.1 Approaches for Nanoscale Surface Modification in Dental Implants

Dental implant therapy constitutes a common and successful treatment for the replacement of missing teeth. Although largely effective, dental implants still need significant improvement, particularly in their capacity to selectively influence and guide tissue regeneration and homeostasis at the implantation site [63]. The surface properties of dental implants can be modified at the

nanolevel by various techniques, with the ultimate aim of creating a more efficient implant integration in the alveolar bone [64,65]. It is well established that surface features enhance biological events both *in vitro* [66–68] and *in vivo* [69–72]. Furthermore, it has been demonstrated that interactions between the material and the host tissue are principally governed by nanometric surface cues [73–77]. Therefore, various strategies have been developed and implemented to nanoengineer surfaces that can directly influence the biological functions of implantable metals [75,78].

A) *Chemical methods:* Electrochemical modification is one of the most common ways to modify metallic surfaces at the nanoscale level [79]. Indeed, anodic oxidation has been successfully used to transform smooth titanium surfaces into nanotubular structures with diameters inferior to 100 nm. Similarly, nanostructured layers have been created on various metallic surfaces using electrophoretic deposition [79]. For example, nanocrystalline (crystal size in the 15–25 nm range) hydroxyapatite (nanoHA) coatings and multiwalled carbon nanotubes have been successfully deposited on titanium-based metals, thus improving their bioactivity [80,81]. Furthermore, combinations of strong acids and oxidants have been applied for generating networks of nanopits (diameter 20–100 nm) on the titanium surface [82,83]. According to the nature of the etching solution it is possible to incorporate selected elements with antibacterial and bone regenerative properties (e.g., fluorine) in nanotopographic surfaces created by oxidative treatment [82]. Further chemical methods include the combination of anodic oxidation and chemical etching to create metal/polymer composites and modification at the nanometric level by sol–gel chemistry and chemical vapor deposition [84,85]. Another strategy to improve implants is the grafting of bioactive molecules such as peptides and growth factors in order to reproduce the natural biochemical environment of the host tissue [86].
B) *Physical methods:* Bioactive nanotopography on metal surfaces can be generated using plasma [87] and physical vapor deposition (PVD) [88,89]. A particular category of physical methods includes technologies that provoke atomic rearrangements such as ion implantation (e.g., $Ca^{2+}$, $F^{-}$, $Na^{+}$, $P^{+}$) and thermal oxidation [90,91]. Moreover, annealing and thermal oxidation have been explored on titanium-based metals to enhance their bioactivity by changing the crystalline structure of the nanometric native oxide layer.

### 13.6.2 Biological Surfaces Principles

The application of nanotechnology to biomedical surface science correlates with the capacities of cells to sense and recognize specifically designed substrate features. Well before cell colonization, water adsorption takes place at the surface contacting the biological environment [92]. The properties of the surface water shell dictate the adsorption of plasma and extra-cellular matrix proteins,

thus determining their orientation, coverage, and potential denaturation [92–96]. Therefore, the subsequent protein adlayer will act as a scaffold on which cells can adhere, proliferate, and differentiate. In addition, *in vitro* studies have shown that the adsorbed protein layer is sensitive to specific physical and chemical properties of the nanostructured surface, thus determining the biochemical characteristics of the adlayer [97]. Nanoscale modifications of the surface structuring may result in energy fluctuations, hydrophilicity, and oxide composition [98–101]. These topographical nanofeatures can significantly affect cell colonization, morphology, and activity [97]. For example, it is well established that nanorough surfaces generally enhance the adsorption of proteins such as fibrinogen, albumin, and fibronectin [102]. Similarly, the vertical dimension of nanometric surface features appears to be critical in determining the adsorption profile of fibronectin [102], thus having an impact on the distribution of focal adhesion of osteoblastic and endothelial cells [103,104].

### 13.6.3 Cellular Responses to Nanostructured Surfaces

It has been demonstrated that modifications of the surface texture or roughness of the implants alter cell shape and cytoskeleton, thus influencing specific gene expression [105–108]. Topographical features with dimensions similar to those of surface-bound proteins (~10 nm) can significantly affect protein orientation and denaturation, which determines the outcome of cell colonization [109–111]. Various *in vitro* cell models have been used to better understand the effects that nanostructured surfaces exert on cellular reactions. For instance, osteoblasts are used to evaluate the capacity of materials to promote bone formation for future dental implants [102,109,112–116]. Similarly, fibroblasts and endothelial cells are used to allow an assessment of fibrous and vascular repair capacities, thus evaluating the ability to promote or limit the growth of various tissues. Ultimately, stem or progenitor cells are generally used to determine whether a given nanotopography can induce differentiation along selected pathways [117].

It has been shown that anodized titanium surfaces, treated by the electrochemical technique, increased osteogenic activity *in vitro* [118–120]. Oxidative nanopatterning conferred titanium-based metals the capacity to selectively guide cell behavior, by favoring the growth of cells having the osteoblastic potential [78,121]. Indeed, the *in vitro* growth and osteogenic differentiation of human mesenchymal stem cells (hMSCs) were promoted on anodized titanium surfaces, suggesting an exciting potential for improving osseointegration of implants [122].

A significant upregulation of genes associated with cell adhesion and migration has been observed in osteogenic cells grown on nanostructured titanium surfaces shaped by either $H_2SO_4/H_2O_2$ or $NH_4OH/H_2O_2$ etching [82]. It has been shown that MSCs grown on nanopatterned titanium surfaces exhibit a bone-specific gene expression profile (e.g., alkaline phosphatase and Runx2) [82,123]. Therefore, anodization and oxidative surface nanopatterning techniques are important

for tissue regeneration and could be applied for achieving predictable tissue healing around dental implants.

Similarly, nanostructured bioactive coatings generated by sol–gel and chemical vapor deposition enhanced osteoblastic cell adhesion and proliferation [124–126]. In addition, the biocompatibility can be improved by creating superficial polyanionic films and collagen coatings [127,128].

Concomitant with these chemical methods, physical approaches confer an enhanced biocompatibility on implantable materials. For example, PVD was used to modify titanium surfaces with different nanotopographical coatings for evaluating the *in vitro* effects of surface chemistry and topography on cellular and/or tissue responses [88,129]. Moreover, electron-gun evaporation has been used to deposit coatings of biocompatible metals (e.g., nanostructured tantalum) with well-controlled roughness on various substrates, for protein adsorption *in vitro* studies [130].

### 13.6.4
### Clinical Applications of Nanostructured Dental Implants

Significant efforts have been made so far to integrate surface modification approaches with implant manufacturing in order to ensure superior clinical performance of current implant-supported prostheses [131–133]. Indeed, tissue integration and stability will result from the interactions between the implant surface and the surrounding tissues at both the cellular and the molecular level [134–137].

Based on the *in vitro* results, nanostructured metals undoubtedly have the potential to yield a faster and more stable integration of dental implants [73,138]. The *in vivo* effects of several nanoscale surface modification approaches and a potential applicability of these techniques to already commercialized dental implants are currently under investigation [73,139–141]. In fact, controlled anodization has endowed the surfaces of titanium implants with highly ordered nanotubes (30 nm diameter) that were able to stimulate collagen type I synthesis in pigs, thus increasing significantly the amount of the forming bone around the implant [139]. However, other *in vitro* [120] and *in vivo* [142] studies dealing with similarly treated surfaces but different nanotube diameters (70–80 nm and 250–800 nm) concluded that anodized titanium does not impact the total collagen content but enhances the peri-implant bone formation [120,142].

Anodic oxidation also allows deposition of nanohydroxyapatite (nanoHA) coatings [143]. Histomorphometric evaluation has shown that nanoHA-modified implants have significantly greater bone to implant contact (BIC) values when compared to acid-treated implants. The enhancement of BIC by nanoHA is due to the early bone formation, which depends on the size and diameter of the nanoHA [144]. A similar effect on BIC increase has been observed after depositing nanotopographic titanium dioxide coatings by a sol–gel technique [145]. Oxidative nanopatterning with $H_2SO_4/H_2O_2$ creates nanotopography on both bulk metals [82] and titanium screw-shaped implants. Oxidative treatment of

commercial screw-shaped titanium implants placed in dog mandibles resulted in enhanced BIC values and osteogenesis [146].

The combination of $TiO_2$ blasting and hydrofluoric acid treatment has been used to create a commercial endosseous titanium implant with nanorough surfaces containing features of 50–100 nm [147]. These implants stimulated osteoblastic gene expression and enhanced *in vivo* bone formation, osseointegration, and bone-implant fixation [148–150]. While some inflammatory reactions were reported [151], the overall success rate was satisfactory, with the majority of implants yielding good osseointegration and stability after 1 year post-surgery. Noteworthy, a high success rate was also reported under challenging clinical conditions such as early masticatory loading [152].

Dual-acid etching (DAE) followed by discrete-crystalline deposition (DCD) method has been used for the coating of titanium implants with calcium phosphate (CaP) nanocrystals (20–100 nm) [153] (Figure 13.3). These implants were clinically evaluated in a randomized controlled trial (RCT), which concluded that BIC increased by about 12% [154]. In addition, bone formation around CaP nanocrystal-coated implants was enhanced [155]. A study in dogs comparing bone formation around DAE and CaP nanocrystal-coated implants showed that

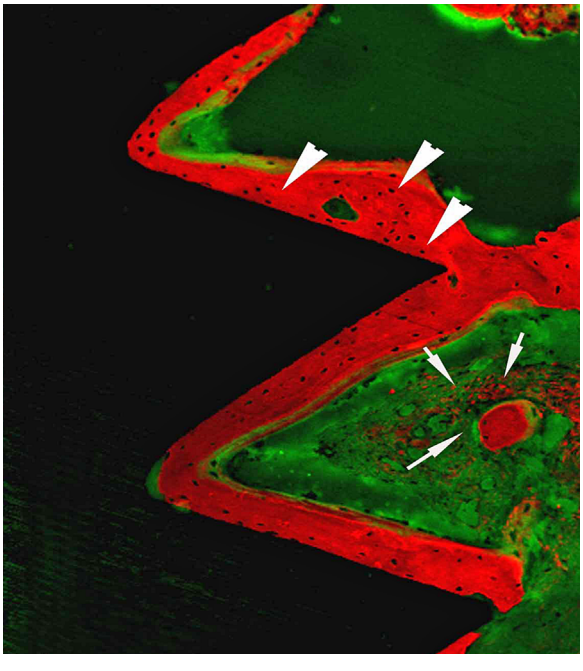

**Figure 13.3** Confocal scanning electron micrograph showing newly formed bone (arrows) closely adhering to the implant nanomodified surface (arrowheads) Photo taken from Ref. [157].)

there was no statistical difference in BIC in the early healing phase (1–4 weeks) [156]. However, bone resorption was reduced at the test sites containing implants coated with nanoparticles.

Nanostructured surfaces presenting uncharacterized "features" of approximately 100 nm have been obtained on nanorough titanium implants by hydrothermal alkaline treatment [158]. This method also caused incorporation of calcium as $CaTiO_3$ in the protective surface oxide layer. Titanium implants with treated surfaces significantly increased BIC and removal torque forces in rabbit tibiae [159–161]. Bioceramic grit-blasting and acid etching (BGB/AA) technologies have been integrated to endow titanium implants with nanometric topography [162]. Histological evaluation after 2 months postsurgery showed significantly higher BIC and osteocyte density around modified implants when compared to dual acid-etched implants [163].

### 13.6.5
### Nanomodifications of Bone Replacements Materials

Bone could be considered as a natural nanocomposite made up of organic compounds (mainly collagen) toughened with inorganic compounds like hydroxyapatite. When alveolar bone volume is limited, bone grafts are required prior to dental implant placement [164]. However, autologous bone grafts are available in limited amounts and may provoke morbidity. Therefore, allografts (e.g., demineralized freeze-dried bone or fresh frozen bone), xenografts (e.g., animal bone grafts), and synthetic biomaterials (e.g., calcium phosphate ceramics, bioactive glasses, porous hydroxyapatite, and polylactic-polyglycolic acid polymers) have been developed and introduced into the clinics during the last decades [165–168]. Synthetic biomaterials have to be biocompatible, osteoinductive, integrative, porous, and mechanically compatible with native bone to fulfill their desired role in bone regeneration and physiology. Improved biomaterials for bone reconstruction around implants could be induced by exploiting the ability of nanostructured surfaces to activate stem/progenitor cells, thus promoting fast bone regeneration [83,121,169]. These biomaterials offer cell anchorage sites, mechanical stability, and structural guidance, providing the interface to respond to physiological changes by remodeling the ECM [170]. Numerous studies have confirmed the success of the above-mentioned substitutes for bone regeneration in diverse reconstructive surgery techniques such as maxillary sinus augmentations, atrophic maxillaries reconstruction, and periodontal defects repair [166,171–175].

Synthetic biomaterials undergo limitations (e.g., poor osteoinductivity, osseointegration) that could be resolved by a common effort of tissue engineering and nanotechnology sciences for the development of new "smart" biomaterials [176]. The principle is to incorporate autologous stem cells and growth factors to nanofeatured scaffolds in order to enhance ECM production and tissue maturation before deposition of the dental implant. This novel approach

has shown some clinical advantages, but several technical issues still remain to be resolved before their use in clinics [63]. For example, newly formed tissue is not always efficient in these scaffolds and most of the grafted stem cells do not survive after implantation. Nanotechnology can provide a promising way of enhancing bioactivity of these new biomaterials that could also serve for cell and/or protein delivery systems [63]. For example, nanoporous surfaces could be further functionalized with molecular arrays or multilayered coatings that could provide specific signals to the cells and expose nanostructures capable of physical cueing or drug release.

### 13.6.6
### Nanofillers in Dental Restorative Materials

Resin-based composite materials are used for restoring missing parts of enamel and dentin. This technology is based on associating three main components that are chemically different from each other: the organic matrix (usually a synthetic monomer or resin), the inorganic matrix (the filler), and a coupling agent (usually silane) that bonds the inorganic to the organic matrix [177]. New materials such as phosphine oxide initiators and monomethacrylate diluents, but most importantly the introduction of nanofillers, have significantly improved the properties of dental composites [177]. The aim of incorporating fillers into resin is to optimize the properties and performance of the restorative material. Indeed, the addition of fillers can improve handling, offer radiopacity, enhance the mechanical properties thus providing composites with wear resistance, reduced polymerization shrinkage, and adapted to the tooth thermal expansion coefficient [178]. Conventional composites contain a range of fillers including quartz and silica particles based on the oxides of barium, strontium, zinc, aluminum, and zirconium. According to the diameter of their filler particles, composites could be classified as macrofiller (0.1–100 μm), microfiller (0.04–0.1 μm), and hybrid (variable sizes) [179]. Commonly, current composites are composed by 0.04–0.7 μm diameter filler particles, which cannot optimally interact with the nanoscopic (1–10 nm) structural elements of enamel (e.g., enamel rods, HA crystals) and dentin (e.g., dentinal tubules and collagen fibers). This lack of interaction compromise the optimal adhesion between the restorative material and the hard dental tissues [180]. Therefore, new composites containing nanofillers (particle size 1–100 nm) have been manufactured in the last years [181,182]. The nanosize of the particles diminishes polymerization shrinkage, offers uniform particle distribution, reduces viscosity, and offers better handling, while the mechanical properties remain intact [180]. However, the most important innovation in nanofillers is their ability to increase the load of the inorganic phase. Microfilled composites have a 50% in weight (wt) filler load, while nanofilled composites possess a 80 wt% filler load [183].

Currently, one nanocomposite system with three different types of fillers (i.e., nonagglomerated “discrete” silica nanoparticles, barium glass, prepolymerized nanoclusters) is used by dentists. Further nanoproducts include nanofillers

composed by aluminosilicate powder with a mean particle size of 80 nm and a 1:4 ratio of alumina to silica [184]. Recently, in order to enhance the physical–mechanical properties of resin-based composites, bimodal silica nanostructures made by $SiO_2$ nanoparticles (~70 nm) and $SiO_2$ nanoclusters (0.07–2.70 μm) were introduced to the market [185]. Improvements in flexural modulus and fracture toughness as well as lower surface roughness have been demonstrated by composites containing porous thermally sintered nanosilica as filler [186]. Another recent development in dental resin-based nanocomposites is the generation of the "bulk-fill" composites. These materials possess decreased polymerization shrinkage stress, reduced cusp deflection, good bond strengths, and can be applied in increments up to 4 mm thickness [187,188]. However, nanofilled composites might not always improve mechanical properties compared to microfilled and hybrid composites [189].

The esthetic aspect of composites is also a critical issue since the matching of composite's color with that of the natural teeth is desirable (Figure 13.4). Nanofillers are employed to increase gloss and improve surface characteristics and translucency that are important esthetic characteristics for dental materials [190]. To date, nanofillers are applied in almost all new resin-based restorative dental materials, thus providing extremely beautiful esthetic restorations with micromechanical properties similar to or even better than those exhibited by traditional composites [191].

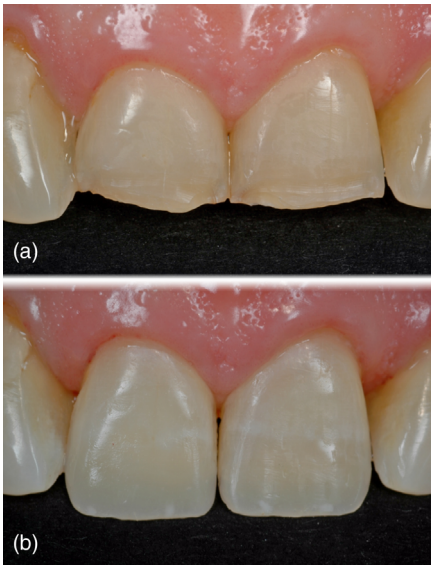


**Figure 13.4** (**a**) Preoperative view of a patient with broken central maxillary incisors. (**b**) Postoperative image of the restorations performed using nanohybrid resin-based composites. (Photo given by Prof. A. Putignano, Unit of Restorative Dentistry and Endodontics, Polytechnic University of Marche, Ancona, Italy.)

### 13.6.7 Nanoscale Modification in the Treatment of Dentin Hypersensitivity and Enamel Remineralization

The use of nanotechnology in products of oral health that may prevent dental caries, enamel erosion, and dentin hypersensitivity (e.g., toothpaste, mouthrinse) is of increasing interest [183,192,193]. Dentin hypersensitivity has increased considerably over the last decades mainly due to the bigger consumption of acidic drinks that cause daily enamel degradation and result in dentin exposure. Nanomodified materials could be used to support enamel and dentin mineralization, control bacterial plaque formation and microbial invasion, and abolish tooth hypersensitivity [194,195]. Employing synthetic nanoHA particles in dentifrices might result in a protective nanostructured layer on the tooth surface and even restore lost mineral contents of enamel and dentin [195,196]. NanoHA and Ca-based nanomodified materials have been used for dentin hypersensitivity by occluding the dentinal tubules and providing enamel remineralization [197] (Figure 13.5). Clinical randomized trials have shown the efficacy of zinc-substituted carbonate-hydroxyapatite (CHA) nanostructured crystals in reducing dentin hypersensitivity after three days of application and to maintain this relief after 4 and 8 weeks [198,199]. It has been shown that enamel surface can be remineralized using CHA-based toothpastes [197]. Toothpastes composed by nanoHA can enhance enamel remineralization and reduce bacterial colonization of the tooth surfaces [183]. Other nanomaterials containing nanoparticulate bioactive glass, nanosized carbonated apatite alone or in combination with silica, nanosized calcium fluoride, carbonate-hydroxyapatite nanocrystals, and nanoprecursors of amorphous calcium phosphates have been tested on enamel and dentin

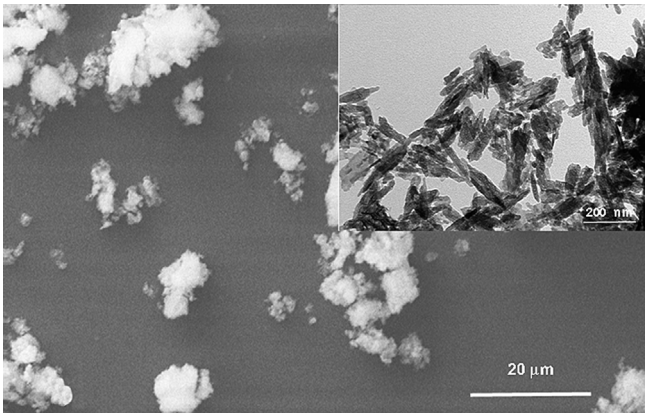


**Figure 13.5** Scanning electron micrograph of synthetic biomimetic carbonate hydroxyapatite (CHA) nanocrystals forming microclasters. The inset shows a transmission electron micrograph of CHA nanocrystals with characteristic acicular morphology. (Photo taken from Ref. [203].)

remineralization [183,195,196]. The nanocomplex of casein phosphopeptide (CPP), which carries calcium and phosphate ions bound to it in the form of amorphous calcium phosphate (ACP), has been also suggested to promote enamel remineralization [200]. When in mouth, the CPP–ACP nanocomplexes adhere to the enamel, bacterial plaque, and soft oral tissues delivering calcium and phosphate ions. Thereafter, the released ions enter the enamel rods and reform apatite crystals that are necessary for enamel remineralization [201]. The recently introduced nanoparticle-based biomimetic dentin remineralization strategy, which is based on the polymer-induced liquid-precursors process, demonstrates great potential in remineralizing faulty hybrid layers (the so-called interdiffusion zone between dentin and resin-based composite restorations) or carious-like dentin [202].

The plethora of scientific and clinical reports have shown positive effects of these new products, making thus evident that there is an emerging market for the use of nanotechnology in dental health care products. However, more controlled and reproducible studies are needed to prove safety and long-term efficacy.

## 13.7 Concluding Remarks

Stem cell-based therapies in dental clinics are not applicable yet. There is a need to develop accurate techniques that will allow monitoring the fate and behavior of transplanted stem cells at the sites of dental injury or loss. Nanotechnology offers a plethora of exciting perspectives to regenerative dentistry, and combined with tissue engineering and stem cell biology might provide novel techniques for dental tissue regeneration.

Nanoscale surface modification approaches are likely to foster profound changes in the ways dental biomaterials are designed and manufactured. These modifications introduce novel bioactive capacity into the arena of dental biomaterials that should be actually produced in a large industrial scale. However, many of the approaches described above still remain to be tested *in vivo*. To date, there are only few animal and clinical studies on the long-term effects of such nanomodifications in the complex *in vivo* environment [204]. *In vivo* studies involving medium- and large-size animals are essential to screen potentially successful treatments for subsequent human trials. Before arriving at clinics, measurements and evaluation techniques need to be standardized [205]. Indeed, dental implants advertised as nanostructured are often characterized by inhomogeneous “nanofeatures” that lack statistical distribution and/or precise reproducibility. In this context, even smooth biomaterials could be considered nanostructured if they exhibit some kind of nanometric “feature” (i.e., natural defects of materials) [204]. Therefore, the need of a distinction between engineered nanostructures and the native topography of materials at the nanoscale

level is legitimate. It will be also important to optimize current and future nanotechnology approaches in order to generate dental materials with controlled and uniform surface nanofeatures.

The application of dental implants will continue to grow until nanotechnology, stem cell biology, and tissue engineering techniques reach a level allowing the regeneration of entire new tissues and organs. Until then, any procedure that could improve biomaterials will have a major impact on the quality of life. Advances in surface-engineering techniques and nanotechnology promise a new generation of improved prosthetic devices with bioactive surfaces.

## Acknowledgments

This work was supported by funds of the University of Zurich, Polytechnic University of Marche, and by the COST Action NAMABIO MP1005. The authors contributed to the planning, writing, critical reading, and editing of the this chapter. The authors confirm that there are no conflicts of interest associated with this work.

## References

1 Mitsiadis, T.A., Woloszyk, A., and Jimenez-Rojo, L. (2012) Nanodentistry: combining nanostructured materials and stem cells for dental tissue regeneration. *Nanomedicine (Lond)*, **7** (11), 1743–1753.
2 Kim, B.Y., Rutka, J.T., and Chan, W.C. (2010) Nanomedicine. *N. Engl. J. Med.*, **363** (25), 2434–2443.
3 Xia, Y. (2008) Nanomaterials at work in biomedical research. *Nat. Mater.*, **7** (10), 758–760.
4 Huebsch, N. and Mooney, D.J. (2009) Inspiration and application in the evolution of biomaterials. *Nature*, **462** (7272), 426–432.
5 Moghimi, S.M., Hunter, A.C., and Murray, J.C. (2005) Nanomedicine: current status and future prospects. *FASEB J.*, **19** (3), 311–330.
6 Moghimi, S.M., Hunter, A.C., and Andresen, T.L. (2012) Factors controlling nanoparticle pharmacokinetics: an integrated analysis and perspective. *Annu. Rev. Pharmacol. Toxicol.*, **52**, 481–503.
7 Wang, Y., Brown, P., and Xia, Y. (2011) Nanomedicine: swarming towards the target. *Nat. Mater.*, **10** (7), 482–483.
8 Forsberg, M. and Hovatta, O. (2012) Challenges for the therapeutic use of pluripotent stem derived cells. *Front. Physiol.*, **3**, 19.
9 Jimenez-Rojo, L., Granchi, Z., Graf, D., and Mitsiadis, T.A. (2012) Stem cell fate determination during development and regeneration of ectodermal organs. *Front. Physiol.*, **3**, 107.
10 Caton, J., Bostanci, N., Remboutsika, E., De Bari, C., and Mitsiadis, T.A. (2011) Future dentistry: cell therapy meets tooth and periodontal repair and regeneration. *J. Cell Mol. Med.*, **15** (5), 1054–1065.
11 Mitsiadis, T.A., and Graf, D. (2009) Cell fate determination during tooth development and regeneration. *Birth Defects Res. C*, **87** (3), 199–211.
12 Papagerakis, P., and Mitsiadis, T. (2013) *Development and Structure of Teeth and Periodontal Tissues* (ed. C.J. Rosen), John Wiley & Sons, Inc, Hoboken.

13 Mitsiadis, T.A., Massa, A., and Orsini, G. (2016) Le cellule staminali del dente. In: Cellule Saminali (ed. L. Bonsi and F. Alviano), Esculario, Bologna, Italy. In press.

14 Murray, P.E., and Garcia-Godoy, F. (2006) The outlook for implants and endodontics: a review of the tissue engineering strategies to create replacement teeth for patients. *Dent. Clin. North Am.*, **50** (2), 299–315.

15 Mitsiadis, T.A., and Harada, H. (2015) Regenerated teeth: the future of tooth replacement. An update. *Regen. Med.*, **10** (1), 5–8.

16 Mitsiadis, T.A., and Papagerakis, P. (2011) Regenerated teeth: the future of tooth replacement? *Regen. Med.*, **6** (2), 135–139.

17 Takahashi, K., Okita, K., Nakagawa, M., and Yamanaka, S. (2007) Induction of pluripotent stem cells from fibroblast cultures. *Nat. Protoc.*, **2** (12), 3081–3089.

18 Takahashi, K. and Yamanaka, S. (2006) Induction of pluripotent stem cells from mouse embryonic and adult fibroblast cultures by defined factors. *Cell*, **126** (4), 663–676.

19 Ikeda, E., Morita, R., Nakao, K., Ishida, K., Nakamura, T., Takano-Yamamoto, T. *et al.* (2009) Fully functional bioengineered tooth replacement as an organ replacement therapy. *Proc. Natl. Acad. Sci. USA*, **106** (32), 13475–13480.

20 Oshima, M., Inoue, K., Nakajima, K., Tachikawa, T., Yamazaki, H., Isobe, T. *et al.* (2014) Functional tooth restoration by next-generation bio-hybrid implant as a bio-hybrid artificial organ replacement therapy. *Sci. Rep.*, **4**, 6044.

21 Oshima, M., Mizuno, M., Imamura, A., Ogawa, M., Yasukawa, M., Yamazaki, H. *et al.* (2011) Functional tooth regeneration using a bioengineered tooth unit as a mature organ replacement regenerative therapy. *PLoS One*, **6** (7), e21531.

22 Oshima, M., Ogawa, M., Yasukawa, M., and Tsuji, T. (2012) Generation of a bioengineered tooth by using a three-dimensional cell manipulation method (organ germ method). *Methods Mol. Biol.*, **887**, 149–165.

23 Mitsiadis, T.A., Barrandon, O., Rochat, A., Barrandon, Y., and De Bari, C. (2007) Stem cell niches in mammals. *Exp Cell Res.*, **313** (16), 3377–3385.

24 Gronthos, S., Mankani, M., Brahim, J., Robey, P.G., and Shi, S. (2000) Postnatal human dental pulp stem cells (DPSCs) *in vitro* and *in vivo*. *Proc. Natl. Acad. Sci. USA*, **97** (25), 13625–13630.

25 Miura, M., Gronthos, S., Zhao, M., Lu, B., Fisher, L.W., Robey, P.G. *et al.* (2003) SHED: stem cells from human exfoliated deciduous teeth. *Proc. Natl. Acad. Sci. USA*, **100** (10), 5807–5812.

26 Sonoyama, W., Liu, Y., Fang, D., Yamaza, T., Seo, B.M., Zhang, C. *et al.* (2006) Mesenchymal stem cell-mediated functional tooth regeneration in swine. *PLoS One*, **1**, e79.

27 Sonoyama, W., Liu, Y., Yamaza, T., Tuan, R.S., Wang, S., Shi, S. *et al.* (2008) Characterization of the apical papilla and its residing stem cells from human immature permanent teeth: a pilot study. *J. Endod.*, **34** (2), 166–171.

28 Morsczeck, C., Gotz, W., Schierholz, J., Zeilhofer, F., Kuhn, U., Mohl, C. *et al.* (2005) Isolation of precursor cells (PCs) from human dental follicle of wisdom teeth. *Matrix Biol.*, **24** (2), 155–165.

29 Seo, B.M., Miura, M., Gronthos, S., Bartold, P.M., Batouli, S., Brahim, J. *et al.* (2004) Investigation of multipotent postnatal stem cells from human periodontal ligament. *Lancet*, **364** (9429), 149–155.

30 Wang, L., Shen, H., Zheng, W., Tang, L., Yang, Z., Gao, Y. *et al.* (2011) Characterization of stem cells from alveolar periodontal ligament. *Tissue Eng. A*, **17** (7–8), 1015–1026.

31 Bluteau, G., Luder, H.U., De Bari, C., and Mitsiadis, T.A. (2008) Stem cells for tooth engineering. *Eur. Cell Mater.*, **16**, 1–9.

32 Graziano, A., d'Aquino, R., Laino, G., and Papaccio, G. (2008) Dental pulp stem cells: a promising tool for bone regeneration. *Stem Cell Rev.*, **4** (1), 21–26.

33 Gronthos, S., Brahim, J., Li, W., Fisher, L.W., Cherman, N., Boyde, A. *et al.*

(2002) Stem cell properties of human dental pulp stem cells. *J. Dent. Res.*, **81** (8), 531–535.

34 Shinmura, Y., Tsuchiya, S., Hata, K., and Honda, M.J. (2008) Quiescent epithelial cell rests of Malassez can differentiate into ameloblast-like cells. *J. Cell. Physiol.*, **217** (3), 728–738.

35 Pagella, P., Neto, E., Lamghari, M., and Mitsiadis, T.A. (2015) Investigation of orofacial stem cell niches and their innervation through microfluidic devices. *Eur. Cell. Mater.*, **29**, 213–223.

36 Huang, G.T., Gronthos, S., and Shi, S. (2009) Mesenchymal stem cells derived from dental tissues vs. those from other sources: their biology and role in regenerative medicine. *J. Dent. Res.*, **88** (9), 792–806.

37 Batouli, S., Miura, M., Brahim, J., Tsutsui, T.W., Fisher, L.W., Gronthos, S. *et al.* (2003) Comparison of stem-cell-mediated osteogenesis and dentinogenesis. *J. Dent. Res.*, **82** (12), 976–981.

38 Huang, G.T., Yamaza, T., Shea, L.D., Djouad, F., Kuhn, N.Z., Tuan, R.S. *et al.* (2010) Stem/progenitor cell-mediated *de novo* regeneration of dental pulp with newly deposited continuous layer of dentin in an *in vivo* model. *Tissue Eng. A*, **16** (2), 605–615.

39 d'Aquino, R., De Rosa, A., Lanza, V., Tirino, V., Laino, L., Graziano, A. *et al.* (2009) Human mandible bone defect repair by the grafting of dental pulp stem/progenitor cells and collagen sponge biocomplexes. *Eur. Cell Mater.*, **18**, 75–83.

40 Handa, K., Saito, M., Tsunoda, A., Yamauchi, M., Hattori, S., Sato, S. *et al.* (2002) Progenitor cells from dental follicle are able to form cementum matrix *in vivo*. *Connect. Tissue Res.*, **43** (2–3), 406–408.

41 Yokoi, T., Saito, M., Kiyono, T., Iseki, S., Kosaka, K., Nishida, E. *et al.* (2007) Establishment of immortalized dental follicle cells for generating periodontal ligament in vivo. *Cell Tissue Res.*, **327** (2), 301–311.

42 Honda, M.J., Shinohara, Y., Hata, K.I., and Ueda, M. (2007) Subcultured odontogenic epithelial cells in combination with dental mesenchymal cells produce enamel-dentin-like complex structures. *Cell Transplant.*, **16** (8), 833–847.

43 Honda, M.J., Sumita, Y., Kagami, H., and Ueda, M. (2005) Histological and immunohistochemical studies of tissue engineered odontogenesis. *Arch. Histol. Cytol.*, **68** (2), 89–101.

44 Young, C.S., Terada, S., Vacanti, J.P., Honda, M., Bartlett, J.D., and Yelick, P.C. (2002) Tissue engineering of complex tooth structures on biodegradable polymer scaffolds. *J. Dent. Res.*, **81** (10), 695–700.

45 Nam, H. and Lee, G. (2009) Identification of novel epithelial stem cell-like cells in human deciduous dental pulp. *Biochem. Biophys. Res. Commun.*, **386** (1), 135–139.

46 Arakaki, M., Ishikawa, M., Nakamura, T., Iwamoto, T., Yamada, A., Fukumoto, E. *et al.* (2012) Role of epithelial-stem cell interactions during dental cell differentiation. *J. Biol. Chem.*, **287** (13), 10590–10601.

47 Otsu, K., Kumakami-Sakano, M., Fujiwara, N., Kikuchi, K., Keller, L., Lesot, H. *et al.* (2014) Stem cell sources for tooth regeneration: current status and future prospects. *Front Physiol.*, **5**, 36.

48 Otsu, K., Kishigami, R., Oikawa-Sasaki, A., Fukumoto, S., Yamada, A., Fujiwara, N. *et al.* (2012) Differentiation of induced pluripotent stem cells into dental mesenchymal cells. *Stem Cells Dev.*, **21** (7), 1156–1164.

49 Sun, H.H., Jin, T., Yu, Q., and Chen, F.M. (2011) Biological approaches toward dental pulp regeneration by tissue engineering. *J. Tissue Eng. Regen. Med.*, **5** (4), e1–16.

50 Zhu, X., Zhang, C., Huang, G.T., Cheung, G.S., Dissanayaka, W.L., and Zhu, W. (2012) Transplantation of dental pulp stem cells and platelet-rich plasma for pulp regeneration. *J. Endod.*, **38** (12), 1604–1609.

51 About, I., Bottero, M.J., de Denato, P., Camps, J., Franquin, J.C., and Mitsiadis, T.A. (2000) Human dentin production *in vitro*. *Exp. Cell Res.*, **258** (1), 33–41.

52 Huang, G.T., Shagramanova, K., and Chan, S.W. (2006) Formation of odontoblast-like cells from cultured human dental pulp cells on dentin *in vitro*. *J. Endod.*, **32** (11), 1066–1073.

53 Howell, T.H., Fiorellini, J.P., Paquette, D.W., Offenbacher, S., Giannobile, W.V., and Lynch, S.E. (1997) A phase I/II clinical trial to evaluate a combination of recombinant human platelet-derived growth factor-BB and recombinant human insulin-like growth factor-I in patients with periodontal disease. *J. Periodontol.*, **68** (12), 1186–1193.

54 Selvig, K.A., Sorensen, R.G., Wozney, J.M., and Wikesjo, U.M. (2002) Bone repair following recombinant human bone morphogenetic protein-2 stimulated periodontal regeneration. *J. Periodontol.*, **73** (9), 1020–1029.

55 Veis, A., Tompkins, K., Alvares, K., Wei, K., Wang, L., Wang, X.S. *et al.* (2000) Specific amelogenin gene splice products have signaling effects on cells in culture and in implants *in vivo*. *J. Biol. Chem.*, **275** (52), 41263–41272.

56 Yang, B., Chen, G., Li, J., Zou, Q., Xie, D., Chen, Y. *et al.* (2012) Tooth root regeneration using dental follicle cell sheets in combination with a dentin matrix-based scaffold. *Biomaterials*, **33** (8), 2449–2461.

57 Oshima, M. and Tsuji, T. (2014) Functional tooth regenerative therapy: tooth tissue regeneration and whole-tooth replacement. *Odontology*, **102** (2), 123–136.

58 Petros, R.A. and DeSimone, J.M. (2010) Strategies in the design of nanoparticles for therapeutic applications. *Nat. Rev. Drug Discov.*, **9** (8), 615–627.

59 Ferreira, L., Karp, J.M., Nobre, L., and Langer, R. (2008) New opportunities: the use of nanotechnologies to manipulate and track stem cells. *Cell Stem Cell*, **3** (2), 136–146.

60 Mooney, D.J. and Vandenburgh, H. (2008) Cell delivery mechanisms for tissue repair. *Cell Stem Cell*, **2** (3), 205–213.

61 Dickinson, L.E., Kusuma, S., and Gerecht, S. (2011) Reconstructing the differentiation niche of embryonic stem cells using biomaterials. *Macromol. Biosci.*, **11** (1), 36–49.

62 Kraehenbuehl, T.P., Langer, R., and Ferreira, L.S. (2011) Three-dimensional biomaterials for the study of human pluripotent stem cells. *Nat. Methods*, **8** (9), 731–736.

63 Variola, F., Brunski, J.B., Orsini, G., Tambasco de Oliveira, P., Wazen, R., and Nanci, A. (2011) Nanoscale surface modifications of medically relevant metals: state-of-the art and perspectives. *Nanoscale*, **3** (2), 335–353.

64 Barbucci, R., Pasqui, D., Wirsen, A., Affrossman, S., Curtis, A., and Tetta, C. (2003) Micro and nano-structured surfaces. *J. Mater. Sci.Mater. Med.*, **14** (8), 721–725.

65 Liu, X., Chu, P.K., and Ding, C. (2004) Surface modification of titanium, titanium alloys, and related materials for biomedical applications. *Mater. Sci. Eng. R.*, **47**, 49–121.

66 Anselme, K. and Bigerelle, M. (2006) Statistical demonstration of the relative effect of surface chemistry and roughness on human osteoblast short-term adhesion. *J. Mater. Sci.Mater. Med.*, **17**, 471–479.

67 Kim, M.-J., Choi, M.-U., and Kim, C.-W. (2006) Activation of phospholipase D1 by surface roughness of titanium in MG63 osteoblast-like cell. *Biomaterials*, **27**, 5502–5511.

68 Aparicio, C., Gil, F.J., Planell, J.A., and Engel, E. (2002) Human-osteoblast proliferation and differentiation on grit-blasted and bioactive titanium for dental applications. *J. Mater. Sci. Mater. Med.*, **13**, 1105–1111.

69 Park, J.-W., Jang, I.-S., and Suh, J.-Y. (2008) Bone response to endosseous titanium implants surface-modified by blasting and chemical treatment: a histomorphometric study in the rabbit femur. *J. Biomed. Mater. Res. B.*, **84** (2), 400–407.

70 Daugaard, H., Elmengaard, B., Bechtold, J.E., and Soballe, K. (2008) Bone growth enhancement in vivo on press-fit titanium alloy implants with acid etched

microtexture. *J. Biomed. Mater. Res. A.*, **87** (2), 434–440.

71 Piattelli, A., Celletti, R., Marinho, V.C., Traini, T., Orsini, G., Bracchetti, G. *et al.* (2006) Bone Contact Around Osseointegrated Implants: A Histologic Study of Acid-Etched and Machined Surfaces. *J. Long-Term. Eff. Med. Implants*, **16** (2), 131–143.

72 Piattelli, M., Scarano, A., Paolantonio, M., Iezzi, G., Petrone, G., and Piattelli, A. (2002) Bone response to machined and resorbable blast material titanium implants: an experimental study in rabbits. *J. Oral Implantol.*, **28** (1), 2–8.

73 Khang, D., Lu, J., Yao, C., Haberstroh, K.M., and Webster, T.J. (2008) The role of nanometer and sub-micron surface features on vascular and bone cell adhesion on titanium. *Biomaterials*, **29**, 970–983.

74 Mendonça, G., Mendonça, D.B.S., Aragao, F.J.L., and Cooper, L.F. (2008) Advancing dental implant surface technology – from micron to nanotopography. *Biomaterials*, **29**, 3822–3835.

75 Liu, H. and Webster, T.J. (2007) Nanomedicine for implants: a review of studies and necessary experimental tools. *Biomaterials*, **28**, 354–369.

76 Horley, G.A. (2006) The importance of being nano. *Small*, **1**, 3–5.

77 Whitesides, G.M. (2003) The "right" size in nanobiotechnology. *Nat. Biotechnol.*, **21** (10), 1161–1165.

78 Variola, F., Vetrone, F., Richert, L., Jedrzejowski, P., Yi, J.-H., Zalzal, S. *et al.* (2009) Improving biocompatibility of implantable metals by nanoscale modification of surfaces: an overview of strategies, fabrication methods, and challenges. *Small*, **5** (9), 996–1006.

79 Kim, K.-H. and Ramaswamy, N. (2009) Electrochemical surface modification of titanium in dentistry. *Dent. Mater. J.*, **28** (1), 20–36.

80 Narayanan, R., Kim, S.-Y., Kwon, T.-Y., and Kim, K.-H. (2008) Nanocrystalline hydroxyapatite coatings from ultrasonated electrolyte: Preparation, characterization, and osteoblast responses. *J. Biomed. Mater. Res. A*, **87** (4), 1053–1060.

81 Lin, C., Han, H., Zhang, F., and Li, A. (2008) Electrophoretic deposition of HA/MWNTs composite coating for biomaterial applications. *J. Mater. Sci. Mater. Med.*, **19**, 2569–2574.

82 Vetrone, F., Variola, F., Oliveira, P.T.d., Zalzal, S.F., Yi, J.-H., Sam, J. *et al.* (2008) Nanoscale oxidative patterning of metallic surfaces to control cell activity and fate. *Nano Lett.*, **9** (2), 659–665.

83 Variola, F., Yi, J.-H., Richert, L., Wuest, J.D., Rosei, F., and Nanci, A. (2008) Tailoring the Surface Properties of Ti6Al4V by Controlled Chemical Oxidation. *Biomaterials*, **29**, 1285–1298.

84 Eisenbarth, E., Velten, D., and Breme, J. (2007) Biomimetic implant coatings. *Biomol. Eng.*, **24** (1), 27–32.

85 Popescu, S., Demetrescu, I., Sarantopoulos, C., Gleizes, A.N., and Iordachescu, D. (2007) The biocompatibility of titanium in a buffer solution: compared effects of a thin film of TiO2 deposited by MOCVD and of collagen deposited from a gel. *J. Mater. Sci. Mater. Med.*, **18** (10), 2075–2083.

86 Morra, M. (2006) Biochemical modification of titanium surfaces: peptides and ECM proteins. *Eur. Cell. Mater.*, **12**, 1–15.

87 Reising, A., Yao, C., Storey, D., and Webster, T.J. (2008) Greater osteoblast long-term functions on ionic plasma deposited nanostructured orthopedic implant coatings. *J. Biomed. Mater. Res.*, **87A**, 78–83.

88 Großner-Schreiber, B., Herzog, M., Hedderich, J., Duck, A., Hannig, M., and Griepentrog, M. (2006) Focal adhesion contact formation by fibroblasts cultured on surface-modified dental implants: an *in vitro* study. *Clin. Oral. Impl. Res.*, **17**, 736–745.

89 Ogawa, T., Saruwatari, L., Takeuchi, K., Aita, H., and Ohno, N. (2008) Ti nano-nodular structuring for bone integration and regeneration. *J. Dent. Res.*, **87** (8), 751–756.

90 Hanawa, T. (1999) *In vivo* metallic biomaterials and surface modification. *Mater. Sci. Eng. A*, **267** (2), 260–266.

91 Hanawa, T., Kamiura, Y., Yamamoto, S., Kohgo, T., Amemiya, A., Ukai, H. *et al.* (1997) Early bone formation around calcium-ion-implanted titanium inserted into rat tibia. *J. Biomed. Mater. Res.*, **36** (1), 131–136.

92 Kasemo, B. (2002) Biological surface science. *Surf. Sci.*, **500**, 656–677.

93 Anselme, K. (2000) Osteoblast adhesion on biomaterials. *Biomaterials*, **21**, 667–681.

94 Puleo, D.A. and Nanci, A. (1999) Understanding and controlling the bone-implant surface. *Biomaterials*, **20**, 2311–2321.

95 Davies, J.E. (1996) *In vitro* modeling of the bone/implant interface. *Anat. Rec.*, **245**, 426–445.

96 Davies, J.E. (1998) Mechanisms of endosseous integration. *Int. J. Prosthodont.*, **11**, 391–401.

97 Kasemo, B. and Gold, J. (1999) Implant surfaces and interface processes. *Adv. Dent. Res.*, **13**, 8.

98 Hori, N., Att, W., Ueno, T., Sato, N., Yamada, M., Saruwatari, L. *et al.* (2009) Age-dependent degradation of the protein adsorption capacity of titanium. *J. Dent. Res.*, **88**, 663–667.

99 Nagassa, M.E., Daw, A.E., Rowe, W.G., Carley, A., Thomas, D.W., and Moseley, R. (2008) Optimisation of the hydrogen peroxide pre-treatment of titanium: surface characterisation and protein adsorption. *Clin. Oral Implants Res.*, **19**, 1317–1326.

100 Wilson, C.J., Clegg, R.E., Leavesley, D.I., and Pearcy, M.J. (2005) Mediation of biomaterial-cell interactions by adsorbed proteins: a review. *Tissue Eng.*, **11**, 1–18.

101 Gugutkov, D., Altankov, G., Hernández, J.C.R., Pradas, M.M., and Sánchez, M.S. (2010) Fibronectin activity on substrates with controlled –OH density. *J. Biomed. Mater. Res. A.*, **92** (1), 322–331.

102 Cai, K., Bossert, J., and Biointerfaces, K.D. J.C.S.B. (2006) Does the nanometre scale topography of titanium influence protein adsorption and cell proliferation? *Colloids Surf. B Biointerfaces*, **49**, 136–144.

103 Carpenter, J., Khang, D., and Webster, T.J. (2008) Nanometer polymer surface features: the influence on surface energy, protein adsorption and endothelial cell adhesion. *Nanotechnology*, **19**, 505103.

104 González-García, C., Sousa, S.R., Moratal, D., Rico, P., and Salmerón-Sánchez, M. (2010) Effect of nanoscale topography on fibronectin adsorption, focal adhesion size and matrix organisation. *Colloids Surf. B Biointerfaces*, **77** (2), 181–190.

105 Leven, R.M., Virdi, A.S., and Sumner, D.R. (2004) Patterns of gene expression in rat bone marrow stromal cells cultured on titanium alloy discs of different roughness. *J. Biomed. Mater. Res. A.*, **70**, 391–401.

106 Masaki, C., Schneider, G.B., Zaharias, R., Seabold, D., and Stanford, C. (2005) Effects of implant surface microtopography on osteoblast gene expression. *Clin. Oral. Implants Res.*, **16**, 650–656.

107 Ogawa, T. and Nishimura, I. (2006) Genes differentially expressed in titanium implant healing. *J. Dent. Res.*, **85** (6), 566–570.

108 Isa, Z.M., Schneider, G.B., Zaharias, R., Seabold, D., and Stanford, C.M. (2006) Effects of fluoride-modified titanium surfaces on osteoblast proliferation and gene expression. *Int. J. Maxillofac Implants*, **21** (2), 203–211.

109 Sela, M.N., Badihi, L., Rosen, G., Steinberg, D., and Kohavi, D. (2007) Adsorption of human plasma proteins to modified titanium surfaces. *Clin. Oral. Implants Res.*, **18**, 630.

110 Roach, P., Farrar, D., and Perry, C.C. (2006) Surface tailoring for controlled protein adsorption: effect of topography at the nanometer scale and chemistry. *J. Am. Chem. Soc.*, **128**, 3939.

111 Hemmersam, A.G., Foss, M., Chevallier, J., and Besenbacher, F. (2005) Adsorption of fibrinogen on tantalum oxide, titanium oxide and gold studied by the QCM-D technique. *Colloids Surf.*, **43**, 208.

112 Denis, F.A., Hanarp, P., Sutherland, D.S., Gold, J., Mustin, C., Rouxhet, P.G. *et al.* (2002) Protein Adsorption on Model

Surfaces with Controlled Nanotopography and Chemistry. *Langmuir*, **18**, 819–828.

113 Dolatshahi-Pirouz, A., Rechendorff, K., Hovgaard, M.B., Foss, M., Chevallier, J., and Besenbacher, F. (2008) Bovine serum albumin adsorption on nano-rough platinum surfaces studied by QCM-D. *Colloids Surf. B.*, **66**, 53–59.

114 Hovgaard, M.B., Rechendorff, K., Chevallier, J., Foss, M., and Besenbacher, F. (2008) Fibronectin adsorption on tantalum: the influence of nanoroughness. *J. Phys. Chem. B.*, **112**, 8241–8249.

115 Rechendorff, K., Hovgaard, M.B., Foss, M., Zhdanov, V.P., and Besenbacher, F. (2006) Enhancement of protein adsorption induced by surface roughness. *Langmuir*, **22**, 10885–10888.

116 Richert, L., Variola, F., Rosei, F., Wuest, J.D., and Nanci, A. (2010) Adsorption of proteins on nanoporous Ti surfaces. *Surf. Sci.*, **604** (17), 1445–1451.

117 Pollard, T.D. and Earnshaw, W.C. (2002) *Cell Biology*, Saunders.

118 Das, T., Ghosh, D., Bhattacharyya, T.K., and Maiti, T.K. (2007) Biocompatibility of diamond-like nanocomposite thin films. *J. Mater. Sci. Mater. Med.*, **18**, 493–500.

119 Ercan, B. and Webster, T.J. (2008) Greater osteoblast proliferation on anodized nanotubular titanium upon electrical stimulation. *Int. J. Nanomed.*, **3** (4), 477–485.

120 Yao, C., Slamovich, E.B., and Webster, T.J. (2008) Enhanced osteoblast functions on anodized titanium with nanotube-like structures. *J. Biomed. Mat. Res. A.*, **85** (1), 157–166.

121 Richert, L., Vetrone, F., Yi, J.-H., Zalzal, S.F., Wuest, J.D., Rosei, F. *et al.* (2008) Surface nanopatterning to control cell growth. *Adv. Mat.*, **20**, 1488–1492.

122 Chiang, C.-Y., Chiou, S.-H., Yang, W.-E., Hsu, M.-L., Yung, M.-C., Tsai, M.-L. *et al.* (2009) Formation of TiO2 nano-network on titanium surface increases the human cell growth. *Dental Mater.*, **25**, 1022–1029.

123 Mendonça, G., Mendonça, D.B., Aragão, F.J., and Cooper, L.F. (2010) The combination of micron and nanotopography by H2SO4/H2O2 treatment and its effects on osteoblast-specific gene expression of hMSCs. *J. Biomed. Mater. Res. A*, **94** (1), 169–179.

124 Bajgai, M.P., Parajuli, D.C., Park, S.-J., Chu, K.H., Kang, H.-S., and Kim, H.Y. (2010) *In vitro* bioactivity of sol–gel-derived hydroxyapatite particulate nanofiber modified titanium. *J. Mater. Sci. Mater. Med.*, **21**, 685–694.

125 Amaral, M., Dias, A.G., Gomes, P.S., Lopes, M.A., Silva, R.F., Santos, J.D. *et al.* (2008) Nanocrystalline diamond: *in vitro* biocompatibility assessment by MG63 and human bone marrow cells cultures. *J. Biomed. Mater. Res. A*, **87**, 91–99.

126 Roy, R.K. and Lee, K.-R. (2007) Biomedical applications of diamond-like carbon coatings: a review. *J. Biomed. Mat. Res. B.*, **83**, 72–84.

127 Dolder, J.V.D. and Jansen, J.A. (2007) The response of osteoblast-like cells towards collagen type I coating immobilized by *p*-nitrophenylchloroformate to titanium. *J. Biomed. Mater. Res. A.*, **83**, 712–719.

128 Pelsoczi, I., Turzo, K., Gergely, C., Fazekas, A., Dekany, I., and Cuisinier, F. (2005) Structural characterization of self-assembled polypeptide films on titanium and glass surfaces by atomic force microscopy. *Biomacromol*, **6**, 3345–3350.

129 Hacking, S.A., Zuraw, M., Harvey, E.J., Tanzer, M., Krygier, J.J., and Bobyn, J.D. (2007) A physical vapor deposition method for controlled evaluation of biological response to biomaterial chemistry and topography. *J. Biomed. Mater. Res. A*, **82**, 179.

130 Hovgaard, M., Chevallier, J., Foss, M., and Besenbacher, F. (2005) Tantalum films with well-controlled roughness grown by oblique incidence deposition. *Appl. Phys. Lett.*, **87**, 073105.

131 Albrektsson, T. and Wennerberg, A. (2004) Oral implant surfaces: part 2–review focusing on clinical knowledge of different surfaces. *Int. J. Prosthodont.*, **17**, 544–565.

132 Shalabi, M.M., Gortemaker, A., Hof, M.A.V.T., Jansen, J.A., and Creugers, N.H. (2006) Implant surface roughness

and bone healing: a systematic review. *J. Dent. Res.*, **85** (6), 496–500.

**133** Sul, Y.T., Johansson, C., Wennerberg, A., Cho, L.R., Chang, B.S., and Albrektsson, T. (2005) Optimum surface properties of oxidized implants for reinforcement of osseointegration: surface chemistry, oxide thickness, porosity, roughness, and crystal structure. *Int. J. Oral Maxillofac Implants*, **20** (3), 349–359.

**134** Davies, J.E. (2003) Understanding peri-implant endosseous healing. *J. Dent. Educ.*, **67**, 932–949.

**135** Park, J.Y. and Davies, J.E. (2000) Red blood cell and platelet interactions with titanium implant surfaces. *Clin. Oral Implants Res.*, **11**, 530–539.

**136** Boyan, B.D., Lossdorfer, S., Wang, L., Zhao, G., Lohmann, C.H., Cochran, D.L. *et al.* (2003) Osteoblasts generate an osteogenic microenvironment when grown on surfaces with rough microtopographies. *Eur. Cell Mater.*, **6**, 22–27.

**137** Kieswetter, K., Schwartz, Z., Hummert, T.W., Cochran, D.L., Simpson, J., Dean, D.D. *et al.* (1996) Surface roughness modulates the local production of growth factors and cytokines by osteoblast-like MG-63 cells. *J. Biomed. Mater. Res.*, **32**, 55–63.

**138** Smith, L.J., Swaim, J.S., Yao, C., Haberstroh, K.M., Nauman, E.A., and Webster, T.J. (2007) Increased osteoblast cell density on nanostructured PLGA-coated nanostructured titanium for orthopedic applications. *Int. J. Nanomedicine*, **2**, 493–499.

**139** Wilmowsky, C.v., Bauer, S., Lutz, R., Meisel, M., Neukam, F.W., Toyoshima, T. *et al.* (2009) *In vivo* evaluation of anodic TiO2 nanotubes: an experimental study in the pig. *J. Biomed. Mater. Res. B Appl. Biomater.*, **89**, 165–171.

**140** Jäger, M., Zilkens, C., Zanger, K., and Krauspe, R. (2007) Significance of nano- and microtopography for cell-surface interactions in orthopaedic implants. *J. Biomed. Biotechnol.*, **2007**, 69036.

**141** Guehennec, L.L., Soueidan, A., Layrolle, P., and Amouriq, Y. (2007) Surface treatments of titanium dental implants for rapid osseointegration. *Dental Mat.*, **23**, 844–854.

**142** Park, K.H., Heo, S.J., Koak, J.Y., Kim, S.K., Lee, J.B., Kim, S.H. *et al.* (2007) Osseointegration of anodized titanium implants under different current voltages: a rabbit study. *J. Oral Rehab.*, **34** (7), 517–527.

**143** Yang, G.L., He, F.M., Hu, J.A., Wang, X.X., and Zhao, S.F. (2009) Effects of biomimetically and electrochemically deposited nano-hydroxyapatite coatings on osseointegration of porous titanium implants. *Oral Surg. Oral Med. Oral Pathol. Oral Radiol. Endod.*, **107**, 782–789.

**144** Meirelles, L., Arvidsson, A., Andersson, M., Kjellin, P., Albrektsson, T., and Wennerberg, A. (2008) Nano hydroxyapatite structures influence early bone formation. *J. Biomed. Mater. Res. A.*, **87**, 299–307.

**145** Meirelles, L., Melin, L., Peltola, T., Kjellin, P., Kangasniemi, I., Currie, F. *et al.* (2008) Effect of hydroxyapatite and titania nanostructures on early *in vivo* bone response. *Clin. Implant Dent. Relat. Res.*, **10**, 254.

**146** Tavares, M.G., Oliveira, P.T.d., Nanci, A., Hawthorne, A.C., Rosa, A.L., and Xavier, S.P.r. (2007) Treatment of a commercial, machined surface titanium implant with H2SO4/H2O2 enhances contact osteogenesis. *Clin. Oral Impl. Res.*, **18**, 452–458.

**147** Guo, J., Padilla, R.J., Ambrose, W., Kok, I.J.D., and Cooper, L.F. (2007) The effect of hydrofluoric acid treatment of TiO2 grit blasted titanium implants on adherent osteoblast gene expression *in vitro* and *in vivo*. *Biomaterials*, **28**, 5418–5425.

**148** Ellingsen, J.E., Johansson, C.B., Wennerberg, A., and Holmen, A. (2004) Improved retention and bone-to-implant contact with fluoride-modified titanium implants. *Int. J. Oral Maxillofac Implants.*, **19**, 656–666.

**149** Berglundh, T., Abrahamsson, I., Albouy, J.P., and Lindhe, J. (2007) Bone healing at implants with a fluoride-modified surface: an experimental study in dogs. *Clin. Oral Implants Res.*, **18**, 147–152.

150 Abrahamsson, I., Albouy, J.P., and Berglundh, T. (2008) Healing at fluoride-modified implants placed in wide marginal defects: an experimental study in dogs. *Clin. Oral Implants Res.*, **19** (2), 153–159.

151 Stanford, C.M., Johnson, G.K., Fakhry, A., Gratton, D., Mellonig, J.T., and Wanger, W. (2006) Outcomes of a fluoride modified implant one year after loading in the posterior-maxilla when placed with the osteotome surgical technique. *Appl. Osseointegration Res.*, **5**, 50–55.

152 Oxby, G., Lindqvist, J., and Nilsson, P. (2006) Early loading of Astra Tech OsseoSpeed implants placed in thin alveolar ridges and fresh extraction sockets. *Appl. Osseointegration Res.*, **5**, 68–72.

153 Mendes, V.C., Moineddin, R., and Davies, J.E. (2007) The effect of discrete calcium phosphate nanocrystals on bone-bonding to titanium surfaces. *Biomaterials*, **28**, 4748–4755.

154 Orsini, G., Piattelli, M., Scarano, A., Petrone, G., Kenealy, J., Piattelli, A. *et al.* (2007) Randomized, controlled histologic and histomorphometric evaluation of implants with nanometer-scale calcium phosphate added to the dual acid-etched surface in the human posterior maxilla. *J. Periodontol.*, **78**, 209.

155 Goené, R.J., Testori, T., and Trisi, P. (2007) Influence of a nanometer-scale surface enhancement on de novo bone formation on titanium implants: a histomorphometric study in human maxillae. *Int. J. Periodontics Restorative Dent.*, **27**, 211–219.

156 Vignoletti, F., Sanctis, M.d., Berglundh, T., Abrahamsson, I., and Sanz, M. (2009) Early healing of implants placed into fresh extraction sockets: an experimental study in the beagle dog. II: ridge alterations. *J. Clin. Periodontol.*, **36**, 688–697.

157 Orsini, E. *et al.* (2007) Randomized, controlled histologic and histomorphometric evaluation of implants with nanometer-scale calcium phosphate added to the dual acid-etched surface in the human posterior maxilla. *J Periodontology*, **78**, 209–218.

158 Park, J.W., Kim, H.K., Kim, Y.J., An, C.H., and Hanawa, T. (2009) Enhanced osteoconductivity of micro-structured titanium implants (XiVE S CELLplus) by addition of surface calcium chemistry: a histomorphometric study in the rabbit femur. *Clin. Oral Implants Res.*, **20**, 684–690.

159 Park, J.-W., Suh, J.-Y., and Chung, H.-J. (2008) Effects of calcium ion incorporation on osteoblast gene expression in MC3T3-E1 cells cultured on microstructured titanium surfaces. *J. Biomed. Mater. Res. A.*, **86**, 117–126.

160 Park, J.-W., Park, K.-B., and Suh, J.-Y. (2007) Effects of calcium ion incorporation on bone healing of Ti6Al4V alloy implants in rabbit tibiae. *Biomaterials*, **28**, 3306–3313.

161 Suh, J.-Y., Jeung, O.-C., Choi, B.-J., and Park, J.-W. (2007) Effects of a novel calcium titanate coating on the osseointegration of blasted endosseous implants in rabbit tibiae. *Clin. Oral Impants Res.*, **18**, 362–369.

162 Marin, C., Granato, R., Suzuki, M., Gil, J.N., Piattelli, A., and Coelho, P.G. (2008) Removal torque and histometric evaluation of bioceramic grit-blasted/acid-etched and dual acid-etched implant surfaces: an experimental study in dogs. *J. Periodontol.*, **79**, 1942–1949.

163 Shibli, J.A., Grassi, S., Piattelli, A., Pecora, G.E., Ferrari, D.S., Onuma, T. *et al.* (2009) Histomorphometric evaluation of bioceramic molecular impregnated and dual acid-etched implant surfaces in the human posterior maxilla. *Clin. Implant Dent. Relat. Res.*, **12** (4), 281–288.

164 Scarano, A., Degidi, M., Iezzi, G., Pecora, G., Piattelli, M., Orsini, G. *et al.* (2006) Maxillary sinus augmentation with different biomaterials: a comparative histologic and histomorphometric study in man. *Implant Dentistry.*, **15** (2), 197–207.

165 Imbronito, A.V., Scarano, A., Orsini, G., Piattelli, A., and Arana-Chavez, V.E. (2005) Ultrastructure of bone healing in defects grafted with a copolymer of polylactic/polyglycolic acids. *J. Biomed. Mater. Res. A*, **74** (2), 215–221.

166 Orsini, G., Traini, T., Scarano, A., Degidi, M., Perrotti, V., Piccirilli, M. *et al.* (2005) Maxillary sinus augmentation with Bio-Oss particles: a light, scanning, and transmission electron microscopy study in man. *J. Biomed. Mater. Res. B, Appl. Biomater.*, **74** (1), 448–457.

167 Guarnieri, R., Pecora, G., Fini, M., Aldini, N.N., Giardino, R., Orsini, G. *et al.* (2004) Medical grade calcium sulfate hemihydrate in healing of human extraction sockets: clinical and histological observations at 3 months. *J. Periodontol.*, **75** (6), 902–908.

168 Scarano, A., Iezzi, G., Petrone, G., Orsini, G., Degidi, M., Strocchi, R. *et al.* (2003) Cortical bone regeneration with a synthetic cell-binding peptide: a histologic and histomorphometric pilot study. *Implant Dentistry.*, **12** (4), 318–324.

169 Webster, T.J., Ergun, C., Doremus, R.H., Siegel, R.W., and Bizios, R. (2000) Specific proteins mediate enhanced osteoblast adhesion on nanophase ceramics. *J. Biomed. Mater. Res.*, **51** (3), 475–483.

170 Brunski, J.B., Puleo, D.A., and Nanci, A. (2000) Biomaterials and biomechanics of oral and maxillofacial implants: current status and future developments. *Int. J. Oral Maxillofac. Implants*, **15** (1), 15–46.

171 Wallace, S.S., Tarnow, D.P., Froum, S.J., Cho, S.C., Zadeh, H.H., Stoupel, J. *et al.* (2012) Maxillary sinus elevation by lateral window approach: evolution of technology and technique. *J. Evid. Base Dent. Pract.*, **12** (3 Suppl), 161–171.

172 Testori, T., Wallace, S.S., Trisi, P., Capelli, M., and Zuffetti, F. (2013) Del Fabbro M. Effect of xenograft (ABBM) particle size on vital bone formation following maxillary sinus augmentation: a multicenter, randomized, controlled, clinical histomorphometric trial. *Int J. Periodontics Restorative Dent.*, **33** (4), 467–475.

173 Orsini, G., Ricci, J., Scarano, A., Pecora, G., Petrone, G., Iezzi, G. *et al.* (2004) Bone-defect healing with calcium-sulfate particles and cement: an experimental study in rabbit. *J. Biomed. Mater. Res. B, Appl. Biomater.*, **68** (2), 199–208.

174 Orsini, G., Scarano, A., Degidi, M., Caputi, S., Iezzi, G., and Piattelli, A. (2007) Histological and ultrastructural evaluation of bone around Bio-Oss particles in sinus augmentation. *Oral Diseases*, **13** (6), 586–593.

175 Orsini, G., Stacchi, C., Visintini, E., Di Iorio, D., Putignano, A., Breschi, L. *et al.* (2011) Clinical and histologic evaluation of fresh frozen human bone grafts for horizontal reconstruction of maxillary alveolar ridges. *Int J. Periodontics Restorative Dentistry*, **31** (5), 535–544.

176 Hench, L.L. and Polak, J.M. (2002) Third-generation biomedical materials. *Science*, **295** (5557), 1014–1017.

177 Cramer, N.B., Stansbury, J.W., and Bowman, C.N. (2011) Recent advances and developments in composite dental restorative materials. *J. Dent. Res.*, **90** (4), 402–416.

178 Chen, M.H. (2010) Update on dental nanocomposites. *J. Dent. Res.*, **89** (6), 549–560.

179 Lutz, F. and Phillips, R.W. (1983) A classification and evaluation of composite resin systems. *J. Prosthet. Dent.*, **50** (4), 480–488.

180 Terry, D.A. (2004) Applications of nanotechnology. *Pract. Proced. Aesthet. Dent.*, **16** (3), 220–222.

181 Lohbauer, U., Wagner, A., Belli, R., Stoetzel, C., Hilpert, A., Kurland, H.D. *et al.* (2010) Zirconia nanoparticles prepared by laser vaporization as fillers for dental adhesives. *Acta Biomater.*, **6** (12), 4539–4546.

182 Canche-Escamilla, G., Duarte-Aranda, S., and Toledano, M. (2014) Synthesis and characterization of hybrid silica/PMMA nanoparticles and their use as filler in dental composites. *Mat. Sci. Eng. C-Biomim.*, **42**, 161–167.

183 Besinis, A., De Peralta, T., Tredwin, C.J., and Handy, R.D. (2015) Review of nanomaterials in dentistry: interactions with the oral microenvironment, clinical applications, hazards, and benefits. *ACS Nano*, **9** (3), 2255–2289.

184 Kanaparthy, R. and Kanaparthy, A. (2011) The changing face of dentistry: nanotechnology. *Int. J. Nanomedicine*, **6**, 2799–2804.

185 Wang, R., Zhang, M., Liu, F., Bao, S., Wu, T., Jiang, X. *et al.* (2015) Investigation on the physical-mechanical properties of dental resin composites reinforced with novel bimodal silica nanostructures. *Mat. Sci. Eng. C-Biomim.*, **50**, 266–273.
186 Atai, M., Pahlavan, A., and Moin, N. (2012) Nano-porous thermally sintered nano silica as novel fillers for dental composites. *Dent. Mater.*, **28** (2), 133–145.
187 Ilie, N., Kessler, A., and Durner, J. (2013) Influence of various irradiation processes on the mechanical properties and polymerisation kinetics of bulk-fill resin based composites. *J. Dentistry*, **41** (8), 695–702.
188 Goracci, C., Cadenaro, M., Fontanive, L., Giangrosso, G., Juloski, J., Vichi, A. *et al.* (2014) Polymerization efficiency and flexural strength of low-stress restorative composites. *Dent. Mater.*, **30** (6), 688–694.
189 Ruttermann, S., Wandrey, C., Raab, W.H., and Janda, R. (2008) Novel nano-particles as fillers for an experimental resin-based restorative material. *Acta Biomater.*, **4** (6), 1846–1853.
190 Kim, J.J., Moon, H.J., Lim, B.S., Lee, Y.K., Rhee, S.H., and Yang, H.C. (2007) The effect of nanofiller on the opacity of experimental composites. *J. Biomed. Mater. Res. B, Appl. Biomater.*, **80** (2), 332–338.
191 Ilie, N., Rencz, A., and Hickel, R. (2013) Investigations towards nano-hybrid resin-based composites. *Clin. Oral Invest.*, **17** (1), 185–193.
192 Najibfard, K., Ramalingam, K., Chedjieu, I., and Amaechi, B.T. (2011) Remineralization of early caries by a nano-hydroxyapatite dentifrice. *J. Clinical Dentistry*, **22** (5), 139–143.
193 Rimondini, L., Palazzo, B., Iafisco, M., Canegallo, L., Demarosi, F., Merlo, M., and Roveri, N. (2007) The remineralizing effect of carbonate-hydroxyapatite nanocrystals on dentine. *Mat. Sci. Forum.*, **539–543**, 602–605.
194 Docimo, R., Montesani, L., Maturo, P., Costacurta, M., Bartolino, M., DeVizio, W. *et al.* (2009) Comparing the efficacy in reducing dentin hypersensitivity of a new toothpaste containing 8.0% arginine, calcium carbonate, and 1450ppm fluoride to a commercial sensitive toothpaste containing 2% potassium ion: an eight-week clinical study in Rome, Italy. *J. Clin. Dent.*, **20** (1), 17–22.
195 Roveri, N., Battistella, E., Foltran, I., Foresti, E., Iafasco, M., Lelli, M., Palazzo, B., and Rimondini, L. (2008) Synthetic biomimetic carbonate-hydroxyapatite nanocrystals for enamel remineralization. *Adv. Mater. Res.*, **47–50**, 821–824.
196 Roveri, N., Battistella, E., Bianchi, C.L., Foltran, I., Foresti, E., Iafasco, M., Lelli, M., Naldoni, A., Palazzo, B., and Rimondini, L. (2009) Surface enamel remineralization: biomimetic apatite nanocrystals and fluoride ions different effects. *J. Nanomaterials*, **2009**, 1–9.
197 Lelli, M., Putignano, A., Marchetti, M., Foltran, I., Mangani, F., Procaccini, M. *et al.* (2014) Remineralization and repair of enamel surface by biomimetic Zn-carbonate hydroxyapatite containing toothpaste: a comparative *in vivo* study. *Front Physiol.*, **5**, 333.
198 Lacruz, R.S., Smith, C.E., Moffatt, P., Chang, E.H., Bromage, T.G., Bringas, P. Jr. *et al.* (2012) Requirements for ion and solute transport, and pH regulation during enamel maturation. *J. Cell Physiol.*, **227** (4), 1776–1785.
199 Orsini, G., Procaccini, M., Manzoli, L., Sparabombe, S., Tiriduzzi, P., Bambini, F. *et al.* (2013) A 3-day randomized clinical trial to investigate the desensitizing properties of three dentifrices. *J. Periodontol.*, **84** (11), e65–73.
200 Thepyou, R., Chanmitkul, W., Thanatvarakorn, O., Hamba, H., Chob-Isara, W., Trairatvorakul, C. *et al.* (2013) Casein phosphopeptide-amorphous calcium phosphate and glass ionomer show distinct effects in the remineralization of proximal artificial caries lesion *in situ*. *Dent. Mater. J.*, **32** (4), 648–653.
201 Reynolds, E.C. (1998) Anticariogenic complexes of amorphous calcium phosphate stabilized by casein phosphopeptides: a review. *Spec. Care Dentist.*, **18** (1), 8–16.
202 Niu, L.N., Zhang, W., Pashley, D.H., Breschi, L., Mao, J., Chen, J.H. *et al.*

(2014) Biomimetic remineralization of dentin. *Dent. Mater.*, **30** (1), 77–96.

**203** Lelli, M. *et al.* (2014) Remineralisation and repair of enamel surface by biomimetic Zn-carbonate hydroxyapatite containing toothpaste: a comparative in vivo study. *Front. Physiol.*, **5**, 333.

**204** Svanborg, L.M., Andersson, M., and Wennerberg, A. (2010) Surface characterization of commercial oral implants on the nanometer level. *J. Biomed. Mater. Res. B Appl. Biomater.*, **92** (2), 462–469.

**205** Wennerberg, A. and Albrektsson, T. (2009) Effects of titanium surface topography on bone integration: a systematic review. *Clin. Oral Implants Res.*, **4**, 172–184.

# 14
# Nanostructured Polymers for Medical Applications

*Prabitha Urwyler*[1] *and Helmut Schift*[2]

[1]*University of Bern, ARTORG Center, Murtenstr. 50, 3010 Bern, Switzerland*
[2]*Paul ScherrerInstitut, Laboratory for Micro- and Nanotechnology, ODRA/103, 5232 Villigen PSI, Switzerland*

## 14.1
## Introduction

Nanotechnology has raised expectations in a variety of applications ranging from electronics to medicine. It provides us opportunities to create smart surfaces and materials using nanostructures. Nanofabrication technologies have made it possible to develop nanostructures with exquisitely controlled geometrical, chemical, and physical properties. The ability to structure materials and devices at the molecular scale can eventually bring enormous immediate benefits in the research and practice of medicine. Nanotopographies on surfaces are of particular interest because of their wide range of application from scaffolds for tissue replacement, control of wetting behavior, color, adhesion, and cell mechanics. Nanostructures provide noninvasive observation modalities into the cellular machinery. It allows for the analysis of parameters such as cellular mechanics, morphology, and cytoskeleton. Furthermore, nanostructuring of materials and their surfaces can play an essential role in the interaction of materials and devices with the human body.

### 14.1.1
### Nanostructured Polymers – A Promising Approach in Biomedical Applications

Polymers have attracted great interest in biomedical applications owing to their low cost and tailorable properties. High-performance polymers such as polyetheretherketone (PEEK) [1] and polyetherketoneketone (PEKK) are used as bone implants and screws, while biodegradable polymers like poly lactic acid (PLA), poly(lactic-co-glycolic acid) (PLGA) are actively used as scaffolds in regenerative medicine [2]. They have replaced metallic, ceramic, and glass products, and their main advantage lies in the fact that they can be fabricated in one single fabrication step, which includes complex, design-based functionality in length-scales

*Nanoscience and Nanotechnology for Human Health,* First Edition. Edited by Bert Müller and Marcel Van de Voorde.

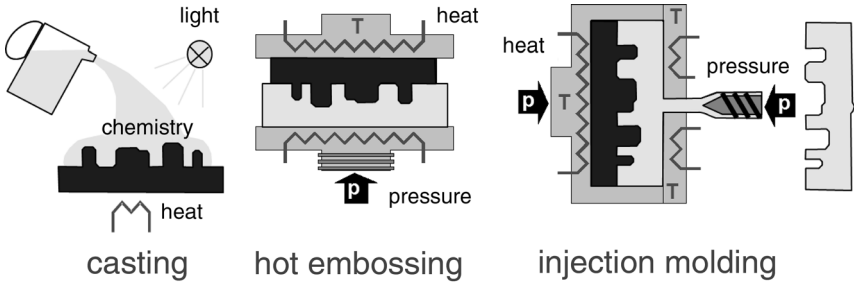


**Figure 14.1** Replication processes for surface patterning of polymer materials by molding. The topography of a mold is transferred into the surface of a viscous material.

from macroscopic outlines for automated handling to nanoscopic surface topographies. Therefore, polymer-based nanostructures have enormous potential that might change the way, how diseases are diagnosed and treated correctly and efficiently. Today, polymers are not only the backbone of lab-analytics and instrumentation, using single-use disposable labware, but also the base material of functional parts with mechanical or chemical properties either comparable or even superior to metal alternatives. Due to their inherent properties and easy way of manufacturing, they can be functionalized by simply adding micro- and nanostructures to the surface, either during manufacturing by molding or during a postprocessing step.

In this chapter, we give an overview of the numerous possibilities to implement functionalities into the surface of polymer components. We present physical nanoeffects, which can be exploited for biomedical applications with a specific emphasis on those effects, which are due to surface topography. We will focus on the creation of topological structures on surfaces in an artificial way, not forgetting that inherent nanocharacteristics also play a role in surfaces, subsurfaces, and material bulk. Due to the specific advantage of using molding, *cf.* Figure 14.1, as the main manufacturing method, we present applications, where such effects have already been realized in polymeric products. For this, it is essential to present the main methods for the fabrication of suitable molds. In combination with the enormous freedom of design and the wide range of processing capabilities, this enables to advance into different, still unexplored applications.

### 14.1.2 Strategies for Creation of Surface Nanotopographies

Polymer parts as applied for bioanalytic devices and medical implants are generally monolithic. This means that they are made from a single material and their function is not only given by their geometry, but also by their material and surface properties. Avoiding welding, gluing, and mechanical connectors is advantageous to guarantee biocompatibility and sterilization. Replicas are cast from

liquid resins, molded from viscous melts, or hot embossed and thermoformed from thermoplastic foils taking advantage of a variety of processes, see Figure 14.1 [3,4]. The obtained products are light-weight and generally low-cost. Polymers offer tailored physical and chemical properties, which can be achieved at the bulk by using different polymers or compositions, as well as surfaces altered by physical and chemical means. As mentioned above, for specific functionalities of the surface, various topographies are often needed. This can be done by including such surface topographies into the mold, from which a number of identical negatives are molded, or by using post-processing techniques, which create such topographies in each individual part after molding is completed. In the first case, the surface topography can be replicated once a mold is available that exhibits a surface structure with exactly the inverse surface shape as the desired component. In the second case, each part assumes a similar surface texture within specifications given by the process parameters. For example, in injection molding one can add an exchangeable insert into a mold cavity to produce polymer parts with microstructures such as pillars, holes, pyramids, and line gratings [5–9]. Such microstructures can represent natural surface textures including that of cortical bone, but also structures, which guide and orient the adherent cells [10,11]. However, for implants with nonflat surfaces or even arbitrary three-dimensional shapes, such inserts are less common because of the complexity in manufacturing. Therefore, treatments including sandblasting and etching have been established to generate more or less defined micro- and nanostructures in each molded part. Plasma treatments are especially interesting, since the size and density of nanostructures can be tailored by controlling the process parameters, that is, plasma power, treatment duration, and the selection of the process gas [12]. Other postprocessing or treatments by electrons, ions, chemicals, X-rays, or UV-light of individual components after molding may be a choice for such components too.

## 14.2 Applications of Nanostructures

Nanotechnology is a transverse technology, combining different fields and disciplines of physics, chemistry, biology, and materials science [13]. In technology, we talk about *nano*, when the surface structures have characteristic length scales below 100 nm, in contrast to structures with length scales in the micrometer range. This makes it possible to generate optical gratings with subwavelength characteristics, for example, for polarization and antireflection of visible light, or to observe plasmonic effects in metal structures with an enhanced sensitivity, if these structures have features below 20 nm. In biology, however, the size ranges needed for manipulation of cells and molecules are quite diverse, and often, it is not understood whether the interaction of a biological cell with a surface topography is based on μm scale, corresponding to the cell size, sub-μm scale, which fits components of the intracellular matrix, or even sub-10 nm size level

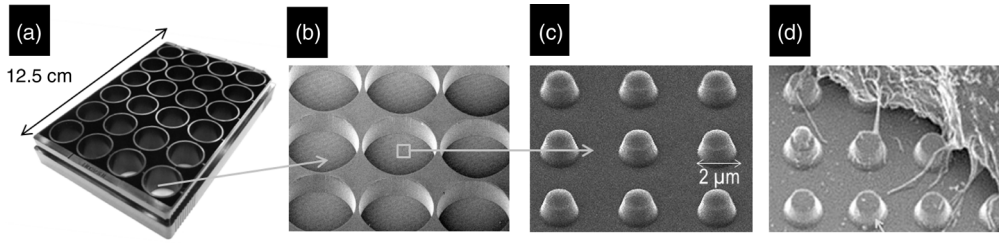


**Figure 14.2** Nanopillar cell culture plate by Hitachi (a), displaying the range of sizes needed from millimeter-sized containers (b), in a macroscopic plate to micrometer-sized pillars (c), fostering primary rat hepatocyte spheroids growth on the container (d). The *nanopillars* are 2 µm wide and 1 µm high [15]. (Reproduced with permission. Copyright Hitachi Ltd.)

corresponding to the morphological nature of contact points. This is dependent on whether cell growth is based on the available contact area, wetting, and containment, the distance between focal adhesion and the extracellular matrix, the interaction at molecular level, and so on. For the interaction of surface topographies and chemical structures with large molecules often similar size range of these molecules is needed, which for proteins is below 10 nm. Then, real *nanoeffects* may be observed, which are difficult to be seen with larger structures. In contrast to this, for the guiding of nerve cells, micrometer sized guiding rails or channels have been found to be appropriate [14]. The same applies for cell culture substrates and containers, where micrometer-sized pillars were found suitable to foster cell growth (see Figure 14.2). The range between 10 and 100 nm, however, is most important for many applications. It is not only the range in which many physical nanoeffects are most prominent, but also in which current technologies allow reproducible manufacturing. Furthermore, microscopy is able to perform reliable analysis. While many effects presented in Table 14.1 are based on sub-µm structuring and not on nanostructures with molecular sizes, real *nanoeffects* relying on mesoscopic effects are given, if single molecules are oriented due to surface patterning (see Figure 14.3).

### 14.2.1 Which Nanoeffects Will Be Exploited for Biomedical Applications?

In biomedical applications, several fields of nanotechnology became apparent; in the molecular nanotechnology, biological systems are subjects of research by controlled use of molecular structures. This will be needed in medical fields for diagnostics and therapy. As the sizes of these molecular structures are in the range below 10 nm, the probes used to host or manipulate these structures are often in the same range. This can be done by nanoparticles, by surface patterns with appropriate length scales, or by materials with structural sizes in the nanometer range.

**Table 14.1** Functionalization using surface nanostructuring.

| **Nanoeffects**: photographs, SEM micrographs, and schematics | | | | |
|---|---|---|---|---|
| Physical effect in nature | Opt. diffraction | Self-cleaning | Cell growth | Draping adhesion |
| |  |  | 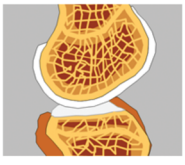 |  |
| | Butterfly with blue color | Lotus-effect due to roughness | Differentiation into bone/cartilage | Gecko-effect based on large surface |
| Nanoeffect | 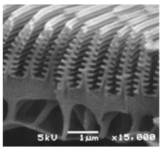 | 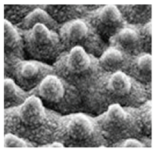 | 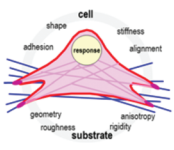 | 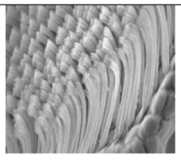 |
| | Subwavelength 3D gratings | Hierarchical surface pattern | Nanomechanical stimulus for cells | Hairs act as a soft substrate that can conform to surfaces |
| Products with artificial nanoeffect |  |  | 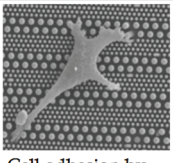 | 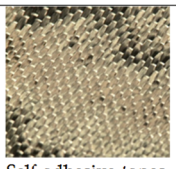 |
| | Structural colors due to surface nanogratings | Complete dewetting due to textured surface | Cell adhesion by size, period and order of pillars | Self-adhesive tapes and bandages with soft nanopillars |

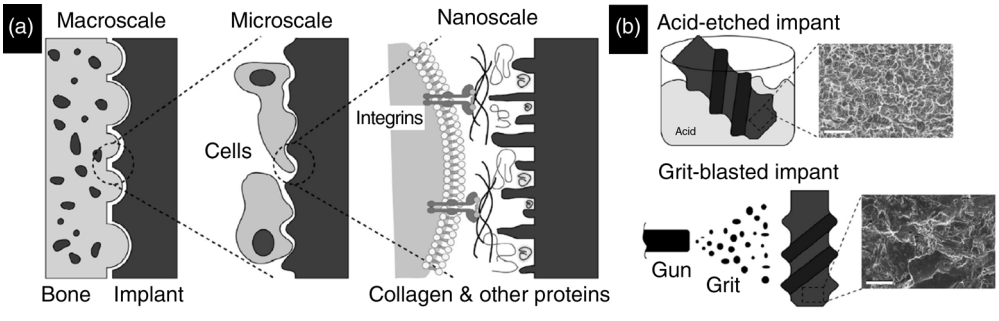


**Figure 14.3** (a) Different size-effects needed for cell growth and differentiation. (b) Schematic and SEM images of examples of surface modification treatments that can be applied to machined implants, including acid etching and grit blasting [16]. SEM scale bar is 3 µm. (Reproduced with permission. Copyright Elsevier.)

Most biological applications deal with aqueous liquids; therefore, the control of the wetting behavior on surfaces or in micro- and nanochannels becomes essential, for enhancing or prohibiting liquid transport. This is done by choosing a material with the desired surface chemistry or by modifying it by surface structuring. If the use of hydrophobic materials, for example, coatings, is impossible, similar properties can be – at least partly – created by topographical means, for example, by adding a specific roughness to the material surface. It arises from pure surface-dependent influence, for example, for biological interaction of cells with the surface by stimulation of cell growth through mechanical stress. The water contact angle of a hydrophobic surface can be enhanced by adding surface roughness with micro- and nanoscale features. If it is above 160°, this effect is called superhydrophobic, because it allows water droplets to form on the surface, which can roll-off. As *Lotus-effect,* it refers to the self-cleaning property of its leaves [13]. This is due to the reduced contact area available for solid contamination, that is, dust particles, and enables easy removal during wet cleaning by rain. It is caused by the hydrophobic water-repellent double structure of the surface. This hierarchical double structure is formed out of a characteristic epidermis and the covering waxes, that is, nanopillars of few 100 nm on top of microbumps (papillae) with 10–20 μm size. The Lotus-effect is also known for rejection of germs and fungi and therefore reduces or even prevents biofouling. To exploit such effects for biomedical applications, not only material and manufacturing issues have to be considered but also the environments of use, for example, body liquids, additives, and contamination.

#### 14.2.1.1 Combined Effects

Surface topographies in the sub-μm range often do not only modify wetting behavior, but also optical diffraction, for example, for color filtering [17,18]. This way, microfluidic elements can integrate micro- and nanochannels, optical readout and light guiding, mechanical interface, and antiwetting behavior. Such solutions are often preferred, because they enable the fabrication of a monolithic component without the addition of chemicals. This is particularly important in diagnostics or for interaction with living cells, for example, for enhancement of cell adhesion on implants.

#### 14.2.1.2 Cell Proliferation and Differentiation

Cells grow and orient themselves. They find not only the right physiological environment, but also surfaces, on which the focal points within the internal cytoskeleton can interact. If these surfaces have structures with the appropriate sizes and distances, often in the nanometer range, stimuli for growth can be created [19–21]. Templates are both needed to stimulate this growth and to measure quantitatively the forces involved in such growth [22,23]. Depending on the structural size and conformation, some cell types are favored while others senescence. When using stem cells, for example, from bone marrow, cells can either differentiate into bone or cartilage. For example, in the experiments shown in Ref. [24], stem cells were seeded on a substrate with a surface nanotopography

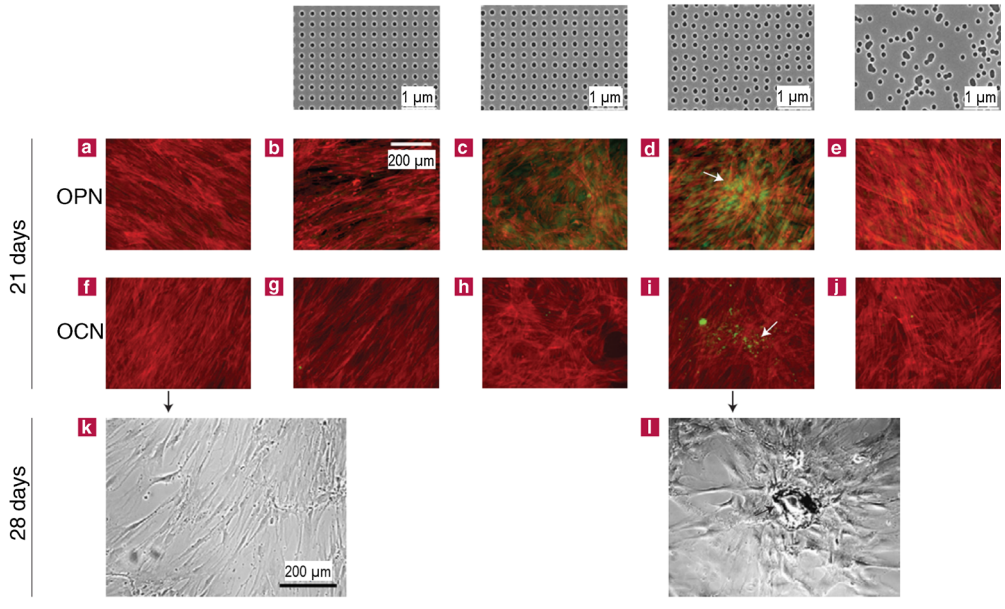


**Figure 14.4** Osteopontin (OPN) and osteocalcin (OCN) staining of MSC cells after 21 days and phase-contrast/bright-field images of alizarin-red-stained cells after 28 days. The top row shows images of nanotopographies fabricated by electron beam lithography. All have 120-nm-diameter pits (100 nm deep, absolute or average 300 nm center–center spacing) with square, displaced square 20 (±20 nm from true center), displaced square 50 (±50 nm from true center), and random placements. (a–j) MSCs on the control. (a and f), note the fibroblastic appearance and no OPN/OCN positive cells; on SQ (b and g), note the fibroblastic appearance and no OPN/OCN positive cells; on DSQ20 (c and h), note OPN positive cells; on DSQ50 (d and i), note OPN and OCN positive cells and nodule formation (arrows); on RAND (e and j), note the osteoblast morphology, but no OPN/OCN positive cells. (k and l), phase-contrast/bright-field images showing that MSCs on the control; (k) had a fibroblastic morphology after 28 days; whereas on DSQ50 (l), mature bone nodules containing mineral were noted [24]. (Reproduced with permission. Copyright Nature Publishing Group.)

(see Figure 14.4). The pits with a diameter of 120 nm and a depth of 100 nm were arranged both in a regular array with 300 nm period and with random displacements of pit positions, that is, with deviations from orthogonal order. After 28 days, mature bone nodules containing mineral were noted for average displacements of 50 nm, while fibroblasts were forming on substrates with smaller or much larger displacements. Such experiments show that interaction of cells and surface texture is complex, but can be controlled by carefully designing surface topographies. Nanopattern on flexible surfaces has been demonstrated to be an excellent tool to study cell mechanics and cell function. Nanostructured polymers are mainly found in sutures, scaffolds, implants, and drug delivery systems. Patterned surfaces in materials such as polydimethylsiloxane (PDMS) have been extensively used in cell attachment studies [25–30].

Nanotopography seems to play an essential role in guiding cell behavior *in vivo*, and is now being used in biomaterials science as a tool for controlling tissue regeneration. A wide variety of techniques have been used to produce nanotopography on biomaterial surfaces. Polymer demixing, chemical etching, and colloidal lithography are some of the most relevant techniques to obtain randomly organized patterns. Conversely, soft-lithography techniques and other methods using different sources of radiation, that is, electrons, ions, or photons, to etch the substrate are among the techniques used most commonly to produce regular geometries.

The potential of nanostructures in regenerating tissues such as bone, cartilage, bladder, nerves, and vessels by enhancing the biological performance of the cells, for example, increased adhesion, proliferation, migration, have been demonstrated in numerous *in vitro* and *in vivo* studies. *Bone*: increased osteoblast adhesion and decreased fibroblast adhesion were seen on mold-casted nanostructured PLGA [31]. *Nerves*: nanopatterned PDMS by replica molding induce differentiation of adult mesenchymal stem cells into a neuronal lineage [32]. *Bladder*: nanostructured PLGA, poly-ether-urethane (PU), and poly-caprolactane (PCL) by chemical etching leads to greater adhesion and proliferation of bladder smooth muscles compared with conventional materials [33]. *Cartilage*: nanostructured PLGA by chemical etching leads to better chondrocyte functions than conventional materials [34,35]. *Vessels*: nanostructured PLGA by chemical etching increased endothelial and smooth muscle cell densities compared with untreated PLGA [35].

#### 14.2.1.3 **Protein Nanopattern**

Patterning proteins on the nanoscale is important as templates with surface structures in the same range as the size of the protein enable self-assembly and orientation of molecules along them. Such directed self-assembly (DSA) is already widely used in semiconductor manufacturing with block copolymers and is a characteristic example of a combination of top-down (lithography) and bottom-up (self-assembly) [27,36–39]. Protein nanopattern in two- or three-dimensions (2D and 3D) on polymer substrates have been created using electron beam [37] or colloidal lithography [36,39]. The nanoarchitecture of the polymer pattern can be tuned for protein patterns leading to applications such as glucose sensors [37] or cell culture guides or immunosensing devices [40]. Cellular adhesion complexes have been studied using protein nanopatterns prepared by colloidal lithography. Multicomponent protein patterning are used to generate complex bioactive surfaces for investigating fundamental questions about protein–protein interactions, as well as studying the effect of geometry on cell behavior [39].

### 14.2.2
### Mimicking Nature

Biomedical applications often try to mimic bioeffects observed in nature. If they are primarily based on surface structuring, the aim is to equip surfaces with

exactly the same shapes of surface patterns and to adapt the surface energy by choosing an appropriate material similar to that used by nature. For technical applications, this copying is impossible or advisable. For example, the Lotus-effect is based on wax nanopillars, which are produced by the leave surface and are regenerated once they are damaged. On technical surfaces such as windows, screens, or implant surfaces these solutions are impossible. Instead of a soft, regenerative solution, a hard coating with hydrophobic properties would be preferred. As we are focusing on molding techniques, with surfaces having the same properties as the bulk, a reasonable compromise needs to be found for intended use and lifetime. For example, for implants, this would be up to the point, when some layers of cells are grown. Besides polymers, compound materials including nanogranular ceramic materials dispersed in a polymeric matrix are of high interest if higher robustness of the surface is needed. This enables to produce the components by injection molding. Afterwards they are converted into hard components by removing the organic components by firing and sintering. Components with such properties were replicated from natural surfaces, for example, a snake's skin with microstructures reducing friction or from artificially generated topographies [41,42].

### 14.2.3
### Gecko-Inspired Bandage as an Example

One example of a bio-inspired effect for medical applications, in which nanostructures play a role, is the gecko-effect. The gecko is a small lizard able to climb on flat, glass-like surfaces, where mechanical interlocking is impossible. The adhesion is guaranteed by surface topographies. It is based on the large surface of thousands of nanofibers, assembled in hierarchical structures, which enable to hold large weights due to added van der waals forces when being in contact with the substrate. Such structures are fabricated in an artificial way, for example, by hot embossing techniques [43].

By using a clever combination of chemical surface and gecko-effect-inspired surface structures, bandages have been developed by different research teams [44], which allow the fabrication self-adhesive tapes without any skin irritation by the chemical glue. It is possible to use such bandages in wet environment, where most glue fail [45].

## 14.3
## Processes for Generation of Nanotopographies

The vast number of processes for the generation of nanosize topographies, that is, trenches and ridges, holes and pillars, concave and convex shapes, ordered and random surface textures can be divided into top-down or bottom-up processes. In top-down technology, the fabrication of nanostructures using lithographic patterning is assisted by tools that mold, erode, or etch base materials to

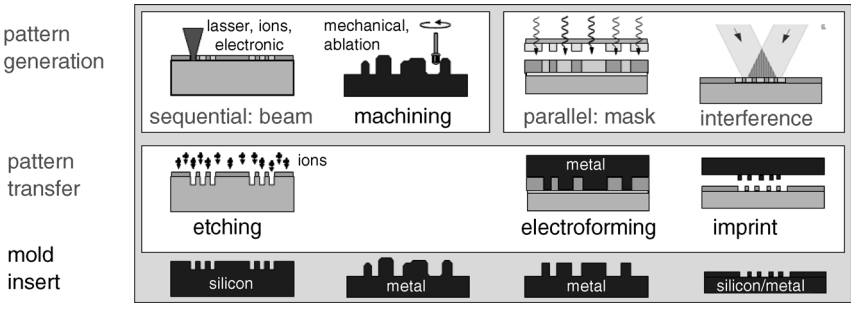


**Figure 14.5** For the fabrication of a mold insert, to be used in replication processes for surface patterning, different methods for origination (pattern generation and transfer) and tooling (by casting or electroplating) are employed.

produce nanostructures with the desired geometry. In bottom-up technology, self-assembly processes or self-organization mechanisms are employed to grow nanostructures from smaller elements and base materials. Due to the fact that many of the processes rely on cleanroom-based equipment and processing, wafer-sized silicon or glass substrates, for example, 100 mm round or square, as well as small chips ($10 \times 10\,mm^2$) are used.

### 14.3.1
### Top-Down Manufacturing by Origination, Tooling, Replication

Top-down processes rely on the constant development of technological processes and tools that originate from precision mechanics and microtechnology. These tools enable locally defined modification of surfaces, by removal and addition of material, or generation and transformation of the shape with defined replications tools (see Figure 14.5). For nanostructuring, often processes are scaled down, which have already been established for mass manufacturing, such as milling, lasing, etching, coating, and molding. The challenges of downscaling are to not achieve only higher precision, but also reproducibility, parallel fabrication, throughput, and versatility. For structures below 100 µm, lithographic techniques, derived from microchip fabrication, are now applied. They are used for the generation of fluidic channels, but also for the definition of nanotopographies. In general, for top-down processes, there is a general problem: The finer the structures, the more complex, demanding, and time-consuming is their fabrication. In addition to this, between 1 mm and 1 nm structural size, several generations of patterning methods have to be used, with disruptive changes between the sizes. As an example for mechanical tooling, milling applies from structures down to 50 µm. For surface patterning with a masking process, photolithography applies down to 2 µm. Electron beam lithography applies down to 20 nm.

Examples with typical resolutions and area are (i) conventional lithography, (ii) electron lithography, (iii) photolithography, (iv) interference lithography, and (v) nanoimprint lithography. The pattern transfer is done via electroplating or

etching into substrate for mold/stamp manufacturing or casting for working stamp fabrication. Some of the equipment including photolithography and etching is standard in cleanrooms. Other process steps require specific and sometimes costly equipment. Specific shops provide masks or stamps.

### 14.3.2
### Bottom-Up Manufacturing By Self-Organization and Surface Postprocessing

Bottom-up processes use self-ordering mechanisms that create complex surface structures by arrangement of small entities, for example, macromolecules and particles, like growth processes in nature. Often these small entities are self-confining or have specific length scales, which enable the generation of quasi-crystals in 2D and 3D. A 2D arrangement could be an orthogonal or hexagonal array of monodisperse beads or in 3D an opal structure, both with a proximity ordering over a few *crystalline periods* or even covering large areas with almost perfect ordering. Furthermore, gratings and dot arrays can be achieved by alignment of block-copolymers with specific sections of different chemical composition along a polymer chain. In addition, self-limiting etching processes can be used, which enable generating surface topographies that can range from well-defined roughness up to ordered pillars of cavities. The mechanisms for self-assembly are diverse and often not well understood. Small entities order because of specific topological and chemical properties of a surface, but also due to their interaction, conformation, and intermolecular forces. Self-assembly mechanisms often possess the ability of self-healing, because they have a strong tendency to order in short-range with energetically favorable shape. When used in 3D, artificial material can be created. Although many bottom-up techniques allow for the reproducible creation of almost perfect ordered surface topographies, they often lack the freedom in design possible with top-down methods. Some of these methods can be used in combination with top-down methods or for generation of stamps.

Examples are nanoparticle self-ordering and assembly typically with 500 nm beads down to 50 nm, nanopore self-ordering by anodic alumina oxidation (AAO), and self-confined plasma etching [46–49]. Often these methods do not need expensive equipment and can be done in chemical labs. However, for production of defect-free large areas, combined bottom-up/top-down approaches are of advantage (see Figures 14.6 and 14.7).

## 14.4
## Surface Patterning of Microcantilevers Using Mold Inlays

In the field of bioanalytics, microcantilevers (μC) are currently being introduced as ultrasensitive elements for cell-force-measurements and bio-analytical sensors. A μC array is a micromechanical device, which exhibits flexible, finger-like extensions from a macroscopic carrier, which can bend if subjected to surface stress or excited by mechanical forces [22,50–52]. This can, for example, be by

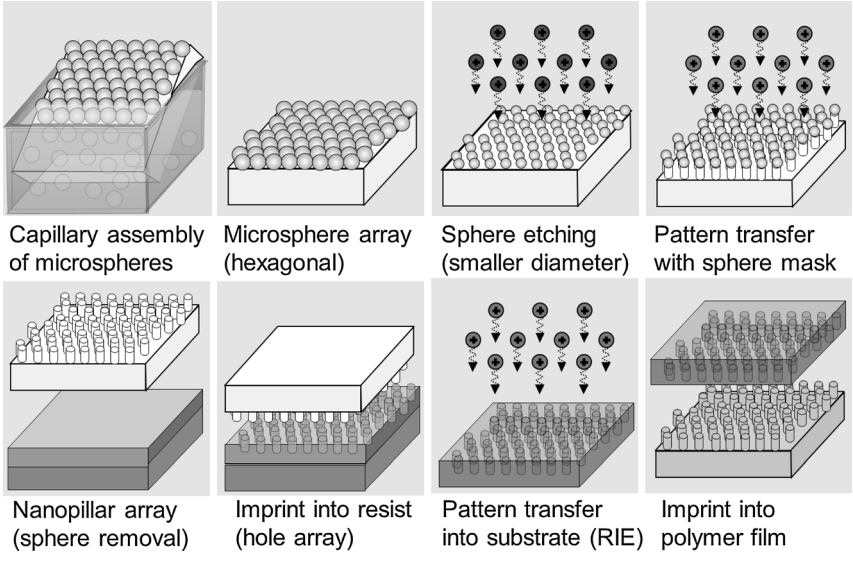


**Figure 14.6** Schematic diagram of a fabrication process using combined bottom-up (self-assembly) and top-down techniques (replication by nanoimprint lithography). Upper row: Si nanopillars are fabricated through PS-sphere dry etching. Lower row: the polarity of the pillar structure is inverted, resulting in holes in a working stamps, by imprint and etching, then polymer films with nanopillars are imprinted into a polymer foil [46,47].

loading a μC with biomolecules, which results in a decrease of its resonance frequency. To achieve local chemical sensitivity, the μC is coated on one side with a thin gold film. This serves both as a layer for selective adsorption of biomolecules, for example, by using thiol-based chemistry, and for enhancing the reflection of a laser beam, which is used to measure the deflection of the μC. Typically, a silicon μC is 500 μm long, 50–100 μm wide and around 1 μm thick (see Figure 14.8). As a device with multiple sensors, an array of μC is attached to a 2.5 mm × 3.5 mm × 0.5 mm carrier. While the size of the carrier is determined by practical considerations, including handling with tweezers, economy of space, and thickness of standard silicon wafers, the size of the μC is often determined by the selectivity needed to detect small amounts of loaded biomolecules and variations thereof. Silicon is the preferred material for these micromechanical elements due to the established capabilities of cleanroom-based micromachining technologies. However, particularly for sensors in a modern biolab environment, single-use low-cost devices are highly desired. For this purpose, polymeric alternatives are most promising. The preferred manufacturing process for the μC is polymer injection molding, and for elements of micrometer size special micro-injection molding (μIM) tools and concepts have been developed. To achieve comparable mechanical properties, the polymer μC need to be around seven times thicker than the silicon counterpart. However, even a cavity height of 10 μm, that is, with an aspect ratio of 50, it is difficult to fill a polymer melt in an

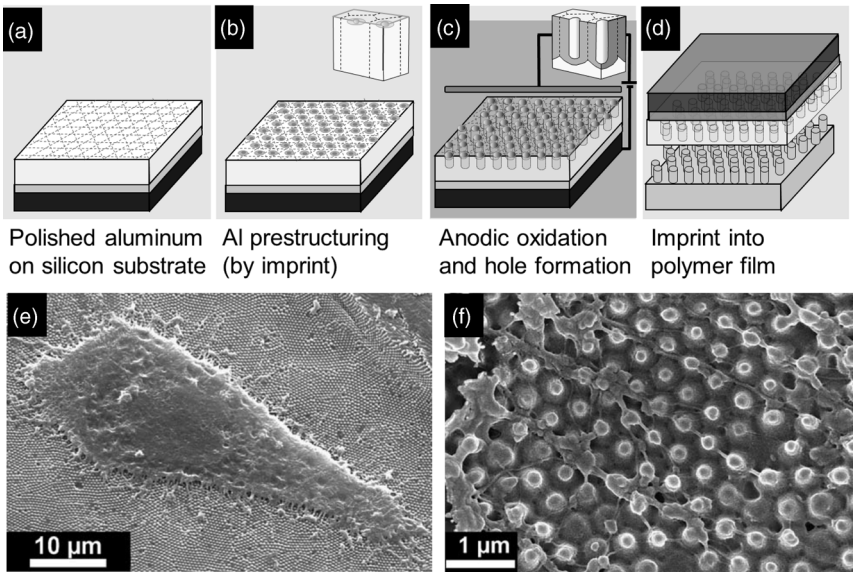


**Figure 14.7** Nondestructive fabrication of nanopillar-based foil using recyclable hard templates. (a–d) Schematic diagrams of a self-limiting etching process in anodic aluminum oxide (AAO). These templates can be used for molding poly-DL lactic acid (PDLLA). After coating with heparin/gelatin, the pillar arrays can be used for cell culturing. (e–f) SEM images of a single fibroblast cell from human skin on heparin/gelatin-functionalized PDLLA nanorod arrays extracted from AAO (pore diameter: 180 nm; pore depth: 1 mm; lattice period: 500 nm) obtained by culturing for one day: (e) Large-field view and (f) detail showing filopodia protruding from the cell body [48,49]. (Reproduced with permission. Copyright 2015, Royal Society of Chemistry.)

isothermal process, that is, in which the mold is kept at a temperature below the melt's glass transition temperature. Here, the thermoplastic polymer needs to keep its ability to flow and fill the extended cavity, while it is freezing upon contact with the mold surface. However, as demonstrated, complete filling can be achieved if the mold cavity height is chosen between 30 and 50 µm (see Figure 14.8.

For a range of reasons, it is of advantage if the surface of a µC is patterned. This can be surface enlargement for higher sensitivity, directional gratings for preferential cell growth and cell contraction, refractive and diffractive elements for optical and plasmonic effects, and fluidic channels for a fountain pen. From the processing point of view, the molding of surface structures onto a µC 500 µm long and 25 µm thick is not different from the molding of data pits on a compact disc. Therefore, by applying a thin micro- or nanopatterned mold insert into one side of the molding tool, surface structures can be added to the mold, while the outline of the macroscopic element is preserved (see Figure 14.9). Since the surface patterning is achieved by using a NIL fabricated hybrid mold, the NIL toolbox approach is needed. Opposite to the microcavity with the µC outlines on the

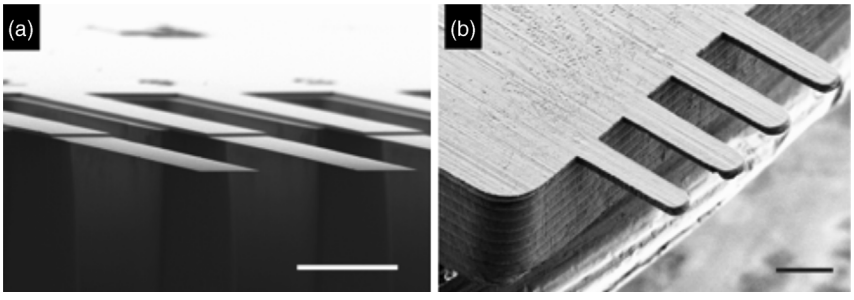


**Figure 14.8** SEM micrographs of an array of (a) silicon and (b) polymer μC with 1 μm and 25 μm thickness, respectively. On the polymer surface, the roughness of the metal mold is well replicated. Scale bars 100 μm [4]. (Reproduced with permission. Copyright 2015, SPIE.)

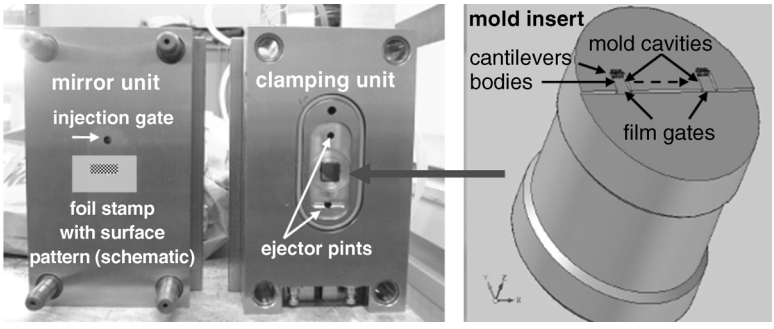


**Figure 14.9** Molding tools for injection molding, left side: while the clamping unit contains the mold insert with two mold cavities and channels, right side on the mirror unit a foil-like stamp can be placed. By placing both units face to face in an injection-molding machine, two closed microcavities are formed, which can be filled with viscous polymer through the injection gate [50]. (Reproduced by permission. Copyright 2015, Elsevier.)

tool side, a foil containing the surface pattern is attached to the injection mirror side of the mold. Thus, by composing a hybrid mold cavity during closing of the tool, instead of the flat surface, a surface pattern is generated on the μC during molding. In Figure 14.10, a variety of surface pattern is shown [6,53–55].

## 14.5 Surface Patterning Using Plasma Etching

Load-bearing implants made of titanium are sandblasted and etched to obtain the micro- and nanometer-scale roughness for osseointegration. In order to reach the same for polymers and extend the applications beyond spinal disc cages and housings of pacemakers, the necessary roughness has to be generated in the finished parts. It has been shown that plasma treatments do not only chemically

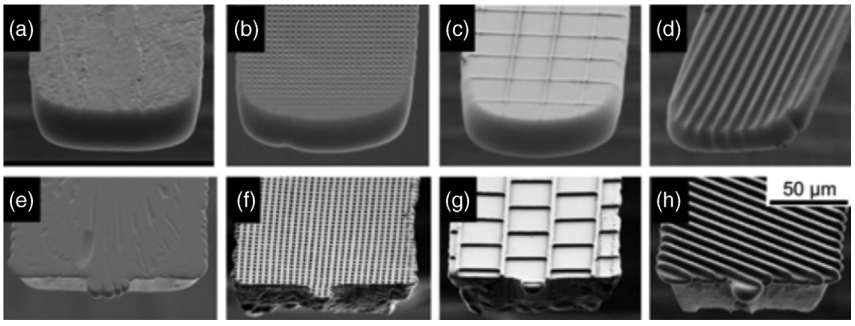


**Figure 14.10** SEM micrographs of (a–d) incompletely molded polymer µC, (a) with bare steel *mirror*, (b) with pyramids of 2 µm footprint, (c) shallow compartments, (d) periodic 5 µm-wide ridges, (e–g) completely molded polymer µC, (e) with polished steel *mirror* [6]. (Reproduced with permission. Copyright 2015, SPIE.)

activate the polymer surfaces but also induce etching processes (see Figure 14.11), which result in well-defined nanostructures (see Figure 14.12) [12,56,57]. The density and size of the nanostructures can be tailored by the choice of the process gas, the plasma power, and the duration of the plasma treatment [12,56]. The nanostructures derived from plasma treatment neither classify as the randomly

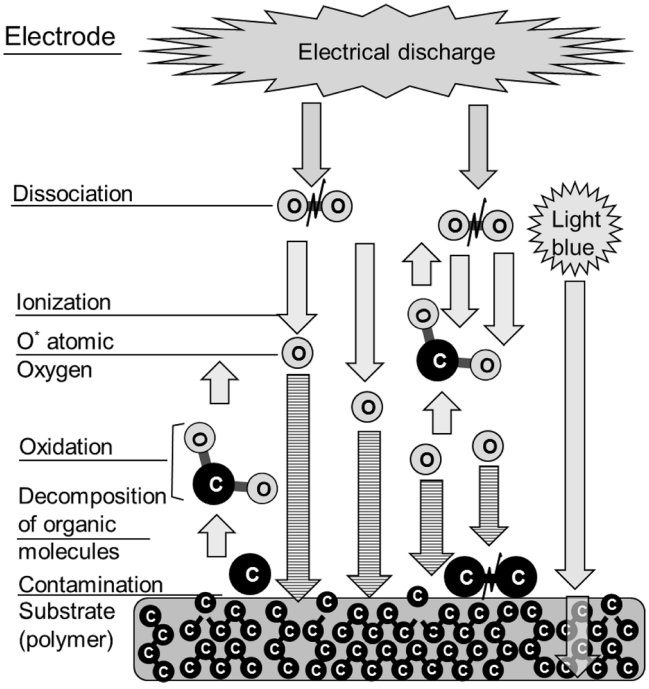


**Figure 14.11** Schematics displaying the interaction of oxygen plasma with a polymer surface.

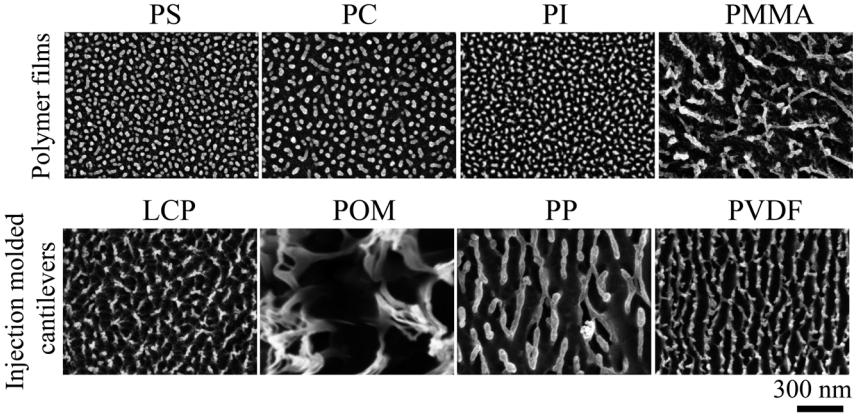


**Figure 14.12** The SEM images of polymer films and injection-molded cantilevers after 50 W oxygen plasma treatment show the occurrence of homogeneously distributed nanostructures with material-specific size and shape. Polystyrene (PS), polypropylene (PP) and polyimide (PI) give rise to circularly shaped nanostructures, while polymethylmetacrylate (PMMA) substrates show large ramified nanostructures with an arm width comparable to the diameter of the compact morphologies of the polymer films investigated. The nanostructures on liquid crystal polymer (LCP) and polyoxymethylene (POM) appear to be isotropic, whereas the ones on < PP and polyvinylidene (PVDF) show an elongated shape with a clear preferential orientation. Size and density of the nanostructures depend on the material selected [12]. (Reproduced with permission. Copyright 2015, SPIE.)

arranged nanostructures, which have been found to induce osteogenic differentiation in contrast to highly ordered nanostructures [24]. The isotropy of the nanostructures depend on the substrate below. Isotropic nanostructures showing preferential orientation of the molecules as result of the film casting process are seen on plasma-treated polymer films, while anisotropic nanostructures are derived by plasma treatments of injection-molded polymers.

In addition to the stochastic patterning of polymeric end-products by etching, these processes can also be applied to obtain molds. Origination ranges from stochastic processes to self-organization using anodic porous alumina, block-copolymers, and controlled particle placement by capillary assembly [58–61].

## 14.6 Cell Response to Surface Patterning

Introducing cell growth via tailoring surface topography on the nanometer scale is a promising approach for repair, growth, as well as for controlling cocultures of cell populations. Regular line pattern, nanogrooves, with feature sizes between 100 and 1000 nm produced on polymers showed that neuronal cells preferentially orient themselves parallel to the nanogrooves [14]. Furthermore, structure depth have been shown to play a crucial role with an aspect ratio greater than 0.6 inducing higher degree of alignment than shallower grooves [14].

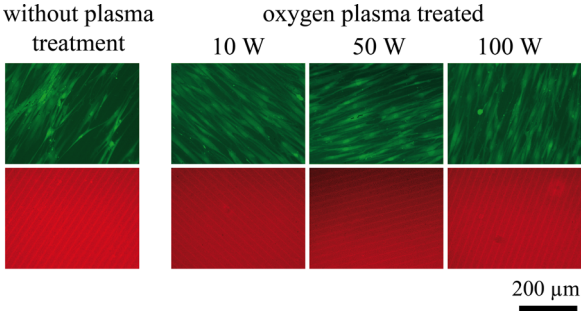


**Figure 14.13** ASC aligned along grooves on oxygen plasma-treated PEEK substrate 48 h after seeding. Vital cells were stained with calcein-AM. The grooves including their orientation are visible in the red-colored images [12]. (Reproduced with permission. Copyright 2015, SPIE.)

Nanostructuring the substrate also allows differentiation of stem cells in the absence of chemical growth factors to become osteoblasts. Arrays of pillars 35 nm tall with a diameter of 193 nm and a distance of about 30 nm have shown conditions for MSCs to form bone cells [62]. Very recently, it has been demonstrated that adipose tissue-derived MSCs seeded on plasma-treated PEEK films show an increased adhesion, a higher degree of proliferation, and an improved osteogenic differentiation compared to untreated films. When these cells were grown on films treated with 10 and 50 W oxygen and ammonia plasmas for duration of 5 min, they exhibit a doubled mineralization degree relative to the untreated PEEK [20]. The effect of nanostructures from plasma treatment in combination with structured grooves from hot embossing showed that adipose tissue derived stem cell (ASC) stretched and aligned parallel to the grooves (see Figure 14.13). The nanostructuring from plasma treatment allowed a homogenous ASC adhesion [56], which is required for proliferation and differentiation to the required phenotype. As the plasma-treated PEEK films supported the osteogenic differentiation of stem cells *in vitro*, one can reasonably assume that plasma-treated PEEK implants hold perspective for suitable osseointegration of load-bearing PEEK implants *in vivo*. Encouraging results have also been reported in the field of vascular grafts, where an improved human umbilical vein endothelial cell (HUVEC) adhesion was seen on plasma-modified polymer films compared with untreated samples [63].

## 14.7 Conclusion

The use of nanosized surface topographies is attractive in biomedical applications, because surface functionalization can be done without change of material and its chemical composition. Moreover, surface nanostructuring can lead to a class of materials for load-bearing or structural implants that incorporate tunable surface features, which can drive cell-specific behavior without the use of

exogenous factors. These nanostructured materials will also continue to improve biocompatibility of a growing range of devices and scaffolds for tissue-engineered products. Nanostructuring can lead to the development of scaffold materials that can stimulate stem cell differentiation to produce bone mineral.

Applications will largely depend on whether effects based on surface topography can be quantified and reproducibly applied to surfaces of existing components. This implies that a range of topographies ranging from μm to nm sizes need to be generated with the same manufacturing methods, and molds or inlays can be fabricated for nonflat surfaces [64]. Polymers are particularly advantageous, because the molds provided for standard replication can be decorated with nanostructures without changing the overall shape of the manufactured component. Nanotopographies, which can be precisely replicated, allow reproducibility of cellular response, thus being an important tool in analyzing how cells process nanoscale information. The nanostructures that can be tailored by the choice of the plasma power and the treatment time are promising for many biomedical applications. It is one promising way of integration, needed to path the way of functional nanostructuring in biomedical areas.

## References


1 Kurtz, S.M. and Devine, J.N. (2007) PEEK biomaterials in trauma, orthopedic, and spinal implants. *Biomaterials*, **28** (32), 4845–4869.

2 Ma, P.X. (2004) Scaffolds for tissue fabrication. *Mater. Today*, **7** (5), 30–40.

3 Heckele, M. and Schomburg, W.-K. (2004) Review on micro molding of thermoplastic polymers. *J. Micromech. Microeng.*, **14**, R1.

4 Giboz, J., Copponnex, T., and Mélé, P. (2007) Microinjection molding of thermoplastic polymers: a review. *J. Micromech. Microeng.*, **17**, 96–109.

5 Stormonth-Darling, J.M. and Gadegaard, N. (2012) Injection moulding difficult nanopatterns with hybrid polymer inlays. *Macromol. Mater. Eng.*, **297** (11), 1075–1080.

6 Schift, H., Urwyler, P., Kristiansen, P.M., and Gobrecht, J. (2014) Nanoimprint lithography process chains for the fabrication of micro- and nanodevices. *J. Micro/Nanolith. MEMS MOEMS*, **13** (3), 031303.

7 Schift, H., David, C., Gabriel, M., Gobrecht, J., Heyderman, L.J., Kaiser, W. *et al.* (2000) Nanoreplication in polymers using hot embossing and injection molding. *Microelectron. Eng.*, **53**, 171–174.

8 Schift, H., D'Amore, A., David, C., Gabriel, M., Gobrecht, J., Kaiser, W. *et al.* (2000) Quantitative analysis of the molding of nanostructures. *J. Vac. Sci. Technol. B*, **18** (6), 3564–3568.

9 Matschuk, M. and Larsen, N.B. (2013) Injection molding of high aspect ratio sub-100 nm nanostructures. *J. Micromech. Microeng.*, **23** (2), 025003.

10 Kane, R. and Ma, P.X. (2013) Mimicking the nanostructure of bone matrix to regenerate bone. *Mater. Today*, **16** (11), 418–423.

11 Gadegaard, N., Dalby, M.J., Martines, E., Seunarine, K., Riehle, M.O., Curtis, A.S.G. *et al.* (2006) Nano patterned surfaces for biomaterial applications. *Adv. Sci. Technol.*, **53**, 107–115.

12 Althaus, J., Urwyler, P., Padeste, C., Heuberger, R., Deyhle, H., Schift, H. *et al.* (2012) Micro- and nanostructured polymer substrates for biomedical applications. *Proc. SPIE*, **8339**, 83390Q.

13 Bhushan, B. (2010) *Handbook of Nanotechnology*, 3rd edn, Springer, Heidelberg.

14 Bremus-Koebberling, E. A., Beckemper, S., Koch, B., Gillner, A. (2012) Nano structures via laser interference patterning for guided cell growth of neuronal cells. *J Laser Applications* **24** (4), 042013-1-6.

15 Hitachi. Nanopillar Plate (2015) Available from: http://www.hitachi-hightech.com/global/about/corporate/research/cuttingedge/nanopillar/index.html/.

16 Gittens, R.A., Olivares-Navarrete, R., Schwartz, Z., and Boyan, B.D. (2014) Implant osseointegration and the role of microroughness and nanostructures: lessons for spine implants. *Acta Biomater.*, **10** (8), 3363–3371.

17 Vukusic, P. and Sambles, J.R. (2003) Photonic structures in biology. *Nature*, **424**, 852–855.

18 Hojlund-Nielsen, E., Weirich, J., Norregaard, J., Garnaes, J., Mortensen, A., and Kristensen, A. (2014) Angle-independent structural colors of silicon. *J. Nanophotonics*, **8** (1), 083988.

19 Vogel, V. and Sheetz, M.P. (2006) Local force and geometry sensing regulate cell functions. *Nat. Rev. Mol. Cell Biol.*, **7**, 265–275.

20 Waser-Althaus, J., Salamon, A., Waser, M., Padeste, C., Kreutzer, M., Piles, U. *et al.* (2014) Differentiation of human mesenchymal stem cells on plasma-treated polyetheretherketone. *J. Mater. Sci.-Mater. Med.*, **25**, 515–525.

21 Gadegaard, N., Thoms, S., Macintyre, D.S., McGhee, K., Gallagher, J., Casey, B. *et al.* (2003) Arrays of nano-dots for cellular engineering. *Microelectron. Eng.*, **67** (8), 162–168.

22 Köser, J., Gaiser, S., and Müller, B. (2011) Contractile cell forces exerted on rigid substrates. *Eur. Cell Mater.*, **21**, 479–487.

23 Köser, J., Gobrecht, J., Pieles, U., and Müller, B. (2008) Detection of the forces involved and modulation of cell-substrate interactions. *Eur. Cell Mater.*, **16**, 38.

24 Dalby, M.J., Gadegaard, N., Tare, R., Andar, A., Riehle, M.O., Herzyk, P. *et al.* (2007) The control of human mesenchymal cell differentiation using nanoscale symmetry and disorder. *Nat. Mater.*, **6** (12), 997–1003.

25 Aizenberg, J., Black, A.J., and Whitesides, G.M. (1998) Controlling local disorder in self-assembled monolayers by patterning the topography of their metallic supports. *Nature*, **394**, 868–871.

26 Chen, C.S. *et al* (1998) Micropatterned surfaces for control of cell shape, position, and function. *Biotechnol. Prog.*, **14**, 356–363.

27 Mrksich, M. and Whitesides, G.M. (1996) Using self-assembled monolayers to understand the interactions of man-made surfaces with proteins and cells. *Annu. Rev. Biophys. Biomol. Struct.*, **25**, 55–78.

28 Takayama, S., McDonald, J.C., Ostuni, E., Liang, M.N., Kenis, P.J.A., Ismagilov, R.F. *et al.* (1999) Patterning cells and their environments using multiple laminar fluid flows in capillary networks. *Proc. Natl. Acad. Sci. USA*, **96**, 5545–5548.

29 Zhang, S.G., Yan, L., Altman, M., Lassle, M., Nugent, H., Frankel, F. *et al.* (1999) Biological surface engineering: a simple system for cell pattern formation. *Biomaterials*, **20**, 1213–1220.

30 Whitesides, J.G. and Lamantia, A.S. (1995) Distinct adhesive behaviors of neurons and neural precursor cells during regional differentiation in the mammalian forebrain. *Dev. Biol.*, **169**, 229–241.

31 Palin, E. (2005) Mimicking the nanofeatures of bone increases bone-forming cell adhesion and proliferation. *Nanotechnology*, **16**, 1828–1835.

32 Yim, E.K.F. (2007) Synthetic nanostructures inducing differentiation of human mesechymal stem cells into neuronal lineage. *Exp. Cell Res.*, **313**, 1820–1829.

33 Thapa, A. (2003) Nano-structured polymers enhance bladder smooth muscle cell function. *Biomaterials*, **24**, 2915–2926.

34 Kay, S., Thapa, A., Karen, M.H., and Webster, J.T. (2002) Nanostructured polymer/nanophase ceramic composites enhance osteoblast and chondrocyte adhesion. *Tissue Eng.*, **8** (5), 753–761.

35 Miller, D.C. (2004) Endothelial and vascular smooth muscle cell function on poly(lactic-co-glycolic acid) with nano-structured surface features. *Biomaterials*, **25**, 53–61.

36 Li, Y., Zhang, J., Fang, L., Jiang, L., Liu, W., Wang, T. *et al.* (2012) Polymer brush nanopatterns with controllable features for protein pattern applications. *J. Mater. Chem.*, **22**, 25116–25122.

37 Borini, S., D'Auria, S., Rossi, M., and Rossi, A.M. (2005) Writing 3D protein nanopatterns onto a silicon nanosponge. *Lab. Chip.*, **5** (10), 1048–1052.

38 Christman, K.L., Broyer, R.M., Schopf, E., Kolodziej, C.M., Chen, Y., and Maynard, H.D. (2011) Protein nanopatterns by oxime bond formation. *Langmuir*, **27** (4), 1415–1418.

39 Bat, E., Lee, J., Lau, U.Y., and Maynard, H.D. (2015) Trehalose glycopolymer resists allow direct writing of protein patterns by electron-beam lithography. *Nat. Commun.*, **6**, 6654.

40 Valsesia, A., Mannelli, I., Colpo, P., Bretagnol, F., and Rossi, F. (2008) Protein nanopatterns for improved immunodetection sensitivity. *Anal. Chem.*, **80** (19), 7336–7340.

41 Mühlberger, M., Rohn, M., Danzberger, J., Sonntag, E., Rank, A., Schumn, L. *et al.* (2015) UV-NIL fabricated bio-inpsired inlays for injection molding to influence the friction behavior of ceramic surfaces. *Microelectron. Eng.*, **141**, 140–144.

42 Kirchner, R., Guzneko, V.A., Rohn, M., Sonntag, E., Mühlberger, M., Bergmair, I. *et al.* (2015) Bio-inspired 3D funnel structures made by grayscale electron-beam patterning and selective topography equilibration. *Microelectron. Eng.*, **141**, 107–111.

43 Röhrig, M., Schneider, M., Etienne, G., Oulhadj, F., Pfannes, F., Kolew, A. *et al.* (2013) Hot pulling and embossing of hierarchical nano- and micro-structures. *J. Micromech. Microeng.*, **23** (105014), 7.

44 McKeag, T. (2015) Sticky wicket: a search for an optimal adhesive for surgery. *Zygote Q.*, **1**, 18–41.

45 Bartlett, M.D., Croll, A.B., King, D.R., Paret, B.M., Irschick, D.J., and Crosby, A.J. (2012) Looking beyond fibrillar features to scale gecko-like adhesion. *Adv. Mater.*, **24**, 1078–1083.

46 Cheung, C.L., Nikolic, R.J., Reinhardt, C.E., and Wang, T.F. (2006) Fabrication of nanopillars by nanosphere lithography. *Nanotechnology*, **17** (5), 1339–1343.

47 Vogel, N., Goerres, S., Landfester, K., and Weiss, C.K. (2011) A convenient method to produce close- and non-close-packed monolayers using direct assembly at the air-water interface and subsequent plasma-induced size reduction. *Macromol. Chem. Phys.*, **212**, 1719–1734.

48 Choi, J., Nielsch, K., Reiche, M., Wehrspohn, R.B., and Gösele, U. (2003) Fabrication of monodomain alumina pore arrays with an interpore distance smaller than the lattice constant of the imprimt stamp. *J. Vac. Sci. Technol. B*, **21** (2), 763–766.

49 Grimm, S., Martin, J., Rodriguez, G., Fernandez-Gutierrez, M., Mathwig, K., Wehrspohn, R.B. *et al.* (2010) Cellular interactions of biodegradable nanorod arrays prepared by nondestructive extraction from nanoporous alumina. *J. Mater. Chem.*, **20**, 3171–3177.

50 Urwyler, P., Schift, H., Gobrecht, J., Häfeli, O., Altana, M., Battiston, F. *et al.* (2011) Surface patterned polymer micro-cantilever arrays for sensing. *Sensor Actuat. A-Phys.*, **172** (1), 2–8.

51 Urwyler, P., Pascual, A., Kristiansen, P.M., Gobrecht, J., Müller, B., and Schift, H. (2013) Mechanical and chemical stability of injection-molded microcantilevers used for sensing. *J. Appl. Polym. Sci.*, **127**, 2363–2370.

52 Urwyler, P., Koser, J., Schift, H., Gobrecht, J., and Muller, B. (2012) Nano-mechanical transduction of polymer micro-cantilevers to detect bio-molecular interactions. *Biointerphases*, **7** (1–4), 6.

53 Schleunitz, A., Spreu, C., Mäkelä, T., Haatainen, T., Klukowska, A., and Schift, H. (2011) Hybrid working stamps for high speed roll-to-roll nanoreplication with molded sol-gel relief on a metal backbone. *Microelectron. Eng.*, **88** (8), 2113–2116.

54 Schift, H., Urwyler, P., and Kristiansen, P.M. (2013) Nanoimprint lithography process chains for the fabrication of micro- and nanodevices. *J. Vac. Sci. Technol. B*, **31** (6), 06FD1.

55 Al-Azawi, A., Smistrup, K., and Kristensen, A. (2014) Nanostructuring

steel for injection molding tools. *J. Micromech. Microeng.*, **24**, 055023.
56 Althaus, J., Padeste, C., Köser, J., Pieles, U., Peters, K., and Müller, B. (2012) Nanostructuring polyetheretherketone for medical implants. *Eur. J. Nanomed*, **4** (1), 7–15.
57 Urwyler, P., Zhao, X., Pascual, A., Schift, H., and Müller, B. (2014) Tailoring surface nanostructures on polyaryletherketones for load-bearing implants. *Eur. J. Nanomed.*, **6** (1), 37–46.
58 Christiansen, A.B., Clausen, J.S., Mortensen, N.A., and Kristensen, A. (2014) Injection moulding antireflective nanostructures. *Microelectron. Eng.*, **121**, 47–50.
59 Malaquin, L., Kraus, T., Schmid, H., Delamarche, E., and Wolf, H. (2007) Controlled particle placement through convective and capillary assembly. *Langmuir*, **23** (23), 11513–11521.
60 Stoykovich, M.P. and Nealey, P.F. (2006) Block copolymers and conventional lithography. *Mater. Today*, **9** (9), 20.
61 Yanagishita, T., Nishio, K., and Masuda, H. (2009) Anti-reflection structures on lenses by nanoimprinting using ordered anodic porous alumina. *Appl. Phys. Expr.*, **2**, 022001.
62 Gadegaard, N., Dalby, M.J., Riehle, M.O., and Wilkinson, C.D.W. (2008) Optimizing substrate disorder for bone tissue engineering of mesenchymal stem cells. *J. Vac. Sci. Technol. B*, **26** (6), 2554–2557.
63 Chong, D.S.T., Turner, L.-A., Gadegaard, N., Seifalian, A.M., Dalby, M.J., and Hamilton, G. (2015) Nanotopography and plasma treatment: redesigning the surface for vascular graft endothelialisation. *Eur. J. Vasc. Endovasc. Surg.*, **49**, 335–343.
64 Rytka, C., Kristiansen, P.M., and Neyer, A. (2015) Iso- and variothermal injection compression moulding of polymer micro- and nanostructures for optical and medical applications. *Micromech. Microeng.*, **25**, 065008.

# 15
# Nanotechnology in the Treatment of Incontinence

*Vanessa Leung and Christian Gingert*

*University of Basel, Biomaterials Science Center, Gewerbestrasse 14, 4123 Allschwil, Switzerland*

Multiple factors and interrelated mechanisms contribute to natural urinary and fecal continence, a key part of which is played by the urinary and fecal sphincters, respectively. From the engineering point of view, sphincters are simple due to their binary nature: they are either on or off. Thus, engineers see sphincters as analogically even simpler than a water faucet, since no flow regulation is required. From the anatomical point of view, sphincters have multiple interacting parts. The urinary sphincter muscle ensures urinary continence during the filling phase of the bladder. Sphincter abnormalities lead in particular to stress urinary incontinence (SUI), which is defined as involuntary loss of urine during coughing, sneezing, or any other kind of related physical exertion. In severe cases, it presents a continuous loss of urine. Approximately 50% of women older than 20 years have reported urinary incontinence (UI) symptoms, of which 50% of patients are classified as having SUI [1].

Natural fecal continence relies on a complex interplay between the central, peripheral, and autonomous nervous systems, a functioning gastrointestinal (GI) tract, and the anal sphincter complex. The dysfunction of only one of these components can cause the loss of continence control. The overall prevalence of fecal incontinence in adults is reported to be 11–15% and increases with age [2]. Common sources of dysfunction are injuries such as birth trauma, psychological and neurological disorders, and inflammatory diseases of the bowel.

Up to now, nanomedicine in urology and colorectal surgery has primarily been applied in the areas of gene therapy, drug delivery, medical imaging, and thermal ablation of tumors. The application of nanotechnology to the regeneration or replacement of structures in the body is only beginning to progress toward clinical trials. The use of structures with 1–100 nm size features promises to give a specific functionality in the mechanical, electrical, or biochemical regime that is commonly inaccessible on the macroscale. Cellular protein structures and cellular receptor–ligand interactions all exist in the nanoscale regime; nanotechnology can thus be used to provide ligands for cell adhesion. Such integration can lead to an implant

*Nanoscience and Nanotechnology for Human Health,* First Edition. Edited by Bert Müller and Marcel Van de Voorde.

that is capable of allowing cellular infiltration and the growth of new tissue and blood vessels. A tissue-integrated implant has the advantage of being accessible to defense by the host's immune system. In addition, a biocompatible implant that can be remodeled by macrophages may lead to a reduced inflammatory response directly after implantation.

The application of nanoscale materials to the treatment of incontinence falls into two main functional categories. Within the scope of regenerative medicine, nanotechnology can first be applied to tissue engineering to replace key functions of the organs responsible for continence. This ranges from the development of an improved material for a pubovaginal sling that eventually integrates into host tissue, to a complete sphincter reconstruction. Second, nanotechnology can be applied to the development of artificial sphincter implants for cases of severe incontinence. Based on their versatility, reaction speed, reaction forces, as well as energy consumption, smart materials such as low-voltage electroactive polymers can be used to produce artificial muscles for sphincter replacement.

In this chapter, we examine the treatment of urinary and fecal incontinence, from the perspective of nanotechnology-based interventions. Both sections are arranged according to the same structure. We first introduce the incontinence etiology and assessment, as well as the underlying physics of incontinence. This forms the basis for the subsequent discussion on the application of nanotechnology to incontinence treatment by tissue engineering or alternatively through the engineering of a sphincter replacement device.

## 15.1 Urinary Incontinence

### 15.1.1 Urinary Incontinence Etiology

An intact urinary continence consists of a complex interplay of the central, peripheral, and autonomous nervous systems. The dysfunction of only one of these components can cause UI. Congenital or acquired anatomical malformations can also cause UI. In general, five types of UI can be differentiated. Most frequent are SUI and urge incontinence, which together account for 90% of instances. The other 10% of instances are the result of the three less frequent causes: neurogenic incontinence, overflow incontinence, and anatomical malfunctions. A clinician has to distinguish between two main categories of urinary incontinence: temporary or persistent UI (see Table 15.1). The general risk factors are listed in Table 15.2 [3].

### 15.1.2 Urinary in-/Continence Assessment

It is important to determine, which of the five types of UI, that is, stress, urge, overflow, neurogenic, or anatomical UI, the patient has, as this identification will

**Table 15.1** Possible causes of UI are classified into two main groups: temporary and persistent.

| | |
|---|---|
| Temporary UI | Diuretic drinks, food or medications:<br>Caffeine<br>Decaffeinated and/or carbonated drinks<br>Alcohol<br>Artificial sweeteners<br>Blood pressure medications, sedatives<br>Large doses of vitamins B or C<br>Fruits high in spice, acid, or sugar<br>Urinary tract infection: Due to irritation of the bladder a strong urge to urinate can be caused. |
| | Constipation: Rectum and bladder share some nerves that can be irritated by stool impaction. This can cause an increase in urination. |
| Persistent UI | Pregnancy: Increased weight of uterus and changes in hormones may increase UI.<br>Childbirth: Muscles needed for bladder control may be weakened by vaginal delivery.<br>Age: With age muscles need for bladder control may be weakened.<br>Menopause: Loss of estrogen can cause a deterioration of the urogenital tract and thereby an increase of UI.<br>Hysterectomy: Removal of the uterus can damage supporting pelvic floor muscles.<br>Enlarged prostate: Especially in older men benign prostate hyperplasia can cause UI.<br>Prostate cancer: UI can be caused by prostate cancer itself because of infiltration and because of medication or radiation.<br>Obstruction: Any obstruction can lead to overflow incontinence.<br>Neurological disorders: Parkinson's disease, stroke, brain tumours, multiple sclerosis and spinal injuries can interfere with pelvic floor innervation. |

guide treatment decisions. The most essential step to UI identification is a detailed anamnesis, in which questions regarding frequency of urination and the ability to hold back urine play an important role. Quite frequently, physicians recommend that patients fill out *bladder diaries* to record the amount of drinks

**Table 15.2** General risk factors for UI are gender, age, body weight, and diseases.

| | |
|---|---|
| Gender | Women > men (pregnancy, childbirth, changes in hormones, and normal female anatomy) |
| Age | With age muscles shrink. So with age muscles of bladder and urethra lose their strength. |
| Body weight | With overweight pressure on the bladder increases and urine may get released. |
| Diseases | Neurological disorders including stroke or metabolic diseases such as diabetes may increase risk of UI by reducing nerve functions. |

and urine, the frequency of urination, or whether the patient felt urge to urinate. The patient is also requested to record episodes of incontinence.

The determination of the patient's history is followed by physical examinations. Conditions such as prolapses and loss of urine, while coughing, can be easily assessed. Further exams include a urinalysis to check on signs of infection and other abnormalities and a postvoid urination residual measurement using a catheter or ultrasound to evaluate the amount of leftover urine in the patient's bladder. A large amount of leftover urine may be a sign of an obstruction in the urinary tract. Nerve or muscular problems can also cause urinary leftover.

Further specialized tests may be recommended including urodynamic testing and cystoscopy. With an urodynamic test, the strength and urinary sphincter health can be assessed and the type of UI can be distinguished. After application of a catheter, the patient's bladder is filled with water, while the pressure within the bladder is measured. In a cystoscopy test, a thin scope is inserted into the urethra and bladder to check the structure of these organs and, if necessary, to remove abnormalities. A cystogram reveals structural and functional problems of the urinary tract through injecting a radiopaque material in the urethra and bladder.

Finally, a pelvic ultrasound can be used to check for abnormalities of the patient's genitals and urinary tract, and magnetic resonance imaging (MRI) can give evidence of dyssynergies and further pathologies of the pelvic floor such as entero-, recto-, or cystoceles. An MRI examination is extensive and relatively expensive, therefore, it is usually only used in cases, where more complex pathologies are suspected [4–6].

### 15.1.3 Physics of Urinary Continence

The urinary sphincter is composed of a thin inner layer and a thick outer layer. The inner layer consists of smooth muscle cells, whereas the outer layer consists of striated muscle (RS) cells, which supports slow contractions around the urethra. The mechanical properties of urethral tissue are characterized by the tissue's stress–strain relation. The stress–strain relation can be measured by a conventional tensile testing machine, by compression, and *in vivo* by aspiration. In the simplest case, from the stress–strain curve measured by these methods, the Young's modulus can be determined by inverse finite element modeling.

The human urethra consists of anisotropic, viscoelastic tissue exhibiting an inner diameter of about 5 mm and an outer one of about 12 mm. As a rough approximation, one can assume that the leakage starts, when the external sphincter pressure equals the intravesical pressure. The tissue of the urethra, however, can act against or with the external pressure. This means that a higher or lower external pressure is necessary to close the urethra. This difference arises from the wall pressure $p_W$ along the sphincter length $L$ and from the stress of the urethra at both ends characterized by the rim force $F_R$. Since the inner part of the urethra can be closed on the length, which is smaller or larger than the

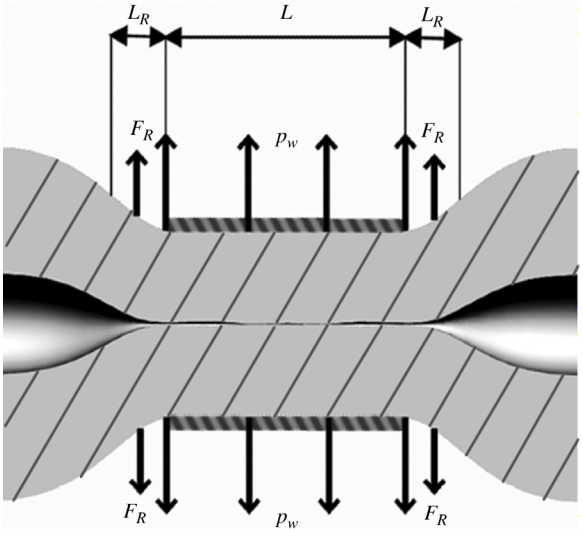


**Figure 15.1** Physical parameters of the urethral compression. (Model from Ref. [7].)

sphincter length $L$, one has introduced the rim length $L_R$ equally present on both sides of the sphincter. This empirical model, known as the *urethra compression model*, contains three parameters, which can be positive and negative, to be determined on the basis of well-defined experiments (see Figure 15.1) [7].

### 15.1.4
### Tissue Engineering and Sling Material for Sphincter Regeneration

The most common surgical treatment for SUI is the placement of a suburethral pubovaginal sling. Sling placement helps to stabilize the urethrovescial junction and compresses the urethral lumen during stress manuveurs. Sling materials include autografts, allografts, that is, cadaveric tissues, xenografts including porcine small intestinal submucosa, and synthetic materials. However, the ideal sling material has still not been identified. Such a material would be strong, readily available, with low occurrences of infection, immunologic rejection, and erosion. Potential advantages of a tissue engineered sling material include reduced donor site morbidity and customizable biomechanical properties.

A key application of tissue engineering (TE) is to replace diseased tissue with a highly porous three-dimensional scaffold that mimics some functions of the extracellular matrix (ECM) so as to promote cell growth and host tissue infiltration. Synthetic polymeric scaffolds such as electrospun polyethylene terephthalate and polyurethane, for example, have a fibrous microarchitecture similar to the ECM. Two potential scaffolds that have been proposed as optimal sling materials for SUI treatment are poly(L)lactic acid (PLA) and small intestinal submucosa (SIS) [8–10]. Both were found to support cell attachment and

proliferation, and had biomechanical properties similar to that of the pelvic floor. Unlike SIS, often derived from porcine sources, PLA is a synthetic material.

Engineering a synthetic sling material with nanometer scale features requires suitable microfabrication techniques, such as electrospinning and 3D printing. Electrospinning is one variation of electrospray techniques and is commonly used to produce nano- and micrometer-size fibers suitable for the fabrication of a scaffold. A syringe is loaded with polymer solution, and a high voltage source is used to extract a stream of polymer from the needle tip toward a collector plate. The plate can be moved to create various fiber orientations, allowing the formation of three-dimensional scaffolds. Electrospinning in combination with heat annealing has been used to produce a PLA scaffold with mechanical properties comparable to native tissue [8].

As less invasive alternatives to sling placement, research directions analogous to those for the application of TE to fecal sphincter regeneration have also been pursued. These directions aim toward directly improving urinary sphincter defects by injection of bulking agents, or by the injection of stem cells, progenitor cells, or adult cells [11]. For both approaches, nanotechnology has the potential to advance progress through structures that are bioengineered down to the nanometer scale.

Bulking agents with nanofeatures have demonstrated advantages [12,13]. Kim *et al.* used growth factor-immobilized porous beads with sizes of 200–300 μm and pores of 25–50 μm as a bioactive bulking agent to treat SUI. They were found to be effective for the regeneration of smooth muscle around the urethra, and lead to functional recovery through an improved contractile response [12]. This is likely due to the combination of (i) the bead's high porosity and the interconnectivity provides an appropriate environment for cell adhesion and proliferation, and (ii) the sustained release of growth factors promotes differentiation into target cells. Similarly, Park *et al.* showed that a hybrid hydrogel consisting of *in situ* forming gelation-based macrogels and self-assembled heparin-based nanogels as a carrier allowed for sustained release of growth factors as well as a bulking effect [13]. In a similar manner, the effective introduction of stem cells relies on seeding onto the appropriate structural support, the fabrication of which can be aided by nanotechnology. Designing features in the natural length scale of proteins can make available better cell-substrate interaction, thus leading to improved biocompatibility. In a recent study, adipose derived stem cells (ADSC) were harvested and seeded onto poly (lactic-coglycolic acid) (PLGA) microparticles containing nerve growth factor (NGF). The preparation was injected periurethrally into mice, and improved the leak-point pressure (LPP) to $(22.5 \pm 6.1)$ cm $H_2O$ over treatments without either PLGA or NGF [14]. PLGA is a copolymer of PLA and poly glycolic acid (PGA), and is a well-introduced biomaterial often used for drug delivery. With continuing advancement in nanofabrication techniques, promising scaffold materials such as PLGA and PLA can be engineered with increasingly advanced nanoscale features conducive to cell growth and proliferation as well as oxygen exchange and nutrient delivery.

## 15.2
## Fecal Incontinence

### 15.2.1
### Fecal Incontinence Etiology

An intact continence consists of a complex interplay of central, peripheral, and autonomous nervous system, a functioning GI tract and anal sphincter complex. A dysfunction of only one of these components can cause a fecal incontinence (FI). A clinician has to distinguish between congenital and acquired risk factors of FI. Congenital risk factors include Hirschsprung's disease or anorectal malformations, whereas acquired risk factors may be conditions after sphincter lesions during delivery, radiation, or previous surgeries (cf. Table 15.3) [15].

### 15.2.2
### Physics of Fecal Continence

The mechanisms and factors contributing to normal continence are multiple and inter-related. Loss of control of continence is called fecal incontinence that for instance may be caused by injuries like birth trauma or previous surgeries, psychological or neurological disorders or inflammatory diseases of the bowel [15]. The curved anatomy of the rectum and the three layers of closure mechanism enable continence. A schematic illustration of the main continence structures is shown in Figure 15.2. The curved anatomy of the rectum is caused by the puborectal sling, which pulls the rectum towards the *os pubis*. The closing mechanism includes an outer, middle, and inner layer. The outer layer narrows the anal canal, and consists of the puborectal sling, *m. levator ani*, and the circular external anal sphincter muscle (EAS). The EAS is a voluntary muscle that can double the pressure in the anal canal during contraction for a short period of time. The pudendal nerve originating from the sacral cord S4 innervates the EAS.

**Table 15.3** Risk factors for FI can be classified as either congenital or acquired.

| | |
|---|---|
| Congenital risk factors | Hirschsprung's disease |
| | Spina bifida |
| | Anorectal malformations |
| Acquired risk factors | Surgeries of the lesser pelvis (rectum resection; hysterectomy) |
| | Radiation |
| | Injuries of the sphincter organ (iatrogenic, i.e., hemorrhoidectomy, surgery of fistula, sphincterotomy; trauma during delivery) |
| | Gastrointestinal diseases (inflammatory bowel diseases; irritable colon) |
| | Neurological incontinence (diabetes mellitus; cerebral insult; spinal trauma; Parkinson's disease; multiple sclerosis) |
| | Age |

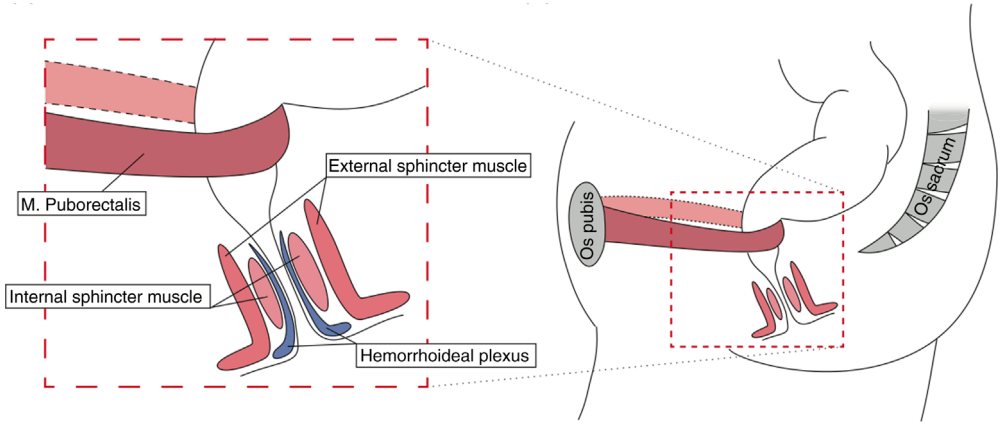


**Figure 15.2** Schematic representation of the anatomical structures involved in continence (adapted from Ref. [16]). The three layers forming the closure mechanism are shown in detail in the expanded view. The muscular structures are rose-colored, while the hemorrhoideal plexus is shown in blue.

The middle layer consists of *m. sphincter ani internus* (IAS), an involuntary muscle contributing about 55% of the resting anal pressure. Together with the inner layer consisting of the hemorrhoidal vascular cushion, the IAS maintains continence, notably for gases and liquids. The parasympathetic fibers originating from the sacral cord and the sympathetic fibers originating from the lumbar cord innervate the IAS [17]. The hemorrhoidal vascular cushion consists of arterial–venous vessels that are filled by contraction of the venous vessels. When filled, the hemorrhoidal cushion forms the so-called *corpus cavernosum recti*, and closes the anal canal completely.

The rectoanal inhibitory reflex (RAIR) is an involuntary IAS relaxation in response to the filling of the rectum. Receptors stimulated by distension initiate the reflex, allowing stool to descend into the anal canal, where other specialized receptors respond to stool consistency. To avoid complete evacuation a semi-voluntary rectoanal excitatory reflex (RAER) of the EAS and *m. puborectalis* follows the RAIR. Other mechanisms of continence include the antiperistaltic function of the sigmoid, which causes the rectum to stay empty, and specialized receptors in the rectum and anal canal that detect, where stool is present and its consistency. Finally, rectoanal reflexes and the defecation cycle enable a complete evacuation of stool from the rectum and anal canal [17].

### 15.2.3
### Fecal in-/Continence Assessment

An essential part of diagnosis is a detailed anamnesis. Questions regarding frequency of defecation and the ability to hold back flatus and stool form part of the anamnesis. Inspection is the easiest and often also most important part of

the diagnostic procedure, allowing direct signs of incontinence such as erythema, scars, or smearing to be detected immediately. Also a part of every examination is rectal palpation, as it allows divergent pressures due to lesions of the sphincter or irregularities in the structure of the anal canal to be found.

Sphincter function can be measured and quantified by manometry. A decreased resting pressure, as well as an insignificant increase of squeezing pressure, can be a sign of a dysfunctional sphincter. An extremely elevated resting pressure can embody a pelvic floor dyssynergy. Besides the simple anal manometry, gastroenterologists also use 3D manometry with fillable balloons. In this way, rectal capacity and/or rectal sensibility can be assessed. This information can be used to draw conclusions on the existence of a rectal reservoir or if the patient is already overreacting to minimal volumes. Endoanal ultrasound (EUS) allows the volume and the integrity of the entire sphincter system to be examined. Defects such as scars including their dimension, as well as the different compounds and layers of the sphincter system, can all be detected with relative ease. In addition, contrast agents can be brought into fistulas to determine the extent of disease. MRI, in particular MR-defecography, is a continuous examination technique, delivering dynamic images during evacuation. Examination by MRI can provide evidence of dyssynergies and further pathologies of the pelvic floor. The rectum is first filled with a paste-like contrast agent; evacuation of this contrast agent allows pelvic floor pathologies such as entero-, recto-, or cystoceles to be clearly identified. However, the MRI examination is extensive, relatively expensive, and embarrassing for patients. Therefore, it is only applied for cases, where other clinical examinations and anamnesis substantiate suspicion of more complex pelvic floor pathologies.

### 15.2.4 Tissue Engineering for Sphincter Regeneration

As in the case for the treatment of urinary incontinence, key tissue engineering methods from regenerative medicine have also been applied to the treatment of fecal incontinence. These efforts range from regenerating the fecal sphincter through minimally invasive means using injectable scaffolds [18] to bioengineering transplantable rings of IAS tissue [19,20]. Therapeutic approaches entirely based on injecting cells into the anal sphincter have given mixed results. One of the first was carried out by Frudinger *et al.*, who performed a clinical study with a 12-month follow-up on 10 women with FI [21]. They found that after autologous myoblasts were injected into the EAS, there was an initial increase in anal squeeze pressure, and there was no sustained physiological change observed after one year. The lack of long-term regeneration suggests the failure of the cells to integrate into host tissue.

To increase the likelihood of engrafting viable cells to the injured sphincter, cells can be combined with a biocompatible scaffold. Studies have shown that the three-dimensional structure of a scaffold is of critical importance to cell adhesion, proliferation, and differentiation [22]. Nanotechnology can be applied

to engineer structural elements of the injectable scaffold, including the pore size, porosity, and surface topography. Ahmadi *et al.*, for example, fabricated macroporous PLGA microspheres as a cell carrier for the transplantation of smooth muscle cells to improve sphincter contractility [23]. They reported enhanced attachment, growth, and migration of smooth muscle cells compared to microcarriers of porcine gelatin, due in part to the specific nature of the cell–scaffold interaction on the PLGA microsphere surface.

Nonetheless, further studies are required to find an optimized bioengineered cell–scaffold therapy, as evidenced by the recent study of Kang *et al.*, one of the first studies to examine whether bioengineering can improve fecal incontinence [24]. In this work, porous polycaprolactone beads containing autologous myoblasts were injected into a dog model of FI. Although they used well-characterized microcarriers, Kang *et al.* did not find any significant improvement in sphincter function, as the injected myoblasts failed to integrate into the host sphincter.

Finally, attempts have been made to bioengineer transplantable tissue. Fibrin gels are formed by the self-assembly of fibrin monomers into fibrils, which, under appropriate conditions, organize themselves into a matrix suitable for contractile tissue growth. Cells migrate into the matrix and proliferate, eventually replacing the fibrin with their own extracellular matrix. Hecker *et al.* found that IAS rings bioengineered from smooth muscle cells grown on a fibrin matrix generated a spontaneous basal tone, and demonstrated physiological functionality similar to IAS smooth muscle *in vivo* [19]. Potential limitations include finding suitable sources of smooth muscle cells, and the time required to produce the IAS structures.

As in the case of TE for the treatment of urinary incontinence, nanotechnology has the potential to advance both approaches described in this section through structures that are bioengineered on the nanometer scale. First, by fabricating biocompatible synthetic carriers that promote the transplantation of cells to host tissue, as well as tissue bulking, and second, by providing scaffolds with microenvironments designed to enhance cell proliferation and integration, as well as neovascularization. However, TE solutions for FI, including those involving nanotechnology, are currently less advanced than similar solutions for urinary incontinence.

### 15.2.5
### Dielectric Elastomer Actuators for Sphincter Replacement

Nanotechnology as an advanced tool for the creation of nanoscale-engineered structures is appropriate not only to scaffolds for the regeneration of functional tissue, but also as artificial replacements of the functional tissue itself. In the treatment of incontinence, nanotechnology can be used to fabricate adaptive sphincters. Dielectric elastomer actuators (DEA) are one candidate for these so-called smart implants. Advantages offered by DEAs as artificial sphincter compared to currently available sphincters are superior actuator properties such as millisecond response time, mechanical strain of more than 10%, and the

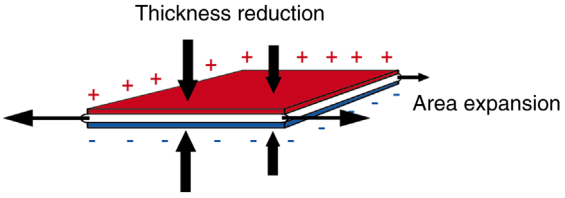


**Figure 15.3** Operating principle of a DEA. A voltage applied across the electrodes results in their attraction by the electrostatic force. The electrodes squeeze the incompressible elastomer between them, resulting in a lateral area expansion.

power-to-mass densities similar to natural muscles. Thus, DEAs are popularly referred to as *artificial muscles*, and offer promising perspectives for biomimetic applications because of the large actuations and sensing ability.

Physically, DEA are capacitors that change their capacitance when a voltage is applied, due to a shape change of the polymer sheet in the electric field, namely, its thickness decreases and its area expands. A stretchable dielectric film is sandwiched between compliant electrodes, forming a planar structure. Applying a voltage across the electrodes induces a mutual electrostatic attraction between them that squeezes the elastomer laterally, as illustrated in Figure 15.3. This lateral expansion is large; depending on the elastomer, a 100% increase in area is possible.

Dielectric elastomer actuators operating at voltages as low as tens of volts will enable their widespread application as medical implants. To reduce the currently used operating voltage by two orders of magnitude or even more, research efforts have primarily been directed toward modifying the elastomers' dielectric permittivity. An alternative, physically motivated approach is to reduce the thickness of the elastomer layer itself. Such an approach is faced with two major technical challenges, both of which can be approached using the tools of nanotechnology. The first technical challenge is in making homogenous elastomer films with thicknesses in the regime of several hundred nanometers or below. This reduction of thickness will allow the actuation voltage to be reduced from the kV regime to medically acceptable values below 42 V. This can be seen by considering the relation between the electromechanical pressure $p_m$, the applied voltage $U$, and the elastomer film thickness $h_{ef}$:

$$p_m = \varepsilon \cdot \varepsilon_0 \cdot E^2 = \varepsilon \cdot \varepsilon_0 \cdot \frac{U^2}{h_{ef}^2},$$

where ε is the relative permittivity of the dielectric elastomer, $\varepsilon_0$ is the free space dielectric permittivity, and $E$ is the induced electric field [25]. By reducing $h_{ef}$ from the micrometer regime to the nanometer regime, the voltage can be similarly reduced from the kV-regime to the order of several volts, while maintaining a comparable strain, which is proportional to $p_m$:

$$s_{x,y} = -0.5\, s_z = \frac{\Delta h_{ef}}{2h_{ef}} = \frac{p_m}{2Y},$$

where $s_{x,y}$ is the strain in the planar directions, $s_z$ is the strain in the thickness direction, and $Y$ is the elastic modulus of the polymer. This relationship is valid for an incompressible polymer and small strains $s_z$ [25].

To give a comparable force to the micrometer-thin actuators, thousands of nanometer-thin layers operating in parallel are required. Such large-scale stacking demands a homogeneity and reproducibility that can be achieved by a well-controlled fabrication process. As known from micro- and optoelectronics, molecular beam deposition (MBD) is such a process. MBD is often the key development step before the establishment of a mass industrial technique such as chemical vapor deposition (CVD). Töpper *et al.* recently presented the use of MBD to fabricate single-layer polydimethylsiloxane (PDMS) nanometer-thick films, showing that these films respond at less than 20 V [26]. The next step to this preliminary result is the growth of reliable actuators by MBD.

Alternative methods are also being investigated. Weiss *et al.* demonstrated that alternating current, electrospray deposition allows for the fabrication of homogenous, flat, nanometer-thin PDMS films [27]. The growth of the PDMS with the average molecular weight of 6000 g/mol at deposition rates ranging from 0.02 to 5.54 nm/s was *in situ* monitored by means of spectroscopic ellipsometry.

The second technical challenge is in making flexible electrodes. Due to the requirement for conductivity, metals are traditionally used as the electrode material. However, even if a metal electrode is 10 times thinner than the elastomer, the mechanical properties of the actuator will still be dominated by the stiffness of its metal electrodes. This is illustrated in Figure 15.4, where the effective

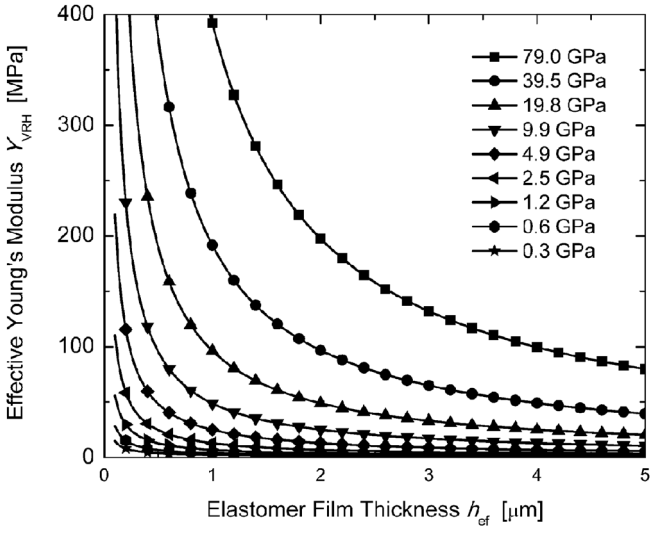


**Figure 15.4** Plot of the Voigt-Reuss-Hill effective Young's modulus as a function of the elastomer film thickness $h_{ef}$, for a 10 nm thick electrode. The elastomer has a constant Young's modulus of 1 MPa. The effect of varying the Young's modulus of the electrode from 0.3 to 79.0 GPa is indicated by the different symbols. (Adapted from Ref. [28].)

Young's modulus (Voigt–Reuss–Hill average) $Y_{VRH}$ of an elastomer with 10 nm of electrode has been calculated as a function of the thickness of the elastomer. In these plots, the Young's modulus of the elastomer is held constant at 1 MPa, while that of the electrode is varied from 0.3 to 79.0 GPa, which is the Young's modulus of gold (square symbols).

Thus, there is a need to find alternative electrodes that are more flexible than isotropic metal electrodes. Electrodes with nanostructured wrinkles have been demonstrated to exhibit a larger actuation and improved stress–strain behavior compared to planar electrodes [28]. Nonconventional electrode materials such as liquid metals or graphene belong to the alternative solutions.

## References


1 Dooley, Y., Kenton, K., Cao, G., Luke, A., Durazo-Arvizu, R., Kramer, H., and Brubaker, L. (2008) Urinary incontinence prevalence: results from the National Health and Nutrition Examination Survey. *J. Urol.*, **179**, 656–661.

2 Macmillan, A.K., Merrie, A.E., Marshall, R.J., and Parry, B.R. (2004) The prevalence of fecal incontinence in community-dwelling adults: a systematic review of the literature. *Dis. Colon Rectum*, **47**, 1341–1349.

3 DuBeau, C.E. (2014) Epidemiology, risk factors, and pathogenesis of urinary incontinence. www.uptodate.com/home (accessed March 5).

4 AskMayoExpert (2013) *What Tests Are Needed to Confirm the Diagnosis or Expedite the Evaluation of Female Incontinence?* Mayo Foundation for Medical Education and Research, Rochester, MN.

5 AskMayoExpert (2013) *What Tests Are Needed to Confirm the Diagnosis or Expedite the Evaluation of Male Incontinence?* Mayo Foundation for Medical Education and Research, Rochester, MN.

6 Hersh, L. and Salzman, B. (2013) Clinical management of urinary incontinence in women. *Am. Fam. Physician*, **87**, 634–640.

7 Marti, F., Leippold, T., John, H., Blunschi, N., and Müller, B. (2006) Optimization of the artificial urinary sphincter: modeling and experimental validation. *Phys. Med. Biol.*, **51**, 1361–1375.

8 Mangera, A., Bullock, A.J., Roman, S., Chapple, C.R., and MacNeil, S. (2013) Comparison of candidate scaffolds for tissue engineering for stress urinary incontinence and pelvic organ prolapse repair. *BJU Int.*, **112**, 674–685.

9 Roman, S., Mangera, A., Osman, N.I., Bullock, A.J., Chapple, C.R., and MacNeil, S. (2014) Developing a tissue engineered repair material for treatment of stress urinary incontinence and pelvic organ prolapse – which cell source? *Neurourol. Urodyn.*, **33**, 531–537.

10 Jankowski, R., Pruchnic, R., Hiles, M., and Chancellor, M.B. (2004) Advances toward tissue engineering for the treatment of stress urinary incontinence. *Rev. Urol.*, **6** (2), 51–57.

11 Lin, C.-S. and Lue, T.F. (2012) Stem cell therapy for stress urinary incontinence: a critical review. *Stem Cell Dev.*, **21** (6), 834–843.

12 Kim, I.G., Oh, S.H., Lee, J.Y., Lee, J.Y., and Lee, J.H. (2011) Bioactive porous beads as an injectable urethral bulking agent: in vivo animal study for the treatment of urinary Incontinence. *Tissue Eng. Part A*, **17** (11–12), 1527–1535.

13 Park, K.M., Son, J.Y., Choi, J.H., Kim, I.G., Lee, Y., Lee, J.Y., and Park, K.D. (2014) Macro/nano-gel composite as an injectable and bioactive bulking material for the treatment of urinary incontinence. *Biomacromolecules*, **15**, 1979–1984.

14 Thaker, H. and Sharma, A.K. (2013) Regenerative medicine based applications

to combat stress urinary incontinence. *World J. Stem Cells*, **5** (4), 112–123.
15 Gingert, C. and Hetzer, F.H. (2014) Stuhlinkontinenz. *Coloproctology*, **36** (2), 125–137.
16 Fattorini, E., Brusa, T., Gingert, C., Hieber, S.E., Leung, V., Osmani, B., Dominietto, M.D., Büchler, P., Hetzer, F., and Müller, B. (2016) Artificial muscle devices: innovations and prospects for fecal incontinence treatment. *Ann. Biomed. Eng.*, **44**, 1355–1369.
17 Fleshman, J.W. and Wolff, B.G. (2007) *The ASCRS Textbook of Colon and Rectal Surgery*, Springer.
18 Bitar, K.N. and Zakhem, E. (2014) Design strategies of biodegradable scaffolds for tissue regeneration. *Biomed. Eng. Comput. Biol.*, **6**, 13–20.
19 Hecker, L., Baar, K., Dennis, R.G., and Bitar, K.N. (2005) Development of a three-dimensional physiological model of the internal anal sphincter bioengineered *in vitro* from isolated smooth muscle cells. *Am. J. Physiol. Gastrointest. Liver Physiol.*, **289**, G188–G196.
20 Raghavan, S., Miyasaka, E.A., Gilmont, R.R., Somara, S., Teitelbaum, D.H., and Bitar, K.N. (2014) Perianal implantation of bioengineered human internal anal sphincter constructs intrinsically innervated with human neural progenitor cells. *Surgery*, **155**, 668–674.
21 Frudinger, A., Kolle, D., Schwaiger, W., Pferfer, J., Paede, J., and Halligan, S. (2010) Muscle-derived cell injection to treat anal incontinence due to obstetric trauma: pilot study with 1 year follow-up. *Gut*, **59**, 55–61.
22 Parmar, N., Kumar, L., Emmanuel, A., and Day, R.M. (2014) Prospective regenerative medicine therapies for obstetric trauma-induced fecal incontinence. *Regen. Med.*, **9**, 831–840.
23 Ahmadi, R., Mordan, N., Forbes, A., and Day, R.M. (2011) Enhanced attachment, growth and migration of smooth muscle cells on microcarriers produced using thermally induced phase separation. *Acta Biomater.*, **7**, 1542–1549.
24 Kang, S.-B., Lee, H.S., Lim, J.-Y., Oh, S.H., Kim, S.J., Hong, S.-M., Jang, J.-H., Cho, J.-E., Lee, S.-M., and Lee, J.H. (2013) Injection of porous polycaprolactone beads containing autologous myoblasts in a dog model of fecal incontinence. *J. Korean Surg. Soc.*, **84**, 216–224.
25 Pelrine, R., Kornbluh, R., and Joseph, J. (1998) Electrostriction of polymer dielectrics with compliant electrodes as a means of actuation. *Sens. Actuators A*, **64**, 77–85.
26 Töpper, T., Weiss, F.M., Osmani, B., Bippes, C., Leung, V., and Müller, B. (2015) Siloxane-based thin films for biomimetic low-voltage dielectric actuators. *Sens. Actuators A*, **233**, 32–41.
27 Weiss, F.M., Töpper, T., Osmani, B., Peters, S., Kovacs, G., and Müller, B. (2016) Electrospraying nanometer-thin elastomer films for low-voltage dielectric actuators. *Adv. Electron. Mater.*, 1500476. doi: 10.1002/aelm.201500476.
28 Osmani, B., Töpper, T., Deschenaux, C., Nohava, J., Weiss, F.M., Leung, V., and Müller, B. (2015) Micro- and nanostructured electro-active polymer actuators as smart muscles for incontinence treatments. *AIP Conf. Proc.*, **1646**, 91–100.

# 16
# Nanomedicine in Dermatology: Nanotechnology in Prevention, Diagnosis, and Therapy

*Kathrin Scherer Hofmeier*[1] *and Christian Surber*[2]

[1]*University Hospital, Department of Dermatology, Basel, Switzerland*
[2]*University Hospitals, Departments of Dermatology, Basel and Zürich, Switzerland*

## 16.1
## Introduction

The use of nanotechnology has spread across the scientific disciplines from electronics via materials and food science to medicine. It has even found applications in cosmetics. In fact, nanotechnology is more prevalent in our day-to-day lives than we might think [1]. Nanotechnology includes the design and engineering of products that interact with biological systems on the molecular level, thus yielding a level of specificity and specialization that was infeasible in the past. Nanomedicine – a subdivision of nanotechnology – opened up entirely new opportunities for highly specific interventions in prevention, diagnosis, and therapy. The key features and benefits are the targeted delivery of nanostructured materials, the inclusion via adsorption/absorption, and protection of actives and their controlled release from the nanostructured materials. The proper design of nanostructured delivery systems ideally enables the distribution of actives in required quantities over desired periods of time to a specific target site without affecting healthy organs and tissues. The latter will potentially increase the safety profile of the actives and may allow reducing the dose as known from conventional delivery systems. The design of the nanostructured delivery system may also protect the active from efflux from the target site or from degradation during delivery [2,3]. The potential of the nanostructured material originates in shaping its size and its surface.

Nanotechnology applied to dermatology represents an advanced field, for which the economic and scientific interest is rising. Even though nanotechnology has probably reached all medical disciplines, it has attracted particular attention in the field of dermatology. As skin is the first point of contact for a whole host of nanostructured materials, hopes in the effects of the *magic bullets* to cure a disease and the fears of harmful particles from sunscreens entering the body often run together.

*Nanoscience and Nanotechnology for Human Health,* First Edition. Edited by Bert Müller and Marcel Van de Voorde.

This chapter discusses (i) the nature of nanoparticles with reference to skin and skin diseases, (ii) the potential of absorption of nanoparticles through skin, (iii) the nanoparticles in prevention, diagnosis and therapy, (iv) some regulatory issues, and (v) the public perception of nanoparticles in topical formulations.

## 16.2 Nature of Nanoparticles

The term *particle* derives from the Latin word *particula*, which means a small part. The prefix *nano* ($10^{-9}$) underlines this notion. The current agreement among the research teams is that the scale from 1 to 100 nm defines the size range of a nanoparticle. Often, however, a more thorough discussion is required to achieve an unambiguous and complete definition [4–6]. A variety of materials including ceramics, metals, polymers, proteins, and lipids have been used. A variety of shapes have been engineered to create nanoparticulate actives and delivery systems. From the point of view of particle interactions with biological surfaces and barriers such as skin, it may be helpful to distinguish between soft and rigid particles. In general, soft particles are made of organic materials such as polymers, proteins, and lipids. They can temporarily alter their shape by stress or contact with surfaces.

### 16.2.1 Soft Particles

Liposomes represent typical soft particles [7]. They are vesicular structures composed of a phospholipid bilayer and a hydrophilic core. Hydrophilic and lipophilic substances can be enclosed into the core. Even though the fate of liposomes, that is, structural stability and functionality, in the delivery vehicle after its application onto the skin is largely unknown, the effect is awarded to the liposomal particle. However, it has been shown that drugs incorporated into liposomes penetrate better into the hair follicle canal or *sebaceous gland* than drugs applied in other nonparticulate formulations [8,9].

Recently, a particular liposome called *transfersome* has attracted attention [10]. It is claimed that these ultradeformable vesicles are able to pass through intact skin as whole aggregates to be distributed throughout the body via the blood circulation. However, the prerequisite is that the formulation is nonocclusively administered onto the skin. The basic principle and driving force for the transfersomes to pass through intact skin was found to be the hydration gradient between the relatively dry skin surface, *stratum corneum* (SC), and the moist viable epidermis and dermis. As phospholipids tend to dehydrate on the skin surface, they need to follow that gradient to stay hydrated. Therefore, nonocclusive application conditions were underlined to be a prerequisite for the principle of hydration gradient-driven barrier permeation [11]. However, clear evidence for whole vesicle permeation through intact skin remains to be established. The ingredients chosen to form a particular liposome have created numerous names such as flexosome, that is, flexible

liposome; ethosome, that is, particle composed of phospholipid, ethanol, and water; niosome, that is, particle composed of nonionic surfactant and cholesterol; invasome, that is, particle composed of terpenes and ethanol; or polymersome, that is, generated through a self-assembly process [12–14].

Virosomes are nanoscaled particles mimicking the nature of viruses. They are hybrids of liposomes and viral proteins [15]. They have been used for a successful vaccination against HBV and HPV [16]. Conceivable is their use in skin cancer treatment [17].

Solid lipid nanoparticles and nanostructured lipid carriers were developed to form more stable systems. They lack the micellar structure of liposomes and make solid lipid nanoparticles and nanostructured lipid carriers more stable both in hydrophilic and in lipophilic environments. This potentially facilitates the transport and delivery of substances including pharmaceutical actives such as retinoids and cosmetic actives such as perfumes to the skin [18,19]. It is also postulated that these particles are particularly suitable to cover the skin surface and hence are ideal for sunscreen products, where coverage is a key issue.

Numerous polymer-based particles have been studied. Accumulation and cytotoxicity of nonbiodegradable particles constitutes major problems and limits their use in humans [20]. Therefore, current interest is focused on biodegradable polymers such as polylactic acid or poly(glycolic-*co*-lactic acid). Polylactic acid is an aliphatic ester of lactic acid, derived from renewable resources such as cornstarch or sugarcanes. This has gained scientific and commercial interest due to its easy manufacturing.

Fullerenes and dendrimers are supramolecular structures that may also be considered as nanoparticles [21,22]. Fullerenes have been investigated for their ability to absorb ultraviolet light and their radical scavenging properties [23,24]. Dendrimers are highly branched structures, the peripheral groups of which can be used both to attach several drug molecules and to target and solublize groups. They may, therefore, be used as drug carrier systems [25]. Poly(amidoamine) dendrimers have also been used as skin permeation enhancers [26].

### 16.2.2 Rigid Particles

Typical rigid nanoparticles consist of metals such as gold or silver, metal oxides including titanium, zinc, or iron oxides, and ceramics such as silica. The encapsulation of drugs in the nanoparticle core or their adsorption on nanoparticle surface allows the transfer and delivery of substances avoiding metabolism and degradation in tissue [27].

Quantum dots are semiconductors with unique electronic and optical properties [28]. Nontoxic quantum dots can be utilized as bioprobes or labels for biological imaging of living cells and tissues [29]. More recently, it has been demonstrated that quantum dots serve not only as imaging agents but also as nanoscaffolds for diagnostic and therapeutic modalities. The combination of these has led to the coining of the term *theranostics* [30–32].

In recent years, much attention has been given to zinc and titanium oxides, which are integral parts of currently distributed sunscreen products. From literature, it is reasonable to conclude that under normal-use conditions on healthy skin, the penetration/permeation of zinc oxide and titanium dioxide nanoparticles poses minimal health concerns [33,34]. However, due to experimental protocols in use, conclusions over the potential penetration/permeation into/through viable skin remain vague [35]. Information from official bodies is often confusing to the consumers. For example, in late 2013 the Therapeutic Goods Administration in Australia stated that studies using animal and human skin have shown that nanoparticles do not penetrate the underlying layers of skin, with penetration limited to the outermost layer of the skin. This suggests that systemic absorption is unlikely [36]. The Cancer Council Australia reported in early 2014 that a recent study found that human immune cells, that is, macrophages, exposed to zinc oxide nanoparticles effectively absorbed the nanoparticles and broke them down [37]. Such reports often remain uncommented by the editors but are broadly reviewed by consumer organizations, are unintelligible to the public, and are hence the source for the perennial health scares in the general public and the media.

### 16.2.3 Surface Functionalization

Nanoparticles come into contact with the biological environment via their surfaces [38]. These surfaces not only may elicit undesired effects but can also be designed to elicit desired effects, such as to targeting specific epitopes. Other applications may demand that nanoparticles are not recognized by the local environment to avoid their clearance by the immune system. To endow nanoparticles with such *stealth* properties, modification of their surfaces with polyethylene glycol (e.g., PEGylation) has become a popular method [39,40]. At present, surface modifications mainly aim at modifying size, surface charge, and their functional groups. Particle surface charge can influence both particle penetration/permeation within the hair follicle canal and the intracellular uptake. Jung *et al.* demonstrated that cationic liposomes could penetrate deeper into the hair follicles than their anionic counterparts [8]. The positive charge influences cellular uptake, since it allows intimate interactions with the negatively charged cell membrane. Nanoparticles can also serve as hosts for functional groups. A promising approach is the design and production of antibody nanoparticles [41]. Biomedical applications of antibody nanoparticles include, for example, targeted drug delivery, gene therapy, cell labeling/tracking, magnetic or optical hyperthermia treatments, and molecular imaging [42]. Key issues are (i) how can the number of captured molecules per nanoparticle be precisely adjusted and (ii) how can the antibodies be attached to nanoparticle surfaces in an oriented way [43,44]. Answers to both questions are key to controlled targeting of nanoparticle bioconjugates in hair follicles and cancer imaging of metastatic melamona.

### 16.2.4
### Formulations with Nanoparticles

Nanoparticles can serve as functional ingredients, e.g., titanium dioxide in sunscreen products, or as vehicles, for example, as carriers of antibodies. They are never applied directly to the skin but incorporated into a carrier system or vehicle. The stability of the nanoparticles in the vehicle is a primary goal of any formulation development and a prerequisite of applied clinical research and subsequent commercialization. When applying formulations with nanoparticles to skin or other biological matrices, the vehicle may undergo significant changes. Volatile ingredients may evaporate or the vehicle may become diluted by the surrounding matrix. This change, coined as metamorphosis of the vehicle, creates a new environment for the nanoparticles that potentially changes their character and functionality [45]. When investigating the interactions of micro- and nanoparticles with biological materials, Graf *et al.* and Racan *et al.* observed instabilities of the colloidal dispersions in physiological media and subsequent particle aggregation [46,47]. Nanoparticles, which were well dispersed in organic solvents or water, often aggregated, when they were transferred to physiological media. This effect is due to the ionic strength and polarity of the used dispersing phase but might also result from complex interactions between the functionalization groups on the surface of the particles and the components of the media, for example, phosphates. Particle aggregation might also reduce the number of nonaggregated particles available for interactions with biological membranes and cellular uptake. Aggregation occurring in body compartments or inside cells could give rise to cytotoxic effects [48]. In many scientific publications, stability and behavior of nanoparticles in its vehicle system and in the biological matrix after application often remains unclear. Potential drugs fail clinically because of insufficient solubility in conventional vehicles. Nanoparticles may help to overcome this handicap, as drugs may be loaded on and into nanoparticles in considerable amounts [49]. Spiked nanoparticles are then incorporated into conventional vehicle systems. Nanoparticles have also helped to improve tolerability to irritation caused by drugs. It has been shown that solid lipid nanoparticles loaded with all-trans-retinoic acid were significantly less irritants than conventional retinoid creams. These particle-based formulations are promising innovations that may help to improve patient treatment adherence [50,51].

## 16.3
## Absorption of Nanoparticles through Skin

### 16.3.1
### Absorption Pathways

There are two general pathways by which any kind of material may penetrate into or permeate through skin: into or through the stratum corneum and the

underlying tissues or along the skin appendages. The stratum corneum is considered to be the main barrier to absorption. The polarity or the hydrophilic/lipophilic character of the absorbent is hereby crucial. The stratum corneum offers two possible pathways for absorption: through the corneocytes (CCs) (bricks) or along the intercellular space (IS) along the lipid matrix (mortar) (Figure 16.1).

Due to the channel-like structures providing higher diffusivity, the latter pathway seems to be more suited for permeation. The stratum corneum as a whole can be considered to be a lipophilic compartment, whereas the underlying tissue is a more hydrophilic compartment. Hence, lipophilic absorbents can partition more easily into the stratum corneum. In addition, these absorbents need to fit into the intercellular space. Hence, the size of the absorbents influences absorption behavior likewise. Partitioning of absorbents into the living, more hydrophilic tissue is in favor of more hydrophilic molecules. It has been shown that the partition coefficient, a ratio of concentrations of a compound in a mixture of two immiscible phases at equilibrium, usually octanol (lipophilic) and water (hydrophilic), is useful in estimating the distribution of drugs within tissues. As a consequence, only substances with partition coefficients (log *P*) between 1 and 3 are well suited for absorption through the skin, see Figure 16.2 [53].

All aspects of absorption, the size of an absorbent and its log *P*, are expressed in the Potts and Guy formula allowing to estimate absorption of a large range of molecules [54]. Empirical findings by Bos and Meinardi [55] known as the *500 Dalton rule* indicate a molar mass cap effect for dermal absorption. It is shown that the diffusion of large-molecule absorbents is drastically impeded in the

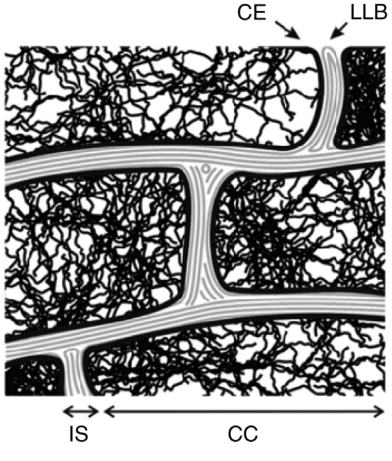


**Figure 16.1** Sketch of the morphology of human stratum corneum (SC): the SC is composed of rigid CCs, dead cells densely packed with keratinous filaments in a matrix of connecting proteins and confined by the cornified envelope (CE), separated by the intercellular space (IS) filled with lipid compounds (fatty acids, ceramides, etc.) and aqueous films to form lamellar lipid bilayers (LLBs) (reproduced with permission from Ref. [52]).

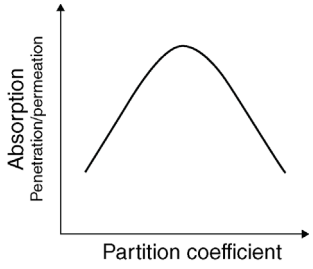


**Figure 16.2** Relation between absorption and polarity (hydrophilicity/lipophylicity). Optimal absorption conditions are given for $1 \leq \log P \leq 3$ with $P$ being the octanol/water partition coefficient.

stratum corneum. As many nanoparticles have molar masses in the order of $10^6$ Da and more, no significant transport over an intact dermal barrier is expected in humans. The role of the appendages in xenobiotic absorption was long considered negligible due to their low surface coverage of about 0.1%. More recently, Otberg *et al.* [56] reevaluated the number and size of follicles of several anatomical sites, that is, lateral forehead, upper arm, forearm, thorax, back, thigh, and calf, and showed that each body region features its own hair follicle characteristics. A maximum surface coverage of 1.28% was found at the forehead and a minimum of 0.09% on the forearm. The available infundibular volume, which determines the potential follicular reservoir, was found to be the highest at the forehead and the calf region. Concurrently, the potential of appendages as targets for nanoparticulate carrier systems was recognized [57,58]. The hair follicles being invaginations of the epidermis may reach deep into the subcutaneous tissue. Nevertheless, an efficient barrier similar to the stratum corneum in the upper part of the follicle and tight junctions in the lower part of the follicle prevent particles from entering into the living cells [59,60]. However, once entered into the follicle openings, particles may be stored there until being cleared by hair growth or sebum production. Clearance is very slow as particles inside the follicles are protected from natural desquamation, textile contact, and washing. This makes the follicles a potential storage site that can be used for targeted drug delivery [61]. Lademann *et al.* also reported that the natural movement of the hair together with the scaly structure of the hair cuticula works like a gear pump, which transports particles having an appropriate size into the follicle. The optimum particle size was reported to be in the range of 400–700 nm [62]. Some of the above observations are waiting to be confirmed.

### 16.3.2
### Risk and Safety Considerations

The absorption of nanoparticulates through the intact skin is limited due to the nature of the SC and the appendages. Nevertheless, the use of nanoparticles in biomedical and cosmetic applications has raised safety and toxicity concerns.

The major concerns about toxicity of nanoparticles are related to their dimensions. As particle size diminishes, its surface-to-volume ratio increases geometrically [63]. If the surface moieties on the particles are biologically reactive, the collective reactivity of the nanomaterial per unit mass also increases geometrically. An often cited example of this type of toxicity is untreated nanoscale titanium dioxide capable of generating reactive oxygen species [64]. These have been shown to contribute to nucleic acid damage, protein damage, and altered proinflammatory protein expression. To mitigate this type of toxicity, one may incorporate the titanium dioxide into antioxidant vehicles or coat the particles. The coating results in the quenching of the produced radicals and significantly reducing photocatalysis and eliminating the hazard of potential carcinogenicity [65]. Whether titanium dioxide or zinc oxide as key components of sunscreen products are properly coated often remains unclear.

In recent decades, the cosmetic industry also began to use and apply the achievements of nanotechnology in their products and since the mid-1990s all major cosmetic companies promote and successfully sell beauty products based on nanotechnology [1]. Quite rightly Simonsson and coworkers raised the question whether the sensitizing capacity of potential allergens could be increased by cosmetic formulations based on nanotechnology [66]. The results of their investigations indicate that there is an elevated risk of sensitization when haptens are delivered in vehicles containing nanoparticulate lipid vesicles [67,68]. It is likely that the enhanced sensitizing capacity is a consequence of the improved penetration or permeation and increased formation of hapten–protein complexes in epidermis, when the allergens are delivered in ethosomal formulations.

Considering the large number of newly emerging applications of nanomaterials, further research looking into both particle-associated effects on living organisms and particle alterations as a result of particle–tissue interactions is essential. The large body of data available from multiple experimental studies using different models and particle types further suggests that the risk assessment has to be done for each particle type or nanomaterial of interest. In fact, particle characteristics such as composition, surface modification, and the manufacturing process itself may influence the behavior of these materials in biological tissues [27].

## 16.4 Nanoparticles in Prevention, Diagnosis, and Therapy

### 16.4.1 Prevention

#### 16.4.1.1 Antisepsis

Antisepsis is an important area of application for nanoparticles. Recent studies describe the topical application of silver, chlorhexidin, and nitric

oxide-releasing nanoparticles for antimicrobial and wound healing applications [69–73]. The inherent antimicrobial properties of silver ions are well known. They are thought to inhibit bacterial enzymes and bind to DNA [74]. Silver nanoparticles and silver ions induce bacterial cell wall and cytoplasmic membrane damage [75,76]. Chlorhexidin-loaded nanoparticles (Nanochlorex®) unfold both an immediate antibacterial effect due to rapid desorption of chlorhexidin from the particle wall and a prolonged effect based on the sustained release from the particle core [77]. The preparation and use of nitric oxide-releasing nanoparticles has been described [78,79]. These nanoparticles were highly effective against methicillin-resistant *Staphylococcus aureus* infection in a mouse model [80].

#### 16.4.1.2 Photoprotection, Color, and Light Reflectance Control

Ultraviolet radiation (UVR) is the major environmental cause of skin cancer. Therefore, it is pivotal to protect the skin from UVR to prevent these skin malignancies. Today, topical sunscreen products have become a quasi-exclusive mode of protection, even though seeking shade and wearing protective clothing provides more protection [81]. At present, organic and inorganic filters as nonparticulate and particulate materials are available for the direct protection against UVR. Titanium dioxide and zinc oxide as inorganic and, for example, bisoctrizole (Tinosorb® M) as organic nanoparticles are widely used in sunscreen products. The particles reflect, scatter, and absorb UVR. Titanium dioxide and zinc oxide in bulk form are opaque white powders poorly miscible in water-based vehicles. They require lipid-based vehicles that persist as whitish films on the skin surface, which users may find messy and cosmetically unacceptable. Titanium dioxide and zinc oxide particles reduced to the nanometer scale confer several advantages. By being smaller than the wavelength of visible light, that is, 400–700 nm, they become transparent, leaving no whitish residue on the skin. Nanosized particles can also be better formulated into cosmetically elegant formulations. Furthermore, these particles are more evenly distributed over the skin leaving a tightly packed invisible film on the skin. To prevent the photocatalytic activity of titanium dioxide or zinc oxide causing the release of DNA-damaging reactive oxygen species and lipid peroxidation, the particles are surface modified by coating them with dimethicone or silica. However, there is limited knowledge about the stability of the coating, once the particles are in contact with skin [82–86]. As the balance of color, light, and shadow on a face determines its shape, volume, and surface appearance, a variety of powders including mica (group of sheet silicate (phyllosilicate) minerals) are being used for skin color and light reflectance control. These powders, that is, plasmonic nanoparticles, are metals with diameters ranging from 10 to 150 nm that are highly efficient at absorbing and scattering light. By changing the size, shape, and surface coating, the color of the nanoparticles can be tuned across the visible and near-infrared region of the electromagnetic spectrum [87]. A mixture of color correcting and reflecting mica powders can alter the balance of incident light, reflecting more in the central face and scattering more light in the periphery of the face. The result

is an optical illusion, which enhances shape and volume of the face [88]. In some populations, skin powdering has a longstanding tradition.

#### 16.4.1.3 Preventive Care

Most preventive care products are regulatory-wise classified as cosmetics. A bewildering array of products is offered claiming to use the specific advantages of nanotechnology. For example, nanoemulsions may be suitable as colloidal carrier systems to deliver various functional and/or therapeutic agents [89,90]. Although there are numerous likely consumer advantages from these products, there is very little information available regarding consumer exposure to the nanoscale materials in these products or any associated risks from these exposures [1].

#### 16.4.1.4 Odor Neutralizers

Odor-reducing properties of nanosilver has led to the rapid commercialization of nanosilver-containing products including clothing [91] and many articles of daily use such as food-storage containers [92], washing machines [93], soaps [94], and surgical masks [95]. This broad use beyond intentional antimicrobial use has raised human health and safety concerns for nanosliver skin exposure, particularly as some of these products may be applied to barrier-defective skin [96,97].

#### 16.4.1.5 Vaccines

The skin provides both innate and adaptive immune response functions to maintain tissue homeostasis and to react promptly to environmental insults [98]. Theoretically every substance that contacts skin may potentially penetrate into or permeate through the skin and produce a physiological change. Skin contains a tight network of immune-competent cells, that is, antigen-presenting cells, dermal dendritic cells, and Langerhans cells. They are especially accessible in the lower *infundibulum* of the hair follicle, that is, tissue in hair follicle canal above sebaceous gland and could, therefore, be a more appropriate target for vaccination purposes than the scarce population of muscle dendritic cells being targeted by i.m. vaccine injections. The ability of nanoparticles to carry antigens and to accumulate in the hair follicles, especially after mechanical stimulation, has generated interest in their use for transcutaneous immune modulation (see Figure 16.3c) [99–101].

Transcutaneous immune modulation by means of nanoparticles represents an innovative application; however, many questions regarding mechanisms by which immunomodulation occurs and regulatory issues remain to be answered [102,103].

### 16.4.2 Diagnosis and Monitoring

The use of nanotechnology in dermatology has also opened up pathways in diagnosing and monitoring. Several nanoparticles are being used in molecular

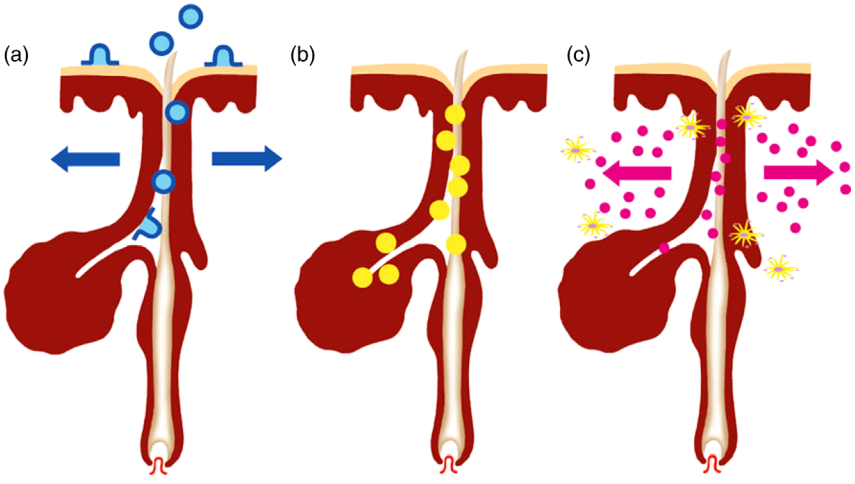


**Figure 16.3** One important feature of the skin as an organ is the function of the stratum corneum as a potent barrier. Since there is evidence that *vellus* and terminal hair follicles can act as a shunt increasing the penetration and absorption of topically applied substances, the selective follicular penetration of topically applied nanoparticles could significantly reform modern dermatotherapy offering a variety of innovative therapeutic strategies: (a) penetration enhancement by nanoparticles of the liposome type. After skin contact and follicular penetration the liposomes dissociate, enabling the diffusion of the released drug with proper physicochemical properties through the skin barrier of the hair follicle as well as the interaction with target cell populations of the follicular epithelium and the dermis or even systemic targets after absorption and blood circulation. (b) The use of drug-loaded microspheres for hair follicle targeting and treatment of hair follicle- and sebaceous-gland-associated disorders. After topical application, particles accumulate within the hair follicle canal, which acts as a depot for the sustained release of the incorporated drug, achieving a constant drug level within the hair follicle and the sebaceous gland. (c) Delivery of particles across the skin barrier and interaction with cell targets. The translocation of small nanoparticles after skin barrier disruption into the viable epidermis and dermis followed by the interaction with cell populations such as the antigen-presenting cells of the follicular epithelium could prove beneficial for therapeutic strategies, for example, particle-based transcutaneous vaccination (reproduced with permission from Ref. [27].)

imaging [104]. Gold nanoparticles are particularly suitable labels for sensors, because a variety of analytic techniques can be used to detect them, including optical absorption, fluorescence, Raman scattering, atomic and magnetic force, and electrical conductivity [105]. Quantum dots are highly fluorescent nanosized solid semiconductor particles that absorb light efficiently over a wide frequency range and reemit it in a single color depending on the particle size [106]. Their fluorescence signal is strong and stable for long periods of time [107]. They have demonstrated their usefulness in identifying sentinel lymph nodes using infrared fluorescence and allow for excellent real-time visualization of the dye travel during a sentinel-node-mapping procedure, for example, in melanoma therapy [108]. Furthermore, they allow nonradioactive detection. Once optimized, they may prove superior to other tracers for sentinel node mapping [109].

## 16.4.3 Therapy

### 16.4.3.1 Sebaceous Gland Disorders

Schaefer and coworkers were the first to demonstrate in the early 1990s a beneficial role of particulate drug delivery systems for intrafollicular drug delivery and for a more successful treatment of sebaceous gland disorders such as acne using adapalene-loaded poly(lactic-*co*-glycolic) acid particles [110]. And adapalene-loaded nanoparticulates for intrafollicular targeting have not lost any of its relevance today [111]. A wide range of products with nanoparticles, including liposomes, solid lipid nanoparticles, and polymer nanoparticles have shown to increase follicular uptake, achieving higher local drug concentrations and optimized therapeutic effects [112]. A major benefit of these delivery systems is their improved tolerability to irritation caused by retinoids and hence the improved patient treatment adherence [113]. Consumer/patient needs and extended research has led to global commercialization of a series of particle-based anti-acne products of benzoyl peroxide. Clinical studies showed increased levels of skin tolerability, esthetic attributes, and patient satisfaction after treatment with BP-loaded microsphere creams [114]. Current research on acne drugs encapsulated into particle-based drug delivery systems is not confined to retinoids and benzoyl peroxide only. It has been demonstrated that liposomal formulations of antiandrogens penetrate deeper into the hair follicle canal and target specifically the sebaceous gland. Various antiandrogens have also been loaded to solid nanoparticles for maximized effect [115].

### 16.4.3.2 Hair Disorders

It has been demonstrated that nanoparticles used for follicular delivery provide a series of advantages over conventional pathways [116]. These include improved local bioavailability, enhanced transport into the follicle and sebaceous gland, increased penetration depth, and prolonged residence time, in brief, precise tissue targeting. Different types of nanoparticulate systems may be employed for management of follicular targeting, such as polymeric nanoparticles, liposomes, and lipid nanoparticles. The sebaceous glands open into the lower *infundibulum* of the hair follicles. Each follicle is associated with a sebaceous gland that releases *sebum*, creating a lipid-enriched environment. Efficient drug transport into the hair follicles depends upon the interaction between the drug and the sebum, but even more importantly on the choice of vehicles [117]. It has been shown that nanoparticles preferentially penetrate into the follicles but not into the stratum corneum, enabling high accumulation within the follicular space. Once deposited in the follicles, the drug may be released from the nanoparticles and exert its effects on the target cells or structures. Additional force such as massage may increase follicular penetration of nanoparticles. Massage induces hair shaft movement, which acts as a geared pump pushing the particles deep into the follicles. An opposite mechanism for follicular delivery is the hair growth and sebum flow, which may slow down the passage of nanoparticles

because of the upward flow compared to the downward delivery of follicular penetration [27,118]. It has been shown that the size of the nanoparticles may also play an important role in the penetration depth of the follicles. Patzelt *et al.* explored the effect of the particulate size between 122 and 860 nm of polyglycolic-*co*-lactic acid nanoparticles on the follicular penetration depth of porcine ear skin *in vitro* [119]. Polyglycolic-*co*-lactic acid nanosystems were prepared in a hydrogel formulation. The results showed that the increased particulate size leads to a significantly deeper penetration into the follicles. The deepest transport was obtained by nanoparticles with a diameter of 643 nm. The penetration depth was significantly decreased for particles 860 nm in diameter. This trend can be explained by the thickness of keratinized cell layers and the surface structure of the hair shafts and follicles. In the recent decade, several groups have demonstrated enhanced delivery of drug-loaded nanoparticles into *pilosebaceous* units compared to conventional formulations of the same drug, for example, minoxidil [120] or finasteride [121]. The incorporation of immunomodulatory agents such as ciclosporin in alopecia areata or psoriasis into nanoparticulate delivery systems could allow replacing systemic administration of drugs causing adverse effects with more selective and effective topical treatments [122,123]. Gene therapy of hair is also gaining importance and recent results emphasize the role of particle-based drug delivery systems for active follicular targeting of disease-related cell populations in the hair follicle [124,125].

#### 16.4.3.3 Inflammatory Disorders

It has been postulated early that controlled drug release would prove beneficial for local therapy of inflammatory skin diseases. Many of the particulate drug delivery systems offer control over drug release. Glucocorticoids show adverse effects such as skin atrophy and hence may limit their extended use. It has been postulated that targeting the epidermis, where the inflammatory process takes place, instead of the dermis, can be achieved using liposomal formulations, thus minimizing skin atrophy [126–128]. Several studies on *psoriasis* indicate that various drugs such as methotrexate, psoralen, and dithranol could be incorporated in nanoparticles to achieve a better tolerability, an increased safety, and an optimal therapeutic effect [129–131]. Many investigations have shown their potential in improving therapeutic benefits of drugs by increasing their therapeutic efficacy with minimal toxicity. However, while the results in animal models using particulate drug delivery systems look promising, the lack of sufficient evidence in clinical setups is a constraint, and more clinical studies on the efficacy and safety are required [132].

#### 16.4.3.4 Cancer

Skin cancer is by far the most common malignancy of humans, particularly in the Caucasian population. The growing incidence of cutaneous malignancies has created the need for multiple treatment options. Even though surgical modalities remain the mainstay of treatment of certain skin cancers, both pharmacological

and pharma-technological innovations are required to further reduce morbidity and mortality. A major necessity of skin cancer patients is still to reduce morbidity and mortality, mainly caused by malignant melanomas [133,134].

Recently, highly targeted therapies and immunotherapies based on pathogenetic knowledge have become available either through clinical trials or commercially [135,136]. As described for other diseases, localized therapy allows for increased substance accumulation in the tumor without toxicity to the rest of the body [137]. The key advantage is that the *in vivo* fate of the drug is no longer mainly determined by the characteristics of the drug, but by the carrier system, which permits a localized and controlled drug release.

Several studies have been performed employing polymers and polymeric nanoparticles in the treatment of skin malignancies, such as quercetin [138], genistein and curcumin [139,140], and 5-aminolevulinic acid [141] or 5-fluorouracil [142]. Liposome-based drug carriers permit both intravenous injection and topical application of lipophilic drugs with low water solubility, as amphotericin B (AmBisome®) [143]. The toxicity of the liposomal system is 1/10 compared to the micelle-based amphotericin formulation. Examples, besides liposomal amphotericin B, are the encapsulation of the UV-DNA repair enzyme T4N5 for topical application in order to prevent skin cancer [144,145]. Tanaka *et al.* demonstrated that the bacteriophage T4 endonuclease V, a 16 500-Da polypeptide isolated from *Escherichia coli* infected with bacteriophage T4, was able to augment nucleotide excision repair in human cells and initiate removal of cyclobutane pyrimidine dimers [146]. Unfortunately, T4N5 never reached the market as a medicinal product. Some cosmetic after-sun products claim to contain enzyme T4 endonuclease. The major evidence of medical utility and efficiency of the liposomal technique is the marketed liposomal doxorubicin (Caelyx®), widely used in clinical practice, for example, monotherapy for patients with metastatic breast cancer or second-line treatment in disseminated melanoma [147].

Advantages of nanoemulsions comprise an elevated content of the lipid phase for increased drug uptake as well as the possibility of relative simple industrial scale production through high-pressure homogenization techniques. They all intend to intensify therapy, for example, photodynamic therapy [148,149]. The main advantages of lipid nanoparticles compared to other colloidal systems are their high biocompatibility, good physical stability, possibility of modified release of drugs, prolonged release from the nanoparticle or adhesiveness and stickiness to biological matrix, easy large-scale production, and economical raw materials. They are used for both systemic [150] and topical applications [151,152]. Magnetic nanoparticles composed of iron derivatives, that is, magnetic, paramagnetic, or superparamagnetic, have the potential to enhance highly localized drug delivery to specific skin/organ locations [153]. The technique has attracted high interest, however, clinical application is still far off.

For clinical use, gold nanoparticles are being studied as carriers both for the delivery of drugs, imaging molecules, and genes and for the development of

cancer therapy products [154–156]. Tumor targeting can be attained by binding tumor-specific recognition molecules such as monoclonal antibodies [157] to the gold nanoparticles. However, toxicity issues have been raised [158]. A significant demonstration of the potential of multifunctional gold nanoparticles for drug delivery was the use of these particles and carriers covalently bound to cetuximab, that is, targeting agent, and gemcitabine, a therapeutic drug in pancreatic cancer [159]. Quantum dots provide a nanoscale scaffold for designing multifunctional nanoparticles with both imaging and therapeutic functions. The surface of quantum dots may be modified to improve specificity, sensitivity, solubility, and visualization of the target tissue [160]. When applied to the skin, quantum dots preferentially accumulate in the upper layers of the stratum corneum and in hair follicles, permeating throughout the skin by getting through intracellular lipid lamellae along the edges of differentiated corneocytes. In addition, quantum dot skin penetration/permeation and toxicity depend on physicochemical properties such as particle size, shape, and chemical structure of the core/shell and surface coating, and charge and pH of the applied vehicle [161,162]. In recent studies nanostructured lipid carriers with quantum dots were used to combine bioimaging and anticancer therapy [163].

It is known that cancer is recognized by the immune system, and under some circumstances, the immune system may control or even eradicate tumors. Different immunotherapeutic approaches are being studied in many cancer types. Topical application of the Toll-like receptor (TLR7) agonist imiquimod, which enhances immune responses and elicits antitumor activity, is approved for immunological treatment of actinic keratoses, which represent a frequently observed carcinoma *in situ*. Likewise, several other TLR agonists such as resiquimod, TLR7/8 agonist, are being considered to help eliminate even micromalignancies: TLR agonists mimic local infections, activate dendritic cells, then, natural killer, and T cells; following the recruitment of lymphocytes into the tumor, cytotoxic activity and immune regulation occurs, which contributes to the immunological clearance of malignant cells [164,165]. Significant systemic exposure to these molecules may evoke severe adverse effect [166,167]. The application of nanotechnological principles to topical TLR agonist formulations could minimize their systemic adverse effects.

#### 16.4.3.5 **Surgery**

Great efforts have been made to incorporate nanoscale materials in the design of surgical materials [168]. It has been demonstrated that aqueous solutions of nanoparticles can be used to introduce strong bonding between the tissues without the need for complex *in situ* polymerization or cross-linking *tissue glues* [169]. These particle solutions adsorb onto the surfaces of tissues and act as a connector between the tissues. Nanoparticle solutions can also be used as hemostatic materials to stop internal bleeding with no requirement for specific preparation or control on polymerization reactions as needed for polymer-based hemostatic agents [170].

## 16.5 Regulatory Issues

Regardless of origin and the variety of nanomaterials, regulatory bodies worldwide are beginning to develop specific Nano Guidance Packages to regulate the aspects of nanomaterials. Considerable regional and national differences do exist, but regulatory harmonization endeavors are ongoing. Even though existing regulations and associated guidance documents may be adapted to nanomaterials, it is often difficult to perform a complete hazard and exposure assessment, since the current legal framework does not account for the complex physicochemical properties of manufactured nanomaterials or the respective analytical requirements [171]. Likewise, there is a lack of suitable toxicological methods [172]. The *European Cosmetic Regulation* has become operative in 2013 [173]. Article 2 (k) of this regulation provides a definition of nanomaterials within the European legislative framework. In this context, nanomaterials are defined as an insoluble or biopersistent and intentionally manufactured material with one or more external dimensions, or an internal structure, on the scale from 1 to 100 nm. The Cosmetics Regulation is the first act in Europe that explicitly considers the putative risks from nanomaterials to consumers. Its Article 16 is solely dedicated to nanomaterials. Each cosmetic product requires a designated *responsible person* for a placement on the European market. This representative is requested to notify the European Commission 6 months in advance before any cosmetics containing nanomaterials are marketed via the Cosmetic Products Notification Portal (CPNP). Required specifications for nanomaterials include particle sizes, used raw materials, and information on product impurities. In addition, a toxicological profile needs to be provided that covers all relevant end points, especially skin and eye irritation, as well as skin sensitization. The European Commission (COM) may request an opinion from the *Scientific Committee on Consumer Safety* (SCCS) in case of safety concerns about the respective product notification or the particular nanomaterial used in the cosmetic product. This opinion has to be provided within 6 months and may ask for additional data, recommend a restricted application, or even propose the ban of the corresponding substance. COM publishes the opinions of the SCCS. Safety concerns initiating a further evaluation process can also be raised after a substance has been placed on the market. Reasons for such action include new scientific knowledge as well as novel data on substance exposure or toxicology as provided by third parties, for example, institutions of the member states. Advancements in nanotechnology may require revising and updating current regulations and guidance in future.

## 16.6 Public Perception of Nanoparticles in Topicals

Lay people are the potential beneficiaries of the advancement of science. However, their benefit–risk perception can be influenced by adverse events, negative

media coverage, and fractious debates. Furthermore, a negative public opinion can seriously jeopardize further technological progress [174]. There are many examples where a failure to understand or align with public opinion has fed a public backlash resulting in reactive policy and regulation and/or an erosion of trust in the government institutions. These include, for example, the debate on genetically modified organisms in Europe and the bovine spondylitis encephalopathy crisis in Britain [175,176]. Concerns have been raised that insensitivity to public opinion could cause similar reactions to real or imagined risks associated with nanotechnology [177,178]. The public has different opinions on the risks associated with the dermal application of nanoparticles. Liposomal formulations are widely used and well received in cosmetic products including sunscreen products. However, the public has developed a considerable mistrust toward nanoparticles in sunscreen products such as titanium dioxide or zinc oxide. Some consumer protection organizations almost annually call attention to potential risks of nanoparticles in cosmetics including sunscreen products. Frequently, the media spreads misleading information, highlighted by flashy headlines, on the topical application of nanoparticles such as *nano – the new asbestos*. To inform the consumer, nanoparticles in cosmetics including sunscreen products have to be declared in the ingredient list by adding to the corresponding ingredient the term *nano* in brackets. Despite this labeling and extensive institutional information, this uncertainty related to nanomaterials in sunscreen products persists in some populations. It is interesting to note that social, national, and regional differences in the perception of nanotechnology and nanoparticles in cosmetics exist [174,179,180].

## 16.7 Conclusions and Future Perspectives

Certainly, the application of nanotechnology to prevention, diagnosis, and therapy in dermatology has generated enthusiasm among scientists and physicians. And the cosmetic industry offers promising claims for their products that are based on nanoparticulate materials. The key features and benefits of nanotechnology are the targeted delivery of nanostructured materials, the inclusion and protection of actives, and their controlled release/delivery from the nanostructured material. Today, the technology offers a broad range of nanostructured materials with characteristics for diverse applications. But the devil is in the detail. Considerable endeavors are still needed to leverage commercial breakthroughs. Furthermore, it should not be forgotten to manage the reputation of the technology that has become hampered by the discussion around the nanoparticulate metal oxides in sunscreen products.

In literature, the discussion on the benefits of nanoparticles is often focused on the particle itself and the particle as a carrier for an active ingredient. However, it often remains unnoticed that the particles are incorporated into another vehicle that is then applied, either systemically or topically. Once applied, the vehicle

of the nanoparticles will change (metamorphosis of the vehicle; the vehicle will be diluted, volatile ingredients will evaporate) and the immediate vicinity of the nanoparticle will change concomitantly. It remains unknown how this affects the character and the functionality and hence the bioavailability of the nanoparticles. The lack of this information may become a major regulatory hurdle.

The exact mechanism of penetration, permeation, and absorption of nanoparticles into and through skin is not fully understood. For example, to take advantage of nanoparticulate delivery to the hair follicle and to bring such a product to regulatory approval and to commercialization, it is mandatory to understand the exact mechanisms of nanoparticulate delivery to the hair follicles. Our present knowledge is still based on qualitative evaluations with moderate objective analysis. Penetration, permeation, and absorption of titanium and zinc oxides are a subject of heated debates among scientists and public alike. From literature, it is reasonable to conclude that under normal use on healthy skin, penetration/permeation of titanium dioxide and zinc oxide nanoparticles pose minimal health concern. Such statements, often presented by the industry, do not resolve uncertainties. Terms like *under normal-use conditions* or *on healthy skin* or *pose minimal health concern* unfold our still limited knowledge on translocation of nanoparticulate materials. Parents with atopic children or adolescents with acne remain rattled. Greater emphasis is urgently needed on quantitative studies that can relate nanoparticulate exposure to nanoparticle penetration, permeation, and absorption and, in case of drugs, to therapeutic efficacy. As an overall consequence, standardized operation procedures are not only desirable but also essential to investigate and eventually predict the behavior of nanoparticulate materials on and in the skin.

Compared to new drug applications only a moderate number of nanoparticulate-based products have reached approval by regulatory bodies. Insufficient understanding of the mechanisms of nanoparticulate delivery and unresolved toxicity issues represent a major challenge and have caused many initiatives in nanomedicine to fail. For many *old* topical drugs, nanoparticulate-based formulations have been proposed and developed to upgrade medical treatment efficacy. Again, only a limited number have appeared in the market. From an entrepreneurial point of view, many nanoparticulate-based formulations of old drugs are economically not viable. Unfortunately, clinical benefits of these products are often not appreciated by restrictive reimbursement policies of many health insurance systems. In fact, this may eventually prevent innovative treatment options.

From the viewpoint of social science, the public perception and awareness of technologies including nanotechnology is vital to innovation, development, and commercialization of nanoproducts. At present, the heated debate concerning nanoparticulate metal oxides in sunscreen products rattle broad sections of the general public. Today, it is of utmost importance that scientists communicate their findings and estimations in a comprehensible way to policymakers, to politicians, to journalists, and to the public. Only this will grant a bright future to nanotechnology.

Despite the hurdles mentioned above, there are still many interesting unanswered questions and technical challenges that provide significant opportunities for further research. The Nanodermatology Society (www.nanodermsociety.org) established in 2010 to promote a greater understanding of the scientific and medical aspects of nanotechnology in skin health and disease will help to increase the communication among scientists, policymakers, regulators, and physicians and will certainly increase the necessary trust and confidence in the public.

## References


1 Kaur, I.P. and Agrawal, R. (2007) Nanotechnology: a new paradigm in cosmeceuticals. *Recent Pat. Drug Deliv. Formul.*, **1** (2), 171–182.
2 Paulo, C.S., Pires das Neves, R., and Ferreira, L.S. (2011) Nanoparticles for intracellular-targeted drug delivery. *Nanotechnology*, **22** (49), 1–11.
3 Manish, G. and Sharma, V. (2011) Targeted drug delivery system: a review. *Res. J. Chem. Sci.*, **1** (2), 135–138.
4 ISO (2008) ISO/TS 27687:2008 Nanotechnologies: terminology and definitions for nano objects – nanoparticle, nanofibre and nanoplate. Available at http://www.iso.org/iso/catalogue_ics (accessed 30 October 2015).
5 ASTM 2456-06 (2015) Standard terminology relating to nanotechnology. Available at http://www.astm.org/Standard/index.shtml (accessed 30 October 2015.
6 HORIBA Scientific (2015) http://www.horiba.com/scientific/products/particle-characterization/applications/what-is-a-nanoparticle/ (accessed 30 October 2015).
7 Bozzuto, G. and Molinari, A. (2015) Liposomes as nanomedical devices. *Int. J. Nanomedicine*, **10**, 975–999.
8 Jung, S., Otberg, N., Thiede, G., Richter, H., Sterry, W., Panzner, S., and Lademann, J. (2006) Innovative liposomes as a transfollicular drug delivery system: penetration into porcine hair follicles. *J. Invest. Dermatol.*, **126** (8), 1728–1732.
9 Bernard, E., Dubois, J.L., and Wepierre, J. (1997) Importance of sebaceous glands in cutaneous penetration of an antiandrogen: target effect of liposomes. *J. Pharm. Sci.*, **86** (5), 573–578.
10 Schroeter, A., Engelbrecht, T., Neubert, R.H., and Goebel, A.S. (2010) New nanosized technologies for dermal and transdermal drug delivery. A review. *J. Biomed. Nanotechnol.*, **6** (5), 511–528.
11 Cevc, G. (2004) Lipid vesicles and other colloids as drug carriers on the skin. *Adv. Drug Deliv. Rev.*, **56** (5), 675–711.
12 Song, Y.K., Hyun, S.Y., Kim, H.T., Kim, C.K., and Oh, J.M. (2011) Transdermal delivery of low molecular weight heparin loaded in flexible liposomes with bioavailability enhancement: comparison with ethosomes. *J. Microencapsul.*, **28** (3), 151–158.
13 Ascenso, A., Raposo, S., Batista, C., Cardoso, P., Mendes, T., Praça, F.G., Bentley, M.V., and Simões, S. (2015) Development, characterization, and skin delivery studies of related ultradeformable vesicles: transfersomes, ethosomes, and transethosomes. *Int. J. Nanomedicine*, **10**, 5837–5851.
14 Anajafi, T. and Mallik, S. (2015) Polymersome-based drug-delivery strategies for cancer therapeutics. *Ther. Deliv.*, **6** (4), 521–534.
15 Schwendener, R.A. (2014) Liposomes as vaccine delivery systems: a review of the recent advances. *Ther. Adv. Vaccines*, **2** (6), 159–182.
16 Ludwig, C. and Wagner, R. (2007) Virus-like particles: universal molecular toolboxes. *Curr. Opin. Biotechnol.*, **18** (6), 537–545.
17 Hufbauer, M., Cooke, J., van der Horst, G.T., Pfister, H., Storey, A., and Akgül, B.

(2015) Human papillomavirus mediated inhibition of DNA damage sensing and repair drives skin carcinogenesis. *Mol. Cancer*, **14** (1), 183.
18 Lauterbach, A. and Müller-Goymann, C.C. (2015) Applications and limitations of lipid nanoparticles in dermal and transdermal drug delivery via the follicular route. *Eur. J. Pharm. Biopharm.*, **97** (Pt A), 152–163.
19 Rizwanullah, M., Ahmad, J., and Amin, S. (2016) Nanostructured lipid carriers: a novel platform for chemotherapeutics. *Curr. Drug. Deliv.*, **13** (1), 4–26.
20 Joshi, V.B., Geary, S.M., and Salem, A.K. (2013) Biodegradable particles as vaccine antigen delivery systems for stimulating cellular immune responses. *Hum. Vaccin. Immunother.*, **9** (12), 2584–2590.
21 Bartelmess, J. and Giordani, S. (2014) Carbon nano-onions (multi-layer fullerenes): chemistry and applications. *Beilstein J. Nanotechnol.*, **5**, 1980–1998.
22 Parat, A., Bordeianu, C., Dib, H., Garofalo, A., Walter, A., Bégin-Colin, S., and Felder-Flesch, D. (2015) Dendrimer–nanoparticle conjugates in nanomedicine. *Nanomedicine (Lond.)*, **10** (6), 977–992.
23 Chirico, F., Fumelli, C., Marconi, A., Tinari, A., Straface, E., Malorni, W., Pellicciari, R., and Pincelli, C. (2007) Carboxyfullerenes localize within mitochondria and prevent the UVB-induced intrinsic apoptotic pathway. *Exp. Dermatol.*, **16** (5), 429–436.
24 Kato, S., Taira, H., Aoshima, H., Saitoh, Y., and Miwa, N. (2010) Clinical evaluation of fullerene-$C_{60}$ dissolved in squalane for anti-wrinkle cosmetics. *J. Nanosci. Nanotechnol.*, **10** (10), 6769–6774.
25 Villalonga-Barber, C., Micha-Screttas, M., Steele, B.R., Georgopoulos, A., and Demetzos, C. (2008) Dendrimers as biopharmaceuticals: synthesis and properties. *Curr. Top. Med. Chem.*, **8** (14), 1294–1309.
26 Venuganti, V.V. and Perumal, O.P. (2009) Poly(amidoamine) dendrimers as skin penetration enhancers: influence of charge, generation, and concentration. *J. Pharm. Sci.*, **98** (7), 2345–2356.
27 Papakostas, D., Rancan, F., Sterry, W., Blume-Peytavi, U., and Vogt, A. (2011) Nanoparticles in dermatology. *Arch. Dermatol. Res.*, **303** (8), 533–550.
28 Zhou, M. and Ghosh, I. (2007) Quantum dots and peptides: a bright future together. *Biopolymers*, **88** (3), 325–339.
29 Snee, P.T. and Das, A. (2016) Synthetic developments of nontoxic quantum dots. *ChemPhysChem.*, **17** (5), 598–617.
30 Onoshima, D., Yukawa, H., and Baba, Y. (2015) Multifunctional quantum dots-based cancer diagnostics and stem cell therapeutics for regenerative medicine. *Adv. Drug Deliv. Rev.*, **95**, 2–14.
31 Wen, C.J., Sung, C.T., Aljuffali, I.A., Huang, Y.J., and Fang, J.Y. (2013) Nanocomposite liposomes containing quantum dots and anticancer drugs for bioimaging and therapeutic delivery: a comparison of cationic, PEGylated and deformable liposomes. *Nanotechnology*, **24** (32), 325101.
32 Chen, J., Shao, R., Zhang, X.D., and Chen, C. (2013) Applications of nanotechnology for melanoma treatment, diagnosis, and theranostics. *Int. J. Nanomedicine*, **8**, 2677–2688.
33 DeLouise, L.A. (2012) Applications of nanotechnology in dermatology. *J. Invest. Dermatol.*, **132** (3 Pt 2), 964–975.
34 Nohynek, G.J., Lademann, J., Ribaud, C., and Roberts, M.S. (2007) Grey goo on the skin? Nanotechnology, cosmetic and sunscreen safety. *Crit. Rev. Toxicol.*, **37** (3), 251–277.
35 Gulson, B., McCall, M.J., Bowman, D.M., and Pinheiro, T. (2015) A review of critical factors for assessing the dermal absorption of metal oxide nanoparticles from sunscreens applied to humans, and a research strategy to address current deficiencies. *Arch. Toxicol.*, **89** (11), 1909–1930.
36 Australian Government, Department of Health Therapeutic Goods Administration. Literature review on the safety of titanium dioxide and zinc oxide nanoparticles in sunscreens. Scientific review report. Version 1.0, August 2013.
37 Wang, B., Zhang, Y., Mao, Z., Yu, D., and Gao, C. (2014) Toxicity of ZnO nanoparticles to macrophages due

to cell uptake and intracellular release of zinc ions. *J. Nanosci. Nanotechnol.*, **14** (8), 5688–5696.

38 Nel, A.E., Madler, L., Velegol, D., Xia, T., Hoek, E.M.V., Somasundaran, P., Klaessig, F., Castranova, V., and Thompson, M. (2009) Understanding biophysicochemical interactions at the nano–bio interface. *Nat. Mater.*, **8**, 543–557.

39 Pelaz, B., Del Pino, P., Maffre, P., Hartmann, R., Gallego, M., Rivera-Fernández, S., de la Fuente, J.M., Nienhaus, G.U., and Parak, W.J. (2015) Surface functionalization of nanoparticles with polyethylene glycol: effects on protein adsorption and cellular uptake. *ACS Nano.*, **9** (7), 6996–7008.

40 He, Q., Zhang, J., Shi, J., Zhu, Z., Zhang, L., Bu, W., Guo, L., and Chen, Y. (2010) The effect of PEGylation of mesoporous silica nanoparticles on nonspecific binding of serum proteins and cellular responses. *Biomaterials*, **31** (6), 1085–1092.

41 Montenegro, J.M., Grazu, V., Sukhanova, A., Agarwal, S., de la Fuente, J.M., Nabiev, I., Greiner, A., and Parak, W.J. (2013) Controlled antibody/(bio-) conjugation of inorganic nanoparticles for targeted delivery. *Adv. Drug Deliv. Rev.*, **65** (5), 677–688.

42 Shi, D. (2009) Integrated multifunctional nanosystems for medical diagnosis and treatment. *Adv. Funct. Mater.*, **19**, 3356–3373.

43 Phillips, E., Penate-Medina, O., Zanzonico, P.B., Carvajal, R.D., Mohan, P., Ye, Y., Humm, J., Gönen, M., Kalaigian, H., Schöder, H., Strauss, H.W., Larson, S.M., Wiesner, U., and Bradbury, M.S. (2014) Clinical translation of an ultrasmall inorganic optical-PET imaging nanoparticle probe. *Sci. Transl. Med.*, **6** (260), 260ra149.

44 Liard, C., Munier, S., Joulin-Giet, A., Bonduelle, O., Hadam, S., Duffy, D., Vogt, A., Verrier, B., and Combadière, B. (2012) Intradermal immunization triggers epidermal Langerhans cell mobilization required for CD8 T-cell immune responses. *J. Invest. Dermatol.*, **132** (3 Pt 1), 615–625.

45 Surber, C. and Smith, E.W. (2005) The mystical effects of dermatological vehicles. *Dermatology*, **210** (2), 157–168.

46 Graf, C., Gao, Q., Schütz, I., Noufele, C.N., Ruan, W., Posselt, U., Korotianskiy, E., Nordmeyer, D., Rancan, F., Hadam, S., Vogt, A., Lademann, J., Haucke, V., and Rühl, E. (2012) Surface functionalization of silica nanoparticles supports colloidal stability in physiological media and facilitates internalization in cells. *Langmuir*, **28** (20), 7598–7613.

47 Rancan, F., Gao, Q., Graf, C., Troppens, S., Hadam, S., Hackbarth, S., Kembuan, C., Blume-Peytavi, U., Rühl, E., Lademann, J., and Vogt, A. (2012) Skin penetration and cellular uptake of amorphous silica nanoparticles with variable size, surface functionalization, and colloidal stability. *ACS Nano.*, **6** (8), 6829–6842.

48 Okuda-Shimazaki, J., Takaku, S., Kanehira, K., Sonezaki, S., and Taniguchi, A. (2010) Effects of titanium dioxide nanoparticle aggregate size on gene expression. *Int. J. Mol. Sci.*, **11**, 2383–2392.

49 Dhar, S., Kolishetti, N., Lippard, S.J., and Farokhzad, O.C. (2011) Targeted delivery of a cisplatin prodrug for safer and more effective prostate cancer therapy in vivo. *Proc. Natl. Acad. Sci. USA*, **108** (5), 1850–1855.

50 Castro, G.A., Oliveira, C.A., Mahecha, G.A., and Ferreira, L.A. (2011) Comedolytic effect and reduced skin irritation of a new formulation of all-trans retinoic acid-loaded solid lipid nanoparticles for topical treatment of acne. *Arch. Dermatol. Res.*, **303** (7), 513–520.

51 Castro, G.A., Coelho, A.L., Oliveira, C.A., Mahecha, G.A., Oréfice, R.L., and Ferreira, L.A. (2009) Formation of ion pairing as an alternative to improve encapsulation and stability and to reduce skin irritation of retinoic acid loaded in solid lipid nanoparticles. *Int. J. Pharm.*, **381** (1), 77–83.

52 Schneider, M., Stracke, F., Hansen, S., and Schaefer, U.F. (2009) Nanoparticles and their interactions with the dermal

barrier. *Dermatoendocrinol.*, **1** (4), 197–206.
53 Moghimi, H.R., Barry, B.W., and Williams, A.C. (1999) Stratum corneum and barrier performance: a model lamellar structural approach, in *Drugs–Cosmetics–Mechanisms–Methodology* (eds R.L. Bronaugh and H.I. Maibach), Marcel Dekker, New York, pp. 515–553.
54 Potts, R.O. and Guy, R.H. (1992) Predicting skin permeability. *Pharma. Res.*, **9**, 663–669.
55 Bos, J.D. and Meinardi, M.M.H.M. (2000) The 500 Dalton rule for the skin penetration of chemical compounds and drugs. *Exper. Dermatol.*, **9**, 165–169.
56 Otberg, N., Richter, H., Schaefer, H., Blume-Peytavi, U., Sterry, W., and Lademann, J. (2004) Variations of hair follicle size and distribution in different body sites. *J. Invest. Dermatol.*, **122**, 14–19.
57 Lademann, J., Richter, H., Teichmann, A., Otberg, N., Blume-Peytavi, U., Luengo, J., Weiss, B., Schaefer, U.F., Lehr, C.M., Wepf, R., and Sterry, W. (2007) Nanoparticles: an efficient carrier for drug delivery into the hair follicles. *Eur. J. Pharm. Biopharm.*, **66**, 159–164.
58 Lademann, J., Richter, H., Schaefer, U.F., Blume-Peytavi, U., Teichmann, A., Otberg, N., and Sterry, W. (2006) Hair follicles: a long-term reservoir for drug delivery. *Skin Pharmacol. Physiol.*, **19**, 232–236.
59 Langbein, L., Grund, C., Kuhn, C., Praetzel, S., Kartenbeck, J., Brandner, J.M., Moll, I., and Franke, W.W. (2002) Tight junctions and compositionally related junctional structures in mammalian stratified epithelia and cell cultures derived therefrom. *Eur. J. Cell Biol.*, **81**, 419–435.
60 Nohynek, G.J., Lademann, J., Ribaud, C., and Roberts, M.S. (2007) Grey goo on the skin? Nanotechnology, cosmetic and sunscreen safety. *Crit. Rev. Toxicol.*, **37**, 251–277.
61 Lademann, J., Richter, H., Schanzer, S., Knorr, F., Meinke, M., Sterry, W., and Patzelt, A. (2011) Penetration and storage of particles in human skin: perspectives and safety aspects. *Eur. J. Pharm. Biopharm.*, **77** (3), 465–468.
62 Lademann, J., Meinke, M., Sterry, W., and Patzelt, A. (2009) How safe are nanoparticles?. *Hautarzt*, **60** (4), 305–309.
63 Nasir, A. (2008) Dermatologic toxicity of nanoengineered materials. *Arch. Dermatol.*, **144** (2), 253–254. Nel, A., Zhao, Y., and Mädler, L. (2013) Environmental health and safety considerations for nanotechnology. *Acc. Chem. Res.*, **46** (3), 605–606.
64 Nakagawa, Y., Wakuri, S., Sakamoto, K., and Tanaka, N. (1997) The photogenotoxicity of titanium dioxide particles. *Mutat. Res.*, **394**, 125–132.
65 Allen, N.S., Edge, M., Sandoval, G., Verran, J., Stratton, J., and Maltby, J. (2005) Photocatalytic coatings for environmental applications. *Photochem. Photobiol.*, **81**, 279–290.
66 Simonsson, C., Madsen, J.T., Graneli, A., Andersen, K.E., Karlberg, A.T., Jonsson, C.A., and Ericson, M.B. (2011) A study of the enhanced sensitizing capacity of a contact allergen in lipid vesicle formulations. *Toxicol. Appl. Pharmacol.*, **252** (3), 221–227.
67 Madsen, J.T., Vogel, S., Karlberg, A.T., Simonsson, C., Johansen, J.D., and Andersen, K.E. (2010) Ethosome formulation of contact allergens may enhance patch test reactions in patients. *Contact Dermatitis*, **63** (4), 209–214.
68 Madsen, J.T., Vogel, S., Karlberg, A.T., Simonsson, C., Johansen, J.D., and Andersen, K.E. (2010) Ethosome formulations of known contact allergens can increase their sensitizing capacity. *Acta. Derm. Venereol.*, **90** (4), 374–378.
69 Elliott, C. (2010) The effects of silver dressings on chronic and burns wound healing. *Br. J. Nurs.*, **19** (15), S32–S36.
70 Chaloupka, K., Malam, Y., and Seifalian, A.M. (2010) Nanosilver as a new generation of nanoproduct in biomedical applications. *Trends Biotechnol.*, **28** (11), 580–588.
71 Jones, M.L., Ganopolsky, J.G., Labbé, A., Wahl, C., and Prakash, S. (2010) Antimicrobial properties of nitric oxide and its application in antimicrobial

formulations and medical devices. *Appl. Microbiol. Biotechnol.*, **88** (2), 401–407.
72 Jones, M.L., Ganopolsky, J.G., Labbé, A., and Prakash, S. (2010) A novel nitric oxide producing probiotic patch and its antimicrobial efficacy: preparation and *in vitro* analysis. *Appl. Microbiol. Biotechnol.*, **87** (2), 509–516.
73 Han, G., Nguyen, L.N., Macherla, C., Chi, Y., Friedman, J.M., Nosanchuk, J.D., and Martinez, L.R. (2012) Nitric oxide-releasing nanoparticles accelerate wound healing by promoting fibroblast migration and collagen deposition. *Am. J. Pathol.*, **180** (4), 1465–1473.
74 Jung, W.K., Koo, H.C., Kim, K.W., Shin, S., Kim, S.H., and Park, Y.H. (2008) Antibacterial activity and mechanism of action of the silver ion in *Staphylococcus aureus* and *Escherichia coli*. *Appl. Environ. Microbiol.*, **74** (7), 2171–2178.
75 Chamakura, K., Perez-Ballestero, R., Luo, Z., Bashir, S., and Liu, J. (2011) Comparison of bactericidal activities of silver nanoparticles with common chemical disinfectants. *Colloids Surf. B*, **84** (1), 88–96.
76 Cameron, P., Gaiser, B.K., Bhandari, B., Bartley, P.M., Katzer, F., and Bridle, H. (2015) Silver nanoparticles decrease the viability of *Cryptosporidium parvum* oocysts. *Appl. Environ. Microbiol.* DOI: 10.1128/AEM.02806-15.
77 Nhung, D.T., Freydiere, A.M., Constant, H., Falson, F., and Pirot, F. (2007) Sustained antibacterial effect of a hand rub gel incorporating chlorhexdine-loaded nanocapsules (Nanochlorex). *Int. J. Pharm.*, **334** (1–2), 166–172.
78 Weller, R. and Finnen, M.J. (2006) The effects of topical treatment with acidified nitrite on wound healing in normal and diabetic mice. *Nitric Oxide*, **15** (4), 395–399.
79 Fang, F.C. (2004) Antimicrobial reactive oxygen and nitrogen species: concepts and controversies. *Nat. Rev. Microbiol.*, **2** (10), 820–832.
80 Martinez, L.R., Han, G., Chacko, M., Mihu, M.R., Jacobson, M., Gialanella, P., Friedman, A.J., Nosanchuk, J.D., and Friedman, J.M. (2009) Antimicrobial and healing efficacy of sustained release nitric oxide nanoparticles against *Staphylococcus aureus* skin infection. *J. Invest. Dermatol.*, **129** (10), 2463–2469. Erratum in *J. Invest. Dermatol.* 2010, **130** (3), 908.
81 Surber, C., Ulrich, C., Hinrichs, B., and Stockfleth, E. (2012) Photoprotection in immunocompetent and immunocompromised people. *Br. J. Dermatol.*, **167** (Suppl 2), 85–93.
82 Carlotti, M.E., Ugazio, E., Sapino, S., Fenoglio, I., Greco, G., and Fubini, B. (2009) Role of particle coating in controlling skin damage photoinduced by titania nanoparticles. *Free Radic. Res.*, **43** (3), 312–322.
83 Wamer, W.G., Yin, J.J., and Wei, R.R. (1997) Oxidative damage to nucleic acids photosensitized by titanium dioxide. *Free Radic. Biol. Med.*, **23** (6), 851–858.
84 Durand, L., Habran, N., Henschel, V., and Amighi, K. (2010) Encapsulation of ethylhexyl methoxycinnamate, a light-sensitive UV filter, in lipid nanoparticles. *J. Microencapsul.*, **27** (8), 714–725.
85 Lademann, J., Richter, H., Golz, K., Zastrow, L., Sterry, W., and Patzelt, A. (2008) Influence of microparticles on the homogeneity of distribution of topically applied substances. *Skin Pharmacol. Physiol.*, **21** (5), 274–282.
86 Xia, Q., Saupe, A., Müller, R.H., and Souto, E.B. (2007) Nanostructured lipid carriers as novel carrier for sunscreen formulations. *Int. J. Cosmet. Sci.*, **29** (6), 473–482.
87 Olson, J., Dominguez-Medina, S., Hoggard, A., Wang, L.Y., Chang, W.S., and Link, S. (2015) Optical characterization of single plasmonic nanoparticles. *Chem. Soc. Rev.*, **44** (1), 40–57.
88 Collins, A. and Nasir, A. (2011) Nanotechnology and dermatology: benefits and pitfalls. *G. Ital. Dermatol. Venereol.*, **146** (2), 115–126.
89 Ribeiro, R.C., Barreto, S.M., Ostrosky, E.A., da Rocha-Filho, P.A., Veríssimo, L.M., and Ferrari, M. (2015) Production and characterization of cosmetic nanoemulsions containing *Opuntia ficus-indica* (L.) mill extract as moisturizing agent. *Molecules*, **20** (2), 2492–2509.

90 Deli, G., Hatziantoniou, S., Nikas, Y., and Demetzos, C. (2009) Solid lipid nanoparticles and nanoemulsions containing ceramides: preparation and physicochemical characterization. *J. Liposome Res.*, **19** (3), 180–188.

91 Walser, T., Demou, E., Lang, D.J., and Hellweg, S. (2011) Prospective environmental life cycle assessment of nanosilver T-shirts. *Environ. Sci. Technol.*, **45** (10), 4570–4578.

92 Costa, C., Conte, A., Buonocore, G.G., and Del Nobile, M.A. (2011) Antimicrobial silver-montmorillonite nanoparticles to prolong the shelf life of fresh fruit salad. *Int. J. Food Microbiol.*, **148** (3), 164–167.

93 Farkas, J., Peter, H., Christian, P., Gallego Urrea, J.A., Hassellöv, M., Tuoriniemi, J., Gustafsson, S., Olsson, E., Hylland, K., and Thomas, K.V. (2011) Characterization of the effluent from a nanosilver producing washing machine. *Environ. Int.*, **37**, 1057–1062.

94 Bansod, S.D., Bawaskar, M.S., Gade, A.K., and Rai, M.K. (2015) Development of shampoo, soap and ointment formulated by green synthesised silver nanoparticles functionalised with antimicrobial plants oils in veterinary dermatology: treatment and prevention strategies. *IET Nanobiotechnol.*, **9** (4), 165–171.

95 Li, Y., Leung, P., Yao, L., Song, Q.W., and Newton, E. (2006) Antimicrobial effect of surgical masks coated with nanoparticles. *J. Hosp. Infect.*, **62** (1), 58–63.

96 Lubick, N. (2008) Nanosilver toxicity: ions, nanoparticles or both? *Environ. Sci. Technol.*, **42**, 8617.

97 Pluut, O.A., Bianco, C., Jakasa, I., Visser, M.J., Krystek, P., Larese-Filon, F., Rustemeyer, T., and Kezic, S. (2015) Percutaneous penetration of silver from a silver containing garment in healthy volunteers and patients with atopic dermatitis. *Toxicol. Lett.*, **235** (2), 116–122.

98 Gallo, R.L. and Nakatsuji, T. (2011) Microbial symbiosis with the innate immune defense system of the skin. *J. Invest. Dermatol.*, **131** (10), 1974–1980.

99 Vogt, A., Mandt, N., Lademann, J., Schaefer, H., and Blume-Peytavi, U. (2005) Follicular targeting: a promising tool in selective dermatotherapy. *J. Investig. Dermatol. Symp. Proc.*, **10** (3), 252–255.

100 Jung, S., Patzelt, A., Otberg, N., Thiede, G., Sterry, W., and Lademann, J. (2009) Strategy of topical vaccination with nanoparticles. *J. Biomed. Opt.*, **14** (2), 021001.

101 Prow, T.W., Grice, J.E., Lin, L.L., Faye, R., Butler, M., Becker, W., Wurm, E.M., Yoong, C., Robertson, T.A., Soyer, H.P., and Roberts, M.S. (2011) Nanoparticles and microparticles for skin drug delivery. *Adv. Drug Deliv. Rev.*, **63** (6), 470–491.

102 Zolnik, B.S., González-Fernández, A., Sadrieh, N., and Dobrovolskaia, M.A. (2010) Nanoparticles and the immune system. *Endocrinology*, **151** (2), 458–465.

103 Jang, J., Lim, D.H., and Choi, I.H. (2010) The impact of nanomaterials in immune system. *Immune Netw.*, **10** (3), 85–91.

104 Zuo, L., Wei, W., Morris, M., Wei, J., Gorbounov, M., and Wei, C. (2007) New technology and clinical applications of nanomedicine. *Med. Clin. North Am.*, **91**, 845–862.

105 Shah, M., Badwaik, V.D., and Dakshinamurthy, R. (2014) Biological applications of gold nanoparticles. *J. Nanosci. Nanotechnol.*, **14** (1), 344–362.

106 Onoshima, D., Yukawa, H., and Baba, Y. (2015) Multifunctional quantum dots-based cancer diagnostics and stem cell therapeutics for regenerative medicine. *Adv. Drug Deliv. Rev.*, **95**, 1.

107 Lovrić, J., Bazzi, H.S., Cuie, Y., Fortin, G.R., Winnik, F.M., and Maysinger, D. (2005) Differences in subcellular distribution and toxicity of green and red emitting CdTe quantum dots. *J. Mol. Med. (Berl.)* **83** (5), 377–385.

108 Doepker, M.P. and Zager, J.S. (2015) Sentinel lymph node mapping in melanoma in the twenty-first century. *Surg. Oncol. Clin. North Am.*, **24** (2), 249–260.

109 Kim, S., Lim, Y.T., Soltesz, E.G., De Grand, A.M., Lee, J., Nakayama, A., Parker, J.A., Mihaljevic, T., Laurence, R.G., Dor, D.M., Cohn, L.H., Bawendi, M.G., and Frangioni, J.V. (2004) Near-infrared fluorescent type II quantum dots

for sentinel lymph node mapping. *Nat. Biotechnol.*, **22** (1), 93–97.

**110** Rolland, A., Wagner, N., Chatelus, A., Shroot, B., and Schaefer, H. (1993) Site-specific drug delivery to pilosebaceous structures using polymeric microspheres. *Pharm. Res.*, **10** (12), 1738–1744.

**111** Bhalekar, M., Upadhaya, P., and Madgulkar, A. (2015) Formulation and evaluation of adapalene-loaded nanoparticulates for epidermal localization. *Drug Deliv. Transl. Res.*, **5** (6), 585–595.

**112** Taglietti, M., Hawkins, C.N., and Rao, J. (2008) Novel topical drug delivery systems and their potential use in acne vulgaris. *Skin Therapy Lett.*, **13** (5), 6–8.

**113** Queille-Roussel, C., Poncet, M., Mesaros, S., Clucas, A., Baker, M., and Soloff, A.M. (2001) Comparison of the cumulative irritation potential of adapalene gel and cream with that of erythromycin/tretinoin solution and gel and erythromycin/isotretinoin gel. *Clin. Ther.*, **23** (2), 205–212.

**114** Bikowski, J. and Del Rosso, J.Q. (2008) Benzoyl peroxide microsphere cream as monotherapy and combination treatment of acne. *J. Drugs Dermatol.*, **7** (6), 590–595.

**115** Münster, U., Nakamura, C., Haberland, A., Jores, K., Mehnert, W., Rummel, S., Schaller, M., Korting, H.C., Zouboulis, ChC., Blume-Peytavi, U., and Schäfer-Korting, M. (2005) RU 58841-myristate: prodrug development for topical treatment of acne and androgenetic alopecia. *Pharmazie*, **60** (1), 8–12.

**116** Fang, C.L., Aljuffali, I.A., Li, Y.C., and Fang, J.Y. (2014) Delivery and targeting of nanoparticles into hair follicles. *Ther. Deliv.*, **5** (9), 991–1006.

**117** Blume-Peytavi, U. and Vogt, A. (2011) Human hair follicle: reservoir function and selective targeting. *Br. J. Dermatol.*, **165** (Suppl 2), 13–17.

**118** Lademann, J., Richter, H., Schanzer, S., Knorr, F., Meinke, M., Sterry, W., and Patzelt, A. (2011) Penetration and storage of particles in human skin: perspectives and safety aspects. *Eur. J. Pharm. Biopharm.*, **77** (3), 465–468.

**119** Patzelt, A., Richter, H., Knorr, F., Schäfer, U., Lehr, C.M., Dähne, L., Sterry, W., and Lademann, J. (2011) Selective follicular targeting by modification of the particle sizes. *J. Control. Release*, **150** (1), 45–48.

**120** Matos, B.N., Reis, T.A., Gratieri, T., and Gelfuso, G.M. (2015) Chitosan nanoparticles for targeting and sustaining minoxidil sulphate delivery to hair follicles. *Int. J. Biol. Macromol.*, **75**, 225–229.

**121** Madheswaran, T., Baskaran, R., Sundaramoorthy, P., and Yoo, B.K. (2015) Enhanced skin permeation of 5α-reductase inhibitors entrapped into surface-modified liquid crystalline nanoparticles. *Arch. Pharm. Res.*, **38** (4), 534–542.

**122** Möller, M. and Kalia, Y.N. (2014) Targeted cutaneous delivery of ciclosporin A using micellar nanocarriers and the possible role of inter-cluster regions as molecular transport pathways. *J. Control. Release*, **196**, 9–18.

**123** Vogt, A., Combadiere, B., Hadam, S., Stieler, K.M., Lademann, J., Schaefer, H., Autran, B., Sterry, W., and Blume-Peytavi, U. (2006) 40nm, but not 750 or 1, 500nm, nanoparticles enter epidermal CD1a+ cells after transcutaneous application on human skin. *J. Invest. Dermatol.*, **126**, 1316–1322.

**124** Nakamura, M., Jo, J., Tabata, Y., and Ishikawa, O. (2008) Controlled delivery of T-box21 small interfering RNA ameliorates autoimmune alopecia (alopecia areata) in a C3H/HeJ mouse model. *Am. J. Pathol.*, **172**, 650–658.

**125** Badea, I., Wettig, S., Verrall, R., and Foldvari, M. (2007) Topical noninvasive gene delivery using gemini nanoparticles in interferongamma-deficient mice. *Eur. J. Pharm. Biopharm.*, **65**, 414–422.

**126** Schlupp, P., Blaschke, T., Kramer, K.D., Höltje, H.D., Mehnert, W., and Schäfer-Korting, M. (2011) Drug release and skin penetration from solid lipid nanoparticles and a base cream: a systematic approach from a comparison of three glucocorticoids. *Skin Pharmacol. Physiol.*, **24** (4), 199–209.

**127** Zhang, J. and Smith, E. (2010) Percutaneous permeation of betamethasone 17-valerate incorporated in lipid nanoparticles. *J. Pharm. Sci.*, **100** (3), 896–903.

128 de Andrade, D.F., Fontana, M.C., Pohlmann, A.R., Guterres, S.S., Carlos, R., and Beck, R. (2015) Nanoencapsulation of clobetasol propionate decreases its penetration to skin layers without changing its relative skin distribution. *J. Nanosci. Nanotechnol.*, **15** (1), 875–879.

129 Ali, M.F., Salah, M., Rafea, M., and Saleh, N. (2008) Liposomal methotrexate hydrogel for treatment of localized psoriasis: preparation, characterization and laser targeting. *Med. Sci. Monit.*, **14** (12), PI66–PI74.

130 Fang, J.Y., Fang, C.L., Liu, C.H., and Su, Y.H. (2008) Lipid nanoparticles as vehicles for topical psoralen delivery: solid lipid nanoparticles (SLN) versus nanostructured lipid carriers (NLC) *Eur. J. Pharm. Biopharm.*, **70**, 633–640.

131 Saraswat, A., Agarwal, R., Katare, O.P., Kaur, I., and Kumar, B. (2007) A randomized, double-blind, vehicle-controlled study of a novel liposomal dithranol formulation in psoriasis. *J. Dermatolog. Treat.*, **18**, 40–45.

132 Rahman, M., Akhter, S., Ahmad, J., Ahmad, M.Z., Beg, S., and Ahmad, F.J. (2015) Nanomedicine-based drug targeting for psoriasis: potentials and emerging trends in nanoscale pharmacotherapy. *Expert Opin. Drug Deliv.*, **12** (4), 635–652.

133 Simões, M.C., Sousa, J.J., and Pais, A.A. (2015) Skin cancer and new treatment perspectives: a review. *Cancer Lett.*, **357** (1), 8–42.

134 Garbe, C., Peris, K., Hauschild, A., Saiag, P., Middleton, M., Spatz, A., Grob, J.J., Malvehy, J., Newton-Bishop, J., Stratigos, A., Pehamberger, H., and Eggermont, A. (2010) Diagnosis and treatment of melanoma: European consensus-based interdisciplinary guideline. *Eur. J. Cancer*, **46** (2), 270–283.

135 Nikolaou, V.A., Stratigos, A.J., Flaherty, K.T., and Tsao, H. (2012) Melanoma: new insights and new therapies. *J. Invest. Dermatol.*, **132** (3 Pt 2), 854–863.

136 Mohan, S.V. and Chang, A.L. (2014) Advanced basal cell carcinoma: epidemiology and therapeutic innovations. *Curr. Dermatol. Rep.*, **3**, 40–45.

137 Tran, M.A., Watts, R.J., and Robertson, G.P. (2009) Use of liposomes as drug delivery vehicles for treatment of melanoma. *Pigment Cell Melanoma. Res.*, **22** (4), 388–399.

138 Sahu, S., Saraf, S., Kaur, C.D., and Saraf, S. (2013) Biocompatible nanoparticles for sustained topical delivery of anticancer phytoconstituent quercetin. *Pak. J. Biol. Sci.*, **16** (13), 601–609.

139 Zhang, Z., Tsai, P.C., Ramezanli, T., and Michniak-Kohn, B.B. (2013) Polymeric nanoparticles-based topical delivery systems for the treatment of dermatological diseases. *Wiley Interdiscip. Rev. Nanomed. Nanobiotechnol.*, **5** (3), 205–218.

140 Mangalathillam, S., Rejinold, N.S., Nair, A., Lakshmanan, V.K., Nair, S.V., and Jayakumar, R. (2012) Curcumin loaded chitin nanogels for skin cancer treatment via the transdermal route. *Nanoscale*, **4** (1), 239–250.

141 Ferreira, D.M., Saga, Y.Y., Aluicio-Sarduy, E., and Tedesco, A.C. (2013) Chitosan nanoparticles for melanoma cancer treatment by photodynamic therapy and electrochemotherapy using aminolevulinic acid derivatives. *Curr. Med. Chem.*, **20** (14), 1904–1911.

142 Sabitha, M., Sanoj Rejinold, N., Nair, A., Lakshmanan, V.K., Nair, S.V., and Jayakumar, R. (2013) Development and evaluation of 5-fluorouracil loaded chitin nanogels for treatment of skin cancer. *Carbohydr. Polym.*, **91** (1), 48–57.

143 Janknegt, R., de Marie, S., Bakker-Woudenberg, I.A., and Crommelin, D.J. (1992) Liposomal and lipid formulations of amphotericin B. Clinical pharmacokinetics. *Clin. Pharmacokinet.*, **23** (4), 279–291.

144 Ceccoli, J., Rosales, N., Tsimis, J., and Yarosh, D.B. (1989) Encapsulation of the UV-DNA repair enzyme T4 endonuclease V in liposomes and delivery to human cells. *J. Invest. Dermatol.*, **93** (2), 190–194.

145 Yarosh, D., Klein, J., O'Connor, A., Hawk, J., Rafal, E., and Wolf, P. (2001) Effect of topically applied T4 endonuclease V in liposomes on skin cancer in xeroderma pigmentosum: a randomised study.

Xeroderma Pigmentosum Study Group. *Lancet*, **357** (9260), 926–929.

**146** Tanaka, K., Sekiguchi, M., and Okada, Y. (1975) Restoration of ultraviolet-induced unscheduled DNA synthesis of xeroderma pigmentosum cells by the concomitant treatment with bacteriophage T4 endonuclease V and HVJ (Sendai virus) *Proc. Natl. Acad. Sci. USA*, **72** (10), 4071–4075.

**147** Fink, W., Zimpfer-Rechner, C., Thoelke, A., Figl, R., Kaatz, M., Ugurel, S., and Schadendorf, D. (2004) Clinical phase II study of pegylated liposomal doxorubicin as second-line treatment in disseminated melanoma. *Onkologie*, **27** (6), 540–544.

**148** Szeimies, R.M., Lischner, S., Philipp-Dormston, W., Walker, T., Hiepe-Wegener, D., Feise, K., Podda, M., Prager, W., Kohl, E., and Karrer, S. (2013) Photodynamic therapy for skin rejuvenation: treatment options – results of a consensus conference of an expert group for aesthetic photodynamic therapy. *J. Dtsch. Dermatol. Ges.*, **11** (7), 632–636.

**149** Avci, P., Erdem, S.S., and Hamblin, M.R. (2014) Photodynamic therapy: one step ahead with self-assembled nanoparticles. *J. Biomed. Nanotechnol.*, **10** (9), 1937–1952.

**150** Souza, L.G., Silva, E.J., Martins, A.L., Mota, M.F., Braga, R.C., Lima, E.M., Valadares, M.C., Taveira, S.F., and Marreto, R.N. (2011) Development of topotecan loaded lipid nanoparticles for chemical stabilization and prolonged release. *Eur. J. Pharm. Biopharm.*, **79** (1), 189–196.

**151** Taveira, S.F., Araújo, L.M., de Santana, D.C., Nomizo, A., de Freitas, L.A., and Lopez, R.F. (2012) Development of cationic solid lipid nanoparticles with factorial design-based studies for topical administration of doxorubicin. *J. Biomed. Nanotechnol.*, **8** (2), 219–228.

**152** Marquele-Oliveira, F., Santana, D.C., Taveira, S.F., Vermeulen, D.M., de Oliveira, A.R., da Silva, R.S., and Lopez, R.F. (2010) Development of nitrosyl ruthenium complex-loaded lipid carriers for topical administration: improvement in skin stability and in nitric oxide release by visible light irradiation. *J. Pharm. Biomed. Anal.*, **53** (4), 843–851.

**153** Rao, Y.F., Chen, W., Liang, X.G., Huang, Y.Z., Miao, J., Liu, L., Lou, Y., Zhang, X.G., Wang, B., Tang, R.K., Chen, Z., and Lu, X.Y. (2015) Epirubicin-loaded superparamagnetic iron-oxide nanoparticles for transdermal delivery: cancer therapy by circumventing the skin barrier. *Small*, **11** (2), 239–247.

**154** Muddineti, O.S., Ghosh, B., and Biswas, S. (2015) Current trends in using polymer coated gold nanoparticles for cancer therapy. *Int. J. Pharm.*, **484** (1–2), 252–267.

**155** Devi, R.V., Doble, M., and Verma, R.S. (2015) Nanomaterials for early detection of cancer biomarker with special emphasis on gold nanoparticles in immunoassays/sensors. *Biosens. Bioelectron.*, **68**, 688–698.

**156** Kodiha, M., Wang, Y.M., Hutter, E., Maysinger, D., and Stochaj, U. (2015) Off to the organelles: killing cancer cells with targeted gold nanoparticles. *Theranostics*, **5** (4), 357–370. Ajith, T.A. (2015) Strategies used in the clinical trials of gene therapy for cancer. *J. Exp. Ther. Oncol.*, **11** (1), 33–39.

**157** Eghtedari, M., Liopo, A.V., Copland, J.A., Oraevsky, A.A., and Motamedi, M. (2009) Engineering of hetero-functional gold nanorods for the *in vivo* molecular targeting of breast cancer cells. *Nano Lett.*, **9** (1), 287–291.

**158** Nel, A., Xia, T., Mädler, L., and Li, N. (2006) Toxic potential of materials at the nano level. *Science*, **311** (5761), 622–627.

**159** Patra, C.R., Bhattacharya, R., Mukhopadhyay, D., and Mukherjee, P. (2010) Fabrication of gold nanoparticles for targeted therapy in pancreatic cancer. *Adv. Drug Deliv. Rev.*, **62** (3), 346–361.

**160** Volkov, Y. (2015) Quantum dots in nanomedicine: recent trends, advances and unresolved issues. *Biochem. Biophys. Res. Commun.*, **468** (3), 18, 419–427.

**161** Desai, P., Patlolla, R.R., and Singh, M. (2010) Interaction of nanoparticles and cell-penetrating peptides with skin for transdermal drug delivery. *Mol. Membr. Biol.*, **27** (7), 247–259.

**162** Tang, L., Zhang, C., Song, G., Jin, X., and Xu, Z. (2013) *In vivo* skin penetration and

metabolic path of quantum dots. *Sci. China Life Sci.*, **56** (2), 181–188.

163 Hsu, S.H., Wen, C.J., Al-Suwayeh, S.A., Huang, Y.J., and Fang, J.Y. (2013) Formulation design and evaluation of quantum dot-loaded nanostructured lipid carriers for integrating bioimaging and anticancer therapy. *Nanomedicine (Lond.)*, **8** (8), 1253–1269.

164 Wenzel, J., Tormo, D., and Tüting, T. (2008) Toll-like receptor-agonists in the treatment of skin cancer: history, current developments and future prospects. *Handb. Exp. Pharmacol.*, **183** (183), 201–220.

165 Rook, A.H., Gelfand, J.C., Wysocka, M., Troxel, A.B., Benoit, B., Surber, C., Elenitsas, R., Buchanan, M.A., Leahy, D.S., Watanabe, R., Kirsch, I.R., Kim, E.J., and Clark, R.A. (2015) Topical resiquimod can induce disease regression and enhance T-cell effector functions in cutaneous T-cell lymphoma. *Blood*, **126** (12), 1452–1461.

166 Meyer, T., Surber, C., French, L.E., and Stockfleth, E. (2013) Resiquimod, a topical drug for viral skin lesions and skin cancer. *Expert Opin. Investig. Drugs*, **22** (1), 149–159.

167 Gnjatic, S., Sawhney, N.B., and Bhardwaj, N. (2010) Toll-like receptor agonists: are they good adjuvants? *Cancer J.*, **16** (4), 382–391.

168 Annabi, N., Tamayol, A., Shin, S.R., Ghaemmaghami, A.M., Peppas, N.A., and Khademhosseini, A. (2014) Surgical materials: current challenges and nano-enabled solutions. *Nano. Today*, **9** (5), 574–589.

169 Rose, S., Prevoteau, A., Elzière, P., Hourdet, D., Marcellan, A., and Leibler, L. (2014) Nanoparticle solutions as adhesives for gels and biological tissues. *Nature*, **505** (7483), 382–385.

170 Meddahi-Pellé, A., Legrand, A., Marcellan, A., Louedec, L., Letourneur, D., and Leibler, L. (2014) Organ repair, hemostasis, and *in vivo* bonding of medical devices by aqueous solutions of nanoparticles. *Angew. Chem. Int. Ed. Engl.*, **53** (25), 6369–6373.

171 Poirot-Mazères, I. (2011) Legal aspects of the risks raised by nanotechnologies in the field of medicine. *J. Int. Bioethique*, **22** (1), 99–118.

172 Henkler, F., Tralau, T., Tentschert, J., Kneuer, C., Haase, A., Platzek, T., Luch, A., and Götz, M.E. (2012) Risk assessment of nanomaterials in cosmetics: a European union perspective. *Arch. Toxicol.*, **86** (11), 1641–1646.

173 Regulation (EC) No 1223/2009 of the European Parliament and of the Council of 30 November 2009 and amendments.

174 Bottini, M., Rosato, N., Gloria, F., Adanti, S., Corradino, N., Bergamaschi, A., and Magrini, A. (2011) Public optimism towards nanomedicine. *Int. J. Nanomedicine*, **6**, 3473–3485.

175 Capon, A., Gillespie, J., Rolfe, M., and Smith, W. (2015) Perceptions of risk from nanotechnologies and trust in stakeholders: a cross sectional study of public, academic, government and business attitudes. *BMC Public Health*, **15**, 424.

176 Vance, M.E., Kuiken, T., Vejerano, E.P., McGinnis, S.P., Hochella, M.F., Rejeski, D., and Hull, M.S. (2015) Nanotechnology in the real world: redeveloping the nanomaterial consumer products inventory. *Beilstein J. Nanotechnol.*, **6**, 1769–1780.

177 Duncan, T.V. (2011) The communication challenges presented by nanofoods. *Nat. Nanotechnol.*, **6** (11), 683–688.

178 Siegrist, M. (2010) Predicting the future: review of public perception studies of nanotechnology. *Hum. Ecol. Risk Assess.*, **16** (4), 837–846.

179 Sechi, G., Bedognetti, D., Sgarrella, F., Van Eperen, L., Marincola, F.M., Bianco, A., and Delogu, L.G. (2014) The perception of nanotechnology and nanomedicine: a worldwide social media study. *Nanomedicine (Lond.)*, **9** (10), 1475–1486.

180 Böl, G., Epp, A., and Hertel, R., Perception of nanotechnology in Internet-based discussions: the risks and opportunities of nanotechnology and nanoproducts: results of an online discourse analysis. Federal Institute for Risk Assessment. Berlin 2010 (BfR-Wissenschaft 08/2010).

# Part Five
# Benefiting Patients

# 17
# Therapeutic Development and the Evolution of Precision Medicine

*Gareth D. Healey and R. Steven Conlan*

*Swansea University, Swansea University Medical School, Swansea, SA2 8PP, United Kingdom*

## 17.1
## Origins of Nanomedicine

In attempting to visualize the scale of 1 nm, that is, a billionth of a meter, it is easier to consider orders of magnitude that allow us to compare our *macro* world to the *nano* world. An aircraft carrier with a length of about 200 m is 100 000 times larger than a 2 mm-long flea, and comparatively, the flea 100 000 times larger than the 2 nm-wide strand of DNA. Here, at the width of just 10 hydrogen atoms, particles no longer behave as solids, liquids, or gases, but rather exist within the world of quantum physics.

The origins of nanomedicine are generally attributed to the Manhatten Project physicist, Richard Feynman, who envisaged the possibility that patients may one day *swallow the surgeon*. His concept related to the idea that tiny robots also termed *nanobots* and related machines could be designed, manufactured, and introduced into the human body to perform cellular repairs at the molecular level [1]. This idea was captured in his lecture, delivered at Caltech in 1959, where he famously said: "There is plenty of room at the bottom. Many of the cells are very tiny, but they are active. They manufacture substance, they walk around, they wiggle, and they do all kinds of marvelous things – all on a very small scale. Consider the possibility that we too can make things very small, which does what we want, when we want – and that we can manufacture an object that maneuvers at that level." – Richard Feynman, 1959.

What has become clear retrospectively is that this lecture actually had little effect on the early development of nanotechnology. The first use of the term *nanotechnology* was by Eric Drexler in his 1986 book, "Engines of Creation: The Coming Era of Nanotechnology," in which he added a crucial aspect to Feynman's idea of miniature factories, suggesting that such entities could self-replicate via computer control [2]. This introduced the idea of a nanoscale assembler and with it the field of molecular nanotechnology, which Drexler

*Nanoscience and Nanotechnology for Human Health,* First Edition. Edited by Bert Müller and Marcel Van de Voorde.

successfully popularized. As molecular nanotechnology and molecular biology evolved into the nanomedicine of today, so it is important to accept that the terms *nano* and *molecular* both deal with manipulations at the same scale. Indeed, frequently the interface in nanomedical systems is between the engineered *nano* and the biological *molecular*. The roots of nanomedicine could arguably be traced to the advances in combinatorial chemistry and polymer therapeutics that paved the way for the rational design of small molecules and the emergence of techniques to improve therapeutic index [3]. These techniques are an integral part of nanomedicine, and as the discipline has evolved, it has added to these techniques combining molecular biology and combinatorial chemistry to create nanoengineered systems with synthetic, biologically inspired molecules. Ultimately, in the author's opinion, this will lead to nanomolecular unification and the development of targeted biological/bioinspired nanoparticles delivering molecular payloads that alter cellular fate.

While Feynman was not solely responsible for the emergence of the field of nanomedicine, the legacy of his ideas, together with the seminal discovery of the structure of DNA by Watson and Crick in 1953 [4], has been to change the way we approach medicine and therapeutic development. Historically, disease was viewed only at the anatomical level, a tumor for example that might consist of about a billion cells. However, advances in molecular medicine mean that we increasingly ascribe diseases to their molecular origins. This in turn has led to the emergence of nanomedicine, which incorporates knowledge of the molecular origins of a disease with rational drug design and the application of nanoscale materials for therapeutic development. Such an approach is essential for future advances in medicine. Providing the potential to increase the sensitivity of our diagnostic techniques down to the single-cell level, while also affording us the opportunity to address key challenges in human health that were previously untouchable with traditional therapeutic/diagnostic development approaches. This is achievable through molecularly targeted, rational drug design and the nanomedicine approach, see Figure 17.1.

## 17.2 Global Nanomedicine Market

In January 2000, US president Bill Clinton, in his State of the Union address, announced that he would seek 475 million USD for nanotechnology research and development via a national nanotechnology initiative, effectively doubling funding for the fiscal year 2001 and marking the beginning of an explosion in the global nanomedicine market. By 2002, funding had increased to greater than 500 million USD and by 2005 had reached 1 billion USD in the United States and 1.3 billion EUR in Europe [1].

This explosion of interest and funding is showing no sign of slowing. In 2012, the US market had reached 79 billion USD with anticancer nanomedicine products making up 5.5 billion USD of the market and oncology as a whole comprising 38% of the market share. Current projections suggest that the US market will

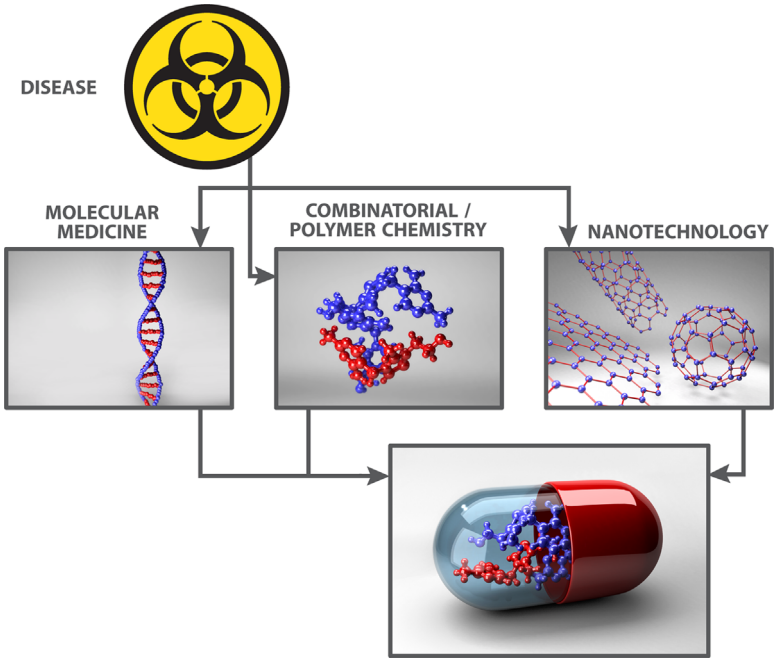


**Figure 17.1** The nanomedicine approach combines molecular medicine to understand the molecular basis of disease with combinatorial/polymer chemistry and nanotechnology to enable the rational design of molecularly targeted therapeutics with high potency and low toxicity.

reach 178 billion USD by 2019. By 2021, the global nanomedicine market is projected to reach 1 trillion USD, with 54 billion USD of that being nanotechnology-enabled diagnostics [1,5,6].

The United Kingdom is also at the forefront of this explosion, with 74 UK Research Council funded projects involving nanomedicine as applied to medicine or life sciences totaling 74 million GBP, currently active. In addition, the United Kingdom currently has 219 nanomedicine-related courses at 61 institutions across the country and in 2011, in recognition of the importance of the nanomedicine field, the United Kingdom government made nanomedicine an integral part of its life science strategy [7].

Across the world, nanomedicine has been embraced by governments, major pharmaceutical companies, and small and medium-sized enterprises as the future of medical advancement.

## 17.3 Nanomedicine Cabinet

Of course, nanoparticles are not new. Biological systems are inherently composed of nanoscale building blocks, and this concatenation means that investigations in

molecular biology are pursued at the nanoscale. What is new is the ability to control production and make particles of specific shapes and sizes. The silicon chip boom of the 1980s gave chemists the technology to begin manipulating materials at the nanoscale, but initially this was done without thought of any biomedical application [1]. Similarly, the advent of the synthetic production of biomolecules, that is, DNA, RNA, and peptides, and artificial derivatives, such as peptide nucleic acids (PNA), gave biologists and physicists the biological building blocks, from which to create novel functional structures and to control molecular responses [8].

Perhaps the most significant technological advancement was the invention of the scanning tunneling microscope by Gerd Binnig and Heinrich Rohrer in 1981 [9]. Based on the concept of quantum tunneling, the scanning tunneling microscope allows the visualization and manipulation of individual atoms. Latterly, the development of the atomic force microscope led to molecular imaging of biological structures that did not require prior crystallization, which hither too had been a limiting factor with X-ray crystallography, in deriving structure–function information [10–12].

Advances in nanoscale manufacture such as atomic layer deposition, for depositing single-atom-thick uniform layers, and nanocrystal synthesis also advanced rapidly during the 1970s and 1980s. These techniques have subsequently become a key technology in the development of biomedical devices, in which the ability to specify surface properties is critical [13]. As nanoscale manufacture techniques continued to evolve, the first nanomaterials also began to emerge. One of the most significant materials to come from this early period was Buckminsterfullerene, which was first discovered in 1985 by Harold Kroto of the University of Sussex, UK, and by James R. Heath, Sean O'Brien, Robert Curl, and Richard Smalley of Rice University, Texas, USA during investigations into the constituents of astronomical dust. Later experimentation revealed laser ablation of graphite as a viable method to produce Buckminsterfullerenes, which are hollow, spherical molecules of carbon [14]. Kroto, Curl, and Smalley were awarded the 1996 Nobel Prize in Chemistry for their roles in the discovery of Buckminsterfullerene and the related class of molecules, the fullerenes. As pharmaceutical agents, soluble derivatives of the fullerenes show great potential with several examples or fullerene-based therapeutics already undergoing clinical trials [15]. Their size, low toxicity, and biocompatibility make them ideal as potential nanoscale delivery vehicles. In addition, there is evidence that fullerenes have antimicrobial properties [16–18].

As with the fullerenes, early nanomedicine products, such as nanocrystals, nanoparticle coatings, and semiconductor nanoparticles, were generally discovered serendipitously without any thought of medical application. By the 1990s, however, the usefulness of these chemical techniques and materials was becoming apparent.

One of the first developments, that found medical application, was the quantum dot. First, discovered in 1981 by Alexey Ekimov, a quantum dot is a nanocrystal of a semiconductor material that exhibits quantum mechanical

properties. They have been studied for many potential applications, including solar cells and diode lasers, but also have several characteristics that make them suitable for medical applications. The electronic characteristics of a quantum dot are closely related to its size and shape. Specifically, the frequency of light emitted by a quantum dot increases as its size decreases, meaning that the color of emitted light shifts from red to blue as the quantum dot size is decreased [19]. In addition, quantum dots are typically 10 times brighter than alternative fluorescent tags such as green fluorescent protein (GFP) and naturally chemically bind human proteins, making them ideal candidates for *in vitro* and *in vivo* labeling and diagnostic platforms [20]. While early generation, selenium- or cadmium-based quantum dots were inherently cytotoxic, a major limiting factor in their development, the recent emergence of ternary I–III–VI quantum dots comprising a variety of alternative molecules offers great potential as nontoxic platforms for development [21]. Single cell, and even single molecule, real-time tracking has been demonstrated using quantum dots due to the fact that they can be targeted to specific proteins. Within mice, the accumulation of quantum dots in lymph nodes has also been observed over a period of 4 months [22]. Further applications of quantum dots within nanomedicine include as a donor fluorophore in Förster resonance energy transfer and as a delivery modality for small interfering RNA [23]. Interestingly, recent advances in optical cell bar-coding using quantum dots have led to the development of a technique that does not require prior knowledge of a molecular target. Relying on the stochastic uptake dynamics of nanoparticles, the technique utilizes three quantum dots to generate over 17 000 unique color codes that are identifiable using a typical laboratory fluorescent microscope. After loading onto a population of cells, the quantum dots are internalized randomly meaning that the cells essentially self-label. The unique combination of each of the three colors within a particular cell allows it to be specifically identified and tracked during time-lapse microscopy experiments. Additionally, the number of quantum dots internalized by a cell can also reveal information about cell function, such as metabolism, cell cycle, or the phenotype of individual cells within a population [24].

As nanomaterials including nanostructured materials have continued to emerge over the last 30 years, the nanomedicine cabinet has expanded rapidly. These materials range from simple surfaces perforated with nanopores or gated nanosieves to highly complex structures such as tectodendrimers or remote-controlled biomolecules [25–27]. Increasingly, these nanomaterials find application in micro/nano devices, whereby microfabrication technologies are adapted to biological purposes. Immunosensors, such as those combining antibodies against the pregnancy biomarker, human chorionic gonadotrophin (hCG), with nanostructured materials, such as graphene, provide an excellent example of this approach [28,29]. Indeed, the versatility of graphene and other carbon-based nanomaterials for these applications is reflected by the significant investment in the graphene industry over the last 20 years.

Nanostructured materials also have potential therapeutic applications by themselves. Lipid-based liquid crystalline nanoparticles, for example, are emerging as a

novel, nontoxic, and highly effective drug delivery platform, particularly for lipophilic drugs [30,31]. Indeed, unpublished work from our laboratory is showing the versatility of this drug delivery modality for infectious diseases of the female genital tract.

Even simple nanomaterials can have life-changing applications. One of the earliest nanomedical devices, described in 1997, involved the fabrication of tiny chambers within single-crystalline silicon wafers. The interface between the chambers and the surrounding biological environment was via nanopores as small as 20 nm, which allow the passage of small molecules such as oxygen, glucose, and insulin, but prevent the passage of larger immune or pathogenic particles. Within these chambers, immune-isolated rat pancreatic cells could be sustained, remaining healthy for weeks, and secrete insulin in response to blood glucose concentration, while remaining hidden from the host immune system [32]. Modifications of this principle have also been demonstrated using pig islet cells encapsulated in nanoporous biocapsules and both techniques carry the advantage of avoiding the use of immunosuppressants that can have significant contraindications [33].

The flow of materials through nanopores can also be externally regulated, as demonstrated by nanopore-based DNA analysis, a single-molecule technique with great potential. By using an applied voltage to drive DNA molecules through a nanopore that separates chambers of electrolyte solution, the size and the structure of molecules can be determined based upon how they block the flow of ions between the chambers [34–36]. The potential of this approach relates to several advantages providing the possibility of label-free, rapid, and low-cost DNA sequencing. It has even been suggested that this technology may achieve the 1000 USD per human genome challenge set by the US National Institutes of Health. The technology is not without problems however, such as the need for ultraprecise, high-speed DNA detection that is beyond current optical and electrical technologies [37].

Nanoshells are another recent addition to the nanomedicine cabinet. These gold-coated silica particles, the size of a poliovirus virion, are unique in that their optical resonance is a function of the thickness of their metal layers. This provides a highly effective cancer drug delivery platform allowing nanoshells to be loaded with a drug embedded in a hydrogel polymer and injected into a host whereby they accumulate within tumors. Subsequent heating of the tumor with an infrared laser causes the nanoshells to melt and release their drug payload. However, nanoshells are just one of an ever growing array of nanomaterials with biomedical applications that continue to enter the nanomedicine cabinet, including graphene oxide, spherical nucleic acids, liposomes, DNA micelles, DNA tetrahedrons, and aptamer-tethered linear DNA nanostructures, the so-called DNA nanotrains [1,15,27,38–40].

Nucleic acid-based nanomedicines, an example of bottom-up molecular self-assembly, have emerged as a new paradigm in nanotechnology [41]. Molecular self-assembly is a fundamental process within biological organisms, but achieving the sophisticated spatial and temporal control required for rationally

designed biomolecules is challenging. Recent advances have led to the ability to control the synthesis of DNA tetrahedrons via the execution of a tightly regulated developmental molecular program. The DNA tetrahedron is constructed from six DNA hairpin strands arranged in such a manner as to maximize the number of correct base pairings. Fundamental to the process is that the structures initially keep key sequence domains inaccessible. Access to these sequences is via specific initiator strands enabling the reaction order to be controlled and the correct shaped molecule assembled [41].

As the technology has continued to evolve, so too has the array of nucleic acid structures that can be rationally designed and manufactured. The application of these products within nanomedicine and nanotechnology, ranges from high-resolution X-ray structural studies of molecular complexes that are difficult to crystallize in isolation, to biophysical studies of enzyme function, to drug delivery. Of particular interest, is that nucleic acid structures can be made to incorporate molecules other than nucleic acids, such as proteins, metallic nanoparticles, quantum dots, and fullerenes. As a result, materials and devices with a wide array of functionalities can potentially be constructed.

## 17.4
## Application of Nanomedicine – A Paradigm Shift

Nanomedicine as a discipline is unique in that its application requires a wide spectrum of skills and knowledge. As a result, a large number of interdisciplinary research programs have emerged across the world to support and exploit developments in the field. Current fields of investigation include nanoelectronics, that is, molecular manufacturing aimed at reducing the size of electronics to increase speed; nanobiotechnology, the combination of nanoscale engineering with biology to manipulate biological systems at the molecular level, or produce biologically inspired materials; targeting, using nanomaterials to deliver pharmaceuticals or diagnostic agents; and biosensing, that is, the interfacing of a nanodevice with the patient [1].

Nanomedicine has also changed the way we approach medicine, meaning that it has also changed our approach to drug discovery and development, perhaps best exemplified within the field of cancer biology. The first example of cancer therapy followed the discovery that rabbit breasts stopped producing milk following oophorectomy by Thomas Beatson at the end of the nineteenth century. Beatson reasoned that since the breast must be under the control of the ovary, oophorectomy might also be beneficial for breast cancer patients. His discovery of the effect of estrogen on breast cancer, despite the hormone not being discovered for another 30 years, followed by Charles Huggins' work demonstrating that prostate cancer in dogs could be stalled by castration or estrogen injection, paved the way for current hormone therapy for cancer [42].

As conventional anticancer drug discovery emerged at the beginning of the twentieth century, there was a heavy focus on cytotoxic agents. Most were

discovered serendipitously, beginning in the 1940s with the observation that WWII soldiers exposed to nitrogen mustards had significant lymphoid and myeloid suppression. US Army Lieutenant Colonel Stewart Francis Alexander, a medical doctor and member of President Eisenhower's medical staff, who was an expert in chemical warfare agents, theorized that since mustard gas suppressed the growth of certain rapidly dividing somatic cells, it could potentially be used in the treatment of certain types of cancers. Using this information, two pharmacologists, Louis Goodman and Alfred Gilman demonstrated that lymphomas within mice could be successfully treated with mustard agents [43]. Further work in humans demonstrated a dramatic, if temporary, effect in human patients, establishing for the first time that the cancer could be treated by pharmacological agents [44]. Although not known at the time, the mechanism of action of nitrogen mustards and their subsequent derivatives is nonspecific DNA alkylation. The result of DNA alkylation is the formation of interstrand cross-links, which are detected by the tumor protein, p53, resulting in the initiation of apoptosis [45].

Subsequent approaches to anticancer therapy included the use of antifolate agents and platinum [46–48]. Folic acid had been discovered in 1937 by Lucy Wills and although its mechanism of action was not understood, it was observed to stimulate the proliferation of acute lymphoblastic leukemia cells when administered to children with the disease. In what was arguably the first rational drug design, Sidney Farber a pathologist working at Harvard Medical School, used folate analogues to block the proliferation of acute lymphoblastic cells and induce remission in children with the disease [49]. The anticancer properties of platinum were discovered by Barnett Rosenberg, who observed the cessation of cell division, while investigating the effect of electric fields on bacterial growth. The effect was mediated by contamination of the growth medium with an electrolysis product of the platinum electrode and led to the development of platinum-based therapies such as mitoxantrone and cisplatin, which continue to this day to be a mainstay of cancer therapy. Cisplatin and other platinum-based cancer therapeutics are classified as alkylating-like compounds. While they have no alkyl group and, therefore, cannot carry out alkylating reactions, they function by inducing DNA cross-links in a number of ways. Cross-links are formed by the binding of platinum ions to DNA bases, usually guanine, which leads to the initiation of apoptosis and cell death.

The early definition of cancer as a disease of uncontrolled cell division meant that efforts were directed towards the identification of cytotoxic, antiproliferative compounds. As a result, tumor size regression became the primary marker of effectiveness in preclinical and clinical testing. The problems with this approach, however, was that it tended to favor the selection of compounds that only targeted rapidly growing tumors, led to far more compounds being discovered than could actually be screened and developed, and meant that the mechanism of action of these compounds became the subject of retrospective investigation.

Nanomedicine, in contrast, offered an opportunity for rational drug design, exemplified by the search for therapeutics targeting the disease

chronic myeloid leukemia (CML), the first cancer to be linked to a specific genetic abnormality.

## 17.5 Targeted Drug Discovery and the Human Kinome

Traditional approaches to cancer drug discovery, with a focus on cytotoxic, antiproliferative molecules, meant that cell screening models were based on cytotoxic or cytostatic activity. Additionally, animal models typically focused on tumor regression and survival advantage, while early human trials were aimed at determining the limiting doses where significant toxicity was observed. Molecularly targeted drugs, however, often act by mechanisms that may not result in direct and significant toxicity. Therefore, molecularly targeted drugs required an altered drug development process to account for their toxicity profile and the fact that their mechanism of action was known.

Although often more complex and laborious, prior knowledge of the mechanism of drug action provided a focus for redefining the drug development process. The use of molecular biology to derive the molecular origins of disease enabled drug evaluation models to be developed that specifically demonstrate the effect of a drug on its molecular target. Although often insufficient to determine clinical efficacy, their use was to validate an approach and provide complete understanding of the mechanism of drug action. The advantage of this approach is that such information could potentially expedite the preclinical phase of drug development. In addition, such drug-specific models often provide surrogate markers to guide escalation studies during human trials, and potential biomarkers. This was exemplified during the development of the first kinase inhibitor, Gleevec™, arguably the first drug developed using a nanomedicine approach.

Protein phosphorylation was discovered in the 1950s by Krebs and Fischer during their studies on glycogen phosphorylase, which led to the discovery of phosphorylase kinase [50]. This discovery paved the way for the discovery of one of the most important groups of enzymes in drug development, protein kinases, which function by transferring a terminal phosphate from adenosine triphosphate (ATP) to a substrate, thereby altering the function of the substrate. These proteins are a set of evolutionary ancient, highly conserved, highly dynamic, and precisely regulated molecular switches that control most biological processes in eukaryotic cells [51]. Following the initial description of phosphorylase kinase, further progress was slow until the 1980s and discovery of the tyrosine kinase Src, which highlighted an as yet unknown diversity to this set of proteins. Subsequently, there was an explosion in the number of kinases discovered, aided in no small part by the rapid improvement in molecular biology techniques during the period. To date, 518 protein kinases, including 90 tyrosine kinases, have been described in what now comprises the human kinome, and corresponds to nearly 2% of the human genome [51,52].

In CML, a chromosomal translocation between the long arms of chromosomes 9 and 22 results in an abnormal chromosome called the Philadelphia chromosome. The molecular consequence of this is the creation of a fusion gene that produces an abnormal protein called the BCR-Abelson protein. Originally described in 1960, the BCR-Abelson (BCR-Abl) protein has a truncated N-terminus resulting in unregulated kinase activity and high enzyme activity. Consequently, hematopoietic stem cells within the bone marrow that contain the translocation gain a proliferative advantage leading to the rapid expansion of cells carrying the Philadelphia chromosome [52].

The identification of the BCR-Abl protein, began a search for kinase inhibitors. The master key, ATP, which following binding causes a conformational change that leads to activation, was the starting point. In 1985, the laborious task of screening compounds that would inhibit the interaction of ATP with kinases was initiated, but it would take until 1990 before the first lead compound, a 2-phenylaminopyrimidine derivative, was identified. The compound had low specificity, inhibiting both serine/threonine and tyrosine kinases, but provided a starting point for a series of further derivatives to be synthesized. Computational modeling enabled several improvements that would enhance the activity of the original lead compound. Key modifications were the addition of a 3′-pyridyl group at the 3′-position of the pyrimidine, which enhanced the cellular activity, and the introduction of a benzamide group at the phenyl ring. This latter modification enabled a specificity shift from serine/threonine kinases to enhance activity against tyrosine kinases, specifically Abl, PDGF-R, and cKit. Further modifications including the introduction of a *flag-methyl* group at the 6-position of the aniline phenyl ring, and the attachment of a highly polar side chain, further enhanced the tyrosine kinase specificity and improved the bioavailability [52,53].

The drug Gleevec (Imatinib mesylate, cf. Figure 17.2) has become a shining example of rational drug design within cancer treatment and the nanomedicine approach to drug development. Gleevec functions by binding the kinase active site, in place of ATP, but sterically inhibiting the conformational change required for activation. X-ray crystallographic and nuclear magnetic resonance imaging studies confirmed that blockage of the conformational change is achieved by the long tail structure of Gleevec that accesses a groove at the back of the molecule. The result being that the kinase is locked in an inactive conformation and cannot phosphorylate its target protein [52,53].

Initial *in vitro* testing confirmed the sensitivity, that is, inhibited cell growth of Philadelphia chromosome positive cell lines to treatment with Gleevec, while Philadelphia chromosome negative cell lines were not affected. In addition, researchers developed a cell assay based upon the interleukin (IL)-13-dependent cell line 32D. These cells require IL-13 to grow in culture, however, by inducing the cells to produce the BCR-Abl protein, via transfection with a plasmid containing BCR-Abl, the cells proliferated uncontrollably, even in the absence of IL-13. Treatment of the 32D cells that now contained the BCR-Abl protein with Gleevec blocked proliferation [52,53].

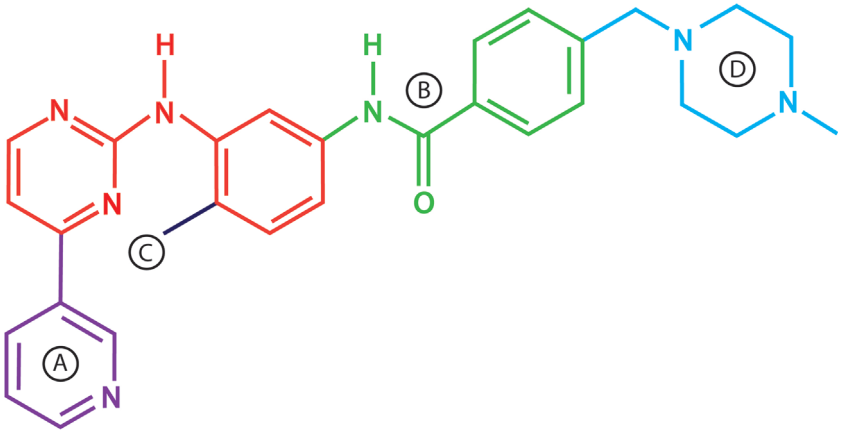


**Figure 17.2** Development of Gleevec from a 2-phenylaminopyrimidine backbone (red). (A) Cellular activity was improved by introducing a 3′-pyridyl group (purple) at the 3′-position of the pyrimidine. (B) Tyrosine kinase specificity was enhanced by addition of a benzamide group (green) to the phenyl ring. (C) Attachment of a "flag-methyl" group (violet) to the diaminophenyl ring reduced activity against PKC. (D) Addition of an *N*-methylpiperazine (blue) increased solubility and oral bioavailability.

In addition to proliferation, researchers also monitored the phosphorylation status of BCR-Abl in cells treated with Gleevec. Since kinases function by transferring a terminal phosphate from ATP to a substrate, kinase activation can be monitored by determining phosphorylation status. Analysis of BCR-Abl phosphorylation demonstrated that concentrations of Gleevec that blocked proliferation also blocked BCR-Abl phosphorylation confirming that Gleevec was working as predicted, and providing the basis of a surrogate marker when translating Gleevec development from the bench to the clinic [52,53].

## 17.6
## Translation from Discovery to the Clinic

The transition from discovery to clinical development is a complex process, a key aspect of which involves the transition from *in vitro* testing to *in vivo*. Traditionally, this takes the form of animal models of disease, which since 1975 for most cancers involves the use xenograft models of human cancer cells grown in nude mice. However, to better represent the human disease, developers of Gleevec undertook a key set of experiments that would ultimately lead to major investment from Sieber Geiger, now Novartis, in the clinical phase of Gleevec development.

Rather than rely on animal models of human CML, researchers developing Gleevec developed an *ex vivo* screening assay that utilized patient samples. Blood and bone marrow cells were taken from CML patients and normal control

patients without CML, and incubated in the presence of methylcellulose, a semi-solid matrix that promotes cell growth, and growth factors. The combination of factors used led to outgrowth of the precursors of granulocytes, myeloid and erythroid lineages, which could be quantified. Undertaking these growth experiments in the presence of Gleevec demonstrated that while in normal control patients there was no effect on cell growth, in the CML patients, cell growth was inhibited. This confirmed that Gleevec was also effective at preventing the growth of Philadelphia chromosome positive primary cells, but that it did not affect normal, Philadelphia chromosome negative cells. Additionally, analysis of the phosphorylation of BCR-Abl not only confirmed the mechanism of action of Gleevec in cells from CML patients, but also suggested that the BCR-Abl phosphorylation status would be a suitable surrogate marker and key element of subsequent clinical studies [51–53].

During phase I clinical studies of Gleevec, hematological responses showed that effective doses *in vivo* matched *in vitro* doses, in which phosphorylation of BCR-Abl was blocked, and monitoring the phosphorylation of BCR-Abl in patient samples over time and at different doses provided a biomarker of target engagement. Following FDA approval for CML patients in blast crisis in 2001, Gleevec reduced the US annual incidence of CML from ~2500 in 2001 to 270 by 2011 [52–54].

The success of Gleevec is attributable to the nanomedicine approach adopted for its development. By beginning from a position of knowledge regarding the molecular origins of CML, a molecularly targeted, low toxicity therapy was developed by using a combination of molecular biology, rational drug design, computational dynamics, and combinatorial chemistry. Indeed, following the emergence of clinically relevant escape mutations in the P- and Acivation-loops of BCR-Abl, a nanomedicine approach provided the solution. Escape mutations are a common occurrence, when selective pressure is placed on highly proliferative diseases. Specifically, they are single-nucleotide polymorphisms that arise within the active site of the molecule being targeted thereby changing the molecular structure of the molecule. For Gleevec, the emergence of escape mutations changed the structure of the BCR-Abl protein sufficiently to prevent binding and rendering the drug ineffective, see Figure 17.3. However, the identification of point mutations in the BCR-Abl gene by cloning and sequencing strategies enabled the rational design of second and third generation, molecularly targeted kinase inhibitors that were either effective in the presence of the mutation, or had higher potency against the primary target, thereby reducing the likelihood of escape mutations [51,55].

## 17.7
## Evolution of Kinase Inhibitors

Following the success of Gleevec, ATP-site-dependent competition binding assays were developed that enable the specificity of inhibitors to be characterized

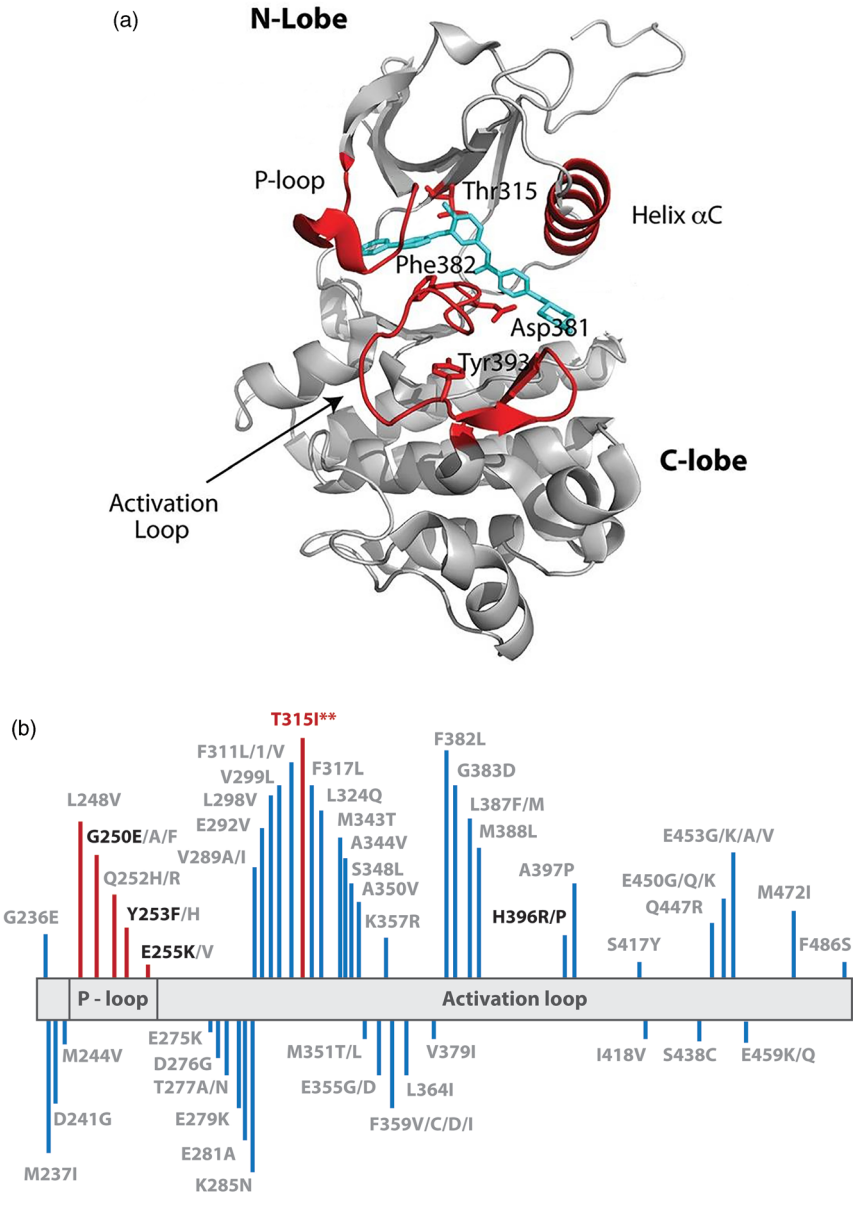


**Figure 17.3** ATP-competitive inhibition. (a) Crystal structure of the Abl kinase domain in complex with Gleevec (cyan) bound to the cleft between the N- and C-lobes of the kinase domain. The P-loop, activation loop, and helix αC are highlighted in red. (Reproduced with permission from Ref. [56].) (b) Diagrammatic Representation of escape mutations within the P-loop and activation loops of the Abl kinase that lead to Gleevec resistance.

for potentially all kinases of the human kinome. A number of methods have been developed for undertaking ATP-site-dependent competition binding assays, although they all aim to identify ligands that effectively bind one or more kinases within the kinome [51]. One such kinase assay employs human kinases expressed as fusions to T7 bacteriophage, a small set of immobilized probe ligands and a set of test *free* ligands. The kinases are essentially fusion proteins that have been tagged to facilitate expression, purification, and detection. The set of immobilized ligands are used to build the assay and, therefore, bind kinases with high affinity. If test compounds bind the kinase directly or indirectly occlude the ATP site, the protein will not bind to the immobilized ligands. Therefore, the read-out is based on the quantification of the amount of bound fusion protein achieved via techniques such as quantitative PCR or traditional phage plaque assays. The accuracy of this technique is sufficient to enable the detection of as few as 10–100 protein molecules [55].

The essential role of kinases in the regulating normal cell functions means that disease, especially cancers, is often a consequence of disrupted kinase activity. Kinase inhibitors have, therefore, become an important target for molecular drug design, reflected in the fact that approximately one third of all protein targets under investigation in the pharmaceutical industry are kinases, and there are currently over 200 kinase inhibitors undergoing clinical trials [57].

## 17.8 Nanoparticle Delivery

As therapeutics continues to evolve, a nanomedicine approach means that molecularly targeted therapeutics can be developed at the level of the drug or at the level of the delivery system. The use of nanoparticles is particularly suited to drug delivery and can in this sense provide a rationale for improving the therapeutic index of several classes of drugs beyond alterations to chemical structure. Over the last three decades, a large number of nanoparticle delivery systems have been developed for cancer therapy, which includes organic and inorganic materials. Liposomal, polymer–drug conjugates, and micellar formulations are becoming routinely used in clinics, and an even greater number of nanoparticle platforms are currently in the preclinical stages of development [40,58,59]. More recently developed nanoparticles are demonstrating the potential sophistication of these delivery systems by incorporating multifunctional capabilities and targeting strategies in an effort to increase the efficacy against the most difficult cancer challenges, including drug resistance and metastatic disease [40].

The first nanoscale delivery systems, liposomes, were described in the 1960s but have subsequently undergone a number of key developments that paved the way for the evolution of modern nanoparticle formulations. Liposomes are spherical vesicles comprising a single lipid bilayer that have become well-established nanocarriers for improving the therapeutic index of anticancer agents. The utility of liposomes springs from their ability to transport

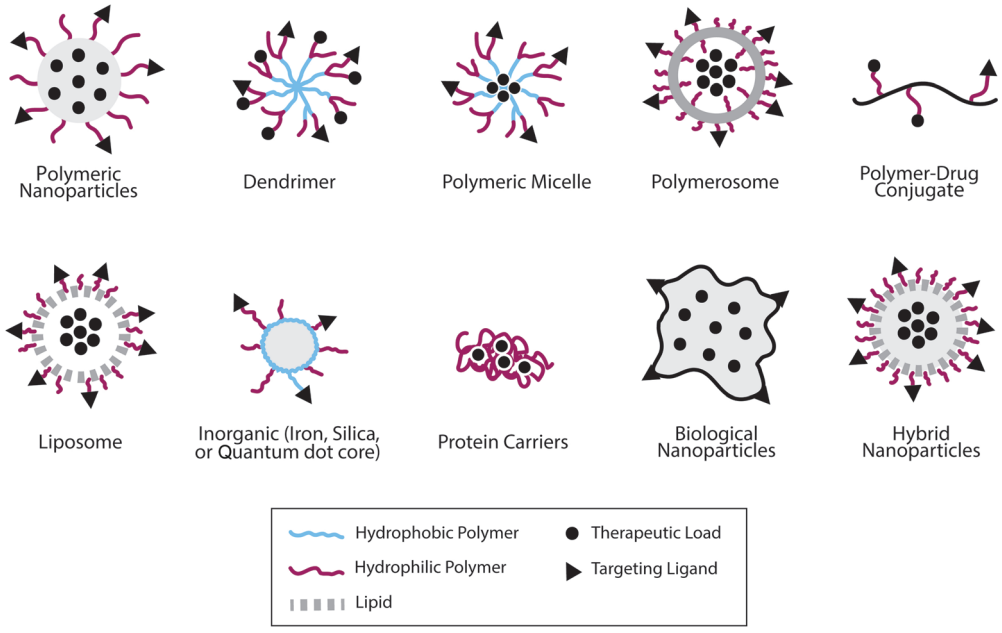


**Figure 17.4** Nanoparticle delivery platforms.

hydrophobic molecules, which associate with the bilayer, or hydrophilic molecules, which can be loaded into the liposome core, across biological membranes. The first demonstration of controlled-release polymer systems in 1976 by Langer and Folkman led to the first application of targeted liposomes in 1980. This was followed by the surface modification of liposomes and polymeric nanoparticles with polyethylene glycol in the early 1990s, which significantly increased *in vivo* half-life and conveyed the first *stealth* properties. The major success from this period of development was the approval of Doxil, a PEGylated, liposome encapsulated form of doxorubicin that is a potent treatment for multiple types of cancer. Indeed, the nanoparticle encapsulation of cytotoxic drugs to improve efficacy has become a well-established approach to cancer treatment. Nanoparticles comprising a polysilsesquioxane polymer cross-linked by a cisplatin prodrug have shown potential in a nonsmall cell lung cancer model, and cisplatin-loaded composite nanoparticles comprising magnetite and folate also show promise [60,61].

Nanomedicines for the treatment of cancer now include a wide array of nanoparticle delivery systems, see Figure 17.4, including polymeric nanoparticles, dendrimers, micelles, polymer conjugates, inorganic nanoparticles, bacterial nanocarriers, lipid-based nanoparticles, protein-based nanoparticles, nucleic acid-based nanoparticles, biological nanoparticles, and hybrid nanoparticles [38,62,63]. Indeed, a recent review of nanomedicine commercialization identified 247 nanomedicine products that are approved or in various stages of

clinical study [39]. As the technologies continue to evolve, nanoparticles are increasingly endowed with multifunctional characteristics enabling increased targeting specificity, controlled drug release profiles, and even the ability to respond to environmental stimuli to facilitate more effective drug delivery. The benefits of nanoparticle delivery systems are exemplified by the development of Gleevec loaded poly(lactide-*co*-glycolide) nanoparticles, which improve drug efficacy against cancer cells, while also reducing cardiotoxicity typically associated with Gleevec [64].

## 17.9 Conclusions

Nanomedicines have the potential to transform the treatment of the challenges faced in human health in major and orphan diseases. There is increasing recognition that heterogeneity within major diseases will only be tackled though the adoption of a precision medicine. The nanomedicine approach described herein encompasses a growing understanding of the molecular origin of disease with the latest advances in nanoengineering, combinatorial chemistry, and nanotechnology. Their combined effect is the potential to not only deliver novel therapeutics to diagnose and treat disease, through new nanotherapeutics and nanoenabled companion diagnostics, and improve quality of life, but also the opportunity to focus nanomedicine development with the aim of producing a streamlined and cost-effective industry.

## References


1 Freitas, R.A. Jr. (2005) What is nanomedicine? *Nanomedicine*, **1** (1), 2–9.
2 (eds) (1986) *Engines of Creation: The Coming era of Nanotechnology*, Doubleday.
3 Haag, R. and Kratz, F. (2006) Polymer therapeutics: concepts and applications. *Angew. Chem., Int. Ed.*, **45** (8), 1198–1215.
4 Watson, J.D. and Crick, F.H.C. (1953) Molecular structure of nucleic acids. *Nature*, **171** (4356), 737–738.
5 [Nanomedicine Market (Neurology, Cardiovascular, Anti-inflammatory, Anti-infective, and Oncology Applications) - Global Industry Analysis, Size, Share, Growth Trends and Forecast, 2013–2019] (2014).
6 [Nanotechnology in Drug Delivery: Global Market] (2012).
7 Reader, A. and Martinez, G. (2014) [UK Nanomedicine Market, Current Status and Future Prospects].
8 Service, R.F. (2002) Nanotechnology. Biology offers nanotechs a helping hand. *Supramol. Sci.*, **298** (5602), 2322–2323.
9 Binnig, G. and Rohrer, H. (1987) Scanning tunneling microscopy – from birth to adolescence. *Rev. Mod. Phys.*, **59** (3), 615–625.
10 Davies, E., Teng, K.S., Conlan, R.S., and Wilks, S.P. (2005) Ultra-high resolution imaging of DNA and nucleosomes using non-contact atomic force microscopy. *FEBS Lett.*, **579** (7), 1702–1706.
11 Dufrene, Y.F. (2014) Atomic force microscopy in microbiology: new structural and functional insights into the microbial cell surface. *MBio*, **5** (4), e01363–14.

12 Francis, L.W., Lewis, P.D., Wright, C.J., and Conlan, R.S. (2010) Atomic force microscopy comes of age. *Biol. Cell.*, **102** (2), 133–143.

13 Purniawan, A., French, P.J., Pandraud, G., and Sarro, P.M. (2010) $TiO_2$ ALD nanolayer as evanescent waveguide for biomedical sensor applications. *Procedia Eng.*, **5**, 1131–1135.

14 Kroto, H.W., Heath, J.R., O'brien, S.C., Curl, R.F., and Smalley, R.E. (1985) C60: Buckminsterfullerence. *Nature*, **318**, 162–163.

15 Partha, R. and Conyers, J.L. (2009) Biomedical applications of functionalized fullerene-based nanomaterials. *Int. J. Nanomed.*, **4**, 261–275.

16 Kolosnjaj, J., Szwarc, H., and Moussa, F. (2007) Toxicity studies of fullerenes and derivatives. *Adv. Exp. Med. Biol.*, **620**, 168–180.

17 Tsao, N., Kanakamma, P.P., Luh, T.Y., Chou, C.K., and Lei, H.Y. (1999) Inhibition of *Escherichia coli*-induced meningitis by carboxyfullerence. *Antimicrob. Agents Chemother.*, **43** (9), 2273–2277.

18 Tsao, N., Luh, T.Y., Chou, C.K., Wu, J.J., Lin, Y.S., and Lei, H.Y. (2001) Inhibition of group A *Streptococcus* infection by carboxyfullerene. *Antimicrob. Agents Chemother.*, **45** (6), 1788–1793.

19 Beane, G., Boldt, K., Kirkwood, N., and Mulvaney, P. (2014) Energy transfer between quantum dots and conjugated dye molecules. *J. Phys. Chem. C*, **118** (31), 18079–18086.

20 Resch-Genger, U., Grabolle, M., Cavaliere-Jaricot, S., Nitschke, R., and Nann, T. (2008) Quantum dots versus organic dyes as fluorescent labels. *Nat. Methods*, **5** (9), 763–775.

21 Subramaniam, P., Lee, S.J., Shah, S., Patel, S., Starovoytov, V., and Lee, K.B. (2012) Generation of a library of non-toxic quantum dots for cellular imaging and siRNA delivery. *Adv. Mater.*, **24** (29), 4014–4019.

22 Ballou, B., Lagerholm, B.C., Ernst, L.A., Bruchez, M.P., and Waggoner, A.S. (2004) Noninvasive imaging of quantum dots in mice. *Bioconjug. Chem.*, **15** (1), 79–86.

23 Algar, W.R. and Krull, U.J. (2008) Quantum dots as donors in fluorescence resonance energy transfer for the bioanalysis of nucleic acids, proteins, and other biological molecules. *Anal. Bioanal. Chem.*, **391** (5), 1609–1618.

24 Rees, P., Wills, J.W., Brown, M.R., Tonkin, J., Holton, M.D., Hondow, N., Brown, A.P., Brydson, R., Millar, V., Carpenter, A.E., and Summers, H.D. (2014) Nanoparticle vesicle encoding for imaging and tracking cell populations. *Nat. Methods*, **11** (11), 1177–1181.

25 Choi, C. (2002) Radio-controlled DNA act as gene switches. *United Press International*, 720.

26 Hamad-Schifferli, K., Schwartz, J.J., Santos, A.T., Zhang, S., and Jacobson, J.M. (2002) Remote electronic control of DNA hybridization through inductive coupling to an attached metal nanocrystal antenna. *Nature*, **415** (6868), 152–155.

27 Leistra, A.N., Han, J.H., Tang, S., Orr, B.G., Banaszak Holl, M.M., Choi, S.K., and Sinniah, K. (2015) Force spectroscopy of multivalent binding of riboflavin-conjugated dendrimers to riboflavin binding protein. *J. Phys. Chem. B*, **119** (18), 5785–5792.

28 Teixeira, S., Burwell, G., Castaing, A., Gonzalez, D., Conlan, R.S., and Guy, O.J. (2014) Epitaxial graphene immunosensor for human chorionic gonadotropin. *Sensor Actuat. B-Chem.*, **190**, 723–729.

29 Teixeira, S., Conlan, R.S., Guy, O.J., and Sales, M.G.F. (2014) Label-free human chorionic gonadotropin detection at picogram levels using oriented antibodies bound to graphene screen-printed electrodes. *J. Mater. Chem. B*, **2** (13), 1852–1865.

30 Chen, Y., Ma, P., and Gui, S. (2014) Cubic and hexagonal liquid crystals as drug delivery systems. *Biomed. Res. Int.*, **2014**, 815981.

31 Zeng, N., Gao, X., Hu, Q., Song, Q., Xia, H., Liu, Z., Gu, G., Jiang, M., Pang, Z., Chen, H., Chen, J., and Fang, L. (2012) Lipid-based liquid crystalline nanoparticles as oral drug delivery vehicles for poorly water-soluble drugs: cellular interaction and *in vivo* absorption. *Int. J. Nanomed.*, **7**, 3703–3718.

32 Desai, T.A., Chu, W.H., Tu, J.K., Beattie, G.M., Hayek, A., and Ferrari, M. (1998)

Microfabricated immunoisolating biocapsules. *Biotechnol. Bioeng.*, **57** (1), 118–120.
33 Leoni, L. and Desai, T.A. (2001) Nanoporous biocapsules for the encapsulation of insulinoma cells: biotransport and biocompatibility considerations. *IEEE Trans. Biomed. Eng.*, **48** (11), 1335–1341.
34 Healy, K. (2007) Nanopore-based single-molecule DNA analysis. *Nanomedicine (Lond)*, **2** (4), 459–481.
35 Meller, A., Nivon, L., Brandin, E., Golovchenko, J., and Branton, D. (2000) Rapid nanopore discrimination between single polynucleotide molecules. *Proc. Natl. Acad. Sci. USA*, **97** (3), 1079–1084.
36 Meller, A., Nivon, L., and Branton, D. (2001) Voltage-driven DNA translocations through a nanopore. *Phys. Rev. Lett.*, **86** (15), 3435–3438.
37 Feng, Y., Zhang, Y., Ying, C., Wang, D., and Du, C. (2015) Nanopore-based fourth-generation DNA sequencing technology. *Genomics Proteomics Bioinform.*, **13** (1), 4–16.
38 Blanco, E., Kessinger, C.W., Sumer, B.D., and Gao, J. (2009) Multifunctional micellar nanomedicine for cancer therapy. *Exp. Biol. Med. (Maywood)*, **234** (2), 123–131.
39 Etheridge, M.L., Campbell, S.A., Erdman, A.G., Haynes, C.L., Wolf, S.M., and McCullough, J. (2013) The big picture on nanomedicine: the state of investigational and approved nanomedicine products. *Nanomedicine*, **9** (1), 1–14.
40 Paliwal, S.R., Paliwal, R., Agrawal, G.P., and Vyas, S.P. (2011) Liposomal nanomedicine for breast cancer therapy. *Nanomedicine (Lond)*, **6** (6), 1085–1100.
41 Lee, H., Lytton-Jean, A.K.R., Chen, Y., Love, K.T., Park, A.I., Karagiannis, E.D., Sehgal, A., Querbes, W., Zurenko, C.S., Jayaraman, M., Peng, C.G., Charisse, K., Borodovsky, A., Manoharan, M., Donahoe, J.S., Truelove, J., Nahrendorf, M., Langer, R., and Anderson, D.G. (2012) Molecularly self-assembled nucleic acid nanoparticles for targeted *in vivo* siRNA delivery. *Nat. Nano*, **7** (6), 389–393.
42 Weisse, A.B. (ed) (1991) *Medical Odysseys: The Different and Sometimes Unexpected Pathways to Twentieth-century Medical Discoveries*, Rutgers University Press.
43 Goodman, L.S., Wintrobe, M.M. *et al.* (1946) Nitrogen mustard therapy; use of methyl-bis(beta-chloroethyl)amine hydrochloride and tris(beta-chloroethyl) amine hydrochloride for Hodgkin's disease, lymphosarcoma, leukemia and certain allied and miscellaneous disorders. *J. Am. Med. Assoc.*, **132**, 126–132.
44 Gilman, A. (1963) The initial clinical trial of nitrogen mustard. *Am. J. Surg.*, **105**, 574–578.
45 Fenn, J.E. and Udelsman, R. (2011) First use of intravenous chemotherapy cancer treatment: rectifying the record. *J. Am. Coll. Surg.*, **212** (3), 413–417.
46 Osborn, M.J., Freeman, M., and Huennekens, F.M. (1958) Inhibition of dihydrofolic reductase by aminopterin and amethopterin. *Proc. Soc. Exp. Biol. Med.*, **97** (2), 429–431.
47 Osborn, M.J. and Huennekens, F.M. (1958) Enzymatic reduction of dihydrofolic acid. *J. Biol. Chem.*, **233** (4), 969–974.
48 Wright, J.C., Prigot, A., Wright, B., Weintraub, S., and Wright, L.T. (1951) An evaluation of folic acid antagonists in adults with neoplastic diseases: a study of 93 patients with incurable neoplasms. *J. Natl. Med. Assoc.*, **43** (4), 211–240.
49 Farber, S. and Diamond, L.K. (1948) Temporary remissions in acute leukemia in children produced by folic acid antagonist, 4-aminopteroyl-glutamic acid. *N. Engl. J. Med.*, **238** (23), 787–793.
50 Fischer, E.H. and Krebs, E.G. (1955) Conversion of phosphorylase B to phosphorylase A in muscle extracts. *J. Biol. Chem.*, **216**, 121–132.
51 Matthews, D.J. and Gerritsen, M.E. (eds) (2010) *Targeting Protein Kinases for Cancer Therapy*, John Wiley & sons, Inc.
52 Deininger, M., Buchdunger, E., and Druker, B.J. (2005) The development of imatinib as a therapeutic agent for chronic myeloid leukemia. *Blood*, **105** (7), 2640–2653.
53 Capdeville, R., Buchdunger, E., Zimmermann, J., and Matter, A. (2002) Glivec (STI571, imatinib), a rationally

developed, targeted anticancer drug. *Nat. Rev. Drug Discov.*, **1** (7), 493–502.

**54** Moen, M.D., McKeage, K., Plosker, G.L., and Siddiqui, M.A. (2007) Imatinib: a review of its use in chronic myeloid leukaemia. *Drugs*, **67** (2), 299–320.

**55** Fabbro, D., Cowan-Jacob, S.W., Mobitz, H., and Martiny-Baron, G. (2012) Targeting cancer with small-molecular-weight kinase inhibitors. *Methods Mol. Biol.*, **795**, 1–34.

**56** Reddy, E.P. and Aggarwal, A.K. (2012) The ins and outs of bcr-abl inhibition. *Genes Cancer*, **3** (5–6), 447–454.

**57** Mariaule, G. and Belmont, P. (2014) Cyclin-dependent kinase inhibitors as marketed anticancer drugs: where are we now? A short survey. *Molecules*, **19** (9), 14366–14382.

**58** Sekhon, B.S. and Kamboj, S.R. (2010) Inorganic nanomedicine – part 2. *Nanomedicine*, **6** (5), 612–618.

**59** Sekhon, B.S. and Kamboj, S.R. (2010) Inorganic nanomedicine – part 1. *Nanomedicine*, **6** (4), 516–522.

**60** Rocca, J.D., Werner, M.E., Kramer, S.A., Huxford-Phillips, R.C., Sukumar, R., Cummings, N.D., Vivero-Escoto, J.L., Wang, A.Z., and Lin, W. (2015) Polysilsesquioxane nanoparticles for triggered release of cisplatin and effective cancer chemoradiotherapy. *Nanomedicine*, **11** (1), 31–38.

**61** Zhang, Y., Wang, X.-j., Guo, M., Yan, H.-s., Wang, C.-h., and Liu, K.-l. (2014) Cisplatin-loaded polymer/magnetite composite nanoparticles as multifunctional therapeutic nanomedicine. *Chin. J. Polym. Sci.*, **32** (10), 1329–1337.

**62** Duncan, R. (2006) Polymer conjugates as anticancer nanomedicines. *Nat. Rev. Cancer*, **6** (9), 688–701.

**63** Wong, P.T., Tang, S., Tang, K., Coulter, A., Mukherjee, J., Gam, K., Baker, J.R., and Choi, S.K. (2015) A lipopolysaccharide binding heteromultivalent dendrimer nanoplatform for Gram negative cell targeting. *J. Mater. Chem. B*, **3** (6), 1149–1156.

**64** Marslin, G., Revina, A.M., Khandelwal, V.K., Balakumar, K., Prakash, J., Franklin, G., and Sheeba, C.J. (2015) Delivery as nanoparticles reduces imatinib mesylate-induced cardiotoxicity and improves anticancer activity. *Int. J. Nanomed.*, **10**, 3163–3170.

# 18
# Benefit from Nanoscience and Nanotechnology: Benefitting Patients

*Bert Müller[1] and Marcel H. Van de Voorde[2]*

*[1]University of Basel, Department of Biomedical Engineering, Biomaterials Science Center, Gewerbestrasse 14, 4123 Allschwil, Switzerland*
*[2]Assembly, Paris Rue du Rhodania, 5, BRISTOL A, Appartement 31, 3963 Crans-Montana, Switzerland*

The key issues treated within this book are medically driven. The related research, however, requires detailed medical knowledge not only in the specific fields but also state-of-the-art materials science, physicochemical methodology, and advanced data analysis. Hence, the book is truly interdisciplinary. It bridges basic science all the way through translation to clinicians. This book connects physicists, chemists, and materials scientists to biologists, dentists, and clinicians across its entire field.

During the first decades of this century, the solvent foundations financially promote the application of nanoscience and nanotechnology in preventing, diagnosing, and treating numerous diseases, as the first part of this book impressively elucidates. These huge investments raise expectations of the society. Especially, the eligible expectations of the suffering patients should become satisfied. The translation of knowledge in nanotechnology to the bedside within a reasonable period of time is an urgent task of our community. The translation can only be successful by a collaborative effort. This book will be of some help.

The pioneers in biology and biochemistry of the last century set the scene for the currently available greater understanding of normal and disordered functions. It has become clearer and clearer that the cells with their extracellular matrix have a complex molecular life, which includes metabolic pathways and signaling. This natural nanoscale machinery can interact with man-made nanostructures with negative and positive feedback. In most cases, the human system recognizes the foreign bodies and develops related reactions. Therefore, it is particularly important to mimic natural counterparts. For example, we can consider the cell membrane formed by phospholipids. Such molecules also constitute the vesicles, which are going to save lives and support healing cardiovascular diseases. The properties of the vesicles can be even better tailored using artificial phospholipids. The discovery of shear-sensitive liposomes is a major milestone

*Nanoscience and Nanotechnology for Human Health,* First Edition. Edited by Bert Müller and Marcel Van de Voorde.

in the development of dedicated drug-delivery containers avoiding the serious side effects. It is, however, known that even FDA-approved liposomal formulations show comparably strong complement activation. Therefore, organic chemists and biochemists have to search for more appropriate formulations. Subsequently, immunologists and veterinary doctors must demonstrate the harmlessness. The current developments in the United States and Europe, often financially supported by donations, are promising but need more intensive efforts to bring the ideas from nanotechnology to the market within less than a decade.

Malignant neoplasms are known as cancers. Their treatment is challenging and many clever strategies have been applied. Since the success of the various therapeutic approaches is still limited and the primary underlying cause of cancer is found in DNA damages, one can reasonably expect serious contributions of nanotechnology to medication and radiation of malignant neoplasms. The widely used photon therapy, for example, will be replaced by particle therapy for an increasing number of cases simply because of physical reasons. This book describes these reasons in the necessary detail understandable for the broad readership. Nanotechnology-based drugs with multifunctional properties are other promising paths to successfully treat cancer patients. As the cancerous tissue grows faster than the healthy one, the supply with nutrients and oxygen is crucial. If one can prevent the growth of malignant neoplasms via significantly reduced supply and the enrichment of species to destroy the diseased tissue, many cancer patients will be cured. The diagnosis of cancer and the precise localization of malignant neoplasms within the body belong to the partly solved challenges. Here, nanomechanical devices will complement conventional pathology.

The interface between the human body and man-made materials is the key to reestablish necessary functions of our body. There are some oxidized metal implants with perfect tissue integration. Medical implants made out of polymers are often better suited than the radio-opaque metallic implants. One chapter elucidates the recent advances in biomimetically structured polymers. Anisotropies as present within the tissues of our body are relatively easy to implement. Such anisotropy is also required in crown repair. Remineralization to reestablish the mechanical performance of the natural dentin and enamel could be achieved within the next decade. The basic ideas in nanodentistry are available.

Dedicated devices based on cutting-edge nanotechnology are known in areas such as optics and electronics. In medicine, their application is more demanding especially because of security issues, wet environment, and encapsulation. The artificial sphincters are certainly such a killer application. Once thousands of nanometer-thin dielectric elastomer layers with compliant electrodes are built, many incontinent people will benefit.

Today, we already benefit from titania and zinc oxide nanoparticles to protect our skin in ultraviolet light. Although one reasonably believes that there is no danger related to these nanoparticles and the currently published studies do not show any serious impact on our body, their application needs caution. A more detailed understanding of the migration of nanoparticles through our skin in health and disease has to be generated.

Some of the important challenges are missing within the book. Tissue engineering, which often roots on the triage between cells, signaling molecules, and three-dimensional scaffolds, is not considered. These scaffolds are often prepared from absorbable materials. Such materials including magnesium alloys are applied for load-bearing implants and will play an important role because of their dedicated micro- and nanostructures. Dedicated features are fabricated by means of advanced nanotechnology.

The neurodegenerative diseases could also benefit from research and development in nanotechnology. Everybody knows that the electrical signals in our brain have amplitudes that well fit the voltages used in our mobile phones and other computers. The creation of suitable interfaces between the neurons and the cables/antenna of the man-made devices is an unsolved challenge and certainly needs ideas from nanosciences.

# Index



*Nanoscience and Nanotechnology for Human Health,* First Edition. Edited by Bert Müller and Marcel Van de Voorde.